



Environmental Engineering and Management Journal

Founding Editor: Matei Macoveanu

Editor-in-Chief: Maria Gavrilescu

Guest Editor: Dan Cascaval

Innovative Materials and Processes (1)



"Gheorghe Asachi" Technical University of Iasi

February 2015 Vol.14 No. 2

ISSN 1582 - 9596



Environmental Engineering and Management Journal

An International Journal

Founding Editor: Matei Macoveanu

Editor-in-Chief: Maria Gavrilescu

Guest Editor: Dan Cascaval

Innovative Materials and Processes (1)



“Gheorghe Asachi” Technical University of Iasi

EcoAdvertising Offer

The **Environmental Engineering and Management Journal** encourages initiatives and actions concerning the improvement of education, research, marketing and management, in order to achieve sustainable development. This journal brings valuable opportunities for those offering products, technologies, services, educational programs or other related activities, creating thus a closer relation with the request of the market in the fields of environmental engineering, management and education.

This journal address researchers, designers, academic staff, specialists with responsibilities in the field of environmental protection and management from government organizations (central and local administrations, environmental protection agencies) or from the private or public companies. Also, graduates of specialization courses or of the Environmental Engineering and Management profile, as well as other specialists may find in this journal a direct linkage between the offer and request of the market concerned with the protection of the environment and the administration of natural resources in the national and international context.

The journal was conceived as a means to develop scientific and technical relationships between people who offer and request solutions for environmental protection and conservation of natural resources, creating thus the premises to enhance the transfer of technology and know-how, the confirmation and implementation of ecological products and services.

Taking these aspects into consideration, we gladly welcome any persons or companies which correspond to the above-mentioned purposes and objectives to use our journal to identify potential collaborators, thus contributing to the support of this self-financed journal, which has a special section for eco-advertising.

Costs of advertising material publication

- I. Color ad – whole page, inside 160 €
Color ad – ½ page, inside 90 €
Color ad – ¼ page, inside 50 €
Color ad – other format, inside 0.50 €/cm²
- II. Black and white ad – whole page, inside 120 €
Black and white ad – ½ page, inside 75 €
Black and white ad – ¼ page, inside 45 €
Black and white ad – other format, inside 0.40 €/cm²
- III. Covers III, IV 220 €
- IV. Advertising article 80 €/page

At a constant publication of the advertising material, the following discounts will be offered:

- ✓ 3 publications 10%
- ✓ 6 publications 15%
- ✓ 12 publications 20%

For subscriptions and orders please contact us at:

**OAIMDD (Academic Organization for Environmental Engineering and Sustainable Development),
71 Mangeron Blvd., PO 10, Box 2111, 700050 Iasi, Romania, CIF: 10150285**

Phone/Fax: 0040-232-271759

E-mail: bmrobu.at.gmail.com mgav_eemj.at.yahoo.com

In LEI:

ALPHA BANK ROMANIA (ABR)

SWIFT Code: BUCUROBU

IBAN: RO87BUCU1032235333663RON

Beneficiary: OAIMDD-EEMJ

Adress: PO 10, Box 2111, 700050 Iasi, Romania

In EURO:

ALPHA BANK ROMANIA (ABR)

SWIFT Code: BUCUROBU

IBAN: RO79BUCU1031215940036EUR

Beneficiary: OAIMDD-EEMJ

Adress: PO 10, Box 2111, 700050 Iasi, Romania

**Department of Environmental Engineering and Management
OAIMDD-EcoZone Publishing House**

73 Prof.Dr.docent Dimitrie Mangeron Street, 700050-Iasi, Romania

Phone/Fax: 0040-232-271759

EDITORIAL BOARD

Founding Editor:

Matei Macoveanu *Gheorghe Asachi* Technical University of Iasi, Romania

Editor-in-Chief:

Maria Gavrilesu, *Gheorghe Asachi* Technical University of Iasi, Romania

Editorial Assistants:

Raluca-Maria Hlihor, *Gheorghe Asachi* Technical University of Iasi, Romania
Laura Bulgariu, *Gheorghe Asachi* Technical University of Iasi, Romania

SCIENTIFIC ADVISORY BOARD

Maria Madalena dos Santos Alves
University of Minho, Braga
Portugal

Abdeltif Amrane
University of Rennes, ENSCR
France

Ecaterina Andronescu
University *Polytechnica* of Bucharest
Romania

Robert Armon
Technion-Israel Institute of Technology, Haifa
Israel

Adisa Azapagic
The University of Manchester
United Kingdom

Hamidi Abdul Aziz
Universiti Sains Malaysia, Penang
Malaysia

Pranas Baltrenas
Vilnius *Gediminas* Technical University
Lithuania

Hans Bressers
University of Twente, Enschede
The Netherlands

Han Brezet
Delft University of Technology
The Netherlands

Dan Cascaval
Gheorghe Asachi Technical University of Iasi
Romania

Aleg Cherp
Central European University, Budapest
Hungary

Yusuf Chisti
Massey University, Palmerston North
New Zealand

Phillippe Corvini
University of Applied Sciences Northwestern Switzerland,
Muttens, Switzerland

Igor Cretescu
Gheorghe Asachi Technical University of Iasi
Romania

Silvia Curteanu
Gheorghe Asachi Technical University of Iasi
Romania

Andrew J. Daugulis
Queen's University Kingston
Canada

Valeriu David
Gheorghe Asachi Technical University of Iasi
Romania

Katerina Demnerova
University of Prague
Czech Republic

Gheorghe Duca
State University of Moldavia, Kishinev
Republic of Moldavia

Emil Dumitriu
Gheorghe Asachi Technical University of Iasi
Romania

Jurek Duszczek
Delft University of Technology
The Netherlands

Anca Duta Capra
Transilvania University of Brasov
Romania

Fabio Fava
Alma Mater Studiorum University of Bologna
Italy

Eugenio Campos Ferreira
University of Minho, Braga,
Portugal

Cristian Fosalau
Gheorghe Asachi Technical University of Iasi
Romania

Anton Friedl
Vienna University of Technology
Austria

Anne Giroir Fendler
University *Claude Bernard* Lyon 1
France

Ion Giurma
Gheorghe Asachi Technical University of Iasi
Romania

Yuh-Shan Ho
Peking University
People's Republic of China

Arjen Y. Hoekstra
University of Twente, Enschede
The Netherlands

Nicolae Hurdac
Gheorghe Asachi Technical University of Iasi
Romania

Ralf Isenmann
Munich University of Applied Sciences
Germany

Marcel Istrate
Gheorghe Asachi Technical University of Iasi
Romania

Ravi Jain
University of Pacific, Baun Hall Stockton
United States of America

Michael Sogaard Jørgensen
Aalborg University
Denmark

Nicolas Kalogerakis
Technical University of Crete, Chania
Greece

Gheorghe Lazaroiu
University *Polytechnica* of Bucharest
Romania

Thomas Lindhqvist
International Institute for Industrial Environmental
Economics, Lund University, Sweden

Andreas Paul Loibner
University of Natural Resources and Life Sciences,
Vienna, Austria

Tudor Lupascu
Academy of Sciences, Institute of Chemistry, Kishinev,
Republic of Moldavia

Antonio Marzocchella
University of Naples *Federico II*,
Naples, Italy

José Mondéjar Jiménez
University Castilla-La Mancha, Cuenca
Spain

Shin'ichi Nakatsuji
University of Hyogo
Japan

Valentin Nedeff
Vasile Alecsandri University of Bacau
Romania

Alexandru Ozunu
Babes-Bolyai University of Cluj-Napoca
Romania

Yannis A. Phillis
Technical University of Crete, Chania
Greece

Marcel Ionel Popa
Gheorghe Asachi Technical University of Iasi
Romania

Marcel Popa
Gheorghe Asachi Technical University of Iasi
Romania

Valentin I. Popa
Gheorghe Asachi Technical University of Iasi
Romania

Tudor Prisecaru
University *Polytechnica* of Bucharest
Romania

Gabriel-Lucian Radu
Polytechnica University of Bucharest
Romania

Ákos Rédey
Pannon University, Veszprém
Hungary

Joop Schoonman
Delft University of Technology
The Netherlands

Dan Scutaru
Gheorghe Asachi Technical University of Iasi
Romania

Bogdan C. Simionescu
Gheorghe Asachi Technical University of Iasi
Romania

Florian Stancu
Gheorghe Asachi Technical University of Iasi
Romania

Carmen Teodosiu
Gheorghe Asachi Technical University of Iasi
Romania

Saulius Vasarevicius
Vilnius Gediminas Technical University
Lithuania

Angheluta Vadineanu
The University of Bucharest
Romania

Colin Webb
The University of Manchester
United Kingdom

Peter Wilderer
Technical University Munich
Germany

Petra Winzer
Bergische University Wuppertal
Germany

Environmental Engineering and Management Journal

Environmental Engineering and Management Journal is included and indexed in

CABI

Chemical Abstracts Service/SciFinder (ACS) (since 2002)

EBSCO Database (since 2002)

EVISA

ICAAP (International Consortium for Advancement of Academic Publications)

Index Copernicus Journal Master List (ICV/2012=16.20)

Journal Citation Reports® (IF=1.258), (*Environmental Sciences*, Ranked **146 of 206**), (5-Year Impact Factor: 0.970

Article Influence® Score: 0.085)

MedSci

ProQuest (since 2002)

The National University Research Council (RO)

Science Citation Index Expanded™ (Thomson ISI)

SJR (SCImago Journal&Country Rank) (*Environmental Sciences*, Ranked **480 of 825**,

H=14, SJR index/2014 = 0.311, SNIP index/2014 = 0.64)

SCOPUS (since 2008)

Thomson ISI Master Journal List

Web of Science® (Thomson ISI) (H=20)

Home page: <http://omicron.ch.tuiasi.ro/EEMJ/>

Full text: <http://www.ecozone.ro>

Founding Editor: Matei Macoveanu, Iasi (RO)

Editor-in-Chief: Maria Gavrilescu, Iasi (RO)

Environmental Engineering and Management Journal is edited by

Gheorghe Asachi Technical University of Iasi and **EcoZone** Publishing House of the **Academic Organization for Environmental Engineering and Sustainable Development (O.A.I.M.D.D.)**

Editorial and Production Office:

Department of Environmental Engineering and Management - Faculty of Chemical Engineering and Environmental Protection

73 Prof.Dr.docent Dimitrie Mangeron Street, 700050 Iasi, Romania

Phone: +40-232-278680, ext. 2259, 2137

Fax: +40-232-271759

e-mail: eemjournal.at.yahoo.com, eem_journal.at.yahoo.com, eemjeditor.at.yahoo.com, eemj_editor.at.yahoo.com,

eemjournal.at.gmail.com, eemj.editor.at.gmail.com, eemj.office.at.gmail.com

Editorial production and secretariat:

Raluca-Maria Hlihor, Editorial Assistant 1

Laura Bulgariu, Editorial Assistant 2

Cristina Ghinea

Isabela Simion

Elena - Diana Comanita

Petronela Cozma

Mihaela Roşca

Camelia Smaranda

Administrative and financial support:

O.A.I.M.D.D., President Brindusa Mihaela Robu

Published 12 issues per year, under the aegis of the

"Gheorghe Asachi" Technical University of Iasi, Romania

by **EcoZone** Publishing House of the **Academic Organization for Environmental Engineering and Sustainable Development (OAIMDD)**, <http://www.ecozone.ro>

Annual subscription rate 2015 (12 issues)

Print:

EURO 500 per volume

EURO 50 per issue

Electronic:

400 per volume

40 per issue

Order directly to the Editorial Office

73 Prof.Dr.docent Dimitrie Mangeron Street, 700050 Iasi, Romania

Phone/Fax: Fax: +40-232-271759

e-mail: bmrobu.at.gmail.com

eemj.office.at.gmail.com

Electronic, full text:

Order or purchase on-line at: www.ecozone.ro

Bank account (EURO):

ALPHA BANK ROMANIA (ABR)

SWIFT Code: BUCUROBU

IBAN: RO79BUCU1031215940036EUR

Beneficiary: OAIMDD-EEMJ

Adress: PO 10, Box 2111, 700050 Iasi, Romania

Bank account (LEI):

ALPHA BANK ROMANIA (ABR), IBAN: RO87BUCU1032235333663RON, Beneficiary: OAIMDD-EEMJ

All rights reserved, including those of translation into foreign languages. No part of each issue may be reproduced in any form (photoprint, microfilm, or any other means) nor transmitted or translated without written permission from the publishers. Only single copies of contributions, or parts thereof, may be made for personal use.

This journal was carefully produced in all its parts. Even so, authors, editors and publisher do not guarantee the information contained there to be free of errors. Registered names, trademarks etc. used in this journal, even when not marked as such, are not to be considered unprotected by law.



“Gheorghe Asachi” Technical University of Iasi, Romania



CONTENTS

ICEEM08 Call

Editorial

- Innovative Materials and Processes
Dan Cascaval 267

Papers

- Study of the synthesis and environmental removal of 4,4'-dipyridine derivatives
Ana Chira, Bogdan Bucur, Toma Galaon, Gabriel-Lucian Radu..... 269
- Development and optimization of water based paint formula in order to reduce VOCs emissions
Andrei Ionut Simion, Irina Ionita, Cristina-Gabriela Grigoras, Lidia Gabriela Favier-Teodorescu, Lucian Gavrilă..... 277
- An improved methodology for determination of radiochemical and chemical impurities in the synthesis process of ^{18}F -FGD(2- ^{18}F) fluoro-2-deoxy-d-glucose)
Mirela Mihon, Catalin Tuta, Radu Leonte, Alina Catrinel Ion, Vasile Lavric, Dana Niculae 289
- Volatiles in *Tămâioasă Românească* via supercritical fluid extraction (SFE) analysis
Lucia Cintia Colibaba, Valeriu V. Cotea, Liliana Rotaru, Bogdan Nechita, Marius Niculău, Ștefan Tudose-Sandu-Ville, Camelia Luchian..... 297
- Development and validation of UV spectrophotometric method for determining the herbicide molinate with and without alginate microparticles
Ana M. Paiva, Berta N. Estevinho, Fernando Rocha, Olga C. Nunes 303
- Influence of hydroxypropyl-beta-cyclodextrin on the physicochemical and biological characteristics of a flavone with important pharmacological properties
Andreia Corciova, Bogdan Cioroiu, Cornelia Mircea, Cristina Tuchilus, Constantin Ciobanu, Cristina Dimitriu, Bianca Ivanescu 311
- Rural development through the optimization of the renewable energy potential
Liliana Topliceanu, Konstantinos Sioulas 321

Environmental impact and risk assessment of the main pollution sources from the Romanian Black Sea coast <i>Brindusa Robu, Oana Jitar, Carmen Teodosiu, Stefan-Adrian Strungaru, Mircea Nicoara, Gabriel Plavan</i>	331
Influence of extraction methods on Caraway (<i>Carum carvi</i> L.) essential oil yield and carvone/limonene ratio <i>Csaba Dezső András, Rozália Veronika Salamon, Imola Barabás, Irina Volf, Alexandru Szép</i>	341
Catalytic and non-catalytic pyrolysis of biologically treated manure <i>Maria Fernandez-Lopez, Maria Magdalena Parascanu, Diego López-González, Gabriela Soreanu, Antonio Avalos-Ramírez, Paula Sanchez, Jose Luiz Valverde, Luz Sanchez-Silva</i>	349
Case study on energy efficiency of biogas production in industrial anaerobic digesters at municipal wastewater treatment plants <i>Alexandrina Zuza, Paul Șerban Agachi, Vasile Mircea Cristea, Abhilash Nair, Nguyen Ngoc Tue, Cristina Horju-Deac</i>	357
Characterization of dyes loaded PVA based hydrogels through CIELAB method <i>Adina Papancea, Silvia Patachia</i>	361
Separation of aromatic intermediates of biological interest using emulsion liquid membranes <i>Alexandra Raluca Miron, Aurelia Cristina Nechifor, Abbas Abdul Kadhim Klaif Rikabi, Szidonia Katalin Tanczos</i>	373
Layered double hydroxides as adsorbents for anionic dye removal from aqueous solutions <i>Maria Celina Alexandrica, Mihaela Silion, Doina Hritcu, Marcel Ionel Popa</i>	381
New complexes of 2-(1H-1, 2, 4-Triazol-3-YL) pyridine with Co(II), Cd(II), Rh(III), ions: Synthesis, structure, properties and potential applications <i>Petronela Horlescu, Daniel Sutiman, Corneliu S. Stan, Carmen Mita, Cristian Peptu, Maria E. Fortuna, Cristina Albu</i>	389
Copper nanoparticles supported on polyether-functionalized mesoporous silica. Synthesis and application as hydrogenation catalysts <i>Constantin Rudolf, Irina Mazilu, Alexandru Chirieac, Brandusa Dragoi, Fatima Abi-Ghaida, Adrian Ungureanu, Ahmad Mehdi, Emil Dumitriu</i>	399
Comparative study of prehydrolysis methods for vegetal materials <i>Corina Măluțan, Adina Elena Pânzariu, Teodor Măluțan</i>	409
Studies on the photocatalytic degradation of organic dyes using CeO ₂ - ZnO mixed oxides <i>Gabriela Antoaneta Apostolescu, Corina Cernatescu, Claudia Cobzaru, Ramona Elena Tataru-Farmus, Nicolae Apostolescu</i>	415
Synthesis and electron transport properties of some new 4,7-phenanthroline derivatives in thin films <i>Cristina M. Al Matarneh, Ramona Danac, Liviu Leontie, Florin Tudorache, Iulian Petrila, Felicia Iacomî, Aurelian Carlescu, Gigel Nedelcu, Ionel Mangalagiu</i>	421

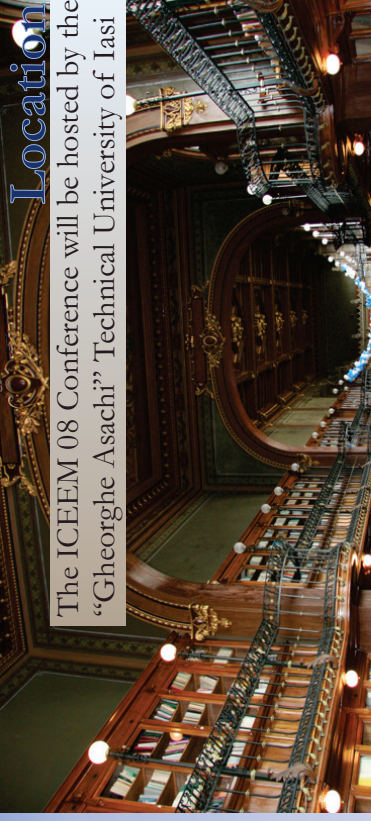
Distribution of oxygen transfer rates in stirred bioreactor for different fermentation broths - oxygen-vector dispersions <i>Anca-Irina Galaction, Alexandra Cristina Blaga, Corina Paraschiva Ciobanu, Marius Turnea, Dan Cașcaval</i>	433
Ion exchange processes on weak acid resins for wastewater containing cooper ions treatment <i>Cristina Modrogan, Alexandra Raluca Miron, Oanamari Daniela Orbulet, Cristina Costache, Giani Apostol</i>	449
Biosorption of antimony by brown algae <i>S.muticum</i> and <i>A.nodosum</i> <i>Gabriela Ungureanu, Silvia Santos, Rui Boaventura, Cidália Botelho</i>	455
Preliminary ecotoxicological evaluation of Erythrosin B and its photocatalytic degradation products <i>Laura Carmen Apostol, Camelia Smaranda, Mariana Diaconu, Maria Gavrilescu</i>	465
Pore structure characterization of chemically modified biochar derived from rice straw <i>Sobhy M. Yakout, Abd El Hakim M. Daifullah, Sohair A. El-Reefy</i>	473
Transformation of technogenic Cu and Zn compounds in chernozem <i>Tatiana M. Minkina, Tatiana V. Bauer, Abdulmalik A. Batukaev, Saglara S. Mandzhieva, Marina V. Burachevskaya, Svetlana N. Sushkova, Tatiana V. Varduni, Alexey K. Sherstnev, Valery P. Kalinichenko</i>	481
Health risk assessment of heavy metals and polycyclic aromatic hydrocarbons in soil at coke oven gas plants <i>Hou Wei, Zhang Le, Li Shuxian, Wu Dan, Li Xiaojun, Ji Lan, Ma Xiping</i>	487
Experimental study on the aeration oxygenation into printing and dyeing wastewater using jet aerator <i>Chunsheng Lei, Xiaofeng Zhu, Meicheng Zhou, Liangfei Dong, Feng e Zhang</i>	497

ICEEM 08

www.iceem.eu

9 - 12 September 2015

Iasi, Romania



Location

The ICEEM 08 Conference will be hosted by the "Gheorghe Asachi" Technical University of Iasi

Abstract Submission

The **extended abstract submission** should be done **no later than March 30, 2015**, via www.iceem.eu. After the review process, the accepted abstracts (2 pages) will be published electronically in a Book of Abstracts.

The 2nd Conference Call and decisions on **abstract acceptance will be available after May 1st 2015**.

Selected papers by the International Scientific Committee will be published in special issues of the journals:

- **Process Safety and Environmental Protection** (ISI impact factor: 1.829) will publish papers with the topics:
 - *Environmental pollution and monitoring*
 - *Water and wastewater treatment and management*
 - *Air pollution, prevention and treatment*
 - *Waste management for resources and energy recovery*

- **Environmental Engineering and Management Journal** (ISI impact factor 1.258) will publish papers with the topics:
 - *Sustainable production and consumption*
 - *Environmental management and sustainability assessments*
 - *Environmental education*

- **New Biotechnology** (ISI impact factor 2.106) will publish papers in:
 - *Environmental biotechnology*

The Conference language is English.

Fees

The fees for the ICEEM 08 Conference will include the conference materials (Program, Abstracts books), coffee breaks, lunches and conference dinner.

- Full fee: **300 EUR**,
- M.Sc. and PhD students fee: **150 EUR**. More details on www.iceem.eu

Contacts

For details please visit the conference site: www.iceem.eu, or contact the Conference Organizing Committee: iceem08@gmail.com



The "Gheorghe Asachi" Technical University of Iasi
Faculty of Chemical Engineering and Environmental Protection
Department of Environmental Engineering and Management



8th INTERNATIONAL CONFERENCE ON ENVIRONMENTAL ENGINEERING AND MANAGEMENT

1st Call for Papers



9 - 12 September 2015
IAȘI, ROMANIA
www.iceem.eu

Partners:

- European Federation of Biotechnology, Environmental Biotechnology section
- InterMEDIU - Information, Consultancy and DL Department, TUIASI, Romania
- Academic Organization for Environmental Engineering and Sustainable Development (OAIMDD), Iași, Romania



EUROPEAN FEDERATION OF BIOTECHNOLOGY

Foreword

After two editions abroad, in Hungary and Austria, the 8th edition of ICEEM will be organized in Iasi, Romania between 9 and 12 September 2015 by the “Gheorghe Asachi” Technical University of Iasi.

This ICEEM edition aims to bring together international researchers, academics, professionals and students activating in the fields of environmental engineering and management and to support knowledge exchange and dissemination of specific research and educational programmes.

Like before, ICEEM 08 strongly encourages contributions that focus on innovation, multidisciplinary and cross-sectorial approaches related to environmental issues and sustainability.

Furthermore, the ICEEM conference welcomes contributions of young and senior scientists, and at the same time it encourages practitioners and specialists in various environmental fields to add a more practical-oriented approach to the conference sessions.

We hope that the plenary sessions, oral and poster presentations, workshops and side-events of ICEEM 08 will enhance multidisciplinary, international cooperation and effective communication of scientists, engineers and managers.

Conference chairperson

Prof.dr., dr.h.c. Carmen Teodosiu
“Gheorghe Asachi” Technical University of Iasi

Topics

- I. Environmental pollution and monitoring
- II. Water & wastewater treatment and management
- III. Air pollution, prevention and treatment
- IV. Environmental biotechnology
- V. Environmental management and sustainability assessments
- VI. Sustainable production & consumption
- VII. Waste management for resources and energy recovery
- VIII. Environmental education, Workshops and Exhibitions

Events

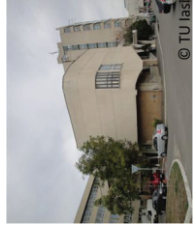
- Key note lectures
- Plenary Sessions
- Seminars
- Workshops
- Posters Sessions
- Social Events

International Scientific Committee

- | | |
|---|---|
| Prof.dr., dr.h.c. Maria Madalena dos Santos Alves
<i>University of Minho, Portugal</i> | Prof.dr. Maria Gavrilescu
<i>Technical University of Iasi, Romania</i> |
| Prof.dr. Tiberiu Apostol
<i>Politehnica University, Bucharest, Romania</i> | Prof.dr. Ion Giurma
<i>Technical University of Iasi, Romania</i> |
| Prof.dr. Adisa Azapagic
<i>The University of Manchester, UK</i> | Assoc. Prof.dr. Almudena Hospido
<i>University of Santiago de Compostela, Spain</i> |
| Prof.dr. Hans Bressers
<i>University of Twente, The Netherlands</i> | Prof.dr. Ovidiu Gabriel Iancu
<i>A.I.Cuza University Iasi, Romania</i> |
| Prof.dr. Han Brezet
<i>Delft University of Technology, The Netherlands</i> | Prof.dr., dr.h.c. Michael Jørgensen
<i>Aalborg University, Denmark</i> |
| Prof.dr. Dan Cascaval
<i>Technical University of Iasi, Romania</i> | Prof.dr. Nikolas Kalogerakis
<i>Technical University of Crete, Greece</i> |
| Prof.dr. Francesc Castells Piqué
<i>University of Rovira i Virgili Tarragona, Spain</i> | Prof.dr. Emmanuel G. Koukios
<i>National Technical University of Athens, Greece</i> |
| Prof.dr., dr.h.c. Yusuf Chisti
<i>Massey University, New Zealand</i> | Prof.dr. Gabriel Lazar
<i>Vasile Alecsandri University of Bacau, Romania</i> |
| Prof. dr. Philippe Corvini
<i>University of Applied Sciences and Arts Northwestern, Switzerland</i> | Prof.dr., dr.h.c. Thomas Lindqvist
<i>IIIIEE, Lund University, Sweden</i> |
| Prof.dr. Cristina Costache
<i>Politehnica University, Bucharest, Romania</i> | Assoc.prof.dr. Florica Manea
<i>Politehnica University Timisoara, Romania</i> |
| Prof.dr. Igor Cretescu
<i>Technical University of Iasi, Romania</i> | Prof.dr. Antonio Marzocchella
<i>University Federico II, Naples, Italy</i> |
| Prof.dr. Camelia Draghici
<i>Transilvania University of Brasov, Romania</i> | Prof.dr. Mircea Nicoara
<i>A.I.Cuza University Iasi, Romania</i> |
| Prof.dr. Fabio Fava
<i>Alma Mater Studiorum-University of Bologna, Bologna, Italy</i> | Prof.dr. Alexandru Ozunu
<i>Babeş Bolyai University, Cluj, Romania</i> |
| Prof.dr. Sorin Filipescu
<i>Babeş Bolyai University, Cluj Napoca, Romania</i> | Prof.dr. Carmen Postolache
<i>University of Bucharest, Romania</i> |
| Prof.dr., dr.h.c. Anton Friedl
<i>Vienna University of Technology, Austria</i> | Prof.dr., dr.h.c. Akos Rédey
<i>Pannonia University, Veszprem, Hungary</i> |
| | Prof.dr. Wilhelm Schabel
<i>Karlsruhe Institute of Technology, Germany</i> |
| | Acad.prof.dr. Bogdan Simionescu
<i>Technical University of Iasi, Romania</i> |

Organizing Committee

- | | |
|----------------------|------------------------|
| Dr. Brindusa Robu | Dr. George Barjoveanu |
| Dr. Adela Buburuzan | Dr. Daniela Gavrilescu |
| Dr. Catalin Balan | Dr. Camelia Smaranda |
| Dr. Daniela Fighir | Dr. Gabriela Sorceanu |
| Dr. Petronela Cozma | Dr. Raluca Hlilor |
| Dr.d. Irina Morosanu | Dr.d. Diana Comanita |





“Gheorghe Asachi” Technical University of Iasi, Romania



INNOVATIVE MATERIALS AND PROCESSES

2nd INTERNATIONAL CONFERENCE ON CHEMICAL ENGINEERING, ICCE 2014, 5 - 8 NOVEMBER 2014, IASI, ROMANIA

As many of us know, ten years ago we started to organize the *Days of Faculty of Chemical Engineering and Environmental Protection*, event focused mainly on the scientific results of the PhD and master students. Every year this initiative has grown and got more and more consistency. Thus, as a consequence of our faculty's position in the national top of scientific research, this conference became an international reference since 2012.

In fact, **the first edition of this international event has been dedicated to the celebration of 100 years of chemical engineering education in Iasi**, and I can affirm that **we represent the promoters of the oldest school on chemical engineering in Romania**, just considering the age, but not only. Because, as the result of its great promoters' initiatives, Moldova was destined for creating and developing the education on technical chemistry, which **appeared in 1882 with the first chemistry laboratory designed by Petru Poni at the University of Iasi**.

The field of chemistry will acquire more and more engineering valences, so the introduction and evolution of the Technological Chemistry Department and its specific courses leading to the approval by the Ministry of Religious Affairs and Public Education of the initiative to create **the Applied Chemistry specialization in 1906**, which will become **the Industrial Chemistry specialization, at the University of Iasi, in 1912**.

The *International Conference on Chemical Engineering (ICCE)* completes successfully the other traditional international event of the Faculty, more experienced and recognized, the *International Conference on Environmental Engineering and Management (ICEEM)*, which will be at the **8th edition** in 2015, being also organized every two years. The continuous alternation of these two important

scientific events underlines the attractiveness of the scientific areas that are found in the activity of our faculty members.

This year, we were happy to consider over 160 papers included in the conference program, an increased number from the previous edition. The authors of these communications or posters were coming from 13 countries. We were also pleased to attend to eight plenary conferences and six key-lectures, presented by scientific personalities in the field, from Romania or abroad.

At few days after Halloween, with any association with, only by coincidence, we celebrated during these three days the Chemical Engineering, which, together with the chemistry is considered a "horror" science for someones, an inaccessible area for others, a not at all easy profession, which apparently loses its attractiveness by many people. This is the trend observed with various magnitudes in different developed geographic regions of the world. However, it is really an artificial trend.

Even in the context of the less favorable economic environment, we never cease to believe that the progress of any human society can not be achieved without engineers and, obviously, without the large contribution of chemical engineers.

We, all the participants to this conference, through which we will present and expose, we have to show that chemical engineering is too far from losing even a bit of its creative and practical potential. Also, we have to underline that **the development of human society depends essentially and dramatically on the development of chemistry and chemical engineering**. Because, if something could give color, flavor, fascination, and trust to such technical field as engineering is, if something can create and perpetuate

life, if something can give value and brightness to an universe and can improve our universe, that "something" is the chemistry and chemical engineering.

Thanks to all colleagues from our country and abroad who have honored us these days and joined our joy to celebrate the Chemical Engineering.

I'd like to thank very much all my colleagues involved in the organization of this conference. Special thanks to the Alumni Association of Industrial Chemistry Faculty for its consistent support.

I am waiting to meet you again in 2016, at the next edition of the International Conference on Chemical Engineering.

Guest editor:

Professor Dan Cascaval
Dean of the Faculty of Chemical Engineering
and Environmental Protection
Gheorghe Asachi Technical University of Iasi, Romania



Professor DAN CAȘCAVAL, PhD, is the Dean of the Faculty of Chemical Engineering and Environmental Protection since 2008, being formerly the Head of the Organic and Biochemical Engineering Department and Director of Doctoral School of the Faculty.

Professor Dan Cascaval is specialist in the fields of biochemical engineering and biotechnology, being the promoter of the biochemical engineering courses in this academic curriculum. His competences and major scientific contributions are focused on bioseparations (*separation of biosynthetic compounds by liquid-liquid extraction with and without chemical reaction, extraction and transport through liquid membranes – free and facilitated pertraction, synergetic extraction and pertraction, direct extraction from unfiltered broths*) and bioreactors (*rheology of fermentation broths, efficiency and distribution of mixing into the stirred bioreactors, optimization of mixing, oxygen and substrate mass transfer, improvement of oxygen transfer by using oxygen-vectors, new bioreactors with mobile and packed beds of immobilized cells/enzymes*).

Professor Dan Cascaval is PhD supervisor and post-doctoral programs coordinator. His main contributions on the research areas are included in over 250 publications (125 papers in ISI ranked journals; 12 books and chapters; 8 patents) and 34 international and national grants. He was invited professor at The University of Manchester, Vienna University of Technology University, Karlsruhe University of Technology, University College London.

Professor Dan Cascaval is member of the Editorial Boards of 11 journals and of the Advisory Boards of over 30 journals, being also member of 5 scientific and professional organizations in the field of chemical and biochemical engineering and biotechnology



“Gheorghe Asachi” Technical University of Iasi, Romania



STUDY OF THE SYNTHESIS AND ENVIRONMENTAL REMOVAL OF 4,4'-DIPYRIDINE DERIVATIVES

Ana Chira^{1,2}, Bogdan Bucur^{1*}, Toma Galaon³, Gabriel-Lucian Radu^{1,2}

¹National Institute of Research and Development for Biological Sciences, Centre of Bioanalysis, 296 Splaiul Independentei, 060031 Bucharest, Romania

²Politehnica University of Bucharest, Faculty of Applied Chemistry and Materials Science, 1-7 Polizu Str., Bucharest 011061, Romania

³National Research and Development Institute for Industrial Ecology – ECOIND, 71-73 Drumul Podu Dambovitei, 060652 Bucharest, Romania

Abstract

Dipyridine derivatives are used on large scale and pose significant environmental problems. We have synthesized dipyridine derivatives with: 5-chlorovaleric acid, α -dichlorohydrin, iodoacetamide and 11-bromoundecanoic acid. The synthesized substituted compounds were investigated by LC-MS. The adsorptive removal of dipyridine derivatives from aqueous solution has been studied using medicinal activated carbon. The adsorption rate has been investigated under the controlled process parameters including adsorption time, carbon and organic compound concentration. The results from this study demonstrated that the activated carbon can be used as a low-cost adsorbent for the removal of environmental cationic dipyridine derivatives from the water environment.

Key words: 4,4'-dipyridine derivatives synthesis, activated carbon adsorption, LC-MS analysis

Received: November, 2014; Revised final: February, 2015; Accepted: February, 2015

1. Introduction

Dipyridine and various dipyridine derivatives are currently synthesized and used on a large scale (Howard et al., 1997). Methylviologen, also named paraquat is a very toxic herbicide to aquatic organisms and may cause long-term adverse effects in the aquatic environment (Chemwatch, 2008). Dipyridine derivatives useful in many applications such as: redox chromophores (Žmija and Małachowski, 2011), electrochromic displays (Cummins et al., 2000), battery half-cells (Michaelis, 1935), sensors (Chira et al., 2014), electron acceptors (Kotani et al., 2006), energy conversion materials (Bocarsly et al., 1980), herbicides (Monk, 1998), neuromuscular agents (Buruiana et al., 1991).

Mono, bi or polymeric dipyridine derivatives compounds may be synthesised from dipyridine and

the desired halogenated reagents. Various symmetrical or asymmetrical, mono or bisubstituted compounds derived from dipyridine are mentioned in literature among which (N-(2-carboxyl-ethyl)-N'-(4-vinylbenzyl)-4,4'-bipyridinium dichloride (Liu et al., 2004), 1-(11-dodecylsulfanyl-undecyl)-[4,4'] bipyridinium bromide (Casillia et al., 2004), alkylthiol-substituted viologen (Tang et al., 1996), polyviologens (Liu et al., 2007). The macrocycle cyclo(paraquat-o-phenylene-paraquat-p-phenylene) was synthesized using an o-xylene bridged bis (4,4'-bipyridinium) salt (Scheytza et al., 1998), cyclobis(paraquat-p-phenylene) ring and methyl viologen radical cation composed triradical tricationic complex (Fahrenbach et al., 2012) or viologen-based cyclophanes was synthesized starting from 1,4-bis-bromomethyl-benzene and 4,4'-dipyridine (Tanabe et al., 2009).

* Author to whom all correspondence should be addressed: e-mail: bucurica@yahoo.com; Phone: +40-021-22-00-900; Fax: +40-021-22-00-900

Dipyridine derivatives are organic pollutants which have attracted much attention due to their slow degradation and potential impact on the environmental.

Among various treatments for the removal of environmental contaminants from an aqueous solution, adsorption is an important retention and purification process eliminating the effluent toxicity (Arsene et al., 2013). Activated carbon is one of the most efficient adsorbents used for removing organic pollutants from industrial waste-waters (Al Duri et al., 1996).

This study reports synthetic strategies to a series of novel derivatives based on the dipyridine. The four syntheses reactions using 5-chlorovaleric acid, α -dichlorhidrin, iodoacetamide and 11-bromoundecanoic acid were studied by refluxing halogenated reagents with 4,4'-dipyridine.

The synthesized substituted compounds were investigated by HPLC-MS and were efficiently removed by adsorption on activated carbon.

2. Material and methods

All of reagents used for synthesis used in this paper 4,4'-dipyridine, 5-chlorovaleric acid, α -dichlorhidrin, iodoacetamide, 11-bromoundecanoic acid were purchased from Sigma-Aldrich. The solutions were analyzed using a UV/Vis-Thermo Evolution 260 Bio (Thermo Fischer Scientific). Adsorption studies were carried out with silica gel 100C8, aminopropyl silicagel (Fluka) and medicinal activated carbon (Carbocit-Biofarm) from a local pharmacy. Acetonitrile (ACN for HPLC) was produced by Biosolve. Aqueous solutions were prepared with purified water (18 M Ω cm⁻¹, Millipore).

HPLC analyses were performed using an Agilent 1260 series LC system (Agilent, Waldbronn, Germany) consisting of: binary pump, micro-degasser, thermostatted autosampler, thermostatted column compartment. The LC instrument was coupled with an Agilent 6410B triple-quadrupole mass analyzer fitted with an electrospray ionization source. Data acquisition and analysis were performed using Mass Hunter software, revision B.05.00. All chromatographic runs were carried out on a Zorbax Eclipse Plus C18 150 x 4.6 mm, 5 μ m column from Agilent Technologies. Column was thermostatted at 27°C.

3. Experimental

3.1. Syntheses of dipyridine derivatives

The reactions used to obtain dipyridine derivatives are shown in Fig. 1. It involves treating the 4,4'-dipyridine with reactive halogenated derivatives. It is interesting to note that reagent II has two chlorine moieties and thus multiple products can be obtained.

The syntheses were carried out in 45 mL acetonitrile and water [2:1] at reflux for 24 H or longer. A mixture of the 5-chlorovaleric acid (10 mmol L⁻¹) and 4,4'-dipyridine (2.5 mmol L⁻¹) was heated under reflux for the 24 h to obtain the product (I). In the similar method different halogenated reagents (2.5 mmol L⁻¹) were refluxed 24 h in the presence of dipyridine (10 mmol L⁻¹) to yield the products (II-1), (III), (IV). The resultant products (II-1, II-2 and II-3) were prepared by mixing solution of 4,4'-dipyridine (20 mmol L⁻¹) with α -dichlorhidrin (2.5 mmol L⁻¹) for the 68 h. The reaction mixtures were then cooled to room temperature and were stored at +4 °C.

3.2. HPLC-MS analysis

The analysis was carried out in isocratic conditions at a constant flow-rate of 0.3 mL/min. Mobile phase composition was a mixture of aq. 0.1% formic acid and acetonitrile in the ratio 40 / 60 (v/v). Sample injection volume was 1 μ L. Mass-spectrometric detection of analytes was made using Selected Ion Monitoring acquisition mode (SIM). Analyte SIM values, fragmentor voltages, ionization source parameters and other MS parameters are shown in Tables 1 and 2.

3.3. Adsorption procedure

The adsorption of the organic molecules obtained after syntheses reactions was carried out in Eppendorf tubes of 1 mL into which different volumes of reaction solutions and 20 mg milled activated carbon were added. The mixtures were shaken with Multi-Vortex for tubes at a temperature of 25 \pm 1°C for 30 min. After vortexing, the obtained solutions were centrifuged through a 30 micron membrane filters Millipore at 14,000 g for 15 min.

Table 1. MS acquisition parameters for dipyridine and investigated reaction products

Compound Name	Mass	MS2 Res	Dwell	Fragmentor	Polarity
4,4'-dipyridine	157.2	Unit	200	100	Positive
5-(4,4'-dipyridinium)-valeric acid	258.1	Widest	200	100	Positive
acetamide-4,4'-dipyridinium	215.1	Widest	200	100	Positive
11-(4,4'-dipyridinium)-undecanoic acid	342.1	Widest	200	100	Positive
1,3-di(4,4'-dipyridinium)-2-propanol	370.2	Widest	100	100	Positive
4,4'-di(3-chlor-2-propanol)-dipyridinium	342.1	Widest	100	100	Positive
1-(4,4'-dipyridinium)-3-chlor-2-propanol	250.1	Widest	100	100	Positive

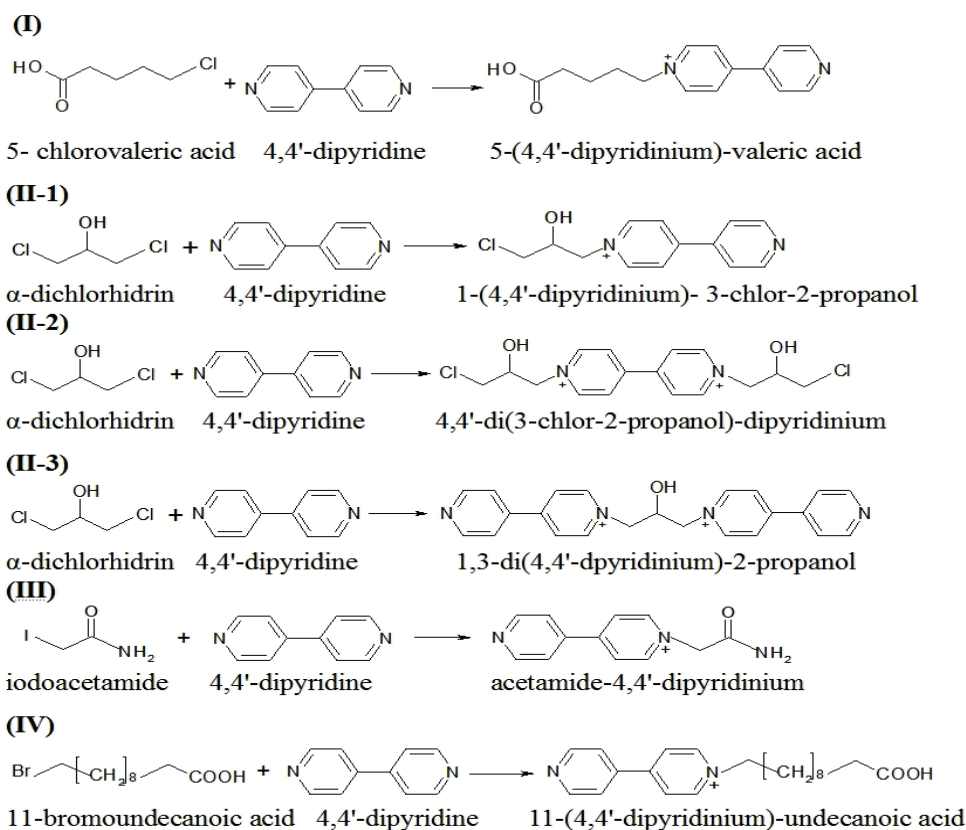


Fig. 1. Synthesis of dipyridine derivatives

Table 2. Electrospray ion source parameters

Drying Gas Flow (L/min)	10
Nebulizer Pressure (psig)	60
Drying Gas Temperature (°C)	300
Capillary Voltage (V)	3000

The all solutions before and after adsorption treatment were analyzed using a UV/Vis by monitoring the absorbance changes at a wavelength of maximum absorbance.

4. Results and discussion

4.1. Synthesis and characterization of dipyridine derivatives

The dipyridine derivatives can be obtained by alkylation with halogenated derivatives that can modify only one or both aromatic nitrogen atoms (mono or bisubstituted derivatives). The reaction yield obtained with different halogenated reagents depends on several factors such as: steric effects, electronic effects and reaction conditions (media, temperature, time). The halogenated reagents used in this work have also other functional moieties (acids, alcohol or amide).

In order to confirm the syntheses and to identify the structure of the obtained resultant products, the reaction mixtures were analyzed by LC-MS. The HPLC-MS analysis results present different peaks with retention time depending on the structure

of synthesized 4,4'-dipyridine derivatives present in the sample. The corresponding peak for 4,4'-dipyridine solution appear at 4.355 min (Fig. 2a).

The chromatograms recorded for a standard solution of 4,4'-dipyridine (277 $\mu\text{g/mL}$) and the refluxing reaction product between 4,4'-dipyridine and 5-chlorovaleric acid (I) are presented below in Fig. 2. For reaction (I) the HPLC-MS data indicated that monoalkylated derivative was obtained by starting 5-chlorovaleric. As it can be observed in Fig. 2b the reaction mixture contains the interest reaction product (5-(4,4'-dipyridinium)-valeric acid). The highest peak found in the sample appears at 3.873 min retention time and the peak area corresponds to 5.7 $\mu\text{g/mL}$ of synthesized compound. From this spectrum, it appears that mass of 258.1 is characteristic for the product of interest. The yield of this reaction was 2.07 %.

The product obtained by refluxing for 24 h of the reaction mixture 4,4'-dipyridine and 1,3-dichloro-2-propanol appears at 3.898 min and has a concentration of 174.1 $\mu\text{g/mL}$ of 1-(4,4'-dipyridinium)-3-chloro-2-propanol (II-1) (Fig. 3a). The reaction yield was 7.73 %. In Fig. 3b different reaction products (II-1, II-2 and II-3) obtained after 68 h refluxing of the same reaction are eluted out at different time intervals (3.898, 3.741 and respectively 3.755 min). These compounds form distinct chromatographic peaks by the mass values: 250.1 (II-1); 342.1 (II-2) and 370.2 (II-3) corresponding to mono and bisubstituted reaction products.

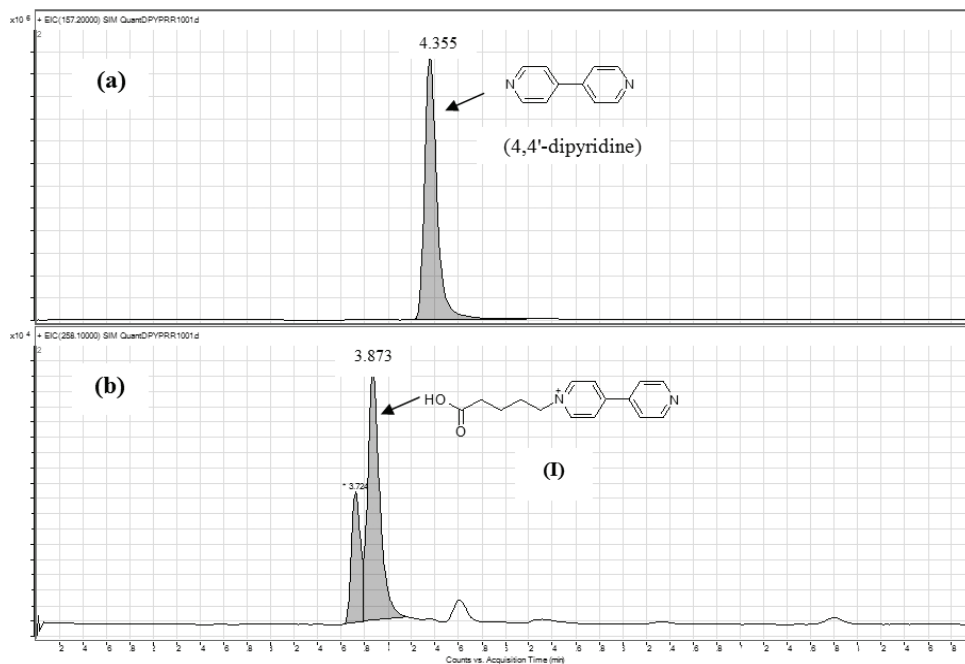


Fig. 2. Chromatograms recorded for the injection of: (a) standard solution of 4,4'-dipyridine (277 $\mu\text{g/mL}$) and (b) product resulted after reaction synthesis: 5-(4,4'-dipyridinium)-valeric acid

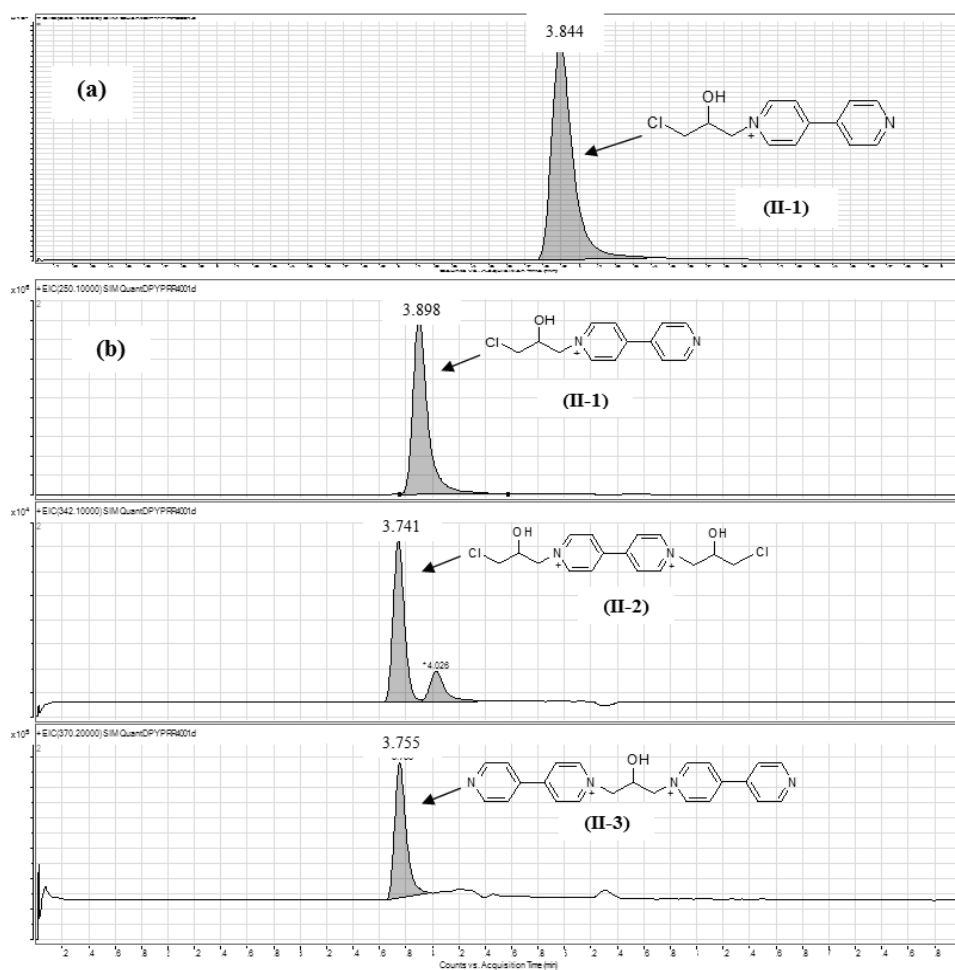


Fig. 3. Chromatograms recorded for the injection of: (a) product mixture resulted after 24 h reaction refluxing: 1-(4,4'-dipyridinium)-3-chlor-2-propanol (II-1) and (b) products mixture resulted after 68 h reaction refluxing: 1-(4,4'-dipyridinium)-3-chlor-2-propanol (II-1), 1,3-di(4,4'-dipyridinium)-2-propanol (II-2) and 4,4'-di(3-chlor-2-propanol)-dipyridinium (II-3)

The reaction compounds 1-(4,4'-dipyridinium)-3-chloro-2-propanol (II-1), 4,4'-di(3-chloro-2-propanol)-dipyridinium (II-2) and trace amount of 1,3-di(4,4'-dipyridinium)-2-propanol (II-3) have reaction yield of 35.82 %, 6.29 %, 0.37 % respectively. The mixture of products contains 710.4 µg/mL of (II-1), 124.7 µg/mL of (II-2) and 7.3 µg/mL of (II-3). The major compound in reaction mixture after 24 h refluxing (II-1) is formed approximately by four times more for the longer reaction time (68 h).

The reaction mixture for reaction (III) was analyzed to characterize the product of interest which is presented in Fig. 4. Excellent yield was obtained for refluxing reaction between 4,4'-dipyridine and iodoacetamide (94.92 %). A significant peak refers to the reaction product that is present in the sample and that is identified with 215.1 mass range and 3.844 min retention time correspond to the formation of acetamide-4,4'-dipyridinium (III). The reaction mixture contain about 1099 µg/mL of acetamide-4,4'-dipyridinium (III).

The structure of synthesis product 11-(4,4'-dipyridinium)-undecanoic acid (IV) obtained by refluxing 4,4'-dipyridine with 11-bromoundecanoic acid was confirmed by recording the chromatogram LC-MS presented in Fig. 5. The chromatogram exhibited a significant peak with m/z 342.1 at 4.021 min. The results indicate about 1036.8 µg/mL. The main reaction product was obtained with a yield of 84.3 %.

The all synthesized 4,4'-dipyridine derivatives (I)-(IV) were successfully obtained in moderate to good yields. It is noteworthy that the syntheses of substituted compounds of 4,4'-dipyridine with halogenated reagents were carried out in a single step

within a reasonable time and the yields were around 2.1-94.9 % (Table 3).

4.2. Adsorption comparison of 4,4'-dipyridine derivatives

In order to investigate the adsorption behavior of synthesized compounds with different functional groups on the activated carbon and silica was quantified by recording the UV-VIS spectra for each reaction mixture before and after adsorption treatment.

The adsorption yield is influenced by structure of the reaction compounds, the concentration of the organic molecules in the analyzed solution and the properties of the absorbent.

The influence of operational parameters such as the mass of activated carbon and the adsorption time were studied for reaction (II for 68 h) because it contained numerous compounds.

In order to investigate the adsorption kinetics of 4,4'-dipyridine derivatives, the stirring time of the solution was investigated between 15 minutes and 1 hour.

The optimum stirring time was chosen 30 minutes as a compromise between a good removal of the organic compounds and a short treatment time. The concentration of activated carbon was studied by varying the carbon mass from 1 to 30 mg/mL and the optimum value was 20 mg/mL.

The reaction products are not absorbed on both silica gel or aminopropyl silicagel even at high quantities (100 mg/mL) and long adsorption time (1 h). The experimental parameters and results are shown in Table 4.

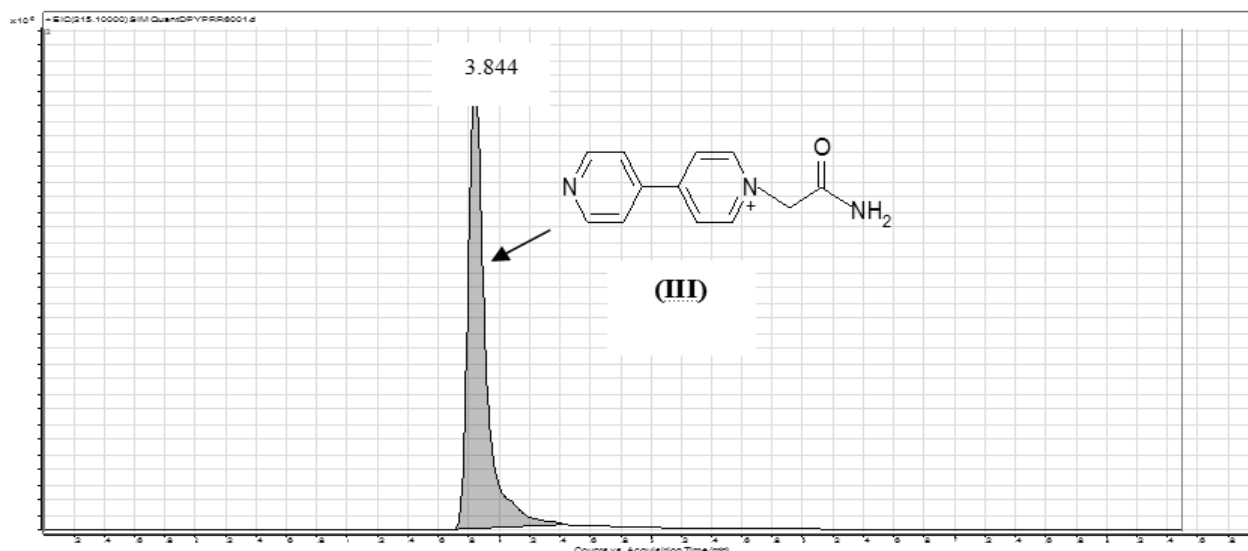


Fig. 4. Chromatogram recorded for the injection of product mixture resulted after 24 h reaction refluxing: acetamide-4,4'-dipyridinium (III)

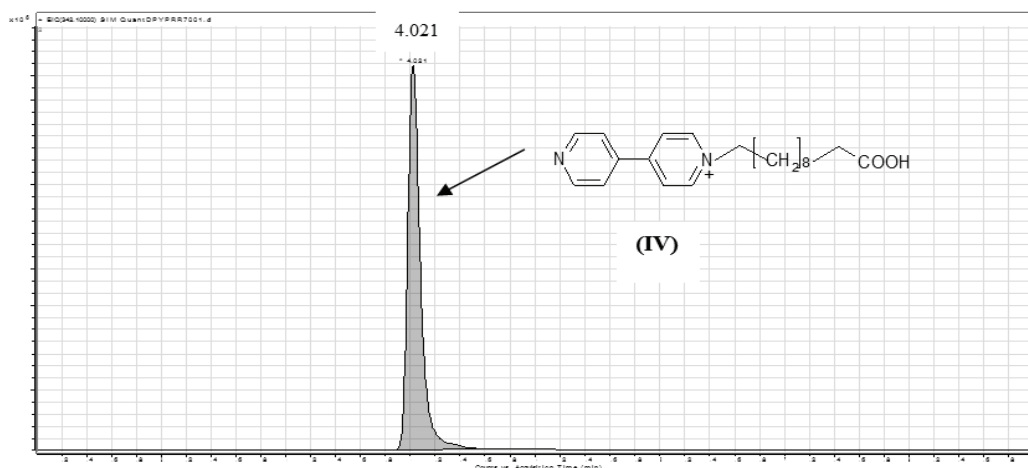


Fig. 5. Chromatogram recorded for the injection of product mixture resulted after 24 h reaction refluxing: 11-(4,4'-dipyridinium)-undecanoic acid (IV)

Table 3. 4,4'-dipyridine derivatives obtained with some halogenated reagents

Compound Name	Molecular mass	Retention time (min)	Solvent	Time (h)	Yield (%)
5-(4,4'-dipyridinium)-valeric acid	258.1	3.873	CH ₃ CN : H ₂ O [2:1]	24	2.1
acetamide-4,4'-dipyridinium	215.1	3.844		24	94.9
11-(4,4'-dipyridinium)-undecanoic acid	342.1	4.021		24	84.3
1-(4,4'-dipyridinium)- 3-chlor-2-propanol	250.1	3.844		24	7.7
		3.898		68	35.8
4,4'-di(3-chlor-2-propanol)-dipyridinium	342.1	3.741		68	6.3
1,3-di(4,4'-dipyridinium)-2-propanol	370.2	3.755	68	0.4	

Table 4. Experimental parameters and results for 4,4'-dipyridine derivatives adsorption onto activated carbon

Reaction	Dilution factors	Activated carbon (mg/mL)	λ (nm)	Absorbance	
				initial	after adsorption
(I)	30	20	250	1.184	0.000
(II-24h)-one derivative	200		238	1.290	0.039
(II-68 h)-tree derivatives	200		238	1.412	0.019
(III)	100		232	1.230	0.009
(IV)	70		246	1.334	0.051

It can be observed that the activated carbon has good capabilities to adsorb dipyrindine derivatives from aqueous solution and can be used for treatment of waste waters.

5. Conclusions

We have synthesized six dipyrindine derivatives using four halogenated reagents: 5-chlorovaleric acid, α -dichlorhidrin, iodoacetamide and 11-bromoundecanoic acid. Mono or bisubstituted compounds were obtained depending on the structure of the halogenated compound and reaction time. The synthesized products were investigated by LC-MS and the reaction yields were between 2.1 and 94.9 %.

This study shows that activated carbon can be used as low-cost adsorbent material for the removal of organic pollutants (dipyrindine derivatives) from water. The procedure for dipyrindine derivatives synthesis can be adapted for the obtaining and characterization of different interested compounds.

Acknowledgements

This work was financed by the program Partnership in priority areas - PN II, supported by the Romanian Department of Education and Research (MEN-UEFISCDI) projects no. PN-II-PT-PCCA-2013-4-0203 and PN-II-PT-PCCA-2013-4-0297.

References

- Al Duri B., (1996), *Introduction to adsorption*, In: *Use of Adsorbents for the Removal of Pollutants from Wastewaters*, McKay G. (Ed.), CRC Press, Boca Raton, Florida, 2-3.
- Arsene D., Teodosiu C., Barjoveanu G., Apreutesei R.E., Apopei P., Musteret C.P., Cailean D., (2013), Combined catalytic oxidation and adsorption of Priority organic pollutants for wastewater recycling, *Environmental Engineering and Management Journal*, **12**, 907-916.
- Bocarsly A.B., Bookbinder D.C., Dominey R.N., Lewis N.S., Wrighton M.S., (1980), Photoreduction at Illuminated p-Type Semiconducting Silicon Photo-Electrodes: Evidence for Fermi Level Pinning, *Journal of the American Chemical Society*, **102**, 3683-3688.

- Buruiana E.C., Diaconu I., Buruiana T., Grigoriu G.E., Caraculacu A., (1991), Synthesis and characterization of some 2,4'-dibenzylidiiisocyanate ionic polymers. VII, Photochromic behavior of ionenes with viologen units, *Die Angewandte makromolekulare Chemie*, **187**, 51–59.
- Casillia S., Malitestab C., Conocic S., Petraliad S., Sortinod S., Vallia L., (2004), Piezoelectric sensor functionalised by a self-assembled bipyridinium derivative: characterisation and preliminary applications in the detection of heavy metal ions, *Biosensors and Bioelectronics*, **20**, 1190–1195.
- CHEMWATCH, (2008), C293LP Version No: 4.1.1.1, 2781-4, On line at: [http://www.biochem.uci.edu/Safety/MSDS/Methyl%20Viologen%20\(Paraquat\)%20MSDS.pdf](http://www.biochem.uci.edu/Safety/MSDS/Methyl%20Viologen%20(Paraquat)%20MSDS.pdf).
- Chira A., Bucur B., Radulescu M.-C., Galaon T., Radu G.-L., (2014), Study of Electrochemically Modified Electrode with Synthesized N-benzyl-4,4'-bipyridine with Anti-Fouling Properties for Oxygen and Hydrogen Peroxide Detection, *International Journal of Electrochemical Science*, **9**, 4493-4511.
- Cummins D., Boschloo G., Ryan M., Corr D., Rao S.N., Fitzmaurice D., (2000), Ultrafast electrochromic windows based on redox-chromophore modified nanostructured semiconducting and conducting films, *The Journal of Physical Chemistry B*, **104**, 11449–11459.
- Fahrenbach A.C., Sampath S., Late D.J., Barnes J.C., Kleinman S.L., Valley N., Hartlieb K.J., Liu Z., Dravid V.P., Schatz G.C., Van Duyne R.P., Stoddart J.F., (2012), A Semiconducting Organic Radical Cationic Host Guest Complex, *ACS Nano*, **6**, 9964–9971.
- Howard P.H., Michalenko E.M., Basu D.K., Hill A., Aronson D., (1997), *Solvents*, In: *Handbook of Environmental Fate and Exposure Data for Organic Chemicals*, Vol. 5, Lewis Publishers: Chelsea, MI.
- Kotani H., Ohkubo K., Takai Y., Fukuzumi S., (2006), Viologen-modified platinum clusters acting as an efficient catalyst in photocatalytic hydrogen evolution, *The Journal of Physical Chemistry B*, **110**, 24047–24053.
- Liu M.O., Chen I. M., Lin J.-L., (2007), Microwave-assisted synthesis of viologens and polyviologens and their preliminary electrochromic effects, *Materials Letters*, **61**, 5227–5231.
- Liu X., Neoh K.G., Lian C., Kang E.T., (2004), Enzymatic activity of glucose oxidase covalently wired via viologen to electrically conductive polypyrrole films, *Biosensors and Bioelectronics*, **19**, 823–834.
- Michaelis L., (1935), Semiquinones, the intermediate steps of reversible organic oxidation reduction, *Chemical Reviews*, **16**, 243–286.
- Monk P.M.S., (1998), *The viologens: Physicochemical Properties, Synthesis and Applications of the salts of 4,4'-bipyridine*, John Wiley & Sons, New York.
- Scheytza H., Reissig H.-U., (1998), Cyclo(paraquat-o-phenylene-paraquat-p-phenylene) - The Missing Isomeric Carbophane of 4,4'-Bipyridine, *Tetrahedron Letters*, **39**, 8637-8640.
- Tanabe K., Kato T., (2009), Self-Assembly of Cyclobis(paraquat-p-phenylene)s, *Chemical Communications*, **14**, 1864-1866.
- Tang X.Y., Schneider T.W., Walker J.W., Buttry D.A., (1996), Dimerized pi-complexes in self-assembled monolayers containing viologens-an origin of unusual wave shapes in the voltammetry of monolayers, *Langmuir*, **12**, 5921-5933.
- Žmija J., Małachowski M.J., (2011), New organic electrochromic materials and their applications, *Journal of Achievements in Materials and Manufacturing Engineering*, **48**, 15-23.



“Gheorghe Asachi” Technical University of Iasi, Romania



DEVELOPMENT AND OPTIMIZATION OF WATER BASED PAINT FORMULA IN ORDER TO REDUCE VOCs EMISSIONS

Andrei Ionut Simion¹, Irina Ionita², Cristina-Gabriela Grigoras¹,
Lidia Gabriela Favier-Teodorescu^{3,4}, Lucian Gavrila^{1*}

¹“Vasile Alecsandri” University of Bacau, Faculty of Engineering, Department of Chemical and Food Engineering,
157 Calea Marasesti, 600115 Bacau, Romania

²“Gheorghe Asachi” Technical University of Iasi, Faculty of Chemical Engineering and Environmental Protection,
Department of Environmental Engineering and Management, 73 Prof.dr.docent D. Mangeron Street, Iasi 700050, Romania

³Ecole Nationale Supérieure de Chimie de Rennes, CNRS, UMR 6226,
Avenue du Général Leclerc, CS 50837, 35700, Rennes Cedex 4

⁴European University of Brittany

Abstract

The interest in waterborne paints amelioration increased lately due to the toxicological effect of certain ingredients on human health, the restrictive environmental legislation and the depletion and escalation in price of raw materials. Research efforts in formulating waterborne paints are directed to insure low volatile organic compounds (VOCs) emission while maintaining and even improving their properties.

This paper presents a waterborne paint formulation process. The required main ingredient was an alkydic resin with 51.3 % w/w non-volatile-matter content, 51.6 mg KOH/g acidity, 8.5 pH, 80 s flow time. Aiming the highest values for paint viscosity, elasticity and hardness and the lowest VOCs emission, the optimal composition concerning the resin neutralization, type and amounts of neutralization agents, co-solvents and water were determined by Response Surface Methodology (RSM). As consequence, the resin was neutralized with a mixture of ammonia and triethylamine in 1:1.8 ratio and solubilized with butanol and butyl glycol co-solvents (2.8:1 ratio). Pigments and filling material were used in a 2.6:1 ratio reported at resin content. The final product can be described as a homogenous, viscos fluid, with 152 s flow time and 22.5% VOCs content. In the optimized drying conditions, it formed a film with a fineness of 40 µm, a semi-gloss aspect, a good adherence, an elasticity (after 7 days) of 5.5 mm and a hardness of 45, 93 and 104 s (after 24 h, 3 and 7 days respectively).

Key words: alkyd resin, enamel, mathematical optimization, primer, waterborne paint

Received: November, 2014; *Revised final:* February, 2015; *Accepted:* February, 2015

1. Introduction

In recent decades, conventional paints are more and more replaced by environmentally friendly formulas (Broek, 1993; Traumann et al., 2014) whose use is recommended due to ecological considerations, specifically the reduction of VOCs emissions) (Tucaliuc, 2014) and economic aspects (low volumes of organic solvents which tend to have a limited availability and are expensive). This type of paints includes powder, high-solids, polyurethanes,

radiation curable, emulsion paints etc. (Barletta et al., 2006; Elhalawany et al., 2014; Klaasen and van der Leeuw, 2006; Kowalczyk et al., 2013; Salleh et al., 2013).

Owing to their reduced solvent content, the water soluble paints are characterized by low toxicity, low VOCs emission, non-inflammability (de Mariz et al., 2010). Even though they could possess a higher viscosity and require more time and heat to dry, the quality of the resulted films are comparable and sometimes superior to those obtained with

* Author to whom all correspondence should be addressed: e-mail: lgavrila@ub.ro; Phone: +40 234 524 411 ext. 145; Fax: +40 234 580 170

solvent soluble paints. Based on the actual requirements for organic solvents emission (Rusu and Dumitriu, 2003) and considering the constant increase performance of existing water-based coatings, this paper was focused on the development of oxidative drying paints, primers, intermediate paints and enamels containing a water soluble resin useful for metal or wood coverage.

The first coatings with water based paints were the emulsion paints containing different resins (Athawale and Nimbalkar, 2011; Crespi et al., 2007). They showed the disadvantages of not being suitable for metal (due to the the small amounts of water remaining in film and on the support, which caused corrosion phenomena) and having a low mechanical stability. The use of additives increases the formulation complexity and affects the film water resistance (Broek, 1993). As consequence, easier to formulate paints were developed using water-soluble synthetic alkyd resins characterized by a low molecular weight and an important number of hydrophilic groups. Their dissolution in water is related to the presence of easily ionizable hydroxyl and carboxyl groups. Ammonia or amines are recommended in this case since they can ensure a good neutralization process without affecting the system rheology or the drying period. Produced by condensation reactions between polyols and polyacids, the mentioned resins contain also fatty acids which use influences in a positive way the mechanical properties of the resulting final film (Hofland, 2012).

The water used in formulation process leads to a longer drying period and support adherence issues. These drawbacks are caused by the water high dipole moment, by its tendency to form hydrogen bonds and by the fact that it reduces the resistance duration of oxygen in the excited stage and the possibility of hydroperoxide stage formation (Dyer and Cummings, 2006). The use of co-solvents such as alcohols or glycol ethers influences the water surface tension (Lisa et al., 2010) ameliorating the support adherence (Khosravi and Connors, 1993). Siccatives and pigments are added in the final step of paint formulations. Additives such as modifiers (Nor et al., 2008), wetting agents, antifoaming agents etc. ameliorate the ingredients dispersion and the film quality but their use remains optional. These paints do not show precipitation phenomena in freeze-thaw cycles or in mechanical shear that can occur during the production process.

This paper was directed to the development of resin water soluble oxidative drying paint, primers, intermediate paint and enamels formulas. An optimization process was leaded by RSM. Parameters such as the resin neutralization percentage, type and amounts of neutralization agents, co-solvents and water were used in order to find the best values able to insure the lowest VOCs content, the highest hardness and the best elasticity values. Various siccatives, pigments and additives were added and

the obtained final paint formulas were submitted to different quality tests.

2. Materials and methods

2.1. Materials and reagents

Water soluble alkyd resin was produced by the Romanian Institute of Advanced Coatings. Luwipal LR 8334, Melarom 31 and Urezit 80 amino resins were supplied by BASF Romania and Rasin Romania respectively.

All reagents and solvents used for the experimental program were of analytical purity. Ethanol, butanol (BuOH), ethylene glycol, ammonia (NH₃), diethanolamine, triethanolamine, triethylamine (Et₃N), cobalt naphthenate, barium hydroxide, titanium oxide, lead (II) chromate, calcium carbonate, phthalocyanine green, phthalocyanine blue, black carbon and talc were purchased from Sigma Aldrich (Romania). Manganese naphthenate and lead naphthenate were bought from TCI Europe (Belgium). Baochemicals (Spain) supplied the butyl glycol (BG). Lithopone, iron oxide yellow, zinc potassium chromate and red iron oxide were provided by Chemos GmbH (Germany). The solutions and dilutions were carried out by using deionized water.

2.2. Paints, primers, intermediate paints and enamels formulations

The products recipes were formulated by using the ingredients listed in Table 1.

Table 1. Ingredients employed for waterborne paint formulations

<i>Ingredients</i>	<i>Required amounts, %</i>
Water thinnable resin (neutralized)	5-60
Water soluble solvents	15-35
Pigments	0-40
Siccatives	0.05-1.5
Slip additive	0.02-5
Wetting agent	0-4
Anti-settling agent	0-4
Rust inhibitor	0-20
Flattening agent	0-20
Water	15-40

The amount of the neutralization agent (amine) was established in order to insure the neutralization of at least 60% of the carboxylic groups existing in the resin. It was calculated from resin acid value by using Eq. (1), where: M_a is the molecular weight of the amine; A is the acid value of the solid resin (defined as milligrams of KOH per gram of solid resin required to give a phenolphthalein titration end point (Howard, 1980)); R is the quantity of the solid resin used and 56100 is 1000 times the molecular weight of KOH.

$$\text{Amine amount} = \frac{M_a \cdot A \cdot R}{56100} \quad (1)$$

The required quantities of siccatives (Eq. 2) were determined knowing that they were purchased as naphthenate salts solutions containing 12% of a given metal (Christhilf et al., 1986).

$$\begin{aligned} \text{Siccative (solution) (wt. \%)} &= \\ &= \frac{\% \text{ metal on vehicle solids desired} \times \text{vehicle solids}}{\% \text{ concentration of metal in siccative solution}} \end{aligned} \quad (2)$$

The established amounts of ingredients were milled for 24 h in a hammer mill. When the mixing process was finalized, certain amounts of resins, neutralizing agents and water were added and mixed with the anterior obtained formulas in order to complete the paint systems.

2.3. Experimental design

The design and analysis of variables were evaluated using NemrodW® v.2000 and XLSTAT-Pro 7.5 version software. Preliminary experiments indicated six main factors affecting the quality of waterborne paints: the alkyd resin neutralization percentage, the type and amount of neutralization agents and co-solvents and the amount of water. In order to establish the appropriate values of these factors two optimization processes were conducted. For each process, the effect of three independent variables on the most important products quality indicators was investigated by RSM. 27 different experiments were carried out each time with three replicates in domain central point.

The independent variables selected in the first case were: the alkyd resin neutralization percentage, the amount of co-solvent (BuOH) and the amount of water. For the second optimization process, the independent variables were: neutralization agents' ratio (NH₃ - Et₃N), co-solvents ratio (BG - BuOH) and the water percentage.

The variation levels of the chosen variables are presented in Tables 2 and 3. Three response functions were followed for each optimization process: product viscosity, film hardness at 7 days and VOCs percentage emission and respectively product elasticity, hardness and VOCs emission. They were fitted in the form of a quadratic polynomial model (Eq. 3), where the values of *n* are between 1 and 3, *nY* is the response function (*1Y* viscosity, *2Y* Persoz hardness, *3Y* VOCs percentage for the 1st RSM set of experiments and *4Y* elasticity, *5Y* Persoz hardness, *5Y* VOCs percentage for the 2nd set), *nA₀*, *nA_i*, *nA_{ii}* and *nA_{ij}* are the regression coefficients of variables for the intercept, linear, quadratic and interaction terms respectively and *X_i* and *X_j* are the independent variables (*i*≠*j*).

$${}_nY = A_0 + \sum_{i=1}^3 A_i \cdot X_i + \sum_{i=1}^3 A_{ii} \cdot X_i^2 + \sum_{i=1}^2 \sum_{j=i+1}^3 A_{ij} \cdot X_i \cdot X_j \quad (3)$$

2.4. Paints, primers, intermediate paints and enamels testing procedure

The obtained products were applied on supports and submitted to different quality analyses (Table 4). All tests were carried out in triplicate at room temperature.

3. Results and discussion

3.1. Water soluble resin choice

The developed waterborne paints were formulated by using a series of ingredients namely water-soluble resins, neutralization agents, co-solvents, deionized water, siccatives, pigments and additives. Their choice and amounts were based on their effects on paint properties (aspect, viscosity, hardness, elasticity, drying time, VOCs emission etc.).

The formulation process consisted in two main phases: pigment dispersion and completion each one divided in several sub-phases.

Table 2. Code and level of independent variables chosen for the 1st RSM optimization

Variables	Symbol		Levels			ΔX _i
	Coded	Uncoded	-1	0	1	
			Actual values			
Percentage of alkyd resin neutralization, %	x ₁	X ₁	60	70	80	10
Co-solvent, % w/w	x ₂	X ₂	15	20	25	5
Deionized water (including water from NH ₃ solution 25% w/w), % w/w	x ₃	X ₃	20	25	30	5

Table 3. Code and level of independent variable chosen for the 2nd RSM optimization

Variables	Symbol		Levels			ΔX _i
	Coded	Uncoded	-1	0	1	
			Actual values			
Neutralization agents (NH ₃ (25% in water) - Et ₃ N) ratio	x ₁	X ₁	1/1.5 (0.33)	1/2 (0.50)	1/3 (0.66)	0.16
Co-solvents (BG - BuOH) ratio	x ₂	X ₂	1/3.3 (0.3)	1/2.6 (0.4)	1/2 (0.5)	0.1
Deionized water (including water from NH ₃ solution 25% w/w), % w/w	x ₃	X ₃	25	27	29	2

Table 4. Tests applied for developed paints, primers, intermediate paints and enamels

<i>Test</i>	<i>Reference method</i>	<i>Apparatus used</i>
Determination of flow time by use of flow cups	ISO 2431 (2012)	Viscosity cups (ISO 2431; $\phi = 4$ mm and 5 mm) (Multilab, Romania)
Determination of fineness of grind	ISO 1524 (2013)	Grindometer ZGR 2024 (Rom Tech, Romania)
Determination of water content	ISO 760 (1994)	-
Determination of non-volatile-matter content	ISO 3251 (2008)	Air oven POL-EKO STD (Nitech, Romania)
Determination of VOCs content	ISO 11890-1 (2007a)	-
Determination of hardness	ISO 1522 (2007b)	Pendulum hardness tester type 707KP (Inspiratech 2000 Ltd., England)
Drying test	ISO 9117-3 (2010a)	Ballotini glass pearls (CDS Consultants, England)
Environmental testing	ISO 60068-2-11 (2001)	-
Determination of resistance to liquids	ISO 2812-1 (2007c) ISO 2812-2 (2007d)	-
Determination of film thickness	ISO 2808 (2007e)	Digital Coating Thickness Gauge (Elcometer Instruments GmbH, Germany)
Cross-cut test	ISO 2409 (2010b)	Cross Hatch Cutter (Paint Test Equipment, England)

For pigment dispersion the most important step was represented by the binder choice. Two types of resins were used to this purpose: an alkydic one for obtaining a classic waterborne paint and a mixture of alkydic resin and different amino resins for the hybrid paint system production.

Preliminary tests were realized in order to establish if alkyd resin alone or its combination with different amino resins represent the best choice for paint formulation. The results (Table 5) revealed no differences between the resins in terms of appearance and drying time. Moreover, the Persoz test indicated higher hardness values in the case of alkyd resin. As respects the resistance to water immersion, a color going from slightly matted for the alkyd resin and its combination with Luwipal resin to matted for combinations of alkyd resin and Melarom or Urezit was observed. As consequence, the alkyd resin was chosen for further experiments.

3.2. Paints, primers, intermediate paints and enamels formulations optimization

Water-soluble alkydic resins are stabilized by anions generated by carboxylic groups which are neutralized by amines or ammonia. If these groups are only weak bases, the pH-values of the neutralized solutions are about 7.5 to 8.2. This fact leads to the saponification of resin ester groups and has as consequence a limited storage time of the resulting paint systems. In order to avoid this inconvenient, the carboxylic groups must be neutralized (Müller and Poth, 2006).

The choice of the agent used to this purpose was based on its ability to insure a good neutralization of carboxylic groups and on its influence on film aspect and drying time. Several preliminary tests were conducted with ammonia solution (25%), triethylamine, triethanolamine and diethanolamine (50%).

The results showed that the neutralization process was satisfactorily realized by all the employed agents. In regard of product appearance, the last two agents led to a sticky film even after 24 h from application. Ammonia conducted to the most reduced drying time but its use affected the paint color a yellowing process being detected.

An opposite effect was observed when triethylamine was used for neutralization. In terms of paint characteristics, the use of ammonia solution led to a higher hardness value (112 s) and to a lower elasticity (3.2 mm) compared to triethylamine which conducted to a hardness of 53 s and an elasticity of 5.3 mm. In order to insure a good solubility of the neutralized alkydic resin and an appropriate final products viscosity various amounts of water and of different solvents such as alcohols and glycol ethers were added. The use of co-solvents, besides of the cited benefits, may also help to the saponification stability.

BG for example, due to its molecular structure, forms solvates of alkyd resins in water phase, which consist of more solvent in the colloidal particles and less water. Other solvents such as ethanol, butanol, ethylene glycol or their mixtures can be employed too. On the other hand, this study was aimed to obtain paint systems with low VOCs emission. Therefore, we have tried to limit as much as possible the amounts of the employed co-solvents. Considering the above related aspects, we have decided to use the RSM in order to establish the ingredients optimal amounts. The values of the independent variables (alkyd resin neutralization percentage, co-solvent amount and water amount) and of the studied response functions (viscosity; hardness at 7 days; VOCs percentage) are reported in Table 6.

The mathematical models generated for the response functions are expressed by Eqs. (4), (5) and (6).

Table 5. Alkyd and amino resins mix characteristics

Characteristics	Alkyd resin	Amino resin		
		Luwipal LR 8334	Melarom 31	Urezit 80
		Alkyd resin and amino resin ratio		
		9/1	10/1	9/1
Appearance	viscous homogenous liquid			
Drying time at 20 °C				
- at dust, min	60	60	60	60
- type C, h	24	24	24	24
Persoz hardness ¹ , s				
- after 24 h	43	34	30	27
- after 3 days	68	58	54	45
- after 7 days	75	65	60	50
Resistance to water immersion ² , 24 h	slightly matted	slightly matted	matted	

¹determined on films applied with hand-drawn scraper, on glass plates, of 120 µm wet thicknesses; ²films sprayed on samples covered with primer based on the same binder as the applied paint

Table 6. 1st RSM test for paint formulation and the observed and predicted values for viscosity, hardness and VOCs

Run	Neutr. agent (NH ₃) ¹		Co-solvent (BuOH)		Water ²		Viscosity, s		Persoz hardness, s		VOCs, %	
	% w. n.r. ³	g	% w. mix ⁴	g	% w. mix	g	Obs. ⁵ ±% (w/w)	Pred. ⁶	Obs. ±% (w/w)	Pred.	Obs. ±2%	Pred.
1	60	0.94	15	23.29	20	31.06	147±6.1	148	107±5.5	107	17.21	17.13
2	60	0.94	15	25.23	25	42.06	144±5.2	141	105±3.7	105	17.10	17.05
3	60	0.94	15	27.53	30	55.06	138±3.2	141	101±7.1	101	17.07	17.13
4	60	0.94	20	33.65	20	33.65	139±5.5	140	109±1.6	109	22.63	22.61
5	60	0.94	20	36.71	25	45.88	133±4.9	133	108±2.1	108	22.58	22.61
6	60	0.94	20	40.38	30	60.56	134±3.3	132	106±2.4	105	22.50	22.76
7	60	0.94	25	45.88	20	36.71	121±3.2	119	107±4.3	107	28.10	28.17
8	60	0.94	25	50.47	25	50.47	109±1.7	112	106±3.3	106	28.00	28.25
9	60	0.94	25	56.08	30	67.29	111±4.8	111	104±4.8	104	28.99	28.48
10	70	1.10	15	23.33	20	31.11	145±5.3	147	112±1.0	112	17.26	17.31
11	70	1.10	15	25.27	25	42.12	144±8.1	140	110±3.8	110	17.22	17.14
12	70	1.10	15	27.57	30	55.14	137±5.5	140	106±3.1	106	17.17	17.12
13	70	1.10	20	33.70	20	33.70	136±5.5	139	113±5.0	114	22.76	22.68
14	70	1.10	20	36.76	25	45.95	133±6.8	133	112±0.9	112	22.66	22.59
15	70	1.10	20	40.44	30	60.66	135±4.6	132	109±4.4	110	22.59	22.65
16	70	1.10	25	45.95	20	36.76	121±8.4	119	112±2.5	111	28.20	28.13
17	70	1.10	25	50.55	25	50.55	110±5.7	112	111±2.7	111	28.13	28.12
18	70	1.10	25	56.16	30	67.40	110±9.2	111	109±2.6	109	28.00	28.25
19	80	1.25	15	23.37	20	31.15	146±4.1	146	112±4.1	112	17.40	17.62
20	80	1.25	15	25.31	25	42.19	144±7.0	140	110±3.2	110	17.38	17.36
21	80	1.25	15	27.61	30	55.23	137±3.2	140	106±0.8	106	17.29	17.24
22	80	1.25	20	33.75	20	33.75	138±6.8	139	114±2.4	114	22.99	22.88
23	80	1.25	20	36.82	25	46.02	131±4.7	133	113±3.0	113	22.72	22.69
24	80	1.25	20	40.50	30	60.75	133±5.6	132	111±6.6	110	22.70	22.66
25	80	1.25	25	46.02	20	36.82	122±5.4	119	112±6.8	112	28.22	28.22
26	80	1.25	25	50.63	25	50.63	108±2.9	112	111±2.1	111	28.12	28.11
27	80	1.25	25	56.25	30	67.50	113±1.1	111	109±3.6	109	28.11	28.15

¹25% aqueous NH₃ solution; ²total amount of water (incorporating water from the NH₃ solution); ³% w. n.r. - percentage of neutralized resin; ⁴mix. - total amount of tested paint; ⁵Obs. - observed value; ⁶Pred. - predicted value

$$1y = 132.556 - 0.222_1x_1 - 14.278_1x_2 - 3.722_1x_3 + 0.333_1x_1x_2 + 0.083_1x_1x_3 - 0.333_1x_2x_3 + 0.333_1x_1^2 - 6.500_1x_2^2 + 2.833_1x_3^2 \quad (4)$$

$$2y = 112.407 + 2.500_2x_1 + 0.667_2x_2 - 2.056_2x_3 + 0.750_2x_2x_3 - 2.056_2x_1^2 - 2.222_2x_2^2 - 0.722_2x_3^2 \quad (5)$$

$$3y = 22.589 + 0.042_3x_1 + 5.487_3x_2 - 0.019_3x_3 - 0.111_3x_1x_2 - 0.094_3x_1x_3 + 0.077_3x_2x_3 + 0.063_3x_1^2 + 0.039_3x_2^2 + 0.076_3x_3^2 \quad (6)$$

The quality of the obtained polynomial model was established by several statistical data: the standard error which estimates the standard deviation of a certain value based on all values mean (Press et al., 1992); the coefficient of determination (R²) which considers all effects; the adjusted coefficient of determination (adj. R²) which considers only square effects and interaction effects between two input variables; the predicted coefficient of determination (pred. R²) which considers all effects for values generated by the employed software; the

predicted residual sum of squares (PRESS) which is a form of cross-validation used in regression analysis to provide a summary measure of the fit of a model to a sample of observations that were not themselves used to estimate the model and the precision adequacy (Adeq. Precision), which measure the ratio of signal to noise. The specific values of these statistical parameters for the studied functions are presented in Table 7. Their values indicate that the mathematical models describe with high accuracy the behavior of the obtained experimental data.

The analysis of variance (ANOVA) served to calculate the significance of the response surface quadratic models coefficients. From data shown in Table 8, it can be observed that the percentage of neutralized resin influences the paint hardness ($p < 0.01$) but does not affect in a significant way the viscosity ($p = 74.7$) and the VOCs emission ($p = 35.1$). This fact can be explained by the small amount of the neutralization agent required (0.94-1.25 g/100 g resin). On the contrary, the co-solvent amount seems to be a very important factor ($p > 0.01$) since it has a great impact on all three studied response functions. In terms of water amount, one can note that it influences only the paint viscosity and hardness ($p < 0.01$). The obtained p values reveal no effect of independent variables interactions on the mentioned functions.

In order to gain a better understanding of the results, the predicted models were presented as 3D surfaces plots (Fig. 1) based on the effects of two factors. Specifically, these plots showed how alkyd resin neutralization, co-solvent and water amounts related to paint viscosity, hardness and VOCs emission. The real values of the independent variables for the optimum results were calculated targeting the highest paint hardness, an appropriate viscosity (aiming values around 127 s) and the lowest

VOCs emission values. From the obtained data (Table 9), it can be noted that for a resin neutralization of 67-72%, 21% co-solvent and 27-28% water (values reported at paint resin content) the product was characterized by a viscosity of ≈ 128 s, a hardness at 7 days of ≈ 110 s and an emission of VOCs of $\approx 23\%$.

The differences in desirability, meaning in finding the best simultaneous conditions of waterborne paint formulation and in the imposed conditions, for all three propose mathematical model are minimal.

In order to validate the mathematical model adequacy and to find the correct paint formulations, 5 replicates of each generated recipe were carried out. After analyzing the recorded values and taking in consideration the averages and values frequency for each characteristic, a compromise formulation composition was adopted: resin neutralization degree 70% (1.10 g NH₃/100 g resin), 21% co-solvent and 27% water (values reported at paint resin content). By testing the obtained paint systems (3 replicates) the following characteristics were measured: 127.1% \pm 1.9% for viscosity, 112.0 s \pm 0.6% for hardness and 23.79 g/L \pm 0.3% for VOCs.

Taking into account these data, we have considered as indicate to ameliorate the obtained characteristics by using a mixture of NH₃ (25% in water) and Et₃N as neutralization agent and a mixture of BG - BuOH as co-solvent.

Thus, another optimization program was established. This time, the three independent variables were represented by the neutralization agent and co-solvent constitutive elements ratios and the percentage of added water. The used values along with the experimental and predicted results obtained for paint elasticity (mm), its hardness at 7 days (s) and VOCs emission (%) are presented in Table 10.

Table 7. Estimates and statistics of the coefficients

Statistical parameters	Equation 4	Equation 5	Equation 6	Equation 7	Equation 8	Equation 9
Standard error	2.903	0.511	0.184	0.11	1.6	0.106
R ²	0.967	0.983	0.999	0.951	0.964	0.741
Adj. R ²	0.950	0.974	0.998	0.925	0.945	0.604
R ² pred.	0.916	0.960	0.996	0.854	0.901	0.348
PRESS	368.042	10.593	1.928	0.573	124.969	0.485
Adeq. Precision	20.93	41.00	102.02	18.52	26.29	4.31

Table 8. Significance of coefficients in the response equations

Coefficient	Significance, p %					
	Equation 4	Equation 5	Equation 6	Equation 7	Equation 8	Equation 9
A ₀	< 0.01	< 0.01	< 0.01	< 0.01	< 0.01	< 0.01
A ₁	74.7	< 0.01	35.1	< 0.01	< 0.01	0.193
A ₂	< 0.01	< 0.01	< 0.01	0.262	< 0.01	68.1
A ₃	< 0.01	< 0.01	66.2	0.166	< 0.01	0.0105
A ₁₁	77.8	< 0.01	41.8	0.0389	< 0.01	62.1
A ₂₂	< 0.01	< 0.01	61.1	2.00	4.28	3.72
A ₃₃	2.74	0.300	32.6	38.9	42.1	40.8
A ₁₂	69.7	100.0	4.96	100.0	0.779	21.7
A ₁₃	91.9	100.0	9.0	60.2	3.30	31.8
A ₂₃	69.7	0.0112	16.3	60.2	0.540	74.7

Table 9. Optimized process variables and related response functions values

<i>Maximum coordinates</i>							
<i>Variable</i>	<i>Coded value</i>			<i>Factor</i>	<i>Real value</i>		
	<i>1st</i>	<i>2nd</i>	<i>3rd</i>		<i>1st</i>	<i>2nd</i>	<i>3rd</i>
X ₁	-0.323209	-0.244171	0.214147	Percentage of neutralized alkyd resin	67	68	72
X ₂	0.214187	0.222248	0.210315	Co-solvent	21	21	21
X ₃	0.389336	0.436502	0.627537	Water	27	27	28
<i>Maximum characteristics</i>							
<i>Response function</i>				<i>Value</i>			
				<i>1st</i>	<i>2nd</i>	<i>3rd</i>	
₁ Y	Viscosity, s			128.22	127.99	128.00	
₂ Y	Hardness at 7 days, s			110.58	110.75	111.42	
₃ Y	VOCs, %			23.79	23.83	23.77	
Desirability, %				98.64	95.39	95.82	

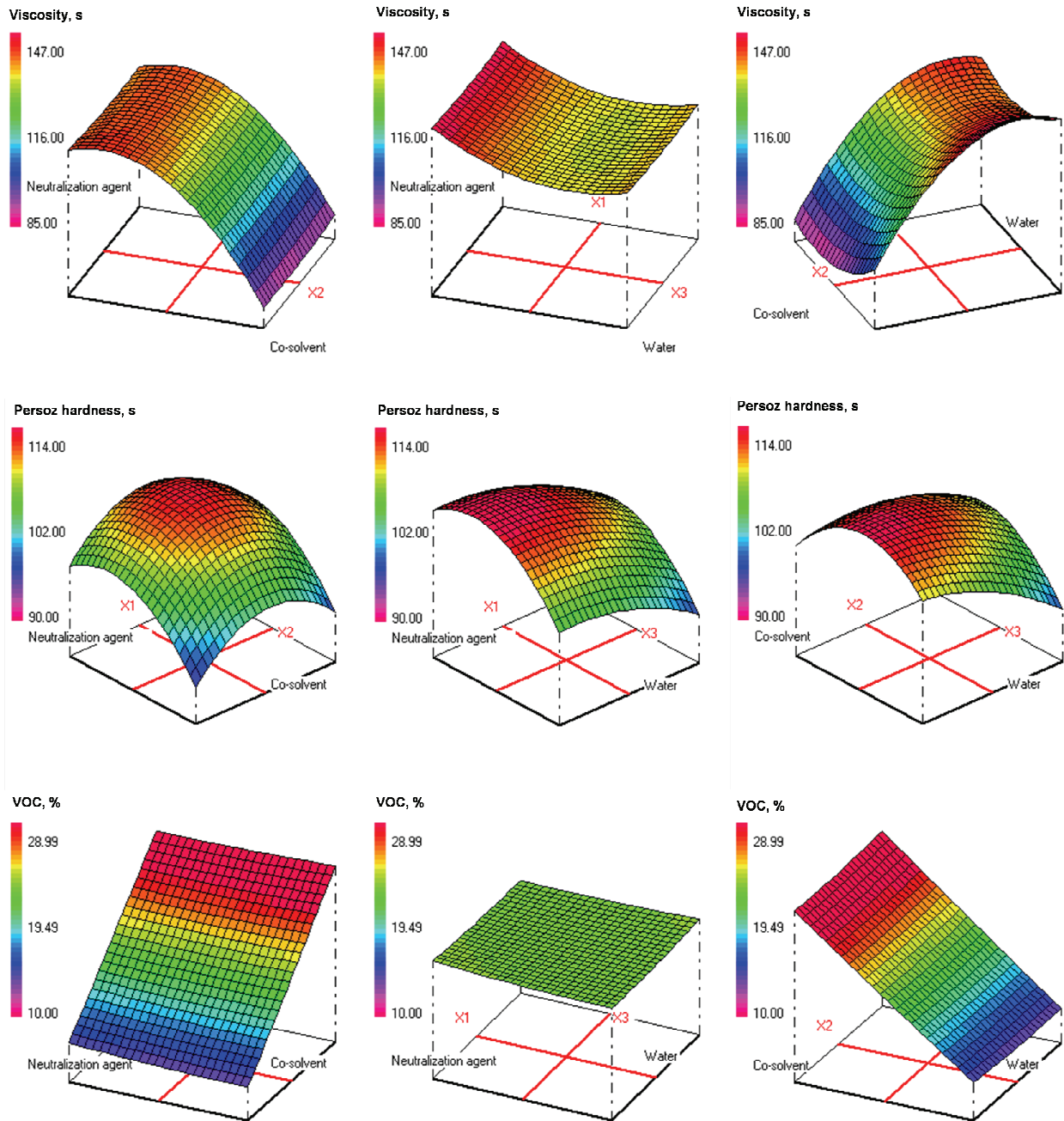


Fig. 1. 3D response surface plots for the 1st process of paint formulation optimization

The Eqs. (7-9) describe the mathematical models obtained for the response functions.

$$4y = 5.27 + 0.42 \cdot 4x_1 + 0.09 \cdot 4x_2 + 0.09 \cdot 4x_3 + 0.02 \cdot 4x_1 \cdot 4x_3 - 0.02 \cdot 4x_2 \cdot 4x_3 - 0.19 \cdot 4x_1^2 - 0.11 \cdot 4x_2^2 + 0.44 \cdot 4x_3^2 \quad (7)$$

$$5y = 88.9 - 6.1 \cdot 5x_1 - 3.3 \cdot 5x_2 - 2.9 \cdot 5x_3 + 1.4 \cdot 5x_1 \cdot 5x_2 - 1.1 \cdot 5x_1 \cdot 5x_3 + 1.5 \cdot 5x_2 \cdot 5x_3 + 4.6 \cdot 5x_1^2 + 1.4 \cdot 5x_2^2 - 0.6 \cdot 5x_3^2 \quad (8)$$

$$6y = 23.861 + 0.092 \cdot 6x_1 + 0.011 \cdot 6x_2 - 0.128 \cdot 6x_3 + 0.039 \cdot 6x_1 \cdot 6x_2 - 0.032 \cdot 6x_1 \cdot 6x_3 + 0.010 \cdot 6x_2 \cdot 6x_3 + 0.022 \cdot 6x_1^2 + 0.097 \cdot 6x_2^2 + 0.037 \cdot 6x_3^2 \quad (9)$$

For these equations, the registered R^2 and adj. R^2 (Table 7) were between 0.741 and 0.951 and between 0.604 and 0.925 respectively. The predicted R^2 and adjusted R^2 in this study indicate that only 7.5, 5.5 and 39.6% respectively of total variations could not be explained by the models. Their values and “Adeq. Precision” reveal an acceptable degree of accuracy for the behavior of the obtained

experimental data. The low values recorded for VOCs emission are due to the fact that the relative difference between minimum (23.7%) and maximum (24.3%) values is of only 2.5% indicating that the variations are influenced only by the neutralization agent (added in small amounts) and that the determined amounts are in the method precision limits.

According to the equations coefficients significance reported by ANOVA test (Table 8), the $NH_3 - Et_3N$ ratio affects ($p > 0.01$) the elasticity and hardness of the resulted paint. In terms of employed co-solvents ratio and water, the statistical analysis shows that they have an influence only on the paint hardness ($p > 0.01$).

It can also be noted that none of the variables has an important impact on the paint VOCs emission. This observation can be explained by the fact that the amount of co-solvents, the main responsible for VOCs emission augmentation, remains constant at 21%, the neutralization agents are in reduced amounts and the water percentage ranges only 2%. Moreover, the interactions between the studied parameters do not affect the followed response functions.

Table 10. RSM test for intermediary paint formulation and the observed and predicted values for elasticity, hardness and VOCs

Run	Neutralization agent 25% NH_3/Et_3N		Co-solvent BG/BuOH		Water ¹		Elasticity, mm		Persoz hardness, s		VOCs, %	
	ratio	g	ratio	g	% w. mix ²	g	Obs. ³ ±% (w/w)	Pred. ⁴	Obs. ±% (w/w)	Pred.	Obs. ±2%	Pred.
1	1/5	5.74	1/3.3	41.12	25	48.95	4.5±2.0	4.4	111±3.8	111	24.10	24.06
2	1/5	5.74	1/3.3	42.70	27	54.90	4.5±0.6	4.5	107±3.7	106	23.88	23.92
3	1/5	5.74	1/3.3	44.41	29	61.33	4.7±1.1	4.6	98±2.9	100	23.80	23.85
4	1/5	5.74	1/2.6	41.12	25	48.95	4.6±1.1	4.6	101±1.9	103	24.00	23.93
5	1/5	5.74	1/2.6	42.70	27	54.90	4.6±0.3	4.7	98±2.2	100	23.81	23.79
6	1/5	5.74	1/2.6	44.41	29	61.33	4.7±2.4	4.8	95±1.5	95	23.75	23.73
7	1/5	5.74	1/2.0	41.12	25	48.95	4.5±1.2	4.6	99±3.7	98	23.89	23.98
8	1/5	5.74	1/2.0	42.70	27	54.90	4.7±0.7	4.6	97±1.1	96	23.90	23.86
9	1/5	5.74	1/2.0	44.41	29	61.33	4.7±0.6	4.7	95±5.1	93	23.80	23.81
10	1/2	5.91	1/3.3	41.19	25	49.03	4.9±0.9	5.0	99±2.5	98	24.10	24.12
11	1/2	5.91	1/3.3	42.77	27	54.99	4.9±0.1	5.1	95±0.8	94	24.00	23.95
12	1/2	5.91	1/3.3	44.48	29	61.43	5.1±0.4	5.2	90±2.1	89	23.88	23.85
13	1/2	5.91	1/2.6	41.19	25	49.03	5.1±0.2	5.2	91±1.6	91	23.92	24.03
14	1/2	5.91	1/2.6	42.77	27	54.99	5.3±0.6	5.3	89±1.1	89	23.70	23.86
15	1/2	5.91	1/2.6	44.48	29	61.43	5.4±0.2	5.4	84±2.7	85	23.88	23.77
16	1/2	5.91	1/2.0	41.19	25	49.03	5.3±1.4	5.2	87±3.3	88	24.30	24.13
17	1/2	5.91	1/2.0	42.77	27	54.99	5.3±0.7	5.3	86±3.3	87	23.87	23.97
18	1/2	5.91	1/2.0	44.48	29	61.43	5.5±0.6	5.4	84±2.6	85	23.91	23.89
19	1/3	6.10	1/3.3	41.26	25	49.12	5.2±0.6	5.2	91±3.3	94	24.20	24.23
20	1/3	6.10	1/3.3	42.85	27	55.09	5.3±0.6	5.3	89±3.8	91	24.10	24.02
21	1/3	6.10	1/3.3	44.56	29	61.54	5.6±0.2	5.5	87±0.6	87	23.83	23.89
22	1/3	6.10	1/2.6	41.26	25	49.12	5.5±0.1	5.4	91±2.7	89	24.25	24.17
23	1/3	6.10	1/2.6	42.85	27	55.09	5.5±0.6	5.5	89±6.2	87	23.91	23.98
24	1/3	6.10	1/2.6	44.56	29	61.54	5.6±0.9	5.6	86±3.3	85	23.89	23.85
25	1/3	6.10	1/2.0	41.26	25	49.12	5.3±0.3	5.4	87±1.5	87	24.20	24.31
26	1/3	6.10	1/2.0	42.85	27	55.09	5.5±0.3	5.5	86±2.1	87	24.30	24.12
27	1/3	6.10	1/2.0	44.56	29	61.54	5.5±1.4	5.6	86±1.1	86	23.91	24.01

¹total amount of water (water from NH_3 solution included); ²mix. - total amount of tested paint; ³Obs. - observed value; ⁴Pred. - predicted value

Fig. 2 depicts the 3D surfaces plots generated for the resulted mathematical models. The figure illustrates how neutralization agents ratio, co-solvents ratio and water percentage related to paint elasticity, hardness and VOCs emission.

The real values of the independent variables for the optimum results were calculated targeting the highest paint hardness and elasticity and the lowest VOCs emission values. The resulted data (Table 11) show that when the ratio between NH_3 (25 % in water) and Et_3N from neutralization agent is comprised between 1/1.45 and 1/2.32; the ratio between BG and BuOH is between 1/1.33 and 1/2.5 and the water percentage is between 26 and 28, the obtained product has an elasticity of ≈ 5.1 mm, a hardness at 7 days of ≈ 91 s and an emission of VOCs of $\approx 23\%$. Once the resin neutralization degree, water, neutralization agent and co-solvents type and amounts were established, the pigments dispersion phase was finalized by the addition of siccatives, pigments and extenders. In regard of utilized pigments, it must be

noted that they have to be stable at the pH of paint formula. From the wide variety of the used substances able to insure a specific coloration we cite the following ones: titanium oxide, lithopone for white paints; black carbon for black paints; iron oxide yellow, lead (II) chromate, zinc potassium chromate for yellow paints; red iron oxide for red paints; phthalocyanine green for green paints and phthalocyanine blue for blue paints. Certain amounts of resins, neutralizing agents and water were mixed with these resulted paint formulas in the completion phase in order to rich the adequate systems composition.

After analyzing the obtained values (averages and frequency) from five replicates of each RSM optimized recipe, a new formulation was adopted: 70% of the neutralized resin with NH_3 (25% in water) and Et_3N in 1/1.8 ratio (1.10 g neutralized agent/100 g resin), 21% BG and BuOH mix in 1/2.8 ratio and 27% water (reported at paint resin content).

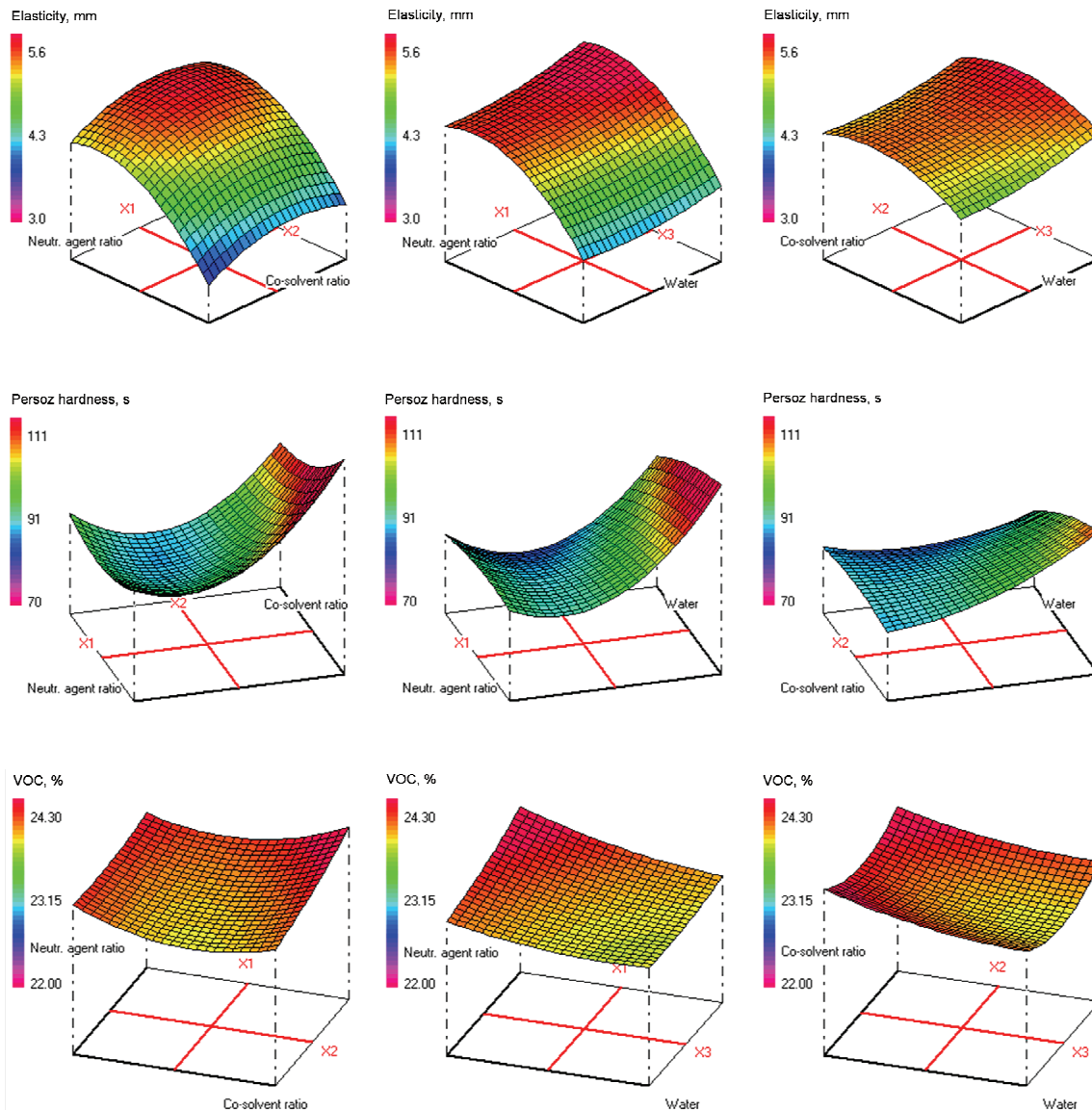


Fig. 2. 3D response surface plots for the 2nd process of paint formulation optimization

The tests of three replicates formulated with the new developed recipe confirmed the model adequacy. The response functions values were: $5.0 \pm 0.1\%$ mm for paint elasticity, 91 s for its hardness and 23.8% for VOCs emission. Considering all the presented results and after different other experimental studies (data not shown) we report below, as example, a possible final composition of a white (Table 12) and a colored (Table 13) waterborne paints. All the products developed in this research were submitted to different analyses (Table 14). The obtained data for both recipes and products characteristics are consistent with those mentioned in literature (Müller and Poth, 2006).

Along to the paint formulations presented above, this study included also the development of different primers, intermediate paints and enamels. They were based on the use of the same water soluble alkydic resin as for paint systems. The resin neutralization was attained with the same neutralization agent (mixture of NH_3 25% in water and Et_3N in 1/1.8 ratio).

For primers, the ratio between binder and pigment with filling materials varied between 1/2 and 1/2.6. They were characterized by a matted aspect, a viscosity of 152 - 187 s (ISO 2431 - cup 5/20 °C) and a fineness of 40 μm . In terms of drying time, the primers required a period of 50 min when the method

called “at dust” was used and of 21 h when type C drying method was employed.

The elasticity registered at 7 days from the application on support was of ≈ 5.3 mm. The recorded hardness after 24 h, 3 and 7 days was of ≈ 45 s, ≈ 91 s and ≈ 105 s respectively. The primers content of VOCs was between 8 and 10%.

In the case of intermediate paints, the resin neutralization process was conducted until the products dispersion fineness attained 30 - 35 μm . The realized analyses revealed a semi glossy aspect; a viscosity (ISO 2431 - cup 4/20 °C) between 172 and 223 s; a drying time of 60 min “at dust” and of 24 h type C; an elasticity between 5.5 and 6.5 mm; and a hardness between 39 and 49 s after 24 h and between 70 and 80 s at 7 days. The resistance to water immersion test showed a matted aspect. The intermediate paints VOCs were between 11.9 and 13%. For enamels the desired dispersion fineness was of 20 to 25 μm . When they were submitted to quality analysis the following results were obtained: glossy aspect; viscosity (ISO 2431 - cup 4/20 °C): 135 - 176 s; drying time: 60 min “at dust” and 24 h type C; elasticity: 6.4 - 6.7 mm; hardness: 80 - 85 s (at 7 days); matted aspect after 24 h of water immersion and unchanged after 24 h of mineral oil immersion.

Table 11. Optimized process variables and related response functions values

<i>Maximum coordinates</i>							
<i>Variable</i>	<i>Coded value</i>			<i>Factor</i>	<i>Real value</i>		
	<i>1st</i>	<i>2nd</i>	<i>3rd</i>		<i>1st</i>	<i>2nd</i>	<i>3rd</i>
X_1	1.202349	-0.514089	-0.407585	Neutralization agent ratio	0.69	0.42	0.43
X_2	-0.785468	0.316674	0.505326	Co-solvent ratio	0.3	0.4	0.5
X_3	-0.256345	0.316809	-0.295560	Water	26	28	26
<i>Maximum characteristics</i>							
<i>Response function</i>		<i>Value</i>					
		<i>1st</i>	<i>2nd</i>	<i>3rd</i>			
${}_1Y$	Elasticity, mm	5.3	5.1	5.1			
${}_2Y$	Hardness at 7 days, s	91	91	91			
${}_3Y$	VOC, %	24.07	23.76	23.85			
Desirability, %		100.00	100.00	100.00			

Table 12. White waterborne paint

<i>Ingredients</i>	<i>Required amounts for 100 g of final product</i>
<i>Pigment dispersion phase</i>	
Water thinnable alkyd resin	19.88
Neutralization agent, NH_3 (25% in water)/ Et_3N = 1/1.8	0.22
Butanol	5.95
Butyl glycol	2.13
Titanium dioxide, rutile type	24.80
Cobalt dryer (Co 6% in solvent system)	0.13
Zinc dryer (Zn 10% in solvent system)	0.13
Talc	1.20
Deionized water	7.56
<i>Completion phase</i>	
Water thinnable alkyd resin	18.35
Neutralization agent, NH_3 (25% in water)/ Et_3N = 1/1.8	0.20
Deionized water	19.44
64.50% solids, 27% water, 155.14 g/L VOC, density 1848 \pm 20 kg/m^3	

Table 13. Red waterborne paint

<i>Ingredients</i>	<i>Required amounts for 100 g of final product</i>
Pigment dispersion phase	
Water thinnable alkyd resin	19.87
Neutralization agent, NH ₃ (25% in water)/Et ₃ N = 1/1.8	0.22
Butanol	5.95
Butyl glycol	2.13
Red iron oxide	10.00
Molybdenum orange	7.50
Manganese dryer (Mn 5% in solvent system)	0.13
Zinc dryer (Zn 10% in solvent system)	0.13
Extender, CaCO ₃	5.50
Talc	3.04
Deionized water	7.55
Completion phase	
Water thinnable alkyd resin	18.34
Neutralization agent, NH ₃ (25% in water)/Et ₃ N = 1/1.8	0.20
Deionized water	19.41
64.50% solids, 27% water, 164.52 g/L VOC, density 1960 ± 20 kg/m ³	

Table 14. Water-borne white and red paints characteristics

<i>Characteristics</i>	<i>White topcoat</i>	<i>Red topcoat</i>
Liquid product		
Appearance	viscous homogenous liquid	
Viscosity, s	190	197
Fineness of dispersion, µm	30-35	
Film product		
Appearance	semi-glossy	
Drying time at 20 °C		
- at dust, min.	60	60
- type C, h	24	24
Elasticity at 7 days	6	6
Adhesion at 7 days (1 mm grid)	good	
Persoz hardness, s		
- after 24 h	35	45
- after 7 days	69	72
Resistance to water immersion, 24 h	slightly matted	
Resistance to mineral oil immersion, 24 h	no modification	

The VOCs of enamels was of 14.9 - 18.25%. All the experiments carried out in this study permitted us to conclude that the followed experimental program was able to establish the adequate ingredients proportions in order to obtain products characterized by an appropriate quality which can be successfully employed for metal or wood coverage.

4. Conclusions

Waterborne paints represents an attractive alternative to those based on organic solvents especially due to the fact that the last ones require expensive ingredients and are responsible for realizing important amounts of VOCs known as affecting the environment and the human health. Even though at the beginning the waterborne paints were classified as not being suitable for all types of supports because of the possible corrosion phenomena, the research conducted to improved formulas able to insure low VOCs emission while maintaining and even improving their properties

(general aspect, rheological characteristics, drying time, resistance at physical, chemical and microbiological actions etc.).

In this paper we successfully developed a waterborne paint formulation process. A water soluble alkydic resin was used to this purpose. Its neutralization percentage, the type and amount of the neutralization agents, co-solvents and water known as parameters affecting some of the main paint characteristics such as viscosity, elasticity, hardness, VOCs emission etc. were chosen as independent variables and optimized in two different steps by RSM. According to the obtained results, it is recommended to neutralize 70 to 80% of the carboxylic groups existing in the employed resin.

A mixture of NH₃ (aqueous solution 25% w/w) and Et₃N in 1/1.8 ratio (1.10 g neutralized agent/100 g resin) can be used to accomplish this objective. Once neutralized, the resin must be solubilized in co-solvents (21% BG and BuOH mix in a ratio of 1 to 2.8) and water (27% reported at the alkyd resin amount) and mixed with siccatives, pigments and other necessary additives (extenders,

wetting agents, anti-settling agents, rust inhibitors, flattening agents etc.). The statistical analysis of the mathematical models obtained for the followed response functions revealed a high similarity between the data acquired experimentally and those predicted by the registered equations. In the established conditions, paint elasticity was of 5.0 mm and its hardness reached 91 s. In terms of VOCs emission, a value of 23.8% was recorded.

Several different paint formulations white or colored along to various primers, intermediate paints and enamels were also developed in the present research work. The analysis of their specific characteristics indicated that the studied parameters and the established experimental program were able to determine the appropriate ingredients types and amounts required for obtaining high quality products useful for metal or wood coverage.

References

- Athawale V.D., Nimbalkar R.V., (2011), Waterborne coatings based on renewable oil resources: an overview, *Journal of the American Oil Chemists' Society*, **88**, 159-185.
- Barletta M., Gisario A., Rubino G., Tagliaferri V., (2006), Electrostatic spray deposition (ESD) of "self organizing" TiO₂-epoxy powder paints: Experimental analysis and numerical modelling, *Surface & Coatings Technology*, **201**, 3212-3228.
- Broek A.D., (1993), Environment-friendly paints: their technical im(possibilities), *Progress in Organic Coatings*, **22**, 55-68.
- Crespi M.S., Hikosaka M.Y., do Amaral G.C.A., Ribeiro C.A., (2007), Kinetic parameters obtained for thermal decomposition of acrylic resins present in commercial paint emulsions, *Journal of Thermal Analysis and Calorimetry*, **88**, 669-672.
- Christhlf H.H., Morrison P.E., Niemczura P.W., (1986), Pipe Varnish Compositions and Use Thereof, USA Patent, No. 4631083.
- de Mariz F.A. I., Millichamp I.S., de la Cal J.C., Reiza J.R., (2010), High performance water-borne paints with high volume solids based on bimodal latexes, *Progress in Organic Coatings*, **68**, 225-233.
- Dyer P.J., Cummings P.T., (2006), Hydrogen bonding and induced dipole moments in water: Predictions from the Gaussian charge polarizable model and Car-Parrinello molecular dynamics, *The Journal of Chemical Physics*, **125**, 1-6.
- Elhalawany N., Saleeb M.M., Zahran M.K., (2014), Novel anticorrosive emulsion-type paints containing organic/inorganic nanohybrid particles, *Progress in Organic Coatings*, **77**, 548-556.
- Hofland A., (2012), Alkyd resins: From down and out to alive and kicking, *Progress in Organic Coatings*, **73**, 274-282.
- Howard J.D., (1980), Resin partially neutralized by an amine or ammonium hydroxide and a water-soluble solvent, USA Patent, No. 4187204 A.
- ISO, (1994), Determination of water – Karl Fisher method (general method), ISO 760, On line at: <https://www.iso.org/obp/ui/#iso:std:iso:760:ed-1:v1:en>.
- ISO, (2001), Environmental testing – Part 2: Tests – Test Ka: Salts mist, ISO 60068-2-11.
- ISO, (2007a), Paints and varnishes – Determination of volatile organic compound content – Part 1: Difference method, ISO 11890-1.
- ISO, (2007b), Paint and varnishes – Pendulum damping test, ISO 1522.
- ISO, (2007c), Paint and varnishes – Determination of resistance to liquids – Part 1: Immersion in liquids other than water, ISO 2812-1.
- ISO, (2007d), Paint and varnishes – Determination of resistance to liquids – Part 2: Water immersion method, ISO 2812-2.
- ISO, (2007e), Paints and varnishes – Determination of film thickness, ISO 2808.
- ISO, (2008), Paints, varnishes and plastics – Determination of non-volatile-matter content, ISO 3251.
- ISO, (2010a), Paint and varnishes – Drying tests – Part 3: Surface-drying test using ballotini, ISO 9117-3.
- ISO, (2010b), Paints and varnishes – Cross-cut test, ISO 2409.
- ISO, (2012), Paints and varnishes – Determination of flow time by use of flow cups, ISO 2431.
- ISO, (2013), Paints and varnishes and printing inks – Determination of fineness of grind, ISO 1524.
- Khosravi D., Connors K.A., (1993), Solvent effects on chemical processes. 3. Surface tension of binary aqueous organic solvents, *Journal of Solution Chemistry*, **22**, 321-330.
- Klaasen R.P., van der Leeuw R.P.C., (2006), Fast drying cobalt-free high solids alkyd paints, *Progress in Organic Coatings*, **55**, 149-153.
- Kowalczyk K., Luczka K., Grzmil B., Szychaj T., (2013), Anticorrosive 2K polyurethane paints based on nano- and microphosphates with high dispersing additive content, *Progress in Organic Coatings*, **76**, 1088-1094.
- Lisa G., Curteanu S., Lisa C., (2010), Artificial neural network for prediction of excess refractive indices of some binary mixtures, *Environmental Engineering and Management Journal*, **9**, 483-487.
- Müller B., Poth U., (2006), *Coatings Formulations*, Vincentz Network GmbH & Co. KG, Hannover, Germany.
- Nor I., Moleavin I., Ibanescu C., Sandu V., Hurduc N., (2008), Smart soluble grafted polysiloxanes with potential applications in waterborne paints, *Environmental Engineering and Management Journal*, **7**, 337-342.
- Press W.H., Flannery B.P., Teukolsky S.A., Vetterling W.T., (1992), *Numerical Recipes in FORTRAN: The Art of Scientific Computation*, Cambridge University Press, Cambridge, England.
- Rusu A.O., Dumitriu E., (2003), Destruction of volatile organic compounds by catalytic oxidation, *Environmental Engineering and Management Journal*, **2**, 273-302.
- Salleh N.G.N., Alias M.S., Glasel H-J., Mehnert R., (2013), High performance radiation curable hybrid coatings, *Radiation Physics and Chemistry*, **84**, 70-73.
- Traumann A., Reinhold K., Tint P., (2014), Environmental and occupational impact on human health of dust and chemicals from modern technologies, *Environmental Engineering and Management Journal*, **13**, 2233-2241.
- Tucaliuc O.M., Cretescu I., Nemtoi G., Breaban I.G., Soreanu G., Iancu O.G., (2014), Monitoring of mercury from air and urban dust in the industrial area of Iasi municipality, *Environmental Engineering and Management Journal*, **13**, 2051-2061.



“Gheorghe Asachi” Technical University of Iasi, Romania



AN IMPROVED METHODOLOGY FOR DETERMINATION OF RADIOCHEMICAL AND CHEMICAL IMPURITIES IN THE SYNTHESIS PROCESS OF ^{18}F -FDG (2- ^{18}F] FLUORO-2-DEOXY-D-GLUCOSE)

Mirela Mihon^{1,2}, Catalin Tuta², Radu Leonte^{2,3},
Alina Catrinel Ion¹, Vasile Lavric¹, Dana Niculae^{2*}

¹University Politehnica of Bucharest, Faculty of Applied Chemistry and Materials Science,
1-7 Polizu Str., 011061 Bucharest, Romania

²National Institute for Physics and Nuclear Engineering “Horia Hulubei”, 30 Reactorului Str., 077125 Magurele Ilfov, Romania

³University Politehnica of Bucharest, Faculty of Applied Sciences, 313 Splaiul Independenței, 060042 Bucharest, Romania

Abstract

^{18}F -FDG is a glucose analog in which the hydroxyl group on the second carbon is substituted with ^{18}F , being used as an indicator of glucose uptake and cell viability.

The aim of this work was to synthesize the ^{18}F -FDG and to validate the methodology for the assessment of its both radiochemical and chemical purities, according to the European Pharmacopoeia. The proposed methodology encompasses three chromatographic methods: radio-HPLC, radio-TLC and HS/GC.

Radiochemical impurities may originate from radionuclide production, incomplete purification and radiolysis after synthesis. Chromatographic methods should effectively separate these species, as radioactive impurities can affect the clinical outcome of positron emission tomography imaging studies because of nonspecific uptake. Chemical impurities, on the other hand, can affect nucleophilic substitution mechanism. Keeping these contaminants at as low concentrations as possible is the key of a successful synthesis. Therefore, the determination of both type of impurities in short time is an essential step in characterizing of each batch, due to the rapid decay of ^{18}F (109.8 min half-life).

By optimizing the operating conditions, both chemical and radiochemical impurities analysis can be done within 12 min. The optimized methodology shows good performance: linearity, specificity, precision, limit of quantification, limit of detection and reproducibility, thus it could be successfully applied in the quality control tests of radiopharmaceuticals according to the European Pharmacopoeia.

Key words: ^{18}F -FDG, chemical impurities, gas chromatography, quality control, radio-HPLC, radio-TLC

Received: November, 2014; Revised final: February, 2015; Accepted: February, 2015

1. Introduction

Positron Emission Tomography (PET) is a technology aimed to obtain *in vivo* biological information quantitatively and noninvasively using radiopharmaceuticals administered intravenously. Chemical and radiochemical impurities may interfere with PET measurements and may cause adverse reactions in the body (Vallabhajosula, 2009).

European Pharmacopoeia (Eur.Ph.) is the official reference source of quality specifications for a pharmaceutical product. The analytical methods predominantly used to assess them are: high performance liquid chromatography (HPLC), thin layer chromatography (TLC), and gas chromatography (GC). For the ^{18}F -FDG radiopharmaceutical, certain quality criteria are required to pass the quality control. For this purpose, the following parameters are to be tested:

* Author to whom all correspondence should be addressed: e-mail: dana.niculae@nipne.ro; Phone: +40 21 404 5033; Fax +40 21 457 4945

radiochemical and chemical purities, endotoxin content, pH, appearance, osmolality, sterility. Analytical methods need to be fast, very accurate and consistent with the usual quality standards of pharmaceuticals, while the detection limit should be as low as *ppm*, due to the short lifetime, and the radiation protection of the operator (special conditions for handling radioactive substances); the latter necessitates a very small amount of chemical compound. The methods should be comparable with the half-life of the radioisotope; in the case of ^{18}F , all tests except the sterility should be performed within 30 minutes post production – a longer analysis time means a loss of radiopharmaceutical's activity (IAEA, 2012).

The radiochemical purity is the ratio, expressed as a percentage, of the radioactivity of the nuclide of interest in the specified chemical form and the radionuclide's total radioactivity in the radiopharmaceutical preparation, respectively (Saha, 2004). A pure radiopharmaceutical compound must not contain other radioactive species. For ^{18}F -FDG, the radiochemical impurities are other species labeled with ^{18}F , such as ^{18}F -fluoride or ^{18}F -acetylglucose (intermediaries). The radiochemical identity can be confirmed by HPLC or TLC. The simplest chromatographic method useful for determination of radiochemical purity is the TLC (Koziorowski, 2010).

The chemical identity and purity address non-radioactive materials in radiopharmaceuticals, including raw materials, solvents and other compounds used in the preparation process (stabilizers, additives etc.). Some examples of non-radioactive core components that require testing in ^{18}F -FDG preparation are: 2-fluoro-2-deoxy-D-glucose (FDG) and 2-chloro-2-deoxy-D-glucose (CIDG), residual solvents (acetonitrile, acetone and ethanol), and Kryptofix 2.2.2 (aminopolyether). Depending on the hydrolysis type in the synthesis path (acidic or alkaline), CIDG impurity could be produced or not (Mosdzianowski et al., 2002).

The aim of this work is the development and validation of faster methods, comparing with those recommended by the Eur.Ph., to determine both radiochemical and chemical purities of ^{18}F -FDG and which can be used in quality control.

The analysis of residual solvents by GC has been widely described concerning some injection techniques, columns and temperature profiles. Apart from different Pharmacopoeia, several methods of analysis have been described (Channing et al., 2001; Fliszar et al., 2004; Klick and Skold, 2004; Qin et al., 2004; Raghani, 2002). A new head-space/gas chromatography (HS/GC) method is presented and validated for the determination of residual solvents (ethanol, acetone and acetonitrile) in this radiopharmaceutical product. Both chemical and radiochemical purities were also validated using a HPLC equipped with electrochemical and radioactive detectors, in accordance with the monograph in Eur.Ph. (EDQM, 2014).

Up to date, several detectors such as UV/VIS, refractive index and pulsed amperometric detector (PAD) coupled with HPLC system were tested for carbohydrates analysis, but each of them has several advantages and disadvantages. For example, the detection of carbohydrates by HPLC with UV/VIS detector is difficult due to the low molar absorbance in the UV/VIS region. Several precolumn or postcolumn derivatizations (i.e., 2-cyanoacetamide and 1-phenyl-3-methyl-5-pyrazolone) of FDG and CIDG have been reported (Nakao et al., 2005, 2008), but derivatizations are not suitable for routine quality control of the ^{18}F -FDG preparations due to the long labeling time, the short half-life of ^{18}F and the radiation exposure of the operator (Nakao et al., 2008).

The refractive index detector can be used only for high concentration of carbohydrates. PAD, working with a gold electrode, could be used if the concentrations of carbohydrates are very low (Jensen et al., 1997; LaCourse et al., 1993). HPLC/PAD has been reported to be a sensitive method, without derivatization, and has been advocated in the Eur.Ph. as the recommended technique.

2. Experimental

2.1. Materials

All solvents were purchased from Merck and used without purification. Ultrapure water was prepared using the Millipore MilliQ Direct 8/16 water purification system. Standards (reference chemicals) were obtained from ABX (Germany).

^{18}F -Fluoride was produced at National Institute for Physics and Nuclear Engineering "Horia Hulubei", Radiopharmaceuticals Research Centre (Ursu et al., 2013), in the Cyclotron TR19 (ACSI).

The synthesis of ^{18}F -FDG was performed according to the nucleophilic substitution method (Hamacher et al., 1986), followed by alkaline hydrolysis of the intermediary product [^{18}F]fluoro-1,3,4,6-tetra-O-acetyl-D-glucose (FTAG) (Fig. 1), on the synthesis module FASTlab (GE Healthcare, USA). The leaving group, triflate is converted to trifluorosulfonic acid ($\text{CF}_3\text{SO}_2\text{OH}$), which is removed at a later stage in the purification process.

2.2. High performance liquid chromatography

HPLC was performed with an Agilent Bio-inert 1260 Series equipped with electrochemical (Decade II, Antec – USA) and radioactive (Gabi, Raytest – Germany) detectors. A CarboPac PA1 column (Dionex) 250x4.5 mm with 1.0 μm internal diameter was used for separation of chemical impurities of FDG by isocratic elution with 0.1 M sodium hydroxide (NaOH) as mobile phase; flow rate 1.2 mL/min, temperature of the column and electrochemical cell 35 $^\circ\text{C}$.

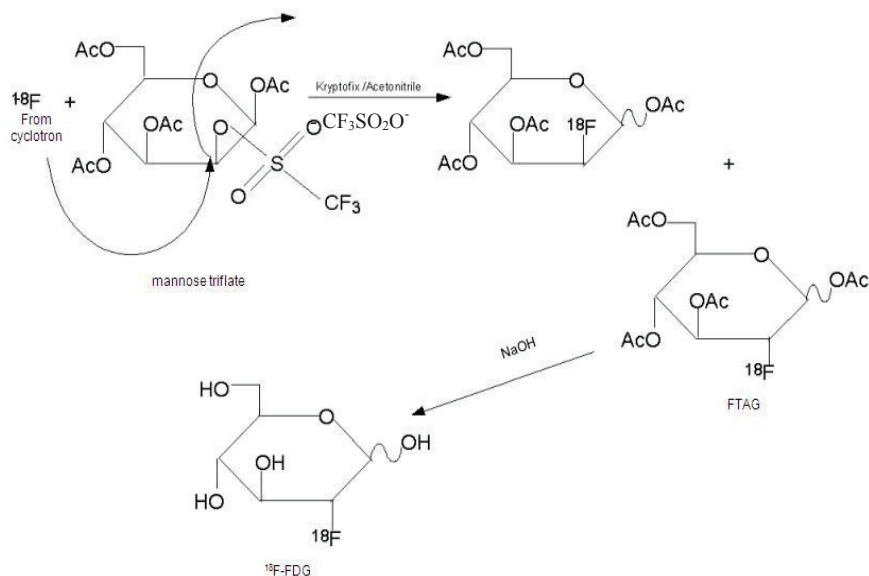


Fig. 1. Synthesis of ^{18}F -FDG by nucleophilic substitution followed by alkaline hydrolysis (Yu, 2006)

Electrochemical detection was performed in pulsed mode used an Au cell with Ag/AgCl reference electrode. Radioactive samples were analyzed using a gamma radioactive detector with NaI cell.

2.3. Gas Chromatography

An Agilent 6890A GC equipped with an FID and a 7694 HS sampler was used for the experiments. The HS/GC system was controlled using Agilent Chem32 software. The GC column was a J&W DB – 624 (6% cyanopropylphenyl / 94% dimethylpolysiloxane) fused silica capillary column, having 30 m length, 0.53 mm internal diameter, 3 μm film thickness.

2.4. Thin Layer Chromatography

The TLC Chromatographic method was applied only to determine the radiochemical purity, as alternative method. A VCS 201 System - Veenstra Instruments Holland was used. The data acquisition was obtained with the VCS 203 software.

2.5. Method validation

The validation of the analytical method was carried out according to ICH Q2 (R1) guidelines (ICH, 2005). The parameters of the validation were: system suitability, specificity, precision, accuracy, linearity, limit of detection (LoD) and limit of quantification (LoQ) (Burlacu et al., 2009; ICH, 2005). The system suitability was evaluated by injecting the blank solution (duplicate) and standard test solution (six injections) using the optimized method.

The chromatograms were recorded, evaluated and the relative standard deviations were computed. The resolution between two successive peaks was

measured. The specificity of the method was performed by injecting standard solutions of each residual solvent and a mixture of standard solutions for these compounds and comparing the retention time of each standard. The precision was performed by injecting six standard test solutions (100%), measuring the response for each solvent peak and calculating its relative standard deviation (%).

The method's accuracy was validated through recovery experiments by spiking with known amount of each solvent at 80%, 100% and 120%. Each concentration was prepared in triplicate and the percent recovery was calculated.

The linearity of the method was investigated using six concentration levels ranging from 100 to 1,000 ppm for ethanol and acetone and 10 to 100 ppm for acetonitrile. The correlation coefficient of determination (R^2) was calculated for each solvent.

The sensitivity of the method was presented as the LoQ with a signal to noise ratio of 10:1 and the LoD with a signal to noise ratio of 3:1. Both LoQ and LoD have been established on the basis of S/N ratio by six injections at LoD level and six injections at LoQ level.

2.6. Standard preparation

For GC determinations, a standard stock solution of solvents was prepared from 2.5 g ethanol, 2.5 g acetone and 0.25 g acetonitrile, accurately weighted and diluted with water in a 10 mL volumetric flask. Working standard solutions were prepared by diluting the standard stock solution with water. Test solutions were obtained by diluting 200 μL of sample to 1.0 mL with water.

For HPLC determinations, 2 mg of FDG standard was weighted and transferred accurately into 10 mL volumetric flask and dissolved in water to obtain the standard stock solution. Working standard

solutions were obtained by serial dilution of standard stock solution. The test sample was directly injected in the chromatographic system.

3. Results and discussion

3.1. Development of the method assessing Residual Solvents using HS/GC

Based on the methods described in Eur.Ph. regarding the analysis of residual solvents in pharmaceutical products, a new and faster method was developed to determine three residual solvents, namely ethanol, acetone and acetonitrile, which may be found in ^{18}F -FDG radiopharmaceutical product.

The proposed method has significant changes in comparison with the method described in Eur.Ph. We varied a number of parameters in the HS system: temperature (oven, transfer line and loop), time (vial equilibration and injection) and pressure. The equilibration temperature was increased from 90 °C to 105 °C. The equilibration time in headspace module was decreased from 45 to 2 minutes. The GC cycle was optimized at 10 min. A number of GC parameters were evaluated during the development of

this method: the oven temperature gradient, the flow rate of the carrier gas and the sample split ratio. The ramp temperature was optimized in the 40–100 °C interval.

All the solutions (standards and samples) were diluted with water. The parameters of the improved HS/GC method are listed in Table 1. In this method the maximal used temperature was 100 °C because all the residual solvents have been eluted before this value. The specificity is the ability of the method to confirm the analyte identity from other interferences. The specificity of the method was confirmed by the resolution between two consecutive peaks, both in sample and in standard solutions.

No interference from the blank at each retention time of analyte peaks was observed. A chromatogram obtained from the standard solution is shown in Fig. 2. The data obtained for standard solutions are presented in Table 2; the resolution between two successive eluting peaks was higher than 2.0, which meets the acceptance criteria. The method has been shown to be linear by a plot of six points in the range 100–1,000 ppm for ethanol and acetone.

Table 1. Chromatographic parameters for HS/GC optimized method

Headspace Parameter	Settings	
	Eur.Ph. method	Optimised method
Equilibration temperature	90 °C	105 °C
Transfer line temperature	105 °C	110 °C
Loop temperature	110 °C	
Vial equilibration time	45 min	2 min
Injection Duration	0.2 min	0.2 min
GC Cycle	30 min	10 min
Volume Injection	1 µL	
GC Parameter		
Inlet temperature	150 °C	
Carrier (He) flow rate	36 mL/min	82.1 mL/min
Pressure	2.3 psi	3.65 psi
Inlet split ratio	10:1	15:1
Oven temperature gradient	40 °C–240 °C	40 °C–100 °C
Ramping to	30 °C / min	15 °C / min.
FID temperature	250 °C	
Detector gas flow	30 mL/min.	

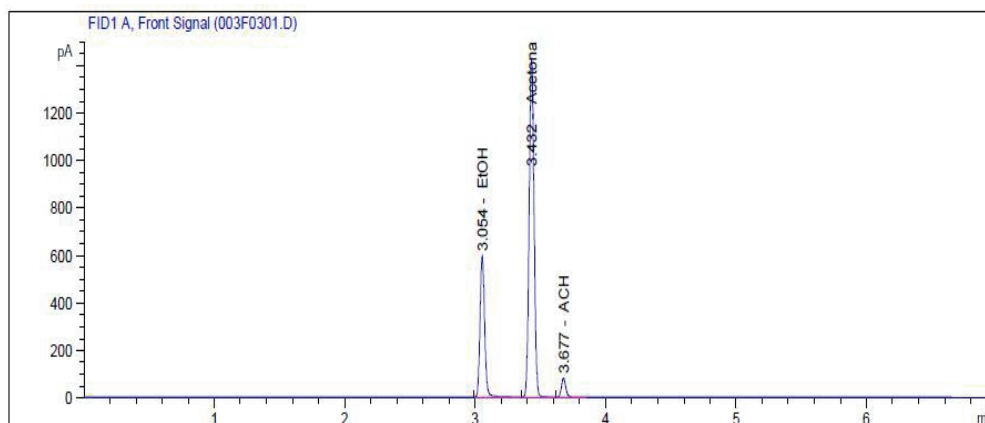


Fig. 2. The chromatogram of the standard residual solvents

The linearity range was determined in between 10–100 ppm for acetonitrile. Good linearity was achieved for all solvents (see Fig. 3). The correlation coefficient (R^2) for each residual solvent had value higher than 0.998.

Table 2. Specificity of the method

Solvent	Retention Time (min)	Relative Retention Time	Resolution
Ethanol	3.05	1.0	-
Acetone	3.43	1.14	5.6
Acetonitrile	3.67	1.22	3.1

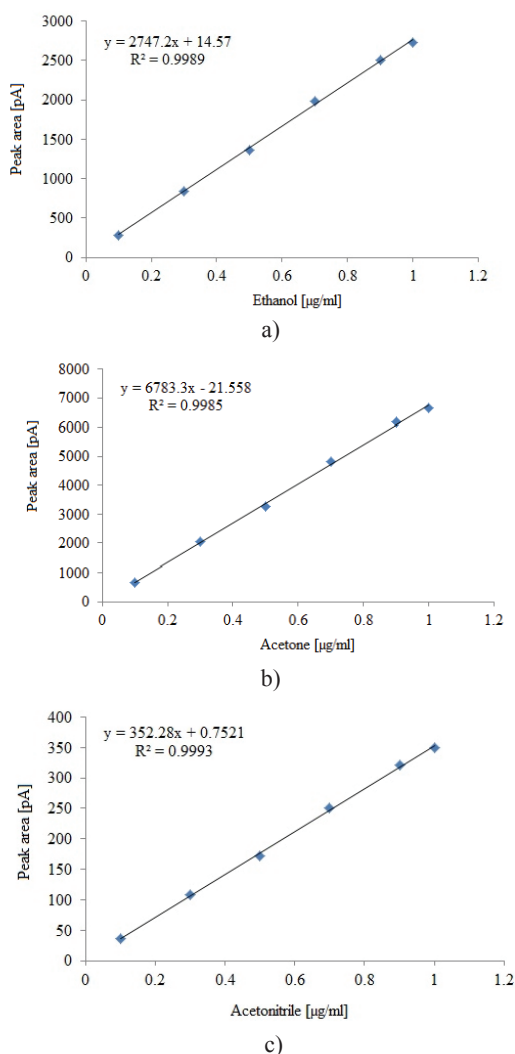


Fig. 3. Calibration curves for residual solvents: a. ethanol; b. acetone; c. acetonitrile

The precision of this method was expressed as relative standard deviation (RSD) data and was performed by injecting six standard test solutions. Both the standard deviation (SD) and RSD were calculated for each solvent. The RSD was found out to be less than 15%. All values are listed in Table 3.

The limits of both LoD and LoQ were calculated following the formulas: $LoD = 3.3 \sigma/S$, and $LoQ = 10 \sigma/S$, respectively, where σ is the SD of

the response and S is the slope of the calibration curve of the solvent. The results are shown in Table 4.

Table 3. The precision of the method

Number of injection	Area		
	Ethanol	Acetone	Acetonitrile
1	1454.6	3562.4	184.5
2	1417.6	3481.8	181.5
3	1446.7	3427.9	180.8
4	1483.2	3421.3	182.8
5	1386	3297.1	174.7
6	1342	3350	174.1
Average	1421.7	3423.4	179.7
SD	43.3	79.4	3.6
% RSD	3.1	2.3	2.0

Table 4. The values of the LoD and the LoQ for the residual solvents

Solvent	Limit of detection [µg/mL]	Limit of quantitation [µg/mL]
Ethanol	0.52	1.57
Acetone	0.39	1.18
Acetonitrile	0.04	0.11

The system suitability has been demonstrated by analyzing the standard solutions during the validation study. The system performance was checked by the resolution, % RSD and asymmetry. The results obtained for the system suitability of this method are presented in Table 5.

3.2. Development of the method for assessing chemical purity using HPLC

The adopted synthesis route of ¹⁸F-FDG product involves a nucleophilic substitution mechanism and a basic hydrolysis. In this case, the 2-chloro-2-deoxy-D-glucose impurity is absent. The limit of FDG standard is 0.5 mg/V, with V being the maximum recommended dose in milliliters. The HPLC analysis's parameters are listed in Table 6.

The detection of FDG was completed in less than 12 minutes (Fig. 4). The range of linearity was determined between 2–200 µg/mL for FDG standard. The calibration line is shown in Fig. 5.

The parameters of the validation process such as precision, accuracy, linearity, LoD and LoQ were determined in conformity with the ICH standard requirements. The results are present in Table 7.

3.3. Complementary TLC method used to identify and to assess the radiochemical purity

The radiochemical purity was evaluated by TLC scanner. TLC mobile phase is a mixture of acetonitrile and water (95:5 v/v). It should be noted that the results of TLC may vary due to different companies producing the paper chromatography and the operating conditions (EDQM, 2014).

Table 5. The system suitability's parameters for the improved HS/GC method

Number	System Suitability Parameters	Value			Specification
		Ethanol	Acetone	Acetonitrile	
1.	Resolution	-	5.6	3.1	>2
2.	% RSD	3.1	2.3	2.0	<15
3.	Asymmetry	0.84–0.94	0.87–0.97	0.85–0.95	0.8–1.2

Table 6. The chromatographic parameters for HPLC/ EC (PAD) method

Chromatographic parameters	Settings
Flow	Isocratic at 1,2 mL/min
Column	Thermo Scientific Dionex Carbopac: PA1, 4x250 mm,1.0 μm i.d.
Temperature	35 °C
Injection volume	5 μL loop
Mobile phase	0.1M Sodium hydroxide (NaOH)
EC parameters (PAD)	Working potential +200 mV vs. Ag/AgCl reference electrode
Range	50 μA

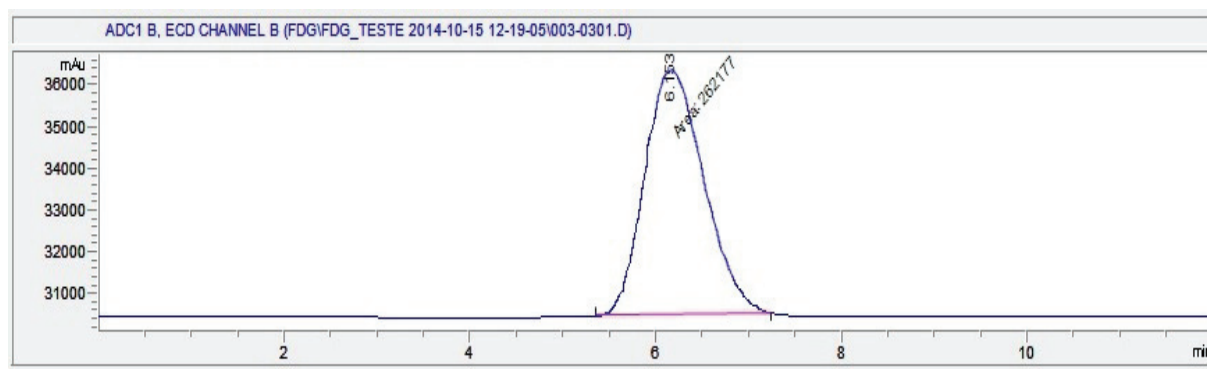


Fig. 4. The HPLC report for the FDG Standard

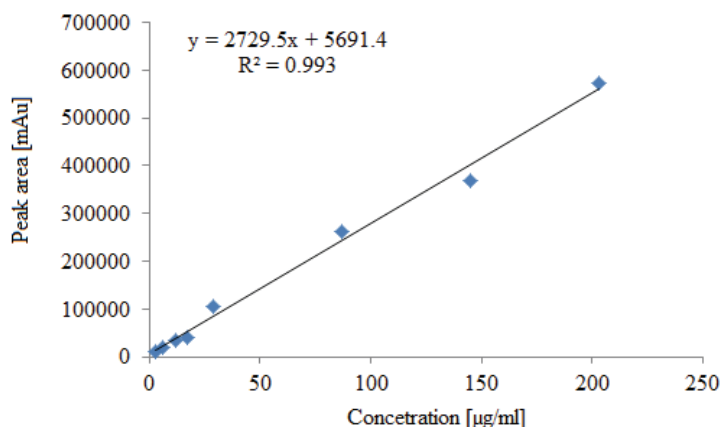


Fig. 5. The calibration line for the FDG standard

Therefore, it is important to use the same type of paper, and also to TLC freshly prepared mobile phase. The size of the spot should be 5 μL. After separation in 95:5 acetonitrile/water mixture, the paper chromatography was dried. Radiochemical purity is defined as the percentage of the radioactivity present in the nuclide of the specified chemical form of interest from the total radioactivity of the radionuclide present in R_f preparation, respectively. In the case of ¹⁸F-FDG synthesis, the

radiochemical impurities are other species marked with ¹⁸F, ¹⁸F such as F or radio-labeled intermediaries.

The radiochemical impurities are separated due to their differing affinities to the mobile phase. The chromatographic paper was dried after separation of the spot in 95:5 acetonitrile/water mixture. The front ratio (R_f) values for ¹⁸F-FDG, free ¹⁸F and acetylated ¹⁸F-FDG are 0.65; 0.00 and, respectively 0.80 to 0.95 (Table 8).

The product migration profile was determined by scanning the chromatogram plate with a suitable collimated radiation detector. The radiochemical purity of the preparation is acceptable if the percent of the area peak of the ^{18}F -FDG is higher than 95%. The radiochemical purity of the synthesized product, i.e. ^{18}F -FDG, was 100% and the radiochromatogram is presented in Fig. 6.

4. Conclusions

The most important aspect of working with ^{18}F -FDG is the short time which can be spent on

quality control in the laboratory, which now is about 30 minutes. The critical factors are the speed, the simplicity and the reliability of the new developed analytical method.

An improved and fast HS-GC method for the quality control of ^{18}F -FDG has been developed and validated, meeting all the acceptance criteria in terms of linearity, specificity, precision, accuracy, as well as LoD and LoQ. The HS-GC method is characterized by the high correlation coefficients and the short time of analysis (10 min), comparing to the 30 min corresponding to the method outlined in the Eur.Ph..

Table 7. The results of HPLC/EC (PAD) validated method

Validation Parameter	
Linearity: The correlation coefficient (R^2) should be > 0.99	
Regression Equation	$y = 2729.5x + 5691.4$
Correlation coefficient (R^2)	0.993
Range ($\mu\text{g/mL}$)	2–200
Precision: %RSD, should be < 5%	
Repeatability	3.47
Intra-day precision	
80%	2.31
100%	1.00
120%	2.43
LoD ($\mu\text{g/mL}$)	1.22
LoQ ($\mu\text{g/mL}$)	3.71
Accuracy: %Recovery should be within 80-120%	
Concentration (%)	Recovery (%)
80	96.32
100	99.13
120	97.88

Table 8. Informative R_f values

$R_f \sim 0$	Free [^{18}F] fluorine ions – $^{18}\text{F}^-$
$R_f \sim 0.65$	2- [^{18}F] fluoro -2-deoxy-D-glucose – [^{18}F]FDG
$R_f \sim 0.9$	Incompletely hydrolyzed sugar derivations – Ac- [^{18}F]FDG

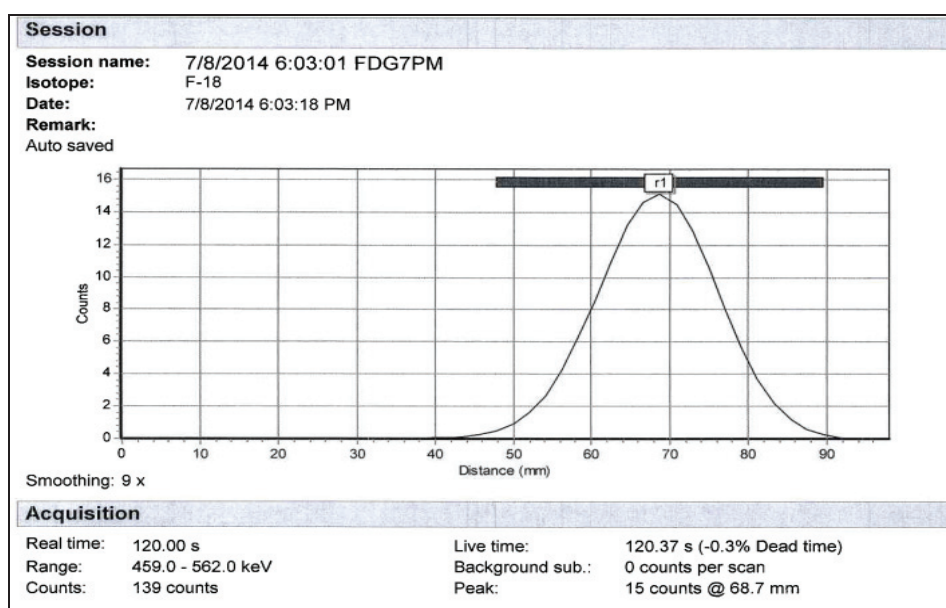


Fig. 6. The TLC report for the synthesized ^{18}F -FDG

The HPLC method for determination of 2-fluoro-2-deoxy-D-glucose (FDG) is specific, precise, accurate, linear and robust. The analysis time is short, just 12 minutes to complete. Also, the determination of the radiochemical purity using TLC is reliable and fast.

These methods are selective and thus can also be used in quality control of other radiopharmaceutical compounds.

Acknowledgements

This work is supported by the Sectorial Operational Program Human Resources Development (SOP HRD), financed from the European Social Fund and the Romanian Government under the contract number POSDRU/159/1.5/S/137390/.

References

- Burlacu A.I., Cuciureanu R., Fitterman P., Larroque M., (2009), Optimisation of gas chromatographic method acrylamide analysis applications for risk management, *Environmental Engineering and Management Journal*, **8**, 315–320.
- Channing M.A., Huang B.X., Eckelman W.C., (2001), Analysis of residual solvents in 2-[F-18]FDG by GC, *Nuclear Medicine and Biology*, **28**, 469–471.
- EDQM, (2014), *European Pharmacopoeia*. 8.0, *Radiopharmaceutical Preparation: Fludeoxyglucose (18F) Injection*, European Directorate for the Quality of the Medicines, 1052 – 1054, Strasbourg.
- Fliszar K., Wiggins J.M., Pignoli C.M., Martin G.P, Li Z., (2004), Analysis of organic volatile impurities in pharmaceutical excipients by static headspace capillary gas chromatography, *Journal of Chromatography A*, **1027**, 83–91.
- Hamacher K., Coenen H., Stocklin G., (1986), Efficient stereospecific synthesis of no-carrier-added 2-[¹⁸F]Fluoro-2-deoxy-D-glucose using aminopolyether supported nucleophilic substitution, *Journal Nuclear Medicine*, **27**, 235–238.
- IAEA, (2012), *Cyclotron Produced Radionuclides: Guidance on Facility Design and Production of [18F]Fluorodeoxyglucose (FDG)*, In: *Radioisotopes and Radiopharmaceuticals*, Series No.3, Vienna, On line at: <http://www.iaea.org/Publications/index.html>.
- ICH, (2005), *Validation of Analytical Procedures: Text and Methodology*, Q2(R1), International Conference of Harmonisation, On line at: <http://www.ich.org/products/guidelines/quality/article/quality-guidelines.html>.
- Jensen M.B., Johnson D.C., (1997), Fast wave forms for pulsed electrochemical detection of glucose by incorporation of reductive desorption of oxidation products, *Analytical Chemistry*, **69**, 1776–1781.
- Klick S., Skold A., (2004), Validation of a generic analytical procedure for determination of residual solvents in drug substances, *Journal of Pharmaceutical and Biomed Analysis*, **36**, 401–409.
- Koziorowski J., (2010), A simple method for the quality control of [18F]FDG, *Applied Radiation and Isotopes*, **69**, 649–716.
- LaCourse W.R., Johnson D.C., (1993), Optimization of waveforms for pulsed amperometric detection of carbohydrates based on pulsed voltammetry, *Analytical Chemistry*, **65**, 50–55.
- Mosdzianowski C., Lemaire C., Simoens F., Aerts J., Morelle J.L., Luxen A., (2002), Epimerization study on [18F]FDG produced by an alkaline hydrolysis on solid support under stringent conditions, *Applied Radiation and Isotopes*, **56**, 871–875.
- Nakao R., Ito T., Yamaguchi M., Suzuki K., (2005), Improved quality control of [18F]FDG by HPLC with UV detection, *Nuclear Medicine and Biology*, **32**, 907–912.
- Nakao R., Ito T., Yamaguchi M., Suzuki K., (2008), Simultaneous analysis of FDG, CIDG and Kryptofix 2.2.2 in [18F]FDG preparation by high performance liquid chromatography with UV detection, *Nuclear Medicine and Biology*, **35**, 239–244.
- Qin L., Hu C.Q., Yin L.H., (2004), Establishment of a knowledge base for prescreening residual solvents in pharmaceuticals, *Chromatographia*, **59**, 475–480.
- Raghani A.R., (2002), High-speed gas chromatographic analysis of solvents in pharmaceuticals using solid phase microextraction, *Journal of Pharmaceutical and Biomedical Analysis*, **29**, 507–518.
- Saha G.B., (2004), *Synthesis of PET radiopharmaceuticals*, In: *Basics of PET Imaging Physics, Chemistry, and Regulations*, Springer, New York, 111–124.
- Ursu I., Craciun L., Niculae D., Zamfir N.V., (2013), The Radiopharmaceuticals Research Centre of IFIN-HH at Start, *Romanian Journal of Physics*, **58**, 1327–1336.
- Vallabhajosula S., (2009), *Quality Control of PET Radiopharmaceuticals*, In: *Molecular Imaging: Radiopharmaceuticals for PET and SPECT*, 1st Edition, Springer, Verlag Berlin Heidelberg, 197–204.
- Yu S., (2006), Review of 18F-FDG synthesis and quality control, *Biomedical Imaging and Intervention Journal*, **2**, e57.



“Gheorghe Asachi” Technical University of Iasi, Romania



VOLATILES IN *TĂMÂIOASĂ ROMÂNEASCĂ* VIA SUPERCRITICAL FLUID EXTRACTION (SFE) ANALYSIS

Lucia Cintia Colibaba¹, Valeriu V. Cotea^{1*}, Liliana Rotaru¹, Bogdan Nechita^{1,2},
Marius Niculaua², Stefan Tudose-Sandu-Ville¹, Camelia Luchian¹

¹“Ion Ionescu de la Brad” University of Agronomic Sciences and Veterinary Medicine Iasi,
3 M. Sadoveanu Alley, 700490 Iasi, Romania

²Oenological Research Center – Iasi Branch of the Romanian Academy, 9 M. Sadoveanu Alley, Iasi, Romania

Abstract

Wine analysis is a complex process, requiring multiple techniques and very in-depth multidisciplinary knowledge. Moreover, when talking about sensorial potent wines, like *Muscat* or *Tămâioasă Românească* (from aromatic Romanian grape variety), the identification and characterization of its volatile compounds is achieved through different methods, most calling for powerful solvents to separate the aroma substances.

Supercritical fluid extraction is a powerful technique with great promise in organic analytical chemistry. To date, little has been published on the use of SFE in the analysis of wine aromas.

The main objective of this study is the analysis of volatiles in samples of *Tămâioasă românească* wines through a custom-made SFE method. The wine variants have been obtained by applying the general technological processes for aromatic wines, using specific oenological products. An in-house SFE analysis method was developed and applied, the obtained extracts were then analyzed by gas chromatography coupled to mass spectrometry (GC-MS) to identify the captured compounds.

Regarding the total number of findings in respect to volatiles, the highest concentrations occur with low molecular weight alcohols, esters and acetic acid. Besides, there were also identified other volatile compounds, such as terpenoids and phenols. These specific compounds originate from the grape variety and give the “varietal” character to the wines.

Key words: supercritical fluid extraction, *Tămâioasă Românească*, volatiles, wines

Received: November, 2014; *Revised final:* February, 2015; *Accepted:* February, 2015

1. Introduction

Wine is largely defined by its appearance (e.g. color, limpidity), volatile as well as non-volatile aroma (flavor), and also what we experience as tactile senses when consuming wine, such as mouth-feel properties. Wine raises most discussions, particularly due to its complex composition of (volatile) compounds responsible for its intricate aromatic nature. Volatile compounds of which some express highly appreciated aroma attributes are the ones that give wine its “genius”, specificity and individuality. Each wine’s individuality or

“personality” is given by a specific and unique combination of characteristic flavor compounds.

Grape-origin compounds provide the basic structure of the wine (sugar, acids, phenols, minerals) and, in addition, the varietal sensory distinction. This is well known for the free floral monoterpenes that define *Muscat*-related and other aromatic wines. For others, monoterpenes may be found primarily in glycosidically bound forms in the grape, and have to be released by enzymes produced during fermentation (Baumes, 2009). Furthermore, depending on wine-style, the overall bouquet of the wine may greatly be influenced by maturing in oak

* Author to whom all correspondence should be addressed: e-mail: vcotea@uaiasi.ro; Phone: +40 232407519; Fax: +40 232407519

barrels, and finally, by the chemical changes observed during aging (Fischer, 2007).

Monitoring volatiles in wines requires complex procedures that usually call for use of solvents that, in high quantities, can be harmful for human health. Therefore, the need of an easier, solvent-free analysis method has risen. The evolution towards Green Analytical Chemistry is to new extraction and sample-preparation processes that should be faster, more reproducible and more environmentally friendly (Herrero et al., 2013).

Supercritical fluid extraction (SFE) is the process of separating one component (the extract) from another (the matrix) using supercritical fluids as the extracting solvent. It is based on the principle that solubility in a supercritical fluid increases dramatically with increasing density, and different solutes have different solubility at the same condition. The major advantage of this method over liquid-liquid extraction is that the supercritical fluid can easily be removed after extraction by lowering the temperature or pressure or both (Válcarcel and Tena, 1997). The essential equipment needed to perform SFE is shown in Fig. 1.

A high pressure pump is used to provide pressurized fluid (at a constant pressure) to the sample which is contained in the extraction vessel or sample cell. The extraction vessel is housed in an oven to maintain the temperature above the critical temperature of the extraction fluid. The extraction fluid is pumped through the extraction vessel, the analytes are partitioned into the supercritical fluid, and the analytes are collected after depressurization of the supercritical fluid. Extracted analytes are most often collected in a small volume of liquid solvent (off-line SFE) or the analytes transferred directly to a chromatographic system (on-line SFE) like SFC or GC. Alternate methods such as cryogenic trapping (Levy et al., 1992; Xie et al., 1989) or collection onto a sorbent cartridge have also been used (Maxwell et al., 1995).

Supercritical fluids exhibit liquid-like (solvent power, negligible surface tension) as well as gas-like (transport) properties above their critical point. This property has led in recent years to great interest in supercritical fluids amongst researchers for their various applications.

CO₂ is used as “supercritical solvent” in the extraction of flavor and fragrance compounds, since it is an odorless, colorless, highly pure, safe, cost effective, nontoxic, nonflammable and recyclable gas allowing supercritical operation at relatively low pressures and near room temperature. Generally speaking, supercritical CO₂ (SC CO₂) behaves like a lipophilic solvent but, compared to liquid solvents, it has the advantage that its selectivity or solvent power is adjustable and can be set to values ranging from gas-like to liquid-like (Reverchon, 1997).

Extraction conditions for supercritical carbon dioxide are above the critical temperature of 31 °C and critical pressure of 74 bar (Jonin et al., 2010). The main advantages of using supercritical fluids for extractions is that they are less expensive, extract the analytes faster and they are also more environmentally friendly than organic solvents.

This study aims at identifying the possibilities of extracting aroma compounds in Tămâioasă românească wines through a newly developed SFE method. In the present work the focus will be on the SFE volatiles’ extraction from Tămâioasă românească wine, one of the most well-known aromatic wines in Romania, which had not been investigated in this respect before. In order to study the volatiles, several trials were made, and the most representative ones are to be seen below. To our knowledge, however, there has been no previous attempt to use this simple technical SFE/SFC procedure (lower pressure and temperature) combined with GC/MS identification for determination of Tămâioasă românească wine aroma compounds.

2. Material and methods

2.1. Grape material and reagents

Grapes of the variety Tămâioasă românească, a Romanian aromatic grape variety were harvested from Cotnari vineyard in 2013, on the 25th of September. The preliminary analysis showed that the grapes had 250 g/L sugars and an acidity of 6.1 g/L tartaric acid.

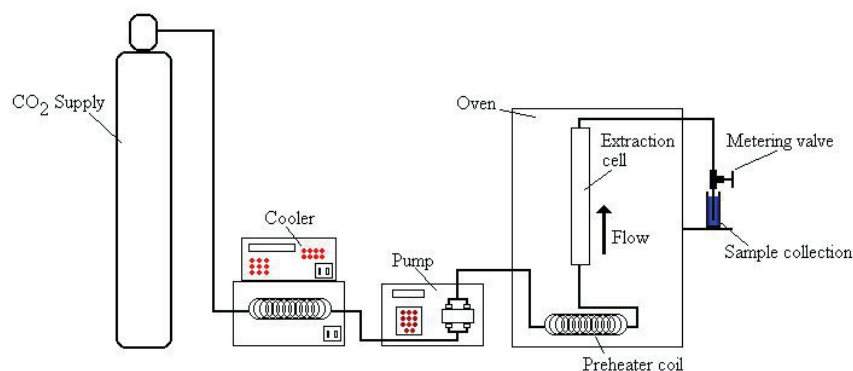


Fig. 1. Diagram of a SFE setup for off-line recovery of analytes (Sewram, 1997)

Solvents: ethanol and dichloromethane, over 99% purity, were purchased from Sigma-Aldrich, Germany. Oenological products were purchased from Sodinal, Paris, France

2.2. Wine samples

The grapes were processed according to the literature, specifically referring to aromatic wine technologies (Cotea and Sauciuc, 1986). After destemming and crushing, the unpressed must was partitioned in three equal parts.

Saccharomyces cerevisiae (Fermactive Ap[®] and Fermactive Muscat[®]), which is recommended for proper vinification of aromatic grapes, such as Muscat, Grasă de Cotnari, Tămâioasă românească and Șarbă was used for fermentation.

Each fermentation vessel (15 L glass jar) was inoculated with 1g/L of dry yeast, previously rehydrated for 15 minutes at 35 °C. The first variant was macerated for 24 hours, with no added enzymes, pressed, and then transferred to glass vessels for fermentation with commercial yeast Fermactive Ap[®]. Second variant of the Tămâioasă românească was macerated for 24 hours with addition of pectolytical enzymes (Zymoclaire High CG[®]). The third variant of Tămâioasă românească was macerated for 24 hours with addition of a different pectolytical enzyme (Endozym Beta-split[®]). Pressing was then done with a hydraulic press. The resulting juice was transferred into glass vessels for fermentation with Fermactive Muscat[®], at 15 °C. The fermentation period took 14 days.

The following experimental wine samples were obtained and registered as follows: TR V1 (Tămâioasă românească wine sample, 24 hours maceration, no enzymes, fermentation with Fermactiv Ap[®]), TR V2 (Tămâioasă românească wine sample, 24 hours maceration with Zymoclaire Aroma High CG[®] enzymes, fermentation with Fermactive Muscat[®] yeasts) and TR V3 (Tămâioasă românească wine sample, 24 hours maceration with Endozym Beta-split[®] enzymes, fermentation with Fermactive Muscat[®] yeasts).

2.3. SFE/GC analysis conditions

An off-line JASCO[®] SFE/SFC custom made procedure was used for supercritical fluid extraction (in house method), while a Shimadzu GC-MS 2010 was used for extracted volatiles' analysis.

2.3.1. SFE analysis of Tămâioasă românească wines

Extractions were performed using an SFE module designed and manufactured by Jasco (Japan). The device has an EV-4 of 10 mL extraction cell for liquid samples in a CO-2060 extraction oven. The chemical modifier was added in to the mixing chamber of the extraction oven with a PU-2089 quaternary gradient pump with a build-in degasser at 20% ratio. Every extraction was 60 minutes long

collected with aid of a BP-2080 back pressure regulator at around 10 MPa. A PU-2080-CO₂ Peltier cooled pump delivered 1 mL/min. liquid carbon dioxide in supercritical mode at more than 10 MPa.

In each 5 mL wine sample were added an amount of 1 g NaCl before SFE extraction, for salting out or increasing aroma compounds' extraction power. The extraction temperature in the oven was 40 °C and the back pressure regulator was set at 60 °C. The temperature of the collected liquid was 20 °C. The modifier used was ethylic ether 25% with 75% dichloromethane. The collected volumes varied from 1.2 to 1.5 mL/h. Also, the most insoluble and less volatile compounds were collected as white solid crystals, fraction recovered with 1 mL of dichloromethane.

2.3.2. GC/MS analysis conditions

The analysis of the obtained extracts was made on a Shimadzu GC-MS 2010plus device. Column oven temperature started at 35 °C where it was maintained for 3 minutes after injection and grew with 5 °C per minute up to 220 °C where it remained for 10 minutes, injection temperature was 250 °C, split mode: 20 for 1 μL injected and column flow was 1 mL/min. The column used is Varian VF-WAXms 30 m length, 0.15 mm diameter, 0.15 μm thickness (Agilent Technologies, Germany). The interface transfer temperature was 250 °C. The mass spectrometer detector had the ion source temperature at 250 °C and acceleration voltage at 0.8 KV. The detected peaks were compared with NIST08, Wiley08 and SZTERP spectra libraries for identification purposes. A similarity percentage of over 70% was considered acceptable.

3. Results and discussion

3.1. SFE/GC analysis

Alcohols and esters were the main identified volatiles of the studied wines. These compounds are mainly produced by yeast metabolism during fermentation (Rapp and Mandery, 1986).

Table 1 shows the aroma compounds in Tămâioasă românească wine samples, obtained from a 24 hours maceration of grapes, with no enzymes addition and using yeast specifically designed for obtaining neutral wines (Fermactiv Ap[®]).

Table 2 shows the aroma compounds in Tămâioasă românească wine samples, obtained from a 24 hours maceration of grapes, with addition of ZYMOCLAIRE High CG[®] which is a highly concentrated pectolytic enzyme preparation, without any cinnamyl-esterase activity, designed for the clarification of grape juice with high turbidity at low temperatures. Fermentation was achieved by using Fermactive Muscat[®] yeasts. In enology, winemakers go for such maceration in order to better extract the bound aroma precursors (Ribereau-Gayon et al., 2000).

In addition, the enzyme added (ZYMOCLAIRE High CG[®]) during maceration aids in cleaving such glycosidic bonds (having glycosidase side-activities). Particularly for bound terpene precursors, this is beneficial for a more pronounced varietal character of the final product.

Table 3 shows the aroma compounds in Tămăioasă românească wine samples, obtained from a 24 hours maceration of grapes, with addition of Endozym Beta-split[®] enzymes that frees up available varietal aromas that are bound with sugars that otherwise would only be available in the case of high over-ripening conditions of the fruit. The same yeasts as in the above sample were used.

The identified compounds are common in wines (Clarke and Bakker, 2004; Ron, 2000), significant for aromatic wines. In previous studies, Tămăioasă românească wines were also analysed from the point of view of volatile composition, therefore, the specific retention time of the identified compounds can be verified. The methods previously used consisted of headspace GC/MS and SPE GC/MS (Nechita, 2010).

As the used SFE method is still in trials, the analysis results of the three samples show some discrepancies according to the analysed wine variants. As seen from the above tables, the number of identified compounds varies from one wine

sample to another. In the first sample, Tămăioasă românească wine obtained through a 24 hours maceration and use of yeasts specific for neutral wine making, 5 compounds were identified, compared to the other two samples (12 compounds in the second and 9 compounds in the third, both latter samples being obtained with use of maceration enzymes and yeasts specific for obtaining aromatic wines).

The identified compounds are from specific chemical classes, as follows: 5 alcohols (propanol, isobutyl alcohol, 3-methyl-1-butanol, 2,3-butanediol, phenylethyl alcohol), 4 esters (ethyl ether, ethyl formate, ethyl acetate and propanoic acid, 2-hydroxyethyl ester), 1 lactone (butyrolactone), 1 acid (acetic acid), 1 terpene (3,7-Dimethyl-octa-1,7-dien-3,6-diol also known as Terpene diol -2) and 1 phenol (4-vinylphenol) (Fig. 2). 4-vinylphenol is a phenolic compound produced by the spoilage yeast *Brettanomyces* in wine. Terpene diol 2 is a specific terpene for Tămăioasă românească wines (Nechita, 2010).

The in-house method described still needs more trials and feedback and possibly this will bring in further optimisation, as modifiers can form aerosols and sweep analyte molecules through the system without the molecules being deposited or collected in traps.

Table 1. Aroma compounds in TR V1

No	R.T. (min.)	Peak area (UA)	Compound name	ID ¹	Sensory descriptor
1	6.04	40205	Propanol	A	slightly sweet fruity nuance of apple and pear
2	7.36	10135	1-Propanol, 2-methyl-	A	ethereal winey
3	10.65	367627	3-Methyl-1-butanol	A	ethereal winey
4	17.40	161821	Acetic acid	A	pungent acidic and dairy-like
5	27.95	665002	Phenylethyl Alcohol	A	floral rose

¹Identification: A = GC retention and MS data in agreement with spectra found in the library; B = tentatively identified by MS matching with library spectra only; nd: not detected, tr: trace. Results are the means of three repetitions.

Table 2. Aroma compounds in TR V2

No	R.T. (min.)	Peak area (UA)	Compound name	ID ¹	Sensory descriptor
1	1.64	286093	Ethyl ether	B	ethereal
2	2.45	67134	Ethyl formate	B	ethereal, sweet, grainy, fruity, winey and cognac
3	3.12	251850	Ethyl acetate	A	ethereal, fruity, sweet, with a grape and cherry nuance
4	6.59	315514	Propanol	A	slightly sweet fruity nuance of apple and pear
5	8.04	186656	Isobutyl alcohol	A	ethereal, winey
6	11.40	2048687	1-Butanol, 3-methyl-	A	ethereal, winey
7	14.78	574334	Propanoic acid, 2-hydroxy-, ethyl ester	A	sweet, fruity, acidic, ethereal with a brown nuance
8	17.40	1909964	Acetic acid	A	pungent acidic and dairy-like
9	19.73	2671696	2,3-Butanediol	A	fruity, creamy, buttery
10	21.74	85006	Butyrolactone	A	creamy, oily with fatty nuances
11	27.94	1082477	Phenylethyl Alcohol	A	floral rose
12	35.47	68742	3,7-Dimethyl-octa-1,7-dien-3,6-diol	B	sweet, floral, citrus

¹Identification: A = GC retention and MS data in agreement with spectra found in the library; B = tentatively identified by MS matching with library spectra only; nd: not detected, tr: trace. Results are the means of three repetitions.

Table 3. Aroma compounds in TR V3

No	R.T. (min.)	Peak area (UA)	Compound name	ID ¹	Sensory descriptor
1	3.00	197532	Ethyl acetate	A	ethereal, fruity, sweet, with a grape and cherry nuance
2	7.21	315014	Propanol	A	slightly sweet fruity nuance of apple and pear
3	8.52	186547	Isobutyl alcohol	A	ethereal, winey
4	11.94	2048874	1-Butanol, 3-methyl-	A	ethereal, winey
5	17.78	1909674	Acetic acid	A	pungent acidic and dairy-like
6	19.64	1066241	2,3-Butanediol	A	fruity, creamy, buttery
7	27.94	70036	Phenethyl alcohol	A	floral, rose
8	35.59	58064	3,7-Dimethyl-octa-1,7-dien-3,6-diol	B	sweet, floral, citrus
9	37.00	153251	4-vinylphenol	B	chemical, phenolic, medicinal with sweet musty and meaty nuances

¹Identification: A = GC retention and MS data in agreement with spectra found in the library; B = tentatively identified by MS matching with library spectra only; nd: not detected, tr: trace. Results are the means of three repetitions.

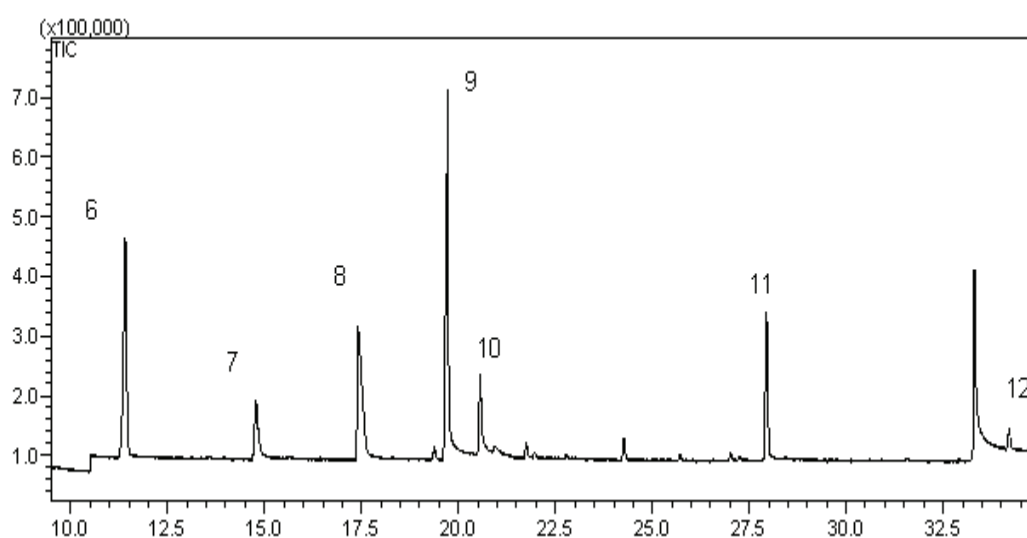


Fig. 2. Excerpt of GC-MS chromatogram of volatiles extracted with supercritical CO₂ from Tămâioasă românească wines. Indicated numbers represent compounds identified: 6) 1-Butanol, 3-methyl-; 7) Propanoic acid, 2-hydroxy-, ethyl ester; 8) Acetic acid; 9) 2,3-Butanediol; 10) Butyrolactone; 11) Phenylethyl Alcohol; 12) 3,7-Dimethyl-octa-1,7-dien-3,6-diol

At the same time, one of the real culprits responsible for low extraction recoveries is inefficient trapping of the analyte once it's extracted. Moreover, variations in pressure and temperature mentioned in literature (Jonin et al., 2010; Reverchon, 1997; Sewram, 1997) have not been applied in our experiment, having maintained these two variables linear for the duration of the process.

4. Conclusions

In summary, we have managed to extract some major aroma compounds in Tămâioasă românească wines and describe the volatiles according to their important sensorial characteristics using a very simple pilot in-house methodology.

The proposed SFE/GC/MS in-house method has successfully extracted the most important volatiles from wines and can thus be used for creating a clear sensorial profile.

The methodology used also portrays the influence of major technological steps in the wine

making process (maceration) but also microbiological faults expressed through specific aroma compounds (4-vinylphenol).

Due to the complexity of wine aroma, the SFE method had to be coupled with GC/MS, sensorial analysis and chemometrics in order to ensure a reproducible volatile profile.

Acknowledgements

Cintia Colibaba and the authors are grateful to the internal research grant 5526/25.04.2013 of USAMV Iasi, allowing this study. The authors would also like to thank the Research Center for Oenology of the Romanian Academy – Iasi Branch, for the material and human resources put at disposal for this research.

References

- Baumes R., (2009), *Wine Aroma Precursors*, In: *Wine Chemistry and Biochemistry*, Moreno-Arribas M.V., Polo M.C. (Eds.), Springer, New York, 251-274.
- Clarke R.J., Bakker J., (2004), *Wine: Flavour Chemistry*, Blackwell Publishing, Oxford, UK.

- Cotea V.D., Sauciu J., (1986), *Oenology Treatise, (in Romanian)*, vol. II, Ceres Publishing House, Bucharest, Romania.
- Fischer U., (2007), *Wine Aroma*, In: *Flavours and Fragrances; Chemistry, Bioprocessing and Sustainability*, Berger R.G. (Ed.), Springer, Berlin, Heidelberg, 241-267.
- Herrero M., Castro-Puyana M., Mendiola J.A., Ibanez E., (2013), Compressed fluids for the extraction of bioactive compounds, *Trends in Analytical Chemistry*, **43**, 67–83.
- Jonin T.M., Adjadj L.P., Rizvi S.S., (2010), *Supercritical Extraction*, In: *Encyclopedia of Life Support Systems (EOLSS)*, Vol. 3 - *Food Engineering*, 210.
- Levy J.M., Ravey R.M., Houck R.K., after SFE, *Fresenius Journal of Analytical Chemistry*, **344**, 517-520.
- Maxwell R.J., Lightfield A.R., Stolker A.A.M, (1995), An spe column teflon sleeve assembly for in-line retention during supercritical-fluid extraction of analytes from biological matrices, *Journal of High Resolution Chromatography*, **18**, 231–234.
- Nechita B., (2010), *Contributions to the studies of volatile compounds in grapes and wines from Cotnari vineyard* (in Romanian), PhD thesis, University of Agricultural Sciences and Veterinary Medicine, Iasi, Romania.
- Reverchon E., (1997), Supercritical fluid extraction and fractionation of essential oils and related products, *Journal of Supercritical Fluids*, **10**, 1–37.
- Ribereau-Gayon P., Glories Y., Maujean A., Dubourdieu D., (2000), *Handbook of Enology: The Chemistry of Wine Stabilization and Treatments*, Vol. 2, Wiley, England.
- Ron S.J., (2000), *Wine Science: Principles, Practice, Perception*, Second Edition, Academic Press, California, USA.
- Sewram V., (1997), *Supercritical fluid extraction and analysis of indigenous medicinal plants for uterotonic activity*, PhD thesis, University of Natal, Durban, South Africa.
- Válcarcel M., Tena M.T., (1997), Applications of supercritical fluid extraction in food analysis, *Fresenius Journal of Analytical Chemistry*, **358**, 561-573.
- Xie Q.L., Markides K.E., Lee M.L., (1989), Supercritical Fluid Extraction - Supercritical Fluid Chromatography with Fraction Collection for Sensitive Analytes, *Journal of Chromatographic Science*, **27**, 365 - 370.



“Gheorghe Asachi” Technical University of Iasi, Romania



DEVELOPMENT AND VALIDATION OF UV SPECTROPHOTOMETRIC METHOD FOR DETERMINING THE HERBICIDE MOLINATE WITH AND WITHOUT ALGINATE MICROPARTICLES

Ana M. Paiva, Berta N. Estevinho*, Fernando Rocha, Olga C. Nunes

LEPABE, Departamento de Engenharia Química, Faculdade de Engenharia da Universidade do Porto,
Rua Dr. Roberto Frias, 4200-465 Porto, Portugal

Abstract

Molinate (S-ethyl-azepane-1-carbothioate) is a thiocarbamate herbicide used in rice cultivation for the control of grass weeds. Environmental contamination with molinate is of major concern due to the adverse effects described both for humans and animals.

Molinate hydrolase, a novel amidohydrolase previously characterized, is responsible for the initial breakdown of molinate, cleaving the thioester bond of molinate, releasing ethanethiol and azepane-1-carboxylate (ACA). Biotechnology is the key for sustainable farming. With advances in biotechnology, bioremediation has become one of the most rapidly developing fields of environmental restoration. Through the microencapsulation of molinate hydrolase, we are aiming to develop a bioremediation process for the effective molinate degradation in rice paddies.

The purpose of this work was to develop and validate an UV method to effectively quantify the substrate (molinate) in further assays with free and microencapsulated molinate hydrolase. The analytical method was validated and the main parameters, as limit of detection, linearity range, precision and accuracy were determined, and compared to those obtained by HPLC (regarding free enzyme kinetics). Both methods show to be linear ($r > 0.999$) over the concentration range of 0.005-0.150 mM molinate. The global uncertainty, estimated accordingly to the bottom-up approach used by Eurachem, was estimated for both methods.

The UV analytical method is effective and seems that it can be applied in future for the quantification of molinate breakdown by free and encapsulated molinate hydrolase.

Key words: microparticles, molinate, molinate hydrolase, uncertainty, UV

Received: November, 2015; *Revised final:* February, 2015; *Accepted:* February, 2015

1. Introduction

Biocatalysis, a crucial component of white or industrial biotechnology, relies on the broad catalytic activity of enzymes leading to the industrial (e.g., food, pharmaceutical) production of value-added compounds, or catalyzing the degradation of several environmental contaminants (e.g., pesticides, hydrocarbons) at low cost (Alcalde et al., 2006). This scientific area relies primarily on the search of microorganisms able to produce/degrade the target compound(s), characterization of the related/involved

metabolic pathway(s), namely the identification, purification and characterization of the enzymes involved, and finally on the optimization of the process.

Thiocarbamates are a sub-group of the carbamate chemical family, which are used worldwide as herbicides (graminicides). Molinate (S-ethyl-azepane-1-carbothioate) is a thiocarbamate used in rice cultivation for the control of grass weeds, such as *Echinochloa spp.*, *Glyceria spp.*, and *Diplachne fusca* (Nunes et al., 2013). Environmental contamination with molinate is of major concern due

* Author to whom all correspondence should be addressed: e-mail: berta@fe.up.pt; Phone: +351225081678; Fax: +351225081449

to the adverse effects described both for humans and animals (Nunes et al., 2013). Molinate hydrolase, a novel amidohydrolase, previously characterized and heterologously expressed, is responsible for the initial breakdown of molinate, cleaving the thioester bond of molinate, releasing ethanethiol and azepane-1-carboxylate (ACA) (Fig. 1) (Duarte et al., 2011).

During the last few years, environmental awareness has been rising all over the world. European authorities aim at the development of a risk assessment system and a sustainable management plan for all types of water (surface, ground, drinking) that combines the requirements as defined by the Directive 414/91/EEC and those defined by the Water Framework Directive 2000/60/EC (EC, 2000; EEC, 1991). In order to address these new restrictions, the research interest was placed on establishing alternative, simple, low-cost technologies for the on-site treatment of wastewaters, natural and ground water, namely with biotechnology. With advances in biotechnology, bioremediation has become one of the most rapidly developing fields of environmental restoration (Dua et al., 2002). One of the techniques that can be used in the bioremediation of soils is the microencapsulation, which is a technique where liquid droplets, solid particles or gas compounds are entrapped in an encapsulating agent, forming small capsules with many useful properties. Microencapsulation can also provide a physical barrier between the core compound and the external environment (Estevinho et al., 2013a). In the case of the microencapsulation of enzymes the microcapsule can give extra protection to the enzyme against undesirable external conditions. Through the microencapsulation of molinate hydrolase, we are aiming to develop a bioremediation process for the effective molinate degradation in rice paddies.

Associated to this work, an adequate analytical method to control the applicability of this process needs to be developed. In industry, where large analytical series of similar samples are frequent and the search for quick, reproducible, precise, inexpensive and easy methods to analyze high amounts of samples is crucial, the UV methods represent an extremely adequate alternative. Nevertheless, literature still lacks information about the validation parameters and the uncertainty of the methodology accordingly to the most recent statistical techniques (Ellison and Williams, 2007; Estevinho et al., 2013b). Hence, the purpose of this

work was to develop and validate an UV method to effectively quantify the substrate (molinate) in aqueous matrices, and aqueous matrices with alginate used in the preparation of microcapsules. The enzyme will be microencapsulated in alginate and the validated method that can be used to evaluate the enzyme's activity and also to test the influence of the biopolymer in the molinate analyses is here in presented. Alginate can also be used as a biopolymer model to test the influence of additional biopolymers in the solutions containing molinate. The analytical method was validated and the main parameters, as limit of detection, linearity range, precision and accuracy were determined, and compared to those obtained by HPLC. The study of the analytical methods focuses also in the determination of the global uncertainty associated to the results.

2. Material and methods

2.1. Reagents

Molinate (S-ethyl azepane-1-carbothioate) was obtained from Herbex, Produtos Químicos (Portugal). Sodium alginate (alginic acid, sodium salt) (180947-100 g) was obtained from Aldrich (USA). All other reagents were analytical grade and from commercial sources.

2.2. Preparation of standard and enzymatic solutions

Standard solutions were prepared from a stock solution of 2.0 M molinate in 50 mM phosphate buffer, pH 7.2. Two different calibration standards were prepared:

a) Calibration standards with 0.150, 0.100, 0.075, 0.050, 0.010 and 0.005 mM molinate prepared from the stock solution in phosphate buffer;

b) Calibration standards with 0.150, 0.100, 0.075, 0.050, 0.010 and 0.005 mM molinate prepared from the stock solution in 50 mM phosphate buffer, containing alginate microparticles (5 mg.mL⁻¹).

2.3. Alginate microparticles preparation

The alginate microparticles were prepared by a spray-drying technique. Spray-drying was performed using a spray-dryer BÜCHI B-290 advanced (Flawil, Switzerland) with a standard 0.5 mm nozzle.

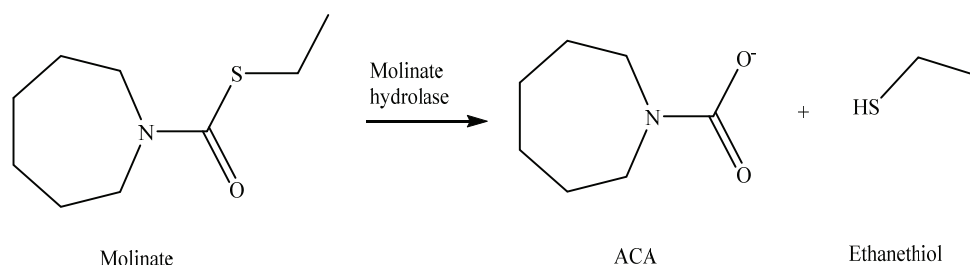


Fig. 1. Transformation of molinate by molinate hydrolase (Duarte et al., 2011)

The spray drying conditions, solution and air flow rates, air pressure and inlet temperature were set at 3 mL/min (10-13%), 35 m³.h⁻¹ (90%), 6.0 bar and 115 °C, respectively. The outlet temperature, a consequence of the other experimental conditions and of the solution properties, was around 45 °C.

2.4. Analytical equipment

The equipment used was a T80/T80+UV-VIS spectrophotometer, (PG Instruments Ltd, England) and measurements were made at 230 nm wavelength, at room temperature.

2.5. Evaluation of the molinate concentration

The evaluation of the concentration of molinate was based on absorbance values, read in an UV-Visible spectrophotometer at 230 nm. Standard solutions were prepared with a concentration between 0.005 mM and 0.150 mM of molinate. The same procedure was used to prepare the standard solutions with molinate and alginate microparticles.

3. Results and discussion

In this work, an UV method was optimised and validated for the analysis of molinate in aqueous solutions with and without alginate microparticles. These analytical methods have been developed with the main objective of evaluating the degradation of molinate with the enzyme molinate hydrolase, in free and microencapsulated form. The method can be further used to evaluate the activity of the enzyme and also to test the influence of the biopolymer in the molinate analyses. Alginate can also be used as a biopolymer model to test the influence of additional biopolymers in solutions containing molinate.

The study of the analytical methods focuses not only the main characteristics of the method (linearity range, detection limit (LOD), accuracy and

precision), but also on the determination of the global uncertainty associated to the results.

3.1. Validation of the UV method in aqueous matrices

The validation of this analytical methodology was performed for the analyses of molinate in a phosphate buffer. A calibration curve was obtained for six molinate standards with concentrations ranging from 0.005 to 0.150 mM. The values of the slope, intercept and correlation coefficient were 6.385, 0.029 and 0.995, respectively (Fig. 2).

The reproducibility of replicated analyses for each standard varied from 0.6 to 12.8%, when expressed as CV%. The LOD estimated from the calibration curve was 0.009 mM.

The intermediate precision of this method was evaluated taking into account the RSD of 6 analyses of each standard, on different days (Table 1). The CV% ranged from 1.2 to 14.1%. In general this value increased with the decrease of molinate concentration.

Accuracy was evaluated based on the recovery factor (%R), that was the ratio between the obtained concentration and the expected one. Accuracy is expressed by the percentage of recovery, for 6 experiments of each concentration level (Table 1).

Table 1. Intermediate precision and accuracy for molinate, at different concentration level, in phosphate solution

[Molinate] (mM)	Intermediate precision (CV %)	Accuracy (Recovery %)
0.150	2.9	98.2
0.100	4.0	103.0
0.075	1.2	106.1
0.050	6.4	102.1
0.010	14.1	70.5
0.005	8.6	29.5

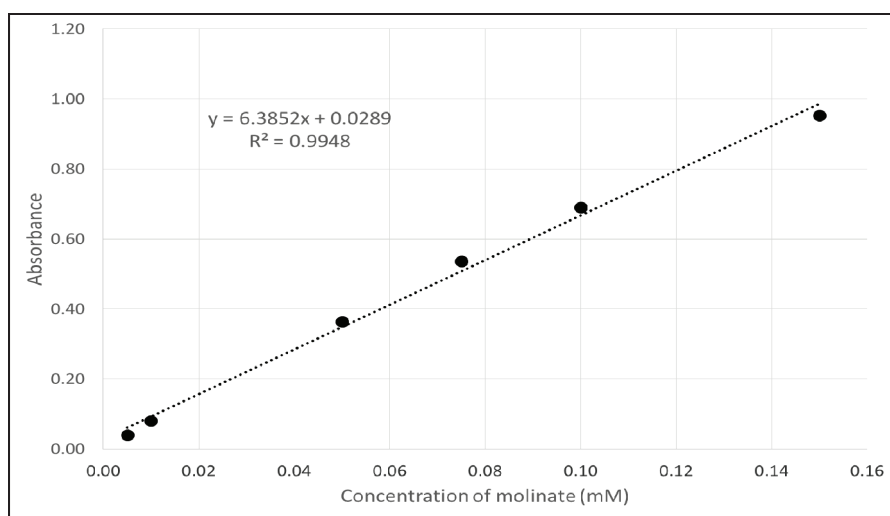


Fig. 2. Calibration curve for molinate in phosphate solution

The global uncertainty combines the contributions of all the sources of error linked to the analytical procedure. In this work, the bottom-up approach, adopted by the International Organisation for Standardisation (ISO), and also initially adapted for the analytical field by the EURACHEM/CITAC Guide (Ellison and Williams, 2007), was used to estimate the overall uncertainty by identifying, estimating and combining all the sources of uncertainty associated to the analytical results. An overestimation of the uncertainty is considered; this has the advantage of weighting the individual contributions and therefore allowing the detection of the most significant sources (Estevinho et al., 2008, 2009).

The global uncertainty (U) can be calculated from the following equation (Eq. 1):

$$U = \sqrt{U_1^2 + U_2^2 + U_3^2 + U_4^2} \quad (1)$$

where: U_1 , U_2 , U_3 and U_4 are the uncertainties associated to, respectively, standard preparation, calibration curve, precision, and accuracy.

The uncertainty associated to the standard preparation (U_1) was calculated for each standard according to Eq. (2), considering the relative error associated to each mass or volume measurement and the law of propagation of uncertainty. The standards were prepared by the method of the successive dilutions, so the lowest concentrations of the standards have incorporated all the errors associated to the preparation of the other standards.

$$U_1 = \sqrt{\left(\frac{\Delta m_{balance}}{m_{molinate}}\right)^2 + \left(\frac{\Delta V_1}{V_1}\right)^2 + \left(\frac{\Delta V_2}{V_2}\right)^2 + \left(\frac{\Delta V_3}{V_3}\right)^2 + \dots + \left(\frac{\Delta V_n}{V_n}\right)^2} \quad (2)$$

where: $\Delta m_{balance}$ is the uncertainty associated to the mass measurement ($m_{molinate}$), ΔV_1 is the uncertainty associated to the preparation of the standard stock solution in a volumetric flask of 250 mL (V_1). ΔV_2 , ΔV_3 ... ΔV_n are the uncertainty associated to the preparation of the standards (6 mL) and V_2 , V_3 , ... V_n are the pipeted volumes to the preparation of the standard.

The uncertainty associated to the calibration curve (U_2) was calculated, for each standard, by the calibration curve, considering the following equations (Eqs. 3 and 4):

$$U_2 = \frac{\left(\frac{S_{y/x}}{b}\right) \times \sqrt{\left(\frac{1}{m}\right) + \left(\frac{1}{n}\right) + \left(\frac{(y_i - y_{av})^2}{b^2 \times \sum (x_i - x_{av})^2}\right)}}{x_0} \quad (3)$$

$$S_{y/x} = \sqrt{\frac{\sum (y_i - y_{ical})^2}{n - 2}} \quad (4)$$

where $S_{\frac{y}{x}}$ represents the standard deviation of the

linearization, b the slope of the regression curve, m the number of replicates performed for each x_i value, n the number of standards used to build the calibration curve ($n = 7$), y_i the experimental value of y (absorbance), y_{ical} the value of y calculated by the regression curve for the concentration x_i , y_{av} the average of y_i values, x_i the concentration of standards (x) used in the calibration and x_{av} the average of x_i values.

The uncertainty associated to the precision (U_3) was estimated considering the precision of the measurement for each standard (Eq. 5). In the following formula, s represents the standard deviation of precision assays.

$$U_3 = \frac{s}{x \times \sqrt{n}} \quad (5)$$

The uncertainty associated to the accuracy (U_4) was calculated from Eq. 6, where η represents the recovery of the assays with spiked solutions at different levels:

$$U_4 = \frac{s(\eta)}{\eta_{average}} \quad (6)$$

In Fig. 3, the relative weight of each individual source of uncertainty for the molinate analysis is represented. The more important sources are the ones related with the calibration curve (U_2) and precision (U_3).

Fig. 4 presents the global uncertainty for the different concentration levels. The global uncertainty is close to 10% for concentrations levels between 0.07 and 0.15 mM. For lower concentrations these values increase to values up to 60% and 90% in the vicinity of the standard of 0.01 and 0.005 mM, respectively. In fact, the 0.005 mM standard presents a concentration smaller than the detection limit (0.009 mM) determined by the method, provoking this high value of uncertainty.

3.2. Validation of the UV method in aqueous matrices with alginate microparticles

This second method consisted in the analytical methodology for the analysis of molinate in a phosphate and alginate microparticles, testing by this way the influence of the alginate in the analysis of molinate. Again, the calibration curve was obtained for six molinate standards with concentrations ranging from 0.005 to 0.150 mM, prepared this time in a phosphate and alginate microparticles suspension. The values of the slope, intercept and correlation coefficient were 6.355 0.011 and 0.9996, respectively (Fig. 5).

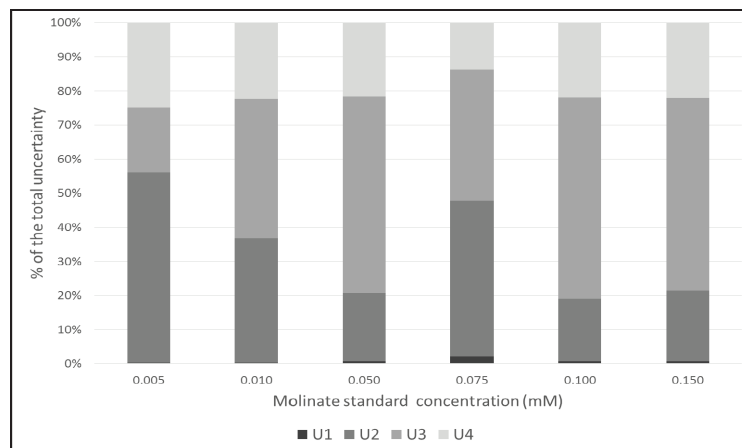


Fig. 3. The relative contribution of the uncertainty sources for different concentration levels of molinate

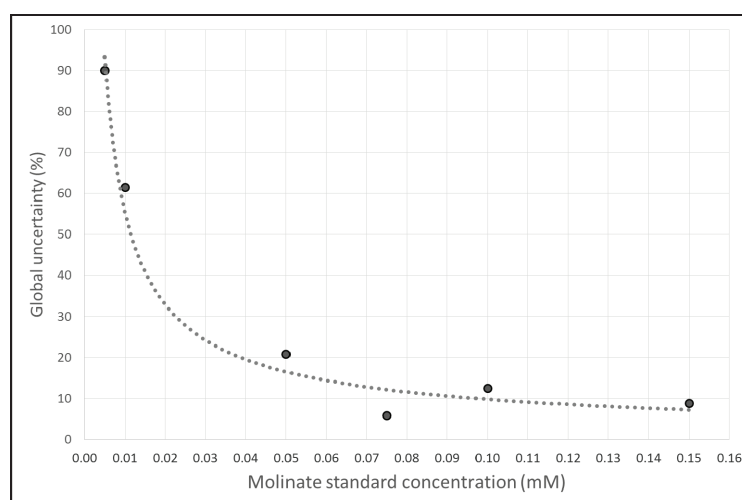


Fig. 4. Global uncertainty for molinate analysis by the UV method

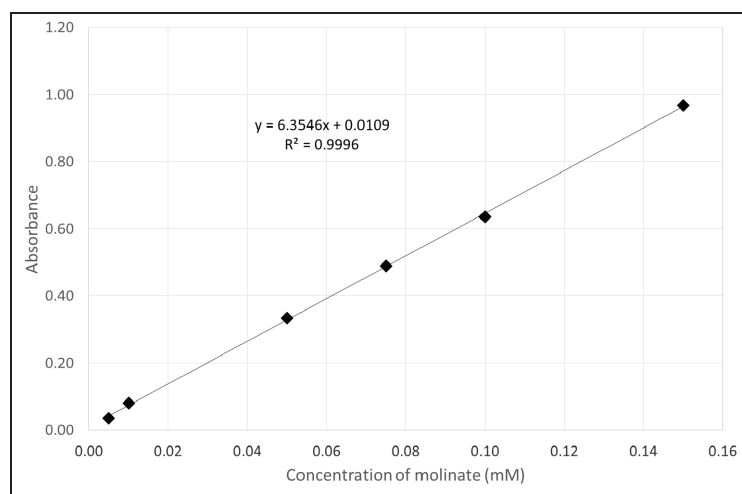


Fig. 5. Calibration curve for molinate in phosphate buffer and alginate microparticles suspension

The calibration curve is similar to the one determined without alginate in solution, this meaning that the interference of alginate is not significant.

The reproducibility of replicated analyses for each standard varied from 0.7 to 5.2%, when expressed as CV%.

The LOD estimated from the calibration curve was 0.002 mM, smaller than the one obtained for the other method. The results of the intermediate precision (CV%) and the accuracy, expressed on the recovery factor (%R of this method) are presented in Table 2.

Table 2. Intermediate precision and accuracy for molinate, at different concentration level, in phosphate and alginate microparticles suspension

[Molinate] (mM)	Intermediate precision (CV %)	Accuracy (Recovery %)
0.150	2.9	99.1
0.100	1.0	99.9
0.075	3.6	98.3
0.050	4.6	101.7
0.010	4.1	109.4
0.005	6.0	69.0

The global uncertainty and the contributions of the uncertainty sources for the different calibration levels in the molinate analysis were also determined. In Fig. 6 it is possible to observe the relative contribution of the uncertainty sources for different concentration levels of molinate measured in phosphate and alginate solution.

The relative contribution of these four sources is decisively dependent on the calibration levels. For

this method the main sources are related to the precision (U_3) and the accuracy (U_4). However, for lower molinate concentrations, the uncertainty associated to the calibration curve (U_2) is the main responsible, almost 45%. For high molinate concentration levels the influences of precision (U_3) and accuracy (U_4) achieved a combined contribution around 90%.

Fig. 7 presents the variation of the global uncertainty, and it is observed that the global uncertainty is less than 10% for concentration levels between 0.05 and 0.15 mM. For lower concentrations the uncertainty increased in an exponential mode, the values increasing significantly to values higher than 25%.

Comparing the two UV methods, it can be observed that the alginate, the matrix that will be further used to microencapsulate the molinate hydrolase, do not influence significantly the precision and the accuracy of the method to determine molinate in aqueous solutions. The calibration curves are similar.

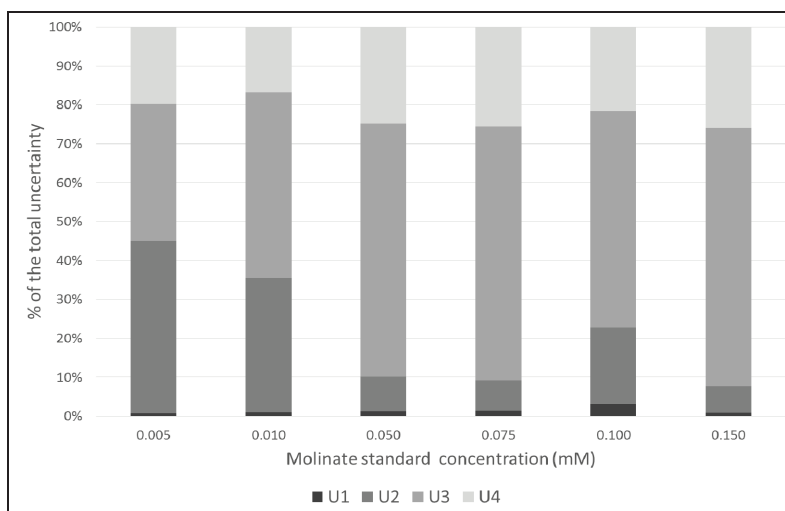


Fig. 6. The relative contribution of the uncertainty sources for different concentration levels of molinate measured in phosphate and alginate microparticles suspension

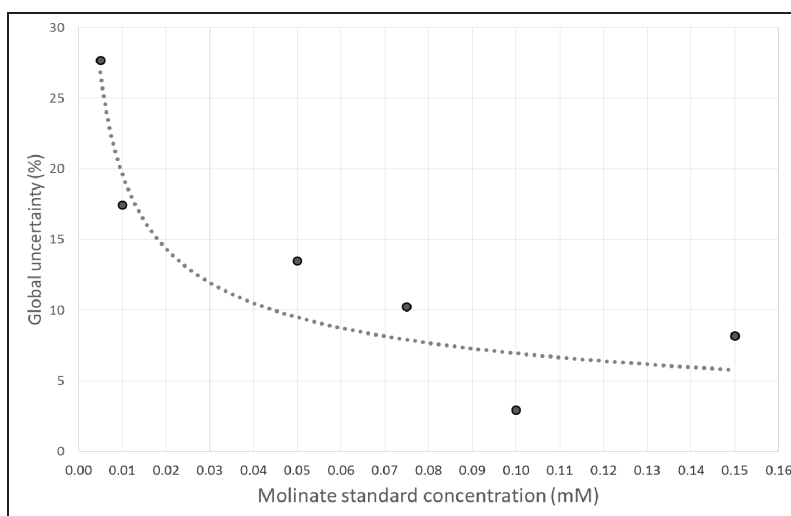


Fig. 7. Global uncertainty for molinate analysis by UV method measured in phosphate and alginate microparticles suspension

3.3. Molinate UV methods versus molinate HPLC method

The HPLC-UV method used by Barreiros et al. (2003) to quantify molinate was performed with a detection limit of 0.9 g/L (4.8 mM). In this work the HPLC-UV methodology was validated to analyse molinate, presenting a linear response between 0.005 and 0.2 mM (standards prepared in phosphate buffer), a correlation coefficient of 0.9999 and a detection limit of 0.001 mM. Global uncertainty associated with the results was around 8%. Some samples were analysed by the two methods (UV and HPLC) and the results obtained by the two methods are very similar. The HPLC method was developed for a more open range (0.005-0.200 mM), presenting a smaller detection limit (0.001 mM). However, the UV method has the advantage of avoiding the problems found in the chromatographic column, provoked by the mucoadhesive properties of alginate. This problem has already been described for other biopolymer, for the analysis of glucose in samples containing chitosan, by Estevinho et al. (2013b). On the other hand, when using the HPLC method, high costs are involved with acquisition and maintenance of the equipment, and acquisition of solvents and columns. The UV methods have smaller costs involved with the equipment.

The UV method is also more flexible and simple in the utilization, allows a large number of sample analyses in a small period of time, and presents less operating problems. The applicability of the UV method on the analysis of molinate in complex alginate samples proved to be a good option.

4. Conclusions

In this work, two UV methods to analyse molinate in phosphate buffer with and without alginate microparticles, were optimized and validated. It can be concluded that the alginate microparticles do not interfere in the molinate analysis, at least in the range of concentration used.

Both methods were shown to be linear ($r > 0.999$) over the concentration range of 0.005-0.150 mM molinate. The global uncertainty, estimated accordingly to the bottom-up approach used by Eurachem, was estimated for the two methods.

The UV analytical method is effective and can be applied for the quantification of molinate breakdown by free and encapsulated molinate hydrolase.

Acknowledgments

This work was supported by Fundação para a Ciência e a Tecnologia (FCT) through LEPABE (PEst-C/EQB/UI0511/2013) and under the project PTDC/AAG-TEC/3909/2012, where A.M. Paiva is recipient of grant

Berta N. Estevinho is recipient of a postdoctoral grant (SFRH/BPD/73865/2010) by FCT.

References

- Alcalde M., Ferrer M., Plou F.J., Ballesteros A., (2006), Environmental biocatalysis: from remediation with enzymes to novel green processes, *Trends in Biotechnology*, **24**, 281–287.
- Barreiros L., Nogales B., Manaia C.M., Ferreira A.C.S., Pieper D.H., Reis M.A., Nunes, O.C., (2003), A novel pathway for mineralization of the thiocarbamate herbicide molinate by a defined bacterial mixed culture, *Environmental Microbiology*, **5**, 944–953.
- Dua M., Singh A., Sethunathan N., Johri A.K., (2002), Biotechnology and bioremediation: successes and limitations, *Applied Microbiology and Biotechnology*, **59**, 143–152.
- Duarte M., Ferreira-da-Silva F., Lünsdorf H., Junca H., Gales L., Pieper D.H., Nunes O.C., (2011), *Gulosibacter molinivorax* AN4T molinate hydrolase, a novel cobalt-dependent amidohydrolase, *Journal of Bacteriology*, **193**, 5810–5816.
- EC, (2000), Directive 2000/60/EC of the European Parliament and of the Council, establishing a framework for Community action in the field of water policy, *Official Journal of the European Communities*, **L327/1**, 22.12.2000.
- EEC, (1991), Directive 414/91/EEC 19, concerning the placing of plant protection products on the market, *Official Journal of the European Communities*, **L 230/1**, 15.07.1991.
- Ellison S.L.R., Williams A., (2007), *Use of uncertainty information in compliance assessment*, EURACHEM/CITAC Guide, First Edition, On line at: <http://www.citac.cc/EURACHEM-CITAC%20Guide%20-%20Use%20of%20uncertainty%20information%20%20in%20compliance%20assessment%20-%202007.pdf>.
- Estevinho B.N., Ferraz A., Rocha F., Alves A., Santos L., (2008), Interference of chitosan in glucose analysis by high-performance liquid chromatography with evaporative light scattering detection, *Analytical and Bioanalytical Chemistry*, **391**, 1183–1188.
- Estevinho B.N., Ferraz A., Rocha F., Santos L., Alves A., (2009), Uncertainty in the determination of glucose in aqueous solutions by high-performance liquid chromatography with evaporative light scattering detection, *Journal of Separation Science*, **32**, 3116–3125.
- Estevinho B.N., Rocha F., Santos L., Alves A., (2013a), Microencapsulation with chitosan by spray drying for industry applications – A review, *Trends in Food Science & Technology*, **31**, 138–155.
- Estevinho B.N., Ferraz A., Santos L., Rocha F., Alves A., (2013b), Uncertainty in the determination of glucose and sucrose in solutions with chitosan by enzymatic methods, *Journal of the Brazilian Chemical Society*, **24**, 931–938.
- Nunes O.C., Lopes A.R., Manaia C.M., (2013), Microbial degradation of the herbicide molinate by defined cultures and in the environment, *Applied Microbiology and Biotechnology*, **97**, 10275–10291.



“Gheorghe Asachi” Technical University of Iasi, Romania



INFLUENCE OF HYDROXYPROPYL-BETA-CYCLODEXTRIN ON THE PHYSICOCHEMICAL AND BIOLOGICAL CHARACTERISTICS OF A FLAVONE WITH IMPORTANT PHARMACOLOGICAL PROPERTIES

Andreia Corciova¹, Bogdan Cioroiu¹, Cornelia Mircea², Cristina Tuchilus³,
Constantin Ciobanu¹, Cristina Dimitriu^{4*}, Bianca Ivanescu⁵

¹“Grigore T. Popa” University of Medicine and Pharmacy, Faculty of Pharmacy, Department of Drugs Analysis,
16 University Str., 700115 Iasi, Romania

²“Grigore T. Popa” University of Medicine and Pharmacy, Faculty of Pharmacy, Department of Pharmaceutical Biochemistry,
16 University Str., 700115 Iasi, Romania

³“Grigore T. Popa” University of Medicine and Pharmacy, Faculty of Pharmacy, Department of Microbiology,
16 University Str., 700115 Iasi, Romania

⁴“Grigore T. Popa” University of Medicine and Pharmacy, Faculty of Medicine, Department of Biochemistry,
16 University Str., 700115 Iasi, Romania

⁵“Grigore T. Popa” University of Medicine and Pharmacy, Faculty of Pharmacy, Department of Pharmaceutical Botany,
16 University Str., 700115 Iasi, Romania

Abstract

The purpose of this study was to investigate the influence of hydroxypropyl- β -cyclodextrin on diosmin, substance from the flavones category with important pharmacological properties. We carried out solubility studies, calculating the solubility constant of the complex formed between diosmin and hydroxypropyl-cyclodextrin at various temperatures (20, 25 and 37 °C) and in the presence of increasing cyclodextrin concentrations. A_L type curves were obtained which suggest the formation of an inclusion compound on a 1:1 molar ratio and the solubility constants had values between 370 and 453 M⁻¹. Knowing that between diosmin, hydroxypropyl-cyclodextrin and the used solvent, thermodynamic interactions occur, we investigated the influence of these interactions on several thermodynamic parameters such as Gibbs free energy change, free energy change, enthalpy change and entropy change. The calculated values showed that the reaction is positively influenced by the cyclodextrin's concentration increment and the temperature, the process being spontaneously. Next, inclusion compounds were obtained by co-evaporation and co-precipitation, and their structures were confirmed by FTIR and MS analysis. The complexes were tested *in vitro* compared with the parent substances, the results indicating improved antioxidant and antimicrobial activities. Moreover, the dissolution of diosmin increased in mediums similar to physiological conditions (simulated gastric and intestinal).

Key words: antimicrobial, antioxidant, beta-cyclodextrin, diosmin, dissolution

Received: November, 2014; *Revised final:* February, 2015; *Accepted:* February, 2015

1. Introduction

Diosmin (D) is a hesperidin semisynthetic derivative that has vasoprotective (Tong et al., 2013),

antioxidant and anti-inflammatory properties (Sezer et al., 2011), antiproliferative and anti-cancer activities (Alvarez et al., 2009). Diosmin exhibits a neuroprotective effect and might have potential in the

* Author to whom all correspondence should be addressed: e-mail: c_dimit@yahoo.com, czvoris@yahoo.com; Phone 0742149580; Fax +40.232.211.820

treatment of neurodegenerative diseases (Abdel-Salam et al., 2012). Also, diosmin manifests antihyperglycemic and hepatoprotective properties (Leelavinothan and Subramani, 2010; Tahir et al., 2013). However, its poor solubility in water increases the difficulty of formulation. In order to overcome this disadvantage, we used the complexation method with "host" substances of cyclodextrins type (Higuchi and Connors, 1965).

Cyclodextrins (CD) are cyclic oligosaccharides which are able to form inclusion compounds in the form of a truncated cone, with the secondary hydroxyl groups present on the lower base and the primary hydroxyl groups on the upper base, resulting in increased water solubility of the cyclodextrins, while the interior cavity is hydrophobic (Davis and Brewster, 2004; Martin Del Valle, 2004). Furthermore, for the improvement of solubility, stability to light and oxygen, and a better control of the chemical reactivity of the guest substance, other cyclodextrin derivatives obtained by esterification and etherification of the primary and secondary hydroxyl groups may be used (Higuchi and Connors, 1965; Liu et al., 2005).

Due to the important pharmacological properties of diosmin, the objective of this study was to investigate the complexation between diosmin and hydroxypropyl- β -cyclodextrin and the influence of this process on some physicochemical and biological characteristics. All determinations were carried out by comparison between the prepared inclusion compounds and parent substances.

2. Experimental

2.1. Materials

The substances used in this study were purchased from Sigma Aldrich (USA), having the following characteristics: diosmin (D) (5-Hydroxy-2-(3-hydroxy-4-methoxyphenyl)-7-[(2*S*,3*R*,4*S*,5*S*,6*R*)-3,4,5-trihydroxy-6-[[[(2*R*,3*R*,4*R*,5*R*,6*S*)-3,4,5-trihydroxy-6-methylloxan-2-yl]oxymethyl]oxan-2-yl]oxychromen-4-one), CAS number 520-27-4, molar mass 608.545 g mol⁻¹, molecular formula C₂₈H₃₂O₁₅, β -cyclodextrin (β -CD) (CAS Number 7585-39-9, empirical formula C₄₂H₇₀O₃₅, molecular weight 1135 g mol⁻¹), hydroxypropyl- β -cyclodextrin (HP- β -CD) (CAS Number 128446-35-5, 0.8 molar substitution, molecular weight 1460 g mol⁻¹), and sulfated- β -cyclodextrin (sulfated- β -CD) (CAS Number 37191-69-8, 7mol per mol β -CD, molecular weight 3277 g mol⁻¹).

2.2. Methods

2.2.1. Phase solubility studies

Solutions with different concentrations of cyclodextrin were prepared (on the range of 0.969 - 16.29 x 10⁻³ M for β -CD, 0.684-13.69 x 10⁻³ M for HP- β -CD and 0.305 - 6.10 x 10⁻³ M for sulfated- β -CD), then an excess of diosmin was added

(Domańska et al., 2011; Higuchi and Connors, 1965). The mixtures were stirred for 24 hours at various temperatures: 20, 25 and 37 ± 1 °C, then the unreacted diosmin was removed through filtering. The concentration of diosmin was determined spectrophotometrically, using a double beam Jasco V 530 spectrophotometer, by measuring the absorbance of samples against a blank containing the same concentration of cyclodextrin as the sample, at 257 nm.

2.2.2. Preparation of inclusion compounds

The inclusion compounds were prepared by co-evaporation and co-precipitation, using a molar ratio of diosmin: cyclodextrin of 1:1. Co-evaporation (CV): to a saturated solution of cyclodextrin was added a solution containing hesperidin in equimolar amount, under continuous stirring. The mixture was stirred at 30 °C for 72 hours, then at room temperature until the solvent evaporated.

Co-precipitation (CP): cyclodextrin was dissolved in a given volume of water to the limit of solubility and solid diosmin was added, with vigorous stirring. The mixture was stirred continuously until a white precipitate was formed. The precipitate was filtered and dried to constant weight.

2.2.3. Physicochemical characterization

- **FTIR spectroscopic analysis:** was performed using a Tensor 27 Optics FT-IR spectrophotometer from Bruker, Germany, with a spectral range of 7500 - 370 cm⁻¹.

- **Mass spectroscopic analysis:** was performed using a triple quadrupole - TSQ Quantum Access Max mass spectrometer. Analysis conditions were: spray discharge voltage 3 kV, vaporizer temperature 400 °C, capillary temperature 375 °C, auxiliary gas pressure 40 mtorr.

2.2.4. Biological characterization

- **Antioxidant activity:** was tested by determining the ability of diosmin to inhibit lipoxygenase activity (Malterud and Rydland, 2000), an enzyme in the oxidoreductases class involved in the metabolism of arachidonic acid and linoleic acid.

The assay was carried out in borate buffer (pH - 9), after the addition of lipoxygenase solution and of the test compounds prepared in DMSO and using linoleic acid as substrate (0.16 mM). The absorbance of the solution was measured at 234 nm in the time interval of 0-120 seconds. The ability to inhibit lipoxygenase was calculated according to Eq. (1) and for each sample IC₅₀ was calculated (mM diosmin in the final solution).

$$\% \text{ activity} = \frac{(A_E - A_{ES})}{A_E} \times 100 \quad (1)$$

where: A_E - the difference between the absorbance of the enzyme without sample at second 90 and the absorbance of the same solution at second 30; A_{ES} -

the difference between the absorbance of the enzyme with sample at second 90 and the absorbance of the same solution at second 30.

- **Antimicrobial activity** of inclusion compounds compared to the parent substances was evaluated by the agar diffusion method (Atilano et al., 2011; LaJean Chaffin, 2008). On the surface of Petri plates, with agar medium Mueller-Hinton for bacteria and agar medium Sabourand for fungi, inoculated with suspension of the test microorganisms, were placed stainless steel cylinders with an inner diameter of 6 mm in which was deposited 100 µl of solutions of the analyzed compounds. The test microorganisms used were: Gram positive bacteria - *Staphylococcus aureus* ATCC 25923, *Sarcina lutea* ATCC 9341, *Bacillus cereus* ATCC 14579, and fungi - *Candida albicans* ATCC 10231, *Candida glabrata* ATCC MYA 2950, *Candida parapsilosis* ATCC 22019. After incubation, for 24 hours at 37 °C, diameters of inhibition zones of microbial growth were registered. Results represent the mean diameters registered on three plates. The antibacterial activity of the investigated compounds was compared with the inhibition zone obtained with a 25 mg ampicillin disc and 30 mg chloramphenicol disc, placed on plates at the same time as the samples. Antifungal activity was compared to a 100 mg nystatin disc.

2.2.5. In vitro dissolution studies

The dissolution rate of diosmin and inclusion compounds was measured using the USP paddle apparatus, at a stirrer speed of 100 rpm, and temperature of 37 ± 0.5 °C. At intervals of 10, 20, 30, 40, 60, 90 and 120 minutes samples were collected, and replaced with the used medium. Samples absorbance was read at 257 nm. The dissolution medium replicated the physiological conditions: 0.1 N hydrochloric acid solutions simulated gastric fluid pH 1.2 and phosphate buffer simulated intestinal fluid pH 6.8 (García et al., 2009; Patil et al., 2008).

3. Results and discussion

3.1. Phase solubility studies

The phase solubility diagram was drawn by plotting the concentration of diosmin to increasing concentrations of cyclodextrin, and it was of A_L type. From the linear portion of the phase diagram Higuchi & Connors (Domańska et al., 2011; Higuchi and Connors, 1965), the stability constants (K_s) were calculated, at each temperature, according to Eq. (2).

$$K_s = \frac{\text{slope}}{S_0(1 - \text{slope})} \quad (2)$$

where: *slope* – was calculated from the graph, *S*₀ – was intrinsic solubility of diosmin in the absence of cyclodextrins.

Fig. 1 shows the solubility diagrams of diosmin, in aqueous solutions of the three

cyclodextrins, at increasing temperature. As can be seen, the solubility of diosmin in water increases linearly with cyclodextrin concentration and with temperature. The highest concentrations are obtained in the presence of HP-β-CD, followed by β-CD and sulfated-β-CD, regardless of temperature. K_s values were between 112-345 M⁻¹ for β-CD, 370-453 M⁻¹ for HP-β-CD and 112 – 333 M⁻¹ for sulfated-β-CD. The slopes obtained from the phase diagrams are less than 1, indicating the formation of inclusion compounds in a 1:1 molar ratio between diosmin and cyclodextrins. The stability of the complex decreases in the following order: HP-beta-CD> beta-CD> sulfated-beta-CD. For this reason, further in the research was used HP-β-CD.

3.1.1. Determination of thermodynamic parameters

Knowing that between diosmin, hydroxypropyl-cyclodextrin and the used solvent, thermodynamic interactions occur, we investigated the influence of these interactions on several thermodynamic parameters such as Gibbs free energy change (Δ*G*_{tr}⁰), free energy change (Δ*G*⁰), enthalpy change (Δ*H*⁰) and entropy change (Δ*S*⁰). The thermodynamic parameters of the reaction depending on the temperature and CD concentration were calculated using the Eqs. (3-7) (Chadha et al., 2012; Domańska et al., 2011).

$$\Delta G_{tr}^0 = -RT \log \frac{S}{S_0} \quad (3)$$

where: *R* = gas constant, *T* = absolute temperature of the reaction, *S*/*S*₀ = the ratio between the solubility of diosmin in cyclodextrin solution and the solubility of diosmin in water.

$$\Delta G^0 = -2.303 RT \log K_s \quad (4)$$

where: *K*_s = equilibrium constant of the complex formed with 1:1 stoichiometry

$$\log K_s = -\frac{\Delta H^0}{RT} + \frac{\Delta S^0}{R} \quad (5)$$

It was graphically represented *log K*_s versus 1/*T*, and the slope of the line obtained gives the value of enthalpy change (Δ*H*⁰) from Eq. (6):

$$\text{Slope} = \frac{\Delta H^0}{2.303R} \quad (6)$$

$$\Delta G^0 = \Delta H^0 - T\Delta S^0 \quad (7)$$

From calculation of thermodynamic parameters, we can assert the following:

- Δ*G*_{tr}⁰ has increasing values, depending on the concentration of the cyclodextrin (mM) and the temperature, with values between - 0733 and - 1420 kJmol⁻¹.

- ΔG^0 ranged between - 14 412 -15. 764 kJmol⁻¹
- ΔS^0 ranged between 52.03 and 53.53 Jmol⁻¹K⁻¹
- the calculated ΔH^0 was 0.833 kJmol⁻¹.

Results indicate a favorable solubilization process of diosmin in the presence of HP- β -CD, influenced by increasing concentrations of cyclodextrin. The formation of inclusion compounds diosmin - HP- β -CD is done through an endothermic process and between the two parent substances hydrophobic interactions are established.

3.2. Physico-chemical characterization

3.2.1. FTIR spectroscopic analysis

One of the methods used to confirm the formation of inclusion compounds is FTIR

spectroscopic analysis (Gajare et al., 2009; Garcia et al., 2014; Liu et al., 2005; Patil et al., 2008). The characteristic spectrum of diosmin (Fig. 2a.) is defined by the following absorption maxima - 3409.43, 1661, 1610 1501, 1448, 1319, 1261, 1182, 1069, 854 and 821 cm⁻¹. The bands specific to free OH groups are wide bands, in the 3200 - 3600 cm⁻¹ domain.

The band at 3409 cm⁻¹ indicates the presence of these groups in the diosmin molecule. The bands characteristic of C-H bonds deflection appear in the domain 1275 - 1000 cm⁻¹, confirmed by the band at 1069 cm⁻¹ (in the case of plane deformation) and at 900-690 cm⁻¹ (in the case of out-of-plane deformation), respectively, bands in the range 854-821 cm⁻¹.

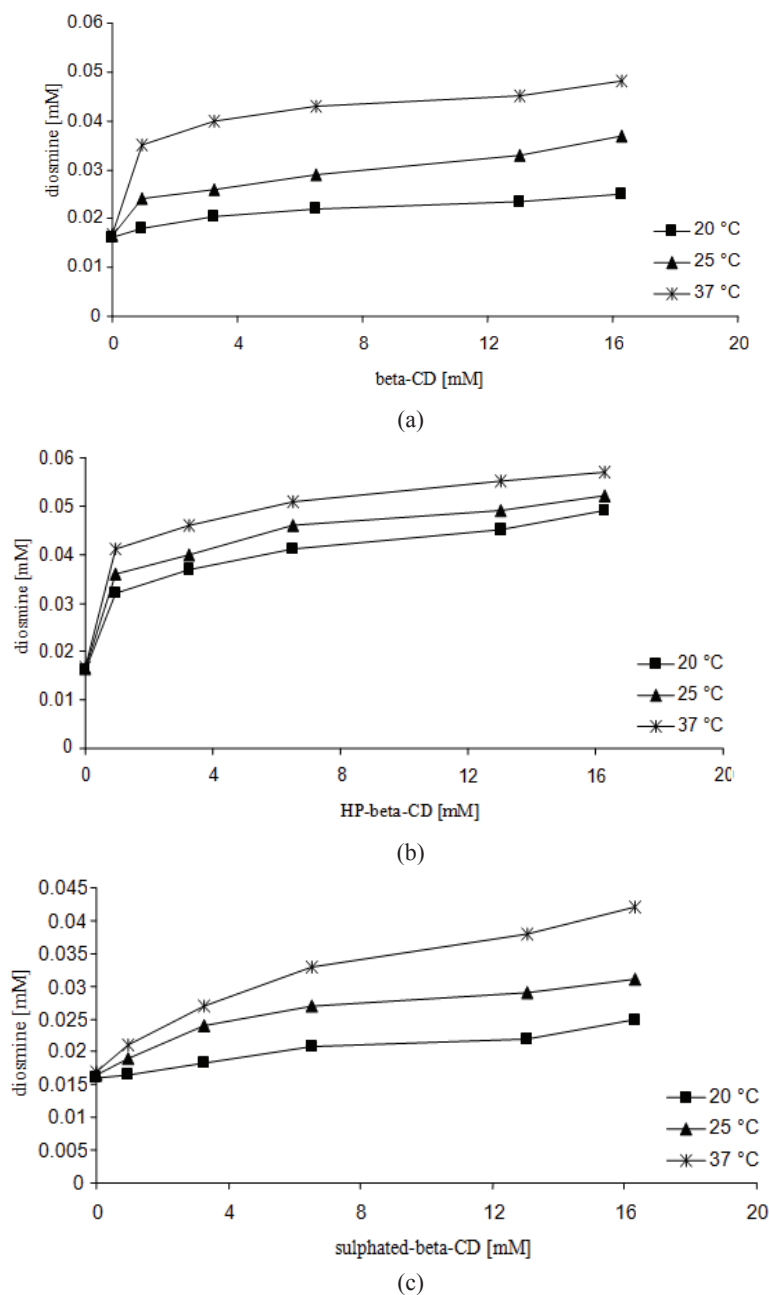


Fig. 1. Phase diagram of diosmin with β -CD (a), HP- β -CD (b) and sulphated- β -CD (c) in water, at different temperatures

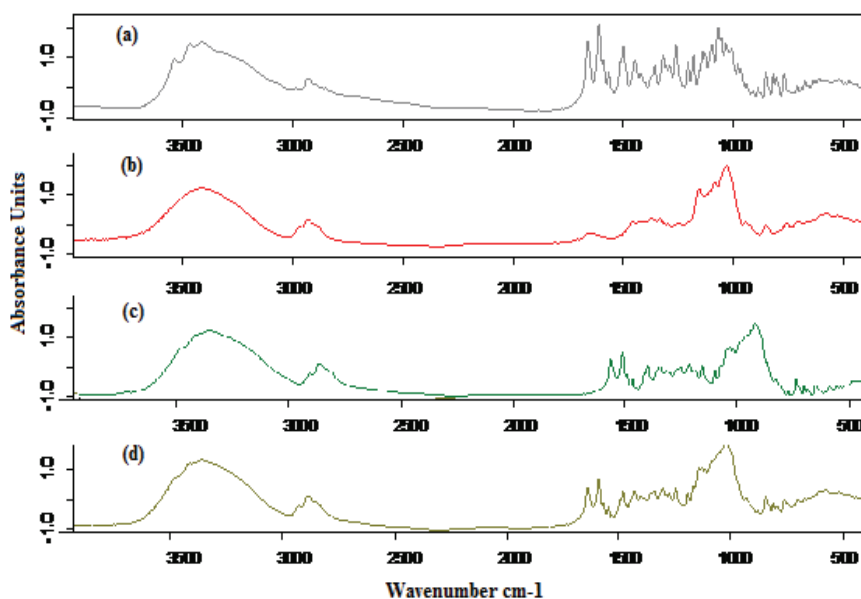


Fig. 2. FTIR spectra of diosmin (a), HP- β -CD (b), inclusion compound CP (c), inclusion compound CV (d)

The spectral line with average intensity is typical of carbonyl group and it is associated with the stretching vibration of the group. Hydroxypropyl-cyclodextrin (Fig. 2b.) shows absorption maxima with higher intensity of bands 865 and 2934 cm^{-1} corresponding to vibrations of asymmetrical stretching for methylene groups and to deformation vibrations of the same C-H bonds.

FTIR spectrum of CP sample (Fig. 2c.) is distinguished by the asymmetry of signal 3410 cm^{-1} that masks OH groups on the surface of the substrate, the shift to 3410 cm^{-1} being also associated with the hydrogen bridges that were created inside the complex. The presence of diosmin is further confirmed by the characteristic signals, 1661, 1610 1501, 1448 cm^{-1} . The substrate is still highlighted by the intense band at 1070 cm^{-1} . CV sample (Fig. 2d.) is similar to the CP sample, but the absorption maxima from 1660 to 1448 cm^{-1} show a lower intensity, confirming the inclusion.

3.2.2. Mass spectroscopic analysis

Prior to the analysis of inclusion complex, was performed the analysis of diosmin in the mass range 100-700 m/z . We noticed the presence of signal 607.8 corresponding to total mass (Fig. 3a). Polarization was negative. MS / MS evaluation (Fig. 3b) at a collision energy of 75eV produced further fragmentation, so fragments are observed at 284.76, 5-hydroxy-2-(3-hydroxy-4-methoxyphenyl)-4H-1-benzopyranone, and 175.75 (theoretical mass 176), 5-hydroxy-1-benzopyranone. With a larger error D-glucopyranosyl was identified at mass 149.67 ($d = -2.67$) (Colombo et al., 2008). Fig. 4a shows the spectrum of the inclusion complex formed by coprecipitation method. Ion 2119.94 is distinguished in the mass spectrum. It can be the adduct (Diosmine + HP- β -CD) which has theoretical mass 2071 at equimolar ratio. For further confirmation, a residual

signal is present at 606.9 that belongs to residual diosmin. High intensity is determined by the higher ionization ability of the substance than of the complex.

Similarly, in case of complex formed by co-evaporation method (Fig. 4b), the signal with mass 2137 is distinguished, whose probability is associated with the mass of theoretical complex 2071. The difference may be associated with Na adduct, since sodium acetate (20 mM) and methanol (50:50) is the dispersion medium (Biernacka et al., 2014; García et al., 2014, Lee et al., 2009).

3.3. Biological characterization

3.3.1. Antioxidant activity

In order to determine the antioxidant activity (Malterud and Rydland, 2000), solutions of the tested samples (CV, CP and D) in DMSO were prepared, with concentrations ranging between 312.5-10000 $\mu\text{g/ml}$ diosmin.

Fig. 5 shows the ability of tested samples to inhibit the activity of lipoxygenase, depending on the concentration of samples. As can be seen from Fig. 5, lipoxygenase activity is influenced by the increase in diosmin concentration. At the same diosmin concentration, inclusion compounds exhibit more intense activity than free diosmin, which demonstrates that the antioxidant activity was influenced by the presence of HP- β -CD.

Calculating IC_{50} values (the ability to inhibit 50 % of lipoxygenase activity) of the analyzed compounds, it was observed that the capacity to inhibit lipoxygenase increased from 76.50 ± 3.89 for free diosmin to 15.73 ± 0.57 (CP) and 16.106 ± 0.586 (CV), showing a 4-fold increase in activity in case of diosmin inclusion in HP- β -CD. Between the inclusion compounds obtained, the differences are insignificant.

3.3.2. Antimicrobial activity

We compared the antibacterial activity against Gram positive bacteria *S. aureus*, *S. lutea*, *B. cereus* and the antifungal activity against *C. glabrata* and *C. parapsilosis* (Fig. 6.) of inclusion compounds in relation to free diosmin. (Atilano et al., 2011; LaJean Chaffin, 2008)

When comparing the antimicrobial activity of inclusion compounds relative to free diosmin, against all tested microorganisms the inclusion compounds showed higher activity due to improved solubility, thus increasing the amount of compound that crosses the microbial membrane. After inclusion, antifungal activity is stronger than antibacterial activity, probably due to the different composition of the cell wall.

Antifungal activity was influenced by the method of preparation of inclusion compounds, those obtained by co-evaporation showing increased activity, as demonstrated by the size of the inhibition zone.

3.4. In vitro dissolution studies

In vitro dissolution tests were performed according to European Pharmacopoeia, 8th edition, at physiological pH simulating the pH of the stomach (Fig. 7a. - acidic pH 1.2) and intestinal pH (Fig. 7b. - alkaline pH 6.8). It can be observed that the dissolution of inclusion compounds was improved compared to the unincluded substance, with similar values for both types of preparation methods

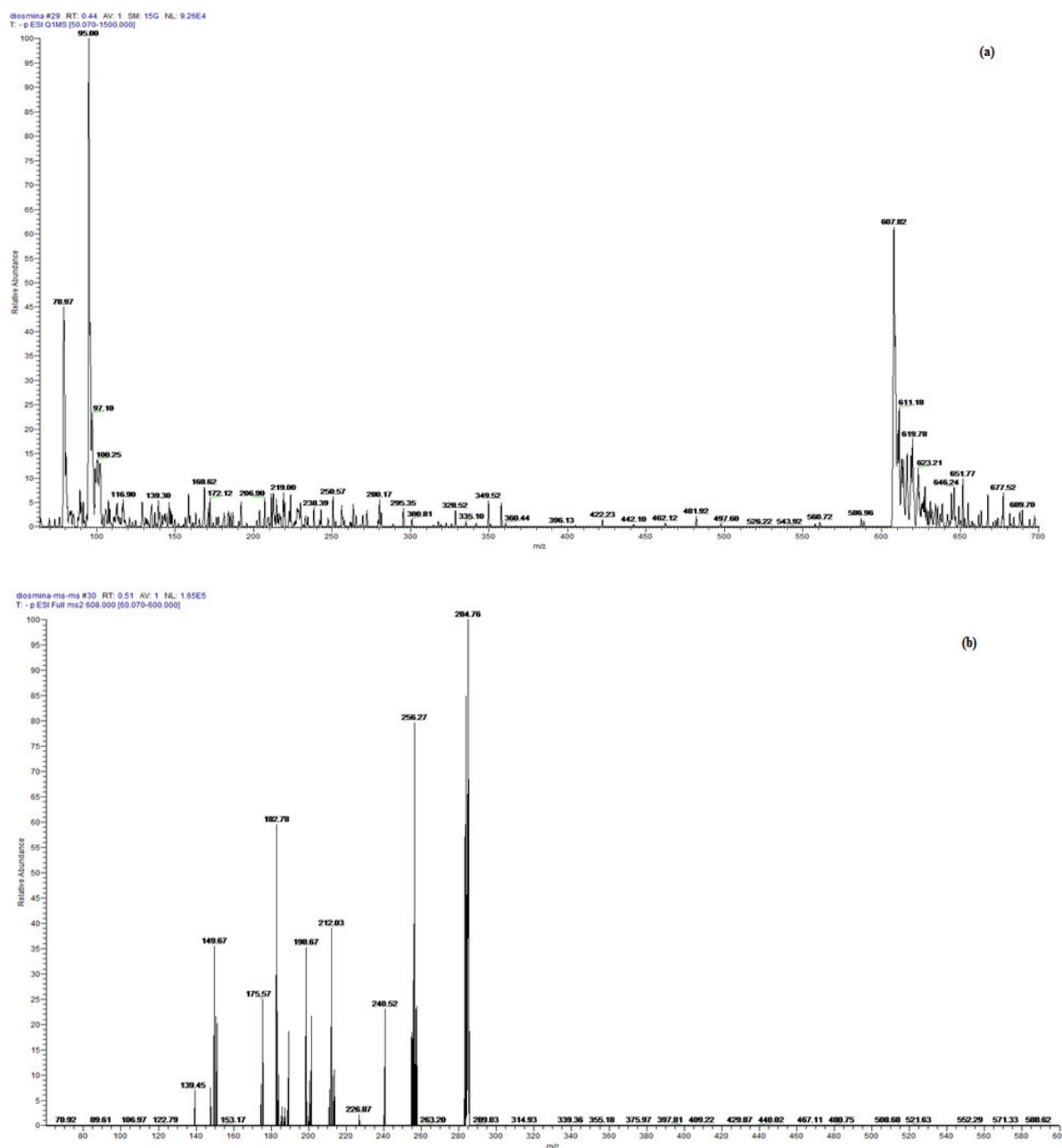


Fig. 3. Full scan MS (a) and MS/MS spectrum (b) of diosmin

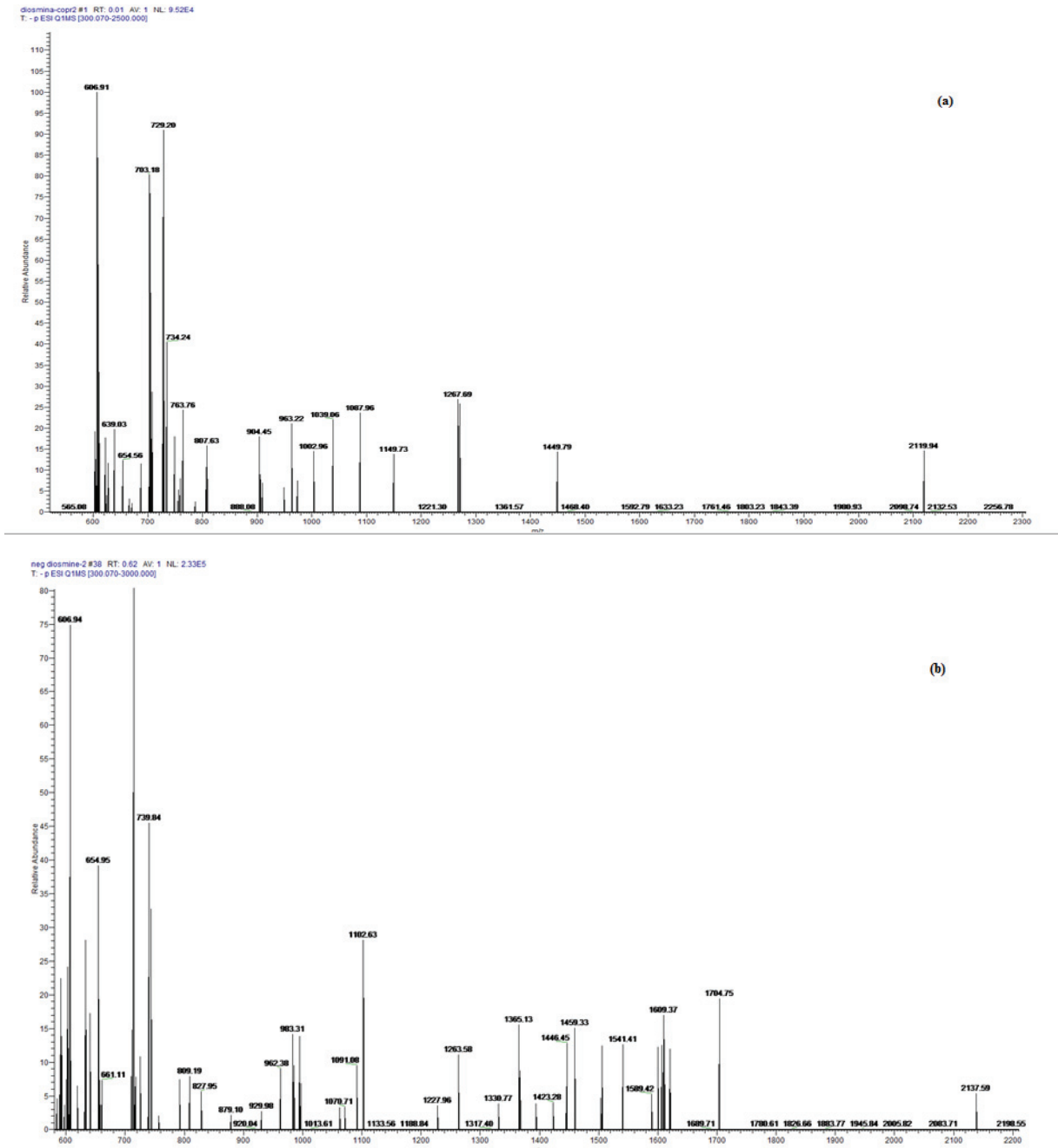


Fig. 4. Full scan MS of complex CP (a), CV (b)

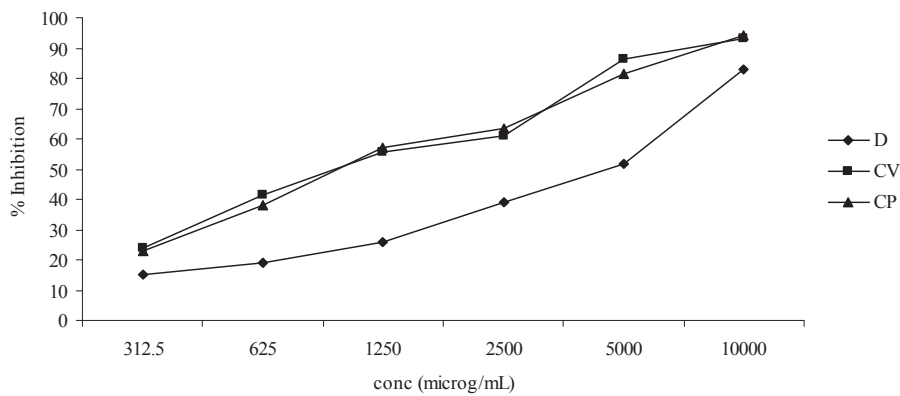


Fig. 5. Lipoxigenase inhibition by diosmin and by inclusion compounds

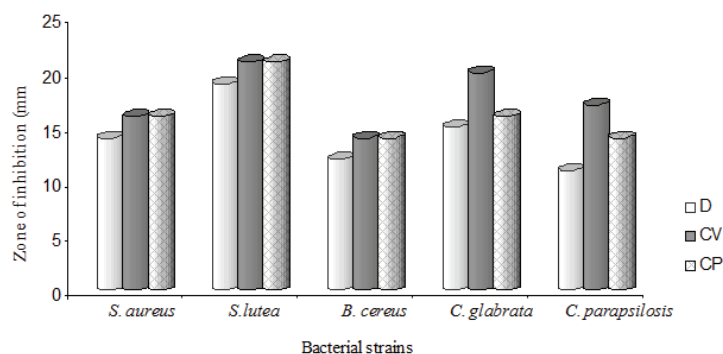


Fig. 6. Antibacterial and antifungal activity of inclusion compounds, relative to free diosmin

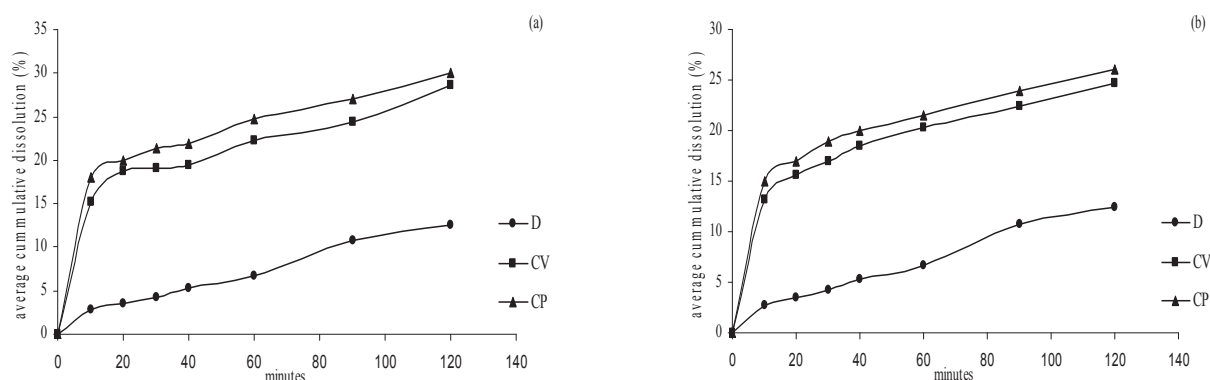


Fig. 7. The in vitro dissolution profile of diosmin and inclusion compounds, at pH 1.2 (a) and pH 6.8 (b)

4. Conclusions

In this work we determined the influence of HP- β -CD on a pharmacologically important flavonoid, diosmin. The phase solubility diagrams in aqueous solution showed a linear increase in water solubility with the increase of cyclodextrin amount and temperature.

The best solubility and stability were obtained in the presence of HP- β -CD at 37 °C. The process takes place spontaneously and it is controlled by enthalpy. The inclusion compounds were characterized physicochemically by FTIR and MS analysis.

Furthermore, antioxidant and antimicrobial activity enhanced after inclusion in HP- β -CD, thereby expanding the possibility of using the inclusion compounds in order to improve pharmacological effects.

Acknowledgments

Scientific research funded by the University of Medicine and Pharmacy "Grigore T. Popa" Iasi, based on the contract no. 4872/18.03.2013.

References

Abdel-Salam O.M., Youness E.R., Mohammed N.A., Abdelmoniem M., Omara E., Sleem A.A., (2012), Neuroprotective and hepatoprotective effects of micronized purified flavonoid fraction (Daflon®) in

lipopolysaccharide-treated rats, *Drug Discoveries & Therapeutics*, **6**, 306-314.

Alvarez N., Vicente V., Martínez C., (2009), Synergistic effect of diosmin and interferon-alpha on metastatic pulmonary melanoma, *Cancer Biotherapy and Radiopharmaceuticals*, **24**, 347-352.

Atilano M.L., Yates J., Glittenberg M., Filipe S.R., Ligoxygakis P., (2011), Wall teichoic acids of *Staphylococcus aureus* limit recognition by the *Drosophila* peptidoglycan recognition protein-SA to promote pathogenicity, *PLoS Pathogens*, **7**, Doi:10.1371/journal.ppat.1002421, On line at: <http://www.plospathogens.org/article/info%3Adoi%2F10.1371%2Fjournal.ppat.1002421>.

Biernacka J., Betlejewska-Kielak K., Witowska-Jarosz J., Kłosińska-Szmurło E., Mazurek A.P., (2014), Mass spectrometry and molecular modeling studies on the inclusion complexes between alendronate and beta-cyclodextrin, *Journal of Inclusion Phenomena and Macrocyclic Chemistry*, **78**, 437-443.

Chadha R., Gupta S., Pissurlenkar R.R.S., Coutinho E.C., (2012), Characterization, thermodynamic parameters, molecular modeling and *in vivo* studies of inclusion complexes of pyrimethamine with native β -cyclodextrin and its derivatives, *International Journal of Pharmacy and Pharmaceutical Sciences*, **4**, 102-112.

Colombo R., Yariwake J.H., McCullagh M., (2008), Study of *C*- and *O*-glycosylflavones in sugarcane extracts using liquid chromatography-exact mass measurement mass spectrometry, *Journal of the Brazilian Chemical Society*, **19**, 483-490.

- Davis M.E., Brewster M.E., (2004), Cyclodextrin-based pharmaceuticals: past, present and future, *Nature Reviews Drug Discovery*, **3**, 1023–1035.
- Domańska U., Pelczarska A., Pobudkowska A., (2011), Effect of 2-hydroxypropyl- β -cyclodextrin on solubility of sparingly soluble drug derivatives of anthranilic acid, *International Journal of Molecular Sciences*, **12**, 2383–2394.
- Gajare P., Patil C., Kalyane N., Pore Y., (2009), Effect of hydrophilic polymers on pioglitazone complexation with hydroxypropyl- β -cyclodextrin, *Digest Journal of Nanomaterials and Biostructures*, **4**, 891 – 897.
- García A., Leonardi D., Salazar M.O., Celina Lamas M., (2014), Modified β -cyclodextrin inclusion complex to improve the physicochemical properties of albendazole. Complete *in vitro* evaluation and characterization, *PlosOne*, **9**, Doi:10.1371, On line at: <http://www.plosone.org/article/info%3Adoi%2F10.1371%2Fjournal.pone.0088234>.
- Higuchi T., Connors A.K., (1965), *Phase Solubility Techniques*, In: *Advances in Analytical Chemistry and Instrumentation*, Reilly C.N. (Ed.), Wiley-Interscience New York, 117-212.
- LaJean Chaffin W., (2008), *Candida albicans* Cell Wall Proteins, *Microbiology and Molecular Biology Reviews*, **72**, 495-544.
- Lee S., Kwon S., Shin H.J., Cho E., Lee K.R., Jung S., (2009), Electrospray ionization mass spectrometric analysis of noncovalent complexes of hydroxypropyl- β -cyclodextrin and β -cyclodextrin with progesterone, *Bulletin of the Korean Chemical Society*, **30**, 1864-1866.
- Leelavinothan P., Subramani S., (2010), Antihyperglycemic effect of diosmin on hepatic key enzymes of carbohydrate metabolism in streptozotocin-nicotinamide-induced diabetic rats, *Biomedicine & Pharmacotherapy*, **64**, 477-481.
- Liu C., Liu C., Desai K.G., (2005), Enhancement of dissolution rate of valdecoxib using solid dispersions with polyethylene glycol 4000, *Drug Development and Industrial Pharmacy*, **31**, 1-10.
- Malterud K.E., Rydland K.M., (2000), Inhibitors of 15-lipoxygenase from orange peel, *Journal of Agricultural and Food Chemistry*, **48**, 5576-5580.
- Martin Del Valle E.M., (2004), Cyclodextrins and their uses: a review, *Process Biochemistry*, **39**, 1033–1046.
- Tong N., Zhang Z., Zhang W., Qiu Y., Gong Y., Yin L., Qiu Q., Wu X., (2013), Diosmin alleviates retinal edema by protecting the blood-retinal barrier and reducing retinal vascular permeability during ischemia/reperfusion injury, *PlosOne*, **8**, 1-10.
- Patil A., Pore Y., Kuchekar B., (2008), Effect of l-arginine on bicalutamide complexation with hydroxypropyl- β -cyclodextrin, *Digest Journal of Nanomaterials and Biostructures*, **3**, 89 – 98.
- Sezer A., Usta U., Kocak Z., Yagci M.A., (2011), The effect of a flavonoid fractions diosmin + hesperidin on radiation-induced acute proctitis in a rat model, *Journal of Cancer Research and Therapeutics*, **7**, 152-156.
- Tahir M., Rehman M.U., Lateef A., Khan R., Khan A.Q., Qamar W., Ali F., O'Hamiza O., Sultana S., (2013), Diosmin protects against ethanol-induced hepatic injury via alleviation of inflammation and regulation of TNF- α and NF- κ B activation, *Alcohol*, **47**, 131-139.



“Gheorghe Asachi” Technical University of Iasi, Romania



RURAL DEVELOPMENT THROUGH THE OPTIMIZATION OF THE RENEWABLE ENERGY POTENTIAL

Liliana Topliceanu^{1*}, Konstantinos Sioulas²

¹“Vasile Alecsandri” University of Bacau, Department of Engineering and Management of Mechanical Systems,
157 Calea Marasesti, 600115 Bacau, Romania

²Centre for Renewable Energy Sources and Saving, 19th km Marathonos Ave, 19009, Pikermi Attiki, Greece

Abstract

The development strategy of the European Union until the year 2020, Europe 2020, militates for an intelligent economy, sustainable and favorable to inclusion. Following these principles, each Member State establishes its targets and action plans at a national level. On the other hand, the rural zones benefit from diverse forms of renewable energy which can assure their development and energetic autonomy, bringing important advantages to the rural community: the diminishing of energy bills, stimulating new investments in the village, the new jobs possibilities, the decline of poverty, the development of access roads, etc. Starting from these presumptions, the paper makes an analysis of the available renewable energy from the rural environment and an evaluation of the way in which this energy can be exploited by the local community. For this study, an advanced methodology is used, methodology which was developed within the Network of Small Rural Communities for Energetic-neutrality, IEE/07/547/SI2.499065/2008 project, financed through the Intelligent Energy Europe program. The necessary steps are presented for the fulfillment of this analysis which is applied, through exemplification, on the actual case of a rural community, community which benefits especially by biomass as renewable energy source. Quite laborious and requiring a rigorous approach and expertise, the method is extremely useful for the local development strategy. It allows the mobilization of the local community in attracting investments to optimize the potential of renewable energy of the area.

Key words: biomass, energetic autonomy, renewable energy, rural communities

Received: November, 2015; *Revised final:* February, 2015; *Accepted:* February, 2015

1. Introduction

The National Rural Development Program for the period of 2014-2020, was realized based on the principles promoted by “Europe 2020” (EC Communication, 2010) and European strategy “Rural development 2014-2020” (EC, 2014).

The program supports the accomplishment of a smart growth through maintaining the technology of agricultural and livestock performance, envisages a durable growth which lays emphasis on the decline of gas emissions with the greenhouse effect, including the advancement of utilizing renewable sources in the rural environment, and the backing of a friendly agriculture, from an environment point of

view. In this sense, the development of exploiting the renewable energy source in the rural environment, for the benefit of the local communities, would contribute to the decline of poverty and to creating new occupation possibilities for the work force available in the rural environment and to making the objectives assumed by Romania, including those in the area of renewable energy.

The EU concern about the conspicuous climate changes greatly influenced its policy in the field of energy and led to setting the targets for 2020. The so-called „20-20-20” objective asks for a reduction of greenhouse gas emissions by 20% compared to 1990, supplying 20% of the energy consumption from renewable sources and increasing

* Author to whom all correspondence should be addressed: e-mail: lili@ub.ro; Phone/Fax: +40234580170

the energetic efficiency by 20%. The EU energy dependence on imports, about 50% of the primary energy consumption comes from imports, is another significant cause for the necessity of switching to alternative energy sources.

The policy of the European Union in the field of renewable energy is relatively recent, and it started by adopting the White Paper in 1997. Over the years, it went from general recommendations to defining certain legally binding objectives, supported by a proper legal framework. The latest Directive concerning the production of energy using renewable sources ensures the necessary regulations for increasing the energy productions using renewable energy sources (EC Communication, 2010; EC Directive, 2009).

The estimations on European level are optimistic, with great chances of achieving the objectives set for 2020, but reaching these objectives cannot be done without the participation of the rural areas.

2. The rural area and the renewable energy sources

The problem of linkage between the rural development and the renewable energy sources was discussed many times (ARE, 2009; Barnes and Floor, 1996; Cherni and Hill, 2009; Kristoferson, 1997; Takase, 1997). Despite the century we live in, there still are rural areas with a weak connectivity to the energy networks or completely isolated, and in such situations, the local production of energy would be a good solution (Havet et al., 2009).

Such systems can be small in size, designed based on the necessities of the area, in places in which the extension of the distribution networks would determine too high of a cost (Kaundinya et al., 2009). At the moment, about 2 billion people of the world, mostly from the countries which are in course of development, do not have access to any forms of modern energy (Alazraque-Cherni, 2008), and their life would be completely different if the local exploitation of the renewable energy sources would commence.

In general, the EU programs for stimulating the use of renewable energy sources and for increasing the energy efficiency, as well as certain flexible financial mechanisms, addressed mainly to the areas with higher population density, to the great cities. A series of large range actions on European level such as Energy Cities, Covenant of Mayors, etc. are also addressed mainly to large cities. However, 56% of the population in the European Union lives in the rural area, over a surface that represents about 91% of the European territory (EC, 2008), and the rural areas have a diversity of renewable energy sources which could ensure their energy autonomy:

- There is plenty of biomass in the rural area, being used especially as a source of thermal energy. In the case of Romania, the biomass covers about 7% of the primary energy demand and about 50% of the

renewable resources potential (Ministry of Economy, 2010);

- The geothermal energy can be exploited in the most common systems for heating (homes, greenhouses, fish culture stations, thermal treatments in the food industry, etc.), but it can also be used in mixed cogeneration systems.

- The solar energy has several applications, being used in the rural area, especially in homes or in isolated houses for producing hot water.

- Life in the rural areas is strictly connected to the existence of a water source, and the hydraulic energy of rivers situated near the villages can be exploited by means of micro hydro plants or turbine engines placed on the rivers, which can be an option for the rural areas that are not connected to the electrical grid;

- The wind energy can also cover the electricity demand in the remote rural areas which are difficult to reach and are non-electrified (Ministry of Economy, 2010).

All these renewable energy sources, largely available in the rural area, can lead to the energetic autonomy of the small rural communities, to reducing the energy bills, increasing investments in the area and creating new jobs (Bhattacharyya, 2006; Gruia, 2011; Karekezi and Kithyoma, 2003; Rourke et al., 2009; Vuckovic, 2014), reducing the greenhouse gas emissions, thus contributing to reaching the EU objectives (Santisirisomboon et al., 2001).

The rural development policy of the European Union for the period 2014-2020 (EC, 2014) is based on three long-term strategic objectives, which are according to the Europe 2020 Strategy, respectively:

- Stimulating the agricultural competitiveness,
- Guaranteeing the sustainable management of the natural resources and fighting the climate changes, as well as
- Encouraging a balanced territorial development of the economy and of the rural communities, creating and maintaining the places of employment.

The rural area has a variety of renewable energy sources which can be used and can ensure energy autonomy on local level. The biomass has a great ratio among these resources. According to the National Renewable Energy Action Plan, the amount of biomass available in Romania is of 318 PJ per year, and it is distributed as follows: „15.5% waste from forest exploitation and firewood, 6.4% wood waste, sawdust and other scrap wood, 7.7% biogas, 7.2% wastes and urban household waste and, most importantly, 63.2% agricultural waste resulting from cereals, corn stalks, vegetal waste, grape vine and others” (Ministry of Economy, 2010).

The biomass can be a good solution for thermal energy as well as for cogeneration. A problem that should be solved is the raw material which should be supplied for a period of time extending over several years.

The projections made for the Renewable Energy Road Map of January 2007 suggested that the use of

biomass can be expected to double, to contribute around half of the total effort for reaching the 20% renewable energy target in 2020.

3. Methodology for the energy assessment of a community.

The methodology presented below has been developed within the project *Network of small RURAL communities for ENERgetic-neutrality*, IEE/07/547/SI2.499065/2008 (Rurener, 2010, 2011), project financed by the program Intelligent Energy Europe and is a good estimation solution for the energy assessment of a community and a good working tool for drawing up future development plans for the community, especially for achieving the Sustainable Energetic Action Plan.

We must specify that this methodology is quite laborious and it requires collecting a great amount of data, the final result and the precision of the assessment depending on the accuracy of the data gathered. Starting from the recorded data for the energy situation at a certain moment, the method allows us to attain a simple and clear view of different energy sources, of the means of using the energy within the community and, being applied successively in the following years, it allows us to observe the evolution of the community from this point of view.

It offers communities the necessary tool for monitoring the production, the conversion and the consumption of energy, enabling them to adapt any future development plans through measures that should ensure environment protection and a sustainable energy development, according to the European provisions and objectives.

Basically, there are two main categories of data that must be collected: the energy consumption and the energy production on community level. By comparing the data, we can determine the degree of energy autonomy of the community, the extent to which it can produce the energy necessary for its normal functioning. The following paragraphs show the method and the type of information that must be collected.

3.1. Data concerning the community- Identifying the community

The energy assessment of the community requires first of all collecting certain preliminary data, involving:

- Setting the physical borders of the community;
- The community surface;
- The number of inhabitants;
- The sectors existing in the community structure and their size: residential, commercial, public services, industry, transport, agriculture, forests, fishing facilities, others.
- The types of transport systems existing in the community: public, private, individual and their extent – if applicable.

Collecting some of this data is not always a simple task. The physical borders of the community have the role to set the area which is subjected to the analysis, which can be part of a place, a district or a whole municipality. Only after setting the physical borders can we start collecting the data.

3.2. Energy production and consumption in the community

The first step in changing the energy policy on community level requires first of all knowing the way in which the energy is produced, if and how much of it comes from fossil or from renewable sources and which are its distribution grids. This information is relatively easy to find out, the energy suppliers being in small numbers on local level.

Only afterwards can we get to the next step which consists in determining the energy consumption on sectors of activity: industrial, agricultural, residential etc. Knowing the way in which a community uses its energy is an important exercise in improving its use and making it more efficient. Gathering data on the energy consumption is a combination between the detailed and the holistic approaches, according to the opportunity of gathering punctual data or just data on large fields of activity. Making an inventory of the energy consumption is the most difficult part of the methodology presented here. The algorithm presented in the following paragraphs is recommended for collecting this data, but each user of this methodology, according to the specific features of the community and to the goal of the analysis, could choose another type of approach.

3.2.1. Identifying all the suppliers of the community and all the types of energy used in the area.

The great suppliers which offer energy through a grid, as well as the small private suppliers will be identified, and an inventory of the quantity and of the types of energy available for that area will be done, as well as an inventory of the fuels used, fossil or renewable fuels: electricity, coal, charred coal, natural gas, wind energy, hydroelectric energy, biomass, solar energy, geothermal energy, gasoline, Diesel fuel, kerosene, etc.

This evidence will separately record the energy produced within a community and the one that comes from outside its physical borders, from the great regional energy suppliers (Fig. 1).

3.2.2. Calculating the energy produced on the level of the community from renewable energy sources

From the data collected previously, we will separate the quantity of energy from renewable sources which will allow us to determine the percentage of this type of energy from the total amount and in what measure the community valorizes the renewable energy sources existing in the area. This quantity of energy will contribute to setting the indicator of the community energetic autonomy.

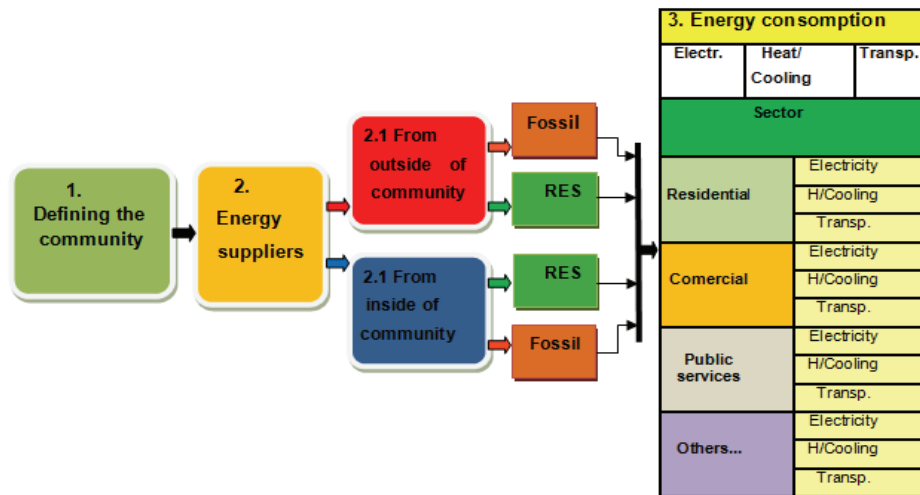


Fig. 1. Data collection chart

The distribution diagram must be drawn up for all the types of energy identified at items 1 and 2, indicating the final consumers, as shown in the chart included in Fig. 1.

On the level of the rural communities, the target of this paper, the energy produced on local level is largely coming from renewable sources. However, the analysis on the possibility of certain conventional energy sources shall not be omitted, for example heating using stoves running on coal.

At this stage there may be certain difficulties in collecting the data, for example if some of the citizens use wood for heating it is necessary to take into consideration the quantity of raw material procured by the suppliers (which can be from outside the community) as well as the one procured by the citizens themselves by individually cutting down trees. In order to solve this problem as accurately as possible, citizen surveys can be done and virtually the statistics offer data on the average amount of wood fuel necessary per month for private houses, reported to the average temperature of the winter months.

3.2.3. Calculating the energy consumption on sectors of activity and types of energy

An important item in building the future action plans for the community is identifying the way of using the energy and the final consumers. Thus, we will know the areas in which the community can work in order to increase the energy efficiency or to cover the consumption demand exclusively from local sources. According to the specific features of the community, the energy consumption is registered for each of the following sectors: residential, commercial, public, small local industry, agriculture, animal husbandry, fishing, forests, etc. In case data is available on the energy consumption in certain sub-sectors, they can be underlined and detailed by creating some more cases in the Tables.

We have analyzed the following objectives:

- The electric energy – meaning the total electric energy consumption on local level, distributed on

different sectors of activity, no matter the source of production: renewable or not, locally produced or not.

❖ The energy produced from the two types of sources will be recorded separately. We will also include here the quantity of energy produced individually, using photovoltaic panels, wind turbines, etc.

- The fossil fuels – including here the fuels used for producing thermal energy such as pit gas, coal, crude oil, as well as the ones used for transport: Diesel fuel, gasoline, kerosene, LPG, etc.

❖ When calculating the energy consumption for transport, we must take into consideration the public transport system, the commercial and the private systems which run on local level. In this case, the community will be completely assessed from the point of view of energy. Or, we may record only the amount of fossil fuel used for producing electric and thermal energy, the transport being considered separately, based on the same methodology but adapting it to the requirements of this type of assessment.

❖ In this category, biofuels will be considered separately, including the ones produced on local level (if applicable), for which separate lines will be introduced in the table.

All this information will be introduced in the first part of the energy balance of the community, as it is presented in Figs. 2 - 3. This step of the methodology is the most difficult and we can collect the necessary information from different sources like: the owner or the manager of the electricity grids, national, regional or local energy centers, independent energy producers, fuel companies, end users, departments of the city halls, etc. In some cases, when a part of the data can't be obtained in another manner, a survey can be conducted directly among the citizens of the area. As we can see in Fig. 3, we also take into consideration the efficiency of the energy production equipment which, in fact, determines the amount of energy that gets to the consumer. In the same way we collect information

concerning the local energy production, which can be from renewable or conventional sources. We also distribute this amount of energy on types of consumers. The report between the local energy production and the total energy consumption within the community allows us to calculate the degree of energy autonomy of this community (Fig. 4).

3.2.4. Setting the conversion factors for different types of energy sources, according to the calorific value / the energy content and the unit of measure

Within this methodology, attention must be given to the units in which the energy is expressed. The production capacity of power plants is usually expressed in units of energy (for example MWh).

ENERGY BALANCE							Community name					
							Country					Template instructions
							Year					All yellow field must be filled in with data
							Population					
Energy Source Input Data												
Fuel type:	Energy (amount)			Total	Units (eg. GWh, tn, litres)	Conversion (Heat Content)	Energy					
	Electricity	Heat	Transportation									
Energy Consumption												
Electricity Consumption 1				0.00	GWh	3,600.00	-	GJ/y				
Electricity Consumption 2				0.00			-					
Electricity consumed in sites off the grid (eg. photovoltaic, wind)				0.00			-					
Coal (eg. Lignite, Pet Coke, etc)				0.00			-					
Heavy oil				0.00			-					
Light oil				0.00			-					
Diesel				0.00	lt		-	GJ/y				
Petrol							-					
LPG				0.00			-					
Gasoline							-					
Kerosane				0.00			-					
Sub Total Petroleum Products							-	GJ/y				
Natural gas				-			-					
Wood and biomass for heating (all types)				-	m3	0.03	-					
Combined Heat and Power (electricity)				-			-					
District heating from waste				-			-					
District heating from biomass				-			-					
District heating from fossil fuels				-			-					
Sub total District heating				-			-					
Solar thermal (heating)				-			-					
Other fuels (specify)				-			-					
Total Energy Consumption							-	GJ/y				
Population								#DIV/0! GJ/y/lt				

Fig. 2. Energy consumption of the community

K	L	M	N	O	P	Q	R	S	T	U	V	W	X
					Sector								
% of Total Energy	Efficiency	End Use	% of Total Final Energy		Residential	Commercial	Public Services	Industry	Transport	Agriculture	Forestry	Fishing	Other use

Fig. 3. Distribution of the consumption on types of users

Local Energy Production													
Energy produced from Renewable fuels													
Wind power									0.00				-
Hydro power									-				-
Wave power									-				-
Solid Biomass Plants and boilers										m3	0.03		- GJ/y
Biomass (mainly wood) used on the territory for individual heating										m3	0.03		-
Biogas													-
Sub Total Energy from Biomass													-
Biomass imported (-) from the territory for energy purposes													-
Biomass exported (+) from the territory for energy purposes													-
Energy from Biomass													- GJ/y
Landfill gas									-				-
Waste Heat and power Recovery									-				-
Geothermal energy									-				-
Solar thermal									-				-
Solar PV									-				-
Other Renewable (please specify)									-				-
Total RES production in the Community													-
Energy produced from non Renewable fuels													
Fossil and nuclear fuels									-				-
Other									-				-
Total non RES production									-				-
Total Energy Production													-
Population									0				#DIV/0!
Autonomy rate													0.00%

Fig. 4. The local energy production

However, the materials used in the power plants (coal, petrol, etc) are often reported using physical units of measure, for example tons of coal or liters of petrol. Thus, in order to be able to use this data, it is necessary to turn them into the same unit of energy, for example GJ.

The methodology presented here has the advantage of allowing for multiple types of analysis, among which we can mention: determining the report between the total quantity of energy consumed and the one coming from renewable sources – we can thus determine how “green” that community is; the ratio of a certain type of energy in the total consumption, the proportion of a certain type of fuel, or of certain economic sector etc. Henceforth we can perform sustainable community development plans.

4. Case study – analysis of a rural community

As the purpose of this paper is to analyse the extent to which the rural environment can ensure energy autonomy with all its advantages, and at the same time to contribute to achieving the targets set by the European Union program, a case study is required. We have chosen Tasca area, located in Neamt County, Romania, as the subject for applying the methodology presented above for calculating the energy autonomy and for drawing conclusions in this direction. Tasca area is situated in a hilly area covered with forests and meadows, along Bicz River and, from an administrative point of view, including the following villages: Tasca, Hamzoaia, Secu, Neagra and Ticos Floarea (Fig. 5). The area has two schools, a police station, a human clinic and a veterinary one, a pharmacy and a public park with a playground for children. At the moment of this study, the area had 2715 inhabitants, 1035 houses. Its surface of 9.563 ha was distributed as follows: 115 ha arable, 1418 ha meadows, 1083 ha grazing ground, 6609 ha forests, 338 ha for other uses.

The main occupations of the inhabitants are in the field of agriculture, raising animals, processing wood, rural tourism and trade, but there are also economic units in the field of construction materials, one of the greatest cement factories in the country being situated in this area. From the geographical point of view, Tasca area is situated at the intersection of the 45°55" parallel north with the 26°27" meridian east and is situated about 600m above sea level, from a climatic point of view being included in the mountain area climate of the Oriental Carpathians. The height of the mountain peaks between 1100 and 1500 m situates it in the medium height mountain climatic area.

The annual average temperature in the lower part of the valley is around 8°C; the coldest month is January, when the average temperature is lower, under -4°C. In the month of July there is the highest thermal value, the average being over 19°C.

Choosing Tasca community for this case study is motivated by the fact that one biomass power plant, co-financed by the Environment Protection Agency Denmark, Neamt County Council and Tasca Local Council, was built here. Moreover, a small photovoltaic system for street lighting was built in this area, system placed within a playground. The thermal power station using sawdust was designed to supply thermal energy for 40% of the inhabitants of Tasca village but, at the date when this study was made, it supplied thermal energy for 132 subscribers, of which: 125 population, 1 economic agent and 6 public institution buildings.

The characteristics of this power plant are presented in Table 1. Other technical characteristics of the power plant are:

- Pressure in the installation - 2 bar;
- Tank capacity - 7600 liters;
- Temperature in the furnace - 700 °C;
- Exit temperature of the water 90 °C;
- $\eta=87\%$.

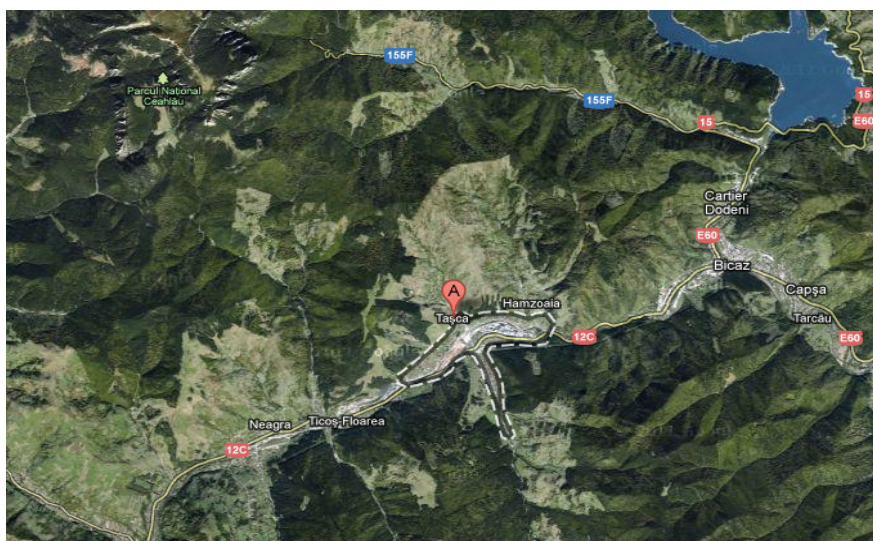


Fig. 5. Position of Tasca area and of its villages (from Google maps)

We must notice that, although the power plant was designed to burn 2500 tons of fuel per year, at the date when this study was made, in November 2011, it used only 1300 tons/year and ensured less than 25% of the thermal energy needs of the village. The reasons for this are connected especially to the reduction of the quantity of sawdust that could be supplied.

When the power plant was designed, the sawdust was for free or it was very cheap, and the construction of the power plant also solved the problem of storing it (Figs. 6, 7). Later on, it was no longer supplied for free, and its price increased continuously. At present, it is purchased for a price that varies between 22-35 euro/ton, which is a high price for the local administration.

The general data regarding the community being already presented, we briefly present below the essential information concerning the energy and the hypotheses that were used in order to apply the methodology for determining the degree of energy autonomy of the community.



Fig. 6. The sawdust warehouse

4.1. Identifying all the suppliers and all the types of energy used in the community

The electricity is supplied through the grid from the local supplier and the average consumption of the community is 1.587 GWh/year. In order to ensure the public lighting in the park area, poles with photovoltaic panels were installed, which produce a

total of 2.044 MWh/year.

The thermal energy is supplied from several sources:

- from the local thermal power plant which uses the sawdust in the area;
- from the regional grid for the distribution of natural gas;
- from wood and agricultural waste, a great proportion of the local people using traditional stoves and in some cases, in the new houses built during the last few years, central heating units using biomass.



Fig. 7. The power plant tank

In order to calculate the energy produced using natural gas, we considered population surveys which were correlated with the statistical data concerning the residential consumption on the level of Neamt County. On the level of Tasca community, the calorific power over the average value taken into consideration (according to the data supplied by E-ON) is of 10.540 kWh/m³, reaching a total of 1.0818 GWh thermal energy per year.

4.2. Calculating the energy produced on community level using renewable energy sources

The energy production on community level refers first of all to the thermal energy, and it is represented by the biomass power plant and the individual heating systems.

Table 1. Characteristics of the biomass plant

Subject	Unit	Data
Heat output capacity of the biomass boiler system	MW	2.5
Fuel		Mostly sawdust, woodchips and bark
Water content of biomass fuel	%	Up to 50
Maximum quantity of wood waste combusted (sawdust)	tons/year	2500
Heat calorific value of wet sawdust	GJ/ton	8.27
Typical emission factor - oil	kg CO ₂ /GJ fuel used (based on lower calorific values)	77.30
Efficiency of flue gas cleaning system (multi cyclone and bag filter unit) at 10% dry oxygen.	mg/Nm ³	CO emissions < 250 NO _x emissions < 500 Dust emissions < 40
CO ₂ emission reduction generated by the demonstration project in Tasca	tons/year	Approx. 1600

At this point, the analysis can become more complicated if we take into consideration the amount of sawdust locally produced and the amount purchased from other sources. The individual heating systems can also be divided into central heating systems with certified biomass and the classical stoves.

As the purpose of this research is to exemplify the way in which a rural community can become energetically autonomous by using wisely the resources existing in the area, we took into consideration the power plant as working according to the initial project, thus ensuring thermal energy for 40% of the population in Tasca village (within the area with the same name), which means hot water and heat during the winter, and during the summer only hot water. Taking into consideration the variations of the consumption necessary during the two seasons, a quantity of thermal energy amounting to 11,167 GWh/year resulted.

As to the private homes with classical individual heating systems, the quantity of wood necessary is between 10-12 m³ per year. As the average annual temperature in Tasca area is quite low, we adopted the value of 12 m³ of biomass per year. During the first stage of the study, we also considered that all the individual homes use certified biomass. This is a problem which has not been thoroughly solved on national level, although some regulations were elaborated (MO 1341, 2012; MO 85, 2013). Having all the necessary data, with the hypotheses listed above, we can now calculate the degree of energetic autonomy of this community.

In the two charts from Figs. 8, 9 we can see that the numbers without decimals are taken but at the conversion to GJ/year, the exact quantity of used and produced energy appears. In our analysis we did not take into consideration the activity of the cement factory situated in the neighborhood, as the local administration could not interfere with its consumption. The analysis aimed at the energetic autonomy of the inhabitants and of the public administration buildings within the community.

It is important to underline that the construction of the biomass power plant and the photovoltaic street lighting system gave rise to 9 temporary jobs and 1 permanent full job.

4.3. Analysis of the case study

According to the hypotheses presented before, the degree of energy autonomy on community level is 66.80 %, most of it being achieved through the use of biomass (Figs. 8, 9).

We thus proved that a rural community can achieve a high degree of energetic autonomy by using the natural resources. The exploitation of renewable energy sources has led to the creation of some temporary and permanent jobs in a different domain than the traditional ones for rural area. Of course, a few problems should be solved first:

- the power plant should work according to the parameters listed in the project;
- the amount of sawdust necessary for the power plant should be supplied;
- the quality of the biomass for the fuel used in the private homes should be certified;
- the classical stoves should be replaced, as much as possible, with high performance heating systems; we should notice that certain classical heating systems, for example certain terracotta stoves which are properly built and used can have quite high energetic efficiency, up to 82%, but there are also heating systems with low efficiency: between 35% (the stoves without a hearth) and 75% (the stoves with a hearth) (Zaharia, 2012) which should be replaced.

In fact, according to the Master Plan for Biomass (document issued in 2010 by the Ministry of Economy - Romania, NL Agency – Netherlands and ENERO – Romania) it is estimated that, until 2020 the main contribution of biomass will be represented by the heating using traditional stoves in the rural area. For this reason, it is recommended that measures should be taken allowing the use of high-performance individual heating systems, with high energetic efficiency by at least 85%. In the present day, systems based on pallets which have an efficiency of 94-95% have been developed and any new construction of a power-station should utilize the latest technologies in the field.

The use of central heating installations leads to increased energetic efficiency, also ensuring hot water, increasing the comfort of the population and reducing the differences between the rural and the urban areas. Starting from the results of the study, a community can better manage its energy consumption and can achieve and orient its strategy for sustainable development in the desired direction.

As to Tasca community, in order to complete the energy need, a plan was initiated concerning the installation of a wind farm placed on Damoc hill, on the boundary of several communities. The wind farm would ensure the energy demand for all the public administration buildings and the street lighting in all the communities which are part of the project.

The study carried out also considered the fuel necessary for transportation. Ensuring the bio-fuel on local level, or the electricity for all the means of transport, are problems which cannot be solved during the next years, and not on local level.

In case the energy necessary for transportation is excluded from the previous calculations, the level of the energy autonomy is of 88.03%. In the situation in which only 10% of the individual stoves (of the new houses) fill into the category of biomass central heating systems, the community energy autonomy is reduced to 40.89%. This fact reveals how important it is to apply the correct technology for the use of the biomass.

ENERGETIC AUTONOMY BALANCE		Community name	TASCA				
		Country	Romania	Template instructions			
		Year	2011	All yellow field must be filled in with data			
		Population	2715				
Energy Source Input Data							
Fuel type:	Energy (amount)			Total	Units (eg. GWh, tn, litres)	Conversion (Heat Content)	Energy
	Electricity	Heat	Transportation				
Energy Consumption							
Electricity Consumption 1	1.59			1.59	GWh	3,600.00	5,713 GJ/y
Electricity Consumption 2	0.00			0.00			-
Electricity consumed in sites off the grid (eg. photovoltaic, wind power...)	0.00			0.00	GWh	3,600.00	7 GJ/y
Coal (eg. Lignite, Pet Coke, etc)				0.00			-
Heavy oil				0.00			-
Light oil				0.00			-
Diesel			412000.00	412000.00	lt	0.03579	14,743 GJ/y
Petrol				0.00	lt	0.03579	- GJ/y
LPG				0.00			-
Gasoline			338000.00	338000.00	lt	0.03185	10,764 GJ/y
Kerosane				0.00			-
Sub Total Petroleum Products			750,000	750,000			25,507 GJ/y
Natural gas		1		1	GWh	3,600.000	3,884
Wood and biomass for heating (all types)		20		20	GWh	3,600.00	70,650
Combined Heat and Power (electricity)							
District heating from waste							
District heating from biomass							
District heating from fossil fuels							
Sub total District heating							
Solar thermal (heating)							
Other fuels (specify)							
Total Energy Consumption				750,022			105,772 GJ/y
Population	2,715						38,958 GJ/y

Fig. 8. Energy consumption of the Tasca community

Local Energy Production							
Energy produced from Renewable fuels							
Wind power				0.00			- GJ/y
Hydro power				-			-
Wave power				-			-
Solid Biomass Plants and boilers		11		11	GWh	3,600.00	40,201
Biomass (mainly wood) used on the territory for individual heating		8		8	GWh	3,600.00	30,449
Biogas		-		-			-
Sub Total Energy from Biomass				20	GWh	3,600.00	70,650
Biomass imported (-) from the territory for energy purposes				-			-
Biomass exported (+) from the territory for energy purposes				-			-
Energy from Biomass				20	GWh	3,600.00	70,650
Landfill gas				-			-
Waste Heat and power Recovery				-			-
Geothermal energy				-			-
Solar thermal				-			-
Solar PV	0			0	GWh	3,600.00	7
Other Renewable (please specify)				-			-
Total RES production in the Community							70,657
Energy produced from non Renewable fuels							
Fossil and nuclear fuels				-			-
Other				-			-
Total non RES production							- GJ/y
Total Energy Production							70,657 GJ/y
Population	2,715						0.19 GJ/y
Autonomy rate							66.80%

Fig. 9. Calculation of autonomy rate of Tasca vilage

5. Conclusions

The methodology presented here, developed within the project Network of small RURAL communities for ENERgetic-neutrality, IEE/07/547/SI2.499065 (Rurener, 2011), allows us to assess the energy consumption necessary within a community, no matter its size, and it does a radiography of the community in question from the point of view of energy. The results are a good starting point for drawing up the sustainable development strategy for any municipality.

The presented case study confirms the fact that intelligent use of the resources which nature offers us, can assure a high degree of energetic

autonomy of the small communities, like the ones in the rural area, with important benefits in terms of environmental protection, the reduction of gas emissions with the greenhouse effect and, by default, the fight against climatic changes.

Another important conclusion which results from this analysis, advises that the exploitation of renewable resources be made through the usage of last generation technologies, with high energetic efficiencies.

In fact, the national policies regarding the renewable energy resources should be headed so that the number of green certificates for 1 MW be granted also by the facts which relate to energy efficiency, higher investments costs having a faster absorption

rate. It is also necessary to specify that according to the statements of specialists in the field (Bizlawer, 2014), in the period 2014-2020, the only renewable resources for which Romania will receive EU funding will be biomass and small hydropower, the targets for wind and solar energy being accomplished.

Acknowledgements

The paper is a result of the project Network of small RURAL communities for ENERgetic-neutrality, IEE/07/547/SI2.499065, acronym RURENER, and the authors gratefully acknowledge for the support of the partners.

References

- Alazraque-Cherni J., (2008), Renewable Energy for Rural Sustainability in Developing Countries, *Bulletin of Science Technology & Society*, **28**, 105-114.
- ARE, (2009), *A green light for renewable energy in developing countries*, Alliance for Rural Electrification Publication, Brussels.
- Bhattacharyya S., (2006), Renewable energies and the poor: niche or nexus? *Energy Policy*, **34**, 659-663.
- Barnes D., Floor W., (1996), Rural Energy in Developing Countries: A Challenge for Economic Development, *Annual Review of Energy and Environment*, **21**, 497-530.
- Bizlawer, (2014), Romanian Legal Business, On line at: <http://www.bizlawyer.ro/stiri/salveazapdf/33921>.
- Cherni J., Hill Y., (2009), Energy and policy providing for sustainable rural livelihoods in remote locations – The case of Cuba, *Geoforum*, **40**, 645–654.
- EC Communication, (2010), Energy 2020 - A strategy for competitive, sustainable and secure energy, Directorate General for Energy, Publications Office of the European Union, 2011, Luxembourg, On line at: http://ec.europa.eu/europe2020/index_en.htm.
- EC Directive, (2009), Directive 28/2009 CE of the European Parliament and of the Council of the 23rd April 2009 on the promotion of the use of energy from renewable sources, *Official Journal of European Union*, **L 140**, 05.06.2009, 16–62, Brussels.
- EC, (2008), Rural Development policy 2007-2013, On line at: http://ec.europa.eu/agriculture/rurdev/index_en.htm.
- EC, (2014), European Commission, Agriculture and Rural Development, Rural development 2014-2020, On line at: http://ec.europa.eu/agriculture/rural-development-2014-2020/index_en.htm.
- Gruia R., (2011), Study on energy resources integration and sustainability of the new modular agriculture pattern, *Environmental Engineering and Management Journal*, **10**, 1213-1219.
- Havet I., Chowdhury S., Takada M., Cantano A., (2009), *Energy in National Decentralization Policies*, New York, United Nations Development Programme, On line at: http://www.undpcc.org/undpcc/files/docs/publications/Energy_Decentralization_r8.pdf.
- Karekezi S., Kithyoma W., (2003), Renewable energy in Africa: Prospects and limits, Workshop for African Energy, Experts on Operationalizing the NEPAD Energy Initiative, Dakar, Senegal, 2-3 June, 1-30, On line at: <http://sustainabledevelopment.un.org/content/documents/nepadkarekezi.pdf>.
- Kaundinya D.P., Balachandra P., Ravindranath N.H., (2009), Grid-connected versus stand-alone energy systems for decentralized power - A review of literature, *Renewable and Sustainable Energy Reviews*, **13**, 2041-2050.
- Kristoferson L., (1997), Seven energy and development myths - are they still alive?, *Renewable Energy for Development*, **10**, 1-6.
- Ministry of Economy, (2010), National Action Plan for Renewable Energy, (in Romanian), 20 iunie 2010, Bucuresti, On line at: http://www.minind.ro/pnaer/PNAER_29%20iunie_2010_final_Alx.pdf.
- MO 1341, (2012), Order No.1341 of 03.05.2012 on the approval of the procedure for issuing certificates of origin for biomass from forestry and related industries, *Romanian Official Monitor*, No. 360 of 28 mai 2012.
- MO 85, (2013), Order No. 85/2013 amending and supplementing the Procedure for issuing of certificates of origin for biomass from forestry and related industries, approved by Ministry of Environment and Forests no. 1341/2012, *Romanian Official Monitor*, Part. 1, 28 January 2013.
- Rourke F.O., Boyle F., Reynolds A., (2009), Renewable energy resources and technologies applicable to Ireland, *Renewable and Sustainable Energy Reviews*, **13**, 8, 1975–1984.
- Rurener, (2010), Energetic Neutrality Template Instructions made by Sioulas, K. from CRESS, On line at: http://rurener.eu/files/2010/07/Template_instructions_excel.pdf.
- Rurener, (2011), Results and perspective, On line at: http://ec.europa.eu/energy/intelligent/projects/sites/iee-projects/files/projects/documents/results_perspectives_rurener_en.pdf.
- Santisirisomboon J., Limmeechokchai B., Chungpaibulpatana S., (2001), Impacts of biomass power generation and CO₂ taxation on electricity generation expansion planning and environmental emissions, *Energy Policy*, **29**, 975–985.
- Takase K., (1997), *The crises of rural energy in developing countries*, In: *Environment, energy and economy-Strategies for sustainability*, Kaya Y., Yokobori K. (Eds.), United Nations University Press, Tokyo, 283-330.
- Zaharia N., (2012), *Market Study on the available biomass heating solutions in rural households* (in Romanian), Chişinău, ProEra Grup Ltd SRL, On line at: http://www.biomasa.md/data/1011/file_1606_0.pdf.
- Vuckovic A., Petrovic D., Mihic M., (2014), Comparative analysis of global trends in energy sustainability, *Environmental Engineering and Management Journal*, **13**, 947-960.



“Gheorghe Asachi” Technical University of Iasi, Romania



ENVIRONMENTAL IMPACT AND RISK ASSESSMENT OF THE MAIN POLLUTION SOURCES FROM THE ROMANIAN BLACK SEA COAST

Brindusa Robu¹, Oana Jitar¹, Carmen Teodosiu^{1*}, Stefan-Adrian Strungaru²,
Mircea Nicoara², Gabriel Plavan²

¹“Gheorghe Asachi” Technical University of Iasi, Faculty of Chemical Engineering and Environmental Protection, Department of Environmental Engineering and Management, 73 Prof. Dr. D. Mangeron Str., 700050, Iasi, Romania

²“Alexandru Ioan Cuza” University of Iasi, Faculty of Biology, Department of Biology, 20 Carol I Blvd., 700505 Iasi, Romania

Abstract

The environmental impact assessment (EIA) is a compulsory evaluation instrument for environmental management and decision making processes and applies to different phases of activities (plans, programmes, projects and /or existing production or services), because it measures the natural and anthropogenic activities effects upon the environment. These impacts may affect the cultural richness, biodiversity, social-economic conditions and human health as well as the ecosystem equilibrium.

The aim of this study was to evaluate the environmental impact generated by the heavy metal pollution from the main sources located in the southern area of the Romanian Black Sea coast. Various pollution sources that discharge contaminated effluents were considered for the impact and risk assessment with concern to water and sediments. The main sources analyzed were the effluents of wastewater treatment plants (4 treatment plants of SC RAJA Constanta) and the effluents of a refinery. The methods applied in order to assess the impact of pollution sources with heavy metals were *Rapid Impact Assessment Matrix* (RIAM) and *Integrated Environmental Impact and Risk* approach.

Environmental indicators used for impact quantification were correlated considering the concentrations of heavy metals from the effluents (generated by the 5 pollution sources), marine water and sediments.

The results obtained in this study provide a general image for the heavy metal pollution caused by considered anthropogenic activities on the Romanian Black Sea Coast. The results showed that the analyzed pollution sources do not have a significant negative impact generated by the heavy metal pollution. However, the presence of other pollution sources should not be overlooked because the ecosystem equilibrium must be maintained even if the concentrations of the heavy metals are below the maximum allowed values.

Key words: Black Sea, heavy metals, impact assessment, pollution sources, risk assessment

Received: November, 2014; *Revised final:* February, 2015; *Accepted:* February, 2015

1. Introduction

Environmental Impact Assessment (EIA) is usually defined as a mandatory assessment procedure that analyzes and evaluates the impacts that human activities can have on the environment (Toro et al., 2013). The environmental impact assessment is defined by the International Association of Impact

Assessment (IAIA) as the “identification, estimation, evaluation and mitigating of the significant effects of the development projects” (Mondal et al., 2010). EIA uses several types of instruments and applies to different phases of activities (projects and /or existing production and services processes), may be applied on a local, national or international scale and has as main deliverable a form of Environmental Impact

* Author to whom all correspondence should be addressed: e-mail: cteo@ch.tuiasi.ro

Statement (EIS) (UNEP, 2002). The environmental impact evaluation relies on both qualitative and quantitative impact evaluation methods that are being used to assign (qualitatively) or compute (quantitatively) numerical values for the environmental impacts (Gavrilescu, 2007; Burger, 2008; Buytaert et al., 2011; Singh et al., 2012).

The international protocols emphasize that one should not act or authorize anthropogenic activities without a serious analysis of the possible negative effects produced to the environment. In some agreements it is mentioned that the environmental impact and risk assessments are working together only. Comprehensive assessments, usually link environmental impact assessment (EIA) with risk assessment (RA) so as to help decision-making processes in water resources management (Teodosiu et al., 2015). Traditionally, risk assessment (RA) refers only to human health (originally referred to occupational health, then public health and safety) but recently it was extended to the environmental level, including freshwater and marine ecosystems (Kiss and Shelton, 2007; Lexer et al., 2006).

In the environmental impact assessment, simple qualitative methods can be easily applied, by working with criteria capable to identify and evaluate the likely environmental changes caused by specific activities such as projects. More than that, the affected community must be informed and invited to debates before the decision making process regarding the project implementation is accomplished.

Toro et al. (2013) have analyzed the limitations of the qualitative environmental impact assessment methods with the purpose to reduce the uncertainties and subjectivity in the assessments regarding the impact importance. Thus, they propose to calculate the *total importance of the impact* ($ImpTotal$) by ponderating the *project importance* ($ImpPro$), the *importance of the activity that generates the impacts* ($ImpAct$), as well as the *importance of the vulnerability of the environmental factors* ($ImpVul$). This proposal has the advantage of calculating the total impact, based on a wider range of information.

The method of Rapid Impact Assessment Matrix (RIAM) is often used in the environmental impact quantification of projects or new activities. Kuitunen et al. (2008) conducted a study that focused on the comparison of results generated by RIAM applied for new projects or activities within EIA process and the results generated within Strategic Environmental Assessment (SEA).

The results are comparable and reliable for both situations thus the method proved to be an objective one. Also, Ijas et al. (2010) applied the RIAM method for projects/new activities, quantifying the positive and negative impact, while other authors such as Mondal et al. (2010) quantified the environmental impact assessment of different municipal solid wastes from Varanasi India, and Upham and Smith (2013) quantified the environmental impact (positive or negative) in the

case of biofuel energy production considering the European Commission recommendations for renewable resources.

The main problems in aquatic environments are caused by the pollution generated by human activities due to industries, agriculture, social development, transportation, mining, etc. and their solving requires integrated approaches based on the water use cycle concept (Teodosiu et al., 2012).

This can damage the entire representative life forms of the ecosystems. The pollution sources should be carefully identified and effective preventive pollution methodologies should be applied along with end-of-pipe treatment processes. The heavy metals are an important category of the priority pollutants that contaminate the aquatic environment and may be generated by wastewaters from the mining, metallurgic, chemical industries as well as from natural sources. They are toxic elements for all life forms and accumulate very fast in the body mass of the marine organisms (Jitar et al., 2012). According to Iordache (2009), the sediments represent the final reservoir of most toxic heavy metals generated by different pollution sources.

The aim of this study was to evaluate the environmental impact generated by the heavy metal pollution from the main sources located in the southern area of the Romanian Black Sea coast. Various pollution sources that discharge contaminated effluents were considered for the impact and risk assessment with concern to water and sediments.

The environmental indicators used for impact quantification were correlated considering the concentrations of heavy metals from the effluents (generated by 5 pollution sources), marine water and sediments. The results obtained from this study provide a general image for the heavy metal pollution caused by considered anthropogenic activities on the Romanian Black Sea Coast.

2. Methodology

2.1. Study area description

The heavy metal pollution of the Black Sea is a multinational problem caused by the anthropogenic activities conducted near the seashore areas and rivers that flow into the sea. It is important to identify each pollution source but it is quite difficult to provide an inventory of *point* and *non-point* pollution sources, due to the numerous and various activities and trans-border discharges.

The natural background concentrations of heavy metals are unknown in many areas of the Black Sea and it is hard to quantify the real ones. The following working strategy was used to achieve the objectives of this study, as presented in Table 1.

The monitoring studies conducted by the National Institute for Marine Research and Development (NIMRD) "Grigore Antipa" Constanta, Romania noticed that the heavy metals

concentrations compared with the maximum values provided by the international regulations represent a risk in the sea water from the shore area.

According to the official information sources provided by the national monitoring program of the Black Sea (NIMRD “Grigore Antipa” and Administratia Bazinala de Apa Dobrogea-Litoral-ABADL) the main sources of heavy metal pollution for the Romanian Black Sea sector are: the Danube River through its pollution loads; local pollution sources from the Romanian shore area; pollution sources located in the Ukrainian Black Sea sector.

The main anthropogenic pollution sources identified for the Romanian coast were: the wastewater treatment plants, the oil refinery, the harbor and the ship construction sites. The agricultural activities were excluded from the main sources of pollution with heavy metals because their influence is not significant. The data were extracted from the official reports published by NIMRD “Grigore Antipa” (INCDM, 2010, 2011, 2012) and Administratia Bazinala de Apa Dobrogea-Litoral (ABADL) available for the years 2010, 2011 and 2012. The main anthropogenic pollution sources are presented in Fig. 1. Jitar et al. (2014), while the associated activities are depicted in Table 2.

2.2. Environmental impact quantification - methods description

Two matrices were applied for the impact and risk quantification induced by the heavy metals (Ni, Cu, Cd, Pb, Cr) on the Romanian Black Sea ecosystem: the Rapid Impact Assessment Matrix (RIAM) and the Integrated Quantification of Impact and Risk matrix (SAB) (Robu and Macoveanu, 2010; Teodosiu et al., 2013). The RIAM method was developed by Christopher Pastakia to quantify the environmental impact (Pastakia, 1998; Pastakia and Jensen, 1998). Since then, it has been tested in many studies for environmental impact assessment (Ijas et al., 2010; Kuitunen et al., 2008; Robu et al., 2007; Suditu and Robu, 2012). RIAM uses specific criteria in quantification the environmental impact, as follows:

- a) criteria that can individually modify the obtained score (group A), and
- b) criteria that cannot individually modify the obtained score (group B).

Each group of criteria (A and B) is calculated considering the specific Eqs. (1) – (2). The Environmental Score (ES) is calculated as the value resulted by multiplying the grades from *group A* with the sum of grades from *group B* (Eqs. 1-3) (Kuitunen et al., 2008; Suditu and Robu, 2012), where: (A_1) , (A_2) are the values assigned to individual criteria from group A; (B_1) , (B_2) , (B_3) are the values assigned to individual criteria from group B; AT is the result of multiplying all *A* grades; BT is the result of summing all *B* grades; ES is the environment score of the environmental assessed components (in this case water and sediments).

$$(A_1) \cdot (A_2) = AT \quad (1)$$

$$(B_1) + (B_2) + (B_3) = BT \quad (2)$$

$$(AT) \cdot (BT) = ES \quad (3)$$

It was assumed that for the assessed sources of pollution, there is a negative influence on the environmental quality. Thus, for the magnitude of the change / effect, values between 0 and (-3) are assigned (Table 3). In order to assure an evaluation system with more certainty, the environmental scores (ES) are classified so that a comparison of quantified impacts for various situations can be done (Table 4).

The second method applied was the Integrated Quantification of Impact and Risk that was performed based on a specific algorithm developed in previous studies (Robu, 2012; Stefanescu et al., 2011; Suditu and Robu, 2012; Teodosiu et al., 2013).

According to these studies, the integrated method may be applied for four environmental components: surface water, ground water, air and soil. The environmental impact quantification is based on two parameters: the *magnitude* of the impact/effect which depends on the measured pollutant concentration in the environment and the *importance* of environmental component that takes values between 0 and 1 (1 representing the most important component - *maximum importance*) (Robu and Macoveanu, 2005; Robu et al., 2005).

In this study there were considered two environmental components: seawater and sediments. The environmental impact (EI) was quantified based on Eqs. (4, 5), where: Q is the quality of the environmental component; UI is the unit of importance for each environmental component; MAC is the maximum admitted concentration for each component according to the environmental standards; C_{det} is the measured concentration in the samples.

$$EI = \frac{UI}{Q} \quad (4)$$

$$Q = \frac{MAC}{c_{det}} \quad (5)$$

The environmental risk was calculated based on Eq. (6), where: EI is the environmental impact; P is the probability of impact occurrence with values between 0 and 1.

$$ER = EI \times P \quad (6)$$

One should notice that if the impact, namely the environmental risk, has a low value, this denotes that the environmental impact is considered to be insignificant and the associated risk is negligible. As a result, the higher the values, the higher the impact risks are.

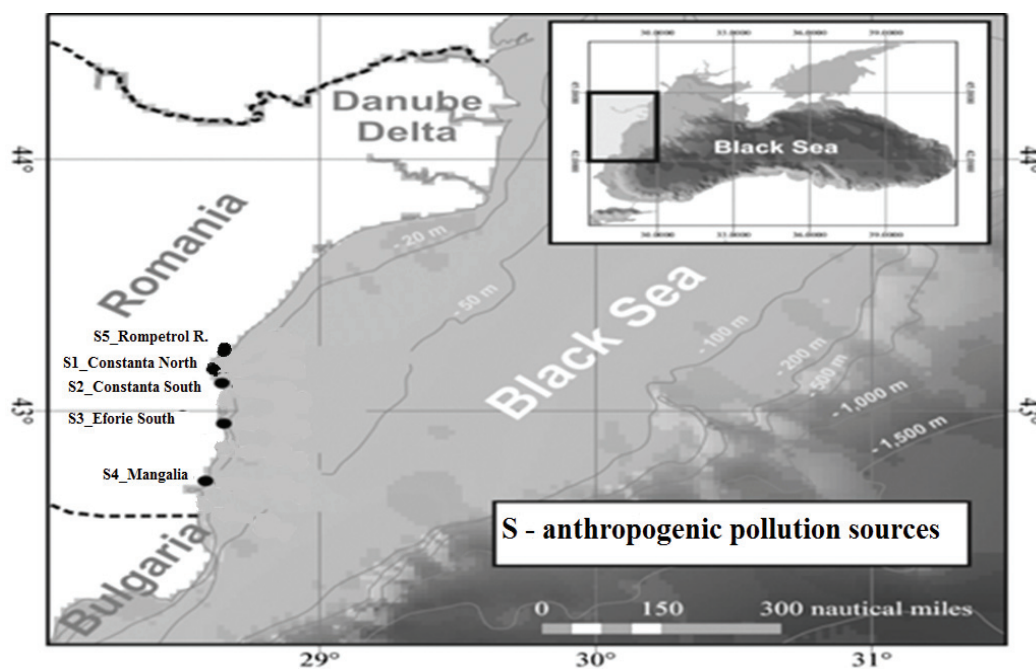


Fig. 1. Anthropogenic sources of pollution with heavy metals identified on the Romanian Black Sea coast

Table 1. The working strategy for the environmental impact and risk quantification

<i>Aim of this study</i>	<i>Objectives</i>	<i>Specific activities (A)</i>
Assessment of the environmental impact and risk generated by the heavy metals pollution	O1: Identification of the main pollution sources (natural and anthropogenic) from the Romanian Black Sea shore	A1: Analysis of the national monitoring programs and inventory of the main pollution sources from the Romanian Black Sea shore
	O2: Identification of the main polluting agents	A2: Data collection from the annual reports databases; A3: Selection of the environmental quality indicators proposed–heavy metals concentrations
	O3: Impact and risk assessment induced by the considered pollution sources on the sea water and sediments	A4: Selection of two assessment matrices for environmental impact and risk caused by the selected indicators; A5: Analyses and processing of collected raw data and elaboration of the evaluation matrices A6: Quantification of the impact and risk induced by the heavy metals in the marine environment

Table 2. The main anthropogenic sources of pollution with heavy metals and the associated activities

<i>Pollution sources</i>	<i>Activities</i>
S ₁ _Wastewater treatment plant Constanta North	This wastewater treatment plant is managed by S.C. Raja S.A. Constanta and collects the wastewater from the Northern district of Constanta town and Mamaia resort.
S ₂ _Wastewater treatment plant Constanta South and the Constanta Harbor area	This wastewater treatment plant is managed by S.C. Raja S.A. Constanta and collects the wastewater and industrial water from the Constanta town and harbor area. The water is mechanically and biologically treated and then discharged in the harbor area of the Black Sea.
S ₃ _Wastewater treatment plant Eforie South	This wastewater treatment plant is managed by S.C. Raja S.A. Constanta and collects the wastewater from Eforie Sud and Eforie Nord resorts, Costinesti resort, Schitu, Agigea and Techirghiol localities.
S ₄ _Wastewater treatment plant Mangalia and the Mangalia Harbor area	This wastewater treatment plant is managed by S.C. Raja S.A. Constanta and collects the wastewater from Mangalia town, and the following resorts: Olimp, Neptun, Jupiter, Venus, Aurora and Saturn.
S ₅ _Rompetrol Refinery	This oil refinery is managed by S.C. Rompetrol Rafinare S.A. Navodari. It is a new chemical oil refinery unit that processes the imported oil.

Table 3. Description of criteria (conventional) (Kuitunen et al., 2008)

<i>Criterion</i>	<i>Scale</i>	<i>Description</i>
A ₁ - The importance of the condition	4	Important for the national/international interests
	3	Important for the regional/national interests
	2	Important only for the zones found near the local zone
	1	Important only for the local condition
	0	No importance
A ₂ - The magnitude of the changing/effect	+3	Major importance benefit
	+2	Meaningful benefit of the quo status
	+1	Benefit of the quo status
	0	Lack of change/status quo / no influence
	-1	Negative change of quo status
	-2	Significant disadvantages or negative changes
	-3	Major disadvantages or changes
B ₁ - Permanence	1	No changes
	2	Temporary
	3	Permanence
B ₂ - Reversibility	1	No changes
	2	Reversible
	3	Irreversible
B ₃ - Cumulatively	1	No changes
	2	Non-cumulative/unique
	3	Cumulative/synergetic

Table 4. Description of the environmental scores calculated (ES)

<i>Environmental score</i>	<i>Class</i>	<i>Description of the category</i>
+72 to +108	+E	Major positive changes/ impact
+36 to +71	+D	Significant positive changes/ impact
+19 to +35	+C	Moderate positive changes/ impact
+10 to +18	+B	Positive changes/ impact
+1 to +9	+A	Slight positive changes/ impact
0	N	Lack of change/status quo/ no impact
-1 to -9	-A	Slight negative changes / impact
-10 to -18	-B	Negative changes / impact
-19 to -35	-C	Moderate negative changes / impact
-36 to -71	-D	Significant negative changes / impact
-72 to -108	-E	Major negative changes / impact

The algorithm of the environmental impact and risk quantification was developed in the Excel program so that it can easily be used and applied under various circumstances (Robu et al., 2007; Stefanescu et al., 2012).

3. Results and discussions

3.1. Rapid Impact Assessment Matrix results

The impact assessment performed by using RIAM method showed that pollution sources (S₁-S₅) (Table 5) have a slight negative impact leading to insignificant negative changes (ES_{total} belongs to category A: *Changes/slight negative impact*), all concentrations of the analyzed pollutants being below the MAC limits according to NTPA 001/2005 (GD 188, 2002; GD 352, 2005).

RIAM method was applied to the average of annual measured concentrations of heavy metals in water and sediment. This data was published in the journal of Marine Research, under the coordination of the “Grigore Antipa” National Institute for Marine Research and Development Constanta. Determination

of the heavy metals concentrations in 2010, 2011 and 2012 was made within a monitoring program by analyzing *seawater* samples (surface horizon of shallow sediments) and *biota* from transitional areas (Sulina – Portita, 5 - 20 m), coastal (Gura Buhaz, Constanța East, Casino Mamaia, Constanța North, Constanța South, Eforie, Mangalia, Vama Veche, 0 – 20 m) and *marine* (depths exceeding 20 m) (*Report on the status of marine and coastal environment in 2010/2011/2012*). According to environmental reports, in all these three years (2010-2012), the concentration values determined in relation with the environmental quality standards for water (Order 161/2006; Directive 2008/105/2008) were below the MAC limits (maximum allowed concentrations), only part of the measurements exceeding MAC. Higher values of Cu were found in the port area and treatment plants. Cu and Pb showed a slight increase in 2011, contrary to the lowered levels of cadmium.

Usually high concentrations of heavy metals are recorded in sediments from areas under anthropogenic impact: ports and wastewater treatment plants. The average concentrations calculated for the coastal zone (0 – 20 m) did not

exceed MAC, but in the sediments from transitional and marine areas were registered average values of Cu, Cd and Ni which exceeded MAC. Close to the Danube River, treatment plants and harbors, all concentrations of heavy metals in sediments were above MAC. Taking into account these aspects, marks for the impact assessment according to RIAM method were awarded. According to these results for the environmental component *water* in 2010 resulted a negative impact, a moderate negative impact in 2011, noting an improvement in 2012 when, as evaluated, water status (ES) showed a slight negative impact (Figs. 2 and 3).

The environmental component *sediment* showed a significant negative impact in 2010, a major negative impact in 2011, while the final values of the average scores still showed an improvement in 2012, as presented in Fig. 2.

3.2. Integrated impact and risk assessment results

The application of the integrated impact and risk assessment method (SAB) for the point sources of pollution (S_1 - S_5), considering the same database as for the RIAM method, led to the same result, namely both the environmental impacts and environmental risks were below the score of 100, which means that the environment is not affected by the activities performed at the sources and the environmental risk is insignificant (Fig. 4).

Although the wastewater treatment plants as a whole do not have a significant impact upon the environment (Fig. 4), it was observed that S_3 had a higher score of environmental impact and risk in 2010 and 2011 (Figs. 5a. and 5b.). This can be explained by the fact that the plant was the subject of rehabilitation works (for two years) in order to introduce the tertiary treatment stages that was completed in 2013.

The results of the environmental impact and risk assessment (by SAB) induced by heavy metal pollution in water and sediments from the Romanian

Black Sea coast revealed that the environmental component “*water*” received the importance grade 1 and probability of impact occurrence of 0.5, while “*sediments*” 0.85 for importance and 0.85 for probability. The integrated method applied for the same quality indicators in 2010 showed an environmental impact due to the effects of anthropogenic activities within allowable limits for water; for sediments, the environmental impact suggested an environment severely affected by human activities.

The environmental risk was negligible for water, with an unacceptable risk for sediments. In 2011 the environmental impact increased both for water and sediment, indicating an impact due to human activities causing discomforts to the environment (Fig. 6). For sediments a major risk was quantified, being necessary measures of prevention, control and remediation. This may be explained by the floods from 2010 that had a significant contribution to the pollution in the Danube River basin, in particular, and reflected in the sediments that accumulated heavy metals.

According to the same method (SAB) applied in 2012 for water, the impact values were 100- 350 which suggests that the environment is subject to the effects of human activities within acceptable limits while the environmental risk is negligible (values less than 100) (Fig. 6). For sediments, the impact showed an environment affected by human activities, causing disturbance for different forms of life (values of 500-700), while the calculated risk is like in 2010 (unacceptable environmental risk, being necessary measures of prevention and control).

The impact and environmental risk assessment considering heavy metals as priority pollutants was performed in order to observe the current state of the marine ecosystem. By using the applied matrices, we highlighted the fact that the point sources of pollution (S_1 - S_5) identified on the mainland do not have a significant contribution to heavy metal pollution of water and sediments.

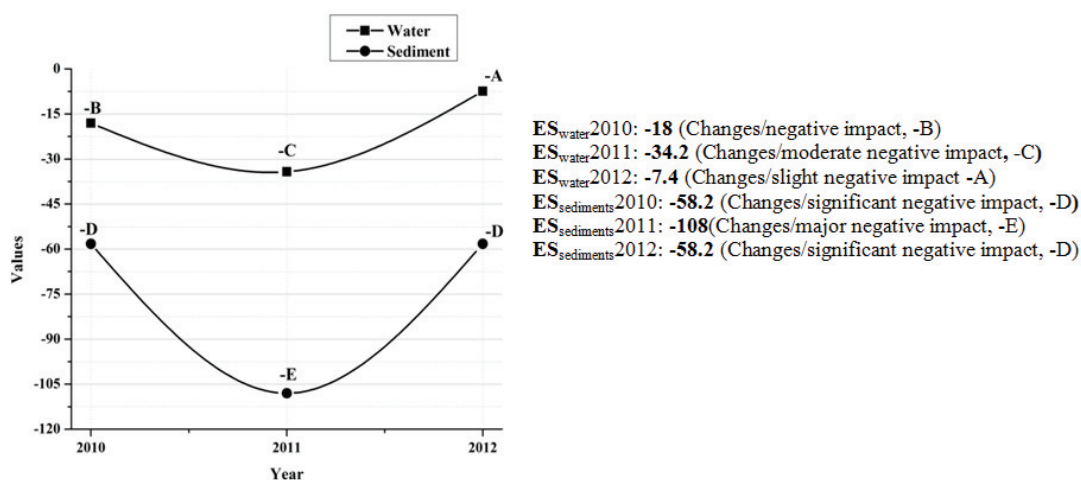


Fig. 2. Environmental scores (ES) for water and sediments from the Romanian Black Sea shore in the years 2010-2012, according to RIAM method

Table 5. The matrix of environmental impact induced by assessed point pollution sources (environmental component *water*)

<i>Pollution source</i>	<i>Year</i>	<i>Quality indicator (i)</i>	A_1	A_2	B_1	B_2	B_3	ES_i	ES_{year}	ES
S ₁	2010	Cd	1	-2	2	1	1	-8	-8.6	-6.67
		Cr	1	-2	2	2	1	-10		
		Ni	1	-2	2	2	1	-10		
		Pb	1	-2	2	2	2	-12		
		Zn	1	-1	1	1	1	-3		
	2011	Cd	1	-1	1	1	1	-3	-4.8	
		Cr	1	-1	1	1	1	-3		
		Ni	1	-1	1	1	1	-3		
		Pb	1	-1	1	1	1	-3		
		Zn	1	-2	2	2	2	-12		
	2012	Cd	1	-1	1	1	1	-3	-6.6	
		Cr	1	-2	2	2	2	-12		
		Ni	1	-1	1	1	1	-3		
		Pb	1	-1	1	1	1	-3		
		Zn	1	-2	2	2	2	-12		
S ₂	2010	Cd	1	-1	1	1	1	-3	-3	-4.05
		Cr	1	-1	1	1	1	-3		
		Ni	1	-1	1	1	1	-3		
		Pb	1	-1	1	1	1	-3		
		Zn	1	-1	1	1	1	-3		
	2011	Cd	1	-1	1	1	1	-3	-3	
		Cr	1	-1	1	1	1	-3		
		Ni	1	-1	1	1	1	-3		
		Pb	1	-1	1	1	1	-3		
		Zn	1	-1	1	1	1	-3		
	2012	Cd	1	-2	2	2	2	-12	-6.17	
		Cr	1	-1	1	1	1	-3		
		Ni	1	-1	1	1	1	-3		
		Pb	1	-1	1	1	1	-3		
		Zn	1	-2	2	2	2	-12		
S ₃	2010	Cr	1	-1	1	1	1	-3	-3.75	-3.64
		Cu	1	-1	1	1	1	-3		
		Zn	1	-1	1	1	1	-3		
		Fe	1	-2	1	1	1	-6		
	2011	Cd	1	-1	1	1	1	-3	-3	
		Cr	1	-1	1	1	1	-3		
		Ni	1	-1	1	1	1	-3		
		Pb	1	-1	1	1	1	-3		
		Zn	1	-1	1	1	1	-3		
	2012	Cd	1	-1	1	1	1	-3	-4.17	
		Cr	1	-1	1	1	1	-3		
		Ni	1	-1	1	1	1	-3		
		Pb	1	-1	1	1	1	-3		
		Zn	1	-2	2	2	1	-10		
S ₄	2010	Cd	1	-1	1	1	1	-3	-3	-4.67
		Cr	1	-1	1	1	1	-3		
		Ni	1	-1	1	1	1	-3		
		Pb	1	-1	1	1	1	-3		
		Zn	1	-1	1	1	1	-3		
	2011	Cd	1	-1	1	1	1	-3	-4.8	
		Cr	1	-2	2	2	2	-12		
		Ni	1	-1	1	1	1	-3		
		Pb	1	-1	1	1	1	-3		
		Zn	1	-1	1	1	1	-3		
	2012	Cd	1	-1	1	1	1	-3	-6.2	
		Cr	1	-2	2	2	2	-12		
		Ni	1	-1	1	1	1	-3		
		Pb	1	-1	1	1	1	-3		
		Zn	1	-2	2	2	1	-10		
S ₅	2010	Cd	1	-1	1	1	1	-3	-5.25	-6.37
		Hg	1	-1	1	1	1	-3		
		Ni	1	-1	1	1	1	-3		
		Pb	1	-2	2	2	2	-12		
	2011	Hg	1	-2	2	2	2	-12	-7.5	
		Ni	1	-2	2	2	2	-12		
		Pb	1	-1	1	1	1	-3		
		Fe	1	-1	1	1	1	-3		

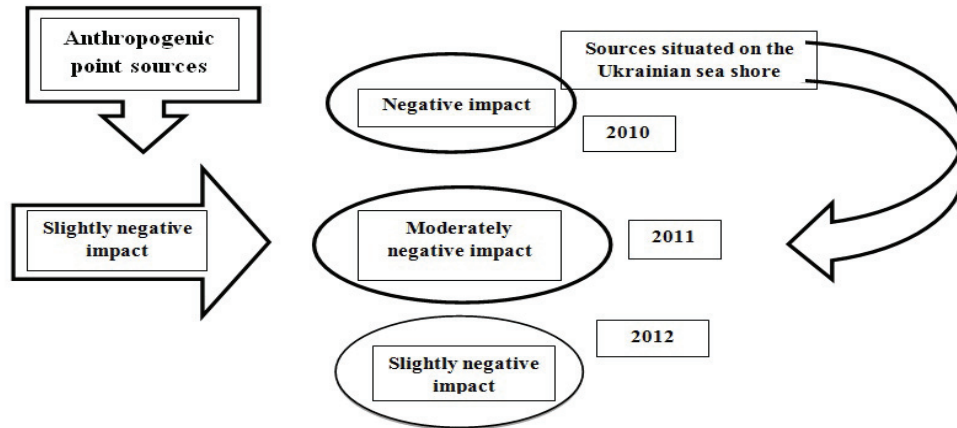


Fig. 3. Graphical representation of environmental impacts induced to water (RIAM method, 2010-2012)

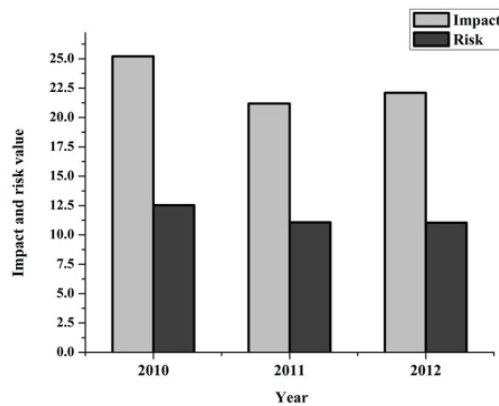


Fig. 4. Graphical representation of the results of the impact assessment and environmental risk by SAB method for the years 2010-2012 for all pollution sources (S1, S2, S3, S4, S5)

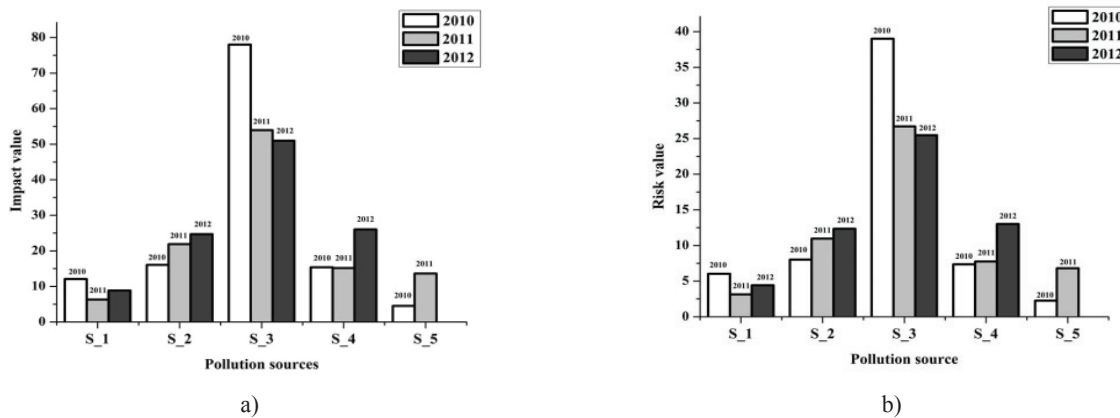


Fig. 5. Graphical representation of the results for: a) impact assessment and b) environmental risk by SAB method for point sources

4. Conclusions

This study was focused on the assessment of the environmental impact and risk on water and sediments, due to heavy metals pollution generated by five point pollution sources of the Romanian Black Sea (S1-S5). This is the first study that analyze and quantifies the integrated impacts and risks caused by

heavy metals in the marine environment through the contribution of each pollution sources based on the monitored quality indicators reported by ABADL and NIMRD institutions, Constanta. To achieve the main goal of this study, two methods were considered for assessing the impact, Rapid Impact Assessment Matrix (RIAM) and the Integrated Quantification of Impact and Risk matrix (SAB).

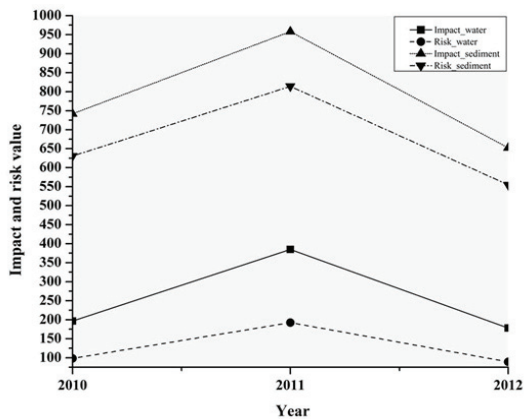


Fig. 6. Graphical representation of the results of environmental impact and risk assessment (SAB method) calculated for environmental components: water and sediment

According to these methods, the point pollution sources (S_1 - S_5) taken into account for the evaluation of the environmental impact and risk do not have a major contribution in terms of heavy metal pollution in the marine environment. Although the wastewater treatment plants do not have significant environmental impacts, it could be observed that S_3 wastewater treatment plant had higher scores for environmental impact and risk in 2010 and 2011, this plant being the subject of rehabilitation works for 2 years.

The results of RIAM method for the environmental component water indicated a negative impact in 2010, a moderate negative impact in 2011 and a noticeable improvement in 2012 when, according to the assessment, the water status (ES) showed a slight negative impact.

By applying the SAB method, in 2010 resulted a significant negative impact for the environmental component “sediments”, the final environmental scores (ES) indicating an improvement for 2012. The SAB method confirmed the results of RIAM method. A significant negative impact due to higher concentrations of heavy metals was observed for sediments, fact which may affect not only benthic organisms, but also the pelagic ones due to the particles re-suspension in the water column. According to the environmental reports there were high concentrations in the sediments from areas under anthropogenic impacts such as harbors and wastewater treatment plants: Constanta South and Mangalia (NRIMD, 2012a; 2012b).

Other sources of pollution of the Black Sea water and sediments should be considered as well. The heavy metals concentrations should not be neglected if the balance of the ecosystem is to be preserved, even if some recorded concentrations were below the MAC levels according to national environmental standards (MO, 2006).

Acknowledgments

This work was supported by a grant of the Romanian National Authority for Scientific Research, CNDI-

UEFISCDI, project no. 60/2012, “Integrated System for Reducing Environmental and Human-related Impacts and Risks in the Water Use Cycle” (WATUSER).

The support of the strategic grant POSDRU/159/1.5/S/133652, co-financed by the European Social Fund within the Sectorial Operational Program Human Resources Development 2007-2013 is also acknowledged.

References

- Burger J., (2008), Environmental management: integrating ecological assessment, remediation, restoration, natural resource damage assessment and long-term stewardship on contaminated lands, *Science of the Total Environment*, **400**, 6-19.
- Buytaert V., Muys B., Devriendt N., Pelkmans L., Kretschmar J.G., Samson R., (2011), Towards integrated sustainability assessment for energetic use of biomass: A state of the art evaluation of assessment tools, *Renewable & Sustainable Energy Reviews*, **15**, 3918-3933.
- Gavrilescu M., (2007), Behaviour of persistent pollutants and risks associated with their presence in the environment – integrated studies, *Environmental Engineering and Management Journal*, **8**, 1517 - 1531.
- GD 188, (2002), Government Decision No. 188/2002 for approving the rules on the conditions of discharging wastewater into the aquatic environment, as amended by HG 352/11.05.2005, *Romanian Official Monitor*, No. 187, 20 March 2002.
- GD 352, (2005), Government Decision No. 352/2005 for modifying Government Decision No. 188/2002 for approving conditions of discharging wastewaters into aquatic environments, *Romanian Official Monitor*, No. 398, 11 May, 2005.
- Ijas A., Kuitunen M. T., Jalava K., (2010), Developing the RIAM method (Rapid Impact Assessment Matrix) in the context of impact significance assessment, *Environmental Impact Assessment Review*, **30**, 82–89.
- INCDM, (2010), State of the Marine and Coastal Environment Report, (in Romanian), On line at: http://www.rmri.ro/Home/Downloads/EnvStatusReport/RaportStareaMediului_2010.pdf.
- INCDM, (2011), State of the Marine and Coastal Environment Report, (in Romanian), On line at: http://www.rmri.ro/Home/Downloads/EnvStatusReport/RaportStareaMediului_2011.pdf.
- INCDM, (2012), Report on the State of the Marine and Coastal Environment in 2012, On line at: <http://www.rmri.ro/Home/Downloads/Publications.RecherchesMarines/2013/paper01.pdf>.
- Iordache V., (2009), *Heavy metals ecotoxicology in Danube Delta*, Ars Docendi Editure.
- Jitar O., Teodosiu C., Nicoara M., Plavan G., (2012), Study of heavy metal pollution and bioaccumulation in the black sea living environment, *Environmental Engineering and Management Journal*, **12**, 271 – 276.
- Jitar O., Teodosiu C., Oros A., Plavan G., Nicoara M., (2014), Bioaccumulation of heavy metals in marine organisms from the Romanian sector of the Black Sea, *New Biotechnology*, <http://dx.doi.org/10.1016/j.nbt.2014.11.004>.
- Kiss A., Shelton D., (2007), *Guide to International Environmental Law*, Martinus Nijhoff Publishers, Leiden/Boston, 190-191.

- Kuitunen M., Jalava K., Hirvonen K., (2008), Testing the usability of the Rapid Impact Assessment Matrix (RIAM) method for comparison of EIA and SEA results, *Environmental Impact Assessment Review*, **28**, 312-320.
- Lexer W., Paluchova K., Schwarz L. B., (2006), Risk Assessment D 3.2 Report WP 3, ÖIR – Austrian Institute for Regional Studies and Spatial Planning, Vienna, Austria.
- MO, (2006), Norms on surface water quality classification in order to establish the ecological status of water bodies, Order no. 161 of 16 February 2006, Ministry of Environmental and Water Management.
- Mondal M.K., Rashmib, Dasgupta B.V., (2010), EIA of municipal solid waste disposal site in Varanasi using RIAM analysis, *Resources, Conservation and Recycling*, **54**, 541–546.
- NRIMD, (2012a), Initial assessment of the marine environment, National Research Institute - Marine Development "Grigore Antipa" Constanța, On line at: http://www.mmediu.ro/beta/wp-content/uploads/2012/07/2012-07-17_evaluare_impact_planuri_evaluareinitialamediumarin.pdf.
- NRIMD, (2012b), Determination of good environmental status for the Romanian Black Sea waters, National Research Institute - Marine Development "Grigore Antipa" Constanta, On line at: http://www.mmediu.ro/beta/wpcontent/uploads/2012/07/2012-07-17_evaluare_impact_planuri_determinarestareecobunamareaneagra.pdf.
- Pastakia C.M.R., (1998), *The rapid impact assessment matrix (RIAM) — a new tool for environmental impact assessment*, In: *Environmental impact assessment using the rapid impact assessment matrix (RIAM)*, Jensen K. (Ed.), Fredensborg: Olsen & Olsen, 8-18.
- Pastakia C.M.R., Jensen A., (1998), The rapid impact assessment matrix (RIAM) for EIA, *Environmental Impact Assessment Review*, **18**, 461–82.
- Robu B., Petruc V., Macoveanu M., (2005), Integrated environmental impact and risk assesement of emissions resulted from oil distribution, *Environmental Engineering and Management Journal*, **4**, 499-513.
- Robu B., Macoveanu M., (2005), *Integration of risk assessment into environmental impact assessment procedure-case study for steel processing*, Proceedings of the 9th International Conference on Environmental Science and Technology, Rhodes Island, Greece, 1-3 September, A-1262-A-1267.
- Robu B.M., Caliman F.A., Betianu C., Gavrilesco M., (2007), Methods and procedures for environmental risk assessment, *Environmental Engineering and Management Journal*, **6**, 573-592.
- Robu B., Macoveanu M., (2010), *Environmental Assessments for sustainable development*, Ecozone Publishing House, Iasi, 148-200.
- Singh R.K., Murty H.R., Gupta S.K., Dikshit A.K., (2012), An overview of sustainability assessment methodologies, *Ecological Indicators*, **15**, 281-299.
- Ștefănescu L., Constantin V., Surd V., Vlad S., Ozunu A., Vlad S., (2011), Assessment of soil erosion potential by the USLE method in Rosia Montana mining area and associated NATECH events, *Carpathian Journal of Earth and Environmental Sciences* **6**, 35-42.
- Suditu G.D., Robu B.M., (2012), Digitization of the environmental impact quantification process, *Environmental Engineering and Management Journal*, **11**, 841-848.
- Teodosiu C., Bârjoveanu G., Robu B., Ene S.A., (2012), Sustainability in the water use cycle: challenges in the Romanian context, *Environmental Engineering and Management Journal*, **11**, 1987-2000.
- Teodosiu C., Robu B., Cojocariu C., Barjoveanu G., (2015), Environmental impact and risk quantification based on selected water quality indicators, *Natural Hazards*, **75**, S89–S105,
- Toro J., Requena I., Duarte O., Zamorano M., (2013), A qualitative method proposal to improve environmental impact assessment, *Environmental Impact Assessment Review*, **43**, 9–20.
- Upham P., Smith B., (2013), Using the Rapid Impact Assessment Matrix to synthesize biofuel and bioenergy impact assessment results: the example of medium scale bioenergy heat options, *Journal of Cleaner Production*, **30**, 1-9.



“Gheorghe Asachi” Technical University of Iasi, Romania



INFLUENCE OF EXTRACTION METHODS ON CARAWAY (*Carum carvi* L.) ESSENTIAL OIL YIELD AND CARVONE/LIMONENE RATIO

Csaba Dezső András^{1*}, Rozália Veronika Salamon¹, Imola Barabás¹,
Irina Volf², Alexandru Szép¹

¹Sapientia Hungarian University of Transylvania, Faculty of Sciences, Department of Food Science,
1 Libertății Square, 530104 Miercurea Ciuc, Romania

²Gheorghe Asachi Technical University Iași, Faculty of Chemical Engineering and Environmental Protection,
Department of Environmental Engineering and Management, 73 Prof. Dr. Docent D. Mangeron Str., 700050 Iasi, Romania

Abstract

The caraway (*Carum carvi* L.) samples were collected from little meadows situated in Harghita Mountain (Mădăraș Ciuc, Harghita Băi, Jigodin, Tușnadu Nou), where a relatively small area was covered by a group of rich populations of wild cumin. The harvested plants are dried by: a) convective laboratory dryer in thick layer, b) static outdoors in sunshine, and (c) static in a warm indoor place in darkness. The hand-picked seeds were separated from debris by sieving and elutriation. The essential oil was obtained with electrically heated Clevenger-type laboratory steam distillation equipment both with and without microwave pretreatment. The variation of the obtained essential oil volume in time was measured and the final yield was determined. For comparison the composition, supercritical fluid extraction of the caraway essential oil with carbon dioxide in a laboratory scale batch supercritical extractor was made. Each sample was analyzed by gas chromatography, following the influence of drying and extraction method on the carvone/limonene ratio. The investigation shows that the essential oil yield is around 7 mL/100 g, less in the case of green plant (6 mL/100 g) and higher in case of the mature plant (10 mL/100 g). The results show that by batch supercritical fluid extraction with CO₂ (at first purge) lowest carvone/limonene ratio was obtained.

Key words: caraway, essential oil, hydrodistillation, supercritical fluid extraction

Received: November, 2014; Revised final: February, 2015; Accepted: February, 2015

1. Introduction

The wild caraway (*Carum carvi* L.) is a well-known spice belonging to Apiaceae family, raw material for food aroma and for pharmaceutical industry (Bernáth, 2000; Csedő, 1980; Sváb, 1992). The caraway is widely used in ethnopharmacology (Johri, 2011), given by effects of their bioactive compounds, namely, the essential oil components.

The health-beneficial properties included carminative (Madisch, 2004), intestinal spasmolytic (Csedő, 1980), antiseptic (i.e. against *Escherichia coli* and *Staphylococcus aureus* (Bonyadian and

Karim, 2002; Seidler-Łożykowska et al., 2013)), antimycotic (Grigore et al., 2012) and antiasthmatic effects (Haggag et al., 2003). Recently, pronounced antiulcerogenic gastroprotective effect of the essential oil extracted with supercritical carbon dioxide was demonstrated (Baananou et al., 2013). The caraway extracts (in special their main components) are used in environmental-friendly organic pest control and vegetable product storage. The insect repellent effect is demonstrated, S-carvone is antisprouting and antifungal agent used in potato storage (de Carvalho et al., 2006; Oosterhaven et al., 1995; Toxopeus and Bouwmeester, 1993). The whole

* Author to whom all correspondence should be addressed: e-mail: csandrasd@gmail.com; Phone: 0745610174

essential oil is effective against crown gall disease of plants (El-Zemity, 2008), caused by *Rhizobium radiobacter* (formerly known as *Agrobacterium tumefaciens*). The essential oil content of the caraway seed has a wide variability: for annual variety are about 2.5% for biennial variety reach even exceed 7% (Bernáth, 2000; Csedő, 1980), and for wild caraway may reach 6.5-7.5 mL/100 g dry material, even higher, about 9-11 mL/100 g dry material (Bouwmeester, 1998; Csedő, 1980).

The factors involved in the essential oil content and composition are: the characteristics and the tillage of soil, the annual precipitation and fertilization amount, breeding, the maturation, harvesting, drying and the extraction technologies (Kolta and Hornok, 1992), and even the microelement content (heavy metals) of the soil (Abu-Darwis and Ofir, 2014). The main quality criterion for caraway essential oil is the carvone/limonene ratio (Kallio et al., 1994; Sedláková et al., 2003), which is variable during ripening. In green, immature seeds the limonene concentration is higher (Chizolla, 2014). The antimicrobial activity of the essential oil is given by its composition, the higher carvone content results the rising of antimicrobial effect (Seidler-Łożykowska et al., 2013). Having antioxidant and antimycotic activity, the essential oil could be used as natural preservative in bakery products containing fats (Darougheh et al., 2014).

The aim of the research is the study of the effects of pretreatment and extraction methods on wild caraway essential oil yield and composition for plant probes from different geographical locations. As the kinetic of the extraction process is an important factor from technological point of view (Ciubota-Roşie et al., 2009) also the kinetic data was represented and a model was fitted.

2. Materials and methods

The wild caraway probes were collected in time period of 2012-2014. The geographical location of the collection point was Mădăraş-Ciuc, Băile Harghita, Jigodin and Tuşnadul Nou (Harghita County). The plant material harvested together with stem was firstly sorted, separating the green and mature shoots, and then it was dried. The seed was picked out and was purified further by sieving and elutriation of the powder-like debris. The such-obtained seeds were stored in a dry place till the extraction of the samples was performed. The seed was ground with Retsch Grindomix GM 200 laboratory scale knife mill, with different milling time, at room temperature. The plant material was dried by three different methods: a) drying in free space; b) drying in closed, cold and dark space; c) convective laboratory drying of the freshly picked seeds. The extraction of the essential oil of the dried (to the equilibrium moisture) caraway seed probes was made by the following, environmentally friendly (so called “green”) extraction methods, without

solvent residues and artefacts (András et al., 2002; Chemat et al., 2013; Sovová et al., 2006; Sovová and Stateva, 2011).

Hydrodistillation (HD): The laboratory-scale hydrodistillation apparatus, described in European Pharmacopoeia (EDQM, 2014), contains 500 mL volume round-bottom flask connected to a slightly modified Clevenger-head (Kapás et al., 2011), capillary collector tube with 1.5 mL (0.01 mL scaling), electric heating power $P=125$ W. Each probe was an amount of 10 g solid suspended in 200 mL distilled water. The heating power was $P=125$ W.

Steam distillation (SD): The steam was generated by electric heating mantle from a 250 mL volume round-bottom flask containing distilled water. The plant material (in 10 g amount) was packed in a glass tube connected to steam generator. The steam leaving the column was condensed in a heat exchanger, and the formed two phases was separated in the Clevenger-head.

Microwave hydrodistillation (MWHd) (Chemat et al., 2013; Kapás et al., 2011): the round-bottom flask containing 200 mL distilled water and 10 g of caraway seed powder in suspension was introduced in a modified domestic microwave oven (Hinari S110) and a Clevenger-head was attached. The hydrodistillation was performed 30 minutes, with heating power of $P=125$ W.

Hydrodistillation with microwave pretreatment (HDMP) (Navarrete et al., 2011): the round-bottom flask containing 200 mL distilled water and 10 g of caraway seed powder in suspension was introduced in a modified domestic microwave oven (Hinari S110) and a reflux condenser was attached, to recycling the steam containing the released essential oil from the plant matrix.

Supercritical fluid extraction (SFE) (András et al., 2002; Sovová et al., 1994; Sovová and Stateva, 2011): The extraction was made with food-grade (99,99% purity) carbon dioxide (Linde, Romania) using SFT 100 laboratory scale extraction apparatus (Supercritical Fluid Technology, Inc., Newark, USA) represented on Fig. 1.

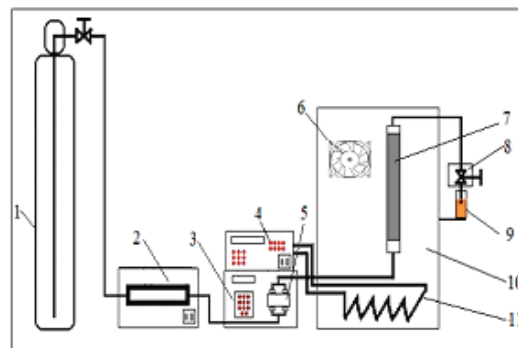


Fig. 1. Schematic representation of the laboratory scale supercritical fluid extraction apparatus (1. Tank of liquid CO₂ with a siphon tube; 2. Peltier-cooler; 3. Pump command module; 4. Command module of the heater; 5. High pressure piston pump; 6. Cooler ventilator; 7. Tubular extraction vessel; 8. Depressurization/restrictor valve; 9. Probe collector; 10. Isothermal oven; 11. Heater resistor)

The apparatus was equipped with a tubular extraction vessel with an effective volume of 10 mL. The extraction was performed batchwise, using extraction parameters $T=40$ °C, and pressure over $p=100$ atm. The condensed essential oil probes were collected from the heated restrictor valve at 42 °C in a glass vial, by purging the extractor content at different moments (purging time was 1 minutes).

3. Qualitative analysis and data processing

The composition (in relative mass percentage) of the essential oil was performed by gas chromatography. For dehydration of the obtained essential oil, anhydrous sodium sulfate was added (Sigma Aldrich) and the probes was stored in sealed glass vials at 2 °C until analysis. In the injected probe ($V=1$ µl) the essential oil was diluted in amount of 1:15 (V/V) with chromatographic grade n-hexane (Sigma Aldrich).

The measurement was made with a Varian CP-3380 gas chromatograph equipped with flame ionization detector (GC-FID). The setting parameters and chromatographic conditions was the same for the each probes, as follows: quartz-capillary column 100×0.25 mm CP-Sil88 (FAME) film-coated stationary phase; Injector and detector temperature: 270 °C; Carrier gas: H_2 at $p=235$ kPa. Heat gradient program: heating to 50 °C in 1 minute; heating with 5 °C/minute gradient to 250 °C. For component peaks identification, a reference chromatogram was used (Kubeczka, 2002). The data analysis was made with Excel (Microsoft, Redmond, USA) and Statistica 8 (Statsoft, Inc., Tulsa, USA).

4. Results and discussion

4.1. The effect of pretreatment and extraction methods on essential oil yield

The yield of the hydrodistillation-obtained essential oil from dried and ground caraway seed was represented on two types of diagrams. On first type of diagrams the yield (V , mL oil/100 g dry matter) variation in time (minutes), on the second type, a linearized function, and the natural logarithm of the relative yield variation ($\ln(1-V/V_0)$) vs. distillation time (τ , min) was represented. As can be seen on Fig. 2, the drying method has little effect on the distillation kinetic. The yield was nearly the same for the three drying method. The effect of grinding times on yield can be observed on Fig. 3 (caraway from Mădăraş).

The kinetic of the essential oil hydrodistillation is well described for many plant materials by the simple, one-term, two parameter exponential model (Kapás et al., 2011; Milojević et al., 2008; Milojević et al., 2013), given by the Eq. (1), where: V_0 - final (maximum) yield (mL/100 g dry matter); V - current yield (mL/100 g dry matter); τ - distillation time (minute); A - integration constant;

k - kinetic constant (minute⁻¹), including the effective diffusion coefficient. The initial distillation rate is given by the Eq. (2).

$$\frac{V_0 - V}{V_0} = A \cdot e^{-k\tau} \quad (1)$$

$$w_0 = \left. \frac{dV}{d\tau} \right|_{\tau=0} = V_0 \cdot A \cdot k \quad (2)$$

Using nonlinear regression, (Statistica 8, quasi-Newton estimation method), the kinetic curves was fitted on experimental points and the kinetic parameters will be obtained for different grinding time. For every case, the value of integration constant A (with the physical mean of remained relative amount of essential oil at the initial moment) was very close to unity. The highest initial distillation rate (0.803 mL/(100 g.min)) and highest yield (8.3 mL/100 g) was obtained at the grinding time of 15 s.

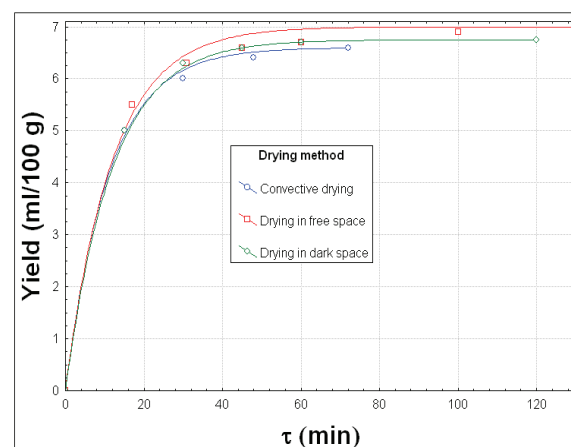


Fig. 2. The effect of drying method on essential oil yield (caraway from Jigodin, ground for 30 s)

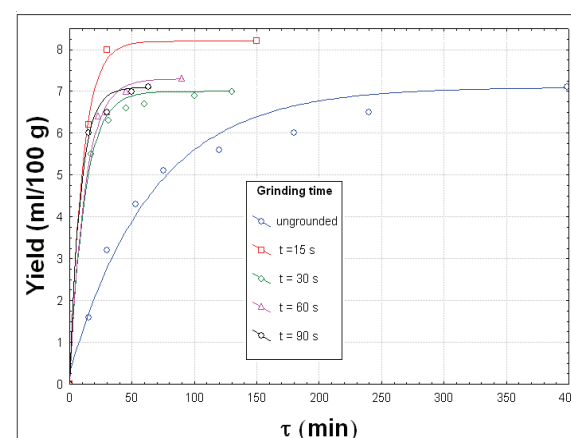


Fig. 3. The effect of grinding time on essential oil yield (ripe caraway dried on free surface, from Mădăraş)

For increased grinding times (30, 60 and 90 s) the initial rate increase (from 0.582 to 0.824 mL/(100 g.min)), but the final yields was close to the value for whole seeds (7.1 mL/100 g). In contrast, the

hydrodistillation of ungrounded seeds was much slower (0.103 mL/(100 g.min)) and the depletion time is more than double and half in comparison with grounded seeds. This behavior is due by two contrary effects. At long grinding time the particle size decrease and the internal diffusion (the velocity determining process) increase, but the increasing temperature cause higher essential oil loss.

By linearization of the Eq. (1) and imposing for A to be equal with unity, the kinetic data vs. distillation time is presented on Fig. 4. The extraction rate was described satisfactory by the two parameter semi-empirical model for HD, MWHD and HDMP of grounded and ungrounded seeds both. Slightly modifying the model, we included the effect of the grinding time. The kinetic constants were further represented in function of grinding time in interval of 30-90 s; a linear regression was made (Fig. 5).

The chosen hydrodistillation model (Eq. 3), with the fitted parameters describes close enough the effect of grinding and distillation time both. To find the optimum grinding time, more experiments are needed.

$$\eta = \frac{V}{V_0} = 1 - e^{-(0.0008t+0.027)\tau} \quad (3)$$

where: η - relative yield; V - current yield (mL/100 g dry matter); V_0 - final yield (mL/100 g dry matter); t - grinding time (s); τ - distillation time (minute).

The fitted equation reflects well the negative effect of the grinding time on essential oil yield. The obtaining methods have more pronounced influence on the yield in comparison with drying method and grinding time (Fig. 6). The rate of the MWHD was the highest, whilst of the HDMP the lowest. The pretreatment with intermittent microwave heating give lower yield, probable due by imbalance between the momentary high steam production during the heating period, and the moderate capacity of the applied condenser. The high loss of essential oil may produce by this effect.

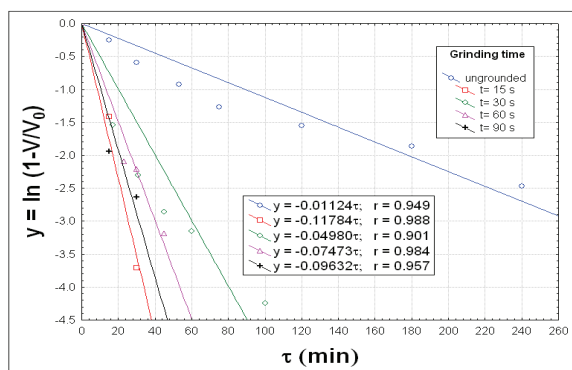


Fig. 4. The validation of the distillation model in function of grinding time ripe caraway from Mădăraș)

Comparing the maximal yields obtained for caraway probes collected from different growing area, harvested years and ripe stage (Fig. 7), it can be

seen that the environmental conditions, the maturation status and growing location have an effect on the essential oil contents.

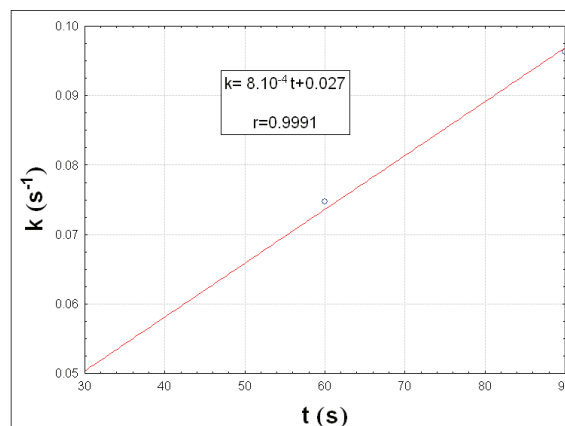


Fig. 5. The correlation between the kinetic constant and grinding time (ripe caraway from Mădăraș)

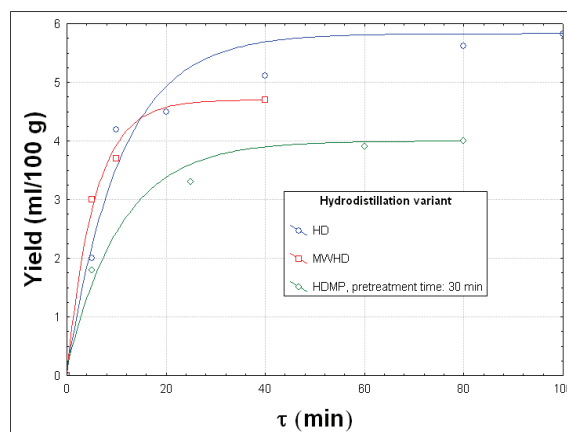


Fig. 6. The effect of distillation method on essential oil yield (caraway collected from Harghita Băi, 2013)

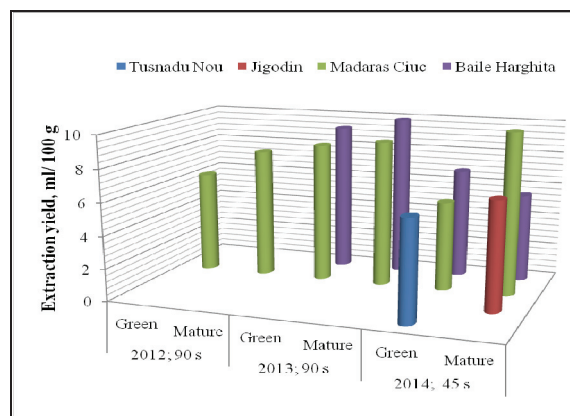


Fig. 7. The maximal hydrodistillation yield in function of growing area and harvesting year

As can be seen from Fig. 7, the meteorological conditions was favorable for caraway in year 2013, for Mădăraș and Harghita Băi growing sites both, since the essential oil yield of the picked seeds approximate the high value of 10 mL/100 g dry matter.

4.2. The effect of pretreatment and extraction methods on the essential oil yield and the ratio of the two main compounds

The pretreatment had the purpose to deteriorate or decompose the plant cellulosic matrix, to enhance the liberation of the volatile compounds by increase the internal diffusion coefficient. By microwave treatment at moderate pressure and dilute acid condition even the hydrolysis occur (Balcu et al., 2009). At atmospheric pressure only the microexplosion of the water-containing plant structures should be considered. This phenomenon was demonstrated by electron microscopic imaging technique (Chemat et al., 2005).

The main quality criterion for caraway essential oil is the carvone/limonene ratio, we determined the composition of the essential oil and studied the variation of the ratio of the two main components. The carvone/limonene ratio is very similar for laboratory convective dried (51.5/47.9) and for overripe caraway (50.3/47.9) and higher for free space dried caraway seeds (58.4/39.3) as seen on Fig. 8.

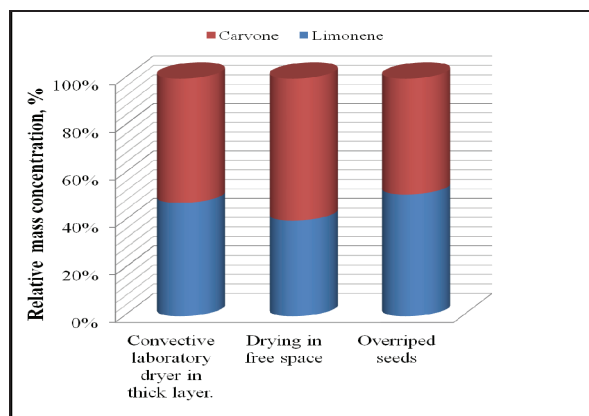


Fig. 8. The effect of pretreatment method on carvone/limonene ratio in the obtained essential oil (caraway from Mădăraș, 2012)

Fig. 9 show that in two cases (HD and MWHD obtained essential oil) the carvone/limonene ratio of was very similar for caraway from Mădăraș location. The microwave pretreatment increase the proportion of the less volatile component (carvone), but, parallel, the total essential oil yield decrease too. This is probable due by the insufficient cooling surface of the condenser. For hydrodistillation variants (HD, SD, HDMP, MWHD) the same trends are observable (Fig. 10). In case of SFE, when high volatile component are extracted, relatively low temperature (40 °C), slightly above the critical value (31.1 °C) and low pressures (in order of 10 MPa) should be used. By this way we assure high selectivity and low solvating power of the supercritical solvent (Marcus, 2006).

This is necessary to avoid the co-extraction of fatty oils and waxes (Kallio et al., 1994; András et al., 2002). With the increasing extraction pressure (up to approx. 207 bar), the limonene amount in the

extract increase. This result is in a good agreement with the literature data (András et al., 2002; Baysal and Starman, 1999; Cabizza et al., 2001; Sovová et al., 1994). The results of SFE experiments showed (Figs. 10 and 11) that independently from the applied pressure, the limonene content of the drained extract decrease with the number of purges.

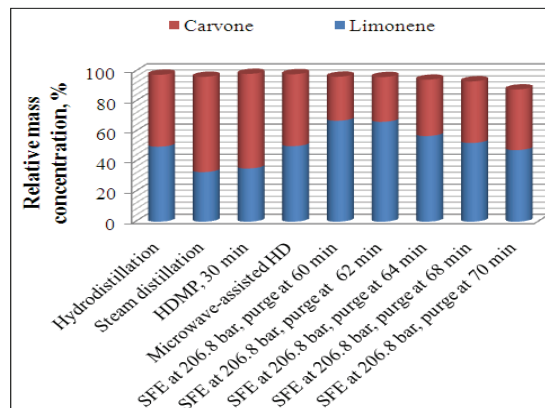


Fig. 9. The effect of obtaining method on carvone/limonene ratio of the essential oil (caraway from Harghita Băi, 2013)

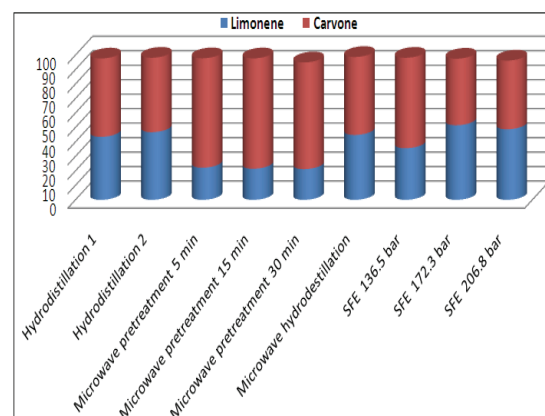


Fig. 10. The effect of extraction method on carvone/limonene ratio (caraway from Mădăraș, 2012)

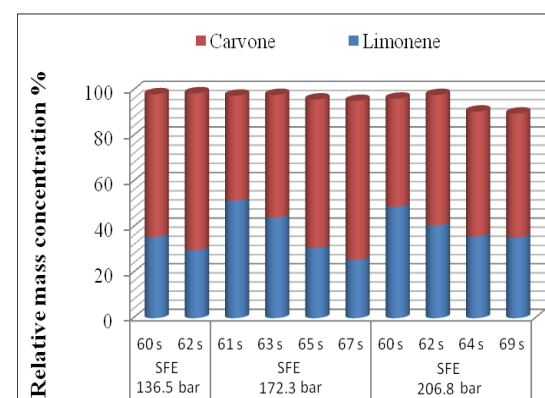


Fig. 11. The effect of pressure and purging time on carvone/limonene ratio in the SFE-obtained essential oil (caraway from Harghita Băi, 2013)

This may be explained with the higher solubility of limonene in supercritical CO₂. The

lower carvone/limonene ratio in case of SFE (first purge) in comparison with SD and MWHD is explained by two facts.

Firstly the solubility of limonene in supercritical CO₂ is higher than the carvone solubility (Sovová et al., 2001) and the easier desorption from the plant matrix of the limonene, comparative to more polar carvone with higher molecular mass. Secondly, despite of the lower boiling point of the limonene comparison with the carvone, given the higher polarity of the carvone, the rate of dissolution in the water is higher. The boiling water penetrate the plant matrix, dissolve some substances, including the essential oil components, too, then the solution diffuse backward through plant matrix in the water pool, this phenomenon is known as hydrodiffusion (Chemat et al., 2006). By this mechanism the amount of the carvone in the formed steam will be higher.

5. Conclusions

The drying methods have the lowest effect on yield comparative with grinding and the extraction modes. The highest yield was obtained with the HD, followed by MWHD and batchwise SFE. The microwave pretreatment decrease the hydrodistillation yield (for the high essential oil containing green and ripe caraway seeds, both), but the carvone/limonene ratio increased.

The quality of the essential oil expressed in the carvone/limonene ratio varies in function of obtaining method. Although the essential oil obtained by SD and MWHD show similar carvone/limonene ratio, this ratio is different for HDMP and SFE function of operation parameters and processing time;

In case of SFE, with pressure increase, the limonene amount increase in the first purge. In the drained extracts obtained by further purges, independently from the extraction pressure, the carvone/limonene ratio increase;

The maximal essential oil yields have high influence the growth location as well as the environmental and meteorological conditions. The highest yield (approx. 10 mL/100 g dry matter) was obtained for the probes harvested in year 2013 (for Mădăraş- and Harghita Băi-harvested caraway). To elucidate the exact correlation between the essential oil content and the meteorological factors, further, more detailed multiannual observation is needed.

References

Abu-Darwish M.S., Ofir R., (2014), Heavy metals content and essential oil yield of *Juniperus phoenicea* L. in different origins in Jordan, *Environmental Engineering and Management Journal*, **13**, 3009-3014.

András C.D., Simándi B., Farsang R., Hamucska K., Héthelyi B.É., Domokos J., Deák A., (2002), The extraction of caraway (*Carum carvi* L.) seeds with supercritical carbon dioxide (in Hungarian), *Journal of Oil Soap Cosmetics*, **51**, 64-68.

Balcu I., Segneanu A.E., Mirica M.C., Iorga M.I., Macarie C., Martagiu R., (2009), Microwave effects in biomass hydrolysis, *Environmental Engineering and Management Journal*, **8**, 741-746.

Baananou S., Bagdonaite E., Marongiu B., Piras A., Porcedda S., Falconeri D., Boughattas N., (2013), Extraction of the volatile oil from *Carum carvi* of Tunisia and Lithuania by supercritical carbon dioxide: Chemical composition and antiulcerogenic activity, *Natural Product Research*, **27**, 2132-2136.

Baysal T., Starmans D.A.J., (1999), Supercritical carbon dioxide extraction of carvone and limonene from caraway seed, *Journal of Supercritical Fluids*, **14**, 225-234.

Bernáth J., (2000), *Medicinal and Aromatic Plants 3rd edition* (in Hungarian), Mezőgazda Kiadó, Budapest, 230-235.

Bonyadian M., Karim G., (2002), Study of the effects of some volatile oils of herbs (pennyroyal, peppermint, tarragon, caraway seed and thyme) against *E. coli* and *S. aureus* in broth media, *Journal of the Faculty of Veterinary Medicine, University of Teheran*, **57**, 81-83.

Bouwmeester H.J., (1998), *Regulation of Essential Oil Formation in Caraway*, In: *Caraway. The Genus Carum*, Németh É. (Ed.), Harwood Academic Publisher, Amsterdam, 83-101.

Cabizza M., Cherchi G., Marongiu B., Porcedda S., (2001), Isolation of a volatile concentrate of caraway seed, *Journal of Essential Oil Research*, **13**, 371-375.

de Carvalho C.C.C.R., da Fonseca M.M.R., (2006), Carvone: Why and how should one bother to produce this terpene, *Food Chemistry*, **95**, 413-422.

Chemat F., Abert-Vian M., Fernandez X., (2013), *Microwave-assisted Extraction of Essential Oils and Aromas*, In: *Microwave-assisted Extraction for Bioactive Compounds. Theory and Practice*, Chemat F., Cravotto G. (Eds.), Springer Science + Business Media, New York, 53-68.

Chemat F., Lucchesi E.M. (2006), *Microwave-assisted Extraction of Essential Oils*, In: *Microwaves in Organic Synthesis, 2nd ed.*, vol. 2, Loupy A. (Ed.), Wiley-VCH Verlag GmbH & Co. KGaA, Weinheim, 959-983.

Chemat S., Ait-Amar H., Lagha A., Esveld C.D., (2005), Microwave-assisted extraction kinetics of terpenes from caraway seeds, *Chemical Engineering and Processing*, **44**, 1320-1326.

Chizolla R., (2014), Composition of the essential oil of the wild grown caraway in meadows of the Vienna region (Austria), *Natural Product Communications*, **9**, 581-582.

Csedő K., (1980), *Medicinal Plants from Harghita County* (in Hungarian), UJCOOP, Tipografia Tg. Mureş, 188-194.

Ciubotă-Roşie C., Diaconescu R., Volf I., Macoveanu M., (2009), Modeling the extraction process of the oil from the seeds of white mustard (*Sinapis alba*), *Environmental Engineering and Management Journal*, **8**, 1429-1432.

Daroughheh F., Barzegar M., Sahari M.A., (2014), Antioxidant and anti-fungal effect of caraway (*Carum carvi* L.) essential oil in real food system, *Current Nutrition & Food Science*, **10**, 70-76.

El-Zemity K., (2008), Antibacterial screening of some essential oils, monoterpenoids and novel N-methyl carbamates based on monoterpenoids against *Agrobacterium tumefaciens* and *Erwinia carotovora*, *Archives of Phytopathology and Plant Protection*, **41**,

- 451-461.
- EDQM, (2014), *Essential Oils in Herbal Drugs* (Monograph 2.8.12.), In: *European Pharmacopoeia (Ph. Eur.)*, 8th Edition, Strasbourg, 273-274.
- Grigore A., Colceru-Mihul S., Paraschiv I., Nița S., Christof R., Iuksel R., Ichim M., (2012), Chemical analysis and antimicrobial activity of indigenous medicinal species volatile oils, *Romanian Biotechnological Letters*, **17**, 7620-7627.
- Haggag E.G., Abou-Moustafa M.A., Boucher W., Theoharides T.C., (2003), The effect of a herbal water extract on histamine release from mast cells and on allergic asthma, *Journal of Herbal Pharmacotherapy*, **3**, 41-54.
- Johri R.K., (2011), *Cuminum cyminum* and *Carum carvi*: An update, *Pharmacognosy Review*, **5**, 63-72.
- Kallio H., Kerrola K., Alhoniemi P., (1994), Carvone and limonene in caraway fruits (*Carum carvi* L.) analyzed by supercritical carbon dioxide extraction-gas chromatography, *Journal of Agricultural and Food Chemistry*, **42**, 2478-2485.
- Kapás A., András C.D., Dobre T.G., Vass E., Székely G., Stroescu M., Lányi S., Ábrahám B., (2011), The kinetic of essential oil separation from fennel by microwave assisted hydrodistillation (MWH), *UPB Scientific Bulletin, Series B: Chemistry and Materials Science*, **73**, 113-120.
- Kolta R., Hornok L., (1992), *Extraction processes for essential oils*, In: *Cultivation and Processing of Medicinal Plants*, Hornok L. (Ed.), John Wiley & Sons, Chichester, 93-104.
- Kubeczka K.H., Formacek V., (2002), *Essential Oil Analysis by Capillary Gas Chromatography and Carbon-13 NMR Spectroscopy*, John Wiley & Sons, Chichester, 37-40.
- Madisch A., Holtmann G., Mayr G., Vinson B., Hotz J., (2004), Treatment of functional dyspepsia with a herbal preparation, *Digestion*, **69**, 45-52.
- Marcus Y., (2006), Are solubility parameters relevant to supercritical fluids?, *Journal of Supercritical Fluids*, **38**, 7-12.
- Milojević S.Ž., Stojanović T.D., Palić R., Lazić M.L., Veljković V.B., (2008), Kinetics of distillation of essential oil from comminuted ripe juniper (*Juniperus communis* L.) berries, *Biochemical Engineering Journal*, **3**, 547-553.
- Milojević S.Ž., Radosavljević D.B., Pavićević V.P., Pejanović S., Veljković V.B., (2013), Modeling the kinetics of essential oil hydrodistillation from plant materials, *Hemijaska Industrija*, **67**, 843-859.
- Navarrete A., Wallraf S., Mato R.B., Cocero M.J., (2011), Improvement of essential oil steam distillation by microwave pretreatment, *Industrial and Engineering Chemistry Research*, **50**, 4667-4671.
- Oosterhaven K., Poolman B., Smid E.J., (1995), S-Carvone as a natural potato sprout inhibiting, fungistatic and bacteristatic compounds, *Industrial Crops and Products*, **4**, 23-31.
- Sedláková J., Kocourková B., Lojtková L., Kubáň V., (2003), Determination of essential oil content in caraway (*Carum carvi* L.) species by means of supercritical fluid extraction, *Plant, Soil and Environment*, **49**, 277-282.
- Seidler-Łożykowska K., Kędzia B., Karpińska E., Bocianowski J., (2013), Microbiological activity of caraway (*Carum carvi* L.) essential oil obtained from different origin, *Acta Scientiarum Agronomy*, **35**, 495-500.
- Sovová H., Komers R., Kučera J., Jež J., (1994), Supercritical carbon dioxide extraction of caraway essential oil, *Chemical Engineering Science*, **49**, 2499-2505.
- Sovová H., Stateva R.P., Galushko A.A., (2001), Essential oils from seeds: solubility of limonene in supercritical CO₂ and how it is affected by fatty oil, *Journal of Supercritical Fluids*, **20**, 113-129.
- Sovová H., Aleskovski S.A., Bocevska M., Stateva, R.P., (2006), Supercritical fluid extraction of essential oils - Results of joint research, *Chemical Industry and Chemical Engineering Quarterly*, **12**, 168-174.
- Sovová H., Stateva R.P., (2011), Supercritical fluid extraction from vegetable materials, *Reviews in Chemical Engineering*, **27**, 79-156.
- Sváb J., (1992), *Caraway*, In: *Cultivation and Processing of Medicinal Plants*, Hornok L. (Ed.), John Wiley & Sons, Chichester, 154-159.
- Toxopeus H., Bouwmeester H.J., (1993), Improvement of caraway essential oil and carvone production in The Netherlands, *Industrial Crops and Products*, **1**, 295-301.



“Gheorghe Asachi” Technical University of Iasi, Romania



CATALYTIC AND NON-CATALYTIC PYROLYSIS OF BIOLOGICALLY TREATED MANURE

Maria Fernandez-Lopez¹, Maria Magdalena Parascanu², Diego López-González³,
Gabriela Soreanu^{2*}, Antonio Avalos-Ramírez⁴, Paula Sanchez¹,
Jose Luiz Valverde¹, Luz Sanchez-Silva^{1*}

¹University of Castilla-La Mancha, Department of Chemical Engineering, Avda Camilo José Cela 12, 13071 Ciudad Real, Spain

²“Gheorghe Asachi” Technical University of Iasi, Department of Environmental Engineering and Management,
73 D. Mangeron Blvd., 700050 Iasi, Romania

³CNRS, IRCELYON, Institut de recherches sur la catalyse et l'environnement de Lyon, France

⁴Centre National en Électrochimie et en Technologies Environnementales, (Québec), Canada

Abstract

The utilization of manure for waste-to-bioenergy conversion processes may be a sustainable development choice rather than its traditional use as a fertilizer. Furthermore, the valorization of manure via thermochemical conversion routes and their integration with biological processes can provide an additional pathway in the utilization of residual biomass. On the other hand, the use of metal oxides might enhance the performance of thermochemical processes such as pyrolysis by either cracking the heavy hydrocarbon chains which turns into the production of a higher quality fuel or increasing the H₂ production by promoting secondary reactions as steam reforming or water-gas shift.

The derivative thermogravimetric (DTG) profiles of manure samples could be divided into four general stages: dehydration, devolatilization, char transformation and inorganic matter decomposition. For samples Pre and Dig R, the maximum DTG peaks were obtained at the same temperature. The first peak was lower for sample Dig R due to the removal of organic matter during the anaerobic digestion. On the other hand, the fourth step was not observed for sample Swine, which could be attributed to its low inorganic components (ash) content. The catalysts used in the catalytic pyrolysis process were: CaO, MgO and ZnO. The addition of these oxides modified the corresponding DTG profiles especially for sample Pre. These effects could be also observed in the mass spectra (MS) profile of the samples leading to a higher production of H₂, especially at high temperatures which could be attributed to the enhancement of secondary reactions that usually take place at temperatures higher than 500 °C.

Key words: derivative thermogravimetry (DTG), manure, pyrolysis, thermochemical processes, waste-to-bioenergy

Received: November, 2014; Revised final: February, 2015; Accepted: February, 2015

1. Introduction

Depletion of fossil fuels reserves and the environmental issues derived from their use are the main cause in the increasing attention of the bioenergy production. Currently, the consumption rate is about 91 million barrels per day of oil and 9 billion cubic metres per day of natural gas (BP, 2013). Therefore, the reserves will satisfy 48 years of

oil and 64 years of natural gas supply. In this context, biomass is considered to be one of the few viable replacement options (Shen et al., 2013), contributing approximately 14% to the world annual energy consumption (Shen et al., 2009).

The organic waste such as manure produced in confined animal feeding operations (CAFO) is potentially valuable as fertilizers (Flotats et al., 2009). Thus, the utilization of manure for waste-to-

* Author to whom all correspondence should be addressed: e-mail: marialuz.sanchez@uclm.es; gsor@tuiasi.ro

bioenergy conversion processes could be a sustainable development choice rather than its traditional use as a fertilizer (Hoppe and Sanders, 2014; Otero et al., 2011). On account of this, a number of bio-processes such as anaerobic digestion (AD) and bio-drying have been proposed in order to value and stabilize these types of wastes. AD has had an increasing attention due to its use for manure stabilization, sludge reduction, odour control and fuel production. AD involves the breakdown of complex organic wastes, producing biogas (mainly composed by methane and carbon dioxide) by a community of anaerobic microorganisms (Callegari et al., 2013; Cantrell et al., 2008). On the other hand, the aim of the bio-drying is the water evaporation by passing air through a waste bed; the heat released by exothermic bio-reactions is captured by an air stream and transferred to water which evaporates (Dufour, 2006). The recovery of the energy released during AD and bio-drying processes is used to obtain high added-value and stabilized products from manure. In this sense, thermochemical conversion such as pyrolysis of biomass is considered to be one of the most direct and promising routes for biomass utilization. Pyrolysis is defined as the thermal decomposition of biomass under an inert atmosphere to obtain three different products: liquid biofuels, gaseous fuel and bio-char.

Thermochemical conversion processes have been widely studied by thermogravimetric analysis (TGA). The valorization of manure as a solid combustible fuel has been recently experienced an increasing attention. Sanchez et al. (2009), compared the combustion of sewage sludge, animal manure and the organic fraction of municipal solid waste by thermogravimetric analysis. Otero et al. (2011) studied the thermal behavior and emissions evolved during swine manure combustion by TGA-MS. It was obtained that the combustion of swine manure started at 390 K and finished at 780 K in two different steps. Moreover, the kinetic behaviour and the activation energy were studied by two different methods: Vyazovkin and Owaza-Flynn-Wall. Wu et al. (2012) examined the pyrolysis and combustion behavior of dairy manure. However, the valorization of manure via thermochemical conversion routes and their integration with biological processes can provide an additional pathway for the utilization of residual biomass that has not been further reported in literature.

In this work, the pyrolysis of two different biologically pretreated manures, dairy (Pre and Dig R) and swine manure (SW), was studied by means of TGA-MS. Finally, the catalytic conversion in the pyrolysis process of manure was compared with that of the non-catalytic one.

2. Material and methods

2.1. Biomasses

In this investigation, the samples used were

animal solid wastes from the province of Québec (Canada). Swine (SW) and dairy manure were the samples selected. They were treated by bio-drying and anaerobic digestion, respectively. Dairy manure was fed into a digester where the anaerobic digestion took place. To evaluate the chemical changes during the biological process, two dairy samples were studied before (sample Pre) and after (sample Dig R) anaerobic digestion.

2.2. TGA-MS analysis

The pyrolysis of manure samples were carried out in a TGA apparatus (TGA-DSC 1, METTLER TOLEDO). The first step is the preheating of the sample at 125 °C; this temperature was kept constant during ten minutes in order to eliminate the moisture content. Subsequently, dynamic runs were carried out up to 1000 °C at a heating rate of 10°C/min under an atmosphere of Ar. TG curves were repeated twice in order to assure reproducibility of results. In previous studies (Sanchez-Silva et al., 2012), the most suitable operating conditions were selected. In this sense, sample weight was kept at 5 mg with a particle size range of 150-200 µm. The flow rate used was 200 Nml/min for pyrolysis tests. The analysis of the gas produced during pyrolysis process was carried out in a mass spectrometer (Thermostar-GSD 320/quadrupole mass analyser; PFEIFFER VACUUM).

2.3. Characterization techniques of manure samples

The manure samples were characterized by Fourier transform infrared spectroscopy (FTIR), bomb calorimeter, elemental analyser and thermogravimetric analyser (TGA).

The IR spectra were recorded on a Perkin-Elmer FTIR Spectrum GX spectrophotometer by accumulating 100 scans (4000 to 800 cm⁻¹) at a resolution of 4 cm⁻¹. 1.5 mg of sample and 150 mg of KBr (spectrometry grade) were homogenized thoroughly in an agate mortar, pelletized and then analysed. The heat of combustion was determined using a Parr 1356 bomb calorimeter according to UNE 164001:2005 EX at constant volume and a reference temperature of 25 °C. The energy equivalent of the calorimeter was determined with a standard reference sample of benzoic acid. A known mass amount of the samples were introduced in a gelatine capsule and combusted under an oxygen atmosphere. The ultimate analysis was used to measure the carbon (C), hydrogen (H), nitrogen (N), oxygen (O) and sulfur (S) content of a sample. This analysis was performed following the standard UNE-EN 15104:2011. The equipment used in this analysis is capable of detecting all elements cited by various mechanisms and the result is obtained as a mass percentage of each element in dry basis.

The proximate analysis was used to determine the ash and the volatile matter content of the samples. The equipment used to perform the proximate

analysis was a thermogravimetric analyzer (TGA / DSC Model 1 METTLER TOLEDO STAR[®]System).

2.4. Catalyst

Calcium oxide, magnesium oxide and zinc oxide were selected as catalysts. Firstly, the oxides were calcined at 1000 °C for 2 h to eliminate the water present both as humidity and bonded with the crystals. Furthermore, the calcination was carried out before experiments to ensure the stability of the oxides at the working temperature range.

3. Results and discussion

3.1. Characterization of dairy and swine manure

The ultimate analysis, the weight percentage of volatile matter (VM) and ash and the calorific values (HHV) of manure samples are shown in Fig. 1. As it can be seen, carbon and hydrogen content were higher for sample Pre whereas sample SW contained a higher content of nitrogen, sulphur and oxygen. The VM content was lower for sample Dig R than for the Pre one which was attributed to the biological degradation of the manure organic matter during the anaerobic digestion (AD) of sample Pre (Tambone et al., 2009). Furthermore, a higher amount of ash was observed for sample Dig R due to its lower volatile matter content (Kobayashi et al., 2013; Thygesen and Johnsen, 2012).

The HHV of sample Pre (18.4 MJ/kg) was higher than that for the SW one (16.1 MJ/kg) which could be associated to the high carbon and hydrogen content of sample Pre. Furthermore, sample SW showed a higher nitrogen and oxygen content which decreased the calorific energy of the sample (Channiwala and Parikh, 2002). On the other hand, the calorific value of sample Dig R was lower than that of sample Pre in spite of the similar values of their ultimate analysis (C, H and N contents). This fact can be explained by the high ash content of sample Dig R which diminished the available energy of the fuel (McKendry, 2002). Nevertheless, calorific values for the samples under study are within a similar range to other types of biomass (12-20 MJ/kg) (Choi et al., 2014) pointing out their suitability for their energetic valorisation.

3.2. Thermogravimetric study on pyrolysis of manure samples

The thermogravimetric (TGA) and derivative thermogravimetric (DTG) profiles of the pyrolysis process of samples Pre and Dig R at a heating rate of 10 °C/min are shown in Fig. 2.

The pyrolysis process of dairy samples (Pre and Dig R) could be divided into five stages. The first one appearing at temperatures below 125 °C represented the drying process of samples (dehydration stage).

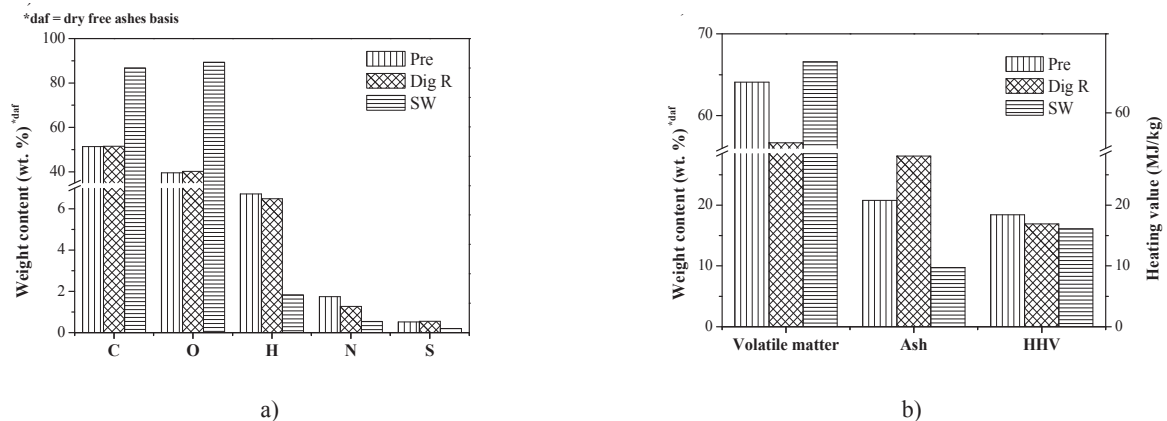


Fig. 1. Manure samples characterization: a) Ultimate analysis and b) Volatile matter, ash and calorific value

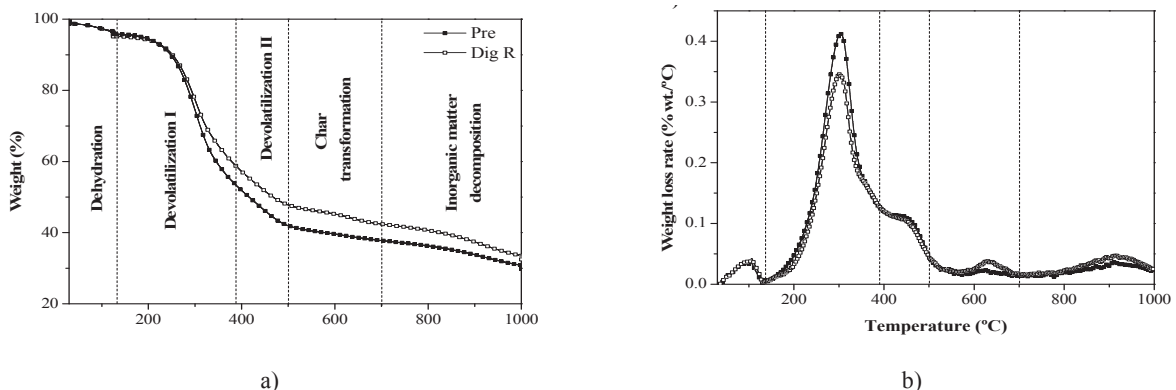


Fig. 2. Thermogravimetric profiles for the pyrolysis process of samples Pre and Dig R: a) thermogravimetric (TGA) profile and b) derivative thermogravimetric (DTG) profile

The second step occurred between 200 and 390 °C where the volatile matter was decomposed. In this stage, the maximum decomposition rate took place at 300 °C, being associated with hemicellulose and glucoside linkage depolymerisation (Wnetrzak et al., 2013). The maximum weight loss in samples Pre and Dig R (approximately 50 wt.% and 40 wt.%, respectively) took place in this stage, being considered the main pyrolytic stage. The lower weight loss and decomposition rate found for sample Dig R pointed out, as above mentioned, the removal of organic matter during the anaerobic digestion.

The third stage was characterized by a shoulder appearing between 390 and 500 °C in the DTG curves. This shoulder was ascribed to the decomposition of lipids and other N-containing compounds (Wnetrzak et al., 2013). Both the second and the third stages were considered as the devolatilization stages.

The last two stages were identified by two peaks between 550-700 °C and 800-1000 °C, associated with the decomposition of the formed char and the decomposition of inorganic matter (López-González et al., 2013).

Sample Dig R presented, in these last stages, peaks more prominent, which was related, as expected, to its higher ash content (Fig. 1). Fig. 3 shows the TGA-DTG profiles for the pyrolysis of sample SW at a heating rate of 10 °C/min.

As it can be seen, the DTG profile for the pyrolysis process of sample SW showed four stages (Fig. 3). The last fifth step was not observed in this sample, which could be attributed to the lower amount of ashes generated (Fig. 1). The main degradation stage was developed in a similar temperature range as that observed for dairy samples. However, this stage was characterized by the presence of two peaks at 280 °C and 320 °C, which could be associated to the thermal decomposition of hemicellulose (Sanchez-Silva et al., 2012).

This result is consistent to the fact that swine are not ruminant and therefore hemicellulose is low degraded in its intestines.

Regarding sample SW, the shoulder of the third stage is smaller than that observed in samples Pre and Dig R. Furthermore, there was a small peak close to 700 °C that could be attributed to the decomposition of some mineral components (Wnetrzak et al., 2013).

3.3. Analysis of gases evolved during pyrolysis of manure samples

Mass spectrometry (MS) profiles for the pyrolysis of samples Pre, Dig R and SW are shown in Fig. 4. MS spectra of manure samples could be divided into different stages associated to their degradations steps studied in the TGA/DTG profiles and described in the previous section. Generally, in the first step (dehydration) water was mainly detected for all the samples.

In the first devolatilization stage, most gaseous products were found, obtaining the highest yields for CO and CO₂ with a higher proportion of the last one. CH₃SH were the only sulphur product detected in this stage. In turn, nitrogen compounds such as amines and cyanides were also identified. In the second devolatilization stage, nitrogen compounds and CH₄ were the main emission peaks found besides aromatic compounds such as toluene. H₂ started evolving in this stage, indicating that char transformation reactions such as thermal cracking and dehydrogenation were taking place (Sanchez-Silva et al., 2012). Additionally, CO, CO₂, HCN and CH₄N were also detected in all samples at 1000 °C (inorganic matter decomposition stage). However, HCN was not detected in sample Pre. Finally, the main gaseous products found in all the stages for dairy samples were similar to those found for SW sample.

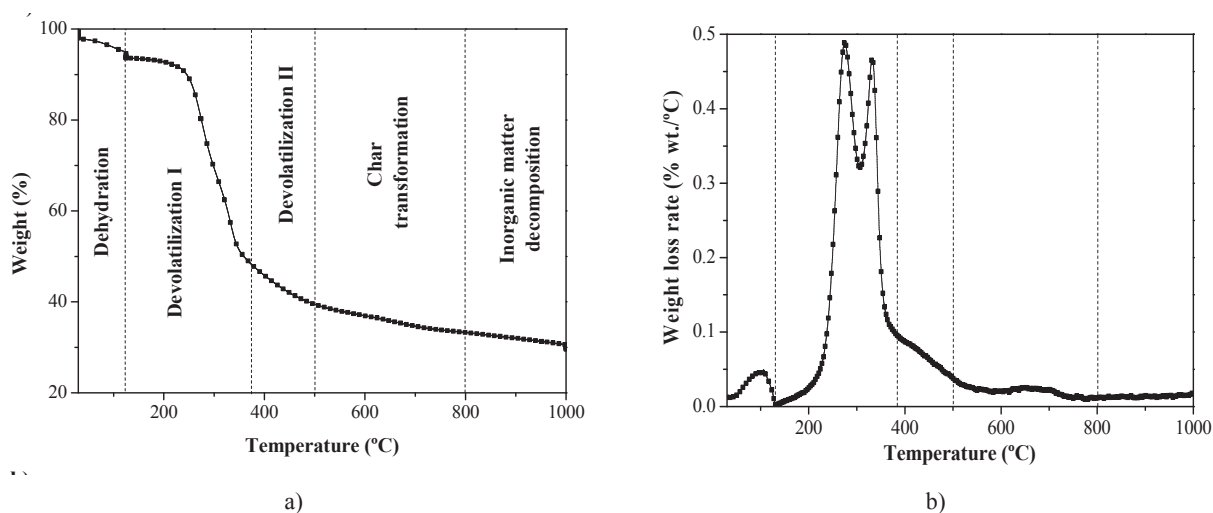


Fig. 3. Thermogravimetric profiles for the pyrolysis process of sample SW: a) thermogravimetric (TGA) profile and b) derivative thermogravimetric (DTG) profile

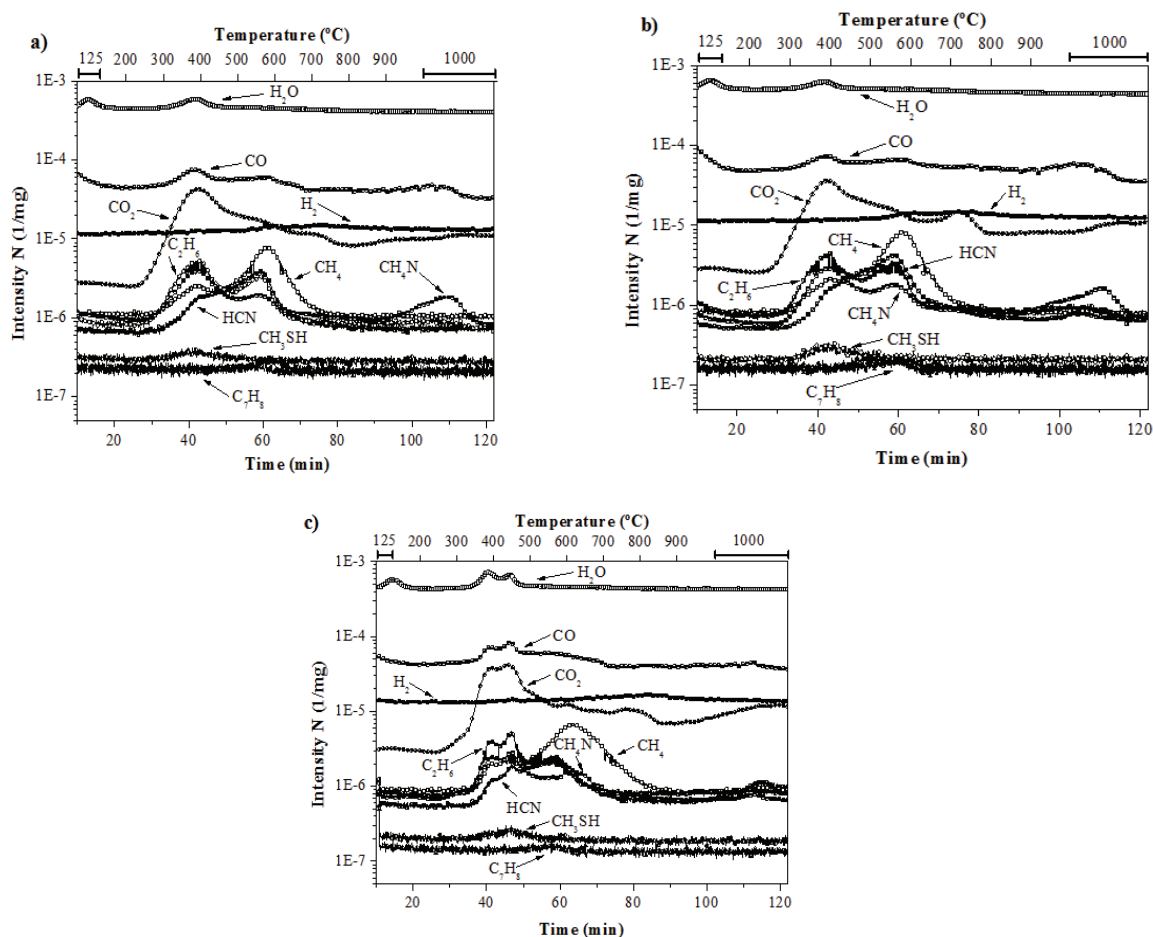


Fig. 4. Mass spectra for the pyrolysis process of manure samples: a) Pre, b) Dig R and c) SW at 10°C/min

3.4. Manure pyrolysis using catalysts

Sample Pre was the sample selected for the study of the pyrolysis using oxides as catalysts.

The derivative thermogravimetric (DTG) curves of the pyrolysis process at a heating rate of 10 °C/min of the sample Pre with and without catalyst are shown in Fig. 5. Mass spectrometry profiles for the pyrolysis of Pre sample by using different catalysts are shown in Fig. 6 (CaO), Fig. 7, (MgO) and Fig. 8 (ZnO). It can be observed that oxides had not effect on the maximum weight loss temperature at the second stage of the pyrolysis process. However, the addition of these oxides decreased the maximum weight loss in all cases, following the decreasing order: Pre>Pre+MgO>Pre+ZnO>Pre+CaO.

In the third stage of the pyrolysis process, this effect was negligible except for the addition of ZnO which reduced the weight loss by a factor of two.

There was a significant weight loss in the fourth stage (between 600 and 700 °C) for the sample with CaO whereas the rest of the samples showed the same behavior. This fact can be attributed to the decomposition of the CaCO₃ formed in previous stage where the CO₂ evolved can be adsorbed by the CaO (Han et al., 2010). The temperature range of the fourth stage is the typical for the degradation of

carbonates (Han et al., 2010). Besides, the MS profile of CO₂ showed a peak between 600 and 700 °C (Fig. 6), pointing out the release of this compound during the carbonate decomposition. In the last stage there was no difference in the DTG profiles of the samples except for ZnO one. This profile showed a prominent peak between 800 and 1000 °C (Fig. 5). The evolved gases at this temperature range were CO₂, CO, H₂, C₂H₅⁺ and C₂H₂. It can also be observed a decrease of the intensity of the water profile (Fig. 8).

Water can react either with the oxygenated hydrocarbons formed during the pyrolysis process or with the char remained, leading to CO and H₂ formation by steam reforming (Eq. 1) in the presence of ZnO (Maciel et al., 2011).

On the other hand, water gas shift reaction could also take place in the present of this catalyst (Maciel et al., 2011). These two reactions could explain the presence of CO₂, CO and H₂ at the last stage of the pyrolysis process (Fig. 8).

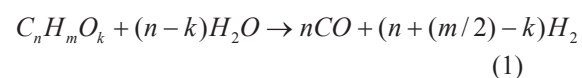


Fig. 9 shows a zoom of the H₂ profiles for sample Pre without and with catalysts. It can be observed that the ZnO was the oxide which best promoted the formation of H₂.

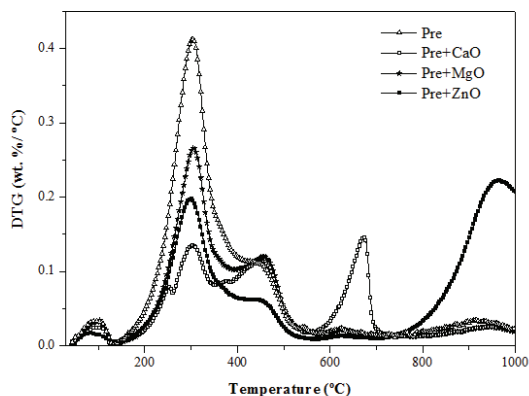


Fig. 5. Derivative thermogravimetric curves for the pyrolysis process of sample Pre without and with catalysts: CaO, MgO and ZnO

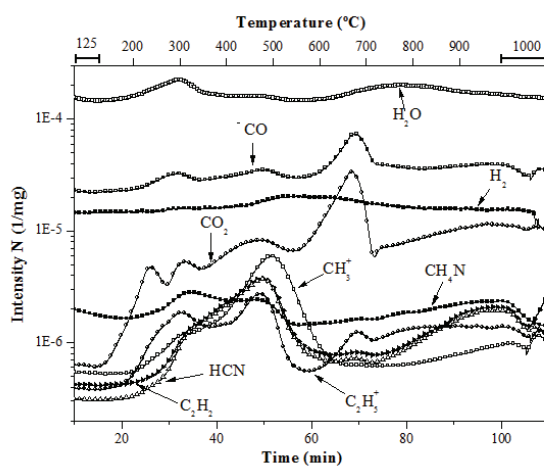


Fig. 6. Mass spectra of the pyrolysis process at 10°C/min of sample Pre with CaO

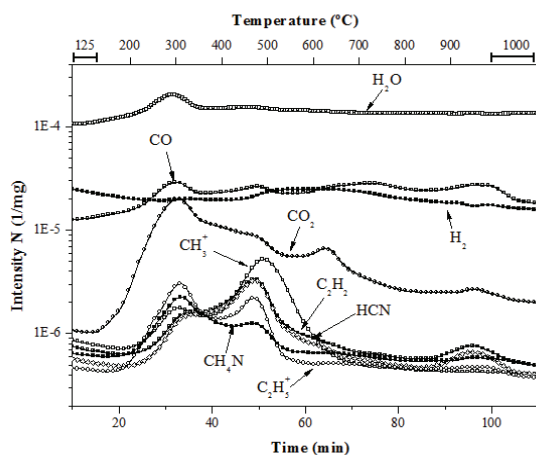


Fig. 7. Mass spectra of the pyrolysis process at 10°C/min of sample Pre with MgO

4. Conclusions

The pyrolysis process of manure samples could be divided into five stages: dehydration, two devolatilization stages, char transformation and inorganic matter decomposition. The fifth step was

not observed for sample SW which could be attributed to its lower amount of ashes. The lowest weight loss and decomposition rate were found for sample Dig R, pointing out the removal of organic matter during anaerobic digestion.

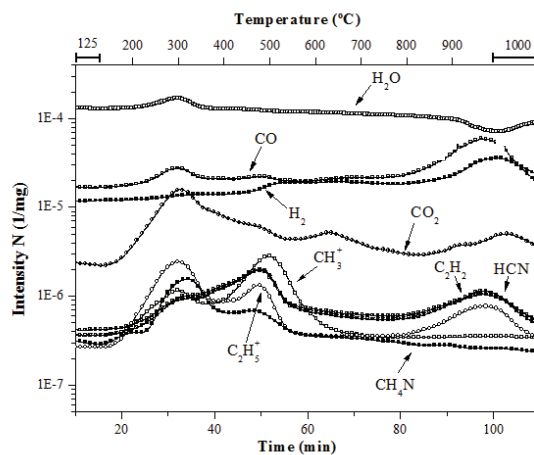


Fig. 8. Mass spectra of the pyrolysis process at 10°C/min of sample Pre with ZnO

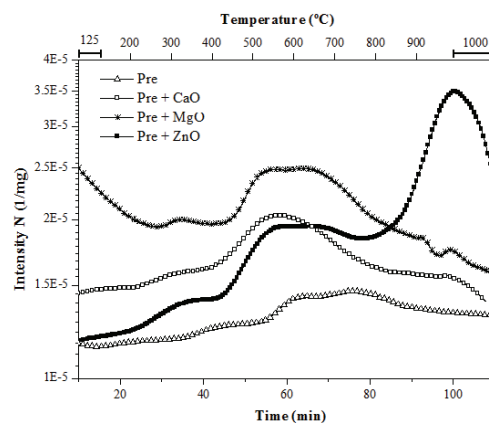


Fig. 9. Zoom of the H₂ production with and without catalysts

The addition of oxides as catalyst during the pyrolysis process of sample Pre decreases the temperature range in which the maximum weight loss was taken place. The maximum weight loss also decreased due to the oxides can adsorb the CO₂ present, leading to carbonates.

The more prominent effect was the H₂ formation at the end of the pyrolysis process with ZnO. The gasification with steam of the char formed at this temperature can take place and could be promoted by the presence of this oxide.

Acknowledgements

The authors acknowledge the financial support from Sociedad Española de Catálisis (Spanish Society of Catalyts, SECAT granted).

References

BP, (2013), BP Statistical Review of World Energy, June 2014, On line at: bp.com/statisticalreview.

- Callegari A., Torretta V., Capodaglio A.G., (2013), Preliminary trial application of biological desulfonation in anaerobic digestors from pig farms, *Environmental Engineering and Management Journal*, **12**, 815-819.
- Cantrell K.B., Ducey T., Ro K.S., Hunt P.G., (2008), Livestock waste-to-bioenergy generation opportunities, *Bioresource Technology*, **99**, 7941-7953.
- Channiwala S.A., Parikh P.P., (2002), A unified correlation for estimating HHV of solid, liquid and gaseous fuels, *Fuel*, **81**, 1051-1063.
- Choi H.L., Sudiarto S.I.A., Renggaman A., (2014), Prediction of livestock manure and mixture higher heating value based on fundamental analysis, *Fuel*, **116**, 772-780.
- Dufour P., (2006), Control engineering in drying technology: Review and trends, *Drying Technology*, **24**, 889-904.
- Flotats X., Bonmatí A., Fernández B., Magrí A., (2009), Manure treatment technologies: On-farm versus centralized strategies. NE Spain as case study, *Bioresource Technology*, **100**, 5519-5526.
- Han L., Wang Q., Ma Q., Yu C., Luo Z., Cen K., (2010), Influence of CaO additives on wheat-straw pyrolysis as determined by TG-FTIR analysis, *Journal of Analytical and Applied Pyrolysis*, **88**, 199-206.
- Hoppe T., Sanders M.Ph.Th., (2014), Agricultural green gas demonstration projects in the Netherlands, A stakeholder analysis. *Environmental Engineering and Management Journal*, **13**, 3083-3096.
- Kobayashi N., Noel E.A., Barnes A., Watson A., Rosenberg J.N., Erickson G., Oyler G.A., (2013), Characterization of three *Chlorella sorokiniana* strains in anaerobic digested effluent from cattle manure, *Bioresource Technology*, **150**, 377-386.
- López-González D., Fernandez-Lopez M., Valverde J.L., Sanchez-Silva L., (2013), Thermogravimetric-mass spectrometric analysis on combustion of lignocellulosic biomass, *Bioresource Technology*, **143**, 562-574.
- Maciel A.V., Job A.E., Da Nova Mussel W., De Brito W., Duarte Pasa V.M., (2011), Bio-hydrogen production based on catalytic reforming of volatiles generated by cellulose pyrolysis: An integrated process for ZnO reduction and zinc nanostructures fabrication, *Biomass and Bioenergy*, **35**, 1121-1129.
- McKendry P., (2002), Energy production from biomass (part 1): Overview of biomass, *Bioresource Technology*, **83**, 37-46.
- Otero M., Sánchez M.E., Gómez X., (2011), Co-firing of coal and manure biomass: A TG-MS approach, *Bioresource Technology*, **102**, 8304-8309.
- Sanchez M.E., Otero M., Gómez X., Morán A., (2009), Thermogravimetric kinetic analysis of the combustion of biowastes, *Renewable Energy*, **34**, 1622-1627.
- Sanchez-Silva L., López-González D., Villaseñor J., Sánchez P., Valverde J.L., (2012), Thermogravimetric-mass spectrometric analysis of lignocellulosic and marine biomass pyrolysis, *Bioresource Technology*, **109**, 163-172.
- Shen D.K., Gu S., Luo K.H., Bridgwater A.V., Fang M.X., (2009), Kinetic study on thermal decomposition of woods in oxidative environment, *Fuel*, **88**, 1024-1030.
- Shen D., Hu J., Xiao R., Zhang H., Li S., Gu S., (2013), Online evolved gas analysis by Thermogravimetric-Mass Spectroscopy for thermal decomposition of biomass and its components under different atmospheres: Part I. Lignin, *Bioresource Technology*, **130**, 449-456.
- Tambone F., Genevini P., D'Imporzano G., Adani F., (2009), Assessing amendment properties of digestate by studying the organic matter composition and the degree of biological stability during the anaerobic digestion of the organic fraction of MSW, *Bioresource Technology*, **100**, 3140-3142.
- Thygesen O., Johnsen T., (2012), Manure-based energy generation and fertiliser production: Determination of calorific value and ash characteristics, *Biosystems Engineering*, **113**, 166-172.
- Wnetrzak R., Kwapinski W., Peters K., Sommer S.G., Jensen L.S., Leahy J.J., (2013), The influence of the pig manure separation system on the energy production potentials, *Bioresource Technology*, **136**, 502-508.
- Wu H., Hanna M.A., Jones D.D., (2012), Thermogravimetric characterization of dairy manure as pyrolysis and combustion feedstocks, *Waste management & research: the journal of the International Solid Wastes and Public Cleansing Association, ISWA*, **30**, 1066-1071.



“Gheorghe Asachi” Technical University of Iasi, Romania



CASE STUDY ON ENERGY EFFICIENCY OF BIOGAS PRODUCTION IN INDUSTRIAL ANAEROBIC DIGESTERS AT MUNICIPAL WASTEWATER TREATMENT PLANTS

Alexandrina Zuza^{1*}, Paul Serban Agachi¹, Vasile Mircea Cristea¹,
Abhilash Nair², Nguyen Ngoc Tue³, Cristina Horju-Deac⁴

¹Faculty of Chemistry and Chemical Engineering, UBB, Cluj-Napoca

²Erasmus Mundus Program, India

³Hanoi University of Science and Technology, Vietnam

⁴Faculty of Materials and Environmental Engineering, Technical University of Cluj-Napoca

Abstract

Anaerobic digestion was analyzed as the biological process that converts the organic matter present in various types of wastes, activated sludge from the wastewater treatment facilities respectively, into biogas. Latest advancements in the mathematical modeling, simulation and control practices have helped in gaining a better insight of the process. In this paper, an energy efficiency and techno-economical investigation of anaerobic digestion technology for the CHP cogeneration unit, has been done to detect maximum concentrations of methane and to minimize the costs at a Municipal Wastewater Treatment Plant.

Key words: anaerobic digestion, biogas, CHP, energy efficiency, wastewater treatment plant

Received: November, 2014; *Revised final:* February, 2015; *Accepted:* February, 2015

1. Introduction

Combined Heat and Power (CHP) involves the simultaneous production of electricity and heat from a single fuel source, such as natural gas, biomass, biogas, coal, or oil. The CHP systems and the technology to treat biogas have improved significantly. CHP systems include different individual components configured into an integrated system as the prime mover, generator, heat recovery setting, and electrical interconnection.

The prime mover that drives the overall system typically identifies the CHP system. With the ability to achieve better results more reliably, cogeneration is a remarkable opportunity for wastewater treatment biogas producers to gain numerous benefits. The main advantages include low-cost electricity production; it also displaces

purchased fuels for thermal needs and enhances power reliability for the plant (Bastian et al., 2011).

2. Properties of biogas as fuel for CHP system

Biogas contains 60% to 70% of CH₄, 0.5 % of H₂ and up to 45% of CO₂ (Table 1). After being cleaned of carbon dioxide, this gas becomes a fairly homogeneous fuel containing up to 80% of methane with the calorific capacity of over 25 MJ/m³. The most important component of biogas, from the calorific point of view is CH₄. The other components are not involved in combustion process, and rather absorb energy from combustion of CH₄ as they leave the process at higher temperature than the one they had before the process (Mihic, 2004).

Thermodynamic properties of CH₄ at 273 K and 1 atm are specific heat $c_p = 2.165$ kJ/kgK, molar mass $M = 16.04$ kg/kmol, density $\rho = 0.72$ kg/m³,

* Author to whom all correspondence should be addressed: e-mail: alexandrinazuza@chem.ubbcluj.ro; Phone: +40-264-593833

individual gas constant $R = 0.518 \text{ kJ/kgK}$, lower calorific value $H_u = 50000 \text{ kJ/kg}$ and $H_{u,n} = 36000 \text{ kJ/Nm}^3$ (Mihic, 2004).

Table 1. Characteristics of anaerobic digester gas (Wiser et al., 2012)

Parameter	Digester Gas	
	Range	Common Value
Methane, CH ₄ , percent (dry basis)	60-70	65
Carbon dioxide, CO ₂ , percent (dry basis)	30-45	39
Nitrogen, N ₂ , percent (dry basis)	0.2-2.5	0.5
Hydrogen, H ₂ , percent (dry basis)	0-0.5	0.2
Water vapor, H ₂ O, percent	5.9-15.3	6
Hydrogen sulfide, H ₂ S, ppmv (dry basis)	200-3,500	500
Siloxanes, ppbv	200-10,000	800
Specific gravity (based on air = 1.0)	0.8-1.0	0.91

The kinetic model of biogas production is described by the modified Gompertz equation (Eq. 1) (Budiyono et al., 2014; Kwanyong, 2013; Yusuf et al., 2011; Zwietering et al., 1990), where: P – cumulative of specific biogas production; A – biogas production potential; U – maximum biogas production rate; \tilde{e} – the lag phase period or minimum time to produce biogas; t – cumulative time for biogas production; $e = \exp(1)$.

$$P = A \exp\left\{-\exp\left[\frac{U \times \tilde{e}}{A}(\lambda - t)\right] + 1\right\} \quad (1)$$

The biogas flowrate can be also calculated by the algebraic equation given in Batstone et al. (2002) (Eq. 2), where: $\rho T_{,8}$, $\rho T_{,9}$ and $\rho T_{,10}$ are the liquid-gas transfer rates and $T_{op} = 308.15\text{K}$.

$$q_{gas} = \frac{RT_{op}}{P_{atm} - p_{gas.H_2O}} V_{liq} \left(\frac{\rho T_{,8}}{16} + \frac{\rho T_{,9}}{64} + \rho T_{,10} \right) \quad (2)$$

3. Energy efficiency of the CHP biogas system and techno-economical investigation

3.1. Materials and methods

At an operating temperature, $T_{op} = 35^\circ\text{C}$, an organic load (OL) between $1.6\text{-}8.0 \text{ kgVSS/m}^3$, retention time of the sludge $RT = 15$ days, volume of the methanetank $V = 3,500 \text{ m}^3$, and an average of $1,800 \text{ m}^3/\text{day}$ of sludge pumped into the anaerobic digesters, for the period considered, it has been produced a maximum of $9,803 \text{ m}^3/\text{day}$ biogas, which represents a biogas flow of approx. $400 \text{ m}^3/\text{h}$. The recirculated biogas, used for mixing purposes inside the digestors is $2,160 \text{ m}^3/\text{day}$, representing 22% of the total biogas produced (Fig. 1). The calculation of total system efficiency is a simple and useful method that evaluates what is produced compared to what is consumed with the following expression (Eq. 3) (Darrow et al., 2014; EPA, 2013), where: W_E – electrical output; Q_{therm} – thermal output; Q_{fuel} – fuel consumption.

$$\eta_0 = \frac{W_E + \sum Q_{therm}}{Q_{fuel}} \quad (3)$$

The biogas flow leads to an electrical energy output of up to $13,328 \text{ kWh/day}$, through the gas engines $2 \times 330 \text{ kW}$ power (P_{ei}), that have an electrical energy efficiency conversion between 34-40% (η_{ei}). The energy efficiency of the gas engine has a conversion of 38% electrical energy, (η_{ei}), 48% thermal energy (η_{therm}) and 14 % losses, with a total CHP generator efficiency of $\eta_0 = 96\%$ (EPA, 2014) (Table 2).

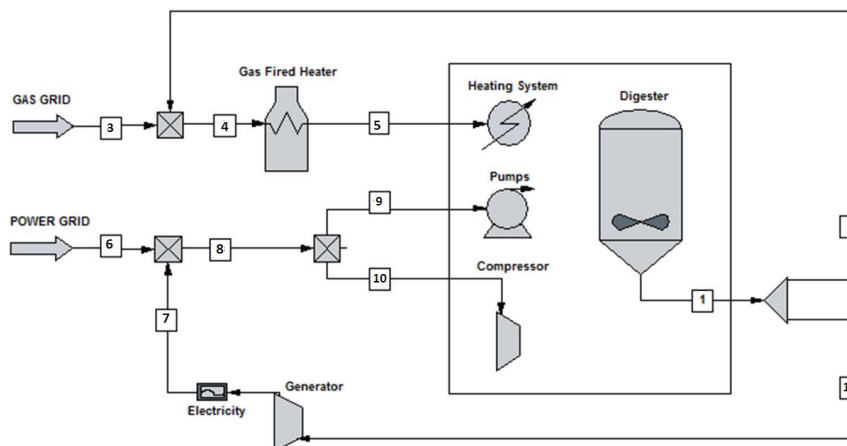


Fig. 1. CHP cogeneration unit scheme: 1. Biogas generated from digesters; 2. Amount of biogas directed to the heating system; 3. Biogas purchased from the national grid; 4. Biogas utilized for the gas fired heater; 5. Thermal energy for the heating system; 6. Electricity purchased from the national grid; 7. Electricity produced by the generator; 8. Total amount of electricity; 9. Electricity utilized for the pumps; 10. Electricity utilized for the compressor; 11. Biogas utilized for the generator

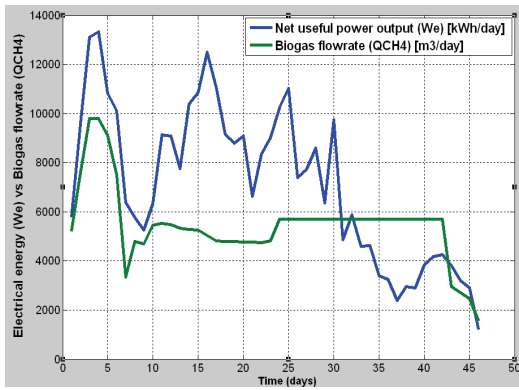


Fig. 2. Electrical energy and biogas flowrate in time

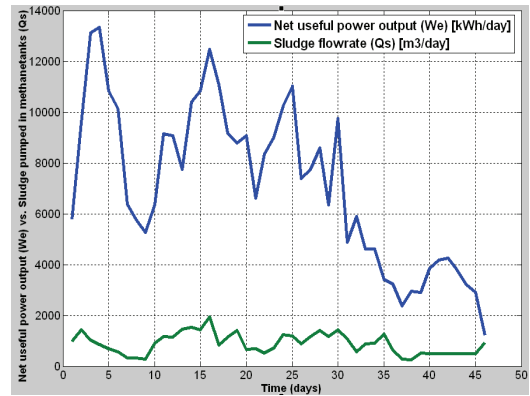


Fig. 3. Electrical energy and sludge flowrate in time

If the total daily average consumption of electricity of the plant reaches 24,570 kWh/day and the electrical energy purchased from the national grid of 11,457 kWh/day at 0.5194 RON (Transelectrica, 2014), the electrical energy output from the biogas brings savings of operational costs which could reach up to a maximum of 46.63% or 6,922 RON/day \approx 1,573 €/day, for the period of time considered. The energy produced by the CHP biogas system can be used or sold to the national grid and savings can be made through an attractive green certificates market.

The amount of green certificates ranges between 37-55 €/MWh and the number of green certificates ranges between 1-4 in the biomass and biogas market (ANRE, 2014; EU Directive 2009/28/CE; OPCOM, 2014).

Table 2. Energy efficiency of the CHP biogas system

Time (min)	Electrical Output (kW)	Thermal Output (kW)	Electrical Efficiency (%)	CHP Generator Efficiency (%)
0	330	369	37.8	96.4
3	330	367	37.8	96.4
15	165	212	34.8	95.6
18	165	208	34.8	95.6
24	248	277	36.8	96.2
27	248	282	36.9	96.2

4. Results and discussion

For an in depth analysis of what specifically influences the biogas production, default electrical energy output and efficiency of the CHP system, the following parameters have been found (Kumar, 2012; Mihic, 2004):

a) Technical Parameters

- Concentration of CH₄, composition of biogas; Calorific value of CH₄ (H_u);
- Process parameters: Input parameters, Sludge composition, OL, Sludge flowrate Q_s, and Hydrolysis stage biodegradation fractions;
- Power demand; Demand of low and medium temperature (cogeneration).

b) Economical Parameters

- Price of biogas;
- Price of electrical energy;

▪ Operational costs.

The rate of decrease in power is largely dependent on the calorific value of the gas. Biogas concentration at 70.10 [%/vol] with a calorific value of H_u = 24.768 kJ/Nm³ ranges as a medium weak gas compared to 76.24 [%/vol] concentration with a calorific value of H_u = 28.723 kJ/Nm³, which causes power reduction.

From the experimental data, for the period considered the maximum net output of electrical power W_e = 13.328 kWh/day is obtained at a biogas flow rate of Q_{CH₄} = 9.803 m³/hr (Fig. 2) and a default sludge flow rate (Q_s) pumped into the methane tanks of 1947.161 m³/day (Fig. 3).

5. Conclusions

The energy (heat+electrical energy) requirements in a WWTP can be significant. Thus the exploitation of both electrical and thermal energy produced from the CHP system (self-consumption for the heat exchangers) assists to a considerable decrease of biogas plant's operational costs. An electrical energy efficiency of the gas generator η_{el} = 38% and η_{therm} = 48% have been found.

A total CHP generator efficiency η_0 = 96% could be observed. The maximum net output of electrical power W_e = 13.328 kWh/day is obtained at a biogas flow rate of Q_{CH₄} = 9.803 m³/hr and a default sludge flow rate (Q_s) pumped into the methane tanks of 1947.161 m³/day.

Augmentation of biogas can be obtained by maximizing the technical parameters discussed, concentrating the sludge with a higher organic load, and adding municipal biodegradable organic waste to the anaerobic digestion process can be further experimented. Future investigation on the parameters that influence the augmentation of biogas could be researched. The green certificates market makes the CHP biogas technology attractive, and it also becomes an option for the EU Directive 2009/28/CE to utilize energy from renewable sources up to 24% until 2020.

Acknowledgements

This paper is a result of a doctoral research made possible by the financial support of the Sectoral Operational

Program for Human Resources Development 2007-2013, co-financed by the European Social Fund, under the project POSDRU/159/1.5/S/132400- “Young successful researchers – professional development in an international and interdisciplinary environment”.

References

- ANRE, (2014), Romanian National Authority for Energy Reglementation, On line at: www.anre.ro.
- Bastian R., Cuttica J., Fillmore L., Hedman B., Hornback C., Levy D., Moskal J., (2011), *Opportunities for Combined Heat and Power at Wastewater Treatment Facilities: Market Analysis and Lessons from the Field*, EPA (Environmental Protection Agency), Combined Heat and Power Partnership, USA, 6-12.
- Batstone D.J., (2002), The IWA Anaerobic Digestion Model No 1 (ADM1), *Water Science & Technology*, **45**, 65-73.
- Budiyono B., Syaichurrozi I., Sumardiono S., (2014), Effect of total solid content to biogas production rate from vinasse, *International Journal of Engineering, Transactions B: Applications* **27**, 177-178.
- Darrow K., Tidball R., Wang J., Hampson A., (2014), *Catalog of CHP Technologies, Appendix A: Expressing CHP Efficiency*, EPA (Environmental Protection Agency), Combined Heat and Power Partnership, USA, 1-3.
- EPA, (2013), *Efficiency Metrics for CHP Systems: Total System and Effective Electric Efficiencies*, Combined Heat and Power Partnership, USA, On line at: http://www.arb.ca.gov/cc/ccei/presentations/CHPEfficiencyMetrics_EPA.pdf.
- EPA, (2014), *Catalog of CHP Technologies*, CHP Combined Heat and Power Partnership, USA, On line at: http://www.epa.gov/chp/documents/catalog_chptech_full.pdf.
- EU Directive, (2009), Directive 2009/28/EC of the European Parliament and of the Council of 23 April 2009 on the promotion of the use of energy from renewable sources and amending and subsequently repealing Directives 2001/77/EC and 2003/30/EC, *Official Journal of the European Union*, **L140**, 16-62.
- Kumar S., (2012), *Biogas*, InTech, Rieka, Croatia.
- Kwanyong L., (2013), Evaluation of methane production and biomass degradation in anaerobic co-digestion of organic residuals, *International Journal of Biological, Ecological and Environmental Sciences (IJBEES)*, **2**, 1-3.
- Mihic S., (2004), Biogas fuel for internal combustion engines, *Annals of Faculty Engineering Hunedoara – International Journal of Engineering*, **2**, 184-187.
- OPCOM, (2014), Electric Energy and Natural Gas Market Operator in Romania, On line at: www.opcom.ro.
- Transelectrica, (2014), Romanian National Electric Grid, On line at: www.transelectrica.ro.
- Wiser J.R., Schettler J.W., Willis J.L., (2012), *Evaluation of Combined Heat and Power Technologies for Wastewater Facilities*, EPA (Environmental Protection Agency), Columbus Water Works, USA, 18-19.
- Yusuf M.O.L., Debora A., Ogheneruona D.E., (2011), Ambient temperature kinetic assessment of biogas production from co-digestion of horse and cow dung, *Research in Agricultural Engineering*, **57**, 97-104.
- Zwietering M. H., Jongenburger I., Rombouts F. M., Van 't Riet K., (1990), Modeling of the bacterial growth curve, *Applied and Environmental Microbiology*, **56**, 2-3.



“Gheorghe Asachi” Technical University of Iasi, Romania



CHARACTERIZATION OF DYES LOADED POLYVINYL ALCOHOL (PVA) BASED HYDROGELS THROUGH CIELAB METHOD

Adina Papancea, Silvia Patachia*

“Transilvania” University of Brasov, Product Design, Mechatronics and Environment Department,
29 Eroilor Str., 500036 Brasov, Romania

Abstract

Hydrogel membranes obtained by neat polyvinyl alcohol (PVA) or PVA with various bio insertions like: Scleroglucan (Scl), Zein (Zein) or Cellulose (Cel), were subjected to diffusion and sorption/desorption experiments using different type of dyes such as: Crystal Violet (CV), Methylene Blue (MB), Congo Red (CR). If the sorption, desorption or diffusion of a dye in/from/through a hydrogel is usually monitored by the dye solution analysis, in this case the transport phenomena are followed by the membrane analysis. Photographic images of colored hydrogels obtained by PVA hydrogel immersion in aqueous solutions of different dyes, with different concentrations have been obtained by using a digital camera CANON Power Shot SX110 with 3456×2592 pixels resolution, in artificial light. The resulted images were processed by using Adobe Photoshop software, CS5 version, and analyzed through CIEL*a*b* system (CIELAB). This method gives the possibility to make difference between two very close colors by taking into account parameters such as: hue, saturation and luminosity.

As a particular case, the present study evidenced, by CIELAB method that all the prepared hydrogels have a good capacity to uptake dyes from aqueous solutions, the highest efficiency being obtained for PVA/Scl hydrogels. Our results are in good agreement with those obtained from SEM and DSC analysis of the loaded gels.

Key words: CIELAB, cryogel, dyes, method, PVA, sorption

Received: November, 2014; *Revised final:* February, 2015; *Accepted:* February, 2015

1. Introduction

Polyvinyl alcohol (PVA) cryogels have the ability to change their color, forming colored complexes in the presence of dyes (Dobritoiu and Patachia, 2013), metallic ions (Papancea et al., 2010b; Patachia et al., 2004), iodine (KI) (Patachia and Rinja, 2005), or some drugs (Patachia et al., 2007). In this paper, we proposed a new application of one method already used in perfume analysis (Korifi et al., 2013), food packaging or medicine but not yet in the gels domain. This is a direct method, that use the color analysis of the colored gels, named CIELAB method, instead of commonly used methods (Luis et al., 2014) which are indirect (through solution analysis, solutions that are light sensitive), expensive (using various reagents) and generating

waste waters.

Since due to its properties, PVA is a good candidate for sorption and transport of dyes (Dobritoiu and Patachia, 2013), three types of PVA biopolymers based materials were used as adsorbents: PVA with scleroglucan (PVA/Scl), PVA with microfibers of cellulose (PVA/Cel) and PVA with zein (PVA/Zein).

To study the dyes sorption through PVA cryogels three dyes were used: Crystal Violet [CV] (due to its medical use as antiseptic) and Methylene Blue [MB] (due to its various applications in biology, chemistry and medicine), both cationic dyes and Congo Red [CR], a diazo dye used in dyeing industry but also in biochemistry and histology to stain microscopic preparations. The change in biobased cryogels color and in aspect after dyes sorption was

* Author to whom all correspondence should be addressed: e-mail: st.patachia@unitbv.ro; Phone: +40 741 649792; Fax: +40 268 410525

analyzed through CIEL*a*b* system (CIELAB). This color model, derived from the CIE system, is based on the way the describe color and not by quantifying it.

CIELAB gives the possibility to make difference between two very close colors by taking into account parameters such as: hue, saturation and luminosity. The CIELAB color space parameters are: L^* , color luminosity, varies from 100 (white) to 0 (black); a^* varies from red (+ a^*) to green (- a^*) and b^* varies from yellow (+ b^*) to blue (- b^*).

In Fig. 1 there is a 3D representation of the CIELAB system, where it can be seen that the brightness scale (L) is centrally placed while C^*ab axis is an open scale with the origin in zero including all neutral color, and the angle hab called "angle hue" can have values between 0 and 360 degrees (Válceanu et al., 2006).

Thus, CIELAB method could find various applications in fields like: environment, for monitoring the sorption of dyes (Confortin et al., 2010; Crini and Badot, 2008; Ikkai et al., 1996) or heavy metal ions from polluted waters (Croitoru et al., 2009; Papancea et al., 2010b; Patachia et al., 2011); sorption of iodine (Patachia et al., 1997) used like disinfectant, from waste-waters; medicine, where the PVA gels can be loaded with active substances, such as: dyes with antiseptic properties (ex. Crystal Violet, ionic liquids) (Patachia and Damian, 2014), porphirines, used in the cancer phototherapy (Patachia et al., 2007; Varga et al., 2008); pharmacy, for the monitoring and controlled release of the drugs or for study the substrate regeneration and substance recovery of some sorbed species.

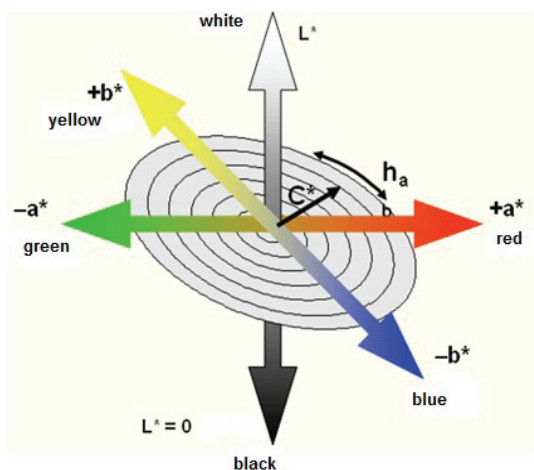


Fig. 1. Three-dimensional representation CIELAB color scale (Globalspec, 2014)

The aim of this paper is to demonstrate that the concentration dependent characteristics such as: adsorption equilibrium, sorption kinetics, sorption mechanism as well as dye-dye or dye-polymer interaction, could be determined through the color analysis of the colored gels, by using CIELAB method.

2. Experimental

2.1. Materials

The following categories of materials were used in our study:

- PVA 98–99% hydrolyzed ($M = 146,000\text{--}186,000$) from Sigma–Aldrich.

- Biopolymers: Scleroglucan (Actigum CS 11, $M_w = 1,000,000$ Da) from Cargill, St-Germain-en-Laye, France. Zein from Sigma–Aldrich. The polymers were used without further purification. Microfibers of cellulose were prepared by the method described by Kim et al. (2009).

- PVA cryogels with biopolymers synthesized according to the method presented by Dobritoiu and Patachia (2013)

- Crystal Violet purchased from Fluka, Methylene Blue, from USP, Powder, American Cyanamid Company, New Jersey and Congo Red was purchased from Merk. All dyes were used as received without further purification. In Fig. 2, the structures of dyes are presented. Solutions of dyes at desired concentrations ($1 \times 10^{-6} - 8 \times 10^{-5}$ mol/L) were prepared by using distilled water. The concentration range considered was selected taking into account the solubility of dyes in water ($S_{MB} = 40$ g/L, $S_{CV} = 16$ g/L, $S_{CR} = 25$ g/L).

2.2. CIELAB method

To analyze the colour of the PVA cryogels after dyes sorption a digital camera (CANON Power Shot SX110 with 3456×2592 pixels resolution) was chosen and was used in artificial light. Unlike other devices that actually measure the colour of small areas (points) on the surface of an object, digital cameras have the advantage on measuring the colour characteristics of the entire object from the global point of view (Hang and Brindley, 1970).

The obtained images were processed by using Adobe Photoshop software, CS5 version, and the colour model: CIELAB. The parameters of the color space (L^* , a^* , b^*) were determined in several points of the samples image (a minimum of ten points for each image), the reported results representing the average of the determinations for each image. Using difference in a^* , b^* and L^* parameters (Eq. 1) the difference in color (ΔE_{ab}^*) (Eq. 2), in chromaticity (ΔC_{ab}^*) (Eq. 3) and in hue (ΔH_{ab}^*) (Eq. 4) were calculated (Schanda, 2007), where: X is one of the color coefficients L^* , a^* or b^* , whereas 1 and 0 indices, are the value for the cryogel dye loaded sample and the value for the reference cryogel (usual that immersed in the lowest concentrated dye solution).

$$\Delta X = X_1 - X_0 \quad (1)$$

$$\Delta E_{ab}^* = \sqrt{\Delta L^{*2} + \Delta a^{*2} + \Delta b^{*2}} \quad (2)$$

$$\Delta C_{ab}^* = \sqrt{\Delta a^{*2} + \Delta b^{*2}} \quad (3)$$

$$\Delta H_{ab}^* = \sqrt{\Delta L^{*2} + \Delta E^{*2} + \Delta C^{*2}} \quad (4)$$

The obtained results for the CIELAB parameters are used to describe the dyes sorption/desorption and diffusion processes and they were compared with the results obtained by VIS spectroscopy.

2.3. Sorption studies

Samples with different masses were immersed in CV, MB and CR solutions (concentrations between: 1×10^{-6} - 8×10^{-5} mol/L). The sorption of dye into the PVA cryogels was monitored using two methods: the analysis of the colored cryogels using CIELAB method and the analysis of the dye immersion solutions at different periods of time after the sample immersion.

The change in solution absorbance was monitored using an UV/VIS Perkin Elmer spectrophotometer, Lambda 25-model ($\lambda_{CV} = 590$ nm, $\lambda_{MB} = 640$ nm, $\lambda_{CR} = 498$ nm). The sorption equilibrium was reached after 20 days. The experiments were made at room temperature.

2.4. Rate of sorption/desorption

To follow the sorption rate of the dye, PVA cryogel circular samples with masses between 0.6 - 0.8 g and 1 cm in diameter were immersed in 5 mL CV solution of 5×10^{-6} mol/L concentration.

The samples were removed from the dye

solution every 15 minutes until one hour and then after 30, 60 minutes and 24 hours, respectively.

After 24 hours of CV sorption, the PVA cryogels were immersed in 5 mL of distilled water. At certain times (15, 30, 45, 60, 120, 150 and 1440 minutes) they were removed from water, whipped with filter paper and then pictures were taken. The sorption/desorption of dye was monitored through the analysis of the immersion solutions.

The change in solution absorbance was monitored using an UV/VIS Perkin Elmer spectrophotometer, Lambda 25-model ($\lambda_{CV} = 590$ nm).

3. Results and discussion

3.1. Analysis of CIELAB parameters used to determine the influence of gel composition on gel color

The change in cryogels color after the dye sorption, from white to: blue for MB, violet for CV or red for CR, is illustrated in Fig. 3 from where it is easy to observe that, at the same dye concentration the cryogels show different shades. This phenomenon could be explained through the dyes-substrate interactions and the substrate morphology, the dyes sorption proving to be dependent not only on the dye type but also on the type of substrate.

Using photographic images from Fig. 3 the color parameters L^* , a^* , b^* were determined for each sample; with the obtained values, ΔL^* , ΔE^* and ΔH^* were calculated. Values for a^* , b^* parameters and their ratio at the highest concentration (c_5), for each dye, are presented in Table 1.

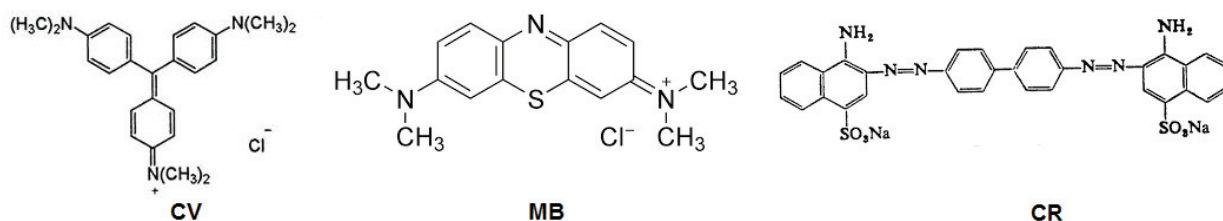


Fig. 2. Structure of Crystal Violet [CV], Methylene Blue [MB] and Congo Red [CR]

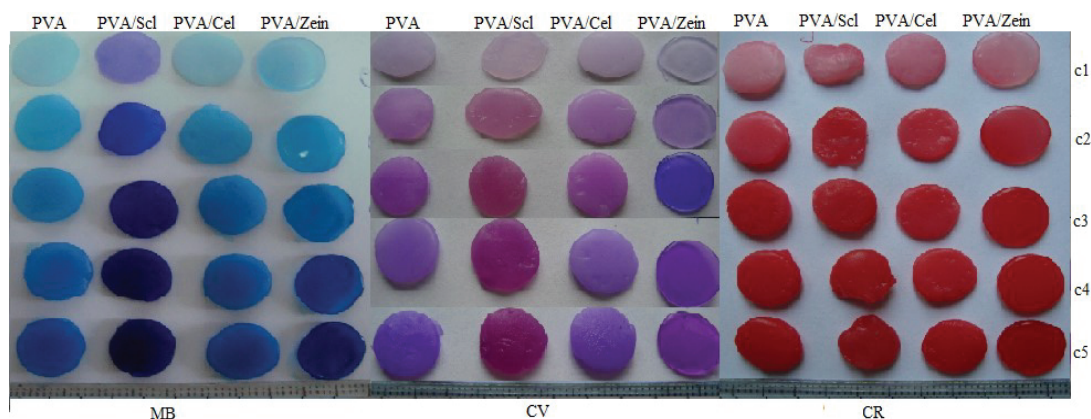


Fig. 3. PVA membranes after MB, CV and CR sorption in five different concentration solutions

Table 1. Values of a*, b* and a*/b* CIELAB parameters for PVA and PVA with bio insertions cryogels after CV, MB and CR sorption

Dye type (concentration)	CIELAB parameters	PVA	PVA/Scl	PVA/Cel	PVA/Zein
CV (1*10 ⁻⁵ mol/L)	a*	36.67	39.33	32.22	45.33
	b*	-50.89	-12.44	-43.00	-47.44
	a*/b*	-0.72	-3.16	-0.75	-0.96
MB (8*10 ⁻⁵ mol/L)	a*	11.44	6.67	6.11	14.56
	b*	-42.00	-18.67	-41.11	-37.00
	a*/b*	-0.27	-0.36	-0.15	-0.39
CR (2*10 ⁻⁵ mol/L)	a*	46.55	45.22	47.67	46.55
	b*	32.22	31.11	29.33	35.22
	a*/b*	1.44	1.45	1.63	1.32

Based on data from Table 1, the following considerations can be made:

- the positive value of parameter a*, (+a*) for CV means absorption of green radiation, so red color of the gel, while the negative value of b* parameter, (-b*), means absorption of yellow radiation, so blue color of the gel. The combination between the two colors is the final color of the cryogel, and is mathematically represented by their ratio. For the membrane with Scl, the ratio value is -3.16, showing 3 times more red than blue color, so a pinkish-violet color of the gel will result, while for the PVA, PVA/Cel and PVA/Zein cryogels the subunit but close to 1 ratio gives a blue-violet color.

- like in CV case, +a* for MB means absorption of green light, so red color of the gels, while -b* means absorption of yellow light, so blue color of the gels. In contrast to the previous case, the value of the ratio a*/b* between the two colors is close to zero, for all four PVA cryogels, showing a much higher proportion of blue than red, the final color of the gels being blue not violet.

- high, positive value of parameter a* (+a*) for CR shows absorption of green light, so red color of the gel, is combining with the positive value of b* parameter (+b*), which shows absorption of blue light, so yellow color of the gel. The value of the ratio a*/b* between the two colors, for all cryogels, is higher than 1 with values between 1.32-1.63, so the final color is an intense red.

Using the method described above, even a person with color-blind deficiency can know the color of the gels after dyes sorption.

3.2. Analysis of CIELAB parameters used to determine the influence of the concentration of the immersion solution on gel colour

Taking the initial concentrations for the each dye solution and the highest values between a* and b* CIELAB parameters for the PVA cryogels, information about cryogel color - solution concentration dependence could be obtained.

From Table 2 it can observe that the parameters a* for CV, and b* for MB, representing red and respectively, blue color, are increasing with the initial concentration of dye solutions, showing a more intense color while the initial solution concentration is increasing. In CR case, the percent

of red color, a* parameter, has a sudden increase but after c₂, the increase is very small, showing the same color intensity.

Table 2. CIELAB a* or b* parameter vs. dye solution initial concentration for PVA cryogels

C _{iCV} [mol/L]	a*	C _{iMB} [mol/L]	-b*	C _{iCR} [mol/L]	a*
1*10 ⁻⁶	7.11	8*10 ⁻⁶	10.33	2*10 ⁻⁶	21.11
3*10 ⁻⁶	20.89	2.4*10 ⁻⁵	29.89	6*10 ⁻⁶	46.00
5*10 ⁻⁶	33.78	4*10 ⁻⁵	36.56	1*10 ⁻⁵	46.00
7*10 ⁻⁶	27.44	5.6*10 ⁻⁵	40.44	1.4*10 ⁻⁵	46.44
1*10 ⁻⁵	36.67	8*10 ⁻⁵	42.00	2*10 ⁻⁵	46.55

Taking into account all above data, the change in the samples luminosity as well as the amount of the dye sorbed in the PVA cryogels at equilibrium (determined through the solution analysis) is shown in Fig. 4. Like a* or b* parameters, the luminosity of the samples is increasing with the initial solution concentration for CV and MB, while for CR, after the increase it remains constant.

Moreover, comparing the samples luminosity with the amount of the sorbed dye at equilibrium/ g PVA, for the three dyes, in the same concentration range (Fig. 4), it can be observed that the amount of CV sorbed is about 15% higher than for CR and double compared to MB.

3.3. Analysis of CIELAB parameters used to determine the type of interaction and the state of the dye into the gel

From the graphical representation of the CIELAB parameters vs. dye solution concentration, type of cryogel and type of dye, information about cryogel-dyes interaction and the aggregation type of dye in the cryogel can be obtained.

Fig. 5a shows the variation of the parameter +a* for all CV concentrations and all types of gels. Absorption of the green color in the visible range is a shift to lower wavelengths or a shift to blue (blue shift) and is correlated with the presence of dimers and molecular aggregates when the concentration of the dye increases (Ibrahim et al., 2010).

In accordance with the literature data (Gyu et al., 1989), for concentrations smaller than 5.10⁻⁶ M

(c_1 - c_3), the dye cation is in the monomeric form CV^+ , while the c_4 - c_5 solutions contain the dye in the dimeric form (Stork et al., 1972). The difference in color (ΔE^*) for CV loaded gels (Fig. 5c) shows the lowest values for PVA/Scl gels and the highest, for the PVA/Zein gels. The lighter color for PVA/Scl gels can be related to a highest contact surface and to a higher porosity (Papancea et al., 2015) that determine a better dye dispersion in the whole mass of the gel, while PVA/Zein gels darker color could be due to a more compact surface with low porosity (Papancea et al., 2015). This would determine a maximum agglomeration of the dye at the gel's surface, equivalent with a higher dye concentration. The lowest luminosity values are, as expected, for the PVA/Scl gel, which has the highest amount of the sorbed dye and for the PVA/Zein gels, which has the most compact structure.

Fig. 6a shows that the increase of the $-a^*$ parameter (green component) followed by a decrease observed for PVA, PVA/Cel, and PVA/Zein cryogels in the small concentrations range, is caused by a shift of the absorption band of MB at higher wavelengths (red-shift) than 664 nm. According with the literature data (Ahmad and Kumar, 2010) the sorbed MB in cryogels is in a monomer form (MB^+). At higher concentration, $+a^*$ parameter increases meaning sorption at the cryogels surface of (MB^+)₂ and respectively (MB^+)₃ forms. For PVA/Scl cryogels, $+a^*$ parameter increases should mean green light color absorption and blue shift in VIS spectrum (Wang and Wang, 2008) and consequently, (MB^+)₂ and (MB^+)₃ sorption on the gel substrate.

In Fig. 6c, the total color difference ΔE^* is the highest for PVA/Scl cryogels at small concentrations, meanwhile at higher concentrations a slight decrease of the ΔE^* parameter could be due to the decrease of samples luminosity. For the other cryogels the parameter increases with the concentration increase. Samples luminosity, ΔL^* evidences a continuous decrease with the increase of MB concentration, but the lowest luminosity is shown by the PVA/Scl cryogels (Fig. 6d). Thus, at small concentrations of

dye, all parameters indicate a maximum dye adsorption for the PVA/Scl samples; at the higher concentrations, the color parameters are not representative, due to luminosity decrease (Fig. 6c).

Fig. 7a shows that the parameter $+a^*$ increases (red component) in all cryogels and for all concentrations. CR has a relatively high ion and is negatively charged for a large range of pH (>5) (Dobrogowska et al., 1991). Correlating the very low concentration gradient of the most diluted solution and the large size of the anion RC, it can be concluded that the adsorption occurs on the surface of the gel by adsorbing a small number of anions. Close values of the parameter a^* for all samples in medium and high concentrations of CR solution could indicate adsorption of monomeric forms of CR, mainly on the surface of the gels.

In contrast to the parameter $+a^*$, the $+b^*$ parameter (yellow component) is changing significantly with increasing concentrations (Fig. 7b). At c_1 , this parameter has very low values, which emphasizes (together with the parameter $+a^*$) that the concentration gradient is very small and adsorption takes place on a small number of active centers. At c_2 - c_5 there is a significant increase in this parameter for PVA/Zein samples. Since these cryogels have the lowest swelling and crystallinity degree (Dobritoiu and Patachia, 2103) and a more compact structure (Papancea et al., 2015), the large dye anions, are adsorbed on the external surface of these gels, causing color intensification. Analysis of the color difference ΔE^* , chromaticity ΔC^* and hue ΔH^* , shows higher values for the PVA/Zein cryogels at medium concentrations while at high concentrations a slight decrease in these parameters can be observed; this decrease could be due to the increased brightness of the samples.

There is a small increase of $+a^*$ parameter (red color) for PVA/Cel cryogel comparing to the other cryogels (Figs. 5a, 6a and 7a) that may be due to a favorable orientation of dye cation plan on the gel surface considering the presence of more ordered micro-cellulose formations contained in the cryogel.

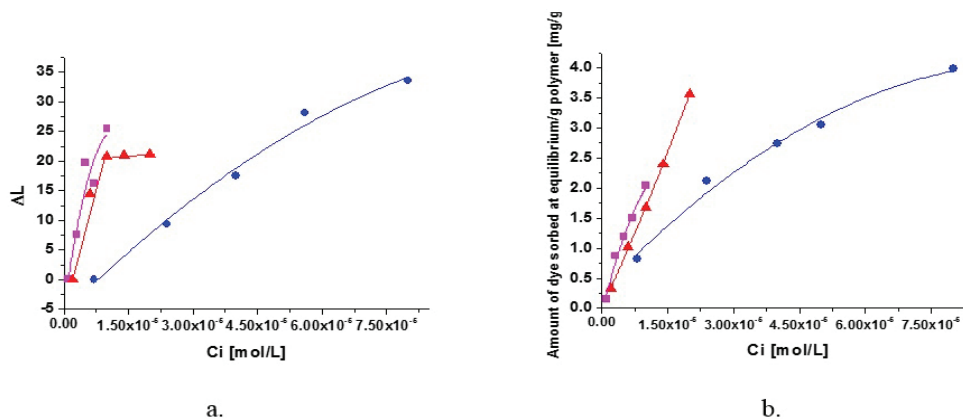


Fig. 4. The samples luminosity variation and the amount of CV (■), CR (▲) and of MB (●) sorbed in PVA cryogels at equilibrium

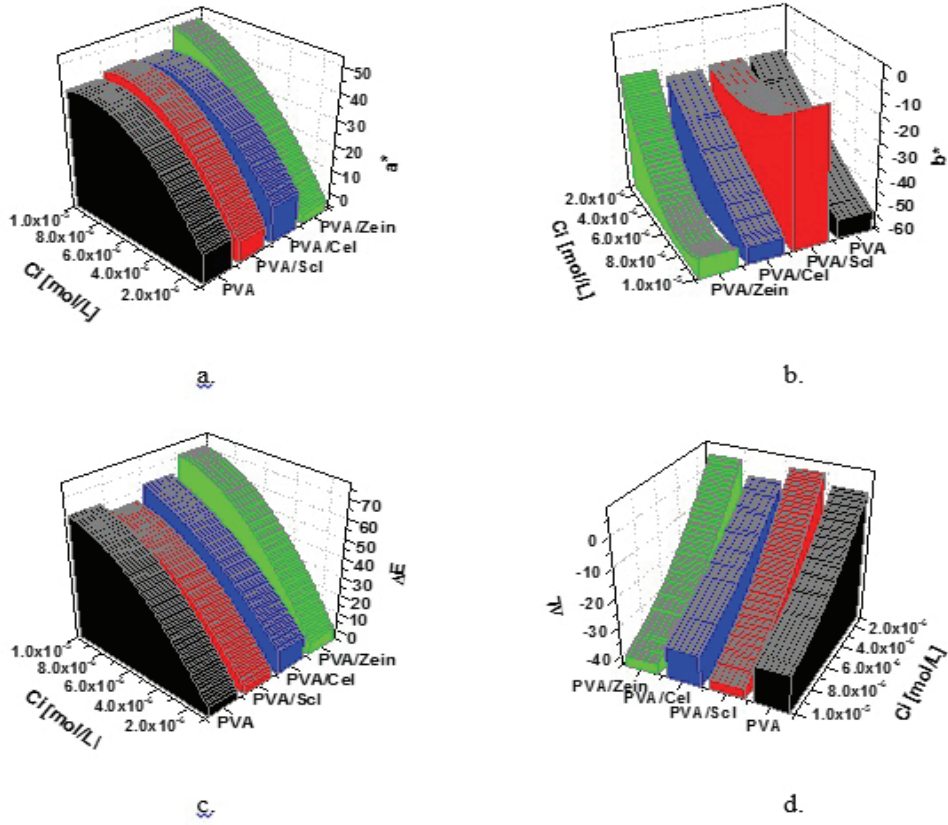


Fig. 5. a^* , b^* , ΔL^* and ΔE^* CIELAB parameters variation vs. CV initial concentration

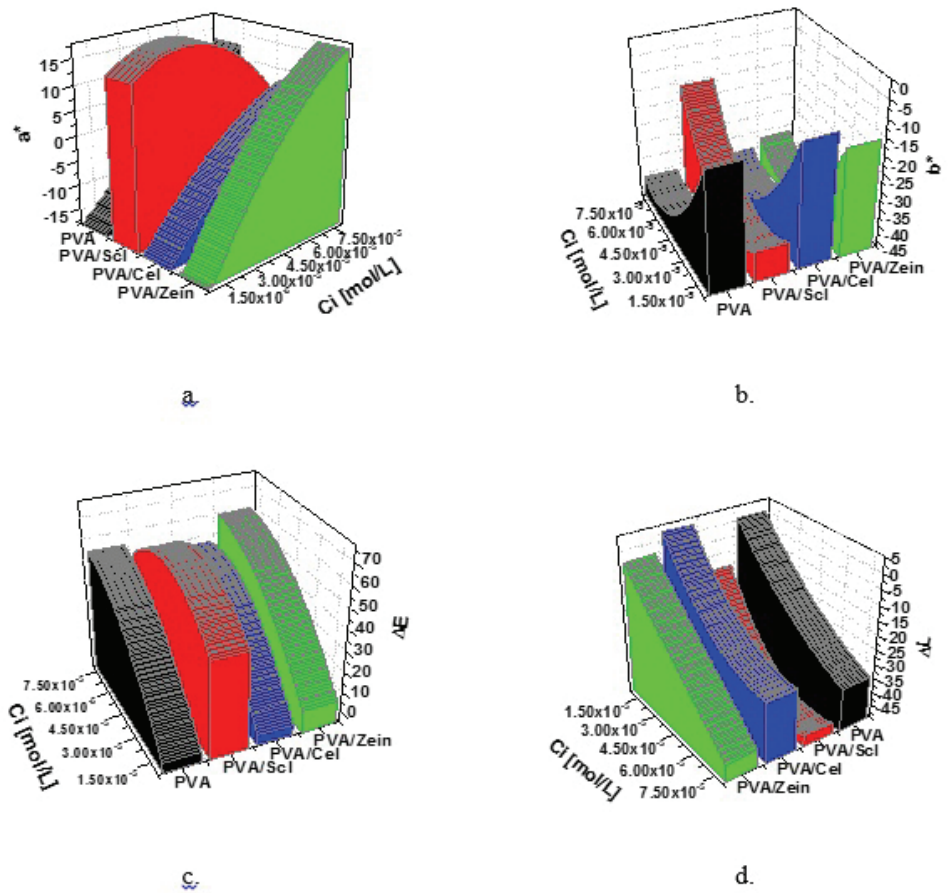


Fig. 6. a^* , b^* , ΔL^* and ΔE^* CIELAB parameters variation vs. MB initial concentration

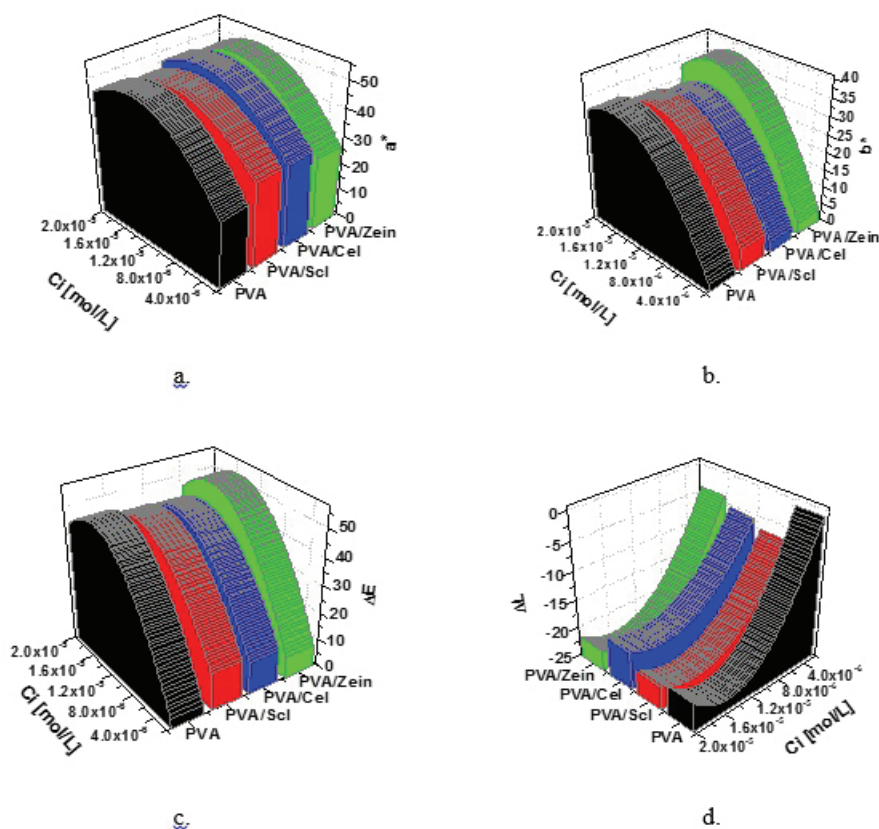


Fig. 7. a^* , b^* , ΔL^* and ΔE^* CIELAB parameters variation vs. CR initial concentration

Comparing the values for the difference in color (ΔE^*) for all samples it can be observed that they are in good agreement with the extinction coefficient, ϵ ($87.000 \text{ M}^{-1}\text{cm}^{-1}$ for CV, $95.000 \text{ M}^{-1}\text{cm}^{-1}$, for MB and $45.000 \text{ M}^{-1}\text{cm}^{-1}$, for CR) (Adams and Rosenstein, 1914; Cenens and Schoonheydt, 1988; Steensma, 2001), the samples with CR having the lowest values. In addition, from the graphical representation of a^*/b^* ratio the following information can be obtained.

The pink-violet color of PVA/Scl cryogels after CV sorption evidenced by the highest value for the ratio between a^*/b^* parameters (Fig. 8) could be explained through the fact that CV is a metachromatic dye (Confortin et al., 2010) that can determine - after its sorption- a shift of the absorption bands (the O-H stretching vibration band in FTIR spectrum of PVA/Scl shows a shift from 3262 cm^{-1} to 3278 cm^{-1} and in PVA case, from 3266.06 cm^{-1} to 3282 cm^{-1}) in the presence of substances with appropriately arranged anionic groups. This is because of the dye molecules that are getting close enough to form dimeric and polymeric aggregates.

For MB, the a^*/b^* ratio represented in Fig. 9, the value is increasing with concentration decrease for PVA, PVA/Cel and PVA/Zein cryogels showing a dependence between color intensification and solution concentration. This dependence can be observed also in Fig. 3. For PVA/Scl the ratio value does not change with concentration (the values are ranging between 0.35-0.47).

The ratio a^*/b^* for CR sorption shows decreasing values with concentration increase for all

cryogels except PVA/Scl where the values remain almost constant (Fig. 10). This could be due to fact that PVA/Scl gels are highly porous (Papancea et al., 2015) and determines a better dye dispersion in the whole mass of the gel. On the other hand, the luminosity parameter is increasing with concentration increase in all cases.

3.4. CIELAB parameters used to determine the permeability of a dye through the gel membrane

In Fig. 11, pictures of the PVA membrane subjected to CR diffusion for 515 hours (Papancea et al., 2010a) in a diffusion cell with two compartments (A- the donor compartment and B- the receptor compartment) are presented. As previously observed (Papancea et al., 2010a), strong interactions between CR and PVA determine the impermeability of the PVA membrane against CR. The both sides of the PVA membrane subjected to the diffusion process were analyzed using CIELAB method and all parameters were calculated and are graphically represented in Fig. 12. Comparing the values for all CIELAB parameters (Fig. 12) for the two sides (side A, membrane in contact with CR solution and side B, membrane in contact with water) of the PVA membrane, higher values are observed for the membrane in contact with the CR solution than for the membrane in contact with water. The high differences (double as values) in luminosity, in hue and in color are confirming the results obtained through solution analysis from B compartment, showing that no permeation occurs.

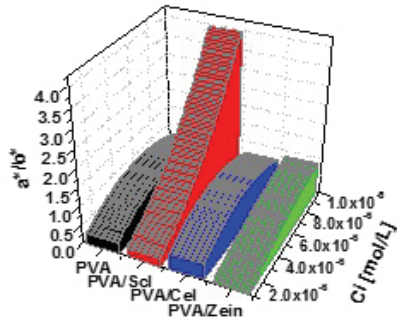


Fig. 8. Variation of a^*/b^* ratio in case of CV sorption vs. cryogel composition

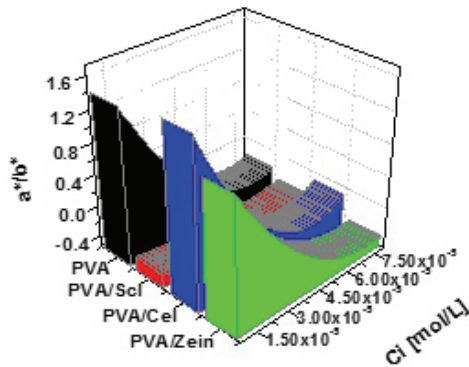


Fig. 9. Variation of a^*/b^* ratio in case of MB sorption vs. cryogel composition

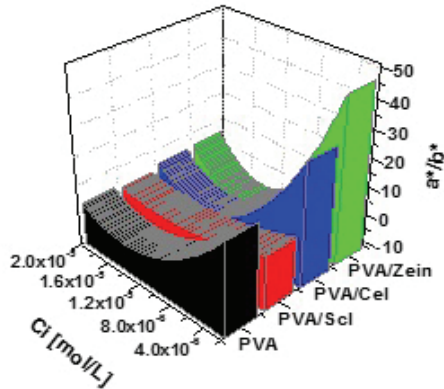


Fig. 10. Variation of a^*/b^* ratio in case of CR sorption vs. cryogel composition

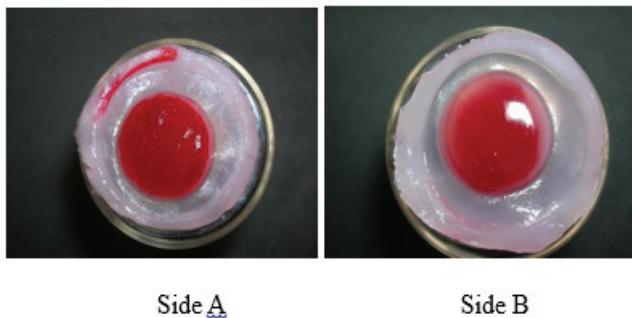


Fig. 11. PVA membranes after CR diffusion: side A – membrane in contact with CR solution; side B – membrane in contact with water

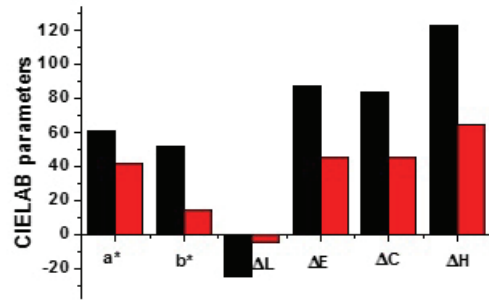


Fig. 12. PVA membranes after CR diffusion: black – side A, membrane in contact with CR solution; red – side B, membrane in contact with water

3.5. CIELAB parameters used to determine the kinetic of the dye sorption and desorption

Photographic images of the samples immersed in 5×10^{-6} mol CV/L solution for a certain period of time are presented in Fig. 13. For these images, CIELAB parameters were calculated and correlated with the values for the mass of CV sorbed /g of polymer obtained by solution analysis (after removing cryogel) through UV-VIS spectrometry. With these data, the sorption rate and the equilibrium time were calculated. The rate of sorption calculated as the slope of a^* vs. time has a value of 0.068 with $R= 0.94$ and for the mass of CV vs. time the rate of sorption is 6.35×10^{-3} mg CV/g PVA*min. Comparing the graphical representation of the a^* parameter vs. time with that of the mass of sorbed dye/g of PVA determined by solution analysis through UV-VIS method, versus time (Fig. 14), the equilibrium time was found to be around 360 minutes in both cases. The photographic images after desorption are presented in Fig. 15.

It can observe that there is a very small difference in color for the first 6 samples but after 24 hours (1440 min) the PVA cryogel has a lighter but more violet color. The slow decrease of $+a^*$ parameter (red component, absorption of green color) together with the slow increase of $-b^*$ (blue component, absorption of yellow color) and the luminosity increase indicates that the color lighten up meaning dye desorption. Like in sorption case, the desorption rate was calculated both as slope of variation of a^* vs. time and of mass of CV dss/g PVA vs. time respectively. The obtained values were 0.04 with $R= 0.89$ and respectively, 5.11×10^{-5} mg/g PVA*min with $R= 0.96$ (Fig. 16). Comparing the values after desorption with the values after sorption, it can observe that a^* , b^* and L values after 24 hours of desorption are comparable with those obtained after 150 minutes of sorption, indicating that a large amount of the dye remains inside of the polymeric matrix, as can be observed in the photographic images from Fig. 15. This hypothesis is confirmed by sorption rate value (6.35×10^{-3} mg CV/g PVA*min), which is two orders of magnitude higher than the desorption rate (5.11×10^{-5} mg/g PVA*min).

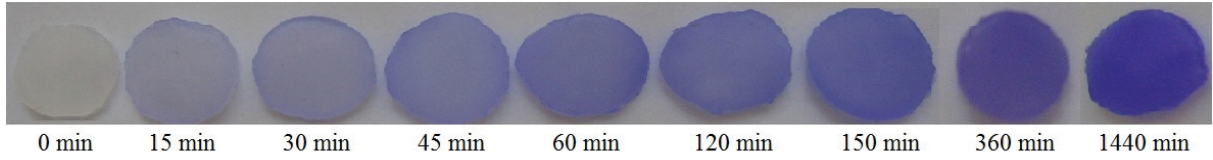


Fig. 13. Photographic images of PVA membranes after CV solution sorption ($C_i=5 \cdot 10^{-6}$ mol/L)

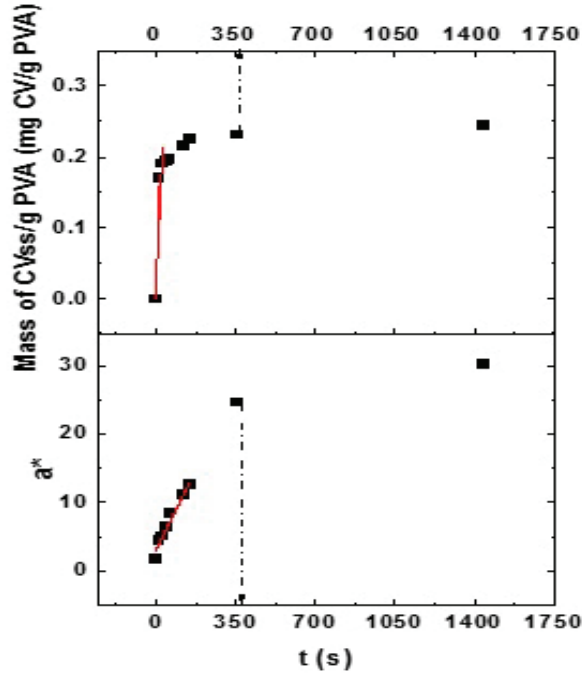


Fig. 14. Variation of a^* parameter vs. time and the mass CV sorbed into PVA vs. time

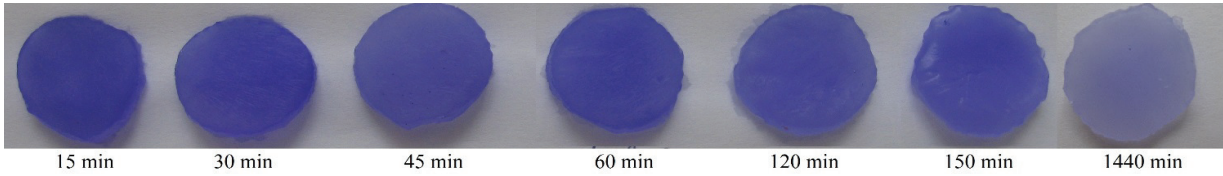


Fig. 15. Photographic images of PVA membranes after CV desorption

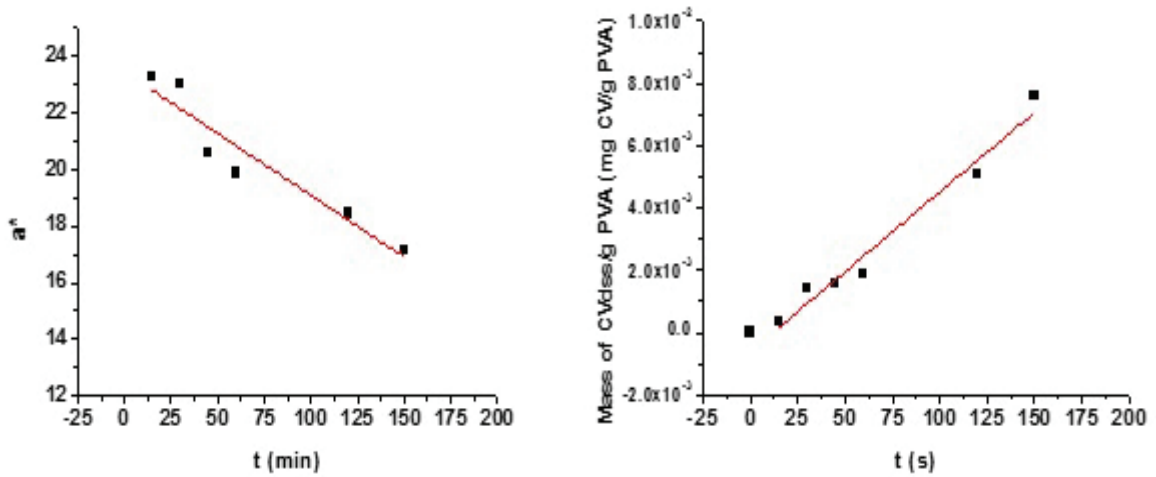


Fig. 16. Variation of a^* parameter vs. time and the mass CV sorbed into PVA vs. time

4. Conclusions

The proposed CIELAB method, applied for colored hydrogels, gives important information concerning the structure and the state of the dye inside of the polymer. It was determined that the color effect is dependent on the dye–dye and dye–polymer interactions, on the chemical composition of the gel, on the crystalline structure of the polymer, and by the nature of the immersion media.

Nevertheless, CIELAB method could be correlated with other methods of analysis and could successfully replace them being easier, time saving, un-expensive and non-polluting. As a case study, it was proved to be very efficient for PVA based hydrogels characterization.

Acknowledgments

This paper is supported by the Sectorial Operational Program Human Resources Development (SOP HRD), financed from the European Social Fund and by the Romanian Government under the project number POSDRU/159/1.5/S/134378.

References

- Adams E.Q., Rosenstein L., (1914), The color and ionization of Crystal-Violet, *Journal of American Chemical Society*, **36**, 1452–1473.
- Ahmad R., Kumar R., (2010), Adsorptive removal of Congo Red dye from aqueous solution using bael shell carbon, *Applied Surface Science*, **257**, 1628–1633.
- Cenens J., Schoonheydt R.A., (1988), Visible spectroscopy of methylene blue on hectorite, Laponite B, and barasym in aqueous suspension, *Clay and Clay Minerals*, **36**, 214–224.
- Confortin D., Neevel H., Brustolon M., Franco L., Albert J., Kettelarij, Williams René M., van Bommel M.R., (2010), Crystal violet: study of the photo-fading of an early synthetic dye in aqueous solution and on paper with HPLC-PDA, LCMS and FORS, *Journal of Physics: Conference Series*, **231**, 012011.
- Crini G., Badot P.M., (2008), Application of chitosan, a natural aminopolysaccharide, for dye removal from aqueous solutions by adsorption processes using batch studies: a review of recent literature, *Progress in Polymer Science*, **33**, 399–447.
- Croitoru C., Patachia S., Moise G., Porzolt A., Scarneciu C., (2009), *Dichromate Anions Sorption from Wastewaters using PVA Cryogels*, Proceeding of 20th DAAAM Conf., Annals of DAAAM and Proceedings, **20**, 1771-1772.
- Dobritoiu R., Patachia S., (2013), A study of dyes sorption on biobased cryogels, *Applied Surface Science*, **285P**, 56– 64.
- Dobrogowska C., Hepler L.G., Ghosh D.K., Yariv Sh., (1991), Metachromasy in clay mineral systems. Spectrophotometric and calorimetric study of the adsorption of crystal-violet and ethyl violet by Namontmorillonit and by Na-kaolinite, *Journal of Thermal Analysis*, **37**, 1347-1356.
- Globalspec, (2014), Three-dimensional representation CIELAB color scale, On line at: http://www.globalspec.com/learnmore/manufacturing_process_equipment/inspection_tools_instruments/color_appearance_instruments.
- Gyu B., Jung R.S., Kim K.J., (1989), Aggregation of crystal violet with tetraphenylborate anions in aqueous solutions, *Bulletin of Korean Chemical Society*, **10**, 148-151.
- Hang P.T., Brindley G.W., (1970), Methylene Blue absorption by clay minerals. Determination of surface areas and cation exchange capacities (Clay-organic studies XVIII), *Clays and Clay Minerals*, **18**, 203-212.
- Ibrahim M.M., El-Zawawya W.K., Nassarb M.A., (2010), Synthesis and characterization of polyvinyl alcohol/nanospherical cellulose particle films, *Carbohydrate Polymers*, **79**, 694–699.
- Ikkai F., Shibayama M., Nomura S., Han C.C., (1996), Complexation of poly(vinyl alcohol)-Congo Red aqueous solutions. 3. Dynamic light scattering study, *Journal of Polymer Science: Part B: Polymer Physics*, **34**, 939-945.
- Kim J., Montero G., Habibi Y., Hinestroza J.P., Genzer J., Argyropoulos D.S., Rojas O.J., (2009), Dispersion of cellulose crystallites by nonionic surfactants in a hydrophobic polymer matrix, *Polymer Engineering Science*, **49**, 2054–2061.
- Korifi R., Le Dreau Y., Antinelli J.-F., Valls R., Dupuy N., (2013), CIEL*a*b* color space predictive models for colorimetry devices – Analysis of perfume quality, *Talanta*, **104**, 58-66.
- Luís P.M.S.S., Cheng C.-Y., Boaventura R.A. R., (2014), Adsorption of a basic dye onto Esmegel clay, *Environmental Engineering and Management Journal*, **13** (2), 395-405.
- Papancea A., Valente A.J. M., Patachia S., (2010a), Diffusion and sorption studies of dyes through PVA cryogel membranes, *Journal of Applied Polymer Science*, **115**, 1445–1453.
- Papancea A., Valente A.J. M., Patachia S., (2010b), PVA cryogel membranes as a promising tool for the retention and separation of metal ions from aqueous solutions, *Journal of Applied Polymer Science*, **118**, 1567-1573.
- Papancea A., Patachia S., Dobritoiu R., (2015), Crystal violet dye sorption and transport in/through biobased PVA cryogel membranes, *Journal of Applied Polymer Science*, DOI: 10.1002/app.41838.
- Patachia S., Tica R., Savin G., (1997), A comparative study on iodine complexing with ethyl alcohol and ethyl acetate, *Revista de Chimie*, **48**, 947-951.
- Patachia S., Isac L., Rinja M., (2004), New methods for copper and sulphide ions retaining from the waste water, *Environmental Engineering and Management Journal*, **3**, 661-667.
- Patachia S., Rinja M., (2005), Ecological method for iodine separation from iodide aqueous solution, *Proceedings of International Symposium EnvEdu*, Brasov, Romania.
- Patachia S., Ion R., Varga St., Rinja M., (2007), Porphyrin encapsulation in nanostructured hydrogels, *Journal of Optoelectronics and Advanced Materials*, **6**, 1816-1820.
- Patachia S., Dobritoiu R., Coviello T., (2011), Determination of the sorption efficiency of Poly(vinyl alcohol)/Scleroglucan cryogels, against Cu²⁺ ions, *Environmental Engineering and Management Journal*, **10**, 193-198.
- Patachia S., Damian N., (2014), Cryogels based on Poly(Vinyl Alcohol) [PVA]/ ionic liquids [ILs]: from obtaining to antimicrobial activity, *Soft Materials*, **12**, 371-379.

- Schanda J., (2007), *Colorimetry: Understanding the CIE System*, John Wiley Sons Ink. Hoboken, New Jersey, USA.
- Steensma D.P., (2001), Congo Red: Out of Africa?, *Archives of Pathology and Laboratory Medicine*, **125**, 250–252.
- Stork W.H.J., Lippits G.J.M., Mandel M., (1972), Association of crystal violet in aqueous solutions, *Journal of Physical Chemistry*, **7**, 1772–1775.
- Vâlceanu A., Vârlan C., Schiller E., (2006), *Physiology and Pathology of Chromatic Dental* (in Romanian), Orizonturi Universitare Press, Timisoara, Romania.
- Varga S., Patachia S., Ion R., (2008), *Analysis of Mass Transfer of Encapsulated Porphyrins from PVA Based Hydrogels: an Experimental Study on Cylindrical Gels and Membranes*, Proceeding of the 5th International Conference HMT'08, Book series: Mathematics and Computers in Science and Engineering, 231-236.
- Wang L., Wang A., (2008), Adsorption properties of congo red from aqueous solution onto N,O-carboxymethyl-chitosan, *Bioresource Technology*, **99**, 1403–1408.



“Gheorghe Asachi” Technical University of Iasi, Romania



SEPARATION OF AROMATIC INTERMEDIATES OF BIOLOGICAL INTEREST USING EMULSION LIQUID MEMBRANES

Alexandra Raluca Miron^{1*}, Aurelia Cristina Nechifor¹,
Abbas Abdul Kadhim Klaif Rikabi^{1,2}, Szidonia Katalin Tanczos^{1,3}

¹Politehnica University of Bucharest, Faculty of Applied Chemistry and Materials Science,
Department of Analytical Chemistry and Environmental Engineering, 1-7 Polizu Str., Bucharest, Romania

²Al-Furat Al-Awsat University, Foundation of Technical Education, Technical College of Al-Mussaib(TCM), Baghdad, Iraq

³Sapientia University, Miercurea Ciuc, 1 Piata Libertatii, 530104 Harghita, Romania

Abstract

Established applications of emulsion liquid membranes (ELM) refer to refining in hydrocarbons and hydrometallurgical processing, rehabilitation of poisoned patients. In this work we investigated the separation of aromatic compounds of biological interest, more often encountered as intermediates in dyes and drugs industry: aniline, nitrobenzene, ortho and para-toluidine, using emulsion liquid membranes. The experimental results showed that in the case of basic substances separation the main physicochemical characteristics which have to be considered are alkalinity and water solubility. Thus, for the liquid emulsion membranes operation it is preferred to have a basicity as high as possible and a solubility as low as possible.

Key words: aromatic intermediates, biological interest compounds, liquid membranes, separation

Received: November, 2014; *Revised final:* February, 2015; *Accepted:* February, 2015

1. Introduction

Nowadays, wastewater is a potential source of pollution causing serious problems to the environments (Gómez et al., 2009; Manea et al., 2013; Modrojan et al., 2014). Thus, the amounts of wastewaters discharged in the environment from a high variety of industrial activities represent an important source of toxic, refractory, carcinogenic and low degradability compounds (Arsene et al., 2013; Santos and Rodrigues, 2014).

Due to the complex composition of the effluents, most of the treatment techniques such as: chemical precipitation, coagulation-flocculation, flotation, ion exchange, electro-oxidation and adsorption have their own limitations (Modrojan and Pincovschi, 2014; Tjoon et al., 2013). In this context, the treatment of wastewater using emulsion or supported liquid membranes represents an intense

process, with a huge application potential (Diaconu et al., 2012).

In particular, emulsion liquid membranes (ELM) are becoming more frequently used in the field of wastewater treatment because they are capable to successfully compete with traditional schemes (Craciun et al., 2009; Kurniawan et al., 2006).

The presence of organic toxic solutes in industrial wastewater is a common environmental problem (Namane et al., 2014; Orbeci et al., 2014). Aniline (amino-benzene) is known to be a harmful and persistent pollutant and its presence in wastewater requires treatment before disposal. Aniline is a carcinogenic chemical common in industry and industrial wastewater (Agrawal et al., 2008). Hence, alternative technique identification is required. Emulsion Liquid Membrane (ELM) is one of the techniques used to remove and recover

* Author to whom all correspondence should be addressed: e-mail: andra3005@yahoo.com

contaminants from wastewaters (Craciun et al., 2011). The field of liquid membrane technology is currently undergoing a rapid expansion in research, as well as its application as an industrial separation process (Zaharia et al., 2013).

Membrane separation, especially ELM enjoys a great success in the field of separation techniques due to its outstanding characteristics such as: simultaneous pollutants removal and materials recovery in a single unit, high efficiency due to large surface area available for mass transfer, high selectivity especially when carrier agents are used in the membrane phase that bind exclusively with target compounds; high fluxes, reusability and low energy consumption compared to other separation processes, low costs (Park et al., 2006; Zaharia et al., 2012).

In this work, the emulsion liquid membrane was employed in removal of biological interest aromatic compounds, more often encountered as intermediates of dyes and drugs industry: aniline, nitrobenzene, ortho and para-toluidine. Also, the research was focused on establishing the influence of operational parameters such as: contact time, pH, HCl concentration in the receiving phase and primary emulsion volume on the extraction yields.

2. Experimental

2.1. Materials and methods

HCl 25% (Merck) and distilled water were analytical grade, while SPAN 20 and SPAN 80 (Sigma-Aldrich) have a technical purity.

2.2. Experimental procedure description

The analysis of aromatic derivatives content in the source, receiving (aqueous) and organic phase was carried out by means of spectrophotometric extractive technique. The aqueous solutions used as source phase in the experiments were prepared in the laboratory.

The characteristics of the chemical substances considered for the extraction and their physical and chemical characteristics are listed in Table 1.

Tehnico-economical considerations require that the primary emulsion volume (toluene or cyclohexanol / acidic aqueous receiving phase) to be as small, in order to avoid the high cost of the surfactant, large emulsion volumes handled and excessive consumption of acids. Through this study, in the case of source phases containing basic and neutral organic compounds the minimum amount of emulsion is determined, or more accurately the volume ratio, R, primary emulsion / source phase, which can be used without seriously affecting the extraction yield.

The extraction yields were calculated based on the initial amount of organic compounds and after 15 minutes of contact, in the source phase, in order to be compared with the conventional solvent extraction yield (Diaconu et al., 2011). The systems used in the experimental studies, as source phase were presented in Table 2. For all the systems the following parameters were maintained constant:

- initial source phase volume $V_{fst} = 200 \text{ cm}^3$,
- contact time $t = 15 \text{ minute}$;
- the composition of primary emulsion.

The emulsion was prepared by mixing equal solution volumes of 5% SPAN 20 in toluene or cyclohexanol and receiving aqueous solution at pH = 1 (made with 0.1 M hydrochloric acid).

3. Results and discussion

3.1. Influence of primary emulsion volume on the extraction yield with ELM

The results of the experimental study conducted at volumetric ratios, R, emulsion phase (V_{fe}) / source phase (V_{si}) ranging from 1/10 and 1/1 are shown in Figs. 1-6.

Table 1. The physicochemical characteristics of the used substances

Substance	Chemical structure	Symbol	P_f °C	K_b^* 10^{-10}	d_{20} g/cm^3	Solubility	
						Water g/L	Cyclohexanol or toluene g/L
Nitrobenzene	$\text{C}_6\text{H}_5\text{-NO}_2$	NB	210.9	-	1.210	0.2	Total miscible
Aniline	$\text{C}_6\text{H}_5\text{-NH}_2$	A	184.4	3.82	1.022	3.6	Total miscible
o-Toluidine	<i>o</i> $\text{C}_6\text{H}_5\text{-NH}_2(\text{CH}_3)$	<i>o</i> -T	192.7	2.50	0.990	1.5	Total miscible
p-Toluidine	<i>p</i> $\text{C}_6\text{H}_5\text{-NH}_2(\text{CH}_3)$	<i>p</i> -T	200.0	1.48	1.010	2.5	Total miscible

Table 2. Chemical composition of the source phases

Symbol	A (ppm)	NB (ppm)	<i>o</i> -T (ppm)	<i>p</i> -T (ppm)
FS ₁	120	-	-	-
FS ₂	-	120	-	-
FS ₃	-	-	120	-
FS ₄	-	-	-	120
FS ₅	60	60	-	-
FS ₆	60	-	60	-
FS ₇	60	-	-	60

At small R ratios (Figs. 1, 2 and 3) it was found that the source systems containing nitrobenzene or lower alkalinity compounds are harder extractable than those containing aniline and p-toluidine. As shown in Figs. 1-6, the higher the volume ratio R is, the yield increase is most important, regardless of the membrane solvent, and the source phase composition. This leads to the conclusion that the extraction yield strongly depends on the volumes ratio, at the same extraction time and acid concentration in the receiving phase, regardless of the organic substances content in the aqueous solution (Figs. 4, 5 and 6).

However, in all the experiments, the best results were obtained using cyclohexanol as solvent, fact that can be explained by its higher polarity compared to toluene.

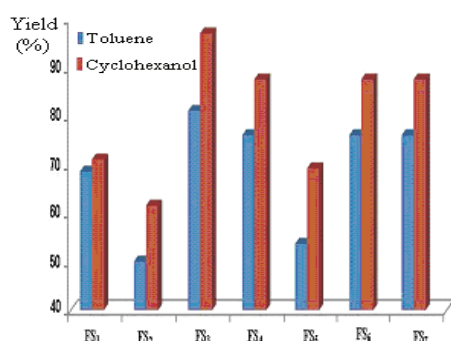


Fig. 1. The extraction yield variation at a volume ratio, R, emulsion phase (V_{fe}) / source phase (V_{si}) = 1/10, F_{SI} system

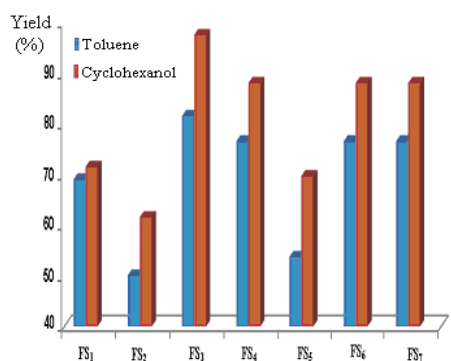


Fig. 2. The extraction yield variation at a volume ratio, R, emulsion phase (V_{fe}) / source phase (V_{si}) = 1/8, F_{SI} system

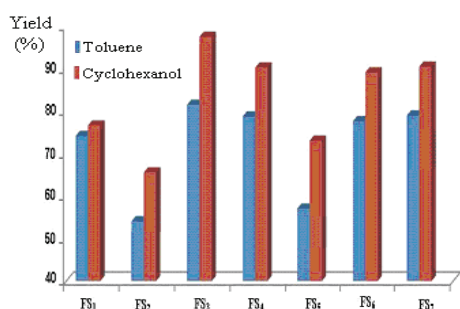


Fig. 3. The extraction yield variation at a volume ratio, R, emulsion phase (V_{fe}) / source phase (V_{si}) = 1/6, F_{SI} system

From the practical point of view, the recommended working conditions for the extraction of basic aromatic derivatives are: polar organic solvent, volume ratio R, emulsion phase (V_{fe}) / source phase (V_{si}) closer to 1, but acceptable, in technologically and economically terms (Fortună et al., 2012).

3.2. The influence of HCl concentration in the receiving phase

For substances having a weakly basic character, respectively aniline, o- and p-toluidine, theoretical, the extraction yield using emulsion liquid membranes is affected by acid concentration in the receiving phase, respectively by its pH.

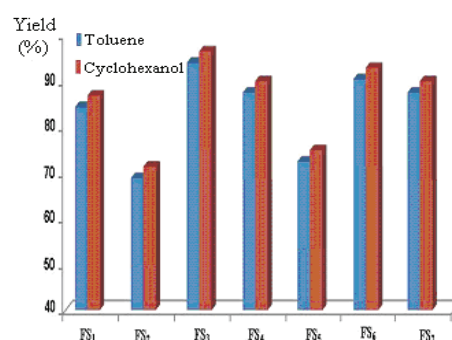


Fig. 4. The extraction yield variation at a volume ratio, R, emulsion phase (V_{fe}) / source phase (V_{si}) = 1/4, F_{SI} system

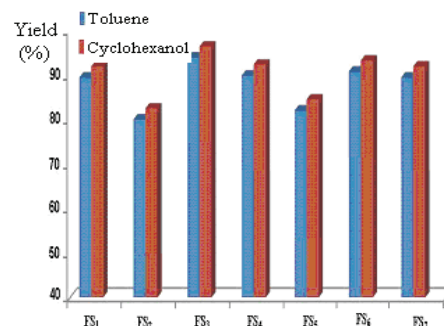


Fig. 5. The extraction yield variation at a volume ratio, R, emulsion phase (V_{fe}) / source phase (V_{si}) = 1/2, F_{SI} system

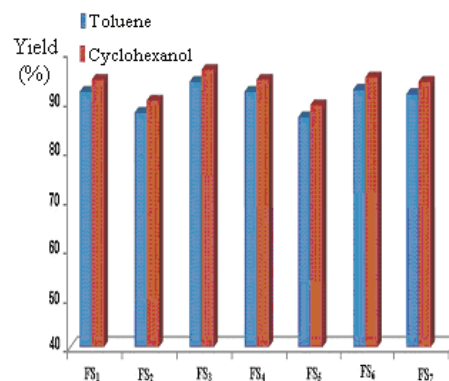


Fig. 6. The extraction yield variation at a volume ratio, R, emulsion phase (V_{fe}) / source phase (V_{si}) = 1, F_{SI} system

In laboratory, the extraction studies have been performed with ELM for FS₁, FS₆ and FS₇ systems with receiving solutions having pH between 1 and 6, adjusted using hydrochloric acid corresponding solutions. Liquid emulsion membranes used in the process were based on SPAN 20 and SPAN 80 in toluene and cyclohexanol (Table 3).

Table 3. Emulsion membranes used in the study

Symbol	Solvent	Surfactant
MTS80	toluene	SPAN 80
MTS20	toluene	SPAN 20
MCHS80	cyclohexanol	SPAN 80
MCHS20	cyclohexanol	SPAN 20

The solvent used for the non-ionic surfactant is toluene or cyclohexanol. The source phase and membrane volumes entered into the system, respectively 200 cm³ and 50 cm³, the contact time, $t = 15$ minutes and the chemical composition of the source phase (Table 2) were kept constant. The results are shown in Figs. 7-9. It is noted that in general for all source phases studied, the extraction yields with ELM increase with pH decreasing, the maximum yields being recorded for pH = 1.

In this case, the organic compounds solubilized in the organic phase, reach to the organic phase / receiving phase interface, where due to the hydrochloric acid presence pass into the aqueous phase, shifting the distribution equilibrium between the three stages to a new organic substance transfer from the source phase to the receiving aqueous phase (Barjoveanu and Teodosiu, 2009).

The negative synergistic effects are, however, unexpected, particularly evident for the membrane systems containing o-toluidine, difficult to explain by means of the distribution coefficients or alkalinity constants. Of course, aromatic amines extraction from source phase into receiving depends on the existing substituents in their aromatic ring. It is noted the higher extraction yield of p-toluidine compared to aniline on the full range of pH. This is not justified because $pK_{b \text{ aniline}} > pK_{b \text{ p-toluidine}}$.

The explanation lies in the lower toluidine solubility in water and therefore an easier passage in toluene or cyclohexanol (membrane). In order to explain the effect of the pK_b value on the aromatic amines separation, beside o-toluidine, p-toluidine experiments were carried out.

The low pH value has a positive influence on all the amine's extraction because favours the amine immobilization in the aqueous receiving phase. However, if the amine is more soluble in water (ex. aniline, toluidine compared with o-toluidine) its extraction is going to be more difficult at less acidic pH. Practically, at low pH (pH <3) the extraction is influenced by pK_b and at pH > 3 the extraction is influenced by the solubility in water.

The most effective p-toluidine separation is achieved at pH = 1, being the strongest base, while o-

toluidine is extracted better in the range $2 < \text{pH} < 4$ being the less soluble in water.

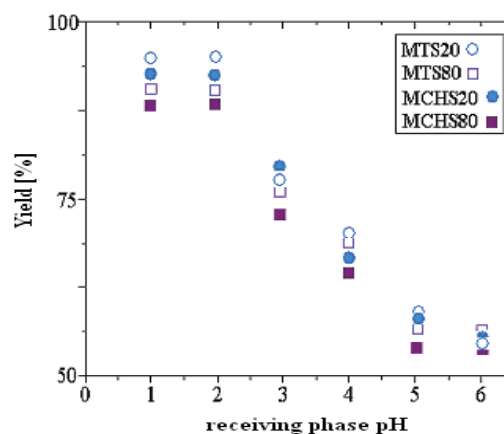


Fig. 7. The pH influence on extraction yield in the FS₁ system

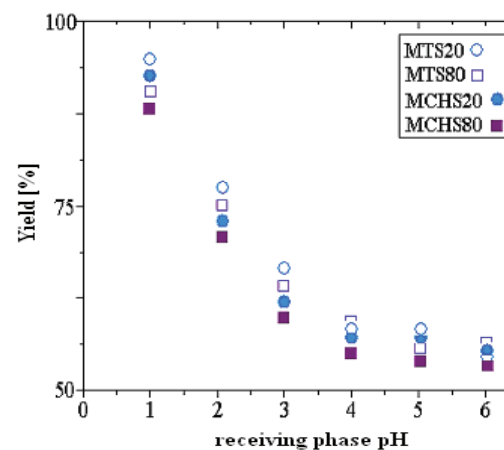


Fig. 8. The pH influence on extraction yield in the FS₆ system

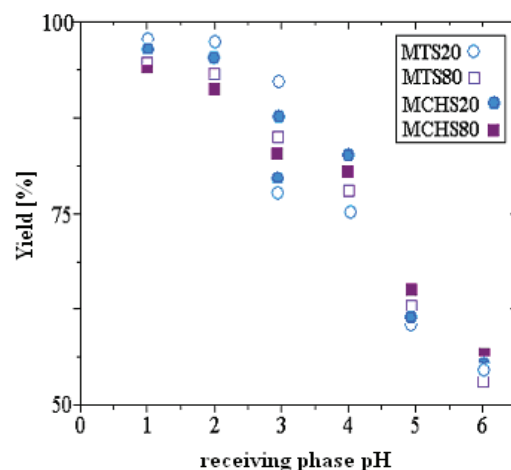


Fig. 9. The pH influence on extraction yield in the FS₇ system

The aniline and o-toluidine extraction yields from the mixture are lower than those obtained for the pure compounds, but the alkalinity influence is the same, o-toluidine extraction efficiency being

higher in this case. The total extraction yield for p-toluidine-aniline mixture is favoured by a positive synergistic effect, but is close to pure components yields. At the same amine content to be extracted, the yield is influenced by the surfactant included in the emulsion membrane, in this case being superior for SPAN 20 compared to SPAN 80 (Fig. 7-9). Favourable influence manifested by SPAN 20 on the extraction is canceled by the osmotic effect leading to swelling of this type of emulsion membrane by water diffusion from the source phase to membrane phase.

Illustrating this effect for FS₆ and FS₇ phases (Figs. 10 and 11), it results that, although the osmotic effect is also observed for the use of SPAN 80 as surfactant, in this case this is much smaller.

The emulsion swelling is an issue that leads to at least three drawbacks:

- ✓ lowering the concentration factor through water transportation into the receiving phase, so is diluted;
- ✓ primary emulsion breakage due to receiving solution particle size increase from the organic solvent, leading to phase mixing;
- ✓ the occurrence of unexplained results in graphs showing the extraction efficiency on pH, making difficult to optimize the working parameters.

3.3. Influence of pH on the concentration factor

For the emulsion membranes extraction, important is the *concentration of the components from the source phase to the receiving phase*, which can be followed, as technological solution, by the application of classical separation and concentration techniques, leading to *classic hybrid membrane technology* (Musteret and Teodosiu, 2007). In the case of primary source phase, solvent extraction would involve the use of high capacity containers, and significant amounts of solvent, which would involve, ultimately, unacceptable operating costs from technical and economical point of view.

Another problem appears when the solvent is contacted with the source phase, thus system performances depend on stirring and container shape. Using emulsion liquid membranes, the contact surface problem is solved, because an enormous surface mass transfer is achieved (Negoescu et al., 2013). In this case, when the concentration is achieved in the internal receiving phase, the problems related to the subsequent extraction with solvents or other separation process, it is solved the operated volumes being a few times lower. In this study was monitored how often the receiving phase was concentrated in aniline, o-toluidine, p-toluidine, and their mixture, depending on the internal phase pH and the surfactant nature used in the primary emulsion preparation, in the case of cyclohexanol as membrane solvent. The results are presented in Table 4. Although the extraction yields are high with MCH S20, however, due to strong swelling of the receiving phase, concentration factors are smaller.

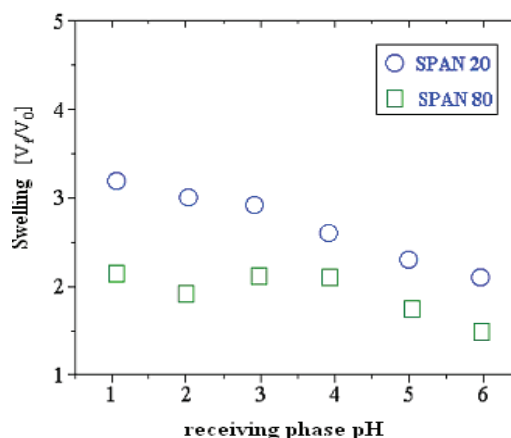


Fig. 10. The pH influence on emulsion membrane swelling for FS₆ system

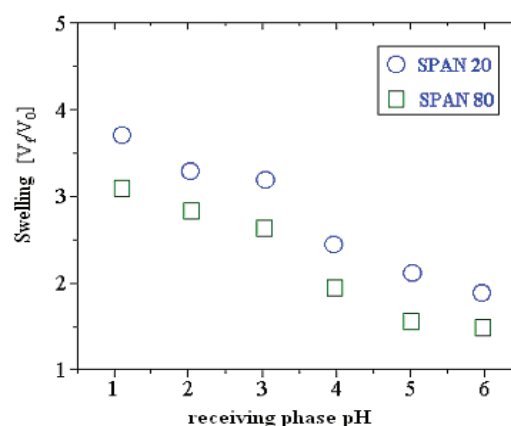


Fig. 11. pH influence on emulsion membrane swelling for FS₇ system

Table 4. The receiving phase pH influence on concentration factor

	$f = \frac{Cf_s}{Cf_R}$					
	pH					
	1	2	3	4	6	Obs
FS ₆	6.2	4.3	0.9	0.8	0.6	SPAN 20
	9.5	7.3	2.4	1.6	0.9	SPAN 80
FS ₇	7.1	3.2	1.8	1.3	0.7	SPAN 20
	8.2	6.7	2.3	1.4	1.0	SPAN 80

It is possible that SPAN 20 to facilitate the aniline and toluidine transport together with an appreciable amount of water. The study done in order to highlight the pH effect reconfirms the previous experiments, namely that at low pH concentration factors are high. The observed differences (especially for SPAN 20) can be justified by breaking the emulsion caused by undesired, retro-osmotic transfer, of water.

3.4. The contact time influence on ELM swelling

It is also interesting the influence of the contact time on the membrane swelling, depending

on the nature of membrane solvent (T - toluene or CH - cyclohexanol). The influence of the receiving phase pH on the swelling, at a determined contact time between the phases was studied.

Maintaining constant the receiving phase pH, SPAN 80 and volume ratio R, was determined the emulsion volume for each source phase type and same type of emulsion. Swelling results are shown in Table 5. It is observed that at a low contact time, swelling varies relatively little according to the source phase composition, but largely depends on the nature of membrane solvent.

Correlating the results and concomitantly following the maximum extraction yield and minimum swelling, the conclusion is that, the optimum working conditions are: contact time, $t \leq 25$ minutes for emulsions with SPAN 80, for all systems FS₁, FS₆, FS₇, and using cyclohexanol as membrane solvent. However at a contact time $t \leq 10$ minutes, for toluene emulsions the results are satisfactory.

Table 5. Contact time influence on emulsion liquid membranes swelling

System		Emulsion swelling at time (min)							
		10	20	30	40	50	60	70	80
FS ₁	MT	1.3	1.4	1.6	1.9	2.0	2.1	2.4	3.2
	MCH	2.0	2.4	2.5	2.6	2.6	2.7	2.8	2.8
FS ₆	MT	1.0	1.5	1.6	1.7	1.9	2.4	3.1	3.3
	MCH	1.9	2.0	2.0	2.1	2.1	2.1	2.2	2.3
FS ₇	MT	2.0	2.1	2.5	2.6	2.8	2.3	2.5	2.9
	MCH	2.0	2.0	2.1	2.1	2.1	2.1	2.2	2.3

4. Conclusions

In this work we aimed to evaluate the influence of operational parameters such as: contact time, pH, HCl concentration in the receiving phase and primary emulsion volume on the biological interest aromatic compounds separation effectiveness, most often found as intermediates in the dyes and drugs industry.

Based on the experimental results it was established that at separation of basic species using emulsion liquid membrane is necessary to provide the following operational conditions:

- surfactant: SPAN 80;
- membrane solvent: cyclohexanol;
- receiving phase/membrane solvent ratio $f_{FR}/S_M = 1$;
- receiving phase pH, close to 1;
- contact time lower than 30 minutes;

The effects of operational parameters above mentioned ensuring consist of:

- concentration factors higher than 2;
- extraction efficiencies higher than 60%.

The primordial physico - chemical characteristics of the basic substances exposed to separation that have to be considered are: alkalinity and water solubility.

Thus, for the operation of liquid emulsion membranes is preferred that: the basicity to be as high as possible and the solubility as low as possible.

Acknowledgements

The work has been funded by the Sectoral Operational Programme Human Resources Development 2007-2013 of the Ministry of European Funds through the Financial Agreement POSDRU/159/1.5/S/134398.

References

- Agrawal A., Manoj M.K., Kumari S., Bagchi D., Kumar V., Pandey B.D., (2008), Extractive separation of copper and nickel from copper bleed stream by solvent extraction route, *Minerals Engineering*, **21**, 1126-1130.
- Arsene D., Teodosiu C., Barjoveanu G., Apreutesei R.E., Apopei P., Musteret C.P., Cailean D., (2013), Combined catalytic oxidation and adsorption of priority organic pollutants for wastewater recycling, *Environmental Engineering and Management Journal*, **12**, 907-916.
- Barjoveanu G., Teodosiu C., (2009), Priority organic pollutants removal by ultrafiltration for wastewater recycling, *Environmental Engineering and Management Journal*, **8**, 277-287.
- Craciun M.E., Mihai M., Nechifor G., (2009), Characteristics of double jet liquid membrane, *Environmental Engineering and Management Journal*, **8**, 771-776.
- Craciun M.E., Badea N.N., Gales O., Aldea F., (2011), Determination of aerosols pollutants on membranes. Evaluation of particle collection efficiency and lead concentration in aerosols, *Environmental Engineering and Management Journal*, **10**, 621-627.
- Diaconu I., Aboul-Enein H.Y., Al-Omar M.A., Nechifor G., Ruse E., Bunaciu A.A., Totu E.E., (2011), Separation of nitrophenols. Equilibriums in bi- and tri-phasic systems, *Arabian Journal of Chemistry*, **4**, 99-103.
- Diaconu I., Zaharia I., Ruse E., Radu D. A., (2012), Kinetic Aspects of Transport para-aminophenol through Agitated Bulk Liquid Membrane, *Revista de Chimie*, **63**, 153-158.
- Fortună M.E., Simion I.M., Ghinea C., Petraru M., Cozma P., Apostol L.C., Hlihor R.M., Fertu Tudorache D., Gavrilescu M., (2012), Analysis and management of specific processes from environmental engineering and protection based on sustainability indicators, *Environmental Engineering and Management Journal*, **11**, 333-350.
- Gómez J.L., León G., Hidalgo A.M., Gómez M., Murcia M.D., Grinan G., (2009), Application of reverse osmosis to remove aniline from wastewater, *Desalination*, **245**, 687-693.
- Kurniawan T.A., Chan G.Y.S., Loa W.H., Babel S., (2006), Physico-chemical treatment techniques for wastewater laden with heavy metals, *Chemical Engineering Journal*, **118**, 83-98.
- Manea E., Manea D., Robescu D.N., (2013), Environmental risks of wastewater sludge disposal, *Environmental Engineering and Management Journal*, **12**, 79-84.

- Modrojan C., Pincovski I., (2014), Depollution of Acid Waste Waters Containing Zinc Ions Using Liquid - liquid Extraction, *Revista de Chimie*, **65**, 1253-1255.
- Modrojan C., Pincovski I., Budea S., (2014), Depollution of Acid Waste Waters Containing Cadmium Ions Using Liquid-Liquid Extraction, *Revista de Chimie*, **65**, 1235-1237.
- Mustereț C.P., Teodosiu C., (2007), Removal of persistent organic pollutants from textile wastewater by membrane processes, *Environmental Engineering and Management Journal*, **6**, 175-187.
- Negoescu C.C., Bunduc N., Iacob Tudose E.T., Mamaliga I., (2013), Aspects on polymer-solvent equilibrium and diffusion in polymeric membranes, *Environmental Engineering and Management Journal*, **12**, 1583-1591.
- Orbeci C., Nechifor G., Stănescu R., (2014), Removing toxic compounds from wastewater, *Environmental Engineering and Management Journal*, **13**, 2153-2158.
- Park Y., Skelland A.H.P., Larry J.F., Kim J.H., (2006), Removal of phenol and substituted phenols by newly developed emulsion liquid membrane process, *Water Research*, **40**, 1763-1772.
- Santos M.P.S., Rodrigues A.E., (2014), Adsorption equilibrium and fixed bed adsorption of aniline onto polymeric resin and activated carbons, *Separation Science and Technology*, **49**, 335-344.
- Tjoon T.T., Muthuraman G., Mubeena K., Sathya M., (2013), Emulsion liquid membrane: removal and recovery of organic and inorganic ions, *Journal of Membrane Science Technology*, **3**, 117-118.
- Zaharia I., Aboul-Enein H. Y., Diaconu I., Ruse E., Bunaciu A.A., Nechifor G., (2013), Facilitated transport of 5-aminosalicylic acid through bulk liquid membrane, *Journal of Iranian Chemical Society*, **10**, 1129-1136.
- Zaharia I., Diaconu I., Ruse E., Nechifor G., (2012), Transport and separation through bulk liquid membrane of some biologic active compounds, *Annals of "Ovidius" University, Constanta – Chemistry Series*, **23**, 53-57.



“Gheorghe Asachi” Technical University of Iasi, Romania



LAYERED DOUBLE HYDROXIDES AS ADSORBENTS FOR ANIONIC DYE REMOVAL FROM AQUEOUS SOLUTIONS

Maria Celina Alexandrica¹, Mihaela Silion², Doina Hritcu¹, Marcel Ionel Popa^{1*}

¹“Gheorghe Asachi” Technical University of Iasi, Faculty of Chemical Engineering and Environmental Protection,
73 Prof.dr.docent D. Mangeron Street, 700050 Iasi, Romania

²“Petru Poni” Institute of Macromolecular Chemistry, 41A Grigore Ghica Voda Alley, 700487 Iasi, Romania

Abstract

Reactive Blue 19 (RB 19) dye removal from aqueous solutions by using layered double hydroxides containing nitrate as the intergallery anion (MgAILDH) as adsorbents was investigated. The adsorption process was found to be influenced by the contact time, the initial dye concentration, the presence of inorganic anions and the temperature. The XRD and FTIR analysis evidence two competitive processes: adsorption and/or intercalation of the molecules may take place, depending on the initial dye concentration. The equilibrium dye adsorption increased from 62 to 350 mg/g as the initial RB 19 concentration was risen from 0.5 to 3.0 mg/mL. The adsorption capacity decreases in the presence of electrolytes. The experimental data are well fitted with the Langmuir isotherm equation. The thermodynamic parameters were calculated. The resulting negative ΔS° value correlated with a positive value of ΔH° indicate that the adsorption process is spontaneous and endothermic. In addition, the regeneration of MgAILDH after RB 19 adsorption was also investigated and proved feasible only in the first cycle.

Key words: adsorption, layered double hydroxide, reactive blue 19, thermodynamic constants

Received: November, 2014; *Revised final:* February, 2015; *Accepted:* February, 2015

1. Introduction

Environmental pollution reduction by implementing ecological technologies is currently a high priority for the scientific community. Large quantities of dyes are annually produced and used in textile, cosmetics, paper, leather, pharmaceutical, food and other industries. Approximately 15% of the dye produced globally is lost during the dyeing process and discharged in the textile effluents (El Gaini et al., 2009).

The presence of dyes in wastewater poses severe problems to the environment, due to their synthetic nature, poor degradability and difficulty to treat by conventional methods. Dyes are stable to light and heat, and some are proven to be toxic to microorganisms, having a negative impact upon photosynthetic activity in aquatic systems (Sumari et al., 2009). Treatments aimed to eliminate dyes from

textile wastewater are prioritized and regulated by government legislation since even small amounts are highly visible and toxic (Salleh et al., 2011).

Many researchers have studied various techniques in order to remove the dyes from wastewaters, for example, the use of coagulant/flocculant agents, advanced processes of oxidation, ozonation, nanofiltration and adsorption on various supports such as solid agriculture waste, gallinaceous feathers (Figueiredo and Freitas, 2013), pumice stone (Samarghandi et al., 2013), different types of activated carbon, montmorillonite impregnated with tensioactive agents, etc. (Itoh et al., 2005). Due to low biodegradability, a conventional biological treatment is not considered efficient, while the adsorption on activated carbon has proven to be an effective process, with the disadvantage of high cost (Purkait et al., 2004). However, among all these methods, the adsorption has been preferred due to the

* Author to whom all correspondence should be addressed: e-mail: mipopa@tuiasi.ro; Phone: +40744496751

high quality of the treated effluents, especially for well-designed sorption processes (Javadian et al., 2014). Low-cost materials, in their natural and modified forms, have been also extensively studied as alternative adsorbents for dyes (Ahmad et al., 2007; Gurses et al., 2006). Among the various adsorbents, layered double hydroxides (LDHs) are promising waste scavengers, particularly for dye molecules (Allmann, 1968).

Recent studies showed that the use of LDHs for the retention of organic anions has shown very good results (De Roy et al., 1992; Lakraimi et al., 2000; Sillion et al., 2013). Adsorption of dyes by LDHs is a facile method for cleaning up effluents and wastewater before discharging them into the environment (Abdelkader et al., 2011; Ahmed and Gasser, 2012; Auxilio et al., 2009; Bouhent et al., 2011; Dos Santos et al., 2013; Elkhatabi et al., 2013; Extremera et al., 2012; Guo et al., 2013; Malek and Yasin, 2012; Monash and Pugazhenth, 2014; Pereira de Sa et al., 2013).

LDHs, also known as anionic clays, are materials of great interest due to their hydrophobic nature and large specific surface area, high anionic exchange capacity and good adsorption ability. The layered structure of the LDHs creates the premises for intercalating large organic or inorganic anions such as dyes, drugs, pesticides, enzymes, polymers, etc. generating hybrid inorganic-organic nanostructures (Chun et al., 2009; De Roy, 1998; Hosni et al., 2009; Nalawade et al., 2009). LDHs are characterised by a lamellar structure similar to that of the brucite $Mg(OH)_2$ in which the Mg^{2+} ions are replaced by trivalent ions like M^{3+} . 3.

The general formula describing these materials is: $[M^{II}_{1-x}M^{III}_x(OH)_2]^{x+}(A^n)_{x/n} \cdot mH_2O$, where: M^{II} and M^{III} are divalent and trivalent cations respectively, A^n is the compensation anion and x is the molar fraction of the trivalent cation ($M^{III}/[M^{II} + M^{III}]$). A large number of divalent and trivalent metals are able to combine to form LDHs layers (Cavani et al., 1991).

The aim of the present work is to assess the adsorption capacity of MgAILDH for the RB 19 dye and to understand the mechanism involved. The influences of contact time, initial dye concentration, amount of LDHs, the temperature and the inorganic anion competition upon the adsorption process have been studied. The localization of the dye in the interlayer space and/or on external surfaces of the LDHs is studied by XRD and FTIR analyses.

2. Materials and methods

2.1. Materials

All chemicals, including $Mg(NO_3)_2 \cdot 6H_2O$, $Al(NO_3)_3 \cdot 9H_2O$ and Reactive Blue 19 (RB 19), were purchased from Sigma-Aldrich and were used without further purification. Deionized water was used for the preparation of all aqueous solutions. The chemical structure of the dye is shown in Fig. 1.

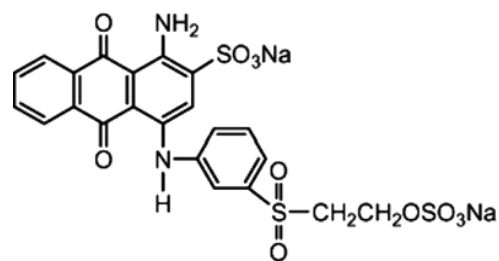


Fig. 1. Structural formula of Reactive Blue 19

2.2. Synthesis of MgAILDH

The MgAILDH was synthesized by coprecipitation method at a constant pH value of 9.7 and a temperature of 60°C (according to the method described by Miyata, 1980). 100 ml aqueous solution containing 0.1 mol of $Mg(NO_3)_2 \cdot 6H_2O$ and 0.05 mol of $Al(NO_3)_3 \cdot 9H_2O$ ($Mg/Al = 2$) was delivered with 0.4 ml/min flow rate into a round bottom flask containing 60 ml deionized water that was previously bubbled with nitrogen for half an hour in order to remove carbonate anion contamination. The pH was maintained constant by simultaneous addition of a 1.0 N NaOH solution, using a TitrLab TIM 854 apparatus. The resulting white precipitate was aged at room temperature for 18 h under stirring and then for 30 h without stirring. After the ageing step, the precipitate was separated by centrifugation, washed extensively several times with deionized water until reaching a pH value of 7, then dried overnight under vacuum at 70°C.

2.3. Characterization techniques

X-ray powder diffraction (XRD) patterns were recorded on a Bruker AXS D8 diffractometer using monochromatic $CuK\alpha$ radiation ($\lambda = 0.154$ nm), operating at 40 kV and 50 mA over a 2θ range from 4 to 70 degree. FTIR spectra were recorded on a FT-IR Bomem MB 104 spectrometer under the following experimental conditions: 200 scans in the mid-IR range (400-4000 cm^{-1}) using KBr (ratio 5 / 95 wt %) pellets, and a resolution of 4.0 cm^{-1} .

2.4. Adsorption experiments

The adsorption experiments were carried out using the batch equilibrium technique at different temperatures in the range of 15°C-45°C, at pH= 6.8 and under a stream of N_2 . 0.4 g of MgAILDH were dispersed in 50 mL of RB 19 solutions. The initial dye concentration was varied between 0.5 and 3 mg/mL. The solution has been washed, filtrated and the solid products obtained have been dried under vacuum at 100°C for 3 hours and used for analysis. The concentration of textile dye RB 19 was determined by the spectrophotometric method. Samples were taken at certain periods of time.

The absorbance for each sample was measured at 594 nm on a Nanodrop 1000 Spectrophotometer. The amount of RB 19 adsorbed

by MgAILDH, Q , was calculated as the difference between initial and equilibrium (final) concentrations of the dye in solution (C_i and C_f , respectively) by a given mass of the adsorbent (m) in the volume of solution, V (Elkhatabi et al., 2013)(Eq. 1):

$$Q = \frac{(C_i - C_f) \times V}{m} \quad (1)$$

3. Results and discussion

3.1. Powder X-ray diffraction

The XRD patterns recorded for the MgAILDH matrix, the corresponding hybrid materials MgAILDH-RB 19, the calcined MgAILDH-RB 19 (CMgAILDH) after the adsorption and for the reconstruction material are presented in Fig. 2. The diffractogram of the original LDH (Fig. 2a) has a typical layered structure similar to those reported in the literature for these materials (Xu and Zeng, 2001). The diffraction peak found at 8.79 Å on the MgAILDH diffractogram corresponds to the basal spacing of LDHs with nitrate anions in the interlayer (Myata, 1983).

The diffractogram recorded for MgAILDH-RB 19 after adsorption in the dye concentration range located below 0.5 mg/mL (Fig. 2b), the crystallinity of the sample is a bit diminished compared with that shown by the original LDH, as indicated by the decrease in the distance of the basal space (d_{003}), that was reduced from 8.79 Å to 8.41 Å (Elkhatabi et al., 2013). At higher dye concentration (more than 1.5 mg/mL), both the adsorption process and the intercalation of anionic molecule of the dye into the LDH structure took place. The intercalation of the dye anions cause an increase in the interlayer space from $d_{003} = 8.79$ Å to $d_{003} = 9.59$ Å. This diffractogram feature is in good agreement with values reported by other authors (Elkhatabi et al., 2013; Rubino, 2001) and it is explained by the exchange of the nitrate anion with the RB 19 anions (Fig. 2c).

The XRD pattern recorded for the CLDH (Fig. 2d) indicated that the layered double hydroxides structure is destroyed and evidenced only the presence of MgO (Crepaldi et al., 2002; Thomas et al., 2006; You et al., 2002). This observation might suggest an almost total decomposition of the MgAILDH and elimination of most interlayer nitrate anions and water. After the dye adsorption onto CLDH, the layered double structure has been mostly reconstructed (Fig. 2e). It was also observed that the intensity of the peaks decreased compared with the original LDH, suggesting a lowered crystallinity due to the calcination and regeneration processes. The basal space of the material after the last cycle of reconstruction was $d_{003} = 8.07$ Å.

3.2. FTIR spectroscopy

The FTIR spectra of the MgAILDH and MgAILDH-RB 19 samples are presented in Fig. 3.

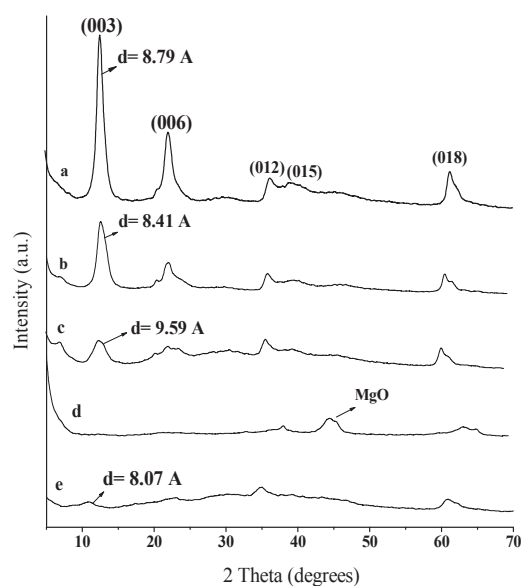


Fig. 2. Powder XRD patterns for MgAILDH (a), MgAILDH-RB19, 0.5 mg/mL (b), MgAILDH-RB19, 3 mg/mL (c), CLDH (d), CLDH after RB 19 adsorption (e)

The broad and strong band in the frequency range of 3600-3200 cm^{-1} , centered at 3466 cm^{-1} , is common for all the hydrotalcite type materials corresponding to the OH stretching vibration due to the presence of water molecules (De Roy et al., 2001). The bands observed in the low-frequency region of the spectrum are associated with the lattice vibration modes in the LDH sheets and may be assigned to the M-O bond in the wavenumber range of 781 to 675 cm^{-1} and respectively to the M-O-M bond located near 447 cm^{-1} (M = Al, Mg) (Cavani et al., 1991). The appearance of a strong band at 1384 cm^{-1} is due to the symmetric vibration of the interlayer nitrate anion belonging to the MgAILDH (Silion et al., 2010). All the vibration bands associated with the organic anion, as well as the adsorption bands characteristic for LDHs are evidenced in the spectra recorded for MgAILDH-RB 19 sample (Fig. 3b, c).

The asymmetric stretching vibration related to the S=O bond appears in the 1273-1155 cm^{-1} region. The adsorption bands at 1674 and 1474 cm^{-1} are assigned to the stretching vibration of the C=C bond belonging to an aromatic ring, while the bands at 1634 and 1182 cm^{-1} are assigned to those of C=O and respectively C-N bond (Elkhatabi et al., 2013). The absence of the 1384 cm^{-1} band from the spectrum of the MgAILDH-RB 19 (Fig. 3c) sample obtained when the initial RB 19 concentration is higher than 1.5 mg/mL, confirms the fact that the interlayer nitrate anions have been displaced (Silion et al., 2012). For the MgAILDH-RB 19 sample obtained when using an initial dye concentration that is lower than 1.5 mg/mL, the band characteristic to the nitrate anion is evidenced (Fig. 3b). In this case, only the adsorption of the dye occurs. The FTIR analysis correlated with the XRD reveal that the interaction between the matrix and the dye is, depending on the initial

concentration of the latter, a competitive process comprising two sides: adsorption and intercalation.

3.3. Adsorption equilibrium

3.3.1. Effect of contact time and initial dye concentration

The dye concentration is an important parameter characterizing the mass transfer of the anionic molecules between the aqueous and solid phase. The effect of initial RB 19 concentration upon the adsorption efficiency was evaluated in the concentration range of 0.5 to 3.0 mg/mL, while the temperature and LDH amount were kept at 25° C and 0.4 g, respectively. The results are presented in Fig. 4. The equilibrium adsorption capacity increased with increasing the initial dye concentration, due to the increase in the amount of anions competing for the available binding sites on the LDH surface.

The equilibrium amount of adsorbed dye increased from 62 to 350 mg/g as the initial RB 19 concentration increased from 0.5 to 3.0 mg/mL. The results show that dye uptake is rapid in the first stage, lasting about 60 minutes, and then changes slowly towards saturation, attained after 240 minutes. The time required for reaching equilibrium increases at higher initial dye concentrations.

3.3.2. Effect of inorganic anion competition

Textile industries generally use large amounts of salts in the fabric dyeing process (Baocheng et al., 2008, Netpradit et al., 2004). Typical formulations involve Na₂SO₄ (50 g/L) and Na₂CO₃ (5g/L) solutions when RB 19 is the dye of choice.

It is therefore important to investigate the effect of these anions upon the dye removal efficiency when MgAILDH is used as an adsorbent. The following procedure was used: 5g Na₂SO₄, 0.5 g Na₂CO₃ and 50 mg MgAILDH were added to 100 mL RB 19 solution with a concentration of 0.15 mg/mL (the parameters are almost similar to the composition of the wastewater from textile industry). Effect of coexisting ions upon the dye adsorption of the MgAILDH is shown in Fig. 5.

The decreased adsorption efficiency in the presence of the electrolytes is due to the interaction between the surface and the added solutes that may block some of the sorption active sites otherwise available for the dye molecules, and probably to the competitive process of intercalation of the inorganic and organic anions of the dye.

The dye uptake was reduced when the dye solution contained Na₂SO₄ and Na₂CO₃, compared to the case where no electrolyte was added. The adsorption efficiency of the dye in the absence of the electrolytes is determined after 420 minutes and it is 71.25 %, while in the presence of SO₄²⁻ anions, the removal efficiency is 58.75 % and it is reached after 480 minutes. The maximum reduction in the removal efficiency was 50 % in the presence of CO₃²⁻ ions. This result is consistent with those reported in the

literature and showed that in the case in which both SO₄²⁻ and CO₃²⁻ coexist, they had a significant effect upon the adsorption of dye (Parsa and Abbasi, 2007). It has been also demonstrated that the interlayer CO₃²⁻ ions in LDHs are difficult to be exchanged by other anions (Goswamee et al., 1988; Inacio et al., 2001; Toraiishi et al., 2002).

3.3.3. Effect of temperature

The adsorption process depends on the temperature and this parameter has the following effect. Increasing the temperature is known to modify the diffusion rate of the adsorbate molecule within the matrix, owing to the decrease in the solution viscosity. Also, changing the temperature will modify the equilibrium capacity of the adsorbant for a particular adsorbate (Khezami and Capart, 2005).

The effect of temperature on the removal of dye was studied by varying adsorption temperatures from 15°C to 45°C by adjusting the temperature controller on the water bath shaker, using 50 mL solution aliquots with initial dye concentrations in the range of 0.5-3 mg/mL.

Fig. 6 displays the adsorption curves obtained under various isothermal conditions. The LDH equilibrium adsorption capacity for RB 19 was higher with increasing temperature, ranging from 172 mg/g at 15°C to 321 mg/g at 25°C, to 451 mg/g at 35°C and to 548 mg/g at 45°C. This trend indicates that the dye adsorption on MgAILDH was favored at higher temperature.

3.4. Thermodynamic study of RB 19 adsorption by MgAILDH

The thermodynamic parameters provide information about the inherent energetic changes associated with the adsorption process.

The standard free energy (ΔG°), standard enthalpy (ΔH°) and standard entropy (ΔS°) were calculated using the following equations (Eqs. 2-4):

$$\Delta G^\circ = -RT \ln K_L \quad (2)$$

$$\Delta G^\circ = \Delta H^\circ - T \Delta S^\circ \quad (3)$$

$$\ln K_L = \Delta S^\circ / R - \Delta H^\circ / RT \quad (4)$$

where R (8.314 J/molK) is the universal gas constant, T (K) is the absolute solution temperature, and K_L (L/mg) is the Langmuir isotherm constant. ΔG° can be calculated from the Langmuir model by using Eq. (3) and the value of the equilibrium constant K_L determined at each temperature. The standard enthalpy (ΔH°) and standard entropy (ΔS°) values can be calculated from the slope and intercept of the plot of $\ln K_L$ versus $1/T$ (Eq. 5).

The values of these parameters are presented in Table 1. The positive value of ΔH° confirms the endothermic nature of the dye adsorption process. Generally speaking, a value of ΔH° between 5 and 40 kJ mol⁻¹ is characteristic for a physisorption

mechanism, while an enthalpy in the range of 40 to 800 kJ mol⁻¹ corresponds to chemisorption mechanism (Crini and Badot, 2008). The negative value of ΔS° indicates a rather good affinity of the material for the dye molecules and it is a sign of an increase in the degree of freedom of the adsorbed species, compared to their unbound state (Hu et al., 2007; Renault et al., 2008; Zhu et al., 2005).

3.5. Regeneration of MgAILDH-RB 19

In order to reuse the adsorbent after completing equilibrium adsorption experiments, the suspensions were recovered, filtered, dried on a thermobalance (Mettler Toledo HG63 Moisture Analyzer) and calcined at 550°C again for 4 h.

The calcined materials (CMgAILDH), in portions of 0.4 g, were re-dispersed in 50 mL of RB

19 solution with 3 mg/mL concentration. This procedure was repeated three times and the amount of RB 19 adsorbed after each dispersion-calcination cycle was determined.

The adsorption of RB 19 using MgAILDH and CMgAILDH after thermal treatment is shown in Fig. 7. After the first-cycle regeneration, CLDH sorption capacity decreased from 281 mg/g to 230 mg/g, a percentage decrease of 13 % compared with the original MgAILDH. This is not in agreement with the LDH adsorption behavior as reported by Zhu et al. (2005). These authors observed that the Brilliant Blue adsorption capacity decreased about 69 % compared with the original calcined LDH after the first regeneration cycle. In the following regeneration cycles, the adsorption capacity decreased significantly, at 122 mg/g in the second cycles and respectively 88 mg/g in the third cycle.

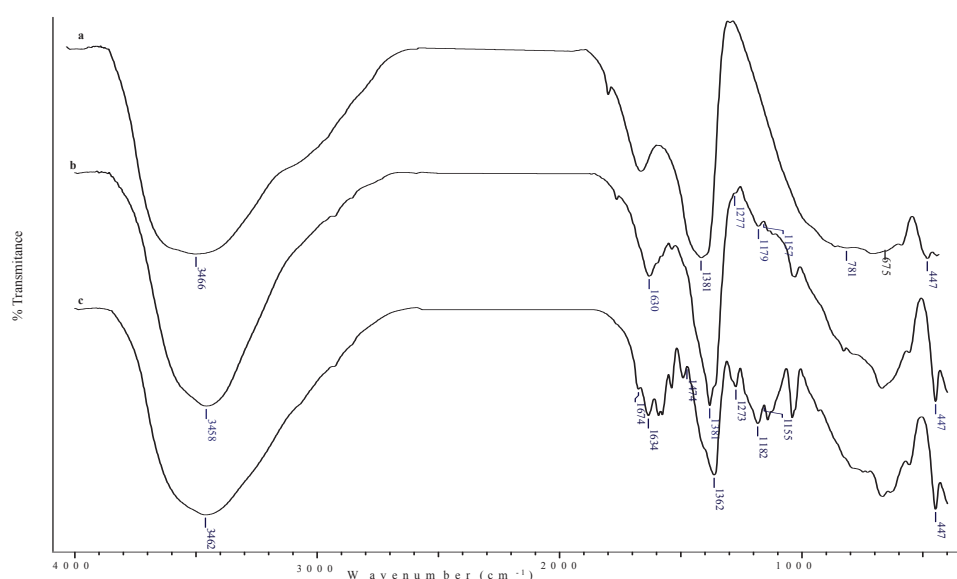


Fig. 3. FTIR spectra of MgAILDH (a), MgAILDH-RB 19, concentration of RB 19- 0.5 mg/mL (b), MgAILDH-RB 19, concentration of RB 19-3 mg/mL (c)

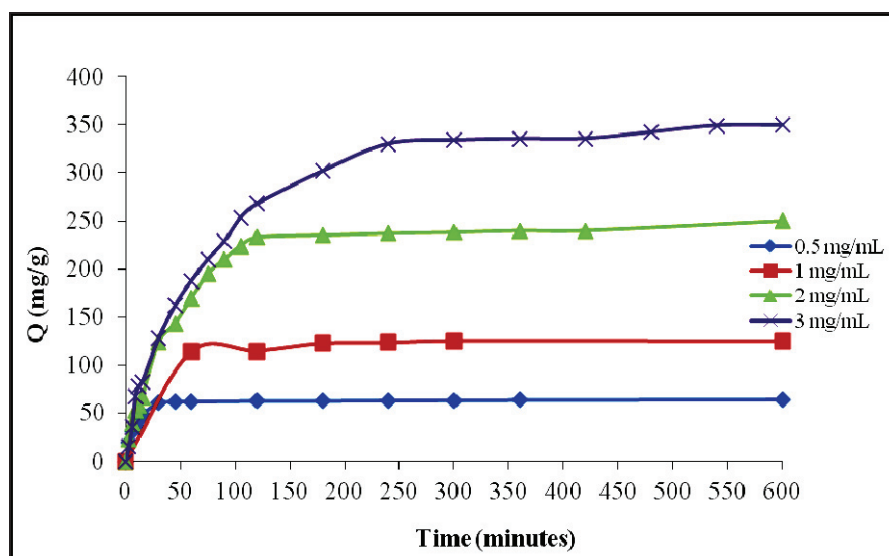


Fig. 4. Effect of contact time and initial concentration of RB 19 on the extent of adsorption

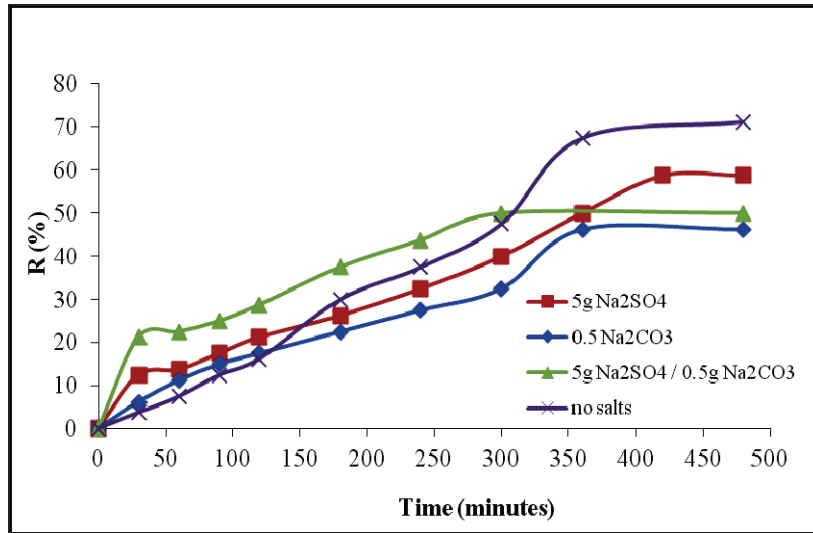


Fig. 5. Effect of co-existing anions on the removal efficiency

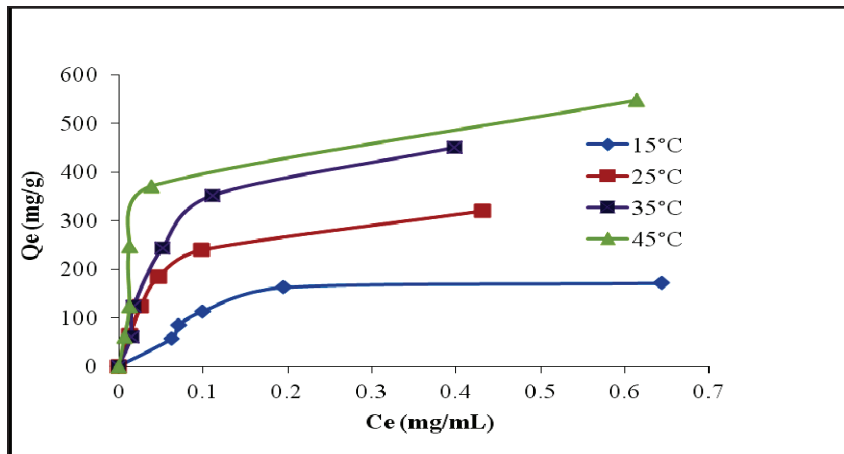


Fig. 6. The adsorption isotherms

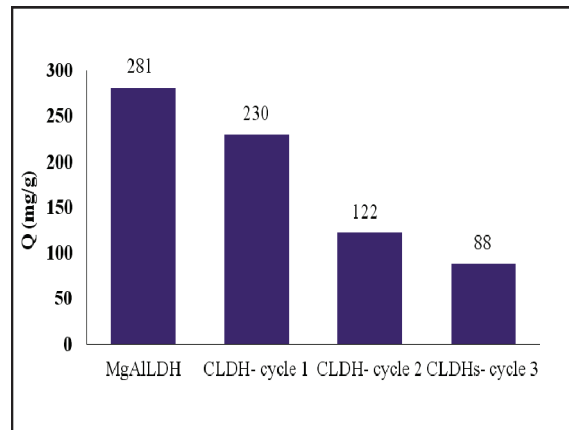
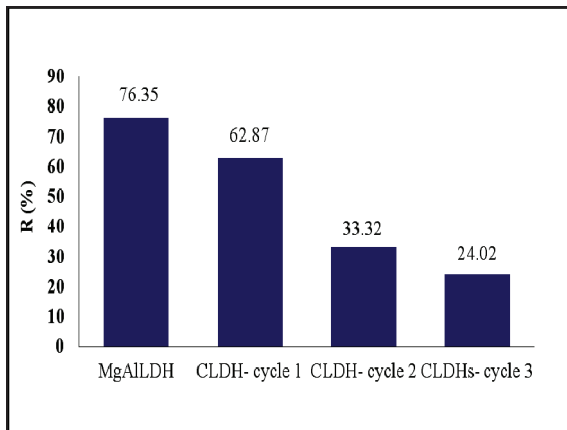


Fig. 7. Adsorption of RB 19 using MgAILDH and CMgAILDH

Table 1. Thermodynamic parameters for the adsorption of RB 19 on MgAILDH

Thermodynamic constants						
MgAILDH	ΔG° (kJ mol ⁻¹)				ΔH° (kJ mol ⁻¹)	ΔS° (J mol ⁻¹ K ⁻¹)
	15°C	25°C	35°C	45°C		
MgAILDH-RB 19	- 1.955	- 4.423	- 5.585	- 6.066	37.18	-135.88

In our experiments, the results are consistent with those reported by Ni et al. (2007) in the adsorption of methyl orange on MgFeLDH. This behavior is probably due to the progressive decreasing in crystallinity of the LDH-like materials in structural reconstruction of the calcined materials, leading to lower adsorption capacity (Ni et al., 2007).

4. Conclusions

This study shows that MgAILDH can be used as an efficient adsorbent for the removal of the RB 19 dye from solutions with compositions that mimic real textile waste-water. The mechanism of adsorption on external surfaces and intercalation by reconstruction of calcined material was confirmed by XRD and FTIR analysis.

The processing parameters such as, contact time and initial dye concentration, inorganic anion competition and temperature can affect the adsorption process. The adsorption data are fitted well with the Langmuir isotherm equation. The thermodynamic parameters were calculated and the negative ΔS° and positive ΔH° indicate that the adsorption process is spontaneous and endothermic under the experimental conditions.

Thermal treatments for regenerating MgAILDH after RB 19 adsorption suggest that this material can be recycled and re-used.

References

- Abdelkader N.B.H., Bentouami A., Derrichea Z., Bettahara N., De Menorval L. C., (2011), Synthesis and characterization of Mg-Fe layer double hydroxides and its application on adsorption of Orange G from aqueous solution, *Chemical Engineering Journal*, **169**, 231-238.
- Ahmad A.A., Hameed B.H., Aziz N., (2007), Adsorption of direct dye on palm ash: kinetic and equilibrium modeling, *Journal of Hazardous Materials*, **141**, 70-76.
- Ahmed I.M., Gasser M.S., (2012), Adsorption study of anionic reactive dye from aqueous solution to Mg-Fe-CO₃ layered double hydroxide (LDH), *Applied Surface Science*, **259**, 650-656.
- Allmann R., (1968), The crystal structure of pyroaurite, *Acta Crystallographica B*, **24**, 972-977.
- Auxilio A.R., Andrews P.C., Junk P.C., Spiccia L., Neumann D., Raverty W., Vanderhoek N., (2009), The adsorption behavior of C.I. Acid Blue 9 onto calcined Mg-Al layered double hydroxides, *Dyes and Pigments*, **81**, 103-112.
- Baocheng Q.U., Jiti Z., Xuemin X., Chunli Z., Hongxia Z., Xiaobai Z., (2008), Adsorption behaviour of azo dye C.I. Acid Red 14 in aqueous solution on surface soils, *Journal of Environmental Sciences*, **20**, 704-709.
- Benselka-Hadj Abdelkadera N., Bentouamib A., Derrichea Z., Bettahara N., de Menorval L.C., (2011), Synthesis and characterization of Mg-Fe layer double hydroxides and its application on adsorption of Orange G from aqueous solution, *Chemical Engineering Journal*, **169**, 231-238.
- Bouhent M.M., Derriche Z., Denoyel R., Prevot V., Forano C., (2011), Thermodynamical and structural insights of orange II adsorption by Mg_RAlNO₃ layered double hydroxides, *Journal of Solid State Chemistry*, **184**, 1016-1024.
- Cavani F., Trifirò F., Vaccari A., (1991), Hydrotalcite-type anionic clays: preparation, properties and applications, *Catalysis Today*, **11**, 173-301.
- Chun X.L., Wan G.H., (2009), Synthesis of layered double hydroxides with novel morphologies, *Journal of Dispersion Science and Technology*, **30**, 174-177.
- Crepaldi E.L., Tronto J., Cardoso L.P., Valim J.B., (2002), Sorption of terephthalate anions by calcined and uncalcined hydrotalcite-like compounds, *Colloids and Surfaces A: Physicochemical and Engineering Aspects*, **211**, 103-114.
- Crini G., Badot P.M., (2008), Application of chitosan, a natural amino polysaccharide for dye removal from aqueous solutions by adsorption processes using batch studies: A review of recent literature, *Progress in Polymer Science*, **33**, 399-447.
- De Roy A., Forano C., El Malki K., Besse J.P., (1992), *Anionic Clays: Trends in Pillaring Chemistry*, In: *Synthesis of Microporous Materials*, Ocelli M.L., Robson H.E. (Eds.), Van Nostrand Reinhold, New York, 108-169.
- De Roy A., (1998), Lamellar double hydroxides, *Molecular Crystals and Liquid Crystals*, **311**, 173-193.
- De Roy A., Forano C., Besse J.P., (2001), *Layered Double Hydroxides: Synthesis and Postsynthesis Modification*, In: *Layered Double Hydroxides: Present and Future*, Rives V. (Ed.) Nova Science, New York, NY, 1-41.
- Dos Santos R.M.M., Gonçalves R.G.L., Constantino V.R.L., Da Costa L.M., Da Silva L.H.M., Tronto J., Pinto F.G., (2013), Removal of Acid Green 68:1 from aqueous solutions by calcined and uncalcined layered double hydroxides, *Applied Clay Science*, **80-81**, 189-195.
- El Gaini L., Lakraimi M., Sebbar E., Meghea A., Bakasse M., (2009), Removal of indigo carmine dye from water to Mg-Al-CO₃-calcined layered double hydroxides, *Journal of Hazardous Materials*, **161**, 627-632.
- Elkhatabi E.H., Lakraimi M., Badreddine M., Legroui A., Cherkaoui O., Berraho M., (2013), Removal of Remazol Blue 19 from wastewater by zinc-aluminium-chloride-layered double hydroxides, *Applied Water Science*, **3**, 431-438.
- Extremera R., Pavlovic I., Perez M.R., Barriga C., (2012), Removal of acid orange 10 by calcined Mg-Al layered double hydroxides from water and recovery of adsorbed dye, *Chemical Engineering Journal*, **213**, 392-400.
- Figueiredo S.A., Freitas O.M., (2013), Adsorption kinetics of removal of Yellow Lanazol dyestuff using gallinaceous feathers, *Environmental Engineering and Management Journal*, **12**, 2061-2070.
- Goswamee R.L., Sengupta P., Bhattacharyya K.G., Dutta D.K., (1988), Adsorption of Cr (VI) in layered double hydroxides, *Applied Clay Science*, **13**, 21-34.
- Guo Y., Zhu Z., Qiu Y., Zhao J., (2013), Enhanced adsorption of acid brown 14 dye on calcined Mg-Fe layered double hydroxide with memory effect, *Chemical Engineering Journal*, **219**, 69-77.
- Gurses A., Dogar C., Yalcin M., Acikyildiz M., Bayrak R., Karaca S., (2006), The adsorption kinetics of the cationic dye, methylene blue, onto clay, *Journal of Hazardous Materials*, **131**, 217-228.

- Hosni K., Srasra E., (2009), Simplified synthesis of layered double hydroxide using a natural source of magnesium, *Applied Clay Science*, **43**, 415-419.
- Hu Q., Xu Z., Qiao S., Haghseresht F., Wilson M., Lu G.Q., (2007), A novel color removal adsorbent from hetero-coagulation of cationic and anionic clays, *Journal of Colloid and Interface Science*, **308**, 191-199.
- Inacio J., Taviot-Gueho C., Forano C., Besse J.P., (2001), Adsorption of MCPA pesticide by MgAl-layered double hydroxides, *Applied Clay Science*, **18**, 255-264.
- Itoh T., Shichi T., Yui T., Takahashi H., Inui Y., Takagi K., (2005), Reversible color changes in lamella hybrids of poly(diacetylenecarboxylates) incorporated in layered double hydroxide nanosheets, *Journal of Physical Chemistry B*, **109**, 3199-3206.
- Javadian H., Angaji M.T., Naushad M., (2014), Synthesis and characterization of polyaniline/ γ -alumina nanocomposite: A comparative study for the adsorption of three different anionic dyes, *Journal of Industrial and Engineering Chemistry*, **20**, 3890-3900.
- Khezami L., Capart R., (2005), Removal of chromium (VI) from aqueous solution by activated carbons: kinetic and equilibrium studies, *Journal of Hazardous Materials B*, **123**, 223-231.
- Lakraimi M., Legrouri A., Barroug A., De Roy A., Besse J.P., (2000), Preparation of a new stable hybrid material by chloride-2,4-dichlorophenoxyacetate ion exchange into the zinc-aluminium-chloride layered double hydroxide, *Journal of Materials Chemistry*, **10**, 1007-1011.
- Malek A.H.A., Yasin Y., (2012), Use of Layered Double Hydroxides to Remove Sunset Yellow FCF Dye from Aqueous Solution, *Chemical Science Transactions*, **1**, 194-200.
- Miyata S., (1975), The Syntheses of Hydrotalcite-Like Compounds and Their Structures and Physico-Chemical Properties I: The Systems Mg^{2+} - Al^{3+} - NO_3^- , Mg^{2+} - Al^{3+} - Cl^- , Mg^{2+} - Al^{3+} - ClO_4^- , Ni^{2+} - Al^{3+} - Cl^- and Zn^{2+} - Al^{3+} - Cl^- , *Clays and Clay Minerals*, **23**, 369-375.
- Miyata S., (1983), Anion-exchange properties of hydrotalcite-like compounds, *Clays and Clay Minerals*, **31**, 305-311.
- Miyata S., (1980), Physico-chemical properties of synthetic hydrotalcites in relation to composition, *Clays and Clay Minerals*, **28**, 50-56.
- Monash P., Pugazhenth G., (2014), Utilization of Calcined Ni-Al Layered Double Hydroxide (LDH) as an Adsorbent for Removal of Methyl Orange Dye from Aqueous Solution, *Environmental Progress & Sustainable Energy*, **33**, 154-159.
- Nalawade P., Aware B., Kadam V.J., Hirlekar R.S., (2009), Layered double hydroxides: A review, *Journal of Scientific & Industrial Research*, **68**, 267-272.
- Nepradit S., Thiravetyan P., Towprayoon S., (2004), Adsorption of three azo reactive dyes by metal hydroxide sludge: effect of temperature, pH and electrolytes, *Journal of Colloid and Interface Science*, **270**, 255-261.
- Ni Z.M., Xia S.J., Wang L.G., Xing F.F., Pan G.X., (2007), Treatment of methyl orange by calcined layered double hydroxides in aqueous solution: Adsorption property and kinetic studies, *Journal of Colloid and Interface Science*, **316**, 284-291.
- Parsa J.B., Abbasi M., (2007), Decolorization of synthetic and real wastewater by indirect electrochemical oxidation process, *Acta Chimica Slovenica*, **54**, 792-796.
- Pereira de Sa F., Cunha B. N., Nunes L.M., (2013), Effect of pH on the adsorption of Sunset Yellow FCF food dye into a layered double hydroxide (CaAl-LDH- NO_3), *Chemical Engineering Journal*, **215-216**, 122-127.
- Purkait M.K., DasGupta S., De S., (2004), Removal of dye from wastewater using micellar-enhanced ultrafiltration and recovery of surfactant, *Separation and Purification Technology*, **37**, 81-92.
- Renault F., Morin-Crini N., Gimbert F., Badot P.M., Crini, G., (2008), Cationized starchbased material as a new ion-exchanger adsorbent for the removal of CI Acid Blue 25 from aqueous solutions, *Bioresource Technology*, **99**, 7573-7586.
- Salleh M.A.M., Mahmoud D.K., Karim W.A.W.A., Idris A., (2011), Cationic and anionic dye adsorption by agricultural solid wastes: A comprehensive review, *Desalination*, **280**, 1-13.
- Samarghandi M.R., Zarrabi M., Amrane A., Soori M.M., Sepehr M.N., (2013), Removal of Acid Black dye by pumice stone as a low cost adsorbent, *Environmental Engineering and Management Journal*, **12**, 2137-2147.
- Silion M., Hritcu D., Popa M.I., (2010), Preparation and characterization of ketoprofen-layered double hydroxide compounds, *Journal of Optoelectronics and Advanced Materials*, **12**, 2150 – 2156.
- Silion M., Hritcu D., Lisa G., Popa M.I., (2012), New hybrid materials based on layered double hydroxides and antioxidant compounds. Preparation, characterization and release kinetic studies, *Journal of Porous Materials*, **19**, 267-276.
- Silion M., Dobrea I.D., Nistor D., Popa M.I., (2013), Environmentally friendly formulations of 2,6-dichlorobenzonitrile pesticide intercalated into calcined layered double hydroxides, *Environmental Engineering and Management Journal*, **12**, 2465-2471.
- Sumari S.M., Yasin Y., Hamzah Z., (2009), Adsorption of anionic amido blank dye by layered double hydroxides ZnAlCO₃-LDH, *The Malaysian Journal of Analytical Sciences*, **13**, 120-128.
- Toraishi T., Nagasaki S., Tanaka S., (2002), Adsorption behavior of IO_3^- by CO_3^{2-} and NO_3^- hydrotalcite, *Applied Clay Science*, **22**, 17-23.
- Xu Z. P., Zeng H. C., (2001), Decomposition Pathways of Hydrotalcite-like Compounds $Mg_{1-x}Al_x(OH)_2(NO_3)_x \cdot nH_2O$ as a Continuous Function of Nitrate Anions, *Chemistry of Materials*, **13**, 4564-4572.
- You Y., Zhao H., Vance G.F., (2002), Adsorption of dicamba (3,6-dichloro- 2-methoxy benzoic acid) in aqueous solution by calcined-layered double hydroxide, *Applied Clay Science*, **21**, 217-226.
- Zhu M.X., Li Y.P., Xie M., Xin H.Z., (2005), Sorption of an anionic dye by uncalcined and calcined layered double hydroxides: a case study, *Journal of Hazardous Materials B*, **120**, 163-171.



“Gheorghe Asachi” Technical University of Iasi, Romania



NEW COMPLEXES OF 2-(1H-1, 2, 4-TRIAZOL-3-YL) PYRIDINE WITH Co(II), Cd(II), Rh(III), IONS: SYNTHESIS, STRUCTURE, PROPERTIES AND POTENTIAL APPLICATIONS

Petronela Horlescu¹, Daniel Sutiman¹, Corneliu S. Stan^{1*}, Carmen Mita²,
Cristian Peptu³, Maria E. Fortuna³, Cristina Albu¹

¹“Gheorghe Asachi” Technical University of Iasi, Faculty of Chemical Engineering and Environmental Protection,
73 Prof. Dr. docent Dimitrie Mangeron Str., 700050 Iasi, Romania

²“Alexandru Ioan Cuza” University of Iasi, Faculty of Chemistry, 11 Carol I Blvd., 700506 Iasi, Romania

³“Petru Poni” Institute of Macromolecular Chemistry, 41A Grigore Ghica Voda Alley, 700487 Iasi, Romania

Abstract

Co(II), Cd(II) and Rh(III) complexes with 2-(1H-1,2,4-triazol-3-yl)pyridine (Htzp) as ligand were synthesized and investigated. The neutral mononuclear complexes with a generic $[M(tzp)_n]$ structure have been prepared from Htzp and corresponding transition metals chlorides at 2:1 and 3:1, respectively molar ratios in H₂O–EtOH. The resulted crystalline complexes were investigated through magnetic and molar conductivity measurements, elemental analysis, FT-IR, mass spectroscopy, thermal analysis, UV-Vis and P-XRD. The experiments indicate that Htzp acts as bidentate anionic ligand, $[Co(tzp)_2] \cdot 1.5H_2O$ and $[Cd(tzp)_2]$ are in the tetragonal coordination, whereas six coordinate octahedral $[Rh(tzp)_3] \cdot H_2O$ complex undergoes a weak tetragonal distortion. In case of Co(II) complex, an interesting feature was revealed through fluorescence spectroscopy, as the fluorescent emission intensity of the free ligand is dependent on the Co(II) solution content. Through complexation, the fluorescence is gradually quenched according to the Co(II) aqueous solution content, which may recommend it as a method of detection of Co(II) presence in waste water.

Key words: Co(II) detection, ligand, transition metal complexes, triazole complexes

Received: November, 2014; *Revised final:* February, 2015; *Accepted:* February, 2015

1. Introduction

Heterocyclic chemistry has now become a separate field of inorganic chemistry with long history, present society and future prospect (Yousif et al., 2013). In recent years, studies on complexes with N containing ligands have attracted considerable interest due to their important role in the development of coordination chemistry as well as inorganic biochemistry, catalysis and optical and magnetic materials.

Triazole classes are considered to be excellent coordinating ligands, because they involved both hard nitrogen and amino group. Furthermore,

compounds containing the nucleus triazole and the pyridine are part of an increased interest from the researchers due their multiple chemical, biological and medical applications, through the chromophore properties (colorants) (Haasnoot, 2000), luminescent (Inkaya et al., 2013; Shan et al., 2013; Shang et al., 2013), catalytic (Bortoluzzi et al., 2013), bacterial activities (Crabtree, 2001; Meek et al., 2011; Liu et al., 2011; Stock and Biswas, 2012), antifungals (Dong et al., 2010; Werner and Stiasny, 1899), antivirals (Chen et al., 2011), antidepressants (Wilson and Wilson, 1955), asthmatics (Meunier et al., 1976) and inflammatory (Bladin, 2006; Potts, 1961). Also, a significant number of compounds were considered,

* Author to whom all correspondence should be addressed: e-mail: stcornel@gmail.com; Phone: 0742208215

because they have antidiabetic (Ding et al., 2005) and diuretics properties (Zhang and Chen, 2006). The organic compound 1, 2, 4 – triazole-3-one, derived from the 1,2,4 – triazole, is particularly interesting due its, antitumor and antibacterial properties. 1,2,4-triazole and 1,2,4-triazol-3-one are important heterocycles being incorporated into a wide variety of drugs like Fluconazole, Itraconazole, Voriconazole, Posaconazole, Letrozole, and Anastrozole used in medical therapy (Pardeshi and Bobade, 2011). Tabatabaee et al. (2012) reported the fact that 1,2,4 – triazoles function as ligands mono-, bi- or tridents, obtaining coordination compounds like the monomers class, dimers and polynuclear species. Reedijks et al. (2011) obtained a series of trinuclear compounds using derivatives from class 1, 2, 4 – triazoles with transition metals M= Mn, Fe, Co, Ni and Zn.

This study presents the synthesis and the structural characterization of new coordinative compounds of the Co(II), Rh(III) and Cd(II) cations with 2-(1H-1,2,4-triazol-3-yl)pyridine, a derivative from 1,2,4 - triazoles class. The research was extended to the possibility of detection of Co(II) presence in water due to the observed fluorescence emission quenching of the free ligand through complexation. The Cd(II) complex is an interesting alternative to be used as precursor in CdSe Quantum Dots synthesis while the Rh(III) complex may be valued in catalytic processes where the presence of rhodium is required.

2. Experimental

2.1. Materials

CdCl_2 (99.9%), $\text{CoCl}_2 \cdot 6\text{H}_2\text{O}$ (99%) and $\text{RhCl}_3 \cdot x\text{H}_2\text{O}$ (99.98%) were purchased from Alfa-Aesar. 2 - (1H-1, 2, 4-triazol-3-yl) pyridine (Htzp) (97%) with the structure presented in Fig. 1 was purchased from Sigma-Aldrich. All the chemicals were of reagent grade and used as received. Solvents used in the synthesis procedure are absolute ethanol (Merck) and high purity MiliQ water.

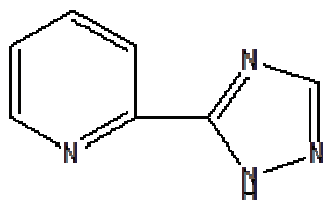
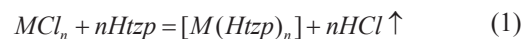


Fig. 1. The structure of 2-(1H-1, 2, 4-Triazol-3-yl) pyridine (Htzp)

2.2. Preparation

First, for the preparation of aqueous solutions of chlorides of Cd, Co and Rh was dissolved 1 mmol of each in 2 mL of double distilled water. The solutions of 2 - (1H-1, 2, 4-triazol-3-yl) pyridine

were prepared by dissolving 3mmol of the ligand in a mixture of 3 mL of water and 1 mL of ethanol. The complexes were prepared by mixing of ligand solution with chloride solution of Cd^{2+} , Co^{2+} , Rh^{3+} , respectively. The complexation reactions (Eq. 1) were carried out under heating (40-45^o C) and stirred for 180 minutes. All complexes were obtained by the reaction of M and Htzp in the 1:2 molar ratio for Co, Cd/Htzp and 1:3 molar ratio for Y, Rh/Htzp.



where: M= Co, Cd, n=2; M= Rh, n=3.

The crystalline complexes were separated by filtration and then washed with double distilled water. The obtained compounds were purified by recrystallization from the ethanol solution. The traces of solvent were removed by drying in the vacuum at room temperature.

2.3. Methods

Elemental analysis was performed with the Thermo Fischer Scientific device Flash EA-1112CHNS/O equipment supplied with the software Eager 300. Metal elemental chemical analysis was performed by atomic absorption. The thermal stability of the prepared complexes was analyzed by TG measurement on a Mettler Toledo TGA-SDTA851e device, under air flow of 20 ml / min, at a heating rate of 10 K min⁻¹. The kinetic parameters have been calculated by Coats-Redfern, Flynn Wall and Urbanovici Segal methods. The conductivity of 2·10⁻⁴ M ethanolic solutions was determined with Consort K912 electrochemical analyzer at 25 °C. Magnetic properties of solid compounds were determined with a magnetic Sherwood Scientific MS auto-balance by Gouy method at room temperature against $\text{Hg}[\text{Co}(\text{SCN})_4]$ as standard.

IR spectra of the ligand and metal complexes were recorded using Digilab FTS-2000 FT-IR spectrophotometer, in the 4000-400 cm⁻¹ range, according to KBr pellet method. The UV-VIS absorption spectra of solid samples were performed with CAMSPEC 501M single beam spectrophotometer provided with a diffuse reflectance sphere, using BaSO_4 as blank, in the 190–1100 nm range. The number and energy of transition bands were resolved by the deconvolution of the original electronic diffuse reflectance spectra (DRS) using OriginLab programs. XRD patterns were recorded in the 5-70^o 2Theta range on a Panalytical X'Pert Pro diffractometer equipped with a Cu-K α radiation source ($\lambda = 0.154060$ nm). Unit cell parameters of the investigated complexes were further refined using software Panalytical X'Pert High Score Plus.

High-resolution MS and MS/MS spectra were acquired on an AGILENT 6520 QTOF mass spectrometer equipped with an ESI source. The ESI MS parameters optimized for the analyzed complexes were set as follows: Vcap = 4000 V,

fragmentor voltage = 175 V, drying gas temperature = 325 °C, drying gas flow = 5 L/min and nebulizer pressure = 35 psig. Nitrogen was used as spraying gas. On this instrument, the MS/MS experiments were conducted in the collision cell using nitrogen as collision gas at a pressure of 18 psig inside the collision cell. The steady state fluorescence spectra were recorded on a Horiba Fluoromax 4P spectrofluorometer.

3. Results and discussion

3.1. Elemental analysis

The results of elemental analysis recorded for [Co(Htzip)₂] (**1**), [Cd(Htzip)₂] (**2**) and [Rh(Htzip)₃] (**3**) are presented in Table 1. The elemental analysis data were correlated with those obtained by thermogravimetric analysis.

3.2. FT-IR analysis

The infrared spectrum of **Htzip** (Fig. 2) shows in the 3350 – 2700 cm⁻¹ range an intense broad band structured in five components assigned to ν(NH)triazole and ν(CH)pyridine/triazole. The ν(NH) stretching vibration is observed at 3082 cm⁻¹ and 3151 cm⁻¹. The shoulder can be attributed to N-H...N intermolecular hydrogen bond. The ν(CH)pyridine stretching vibrations are observed at 2936 and 2866 cm⁻¹, while ν(CH)triazole vibration is located at 2801 cm⁻¹ due to the lower bond order of C-H triazole group. A series of very weak intensity bands were recorded in the 2800 - 1800 cm⁻¹ range which can be attributed to the combined bands of deformation vibration by Fermi resonance (Nakamoto, 1997).

The medium peak centered at 1597 cm⁻¹ was attributed to the ν(C=N) pyridine stretching vibration, but the wider bandwidth can be due to overlapping of ν(C=N)pyridine stretching mode and ν(C=C)pyridine vibration. The ν(C=N)triazole stretching vibration is characterized by a strong sharp band located at 1477 cm⁻¹. The band observed at 1404 cm⁻¹, which can be attributed to the ν(C-N)triazole stretching modes, is partially overlapped with γ(N-H)triazole + γ(C-H)pyridine rocking vibration modes. The C-C, C-N pyridine and N-N triazole stretching vibrations in broad bands of 1300 – 1000 cm⁻¹ range are complicated and mixed with other vibrational modes.

The FTIR spectra of **1** and **3** presents in the 3500 – 3200 cm⁻¹ range two bands centered at 3415 cm⁻¹ and 3431 cm⁻¹, respectively, due to asymmetric and symmetric ν(OH) stretching vibration modes of water. The intensity and broadness of these bands suggest that the water molecules are not coordinated at metal cations but can be involved in the hydrogen bonds with the one of nitrogen atoms of triazole ring. The asymmetric and symmetric ν(OH) stretching vibration modes of water is not present in the infrared spectrum of Cd(II) complex (**2**). After coordination of **Htzip** to metal cation the ν(N-H)triazole can not be identified. This is in agreement with the UV-Vis and

conductance results. Modification of charge density from pyridine and triazole rings determined the shifting of C-H, C=C, C=N and N-N stretching vibration modes. The ν(C-H)pyridine and ν(C-H)triazole generate two separated relatively broad bands centered at 3074 and 2882 cm⁻¹ (for **1**), 3072 and 2887 cm⁻¹ (for **2**), 3084 and 2889 cm⁻¹ (for **3**), respectively.

The hypochromic shift of ν(C-H) indicates the increasing of the covalent character of C-H bonds as a consequence of the decreasing of electronic density on the carbon atoms. The relative high intensity of ν(CH) frequency bands of **3** exceed the intensities of the other IR bands, the position and intensity of the bands being dependent by the vibration modes of tzip⁻ ligand, strongly coupled with other skeletal modes. This could be due to the simultaneous increasing of polarities of both type of C-H bonds (pyridine and triazole) and the steric hindrance of coordinated ligand (Bellagamba et al., 2013). In the 1700 – 1000 cm⁻¹ range the spectra of all complexes revealed the relatively broad bands of free Htzip becoming more intense and sharp after tzip⁻ coordination to metal center.

The process is accompanied by the shift of the ν(C=N)pyridine (1612 cm⁻¹ for **1** and **3**, 1660 cm⁻¹ for **2**) and ν(C=N)triazole (1495 cm⁻¹ for **1**, 1550, 1478 cm⁻¹ for **2**) to higher energy, excepting ν(C=N)triazole of **3** (1466 cm⁻¹), due to the increasing of the C=N bonds, order which is determined by the electrophilic effect of the metal cation. Splitting of frequency of triazole C=N bonds suggest that the Cd(II) cation interacts more with the N atom, derived from the HN group, than the N atom of pyridine. The decrease of electronic density of coordinated nitrogen atom is compensated by decreasing of negative charge density on the nearest atom with low electronegativity. The same effect was observed for the (C-N) triazole and (N-N) triazole: wavenumbers increase from 1404 cm⁻¹ (**Htzip**) to 1427 (**1**) and 1419 cm⁻¹ (**2** and **3**) for ν(C-N) triazole and from 1269 cm⁻¹ (**Htzip**) to 1271 (**1**), 1273 (**2**), 1288 and 1257 cm⁻¹ (**3**) for ν(N-N) triazole. In case of rhodium complex (**3**), the splitting of ν(N-N)triazole band could be due to the Jahn-Teller effect on one direction (equatorial or axial), the steric hindrance and/or influence of the crystalline lattice by symmetry group and formation of a hydrogen bonding between water molecule and a nitrogen atom of one tzip⁻ ligand.

The corresponding deformation band, assigned of δ(H₂O) is overlapped by the strong ν(C=N)pyridine bands. In the 700 – 400 cm⁻¹ range were identified by the deconvolution of original **1**, **2** and **3** spectra, four bands assigned to symmetric and asymmetric ν(M-N) vibrations at 636, 543, 484 and 462 cm⁻¹ for **1**; 683, 476 and 412 cm⁻¹ for **2**; 665, 631, 513 and 459 cm⁻¹ for **3**. These indicate the nonequivalence of the M-N bonds, the high energy vibration being a quantitative parameter of M-N triazole bond strength: Cd²⁺-N > Rh³⁺-N > Co²⁺-N. The position and intensity of ν(M-N) bands are

dependent by the stereochemical configuration of complexes, vibration modes of ligand being strongly coupled with other skeletal modes. As expected from symmetry consideration, the cis-isomer will exhibit two $\nu(\text{M-Npyridine})$ and $\nu(\text{M-Ntriazole})$ modes whereas the trans-isomer only one for each type of these modes. The all complexes exhibit both types of stretching vibrations, but the symmetry of Cd^{2+} coordination center is higher than of Co^{2+} and Rh^{3+} complexes (Zhang and Zhang, 2013).

3.3. Mass spectroscopy

The $[\text{Co}(\text{tzp})_2(\text{H}_2\text{O})_{1.5}]$ complex was analyzed through ESI mass spectrometry. The obtained

spectrum is showed in the Fig. 3A. The peak observed at $m/z = 495$ was associated with the presence of a complex of Co with three ligand molecules [$495 = 59 (\text{Co}) + 145 (\text{L}) \times 3 + 1(\text{H})$]

Also, there may be observed a second peak with higher intensity, at $m/z = 350$ corresponding to the complex of Co with two ligand molecules. This peak is probably formed in ESI MS conditions through the loss of a ligand molecule and represents a more stable form in electrospray conditions. Nevertheless, the performed experiment allows the qualitative identification of the $[\text{Co}(\text{tzp})_2(\text{H}_2\text{O})_{1.5}]$ complex.

Table 1. Theoretical and experimental chemical composition of synthesized compounds

Compound	Experimental (calculated) mass, %				Molecular weight, g/mol	Empirical/ molecular formula
	C	N	O	H		
1	43.98 (44.64)	29.30 (29.76)	6.55 (6.37)	3.88 (3.98)	15.85 (15.67)	$\text{Co}^{2+}\text{C}_{14}\text{H}_{15}\text{N}_8\text{O}_{1.5}$ $[\text{Co}(\text{tzp})_2] \cdot 1.5\text{H}_2\text{O}$
2	41.86 (41.75)	28.22 (27.83)	- -	2.90 (2.98)	28.05 (27.83)	$\text{Cd}^{2+}\text{C}_{14}\text{H}_{12}\text{N}_8$ $[\text{Cd}(\text{tzp})_2]$
3	44.57 (45.28)	29.77 (30.19)	2.95 (2.87)	3.77 (3.59)	18.23 (18.51)	$\text{Rh}^{3+}\text{C}_{21}\text{H}_{20}\text{N}_{12}\text{O}$ $[\text{Rh}(\text{tzp})_3] \cdot \text{H}_2\text{O}$

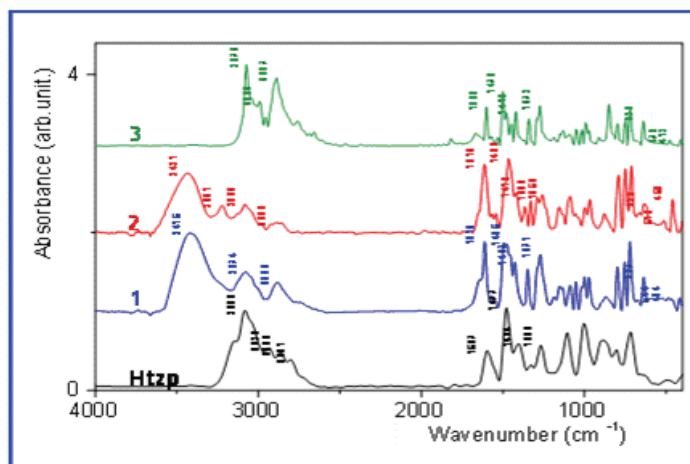


Fig. 2. FTIR spectra of Htzp, $[\text{Co}(\text{tzp})_2] \cdot 1.5\text{H}_2\text{O}$ - 1, $[\text{Cd}(\text{tzp})_2]$ - 2 and $[\text{Rh}(\text{tzp})_3] \cdot \text{H}_2\text{O}$ - 3

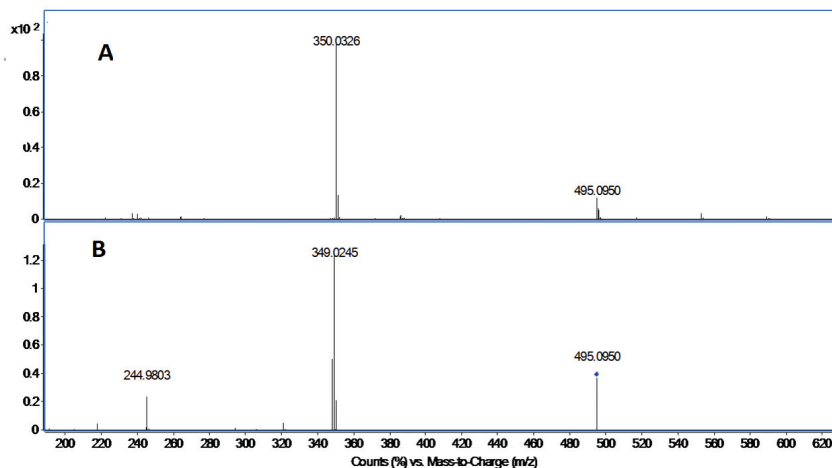


Fig. 3. A: ESI MS spectrum of $[\text{Co}(\text{tzp})_2(\text{H}_2\text{O})_{1.5}]$ complex; B: ESI MS/MS fragmentation of 495 peak

The fragmentation of the 495 peak in MS/MS conditions was attempted to further confirm the MS assignments. The MS/MS spectrum presented in figure 3B shows that the 495 peak losses one ligand molecule (146 m/z corresponds to the mass of the Htzp ligand) and leads to the formation of the ionic species with m/z = 349. A supplementary loss of m/z = 105 (peak found at m/z = 244) is related to further fragmentation of the ligand molecule as confirmed by the MS/MS fragmentation of the ligand molecule (spectra not given).

Overall, the ESI MS and MS/MS experiments confirm at molecular level the formation of the Co complexes with three ligand molecules.

3.4. DRS UV-Vis-NIR analysis

The spectra and values of band maxima for systems obtained are shown in Fig. 4 and Table 2. The DR spectra of all complexes show a number of partial overlapped intense bands in the 200 - 400 nm range (Fig. 4). After the original spectra deconvolution were identified 4 bands assigned to intraligand n- π^* and π - π^* transitions (Fig. 4, Table 2), which are dominated by the π - π^* transitions of the pyridine and the triazol rings. Accordingly, in the electronic spectrum both energies of π_{py} - π^* and π_{tz} - π^* transitions upon coordination are shifted.

The values of energy decrease for the π_{py} - π^* transition from 35336 cm⁻¹ (**1**), 3464 cm⁻¹ (**3**) to 34364 cm⁻¹ (**2**) when the π_{tz} - π^* transition is the same (41152 cm⁻¹) for **1** and **2** complexes. These suggest that the metal cations increase the electronic delocalization of ligand rings, more evident in case of Cd²⁺ complex.

The wavelengths of n- π^* transition bands (Table 4) are also determined by the individual electronegativity of nitrogen atoms of -N=N- and -C=N- groups and the inductive electronic effect of metal cation. The shift of both n_N- π^* transitions to lower energy, imply that the changes in the energy levels of the molecular orbitals of ligand upon coordination substantially originate from the increasing of polarizability of nitrogen atoms.

The electronic spectrum of **1** exhibits two intense bands at 10020 cm⁻¹ and 20576 cm⁻¹ due to d-d transitions. This pair of allowed electronic transitions can be generated by the distorted tetrahedral symmetry of coordination center by the nonequivalent donor atoms and steric hindrance. The tetrahedral Co²⁺-d⁷ high spin ground state is ⁴A₂. Three spin-allowed d-d transitions to the ⁴T₂, ⁴T₁ and ⁴T₁(P) state is predicted but first transition lies at low energy (over detection limit of device).

The gap energy between the two transitions can allowed us to estimate that the tzp⁻ creates a relatively strong ligand field located at the boundary between ⁴F (high spin) and ²G (low spin) ground state. The Cd(II) - d¹⁰ configuration does not have the d-d transitions. In the spectrum of **3** were identified two d-d transitions. The energies and low

intensities of absorption bands as well as the strength of ligand field (as **1**) are specific for the low spin Rh(III) - d⁶ configuration in tetragonally distorted octahedra.

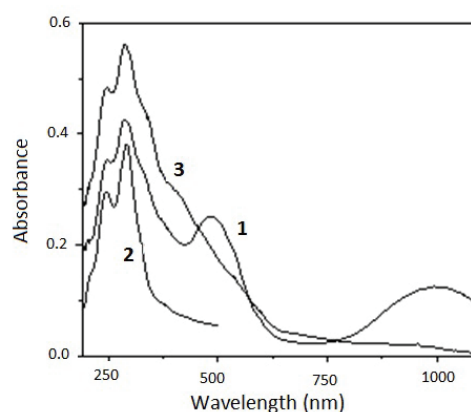


Fig. 4. The diffuse reflectance absorption spectra (DRS) of **1**- [Co(tzp)₂] \cdot 1.5H₂O, **2**- [Cd(tzp)₂] and **3**- [Rh(tzp)₃] \cdot H₂O complexes

Therefore, the two observed bands can be attributed to ¹E_g \leftarrow ¹A_{1g} (19084 cm⁻¹) and ¹A₂ \leftarrow ¹A_{1g} (22676 cm⁻¹) electronic transitions (Alasalvar et al., 2013). All three complexes exhibit in 26000 - 29000 cm⁻¹ domain the charge transfer (CT) transitions (Table 4). The CT absorption bands are superposed with d-d (for **1** and **3**) and intra-ligand transitions. The intensity of CT are relatively high for d(Co²⁺) - π (tzp⁻) and d(Rh³⁺) - π (tzp⁻) transitions compared to π^* (tzp⁻)-d(Cd²⁺) (Fig. 4).

3.5. Electric conductance

The values of molar conductivity, Λ_M , of **1**, **2** and **3** (Table 3) are in agreement with their nature of nonelectrolytes. This behavior suggests the existence of anionic ligands in the coordination sphere which countervail the cation charge and also a relatively low polarization in electric field of the studied complexes.

3.6. Magnetic properties

The magnetic susceptibility values of **2** and **3** (Table 3) are characteristic to the class of diamagnetic compounds, while **1** belongs to paramagnetic class. With equation $\mu = 2.84 \cdot (\chi_M \cdot T)^{1/2}$ (χ_M - molar magnetic susceptibility, T - temperature, K) was calculated the effective magnetic moment for Co²⁺ complex as $\mu_{\text{eff}} = 0.92 \mu_B$. The μ_{eff} value for **1** and negative χ_{exp} of **3** could be explained by existence of a strong ligand field around Co²⁺ (d⁷) and Rh³⁺ (d⁶) cations.

3.7. P-XRD analysis

Calculated unit cell parameters of the Hpz free ligand and prepared complexes are presented in

Table 4. For exemplification, one of the recorded diffractograms (for the $[\text{Cd}(\text{tzp})_2]$ complex) is presented in Fig. 5. The crystallization system is triclinic for the complexes while in case of free ligand, a monoclinic configuration was found.

3.8. Thermal analysis

Thermal analysis revealed significant differences in the decomposition schemes of the free ligand compared with the prepared complexes (Fig. 6 a-d). Thus, in the case of complexes four decomposition stages were recorded while in case of the free ligand only two decomposition stages were noted. Table 5 summarizes the parameters for each decomposition stage recorded for the free ligand and prepared complexes.

In the first stage, the remnant small amounts of physical bonded water and also the coordinated water is lost. In the second stage, the percent of mass losses suggests the breaking of the covalent C-C bond between the two constituent rings of the ligand (Fig. 1) and the elimination of the pyridine ring. This conclusion is sustained by the results recorded from mass spectroscopy investigation which also suggests the fragmentation of the ligand. In the upper stages the decomposition processes evolves with further deconstruction of the complexes accompanied by volatile exhaustions. In each case, the recorded residual mass suggests the presence of Co, Rh, Cd oxides as final decomposition product along with small amounts of residue resulted from decomposition of the ligand (Mészáros et al., 1998; Sasidharan et al., 2011).

Table 2. The electronic spectral data (λ , cm^{-1}) of **1-** $[\text{Co}(\text{tzp})_2] \cdot 1.5\text{H}_2\text{O}$, **2-** $[\text{Cd}(\text{tzp})_2]$, and **3-** $[\text{Rh}(\text{tzp})_3] \cdot \text{H}_2\text{O}$

Compound	Transition						
	Intra-ligand, (cm^{-1})				Charge transfer (cm^{-1})		d-d, (cm^{-1})
1	51546	41152	35336	30960	26954	20576	10020
2	48309	41152	34364	30864	28329	-	-
3	46729	41322	34722	29940	26316	22676	19084

Table 3. The experimental magnetic susceptibility (χ_{exp}) and molar conductivity (Λ_{M}) of the prepared complexes

Compound	Color	$\Lambda_{\text{M}}, \Omega^1 \cdot \text{cm}^2 \cdot \text{mol}^{-1}$	$\chi_{\text{exp}} \cdot 10^6$
1 $[\text{Co}(\text{tzp})_2] \cdot 1.5\text{H}_2\text{O}$	red-orange	35.711	0.319
2 $[\text{Cd}(\text{tzp})_2]$	white	69.021	-6.057
3 $[\text{Rh}(\text{tzp})_3] \cdot \text{H}_2\text{O}$	orange	40.991	-2.065

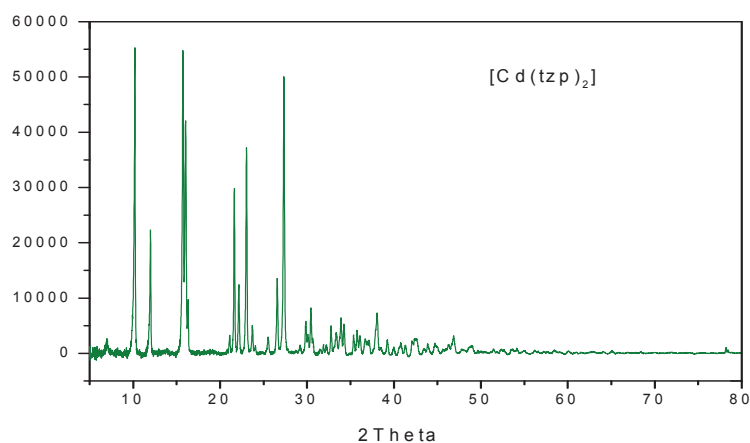


Fig. 5. Diffractogram recorded for the $[\text{Cd}(\text{tzp})_2]$ complex

Table 4. Calculated unit cell parameters of the ligand and prepared complexes

Parameters	Htzp	$[\text{Co}(\text{tzp})_2] \cdot 1.5 \text{H}_2\text{O}$	$[\text{Rh}(\text{tzp})_3] \cdot \text{H}_2\text{O}$	$[\text{Cd}(\text{tzp})_2]$
a [Å]	10.53	5.5	4.672	6.801
b [Å]	3.96	10.5	10.83	15.92
c [Å]	8.90	16.5	10.95	15.28
Alpha [°]	90	38.35	88.6	47.1
Beta [°]	110.7	95.7	83.9	80.15
Gamma [°]	90	89.0	94.58	53.23
Volume [Å ³]	347.15	578.04	548.85	887.68
System	monoclinic	triclinic	triclinic	triclinic

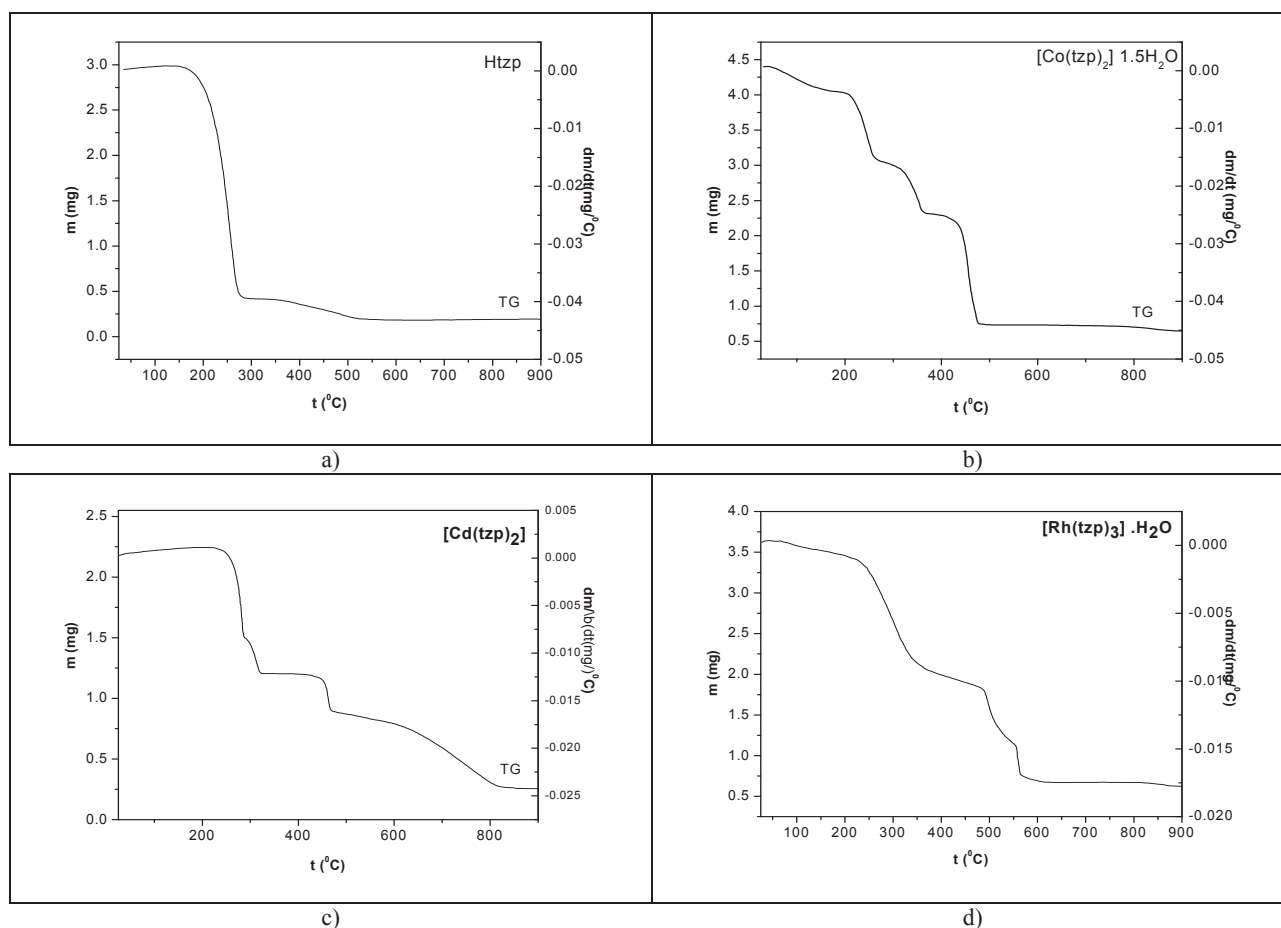


Fig. 6. Thermal analysis curves (TG) of the a) ligand Htzip and complexes b) $[Co(tzp)_2] \cdot 1.5H_2O$, c) $[Cd(tzp)_2]$, d) $[Rh(tzp)_3] \cdot H_2O$

Table 5. Thermal decomposition stages, reaction order and activation energies (kJ/mol) of the ligand and prepared complexes

Decomposition Stage	Parameter	Ligand	$[Co(tzp)_2 \cdot 1.5(H_2O)]$	$[Cd(tzp)_2]$	$[Rh(tzp)_3] \cdot H_2O$
Stage 1	A	$1.62 \cdot 10^{18}$	1.49	$1.36 \cdot 10^{26}$	$0.51 \cdot 10^2$
	Ea/kJ/mol	74.05	18.48	295.01	28.70
	N	0.33	0.57	0.26	0.84
	Ti-Tf	203-272	56-146	253-280	75.4-185
	%loss	88.1	8.00	32.54	5.19
Stage 2	A	$20.1 \cdot 10^{18}$	$3.29 \cdot 10^7$	$9.98 \cdot 10^{15}$	4.95
	Ea/kJ/mol	45.3	94.85	199.37	34.92
	N	0.55	0.44	0.34	0.37
	Ti-Tf	365-516	208.1-256	290.5-317	231.5-340
	%loss	7.93	23.76	12.64	41.67
Stage 3	A	-	$3.02 \cdot 10^9$	$1.59 \cdot 10^{62}$	$1.33 \cdot 10^{32}$
	Ea/kJ/mol	-	137.51	894.5	496.17
	N	-	0.27	0.58	1.47
	Ti-Tf	-	318.9-355	447.8-464	481.2-513.2
	%loss	-	16.76	13.90	22.48
Stage 4	A	-	$5.47 \cdot 10^{35}$	$5.09 \cdot 10^{24}$	$6.18 \cdot 10^3$
	Ea/kJ/mol	-	521.22	56.89	85.55
	N	-	2.05	0.33	0.34
	Ti-Tf	-	431.2-476	613.1-810	545.8-803.1
	%loss	-	35.28	23.32	13.16

3.9. Fluorescence spectroscopy

As stated above, the fluorescent emission intensity of the free ligand, in presence of incremental quantities of Co(II) cations present in an

aqueous solution tend to gradually diminish towards total quenching of the radiative transitions. Fig. 7 presents the variation of the fluorescent emission intensities during the addition of increasing quantities of Co(II).

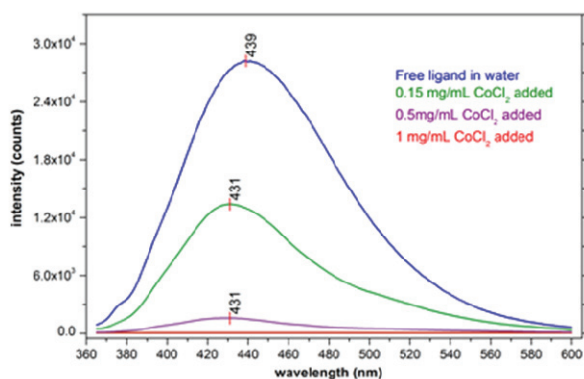


Fig. 7. Intensities of the fluorescence emission spectra recorded under 350 nm excitation for the free ligand and for increasing quantities of CoCl_2 added in the aqueous solution

During complexation, the presence of the central cation influence the excited states of the ligand which are responsible for the radiative transitions. Thus, the intensity of the emission diminishes with the increasing presence of the Co(II) cations in solution due to the commencing of the complexation process. As increasingly higher quantities of free ligand is complexed the emission intensity decreases. This behavior may be useful in such applications where Co(II) cations should be detected and quantitatively evaluated.

4. Conclusions

Three new complexes of Co^{2+} , Cd^{2+} and Rh^{3+} with 2 - (1H-1, 2, 4-triazol-3-yl) pyridine (Htzp) were obtained and studied. The compounds were characterized in the solid state by elemental analysis, XRD analysis, magnetic, conductivity and thermogravimetric measurements, DR and FTIR spectrophotometry. The experimental data show that the HTzpz acts as anionic bidentate ligand, tzp⁻, and complexation reactions led to $[\text{Co}(\text{tzp})_2] \cdot 1.5\text{H}_2\text{O}$, $[\text{Cd}(\text{tzp})_2]$ and $[\text{Rh}(\text{tzp})_3] \cdot \text{H}_2\text{O}$ compounds. The infrared, UV-Vis and P-XRD data indicate that tzp⁻ binds metal cations through nitrogen atom of pyridine and nitrogen 1 atom of triazole group. The thermogravimetric data confirm these bonding modes.

The absorption spectra suggest that the Co^{2+} and Cd^{2+} complexes are tetrahedral and Rh^{3+} complex adopt a distorted octahedral symmetry. In case of Co(II) complex, an interesting feature was noted, as the fluorescent emission intensity of the free ligand is dependent on the Co(II) solution content. Through complexation, the fluorescence is gradually quenched according to the Co(II) content, which may recommend it as a method of detection of Co(II) presence in waste water.

Aknowledgements

This work was supported by the strategic grant POSDRU/159/1.5/S/133652, co-financed by the European

Social Fund within the Sectorial Operational Program Human Resources Development 2007 – 2013.

References

- Alasalvar C., Soylu M.S., Ünver Y., Apaydın G., Ünlüer D., (2013), Spectroscopy studies, X-ray diffraction and DFT, HF calculations of 4-allyl-5-(thiophen-2-ylmethyl)-2H-1,2,4-triazol-3(4H)-one, *Journal of Molecular Structure*, **1033**, 243–252.
- Bellagamba M., Bencivenni L., Gontrani L., Guidoni L., Sadun C., (2013), Tautomerism in liquid 1,2,3-triazole: a combined energy-dispersive X-Ray diffraction, molecular dynamics and FTIR study, *Chemical Physics*, **24**, 933-943.
- Bladin J.A., (2006), Over dicyanophenylhydrazine and related compounds, *European Journal of Inorganic Chemistry*, **18**, 1544–1551.
- Bortoluzzi M., Scrivanti A., Reolon A., Amadio E., Bertolasi V., (2013), Synthesis and characterization of novel gold(III) complexes with polydentate N-donor ligands based on the pyridine and triazole heterocycles, *Inorganic Chemistry Communications*, **33**, 82–85.
- Chen S.C., Zhang Z.H., Zhou Y.S., Zhou W.Y., Li Y.Z., He M.Y., Chen Q., Du M., (2011), Alkali-metal-templated assemblies of new 3D Lead(II) tetrachloroterephthalate coordination frameworks, *Crystal Growth & Design*, **11**, 4190- 4197.
- Crabtree R.H., (2001), *Introduction. The Organometallic Chemistry of the Transition Metals*, 3rd Ed., John Wiley, New York.
- Ding B., Yi L., Gao H.L., Cheng P., Liao D.Z., Yan S.P., Jiang Z.H., (2005), 4-[3-(1,2,4-triazolyl)-1,2,4-triazole complexes of four-coordinated Cu(II) and six-coordinated Fe(II) , *Inorganic Chemistry Communications*, **8**, 102-104.
- Dong B.X., Gu X.J., Xu Q., (2010), Solvent effect on the construction of two microporous yttrium-organic frameworks with high thermostability via in situ ligand hydrolysis, *Dalton Transactions*, **39**, 5683-5687.
- Haasnoot J.G., (2000), Mononuclear, oligonuclear and polynuclear metal coordination compounds with 1,2,4-triazoles derivatives as ligands, *Coordination Chemistry Reviews*, **200–202**, 131–185.
- Inkaya E., Dinçer M., Ekici Ö., Cukurovali A., (2013), 1-(3-Methyl-3-mesityl)-cyclobutyl-2-(5-pyridin-4-yl-2H-[1,2,4]triazol-3-ylsulfanyl)-ethanone: X-ray structure, spectroscopic characterization and DFT studies, *Spectrochimica Acta Part A: Molecular and Biomolecular Spectroscopy*, **101**, 218–227.
- Liu T.F., Lu J., Tian C., Coa M., Lin Z., Cao R., (2011), Porous anionic, cationic, and neutral metal-carboxylate frameworks constructed from flexible tetrapodal ligands: syntheses, structures, ion-exchanges, and magnetic properties, *Inorganic Chemistry*, **50**, 2264- 2271.
- Meek S.T., Greathouse J.A., Allendorf M.D., (2011), Metal-organic frameworks: a rapidly growing class of versatile nanoporous materials, *Advanced Materials*, **23**, 249- 267.
- Meunier-Piret J., Piret P., Putzeys J.P., Van Meerssche M., (1976), Crystalline structure of hexakis-(benzotriazolyl)-hexakis(allylamine)-trisnickel(II) with triphenylphosphine oxide, *Acta Crystallographica*, **B32**, 714–717.

- Mészáros S.K., Ivegeš E.Z., Leovac V.M., Vojinović Lj.S., Kovács A., Pokol G., Madarász J., Jaćimović Ž.K., (1998), Transition metal complexes with pyrazole-based ligands. Part 6: Synthesis, characterization and thermal decomposition of cadmium complexes with 3(5)-amino-5(3)-methylpyrazole, *Thermochimica Acta*, **316**, 79–85.
- Nakamoto K., (1997), *Infrared and raman spectra of coordination compounds*, Part A, 5th Ed., John Wiley and Sons, New York.
- Pardeshi S., Bobade V.D., (2011), Synthesis and biological evaluation of some novel triazol-3-ones as antimicrobial agents, *Bioorganic & Medicinal Chemistry Letters*, **21**, 6559–6562.
- Potts K.T., (1961), The Chemistry of 1,2,4-Triazoles, *Chemical Reviews*, **61**, 87-127.
- Reedijk J., Peerke I.M. van der List, Oldenbroek S.J.L., Lugthart E.N., Albada G.A. van, Gamez P., Haasnoot J.G., Teat S.J., Roubeau O., Mutikainen I., (2011), Coordination network solids based on Cu(II) coordination compounds with 1,4-bis-(1,2,4-triazol-1-yl)-butane as a flexible alkyl spacer ligand: Synthesis, characterization and X-ray structures, *Inorganica Chimica Acta*, **370**, 164–169.
- Sasidharan N., Hariharanath B., Rajendran A.G., (2011), Thermal decomposition studies on energetic triazole derivatives, *Thermochimica Acta*, **520**, 139–144.
- Shan G.G., Li H.B., Cao H.T., Sun H.Z., Zhu D.X., Su Z.M., (2013), Influence of alkyl chain lengths on the properties of iridium(III)-based piezochromic luminescent dyes with triazole-pyridine type ancillary ligands, *Dyes and Pigments*, **99**, 1082-1090.
- Shang X., Han D., Li D., Wuc Z., (2013), Theoretical study of injection, transport, absorption and phosphorescence properties of a series of heteroleptic iridium(III) complexes in OLEDs, *Chemical Physics Letters*, **565**, 12–17.
- Stock N., Biswas S., (2012), Synthesis of metal-organic frameworks (MOFs): routes to various MOF topologies, morphologies, and composites, *Chemical Reviews*, **112**, 933- 969.
- Tabatabaee M., Tahriri M., Tahriri M., Ozawa Y., Neumüller B., Fujioka H., Toriumi K., (2012), Preparation, crystal structures, spectroscopic and thermal analyses of two-co-crystals of [M(H₂O)₆][M(dipic)₂] and (atrH)₂[M(dipic)₂] (M = Zn, Ni, dipic = dipicolinate; atr = 3-amino-1H-1,2,4-triazole) with isostructural crystals system, *Polyhedron*, **33**, 336–340.
- Yousif E., Haddad R., Ahmed A., (2013), Synthesis and characterization of transition metal complexes of 4-amino-5-pyridyl-4H-1,2,4-triazole-3-thiol, *Springer Plus*, **2**, 510.
- Werner A., Stiasny E., (1899), Nitroderivates of Azo-, Azoxy- and Hydrazo-Benzols, *Berichte*, **32**, 3256–3282.
- Wilson R.F., Wilson L.E., (1955), Preparation of Palladium(II) Chloride-1,2,3-Benzotriazole Coordination Compound, *Journal of the American Chemical Society*, **77**, 6204–6205.
- Zhang J.P., Chen X.M., (2006), Crystal engineering of binary metal imidazolate and triazolate frameworks, *Chemical Communications*, **16**, 1689-1699.
- Zhang R.Z., Zhang X.Z., (2013), Molecular structure, NMR parameters of N-(1,3,4-thiadiazol-2-yl)-1-[1-(6-chloropyridin -3-yl) methyl]-5-methyl-1H-[1,2,3] triazol-4-carboxamide by density functional theory and *ab-initio* Hartree-Fock calculations, *Indian Journal of Pure & Applied Physics*, **51**, 164-173.



“Gheorghe Asachi” Technical University of Iasi, Romania



COPPER NANOPARTICLES SUPPORTED ON POLYETHER-FUNCTIONALIZED MESOPOROUS SILICA. SYNTHESIS AND APPLICATION AS HYDROGENATION CATALYSTS

Constantin Rudolf¹, Irina Mazilu¹, Alexandru Chiriac¹, Brandusa Dragoi¹,
Fatima Abi-Ghaida², Adrian Ungureanu¹, Ahmad Mehdi², Emil Dumitriu^{1*}

¹“Gheorghe Asachi” Technical University of Iasi, Faculty of Chemical Engineering and Environmental Protection,
Laboratory of Catalysis, 73 Prof. Dr. docent Dimitrie Mangeron Str., 700050 Iasi, Romania

²University of Montpellier, The Institute Charles Gerhardt of Montpellier, UMR 5253,
Molecular Chemistry and Solid Organisation, cc 1701, Place E. Bataillon, 34095 Montpellier, Cedex 5 France

Abstract

Copper nanoparticles were successfully synthesized on polyether-functionalized mesoporous silica to investigate the effect of metal loading (10, 25 and 35 wt. % Cu) on their structural and catalytic properties. The oxide forms of these nanocomposite materials were thoroughly characterized by nitrogen physisorption, SAXS, WAXS, TEM, EDXS, and TPR, whereas the metallic forms were analysed by N₂O chemisorption. The results indicated that the mesostructured SBA-15-like hybrids favoured the generation of highly dispersed supported copper nanoparticles with average sizes in the range of ~2-6 nm, displaying excellent activity in the hydrogenation of cinnamaldehyde. The average particle size was shown to increase with the metal loading. Among the tested catalysts, the highest activity was obtained for the sample having 25 wt. % Cu (total conversion of cinnamaldehyde in 150 min of reaction). All the catalysts exhibited high selectivity towards hydrocinnamaldehyde (> 85 mol %), which did not appear dependent on the copper particle size.

Key words: Cu-based catalysts, hydrogenation of cinnamaldehyde, polyether-functionalized mesoporous materials

Received: November, 2014; *Revised final:* February, 2015; *Accepted:* February, 2015

1. Introduction

The unique electronic structure and the high active surface of metal (oxide) nanoparticles (NPs) have motivated extensive researches focused on developing new performing heterogeneous catalysts with potential applications in fine chemistry, petrochemistry, pollution prevention (Jansat et al., 2007) and other important fields (Campelo et al., 2009). For such applications, the most common type of catalysts comprises metal (oxide) NPs deposited on inorganic or organic porous supports, which provide high-surface areas and specific local environments to stabilize highly dispersed catalytic active phases. It was reported that the main features

that influence the activity, selectivity, and lifetime of such supported nanocatalysts are the particle structure and morphology (size and shape), their chemical composition and the oxidation state, which in turn, are dependent on many factors such as the nature of metal/catalytic precursor, the nature of the support and the interactions between the metal and support, all of which are in close connection with the preparation method (Cuenya, 2010).

Extensive efforts have been made to control the structure and morphology of NPs on supported catalysts, but the development of a simple strategy for the preparation of highly dispersed metal (oxide) particles remains a challenge, particularly in the case of copper-based catalysts. For instance, it was shown

* Author to whom all correspondence should be addressed: e-mail: edumitri@tuiasi.ro

that bulk copper catalysts are not active in hydrogenation reactions, but reduction in the particle size of metallic copper (up to 10 nm or smaller) changes its electronic structure, the number of defects on the crystal surface, and the distribution of surface sites, thus leading to enhanced catalytic activity (Dragoi et al., 2010; Mäki-Arvela et al., 2005; Ungureanu et al., 2013). It is also known that Cu clusters do not chemisorb H₂ molecules because they need to pass an activation barrier (Andersson et al., 1996; Morse et al., 1985), which could be easily overpassed by small crystals, as also predicted by theoretical calculations (Guvelioglu et al., 2006; Yang et al., 2010).

Therefore, many attempts were reported to control the size and the shape of copper NPs, which to date remains a very challenging goal because of the high mobility of copper ions resulting in significant sintering (even at low temperatures) and formation of large aggregates (Munnik et al., 2011). Furthermore, such lack of control substantially magnifies with increasing copper loading.

In order to achieve high dispersion and stability of copper NPs supported on inorganic supports, various strategies were applied. These include controlled calcination conditions (Munnik et al., 2011), drying at ambient temperature (Toupance et al., 2000), incipient wetness impregnation followed by mild drying (IWI-MD) (Ungureanu et al., 2013) or vacuum-thermal treatment (Liu et al., 2014), the promoting effect caused by a second metal (Dragoi et al., 2013; Ungureanu et al., 2013), mild reduction of Cu²⁺ substituted in a LDH matrix (Chirieac et al., 2012; Dragoi et al., 2011) etc. Nonetheless, the experimental results indicated that the stability of Cu-NPs is far from being resolved, especially at high metal loading. Simultaneously, the most significant strategy is based on the preparation of catalysts by impregnation on silica supports. In the case of incipient wetness impregnation, the water volume used for metal precursors is lower than the pore volume of the support.

Hence, it is often difficult to prepare catalysts with high degrees of metal loading due to the limited amount of solvent. This drawback can be easily overcome by applying the solvent-free melt infiltration method (MI) (de Jongh and Eggenhuisen, 2013). This emergent synthetic methodology not only provides an alternative to the classical wet preparation approaches, but it also facilitates extended control over the spatial distribution of NPs throughout the porosity of support, notably because the drying step to remove solvents is absent, which is known to bring about the redistribution of precursor species and formation of undesired bulky agglomerates. Furthermore, melt infiltration can be successfully applied on as-synthesized mesostructured supports, providing a very significant example on how the microenvironment existing between polymeric fragments and inorganic walls can be rationally explored to include high amounts of metal precursors and generate highly dispersed metal

(oxide) nanoparticles (Tian et al., 2010; Yin et al., 2012).

Therefore, this study is aimed at successfully preparing catalysts with different contents of copper (from 10 up to 35 wt. % Cu) deposited on a functional SBA-15-like mesoporous silica support by using IWI-MD and MI methods followed by investigating the influence of metal loading on the particle size of metallic copper and its impact on the catalytic performances. Mesoporous materials with SBA-15 topology were previously shown to exhibit excellent properties as catalytic supports for metal (oxide) NPs owing to the large specific surface areas and well defined pore structures (Munnik et al., 2011; Sietsma et al., 2008).

Moreover, these materials are prone to one-pot or post-synthetic functionalization with various organic groups, resulting in functional inorganic-organic hybrid mesostructures. Such functionalization offers specific tailoring of the surface chemical properties which improves the interaction between metal precursors and pore surfaces thus leading to high dispersions of copper NPs stabilized within the pores (Athens et al., 2009). For instance, Cu-NPs with 2–6 nm in average size and metal loadings of 7.6–25.2 wt. % can be successfully prepared by immobilization on hybrid SBA-15 supports functionalized with carboxylic acid groups (Chen et al., 2013). Herein, we utilized a different strategy to deposit highly dispersed copper NPs on SBA-15-like mesoporous silica. A functionalized bis-silylated triblock copolymer Pluronic P123 containing triethoxysilyl moieties at the chain ends was prepared, according to a procedure previously reported (Grandsire et al., 2010).

The functionalized Pluronic P123 acted thereafter as both a structure direction agent (SDA) for the two-dimensional hexagonal SBA-15-like mesostructure containing the original polyether groups of the surfactant covalently bound to the silica framework and a dispersing agent for the copper precursors to be subsequently impregnated/infiltrated into the support porosity, respectively. As a novel hybrid SBA-15-like support material, this polyether-functionalized mesoporous silica presented enhanced capacity to stabilize Cu NPs having outstanding catalytic performances in cinnamaldehyde hydrogenation. This reaction is very interesting from a fundamental point of view (control of the chemoselectivity) and it has been largely investigated (Mäki-Arvela et al., 2005). Also, it is of industrial relevance since the products of partial and total hydrogenation are being used in flavour and perfume industry, cosmetics etc.

It is worthy to note that a wide variety of efficient noble metal-based catalysts were reported for the hydrogenation of cinnamaldehyde, amongst which are platinum (Chatterjee et al., 2004; Jung et al., 2009; Li et al., 2008; Richard et al., 1989; Rylander, 1967; Samant et al., 2005), iridium (Giroir-Fendler et al., 1988; López-Linares et al., 1999),

ruthenium (Hájek et al., 2003; Liu et al., 2011; Toebe et al., 2003), and rhodium (Reyes et al., 2000). Albeit their great potential to replace the expensive noble metal-base catalysts, the cost-effective copper-based catalysts were barely reported in cinnamaldehyde hydrogenation (Gutiérrez et al., 2011, 2012).

2. Experimental

2.1. Bis-silylated P123 synthesis

Bis-silylated P123 (Si-P123) was synthesized according to Grandsire et al., 2010 as follows: a solution of 10 g (1.72 mmol) of Pluronic P123 (poly(ethyleneoxide)-block-poly(propyleneoxide)-block-poly(ethyleneoxide)-block), $\text{EO}_{20}\text{PO}_{70}\text{EO}_{20}$, molecular weight of 5800, BASF Corp.) in CH_2Cl_2 (200 mL) was dried with magnesium sulfate and filtered. CH_2Cl_2 was removed and polymer was heated under vacuum at 100 °C for 12 h. Dry P123 was then silylated with 3-isocyanatopropyltriethoxysilane (ICPTES). To a solution of P123 (0.1 M) in dry THF (100 mL), an excess of ICPTES (4 equiv.) and Et_3N (2 equiv.) were added at room temperature. The mixture was stirred at reflux for 72 h under argon. After removal of THF and Et_3N , the obtained crude was washed with pentane four times and dried, giving rise to 9.39 g (1.50 mmol, 87%) of Si-P123 as colourless oil.

2.2. Supports and catalysts preparation

The polyether-functionalized mesoporous silica support was obtained according to the previously reported method (Grandsire et al., 2010). Thus, for 5.6 g of powder, in an Erlenmeyer flask, an amount of 8.6 g (1.36 mmol) of Si-P123 as SDA was solubilized in 300 mL of an aqueous HCl solution having a pH of 1.5. After 2-3 h of stirring, the solution was poured into another flask containing 18.7 g (89.78 mmol) of tetraethylorthosilicate ($\text{Si}(\text{OC}_2\text{H}_5)_4$, TEOS) at room temperature.

The reaction mixture was left for 2 h and 30 min. at room temperature under vivid and regular magnetic stirring to give rise to a microemulsion: the solution is perfectly clear and colourless. The flask was immersed in an oil bath at 60 °C then (after 2 minutes) 150 mg (3.6 mmol) of NaF was added under stirring to allow hydrolysis-polycondensation. A white precipitate formed within few minutes. The reaction mixture was left under stirring for 72 hours at 60 °C, the resulting powder was filtered off and the unbound surfactant was removed by Soxhlet extraction over ethanol for 24 hours and finally dried at 120 °C under vacuum. The polyether-functionalized mesoporous silica was denoted as M100, where "M" stands for mesoporous support and "100" stands for the molar ratio of bis-silylated P123 used in synthesis (no P123 was used). According to thermogravimetric analysis, the organic

fraction in dried M100 material was of ~25 wt. % (weight loss up to 500 °C under air).

Metal oxide-loaded mesoporous support with 10 wt.% zero-valent metal loading was prepared by incipient wetness impregnation, followed by mild drying (IWI-MD) (Ungureanu et al., 2013). A certain amount of M100 support was placed in contact with the corresponding aqueous copper nitrate precursor solution. The metal precursor/hybrid SBA-15 composites were gently dried under air at 25 ± 1 °C for 5 days. The powders were sequentially submitted to calcination under stagnant air in a muffle oven at 500 °C for 6 h (heating ramp of 1.5 °C \cdot min $^{-1}$) to obtain the oxide forms of catalysts and burn off the organic components. The sample was denoted as $\text{Cu}_{10}/\text{M100}$.

To study the effect of metal loading, two samples with 25 and 35 wt. % Cu, respectively were prepared by an optimized melt infiltration (MI) procedure. Basically, the method consists of mixing the appropriate amounts of $\text{Cu}(\text{NO}_3)_2 \cdot 3\text{H}_2\text{O}$ and hybrid support, followed by continuous grinding for 45 minutes. The solid mixture was transferred to a Teflon autoclave and subjected to a heat treatment at 120 °C for several days, followed by cooling down to room temperature. The obtained infiltrates were calcined under the same conditions as above. These samples were denoted as $\text{Cu}_{25}/\text{M100}$ and $\text{Cu}_{35}/\text{M100}$, according to their metal loading.

A mesoporous alumina sample (denoted as MA) was also synthesized via Evaporation-Induced Self-Assembly (EISA) technique by using P123 as SDA (according to Yuan et al., 2008) and used as support. CuO-loaded mesoporous alumina (10 wt. % Cu) was also prepared by MI (sample Cu_{10}/MA) and used as reference.

2.3. Catalyst characterization

Nitrogen physisorption was carried out at -196 °C on an Autosorb 1-MP instrument from Quantachrome. Surface areas and pore volumes were calculated from the corresponding isotherms using conventional algorithms.

Temperature programmed reduction (TPR) and chemisorption experiments were performed on a Chembet Pulsar TPR/TPD from Quantachrome. About 30 mg of calcined sample were inserted in a U-shape microreactor. Before each TPR run, the catalyst was activated at 500 °C for 1 h under a flow of simulated air (40 mL min $^{-1}$). After cooling to 50 °C, the H_2 containing flow was stabilized (40 mL min $^{-1}$, 5 vol. % H_2 in Ar) and the TPR was performed from 50 to 500 °C with a temperature ramp of 5 °C min $^{-1}$.

The dispersion of metallic copper (D_{Cu}), average copper particle size (d_{Cu}) and active surface area (S_{Cu}) were determined using a nitrous oxide chemisorption method using specific algorithms (Chinchen et al., 1987; Evans et al., 1983; Jun et al., 1998; Krishna et al., 1999). The experiments were conducted in a quartz U-tube reactor, where an

amount of about 30 mg of the sample was introduced and fixed with quartz wool. The first reduction was carried out under the same conditions used for TPR, up to 500 °C. After the reduction step, the gas was switched to Ar and the reactor was cooled down to 50 °C, kept for 30 min., and then the gas was switched to N₂O (40 mL min⁻¹) for 30 min. in order to oxidize the surface zero-valent Cu to Cu₂O. The sample was again flushed with pure Ar for 30 min., and then a second TPR run was performed.

Energy X-Ray dispersive spectroscopy (EDXS) analyses were performed with an environmental scanning electronic microscope Quanta 200 coupled with an Oxford INCA analyzer. The Transmission Electron Microscopy (TEM) observations were carried out at 100 kV on a JEOL 1200 EXII microscope at the Service Commun de Microscopie Electronique (UM2, Montpellier, France). The SAXS and WAXS experiments were made on ID02 at 12.4keV with d=1.5m. The samples were inserted between two Kapton glasses. All measurements were dark subtracted and the background was measured with a double empty Kapton glass. All measurements were normalized by the transmission coefficient and by the acquisition time.

2.4. Catalytic activity

The catalytic liquid phase hydrogenation of cinnamaldehyde was carried out at atmospheric pressure in a round-bottom three-necked glass reactor equipped with a bubbler, a magnetic stirrer and a reflux condenser. The following reaction conditions were applied: 0.265 g of catalyst, 1.0 mL of trans-cinnamaldehyde, 25.0 mL of propylene carbonate as solvent, hydrogen flow of 1.0 L.h⁻¹, reaction temperature of 150 °C, and stirring speed of 900 rpm. At certain periods, aliquots of reaction mixture were withdrawn and analyzed with a gas-chromatograph (HP 5890 equipped with a DB-5 capillary column (25 m × 0.20 mm × 0.33 μm) and FID detector).

The products were identified from the retention time of the pure compounds and also verified with a GC-MS (Agilent 6890N system equipped with an Agilent 5973 MSD detector and a DB-5-ms column). For the quantitative analyses, the FID response factors for each compound were taken into consideration. The selectivity towards the products and the total conversion were calculated in a previous paper. (Dragoi et al., 2010)

3. Results and discussion

3.1. Structural and textural properties

The textural characteristics of the metal oxide-loaded samples were evaluated from the nitrogen adsorption-desorption isotherms (Fig. 1) and compared with those of the calcined M100. All materials display isotherms of type IV with hysteresis loops of type H1. The isotherms of both, the metal

oxide samples and the calcined samples are characteristic of ordered SBA-15-like mesostructures having narrow size distributions of the cylindrical mesopores, indicating that the mesoporous structure of the support was retained after the deposition of copper oxide.

However, with the gradual rise in metal loading, a continuous decrease in the nitrogen uptake at high relative pressure can be observed, suggesting a corresponding reduction in pore volume, which can be associated with the successful deposition of more copper oxide NPs within the porosity of the support. Moreover, no forced closures of the hysteresis loops are observed on the desorption branches of the isotherms, suggesting the absence of cavitation effects resulting from the partial blockage of primary mesopores with metal oxide NPs, which usually occurs when all particles are confined within the main mesopores of the support (Ungureanu et al., 2013).

The pore size distribution curves shown in Fig. 2 are in good agreement with the adsorption/desorption isotherms. Thus, all solids have narrow pore size distribution of the main channels (Kruk and Jaroniec, 2001) when compared with the calcined M100 (curve a) where the maxima of the differential pore volume for Cu₁₀/M100 and Cu₂₅/M100 (curves b and c) are slightly shifted to lower values (9.2 vs 9.6 nm), whereas for Cu₃₅/M100 (curve d) the maximum was found to be essentially unchanged (9.8 vs 9.6 nm) owing to the different dispersion degrees of CuO NPs and different particle size distribution as a function of metal loading.

The evaluation of the textural properties of the calcined samples based on the nitrogen adsorption/desorption isotherms reveals a progressive decrease in the specific surface area as a function of the metal loading, from 943 m²/g (M100) to 437 m²/g (Cu₃₅/M100), in parallel with a decrease in the total pore volume, from 1.52 to 0.71 cm³/g (Table 1).

Likewise, the micropore surface area steadily falls from 301 m²/g (M100) to 126 m²/g (Cu₂₅/M100). Further increase in the copper loading (35 wt. %) maintains a nearly constant surface area (121 m²/g). It is therefore likely that a population of CuO crystallites had suffered the nucleation and growth inside/at the mouth of the microporous domains generating stable micropore-encapsulated oxide NPs, whose fraction seems to be maximum at a metal loading of 25 wt. %.

Fig. 3 shows the SAXS results obtained for the calcined Cu/M100 materials with different metal loadings. For all samples, the patterns display very intense peaks indexed to the (100) planes and two less intense peaks indexed to the (110) and (200) planes of highly ordered hexagonal 2D structures with *p6mm* symmetry (Boubekr et al., 2011; Imperor-Clerc et al., 2004), confirming thus the physisorption results. No significant shifts of the *q* values with the increase in metal loading were observed, indicating similar unit cell parameters of the obtained mesostructured composites.

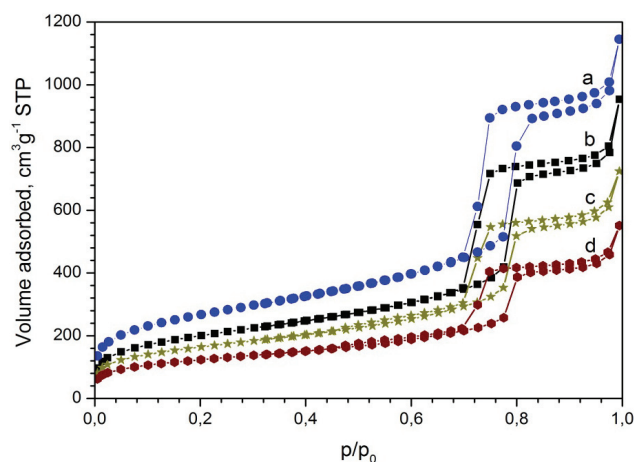


Fig. 1. N₂ physisorption isotherms for calcined a) M100, b) Cu₁₀/M100, c) Cu₂₅/M100 and d) Cu₃₅/M100

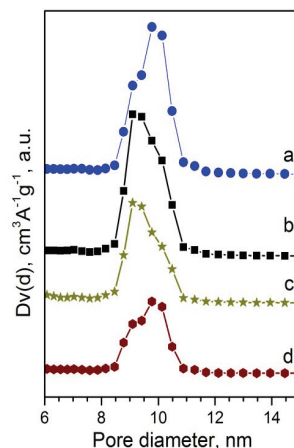


Fig. 2. NL-DFT pore size distributions for calcined a) M100, b) Cu₁₀/M100, c) Cu₂₅/M100 and d) Cu₃₅/M100

Table 1. Textural properties of calcined Cu/M100 materials

Sample	S_{BET} (m^2/g)	D_p (nm)	V_p (cm^3/g)	S_μ (m^2/g)	V_μ (cm^3/g)
M100	943	9.6	1.52	301	0.14
Cu ₁₀ /M100	714	9.2	0.98	188	0.08
Cu ₂₅ /M100	577	9.2	0.95	126	0.06
Cu ₃₅ /M100	437	9.8	0.71	121	0.05

S_{BET} – specific surface area, D_p – mean mesopore diameter, V_p – total pore volume, S_μ – micropore surface area, V_μ – micropore volume

Simultaneously, the relative intensities of the different peaks seem to be unaltered, which is in agreement with the retention of the mesostructural ordering of the support after the deposition of CuO NPs. However, a clear decrease in the overall intensity occurs with the increase in the loading from 10 to 25 wt.% (patterns a and b), note that the intensity does not change at higher loading of 35 wt.% (pattern c).

Since the intensity of the (100) peak is directly proportional to the square of the electron density difference between the silica walls and the oxide phase located inside the pores (Imperor-Clerc et al., 2004), the less intense peaks observed herein at loadings of 25 and 35 wt. % suggests that the extent of filling of the main mesopores with CuO-NPs is higher than those corresponding to 10 wt. %.

The results can be readily explained by taking into account the tendency of copper precursors to aggregate, especially at high loadings, either within the main mesopores forming confined oxidic aggregates or at the external surface of support grains giving rise to bulky oxide particles (Munnik et al., 2011). Indeed, the WAXS patterns of Cu₂₅/M100 and Cu₃₅/M100 solids (Fig. 4, patterns b and c) exhibit diffraction peaks characteristic to monoclinic CuO, whose intensity follows the metal loading of the catalysts.

However, introspection on these two patterns discloses that the diffraction peaks are asymmetric in shape and with obvious broadened onsets, signifying that two populations of CuO crystallites must be present in these composites: (i) intra-porous, highly

dispersed CuO-NPs, which are likely confined in the micropores and/or main mesopores and (ii) extra-porous CuO large aggregates. In contrast, Cu₁₀/M100 sample displays hardly distinguishable CuO diffraction peaks, clearly indicating the presence of only nanosized oxidic crystallites.

Transmission electron microscopy (TEM) images recorded at low-resolution for the copper-based nanocomposites are presented in Fig. 5. As a first observation, both solids exhibit typical highly-ordered mesoporous SBA-15-like structures composed of cylindrical mesochannels with narrow size distribution, in line with SAXS and N₂ physisorption results. No large aggregates on the external surface of silica grains were observed for the sample Cu₁₀/M100 (image a). In contrast, extra-porous large particles (as indicated by an arrow in image b) appeared for the sample Cu₃₅/M100. These observations confirm that as the copper loading increases from 10 wt. % to higher loadings, the distribution of particles sizes becomes more heterogeneous, in good agreement with WAXS. Nevertheless, the highly dispersed intra-porous copper particles cannot be clearly distinguished in the corresponding TEM images.

3.2. Reducible properties and copper dispersion

The EDXS results confirm that the metal loading degrees are close to the calculated ones (Table 2). The reducibility of CuO-loaded materials was analysed by TPR and the results are illustrated in Fig. 6.

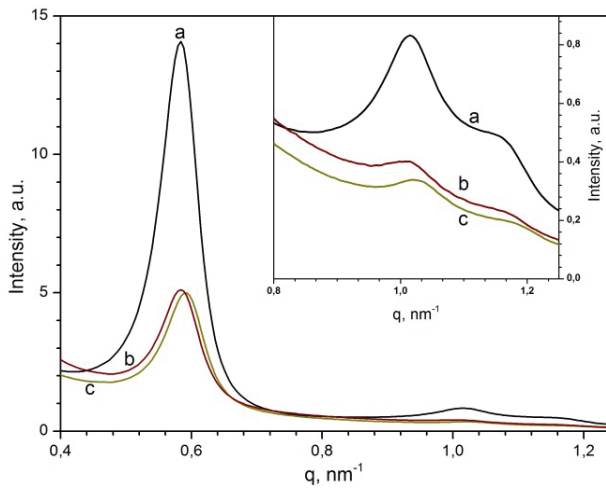


Fig. 3. SAXS patterns for a) Cu₁₀/M100, b) Cu₂₅/M100 and c) Cu₃₅/M100

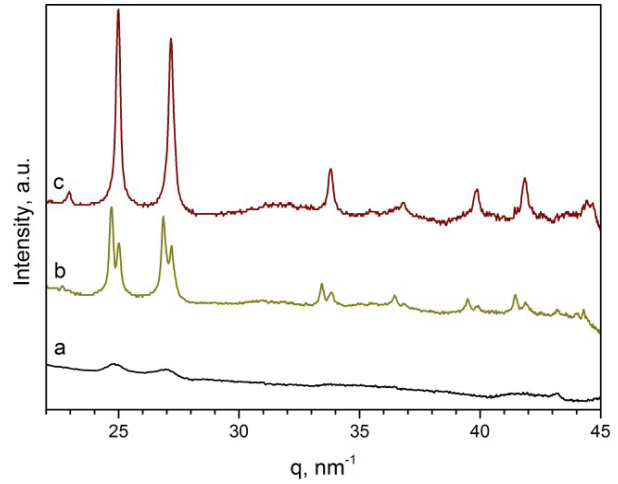


Fig. 4. WAXS patterns for a) Cu₁₀/M100, b) Cu₂₅/M100 and c) Cu₃₅/M100

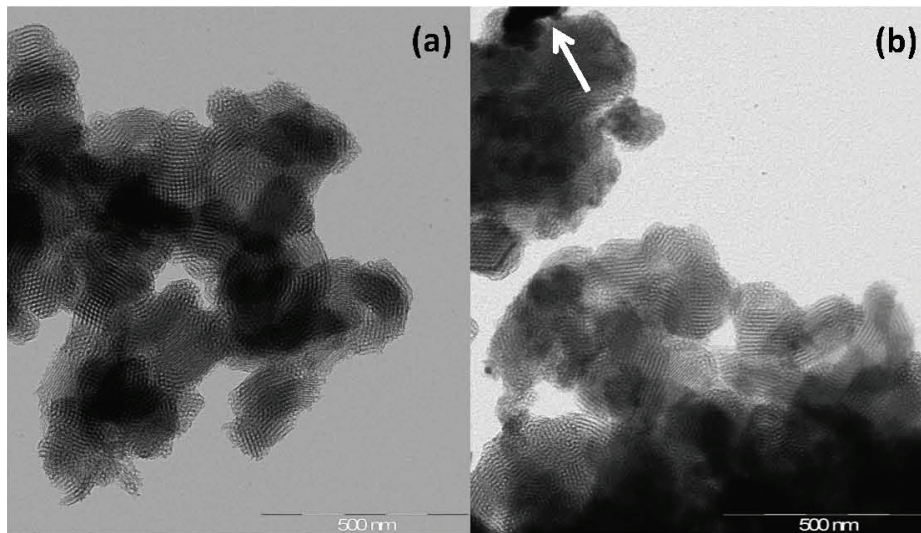


Fig. 5. Low-resolution TEM images for a) Cu₁₀/M100 and b) Cu₃₅/M100

Table 2. EDXS and N₂O chemisorption results

Sample	EDXS Cu (wt. %)	N ₂ O chemisorption			
		D _{Cu} (%)	d _{Cu} (nm)	S _{Cu} (m ² /g _{Cu})	S _{Cu} (m ² /g _{cat})
Cu ₁₀ /M100	12.6	43.5	2.3	294.3	37.1
Cu ₂₅ /M100	23.6	25.1	4.0	169.8	40.1
Cu ₃₅ /M100	33.8	16.7	6.0	113.0	38.2
Cu ₁₀ /MA	10.5	9.0	11.0	60.9	6.4

D_{Cu} - dispersion degree, d_{Cu} - average size of Cu particles, S_{Cu} - Cu surface area

As a first observation, the experimental hydrogen consumption was in good agreement with the theoretical consumption calculated by elemental analysis of the calcined samples, which indicates that the presented TPR profiles reflect the complete reduction of CuO to zero-valent metallic Cu.

The TPR profile for Cu₁₀/M100 (curve b) displays a single step reduction at ~270 °C, which indicates a homogenous distribution of the highly dispersed CuO particles. In contrast, Cu₂₅/M100 and Cu₃₅/M100 samples show two-step reduction profiles, which are characterized by main peaks at

~300 °C and shoulders at ~270 °C. According to literature, the reduction temperature of CuO depends on the particle size and dispersion, lower temperatures being usually associated to higher dispersion (Tu et al., 2006; Zheng et al., 2005). Under these considerations, TPR results for the samples with high metal loadings indicate a heterogeneous distribution of CuO particles sizes, in agreement with TEM: the main peaks are attributed to weakly dispersed CuO probably under the form of extra-porous aggregates whereas the shoulders are due to the highly dispersed intra-porous CuO

particles. On the other hand, Cu₁₀/MA reference material displays a reduction maximum at ~290 °C, pointing out a much lower CuO dispersion, as compared with the copper material obtained on the mesostructured SBA-15-like hybrid.

To evaluate copper dispersion, the titration of superficial copper atoms with N₂O was performed. Table 2 centralizes the dispersion degrees, Cu surface areas, and Cu average particle sizes for all catalysts. Cu/M100 catalysts showed high dispersion degrees that fall from 43.5 to 25.1 and 16.7 % by increasing the metal loading from 10 to 25 and 35 wt.%, respectively.

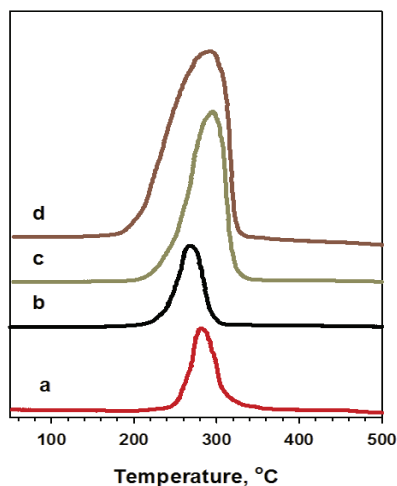


Fig. 6. TPR profiles for Cu₁₀/MA (a), Cu₁₀/M100 (b), Cu₂₅/M100 (c), and Cu₃₅/M100 (d)

In parallel, the estimated values of Cu particle size range between 2.3 and 6.0 nm, indicating that small metallic copper NPs are generated by the reduction of highly dispersed CuO-NPs, as already demonstrated by various techniques. As awaited, the average particle size increases with the copper loading, whereas the active surface per gram of copper decreases. It is however interesting to observe that Cu surface area per gram of catalyst shows a maximum value of 40.1 m²/g for the Cu₂₅/M100 sample, which is thus expected to show the highest catalytic activity. It is also worthy to note that a similar high value of Cu surface area (45.8 m²/g) was

previously reported for 25.2% Cu/SBA-15 prepared by impregnation on hybrid SBA-15 functionalized with carboxylic acid groups (Chen et al., 2013), as a confirmation on the high capacity of our approach to stabilize highly dispersed Cu NPs even at high loading degree. On the other hand, as expected, Cu₁₀/MA showed a much lower dispersion (9 %) and larger particle size (11 nm) as compared with Cu₁₀/M100.

3.3. Catalytic properties

The obtained materials were finally tested in the catalytic hydrogenation of trans-cinnamaldehyde (Fig. 7) with the purpose of investigating the activity and selectivity in relation with the metal loading degree. The evolution of CNA conversion vs time is presented in Fig. 8. It can be observed that all catalysts obtained on M100 supports are highly active in hydrogenation where complete conversion of the substrate takes place in a maximum of 240 min. of reaction duration.

The results are very interesting while considering the mild reaction conditions, especially the atmospheric pressure. Under the same conditions, Cu₁₀/MA displays a poor activity, which can be readily connected with the lowest dispersion and Cu surface area (see Table 2). Although all Cu/M100 materials were very active, the conversion curves shown in Fig. 8 indicate that the catalytic activity follows the order: Cu₂₅/M100 > Cu₁₀/M100 ~ Cu₃₅/M100, these are in good agreement with the evolution of S_{Cu} (m²/g_{cat}) (Table 2), Cu₂₅/M100 sample displaying the highest active surface of 40.1 m²/g. The results clearly demonstrate that a loading of 25 wt. % Cu is optimum to achieve high activity correlated with the highest number of active sites. Regarding the selectivity, as shown in Table 3, it can be concluded that Cu/M100 catalysts are highly selective towards the saturated aldehyde (more than 85 mol % HCNA).

Furthermore, the selectivity profiles were almost identical for all catalysts, suggesting that the chemoselectivity does not depend on the copper particle size, as far as the range of 2.3-6 nm is considered.

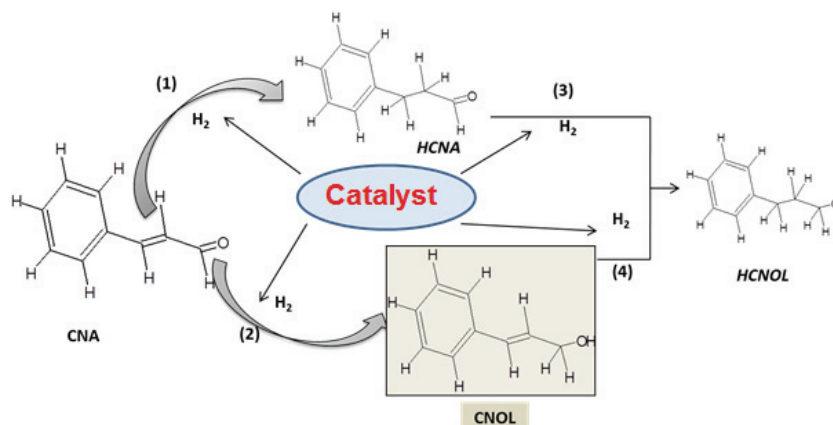


Fig. 7. Reaction pathways for the hydrogenation of cinnamaldehyde

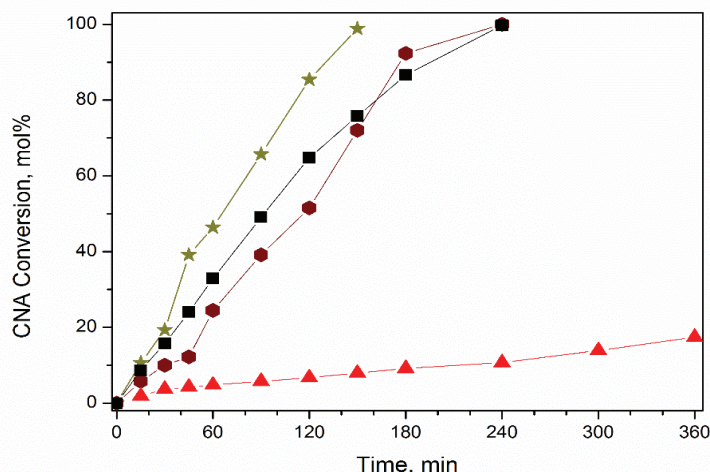


Fig. 8. Catalytic activity of copper NPs supported on M100
 ■-Cu₁₀/M100, ★-Cu₂₅/M100, ●-Cu₃₅/M100, ▲-Cu₁₀/MA

Table 3. Selectivity of copper NPs supported on M100

Sample	Selectivity* (mol %)		
	HCNA	CNOL	HCNOL
Cu ₁₀ /M ₁₀₀	86.5	3.5	10.0
Cu ₂₅ /M ₁₀₀	85.9	1.7	12.4
Cu ₃₅ /M ₁₀₀	88.5	4.6	6.9

*selectivity measured after 120 min

4. Conclusions

Bis-silylated mesoporous silica was successfully loaded with large amounts of copper, up to 35 wt. %, while maintaining good dispersion degrees and very high copper active surfaces. Nevertheless, metal loadings higher than 10 wt. % resulted in lower dispersions of CuO-NPs, which appear heterogeneously distributed on the mesoporous silica support as both large agglomerates and highly dispersed particles, respectively.

As a consequence, the average particle size of metallic copper increased with the metal loading from 2.3 to 6 nm. The catalysts manifested excellent activity in the hydrogenation of cinnamaldehyde, with a maximum for the sample with 25 wt. % Cu, and high selectivity towards hydrocinnamaldehyde (> 85 mol %), which however did not depend on the copper particle size.

Due to these interesting results, bis-silylated mesoporous hybrid materials with different contents in the functionalized P123 were designed and used for detailed investigations on the effect of surface microenvironment on copper particle structure and morphology, which will constitute the subject of a distinct contribution.

Acknowledgments

This work was partially supported by two grants of the Romanian National Authority for Scientific Research, CNCS-UEFISCDI (project numbers PN-II-RU-TE-2012-3-0403 and PN-II-CT-RO-FR-2012-1-0052 - Bilateral program Hubert Curien-Brancusi).

References

- Andersson M., Persson J.L., Rosén A., (1996), Reactivity of Fe_n, Co_n, and Cu_n clusters with O₂ and D₂ studied at single-collision conditions, *The Journal of Physical Chemistry*, **100**, 12222-12234.
- Athens G.L., Shayib R.M., Chmelka B.F., (2009), Functionalization of mesostructured inorganic-organic and porous inorganic materials, *Current Opinion in Colloid & Interface Science*, **14**, 281-292.
- Boubekr F., Davidson A., Casale S., Massiani P., (2011), Ex-nitrate Co/SBA-15 catalysts prepared with calibrated silica grains: Information given by TPR, TEM, SAXS and WAXS, *Microporous and Mesoporous Materials*, **141**, 157-166.
- Campelo J.M., Luna D., Luque R., Marinas J.M., Romero A.A., (2009), Sustainable preparation of supported metal nanoparticles and their applications in catalysis, *ChemSusChem*, **2**, 18-45.
- Chatterjee M., Zhao F.Y., Ikushima Y., (2004), Effect of synthesis variables on the hydrogenation of cinnamaldehyde over Pt-MCM-48 in supercritical CO₂ medium, *Applied Catalysis A: General*, **262**, 93-100.
- Chen C.S., Lai Y.T., Lai T.W., Wu J.H., Chen C.H., Lee J.F., Kao H.M., (2013), Formation of Cu nanoparticles in SBA-15 functionalized with carboxylic acid groups and their application in the water-gas shift reaction, *ACS Catalysis*, **3**, 667-677.
- Chinchen G.C., Hay C.M., Vandervell H.D., Waugh K.C., (1987), The measurement of copper surface areas by reactive frontal chromatography, *Journal of Catalysis*, **103**, 79-86.
- Cuenya B.R., (2010), Synthesis and catalytic properties of metal nanoparticles: size, shape, support, composition, and oxidation state effects, *Thin Solid Films*, **518**, 3127-3150.

- de Jongh P.E., Eggenhuisen P., (2013), Melt infiltration: an emerging technique for the preparation of novel functional nanostructured materials, *Advanced Materials*, **25**, 6672-6690.
- Dragoi B., Ungureanu A., Chiriac A., Hulea V., Dumitriu E., (2010), Hydrogenation of unsaturated carbonyl compounds on non-calcined LDHs. I. Synthesis and characterization of ZnNiCuAl hydrotalcite-like materials, *Acta Chimica Slovenica*, **57**, 677-685.
- Dragoi B., Ungureanu A., Chiriac A., Dumitriu E., (2011), Synthesis of new catalysts by insertion of Co and Cu in the matrix of hydrotalcite-like materials for cinnamaldehyde hydrogenation, *Environmental Engineering and Management Journal*, **10**, 1561-1571.
- Dragoi B., Ungureanu A., Chiriac A., Hulea V., Royer S., Dumitriu E., (2013), Enhancing the performance of SBA-15-supported copper catalysts by chromium addition for the chemoselective hydrogenation of trans-cinnamaldehyde, *Catalysis Science and Technology*, **3**, 2319-2329.
- Chiriac A., Dragoi B., Ungureanu A., Corcodel A.M., Rudolf C., Sasu A., Dumitriu E., (2012), Controlling the activity and chemoselectivity in the cinnamaldehyde hydrogenation by insertion of non-noble metals in the matrix of hydroalcite-like materials, *Environmental Engineering and Management Journal*, **11**, 47-54.
- Evans J.W., Wainwright M.S., Bridgewater A.J., Young D.J., (1983), On the determination of copper surface area by reaction with nitrous oxide, *Applied Catalysis*, **7**, 75-83.
- Giroir-Fendler A., Richard D., Gallezot P., (1988), *Selectivity in Cinnamaldehyde Hydrogenation of Group-VIII Metals Supported on Graphite and Carbon*, In: *Studies in Surface Science and Catalysis*, Guisnet M., Barbier J., Barrault J., Bouchoule C., Duprez D., Pérot G., Montassier C. (Eds.), Elsevier, 171-178.
- Grandsire A.F., Laborde C., Lamaty F., Mehdi A., (2010), Palladium supported on polyether-functionalized mesoporous silica. Synthesis and application as catalyst for Heck coupling reaction, *Applied Organometallic Chemistry*, **24**, 179-183.
- Gutiérrez V.S., Diez A.S., Dennehy M., Volpe M.A., (2011), Cu incorporated MCM-48 for the liquid phase hydrogenation of cinnamaldehyde, *Microporous and Mesoporous Materials*, **141**, 207-213.
- Gutiérrez V., Alvarez M., Volpe M.A., (2012), Liquid phase selective hydrogenation of cinnamaldehyde over copper supported catalysts, *Applied Catalysis A: General*, **413-414**, 358-365.
- Guvelioglu G.H., Ma P., He X., Forrey R.C., Cheng H., (2006), First principles studies on the growth of small Cu clusters and the dissociative chemisorption of H₂, *Physical Review B*, **73**, 155436-1 – 155436-10.
- Hájek J., Kumar N., Mäki-Arvela P., Salmi T., Murzin D. Y., Paseka I., Heikkilä T., Laine E., Laukkanen P., Väyrynen J., (2003), Ruthenium-modified MCM-41 mesoporous molecular sieve and Y zeolite catalysts for selective hydrogenation of cinnamaldehyde, *Applied Catalysis A: General*, **251**, 385-396.
- Imperor-Clerc M., Bazin D., Appay M.D., Beunier P., Davidson A., (2004), Crystallization of β -MnO₂ nanowires in the pores of SBA-15 silicas: in situ investigation using synchrotron radiation, *Chemistry of Materials*, **16**, 1813-1821.
- Jansat S., Pelzer K., García-Antón J., Raucoules R., Philippot K., Maisonnat A., Chaudret B., Guari Y., Mehdi A., Reyé C., Corriu R.J.P., (2007), Synthesis of new RuO₂@SiO₂ composite nanomaterials and their application as catalytic filters for selective gas detection, *Advanced Functional Materials*, **17**, 3339-3347.
- Jun K.-W., Shen W.-J., Rama Rao K.S., Lee K.-W., (1998), Residual sodium effect on the catalytic activity of Cu/ZnO/Al₂O₃ in methanol synthesis from CO₂ hydrogenation, *Applied Catalysis A: General*, **174**, 231-238.
- Jung A., Jess A., Schubert T., Schutz W., (2009), Performance of carbon nanomaterial (nanotubes and nanofibres) supported platinum and palladium catalysts for the hydrogenation of cinnamaldehyde and of 1-octyne, *Applied Catalysis A-General*, **362**, 95-105.
- Krishna R.G., Rama Rao K.S., Kanta Rao P., (1999), Effect of support modification by carbon coverage in the dehydrogenation activity of Cu/Al₂O₃ catalyst, *Catalysis Letters*, **59**, 157-160.
- Kruk M., Jaroniec M., (2001), Gas adsorption characterization of ordered organic-inorganic nanocomposite materials, *Chemistry of Materials*, **13**, 3169-3183.
- Li Y., Ge C.H., Zhao J., Zhou R.X., (2008), Influence of preparation modes on Pt-Ni/CNTs catalysts used in the selective hydrogenation of cinnamaldehyde to hydrocinnamaldehyde, *Catalysis Letters*, **126**, 280-285.
- Liu H.L., Yuan M.L., Guo C.H., Li R.X., Fu H.Y., Chen H., Li X.J., (2011), Selective hydrogenation of cinnamaldehyde to cinnamyl alcohol over Ru/ZrO₂·xH₂O catalyst, *Chinese Journal of Catalysis*, **32**, 1256-1261.
- Liu C.H., Lai N.C., Lee J.F., Chen C.S., Yang C.M., (2014), SBA-15-supported highly dispersed copper catalysts: Vacuum-thermal preparation and catalytic studies in propylene partial oxidation to acrolein, *Journal of Catalysis*, **316**, 231-239.
- López-Linares F., Gonzalez M.G., Páez D.E., (1999), The regioselective biphasic hydrogenation of trans-cinnamaldehyde by meta sulfonatophenyl-diphenylphosphine (TPPMS) Ru(II) and Os(II) species. The influence of ionic strength, ligand tensoactivity and metal nature in the selective production of the unsaturated alcohol, *Journal of Molecular Catalysis A: Chemical*, **145**, 61-68.
- Mäki-Arvela P., Hájek J., Salmi T., Murzin D.Y., (2005), Chemoselective hydrogenation of carbonyl compounds over heterogeneous catalysts, *Applied Catalysis A: General*, **292**, 1-49.
- Morse M.D., Geusic M.E., Heath J.R., Smalley R.E., (1985), Surface reactions of metal clusters. II. Reactivity surveys with D₂, N₂, and CO, *The Journal of Chemical Physics*, **83**, 2293-2304.
- Munnik P., Wolters M., Gabriësson A., Pollington S.D., Headdock G., Bitter J.H., De Jongh P.E., De Jong K.P., (2011), Copper nitrate redispersion to arrive at highly active silica-supported copper catalysts, *The Journal of Physical Chemistry C*, **115**, 14698-14706.
- Reyes P., Rodríguez C., Pecchi G., Fierro J.L.G., (2000), Promoting effect of Mo on the selective hydrogenation of cinnamaldehyde on Rh/SiO₂ catalysts, *Catalysis Letters*, **69**, 27-32.
- Richard D., Gallezot P., Neibecker D., Tkatchenko I., (1989), Characterization and selectivity in cinnamaldehyde hydrogenation of graphite-supported platinum catalysts prepared from a zero-valent platinum complex, *Catalysis Today*, **6**, 171-179.

- Rylander P.N., (1967), *14 - Hydrogenation of Aldehydes*, In: *Catalytic Hydrogenation over Platinum Metals*, Rylander P.N. (Ed.), New York, USA: Academic Press, 238-256.
- Samant P.V., Pereira M.F.R., Figueiredo J.L., (2005), Mesoporous carbon supported Pt and Pt-Sn catalysts for hydrogenation of cinnamaldehyde, *Catalysis Today*, **102**, 183-188.
- Sietsma J.R.A., Meeldijk J.D., Versluijs-Helder M., Broersma A., van Dillen A.J., de Jongh P.E., de Jong K.P., (2008), Ordered mesoporous silica to study the preparation of Ni/SiO₂ ex nitrate catalysts: impregnation, drying, and thermal treatments, *Chemistry of Materials*, **20**, 2921–2931.
- Tian W.H., Sun L.B., Song X.L., Liu X.Q., Yin Y., He G.S., (2010), Adsorptive desulfurization by copper species within confined space, *Langmuir*, **26**, 17398-17404.
- Toebe M.L., Prinsloo F.F., Bitter J.H., Van Dillen A.J., De Jong K.P., (2003), Influence of oxygen-containing surface groups on the activity and selectivity of carbon nanofiber-supported ruthenium catalysts in the hydrogenation of cinnamaldehyde, *Journal of Catalysis*, **214**, 78-87.
- Toupance T., Kermarec M., Louis C., (2000), Metal particle size in silica-supported copper catalysts. influence of the conditions of preparation and of thermal pretreatments, *Journal of Physical Chemistry B*, **104**, 965-972.
- Tu C.-H., Wang A.-Q., Zheng M.-Y., Wang X.-D., Zhang T., (2006), Factors influencing the catalytic activity of SBA-15-supported copper nanoparticles in CO oxidation, *Applied Catalysis A: General*, **297**, 40-47.
- Ungureanu A., Dragoi B., Chiriac A., Ciotonea C., Royer S., Duprez D., Mamede A.S., Dumitriu E., (2013), Composition-dependent morphostructural properties of Ni-Cu oxide nanoparticles confined within the channels of ordered mesoporous SBA-15 silica, *ACS Applied Materials and Interfaces*, **5**, 3010-3025.
- Yang Y., Evans J., Rodriguez J.A., White M.G., Liu P., (2010), Fundamental studies of methanol synthesis from CO₂ hydrogenation on Cu(111), Cu clusters, and Cu/ZnO(0001), *Physical Chemistry Chemical Physics*, **12**, 9909-9917.
- Yin Y., Xue D. M., Liu X.Q., Xu G., Ye P., Wu M.Y., Sun L.B., (2012), Unusual ceria dispersion formed in confined space: a stable and reusable adsorbent for aromatic sulfur capture, *Chemical Communications*, **48**, 9495-9497.
- Yuan Q., Yin A.-X., Luo C., Sun L.-D., Zhang Y.-W., Duan W.-T., Liu H.-C., Yan C.-H., (2008), Facile synthesis for ordered mesoporous γ -aluminas with high thermal stability, *Journal of the American Chemical Society*, **130**, 3465-3472.
- Zheng X.-C., Wu S.-H., Wang S.-P., Wang S.-R., Zhang S.-M., Huang W.-P., (2005), The preparation and catalytic behavior of copper–cerium oxide catalysts for low-temperature carbon monoxide oxidation, *Applied Catalysis A: General*, **283**, 217-223.



“Gheorghe Asachi” Technical University of Iasi, Romania



COMPARATIVE STUDY OF PREHYDROLYSIS METHODS FOR VEGETAL MATERIALS

Corina Măluțan, Adina Elena Pânzariu, Teodor Măluțan*

“Gheorghe Asachi” Technical University of Iasi, Faculty of Chemical Engineering and Environmental Protection,
Department of Natural and Synthetic Polymers, 73 Prof. Dr. docent Dimitrie Mangeron Str., 700050 Iasi, Romania

Abstract

This paper presents the results obtained using the prehydrolysis treatments of rapeseed stalks depending on regime and the catalyst. The vegetal materials were subjected under different temperature conditions and then characterized for the yield reducing substances. The differences between samples have been established by using FTIR and depend on the successive hydrolytic treatments of dynamic and static regime in the presence of various catalysts. The experimental data show that the hydrolysis reaction induces the modification of cellolignin functionality.

Key words: dynamic regime, FTIR, prehydrolysis, rapeseed stalks, static regime

Received: November, 2014; *Revised final:* February, 2015; *Accepted:* February, 2015

1. Introduction

Production of biofuels and “green chemical” from renewable resources is of great interest as an alternative to fuels and fossil chemicals usual. A possible solution to fill the lack of energy in the world is the use of biomass as a sustainable alternative source of energy used to produce chemicals and biofuels with high added value (Xu et al., 2013).

Biomass residues resulting from agricultural crops (such as rapeseed stalks, wheat straw, barley, corn, sugar cane etc.) and wood waste (softwoods, hardwoods) are a significant source of raw materials, untapped properly and present in high quantities. These materials contain polysaccharides (cellulose and hemicellulose), which can be released by hydrolysis for the production of bioethanol and green chemicals. Interest for the use of biomass as a potential source of energy and chemical intermediates increased in recent years (Saxena et al., 2009), because the vegetal materials are biodegradable, not expensive and can be converted to

valuable products with numerous applications in various industrial fields

Thus, we are witnessing currently studies performed for bio-fuels production of second generation in which cellulosic materials play a key role as secondary resources from agriculture or forestry, in particular energy crops on lands without the agricultural value.

The rapeseed stalks (*Brassica napus*) represent an attractive feedstock for several specific applications: production of bioenergy, production of energy with thermal applications, such as pyrolysis (Jeong et al., 2010); production of biodiesel (Šimáček et al., 2009), production of bioethanol due its high content of carbohydrates (more than 60%) (Lu et al., 2009); production of fermentable sugars (Kang et al., 2012); production of chemical compounds, such as glucose, xylose, acetic acid, furfural and 5-hydroxymethylfurfural (Jeong et al., 2010).

These applications involves a step of pretreatment, classified according to catalyst, operating temperature, method of energy supply, hydrodynamic regime, methods for the introduction

* Author to whom all correspondence should be addressed: e-mail: thmalu@tuiasi.ro; Phone: +40 278683; Fax: +40 271311

of reactants and evacuation of products, while not all were sufficiently well developed to become feasible in the application processes are carried out on an industrial scale (Kusch and Morar, 2009).

Most frequently applied methods implies, e.g. the use of water vapors (Cara et al., 2008) or explosions by carbon dioxide (Zheng et al., 1998); hot water treatment (Mosier et al., 2005), chemical processes that involves acidic (Lloyd and Wyman, 2005) or alkaline treatments (Kaar and Holtzapfle, 2000) or the organosolv pretreatment. Thus, at present, vegetal biomass pretreatment methods are divided into physical, chemical, physico-chemical (Zhao et al., 2009) and biological (Kusch and Morar, 2009) processes.

The present paper was performed in order to establish optimal working conditions at the prehydrolysis of the studied vegetal material, namely rapeseed stalks, in the two operating regimes: dynamic, static and moderate pressure.

2. Materials and methods

2.1. Raw materials

Samples of rapeseed stalks were collected from different fields after harvest.

The FTIR analysis were performed using cellolignins obtained after hydrolytic treatments in static and dynamic regime, denoted as: CL_S1-cellolignin obtained by hydrolysis with 3% solution of $\text{Al}_2(\text{SO}_4)_3$ and CL_S2-cellolignin obtained by hydrolysis with 0.5% solution of H_2SO_4 .

2.2. Hydrolysis of the vegetal materials

The prehydrolysis process is preferred for the complex and integral recovery of chemical components of vegetal materials: the polysaccharides towards obtaining the glucose and further bioethanol and lignin as a source of aromatic compounds with added value. In order to evaluate the hydrolytic potential of the vegetal material represented by rapeseed stalks, we performed the prehydrolysis in two operating regimes, namely under dynamic

conditions (reactive flow of 2mL/min at predefined temperature) and static conditions (predefined temperature and time) with 3% $\text{Al}_2(\text{SO}_4)_3$ solution (S1) and 0.5% H_2SO_4 solution (S2) (Liu and Wyman, 2003, 2004). The schematic representation of the hydrolytic conversion during the pretreatment of the vegetal material is shown in Fig. 1 (Panzariu, 2013).

The pretreatment resulted in two fractions: a solid one (cellolignin), and a liquid one, containing oligosaccharides, monosaccharides, decomposition products of sugars, fractions of lignin with low molecular weight. The liquid fractions obtained from these prehydrolytic treatments were analyzed for the content of total reducing substances (TRS).

2.3. Sample analysis

2.3.1. Concentration of the total reducing substances (TRS)

The total reducing substances were determined by the method with dinitrosalicylic acid (DNS) using a JASCO V-550 spectrophotometer at a wavelength of 540 nm.

Prior to determining the total reducing substances the posthydrolysis of the hydrolysates was conducted using NREL standard method No 002 (Adney and Baker, 1996), with 4%(w/w) H_2SO_4 solution, at 120°C and for 60 min residence time.

2.3.2. FTIR spectroscopy

The FTIR spectra of cellolignins were recorded, in a KBr pellet, with a DIGILAB-SCIMITAR FTS 2000 spectrometer, in the 4000-400 cm^{-1} range, with a resolution of 4 cm^{-1} , 32 scans.

3. Results and discussion

3.1. Raw material composition

The raw material used was rapeseed stalks with the following chemical composition: ethanol-benzene extractives=2.43%; cellulose=45.94%; lignin=26.56%; easily hydrolyzable polysaccharides (PUH)=36.28%; slow hydrolyzable polysaccharides (PGH)=36.06% (Panzariu and Malutan, 2012a).

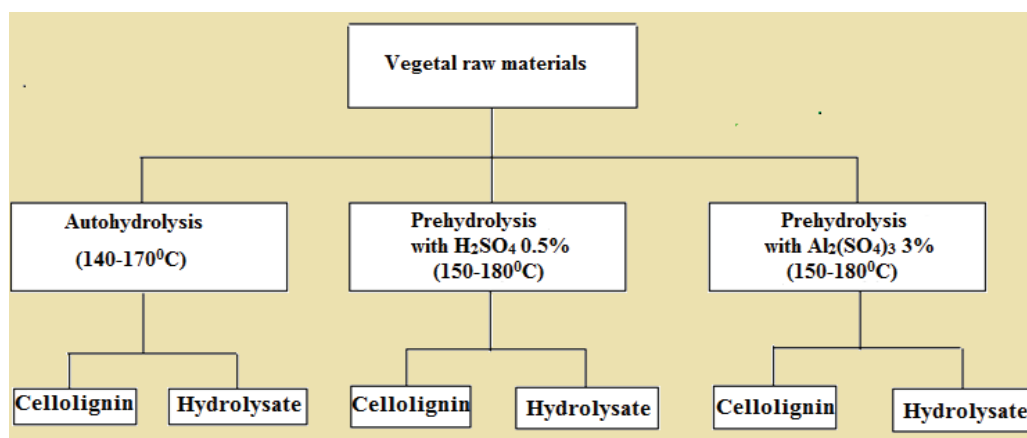


Fig. 1. Schematic representation prehydrolysis of processes

The cellulose, lignin, PUH and PGH contents were determined according to the classic methods of analysis (the cellulose through the nitro-alcoholic method, the lignin through the Klason-Komarov method) (Rozmarin et al., 1984).

3.2. Yield of total reducing substances (TRS)

The prehydrolysis is a preliminary treatment of vegetal material, which may be performed using water or acidic regime, at high temperatures (150°C-160°C). For prehydrolysis different chemicals may be used (mineral acids, organic acids, sulfite solutions etc.), but the most used agent of prehydrolysis is water.

Rogalinski et al. (2008) have achieved a pretreatment of rye straw with hot water in a continuous feeding reactor. The degree of solubilization of the vegetal material was high, the yield of the undesired degradation products increased with increasing with the severity of pretreatment. Ingram et al. (2009) studied the pretreatment of rye straw with hot water in a semi-continuous reactor and concluded that a temperature range between 170°C and 230°C would be optimal.

The experimental data obtained in the autohydrolysis, at the prehydrolysis with acid catalysts and the prehydrolysis with salt of rapeseed stalks are shown in Fig. 2 (a-b). These data are compared, as histograms and show the influence of nature and the addition of the catalyst on the yields of reducing substances in the prehydrolysis, depending on the temperature and prehydrolysis regime applied.

Comparing with other substances reducing yields of prehydrolysate (reported at oven dried material) obtainable from prehydrolysis with three types of catalysts, it is found that, when the temperature rises, this results in increasing yields of reducing substances. It can be observed that, when using dynamic regime, lower values of the reducing substance was obtained in the presence of 3% $\text{Al}_2(\text{SO}_4)_3$ solution, instead using the static regime with saline catalyst to obtain the best performance at 170°C. In the dynamic mode, the yields of reducing substances at autohydrolysis may reach values of up to 11% sugars (reported at the relative content of hemicellulose), which imposes the use of a specific catalyst. Low yields obtained in this case would be due to the high percentage of ash of vegetal material, which plays an important role in catalyst deactivation.

Varying the pH of prehydrolysate within the limits 4-4.5 is insufficiently for a significant depth hydrolysis (Panzariu, 2013). By using a solution of 0.5% H_2SO_4 at prehydrolysis of rapeseed stalks, yields of sugar reach the maximum values of 42%-45% related to hemicellulose at the temperature of 150-160°C. In static regime, at prehydrolysis of rapeseed stalks with 3% solution of $\text{Al}_2(\text{SO}_4)_3$ the yields of sugars can reach a maximum of 44%

reported to hemicelluloses, for temperatures of 170°C.

The treatment of vegetal material with hot water, as well as with hot water under pressure can result in improved yields of pentoses and reduced amounts of by-products.

3.3. FTIR analysis

The following ratios of the relative absorbance for different groups were defined (Malutan et al., 2008):

- Mean value of OH groups = average (A_{3430} , A_{1370} , A_{1165} , A_{1043})/ $A_{1510(1600)}$

- Mean value of phenolic OH groups = $A_{1370}/A_{1510(1600)}$

- Mean value of OCH₃ groups = average (A_{2890} , A_{1460} , A_{1420})/ $A_{1510(1600)}$

- Mean value of C=O groups = $A_{1720}/A_{1510(1600)}$

- Mean value of aromatic ring = average (A_{1510} , A_{1600} , A_{844})

- Ratio of aliphatic to aromatic signals = $A_{2936}/A_{1510(1600)}$

- S/G ratio A_{1330}/A_{1269}

The analysis of the FT-IR absorption spectra of the obtained celollignins shows that the OH total groups relative to the phenylpropane units increase from 0.68 to 2.27 (Table 1), with any increasing of operating temperature between 150-170°C, when using $\text{Al}_2(\text{SO}_4)_3$ as catalyst. At the temperature of 160°C the number of OH alcoholic groups is constant, around 1. Methoxy groups recorded an increase from 0.68 to 1.05 with temperature increasing from 150-170°C. Also the C=O groups vary from 0.72 to 1.54 (a doubling of the C=O). These increases of the number of functional groups are the results of functionalization reactions taking place during continuous hydrolytic treatments in the presence of 3% $\text{Al}_2(\text{SO}_4)_3$ solution.

In the operating temperature range of 160°-180°C it is observed that total OH groups increase significantly at 170°C. The alcoholic OH groups show a decrease from 1.14 to 1.00 (Table 2) with increasing temperature. Methoxyl groups is decreasing at 170°C and the same is carried and C=O groups. These changes are due to functionalization reactions that occur throughout discontinuous hydrolytic treatments in H_2SO_4 solution. By analyzing the data obtained during discontinuous hydrolytic treatments in the presence of $\text{Al}_2(\text{SO}_4)_3$, it is found that the number of Ar-OH groups increases from 1.42 to 2.95 with increasing the operating temperature from 160°C to 180°C (Table 3). In the opposite direction, the number of alcoholic OH groups decreases when the temperature rises. The same is valid for methoxyl groups when the temperature rises there is a gradual decrease in their number. The number of C=O groups show an increase from 0.81 to 4.01 (Table 4). When the temperature rises from 170°C at 180°C there is a

large increase of C=O groups number due to the functionalization reactions, throughout the discontinuous hydrolytic treatments in the presence of $Al_2(SO_4)_3$.

We observed that the number of total OH groups, related to phenyl propane units increases from 1.38 to 2.71 (Table 4) with increasing the operating temperature between 150-170°C, when using H_2SO_4 catalyst. The alcoholic OH-groups occurs an increase low at 160°C compared to other temperatures. The C=O groups show a decrease from

1.67 to 0.78, all these changes being due to functionalization reactions, during the discontinuous hydrolytic treatments in the presence of H_2SO_4 catalyst.

From the analysis of FTIR spectra obtained for cellulignins there are observed these maximum intensity characteristic bands of the valence vibration, $\nu(C-O)$ from 1059 to 1034 cm^{-1} and $\nu(O-H)$ at 3414-3428 cm^{-1} . The maximum decreases in intensity with increasing temperature from 150°C to 170°C (Panzariu and Malutan, 2012b).

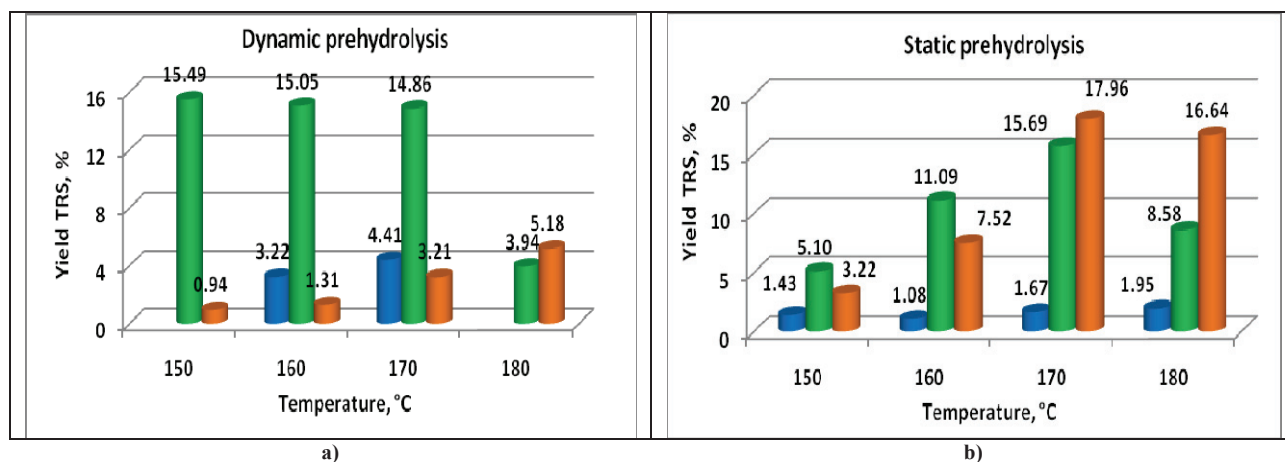


Fig. 2. Yield of total sugars obtained from the prehydrolysis of rapeseed stalks depending on the temperature and the catalyst (a) dynamic regime (b) static regime demineralized H_2O ; 0.5% H_2SO_4 solution; 3% $Al_2(SO_4)_3$ solution

Table 1. Values of the characteristic parameters for cellulignins obtained of dynamic hydrolysis of 3% $Al_2(SO_4)_3$ solution (S1)

Sample	OH total groups	OH alcohol groups	OCH ₃ groups	C=O groups
CL_150_S1	0.68	0.57	0.68	0.72
CL_160_S1	1.45	1.03	0.80	0.83
CL_170_S1	2.27	0.91	1.05	1.54

Table 2. Values of the characteristic parameters for cellulignins obtained of dynamic hydrolysis of 0.5% H_2SO_4 solution (S2)

Sample	OH total groups	OH alcohol groups	OCH ₃ groups	C=O groups
CL_160_S2	2.58	1.14	1.08	1.11
CL_170_S2	2.71	1.13	1.02	0.78
CL_180_S2	2.30	1.00	1.12	1.63

Table 3. Values of the characteristic parameters for cellulignins obtained of static hydrolysis of 3% $Al_2(SO_4)_3$ solution (S1)

Sample	OH total groups	OH alcohol groups	OCH ₃ groups	C=O groups
CL_160_S1	1.42	1.08	1.06	0.81
CL_170_S1	1.47	0.76	0.94	1.10
CL_180_S1	2.95	0.70	0.80	4.01

Table 4. Values of the characteristic parameters for cellulignins obtained of static hydrolysis of 0.5% H_2SO_4 solution (S2)

Sample	OH total groups	OH alcohol groups	OCH ₃ groups	C=O groups
CL_150_S2	1.38	1.00	0.81	1.67
CL_160_S2	2.58	1.14	1.08	1.11
CL_170_S2	2.71	1.13	1.02	0.78

4. Conclusions

The experiments were performed in order to establish the working conditions at the prehydrolysis of the rapeseed stalks, in dynamic and static operating conditions, and moderate pressure.

The ratios of the relative absorbance for different groups were modified during the hydrolysis, probably because due to functionalization reactions which occur throughout hydrolytic treatments.

References

- Adney B., Baker J., (1996), Measurement of cellulase activities, Laboratory Analytical Procedure, (LAP) No. 006, *National Renewable Research Laboratory (NREL)*, Golden, CO, USA.
- Cara C., Ruiz E., Ballesteros M., Manzaneros P., Negro M.J., Castro E., (2008), Production of fuel ethanol from steam-explosion pretreated olive tree pruning, *Fuel*, **87**, 692-700.
- Ingram T., Rogalinski T., Bockemühl V., Antranikian G., Brunner G., (2009), Semi-continuous liquid hot water pretreatment of rye straw, *The Journal of Supercritical Fluids*, **48**, 238-246.
- Jeong T.-S., Um B.-H., Kim J.-S., Oh K.-K., (2010), Optimizing dilute-acid pretreatment of rapeseed straw for extraction of hemicelluloses, *Applied Biochemistry and Biotechnology*, **161**, 22-33.
- Kaar W.E., Holtzapfle M.T., (2000), Using lime pretreatment to facilitate the enzymic hydrolysis of corn stover, *Biomass Bioenergy*, **18**, 189-199.
- Kang K.E., Jeong G.-T., Sunwoo C., Park D.-H., (2012), Pretreatment of rapeseed straw by soaking in aqueous ammonia, *Bioprocess and Biosystems Engineering*, **35**, 77-84.
- Kusch S., Morar M.V., (2009), Integration of lignocellulosic biomass into renewable energy generation concepts, *ProEnvironment*, **2**, 97-102.
- Liu C.G., Wyman C.E., (2003), The effect of flow rate of compressed hot water on xylan, lignin, and total mass removal from corn stover, *Industrial & Engineering Chemistry Research*, **42**, 5409-5416.
- Liu C.G., Wyman C.E., (2004), Impact of fluid velocity on hot water only pretreatment of corn stover in a flowthrough reactor, *Applied Biochemistry and Biotechnology*, **113-116**, 977-987.
- Lloyd T.A., Wyman C.E., (2005), Combined sugar yields for dilute sulfuric pretreatment of corn stover followed by enzymatic hydrolysis of the remaining solids, *Bioresource Technology*, **96**, 18, 1967-1977.
- Lu X., Zhang Y., Angelidaki I., (2009), Optimization of H₂SO₄-catalyzed hydrothermal pretreatment of rapeseed straw for bioconversion to ethanol: Focusing on pretreatment at high solids content, *Bioresource Technology*, **100**, 3048-3053.
- Malutan T., Nicu R., Popa V.I., (2008), Contribution to the study of hydroxymethylation reaction of alkali lignin, *BioResources*, **3**, 13-20.
- Mosier N., Hendrickson R., Ho N., Sedlak M., Ladisch M.R., (2005), Optimization of pH controlled liquid hot water pretreatment of corn stover, *Bioresource Technology*, **96**, 1986-1993.
- Panzariu A.E., Malutan T., (2012a), Analysis of the celloignins obtained from hydrolytic conversion of vegetal materials, *Bulletin of the Polytechnic Institute of Iasi, Section Chemistry and Chemical Engineering*, **LVIII (LXII)**, 173-181.
- Panzariu A.E., Malutan T., (2012b), The flowthrough acid hydrolysis of rapeseed stalks, *Environmental Engineering and Management Journal*, **11**, 2313-2318.
- Panzariu A.E., (2013), *New alternatives for hydrolytic conversion of vegetal materials*, PhD Thesis, „Gheorghe Asachi” Technical University, Iasi, Romania.
- Rogalinski T., Ingram T., Brunner G., (2008), Hydrolysis of lignocellulosic biomass in water under elevated temperatures and pressure, *The Journal of Supercritical Fluids*, **47**, 54-63.
- Rozmarin G., Popa V.I., Grovu-Ivănoiu M., Doniga E., (1984), *Chemistry of Macromolecular Compounds, Chemistry of Wood-Applications*, (in Romanian), Polytechnic Institute Press, Iasi, Romania.
- Saxena R.C., Adhikari D.K., Goyal H.B., (2009), Biomass - based energy fuel through biochemical routes: A review, *Renewable and Sustainable Energy Reviews*, **13**, 167-178.
- Šimáček P., Kubička D., Šebor G., Pospíšil M., (2009), Hydroprocessed rapeseed oil as a source of hydrocarbon-based biodiesel, *Fuel*, **88**, 456-460.
- Xu J.-K., Sun Y.-C., Xu F., Sun R.-C., (2013), Characterization of hemicelluloses obtained from partially delignified *Eucalyptus* using ionic liquid pretreatment, *BioResources*, **8**, 1946-1962.
- Zhao H., Jones C.L., Baker G.A., Xia S., Olubajo O., Person V.N., (2009), Regenerating cellulose from ionic liquids for an accelerated enzymatic hydrolysis, *Journal of Biotechnology*, **139**, 47-54.
- Zheng Y.Z., Lin H.M., Tsao G.T., (1998), Pretreatment for cellulose hydrolysis by carbon dioxide explosion, *Biotechnology Progress*, **14**, 890-896.



“Gheorghe Asachi” Technical University of Iasi, Romania



STUDIES ON THE PHOTOCATALYTIC DEGRADATION OF ORGANIC DYES USING CeO₂ - ZnO MIXED OXIDES

Gabriela Antoaneta Apostolescu, Corina Cernatescu, Claudia Cobzaru, Ramona Elena Tataru-Farmus, Nicolae Apostolescu*

“Gheorghe Asachi” Technical University of Iasi, Faculty of Chemical Engineering and Environmental Protection, 73 Prof. Dr. docent Dimitrie Mangeron Str., 700050 Iasi, Romania

Abstract

A new catalytic mixture of nanosized dioxide (CeO₂) and zinc oxide (ZnO) powders have been synthesized by surfactant-assisted solvo-thermal route, characterized and evaluated for photocatalytic activity. The prepared catalysts were characterized by TG, XRD, SEM and EDAX methods. SEM analysis showed that the catalyst particles have spheroidal shape and their sizes range from 50 to 80 nm, organised as uniform distributed aggregates with large surface area, leading to the existence of a large number of defects. The photocatalytic activity of these materials was evaluated by UV-Vis spectroscopy for degradation of methylene blue (MB) and 4’-(1-methyl-benzimidazolyl-2)-phenylazo-2’’-(8’’-amino-1’’-hydroxy-3’’-6’’-disulphonic)-naphthalene acid (PMBH) in water.

Key words: CeO₂ - ZnO mixed oxides, MB, organic dye photodegradation

Received: November, 2014; *Revised final:* February, 2015; *Accepted:* February, 2015

1. Introduction

Materials based on mixed oxide (CeO₂ - ZnO) nano-powders have been intensive studied in the last years in order to find the best solutions to improve or to fix some environmental problems (Faisal et al., 2013; Lima et al., 2009; Nascimento et al., 2014). Separately, cerium oxide (simple or in matrix) is used as catalyst or catalyst support material, in optical devices as semiconductor or as gas sensor (Ghodsi et al., 2008; Paul et al., 2008; Preetam and Hegde, 2008), and recently have appeared studies about antiseptic properties or UV filter in sunscreen. Also, zinc oxide (simple or in matrix) is studied for its applications as semiconductor, pigment, antiseptic or in sunscreens (Ameen et al., 2012; Ezenwa, 2010; Kashif et al., 2013; Shafaei et al., 2010). Both materials show properties that can be easily exploited. Therefore, it is interesting to study the

behaviour of the material obtained by combining in specific conditions of these two oxides.

Due to the last trends in environmental protection it is required to find some new materials that could be used to purify exhausted waters, mainly the organic compounds well known to be toxic. The degradation of organic compounds produced in industrial processes using the most efficient methods and advanced materials has emerged as a necessity to protect the environment (Arsene et al., 2013). Following this trend, the degradation of organic effluents have been studied by using various catalytic materials based on cerium / zinc oxide simple or doped with various metals or materials.

Studies are reported on photocatalytic degradation of methylene blue dye, Rhodamine B, methyl tert-butyl ether, castor oil or other organic compounds (Abbas et al., 2014; Akyol et al., 2005; Bansal and Sud, 2011; Fan et al., 2008; Khataee et

* Author to whom all correspondence should be addressed: e-mail: napostol@ch.tuiasi.ro

al., 2015; Ko et al., 2014; Kumar et al., 2014; Orbeci et al., 2014; Shidpour et al., 2014; Wang et al., 2009).

Our research is focused on the development of efficient and inexpensive smart materials that can be used in several areas of heterogeneous catalysis, such as the combination of cerium oxide and zinc oxide that generates good results. This material is correlated with low price and low toxicity of zinc oxide that recommend it as promising photocatalyst. Also the possibilities of modelling the structural and textural properties of synthesized catalyst can contribute to the improvement of the photocatalytic activity.

2. Materials and methods

All chemicals used in this study were of analytical grade and used without further purifications. The starting materials were $\text{Ce}_2(\text{C}_2\text{O}_4)_3 \cdot x\text{H}_2\text{O}$, $\text{ZnC}_2\text{O}_4 \cdot x\text{H}_2\text{O}$ (all 99.99% purity, supplied from Aldrich), and PVA (average Mw 89,000 - 98,000, 99 %, Aldrich), ethanol and methylene blue (Chemical Company). The pH was adjusted with NaOH or HCl (Chemical Company). The 4'-(1-methyl-benzimidazolyl-2)-phenylazo-2''-(8''-amino-1''-hydroxy-3'',6''-disulphonic)-naphthalene acid, was synthesized in our laboratory. This compound is abbreviated as PMBH. A SP-870 plus METERTECH UV - Vis spectrophotometer was used to monitor the residue concentration of methylene blue (abbreviated as MB) and PMBH.

Methylene blue is a cationic dye with the structure shown in Fig. 1. It is most commonly used for colouring paper, temporary hair dye, dyeing cotton, wools and so on th. MB, although not considered to be a very toxic dye it can reveal very harmful effects on the living things.

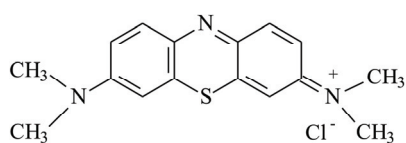


Fig. 1. Methylene blue structure

Methylene blue is a thiazinic dye and could be reduced by X and UV rays, acid pH or by using various salts as catalysts.

4'-(1-methyl-benzimidazolyl-2)-phenylazo-2''-(8''-amino-1''-hydroxy-3'',6''-disulphonic)-naphthalene acid (PMBH)

The PMBH ($\text{C}_{24}\text{H}_{19}\text{N}_5\text{O}_7\text{S}_2$, $M = 553\text{g/mol}$), with the structure shown in Fig. 2) was synthesized in our laboratory, the synthesis being the subject of another paper, the structure of the azoic dye being presented below.

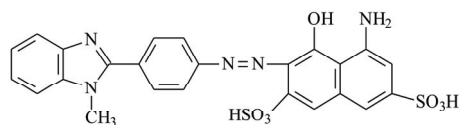


Fig. 2. 4'-(1-methyl-benzimidazolyl-2)-phenylazo-2''-(8''-amino-1''-hydroxy-3'',6''-disulphonic)-naphthalene acid structure

The reaction mixture was heated to 150°C and continuously stirred for 2 h, in a capped reactor and transferred into a 200 mL Teflon-lined autoclave. Then the autoclave was sealed and kept at 160 °C for 8 h, and subsequently cooled down to room temperature naturally. The precipitate was separated by centrifugation (6000 rot/min, 5 min), washed three times with deionized water, and dried in vacuum at 80°C for 6 h. Finally, the product was calcined at 450 °C in air for 4 h.

The final material obtained was a yellowish powder. The sample was examined by SEM (MIRA TESCAN and QUANTA 200 3D), EDAX (Quanta 200 3D electron microscope connected with EDS Ametek/EDAX equipment) thermal analysis (Pyris Diamond TG/DTA PerkinElmer), and XRD (Shimadzu XRD 6100 diffractometer using monochromatic Cu K α radiation ($\lambda = 0.154\text{ nm}$), operating at 40 kV and 30 mA).

3.2. Photocatalytic reaction procedure

The photocatalytic activity measurements were carried out as follows: the absorption mode of UV-Vis spectroscopy was used to measure the absorbance of various MB or PMBH concentration to plot the diagram of absorbance at 664 nm (in a.u., for MB) or 540 nm (in a.u., for PMBH) vs. concentration (mol/L). The reaction system containing 100 mL MB or PMBH aqueous solution with 10^{-5} mol/L MB, 5×10^{-5} mol/L PMBH and 10 mg $\text{CeO}_2 - \text{ZnO}$ photocatalyst was stirred magnetically in darkness at pH=7, for 30 min. To ensure a well dispersing and de-agglomeration of $\text{CeO}_2 - \text{ZnO}$ nanopowder suspended in aqueous solution, a 400 W ultrasonic bath was used for 4 min. Before the irradiation, 3 mL of solution were taken out for adsorption analysis. The stirring was performed to reach the adsorption equilibrium of the MB/PMBH before exposure to UV irradiation from a 25 W Hg lamp. The distance between the lamp and reaction system was 5 cm and the temperature was set on 25 °C. First, some experiments were done in two cases: in the presence of $\text{CeO}_2 - \text{ZnO}$ photocatalyst and without any UV irradiation to identify the catalysis's influence and second, only under UV radiation to probe degradation of MB and PMBH solution.

For recording the first results without any light source, we put the prepared dispersed solution in a dark and cool place under vigorous stirring for 30 min. After beginning the irradiation process, the same amount of solution was taken out for each quantitative analysis, during 200 min. In these two cases there were no changes in the studied systems. A SP-870 plus METERTECH UV-Vis spectrophotometer was used to monitor the residue concentration of methylene blue and benzimidazole dye. All the photocatalytic experiments were repeated three times. The MB and PMBH removal was analysed by measuring the change in absorbance using UV-Visible spectrophotometer at 664 nm

corresponding to maximum absorption wavelength of MB and 540 nm for PMBH.

4. Results and discussion

4.1. Morphology and structure of CeO₂ - ZnO photocatalysts

The surface morphology, shape features and size determination of the synthesized CeO₂ - ZnO nanocomposites were investigated using SEM and results are shown in Fig. 3 a-d, at different magnifications. In the first stage of organization can be observed association parallelepipedic crystals of about 2-5 μm (images a, b). By increasing the magnification is observed the second level of organization, consisting of small spheroidal shape crystals, about 50-80 nm in diameter (images c, d). The agglomeration of nanocrystals is a commonly occurring phenomenon because the nanocrystals follow to decrease the exposed surface in order to minimize the interface energy. CeO₂ - ZnO crystals have specific oriented aggregation of individual nanocrystals, leading to the existence of a large

number of defects. The X-ray patterns of and CeO₂ - ZnO is depicted in Fig. 4. For CeO₂ - ZnO nano powder, the reflection planes perfectly match the indexed CeO₂: cubic system and ZnO: hexagonal system. No peak due to any other phase was observed. In addition, the EDAX analysis (Fig. 5 and Table 1) indicate the presence of all components (Ce, Zn, O). The sharp peaks of Zn, Ce and O were obtained; no other peak related to any other element was detected in the spectrum within the detection limit which confirms that synthesized material composed of Zn, Ce and O only. The thermogravimetric (TG) and differential thermal analysis (DTA) were performed by using a Perkin-Elmer Pyris Diamond TG/DTA thermobalance which records simultaneously T, TG and DTA curves and are shown in Fig. 6 and Table 2. The DTG curves were obtained by numerical differentiation of the TG curves. The working conditions were as follows: sample mass 9.4 mg, heating rate 10 °C min⁻¹, temperature range 30 – 850 °C in air stream (80 mL min⁻¹). There is no obvious weight change at above 420 °C, so that we chose that calcination occurs at 450 °C.

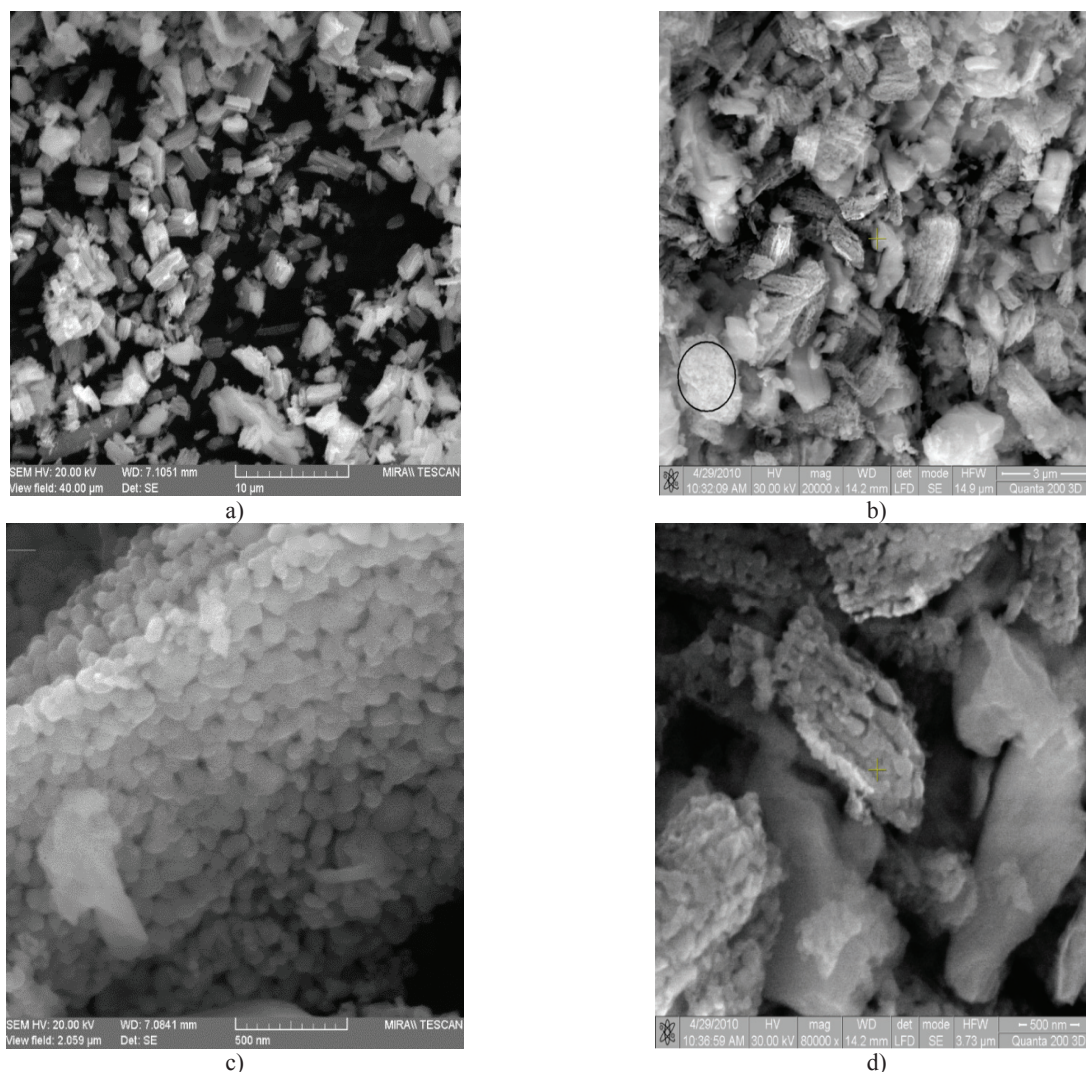


Fig. 3. The SEM images for CeO₂ - ZnO synthesized material

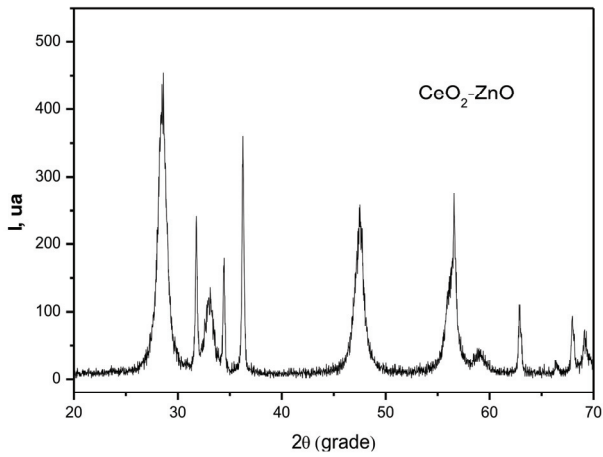


Fig. 4. CeO₂ - ZnO X-ray diffraction pattern

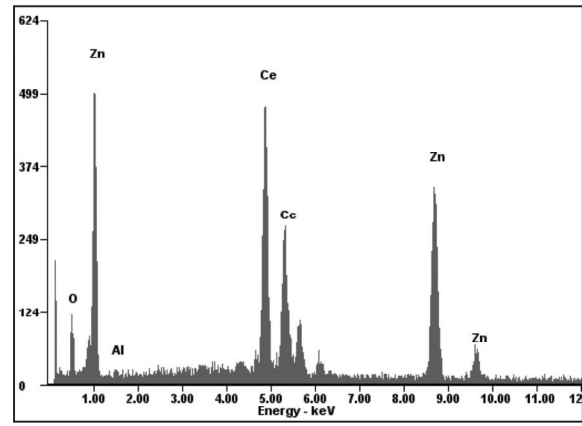


Fig. 5. The EDAX analysis

Table 1. The EDAX analysis

Element	Wt%	At%
O _K	07.81	32.38
AlK	01.48	03.64
CeL	51.91	24.59
ZnK	38.81	39.40
Matrix	Correction	ZAF

Table 2. The TG – DTA results of CeO₂ - ZnO prepared sample

Stage	T _i	T _m	T _f	w _∞	DTA
I	30	66	81	1.38	endo
II	81	116	130	9.27	endo
III	130	143	238	7.51	endo
IV	238	270	291	1.17	exo
V	291	332	366	20.42	exo
VI	366	392	415	12.07	exo
VII	415	423	480	1.41	exo
Residue %				46.77	

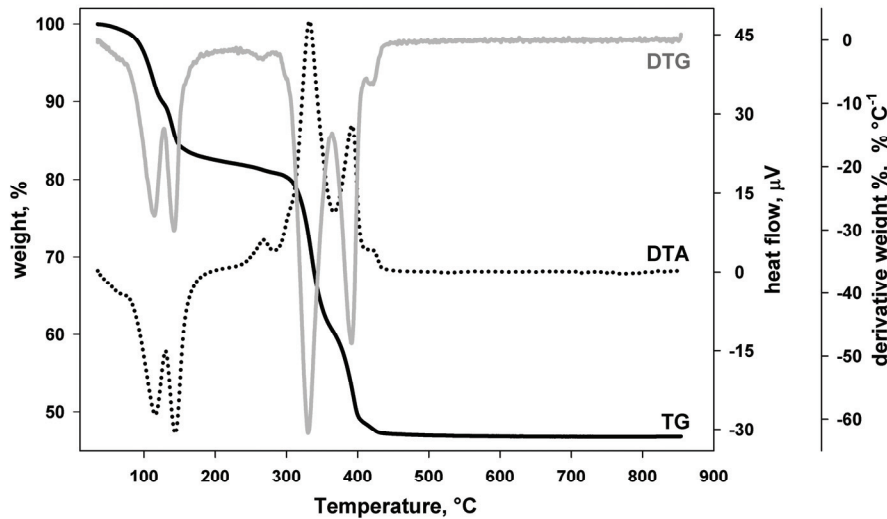
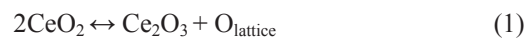


Fig. 6. The TG/DTA curves of CeO₂ - ZnO prepared sample

The catalytic activity of ceria can be related with the oxygen evolution and absorption equilibrium reaction shown in Eqs. (1-2) (Nakatsuji et al., 2013).



4.2. The photocatalytic activity

The photocatalytic activity of CeO₂ - ZnO samples was evaluated by measuring the decomposition rate of MB and PMBH under UV light irradiation. Figs. 7 and 8 show the changes of MB and PMBH concentration with reaction time under UV irradiation and in presence of CeO₂ - ZnO catalyst.

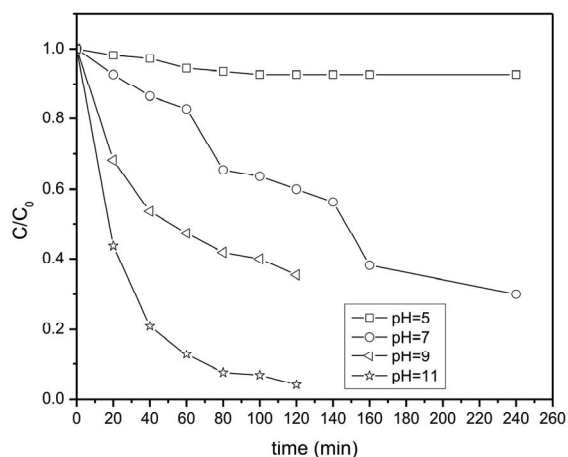
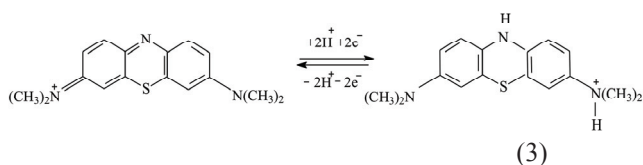


Fig. 7. The MB degradation under UV irradiation, initial MB concentration = 10^{-5} mol/L and 0.1 g/L CeO₂ - ZnO

MB degradation was followed for 260 min. In acidic media were not observed changes in the dye behaviour. After about 3 hours, the MB concentration was only slightly smaller than the initial one. At pH = 7, and pH = 9, the degradation of MB was about 60 %, faster result being reached in basic medium. For pH = 11 MB degradation was achieved in 90 % in just 2 hours, which is remarkable considering the intensity of UV radiation used.

The degradation occurs due to the following reaction (Eq. 3):



The photoreduction is reversible and is measured by decoloration ratio, the leucoderivative formed being white due to the breaking of the double bonds at the nitrogen atom. The leucoderivative has an absorption maximum at 225 nm, while the methylene blue has the absorption maximum at 664 nm. The PMBH dye has an azoic structure, thus it acts different from the MB.

PMBH degradation was also followed at different pH values for 300 min. In neutral and acidic media after 150 min were not observed notable changes in analysed system behaviour. In basic medium, after 300 minutes only 30% of the original compound has been degraded. The azo group is a well-known weak group, so it was a surprise result the fact that only 30% of the dye was decomposed.

The high resistance to UV action occurs due to the extended conjugated system and the electrons transitions, but this hypothesis will be further studied using various analytical methods.

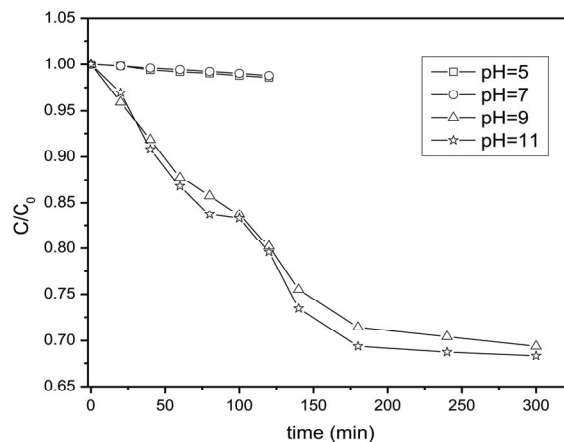


Fig. 8. The PMBH degradation under UV irradiation, initial PMBH concentration = $5 \cdot 10^{-5}$ mol/L and 0.1 g/L CeO₂ - ZnO

5. Conclusions

CeO₂ - ZnO: nanopowder was synthesized by a surfactant-assisted solvo-thermal route. The method is simple and lead to the preparation of ultrafine particles with required characteristics. SEM analysis showed that the particles have spheroidal shape and their sizes range from 50 to 80 nm, which is appropriate for a homogeneous suspension. Moreover, CeO₂ - ZnO systems present photocatalytic activity leading to degradation of two organic substances: MB almost total in basic medium and PMBH less.

References

- Abbas M., Parvatheeswara Rao B., Reddy V., Kim C.G., (2014), Fe₃O₄/TiO₂ core/shell nanocubes: Single-batch surfactantless synthesis, characterization and efficient catalysts for methylene blue degradation, *Ceramics International*, **40**, 11177–11186.
- Akyol A., Bayramoglu M., (2005), Photocatalytic degradation of Remazol Red F3B using ZnO catalyst, *Journal of Hazardous Materials B*, **124**, 241–246.
- Ameen S., Akhtar M.S., Shin S.H., (2012), Growth and characterization of nanospikes decorated ZnO sheets and their solar cell application, *Chemical Engineering Journal*, **195-196**, 307–313.
- Arsene D., Teodosiu C., Barjoveanu G., Apreutesei R.E., Apopei P., Musteret C.P., Cailean D., (2013), Combined catalytic oxidation and adsorption of priority organic pollutants for wastewater recycling, *Environmental Engineering and Management Journal*, **12**, 907-916.
- Bansal P., Sud D., (2011), Photodegradation of commercial dye, Procion Blue HERD from real textile wastewater using nanocatalysts, *Desalination*, **267**, 244–249.
- Ezenwa I.A., (2012), Synthesis and optical characterization of zinc oxide thin film, *Research Journal of Chemical Sciences*, **2**, 26–30.

- Faisal M., Ismail A.A., Ibrahim A., Bouzid H., Al-Sayari S.A., (2013), Highly efficient photocatalyst based on Ce doped ZnO nanorods: Controllable synthesis and enhanced photocatalytic activity, *Chemical Engineering Journal*, **229**, 225–233.
- Fan D.H., Zhu Y.F., Shen W.Z., Lu J.J., (2008), Synthesis and optical properties of hierarchical pure ZnO nanostructures, *Materials Research Bulletin*, **43**, 3433–3440.
- Ghods F.E., Tepehan F.Z., Tepehan G.G., (2008), Optical and structural properties of sol gel made Ce/Ti/Zr mixed oxide thin films as transparent counter electrode for electrochromic devices, *Optical Materials*, **31**, 63–67.
- Kashif M., Ali M.E., Usman Ali S.M., Hashim U., (2013), Sol-gel synthesis of Pd doped ZnO nanorods for room temperature hydrogen sensing applications, *Ceramics International*, **39**, 6461–6466.
- Khataee A., Karimi A., Arefi-Oskoui S., Soltani R.D.C., Hanifehpour Y., Soltani B., Joo S.W., (2015), Sonochemical synthesis of Pr-doped ZnO nanoparticles for sonocatalytic degradation of Acid Red 17, *Ultrasonics Sonochemistry*, **22**, 371–381.
- Ko H.H., Yang G., Cheng H.Z., Wang M.C., Zhao X.J., (2014), Growth and optical properties of cerium dioxide nanocrystallites prepared by coprecipitation routes, *Ceramics International*, **40**, 4055–4064.
- Kumar P.S., Abhinaya R.V., Arthi V., Gayathri Lashmi K., Priyadharshini M., Sivanesan S., (2014), Adsorption of methylene blue dye onto surface modified cashew nut shell, *Environmental Engineering and Management Journal*, **13**, 545-556
- Lima J.F., Martins R.F., Neri C.R., Serra O.A., (2009), ZnO:CeO₂-based nanopowders with low catalytic activity as UV absorbers, *Applied Surface Science*, **255**, 9006–9009.
- Nakatsuji T., Kunishige M., Li J., Hashimoto M., Matsuzono Y., (2013), Effect of CeO₂ addition into Pd/Zr–Pr mixed oxide on three-way catalysis and thermal durability, *Catalysis Communications*, **35**, 88–94.
- Nascimento L.F., Martins R.F., Silva R.F., Serra O.A., (2014), Catalytic combustion of soot over ceria-zinc mixed oxides catalysts supported onto cordierite, *Journal of Environmental Sciences*, **26**, 694–701.
- Orbeci C., Nechifor Gh., Stănescu R., (2014), Removing toxic compounds from wastewater, *Environmental Engineering and Management Journal*, **13**, 2153-2158.
- Paul H., Kessler D., Herr U., (2008), Optical properties of nanocrystalline YAG:Ce, *Solid State Phenomena*, **140**, 9-16.
- Preetam S., Hegde M.S., (2008), Controlled synthesis of nanocrystalline CeO₂ and Ce_{1-x}M_xO_{2-δ} (M = Zr, Y, Ti, Pr and Fe) solid solutions by the hydrothermal method: Structure and oxygen storage capacity, *Journal of Solid State Chemistry*, **181**, 3248–3256
- Shafaei A., Nikazar M., Arami M., (2010), Photocatalytic degradation of terephthalic acid using titania and zinc oxide photocatalysts: Comparative study, *Desalination*, **252**, 8–16.
- Shidpour R., Simchi A., Ghanbari F., Vossoughi M., (2014), Photo-degradation of organic dye by zinc oxide nanosystems with special defect structure: Effect of the morphology and annealing temperature, *Applied Catalysis A: General*, **472**, 198–204.
- Wang L.S., Xiao M.W., Huang X.J., Wu Y.D., (2009), Synthesis, characterization, and photocatalytic activities of titanate nanotubes surface-decorated by zinc oxide nanoparticles, *Journal of Hazardous Materials*, **161**, 49–54.



“Gheorghe Asachi” Technical University of Iasi, Romania



SYNTHESIS AND ELECTRON TRANSPORT PROPERTIES OF SOME NEW 4,7-PHENANTHROLINE DERIVATIVES IN THIN FILMS

Cristina M. Al Matarneh¹, Ramona Danac¹, Liviu Leontie^{2*}, Florin Tudorache³,
Iulian Petrila³, Felicia Iacom², Aurelian Carlescu², Gigel Nedelcu², Ionel Mangalagiu¹

¹Alexandru Ioan Cuza University of Iasi, Faculty of Chemistry, 11 Carol I Blvd., 700506 Iasi, Romania

²Alexandru Ioan Cuza University of Iasi, Faculty of Physics, 11 Carol I Blvd., 700506 Iasi, Romania

³Alexandru Ioan Cuza University of Iasi, Interdisciplinary Research Department - RAMTECH,
11 Carol I Blvd., 700506 Iasi, Romania

Abstract

Temperature-dependent d.c. electric conductivity of some recently synthesized organic compounds, 4,7-phenanthroline derivatives is studied. Thin-film samples ($d=0.34-0.63 \mu\text{m}$) spin-coated from dimethylformamide solutions onto glass substrates have been used. Organic films with reproducible electron transport properties can be obtained if, after deposition, they are submitted to a heat treatment within temperature range of 298–523K. Examined organic compounds in thin films are polycrystalline and display typical n -type semiconductor behavior. The activation energy of d. c. electric conduction ranges between 0.09 and 0.46 eV and is influenced by nature of substituents, degree of conjugation systems and packing capacity of compounds. In the higher temperature range ($T>433 \text{ K}$), the electron transport in examined compounds can be interpreted in terms of the band gap representation model, while in the lower temperature range, the Mott's variable-range hopping conduction model was found to be appropriate. Some of the investigated compounds hold promise for thermistor applications.

Key words: chemical synthesis, electric conductivity, organic compounds, thin films

Received: November, 2014; *Revised final:* February, 2015; *Accepted:* February, 2015

1. Introduction

Organic semiconductor compounds (in form of monomers, polymers, plastics, synthetic rubbers, etc.) represent an emerging class of materials, extensively explored over the past four decades. The ample worldwide research effort addressed divers aspects, from material synthesis and growth (single crystals, thin films, nanostructures), study of electron transport, optical, and photophysical/photochemical properties, to a wide range of technological applications (Iniewski, 2011; Logothetidis, 2012).

The extended π -electron systems of organic semiconductors can be easily tuned through ‘molecular engineering’ (molecular structure

modification by chemical substitution). In this way, divers classes of emerging materials, ranging from superconducting and semiconducting, to conducting ones have been synthesized to date (Fraxedas, 2006; Lebed, 2008).

Due to their remarkable characteristics, significant electroluminescence, high mobilities of charge carriers, energy band gap in the IR–vis domain, relevant photophysical characteristics, combined with high processability and versatility, easy shaping and manufacture, compatibility with mechanically flexible substrates and facile integration with divers physical/chemical/biological functionalities (Bernards et al., 2008; Huang et al., 2014; Turbiez et al., 2005), organic semiconductors

* Author to whom all correspondence should be addressed: email: lleontie@uaic.ro

show great promise for a wide range of solid-state device applications, including: transistors, light-emitting diodes, solar cells, sensors, as well as in nanoelectronics, transparent electronics, electro-optics, photonics and spinics (Deleonibus, 2009; Facchetti and Marks, 2010; Kymissis, 2009; Metzger, 2012; Ohtsu, 2004; Paraschiv 2014; Schols 2011; Sun and Saracftci 2005; Szodrai and Lakatos 2014).

The electron transport properties of organic semiconductor materials employed as active components in semiconductor devices are strongly influenced by their molecular packing, which may significantly affect molecular orbital shapes and interactions (Kazheva et al., 2002). In this respect, study of the of the structure/property relationship of utilized organic materials becomes extremely important, providing understanding of basic transport mechanisms in these materials and consequently, enabling improvement in the performance of new (opto)electronic devices (Coropceanu et al., 2007; Karl, 2003; Stallinga, 2009; Ueno and Kera, 2008).

In our previous works (Danac, 2014; Leontie et al., 2003a; Leontie et al., 2003b; Leontie et al., 2005a; Leontie et al., 2005b; Leontie et al., 2006; Leontie and Danac, 2006; Leontie, 2007; Leontie, 2009; Leontie, 2010; Leontie, 2011; Leontie, 2012; Prelipceanu, 2007; Rusu et al., 2001; Şunel et al., 1995) electronic transport and optical properties of a

great number of organic compounds showing typical semiconducting behavior have been studied. In this paper, we extend these investigations to some recently synthesized organic compounds, 4,7-phenanthroline-4-ium salts (SMC compounds), in form of polycrystalline thin films.

2. Experimental

2.1. Synthesis of compounds

4-(R-2-oxoethyl)-4,7-phenanthroline-4-ium bromides have been recently synthesized in our group by a N-alkylation reaction. These salts have been prepared in excellent yields (67-94%) by reaction of 4,7-phenanthroline (**1**) with reactive halides (**2**) in refluxing acetonitrile.

The reaction of N-quaternization of 4,7-phenanthroline undergoes the following transformation (Fig. 1).

The structure of the compounds was proved by elemental and spectral methods (IR, ¹H-NMR). They showed good chemical stability under normal ambient atmosphere. Investigated organic compounds correspond to the general formula presented in Fig. 2.

The molecular formulas together with other compounds properties are given in Table 1.

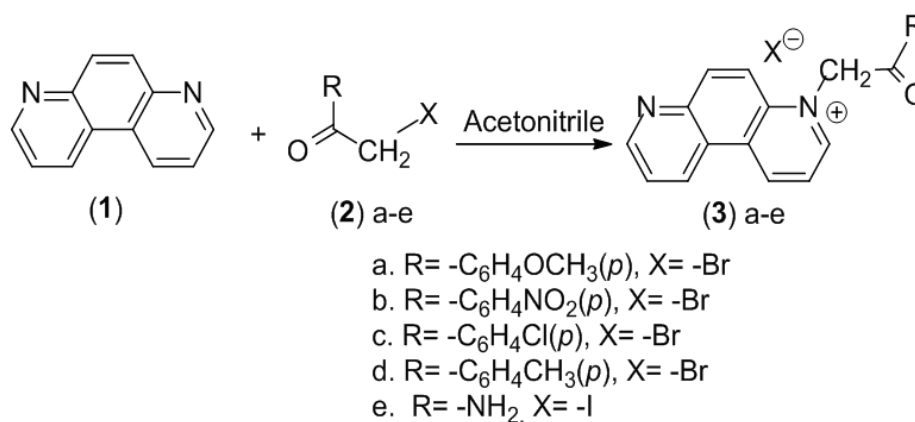


Fig. 1. Synthesis pathway of the investigated compounds

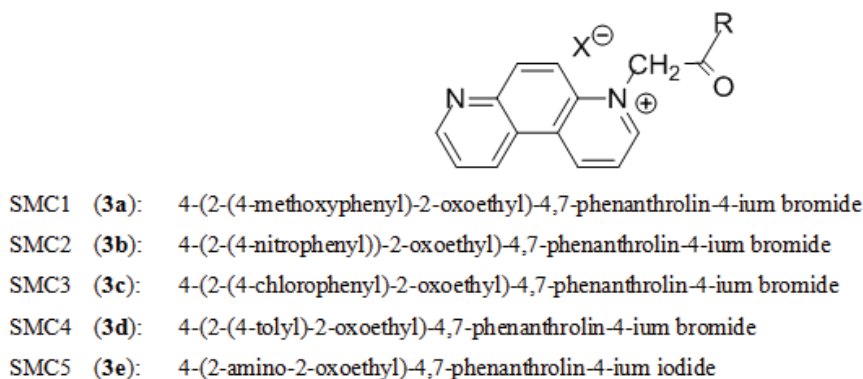


Fig. 2. General structure of the investigated compounds

Table 1. Molecular formula and some properties of the investigated compounds

Compound	Molecular formula	Molecular weight, <i>M</i>	Color	Melting point (K)
SMC1	C ₂₁ H ₁₇ BrN ₂ O ₂	409.28	beige	526–528
SMC2	C ₂₀ H ₁₄ BrN ₃ O ₃	424.25	beige	508–510
SMC3	C ₂₀ H ₁₄ BrClN ₂ O	413.69	beige	515–517
SMC4	C ₂₁ H ₁₇ BrN ₂ O	393.28	beige	519–521
SMC5	C ₁₄ H ₁₂ IN ₃ O	365.17	yellow	537–539

2.2. Sample preparation. Electric conductivity measurements

The d. c. electric conductivity of as-synthesized compounds was investigated using thin-film samples [surface-type cells (Căplănuș, 1999-2000; Rusu, 2001; Şunel et al., 1995)] as thin films deposited by sol-gel (spin-coating) technique, at room temperature, onto glass substrates. Dimethylformamide was used as solvent, in which actual compounds SMC1–SMC5 showed good stability. By adjusting the deposition conditions (solution concentration in the range of 3–10 mg/ml, rotation speed by 1500 rot./min, 5–9 coating-drying cycles, respectively, substrate maintained at room temperature, etc), organic films of a constant thickness on large areas of the substrate surface were obtained.

Thin Ag films (about 1 µm thick), thermally evaporated in vacuum (~10⁻⁵ Torr) onto substrates prior to film deposition, served as electrodes; they were separated by a gap of 2–5 mm. In all performed measurements low-intensity electric fields (under 10² V·cm⁻¹) were applied, so that non-ohmic effects were not noticed.

Thickness (*d*) of thin-film samples was determined with an interferometric microscope MII-4 (LOMO, St. Petersburg) and was found in the range of 0.34–0.63 µm. Surface morphology of organic films was examined by Atomic Force Microscopy (AFM), with a NT-MDT SOLVER PRO-M equipment. The crystal structure of the organic films was investigated by X-ray diffraction (XRD) technique (CuK_α radiation, wavelength λ=1.54182 Å), using a DRON-2.0 diffractometer.

The electric conductivity type of the organic thin films under study was determined by thermal-sonde method (Smith, 1980) and was found to be of *n*-type, for all investigated samples. Experimental arrangements used in the study of temperature dependences of d. c. electric conductivity were similar to those presented in (Căplănuș, 1999-2000; Rusu, 2001; Şunel et al., 1995). A KEITHLEY Model 6517B electrometer was used for resistance measurements of organic thin films. Transmission and reflection spectra, in the spectral range of 300–1400 nm, were recorded with a STEAG ETA-Optik spectrometer.

The absorption coefficient of thin-film samples, α, was determined by using the expression (Pancove, 1979) (Eq. 1), where *d* is the film

thickness and *I*₀ and *I* denote the intensity of incident and emergent beam, respectively.

$$\alpha = \frac{1}{d} \ln \left(\frac{I_0}{I} \right) \quad (1)$$

The above approximate formula (neglecting the effect of reflexion) may be properly used for present organic films, the reflectance of which is below 10 %, for photon energies less than the optical band gap, *E*_{go} (Moss, 1994).

3. Results and discussion

As revealed by the XRD study (Fig. 3, examined organic thin films exhibit a prevailing polycrystalline structure, with a high degree of crystallinity. Structural investigations showed that sample structure depend on the compound nature (molecular structure), thin-film thickness (increased film thickness generally leading to larger grain sizes), and deposition conditions.

All examined samples were found to display the most preferred planes parallel to substrate surface. The interplanar spacings (*d*_{*hkl*}) of studied organic samples were calculated by using the Bragg equation (Cullity and Stock, 2001; Pecharsky and Zavalij, 2009) (Eq. 2), where θ denotes the Bragg diffraction angle, λ=1.54182 Å is the wavelength of the incident X-ray beam and *n* is the reflection order; *h*, *k*, *l* are Miller indices, used to express crystal lattice planes and directions.

$$2d_{hkl} \sin \theta = n\lambda \quad (2)$$

The average crystallite size (*D*) was determined by means of Debye-Scherrer equation, supposing a negligible residual strain effect (Cullity and Stock, 2001; Pecharsky and Zavalij, 2009) (Eq. 3), where *k*=0.9 (Cullity and Stock, 2001) denotes the Scherrer constant, λ=1.54182 Å is the X-ray wavelength, β is the angular full-width at half-maximum (FWHM) of the XRD peak in radians, and θ is the Bragg diffraction angle corresponding to respective peak.

$$D = \frac{k\lambda}{\beta \cos \theta} \quad (3)$$

Values of some typical parameters, determined according to standard method for structural analysis (Cullity and Stock, 2001), are

given in Table 2. As can be observed from this table, investigated organic thin films display rather small crystallites, the size of which is ranged between 15.75 and 60.58 nm. The polycrystalline structure, which is prevalent in the case of actual organic films, exerts a strong influence on the electron transfer mechanism in examined samples: additional scattering produced by film surfaces and small crystallite boundaries tends to substantially diminish the charge carrier mobilities and electric conductivity, with respect to those of the bulk materials (Kazmerski, 1980). The AFM study of organic thin-film samples revealed (Fig. 4) a preponderant grain-like surface morphology, as characteristic topographical feature. Actual organic films display a typical polycrystalline, compact and pinhole-free microstructure; they contain grains of different shapes and sizes, the basis of which lays on the film surface. As resulted from the analysis of AFM micrographs for different organic samples, the mean values of the root mean square (RMS) roughness laid in the range of 6.8–48.3 nm, while the mean grain sizes ranged between 20 and 52 nm.

In our previous works, above-mentioned, we have studied the electron transport properties of many classes of heterocyclic compounds (in polycrystalline thin films, deposited from solution) with similar molecular conformations, which were found to exhibit typical semiconductor properties.

It was experimentally established that organic thin-film samples with stable solid-state structure and reproducible electron transport properties (reversible temperature dependences of electric conductivity, Seebeck coefficient etc.) can be obtained if they are submitted to a heat treatment consisting of several successive heating and cooling cycles within a certain temperature interval, ΔT , characteristic to each compound (Table 3).

The above statement was confirmed by actual experiments. Analysis of temperature (T) dependence of d. c. electric conductivity (σ) for thin organic films with different thickness may provide valuable information on the processes taking place during the heat treatment (Danac, 2014; Leontie et al., 2005a; Rusu, 2001; Şunel et al., 1995).

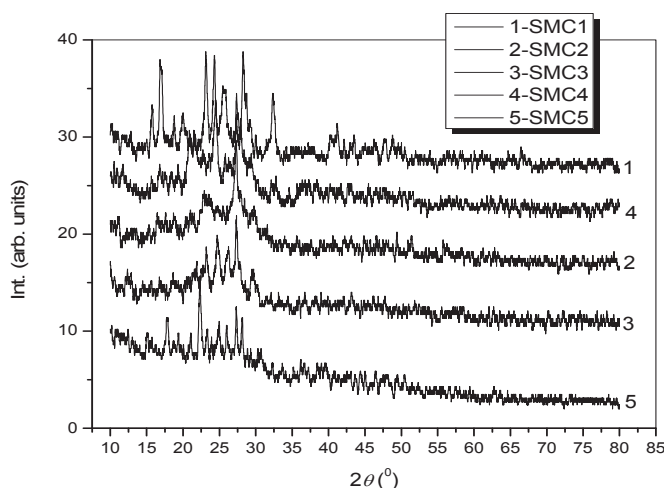


Fig. 3. XRD patterns of examined organic compounds

Table 2. Typical crystallite size values for SMC compounds

Compound	D (μm)	2θ ($^\circ$)	d_{hkl} (nm)	D (nm)
SMC1	0.39	16.85	0.0916	19.53
		23.12	0.0912	24.23
		24.31	0.1928	27.41
		28.26	0.0771	23.8
SMC2	0.44	27.32	0.0868	18.59
SMC3	0.48	23.2	0.0937	60.58
		24.7	0.3591	15.75
		26.25	0.1454	20.81
		27.35	0.0861	18.59
SMC4	0.40	24.45	0.2303	17.71
		27.36	0.0859	29.48
SMC5	0.46	17.79	0.1526	21.56
		22.33	0.0782	23.52
		24.97	0.94845	27.45
		25.99	0.1855	31.58
		27.31	0.0870	32.88
		28.12	0.0773	38.93

d -thin-film thickness; θ -Bragg angle; d_{hkl} -interplanar spacing for a family of atomic planes with (hkl) Miller indices; D -crystallite size

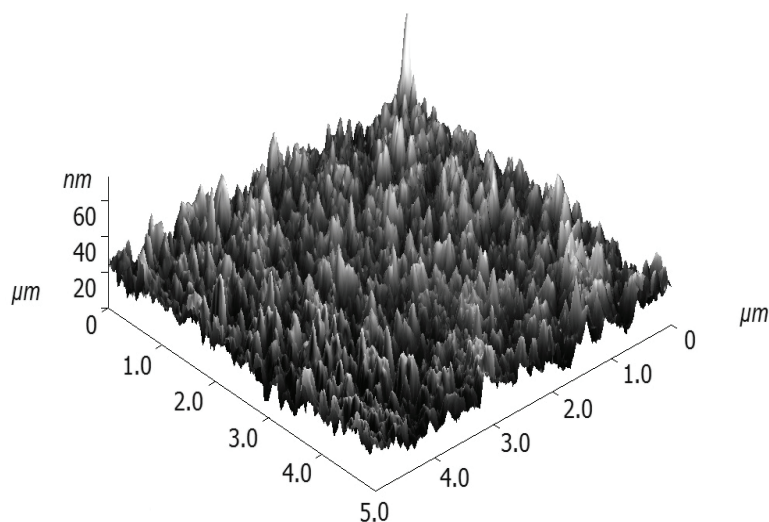


Fig. 4. Typical AFM image for thin-film organic samples: compound SMC4 (RMS=6.85 nm)

Actual experiments indicate that the shapes of the electric conductivity-temperature dependences are similar to those presented and discussed in (Danac, 2014; Leontie et al., 2005b; Leontie, 2011; Rusu, 2001; Şunel et al., 1995).

The electric conductivity of all examined samples was found to increase together with temperature over the whole range investigated. For a large number of organic compounds with similar molecular structures, we found that the well-known exponential law (Meier, 1974; Seeger, 1999) (Eq. 4), can suitably describe the experimental electric conductivity-temperature dependences, where E_a is the thermal activation energy of electric conduction, σ_0 denotes a characteristic parameter depending on the compound nature and k_B is the Boltzmann's constant.

$$\sigma = \sigma_0 \exp\left(-\frac{E_a}{k_B T}\right) \quad (4)$$

According to the band model representation, in the intrinsic conduction domain (for $T > T_c$, where T_c is a characteristic temperature, given in Table 3), the thermal activation energy is equal to half of the forbidden bandwidth of the material, E_g ($E_a = E_g/2$), which coincides with the energy difference between conduction band (CB) minimum and the valence band (VB) top. Besides, within the extrinsic conduction domain ($T < T_c$), it indicates the energy of donor levels measured with respect to the bottom of CB, or that of the acceptor levels with respect to the VB maximum, for n -type or p -type conduction, respectively (Gutman and Lyons, 1981; Kazmerski, 1980; Meier, 1974; Seeger, 1999).

According to Eq. (4), the experimental $\ln\sigma=f(10^3/T)$ plots must be linear, under the assumption of a temperature-independent preexponential factor. We supposed that for examined organic films an exponential temperature

dependence of d. c. electric conductivity, described by law (4), is also possible; consequently, we have examined the shape of $\ln\sigma=f(10^3/T)$ dependences during the heat treatment. The obtained curves, depending on the compound nature, thin-film sample thickness and preparation conditions for organic films, also display some similar trends for all investigated samples. Fig. 5 illustrates a typical experimental $\ln\sigma=f(10^3/T)$ dependence during the heat treatment for one of the organic compounds, subjected to three successive heating/cooling cycles. Some modifications in thin-film microstructure (grain size and shape, characteristics of intergrain boundaries, etc.) and purity (by removal of the adsorbed/absorbed gases, as well as of some accidental impurities) (Danac, 2012; Leontie, 2012; Rusu, 2007) may occur, especially, during the first heating run (Fig. 5).

Our experiments showed that after 2–3 series of successive heating/cooling cycles, the temperature dependences of electric conductivity become reversible. This behavior denotes stabilization of thin-film solid-state structure within the investigated temperature range (Danac, 2012; Rusu et al., 2001).

As can be ascertain from Figs. 4 and 5, the obtained $\ln\sigma=f(10^3/T)$ curves of heat-treated organic thin-film samples are typical for wide band gap semiconductors. They generally exhibit a portion with a smaller slope, within the lower temperature range ($T < T_c$), and a portion with a larger slope in the higher temperature domain ($T > T_c$). The two different slopes denote different activation energies and different conduction mechanisms operating in present organic films in indicated temperature ranges. In the lower temperature region, the organic films display a prevailing extrinsic conductivity. For this temperature range, the slope of the $\ln\sigma=f(10^3/T)$ curves corresponds to the energy of the donor levels, measured with respect to the CB minimum (since actual organic films exhibit a predominant n -type conduction). The values of the thermal activation

energy in the low temperature range (E_{a1}) lay between 0.09 and 0.14 eV (Table 3).

Several models have been proposed to explain the electric conduction mechanisms in organic semiconducting thin films. According to the crystallite boundary trapping theory (Baccarani et al., 1978 ; Leontie and Rusu, 2006), a high density of trap states occurs at the crystallite boundary, which favors capture of the free carriers. So created space charge causes a bending of the energy bands and occurring of potential barriers (usually rather low, under 0.1 eV). These barriers determine a decrease in electric conductivity of polycrystalline samples.

We consider that obtained values for the activation energy in the low temperature range (E_{a1}) are unusually high to use mentioned conduction models, based on grain barrier-limited electron transport. Besides, taking into account the structural features of actual samples, we consider that crystallite boundary trapping models are not applicable to actual organic films, instead the hopping conduction mechanism could be more appropriate for the lower temperature range.

In the higher temperature range, an intrinsic conduction mechanism operates in studied organic films. As our experiments revealed, the intrinsic conduction domain begins at a certain temperature, T_c (Table 3), which depends on the compound nature and organic thin-film thickness. During the heat treatment, T_c values were found shift to the lower temperature range; this behavior indicates a diminution of the impurity and structural defect density in organic films under study (Leontie et al., 2005a; Leontie et al., 2005b; Rusu, 2001).

The values of activation energy for the higher temperature range were found to depend on the compound nature.

As can be inferred from Fig. 5, the slopes of experimental $\ln\sigma=f(10^3/T)$ curves don't change during heat treatment within $T>T_c$ range. Besides, the shape of conductivity-temperature curves registered for a given compound, prepared with different solvents, exhibited certain changes in the lower temperature range, but not in the higher temperature domain. Also, for a series of organic compounds, E_a values, determined from the optical absorption spectra, were found to be close to values obtained from electric measurements (Rusu, 2007). These features confirm that in the respective temperature intervals an intrinsic conduction mechanism does operate. Consequently, we have determined the values of the thermal activation energy for the investigated organic thin films, from the slope of the experimental $\ln\sigma=f(10^3/T)$ curves, within the intrinsic conduction domain, according to Eq. (4) and listed them in Table 3 (E_{a2}). The experimental temperature dependences of electric conductivity (Figs. 5 and 6) suggest that in the higher temperature range ($T>T_c$), the band model representation could be applied for the study of electron transport mechanism in present organic thin-film samples.

Analysis of the d. c. electric conductivity data reveals that the organic compounds under study exhibit a typical *n*-type semiconductor-like behavior, which is determined by the thin-film structure (predominantly polycrystalline), as well as specific molecular configurations.

Table 3. Temperature dependence of the electric conductivity for SMC compounds

Compound	d (μm)	ΔT_1 (K)	E_{a1} (eV)	ΔT_2 (K)	ΔT (K)	T_c (K)	E_{a2} (eV)
SMC1	0.39	298–343	0.14	433–508	298–508	442	0.41
SMC2	0.44	298–353	0.10	423–493	298–493	433	0.41
SMC3	0.48	298–353	0.09	433–498	298–498	434	0.39
SMC4	0.40	298–343	0.12	363–498	298–498	432	0.36
SMC5	0.46	298–363	0.13	453–523	298–523	483	0.46

d -film thickness; ΔT_1 , ΔT_2 : temperature ranges for extrinsic and intrinsic conduction domains, respectively; E_{a1} , E_{a2} -thermal activation energies of electric conduction within temperature ranges ΔT_1 and ΔT_2 , respectively; ΔT -whole temperature range for the heat treatment; T_c -characteristic temperature (for $T>T_c$, conductivity of heat treated samples become intrinsic); E_{a2} -thermal activation energy of electric conduction after the heat treatment.

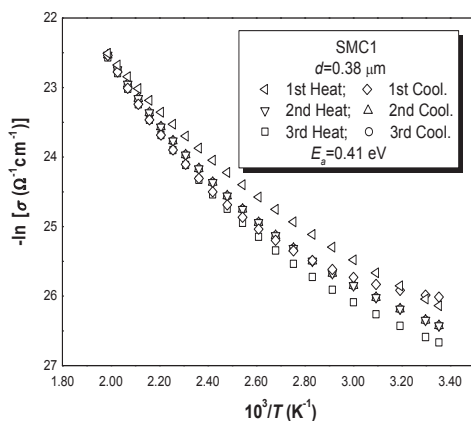


Fig. 5. Temperature dependence of electric conductivity during the heat treatment: compound SMC1

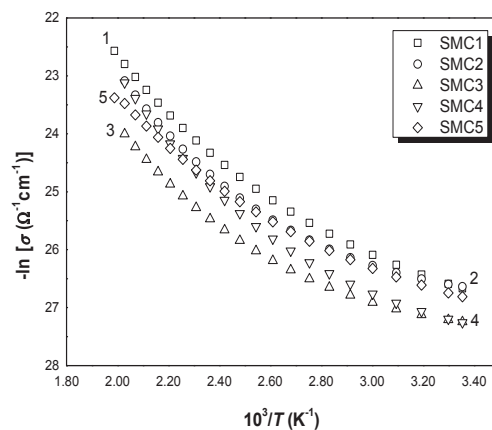


Fig. 6. Temperature dependence of electric conductivity for the heat-treated samples (SMC series)

The examined organic semiconductor materials exhibit extended conjugation systems, which facilitate the electron transfer and serve to the enhancement of the d. c. electric conduction at the intramolecular level. The degree of conjugation can be substantially influenced by the nature and position of the substituents (R) within the organic molecule (Danac, 2012, 2014; Leontie, 2012; Rusu, 2007), which affect the obtained values of the activation energy (E_{a2} , Table 3). These values were found to be smaller for extended conjugation systems.

On the other hand, intermolecular d. c. conduction processes, significantly influenced by intermolecular arrangement, need to be taken into consideration. The small-molecule polycrystalline organic semiconductors contain closed-shell molecular moieties, which are bound to each other by weak Van der Waals forces. The strong coupling between π -electrons of overlapping molecules in present compounds results in an enhanced carrier delocalization, which constitutes another important factor strongly affecting the electric conduction mechanism at the intermolecular level, in these materials. Therefore, molecular packing plays a key role in electron transport behavior of small-molecule organic compounds in polycrystalline thin films (Horowitz, 1998).

The registered differences between obtained thermal activation energies of five investigated compounds can be explained considering both their capacity to enable extended planar conjugation systems and the significant capability of compact packing in overlapping monomolecular layers.

The skeleton of the investigated compounds is the aromatic planar 4,7-phenanthroline heterocycle, possessing a strong and extended conjugation of its π -electrons. This main part of the molecule remains unchanged in the investigated compounds, thus the differences between the values of thermal activation energy of electrical conduction are small. Packing in overlapping molecular layers is enhanced in the case of compounds showing less voluminous phenyl substituents. Thus compound SMC4, having a small methyl group as substituent on the phenyl ring, shows the lowest value of the activation energy of electric conduction. Larger volume substituents may cause steric perturbation of their local environments, leading to a decreased packing capacity.

It is known that in the case of polycrystalline films, the electron transport properties of which are strongly influenced by inter-grain characteristics, determination of the energy band gap from absorption spectra is more appropriate (Harbeck, 1985; Greenaway, 1968). In the region of the fundamental absorption threshold, the absorption coefficient, α , depends on the energy of the incident photon, $h\nu$, according to the relation (5) (Pancove, 1979) where: $n=1/2$ and 2 for optical direct and indirect allowed transitions, respectively, E_{go} is the optical band gap, direct (E_{go}^d) or indirect, and A is a

characteristic parameter which is independent on the photon energy.

$$\alpha h\nu = A(h\nu - E_{go})^n \quad (5)$$

According to the above equation, low energy portions of $\alpha h\nu=f(h\nu)$ curves can be fitted to any of standard dependences, in particular $(\alpha h\nu)^2=f(h\nu)$ for allowed direct transitions. The analysis of actual experimental data (Fig. 7) shows that the best fitting is obtained for $(\alpha h\nu)^2=f(h\nu)$ dependences and consequently, these curves have been used for estimation of the optical band gap values, by extrapolating respective straight lines to $\alpha h\nu \rightarrow 0$. Obtained values are listed in Table 4.

The experimental data indicate that the examined compounds have direct band gaps (E_{go}^d) ranging between 3.82 and 4.33 eV. The obtained values (Table 4) are greater with respect to the $2E_a$ values (Table 3). This fact is due to the quite different nature of the carrier excitation in the respective processes (optical absorption and electric conduction). The values of E_{go}^d correspond to band-to-band transitions, whereas those of the E_a are determined by the electronic transport mechanism in present organic films (Leontie, 2011).

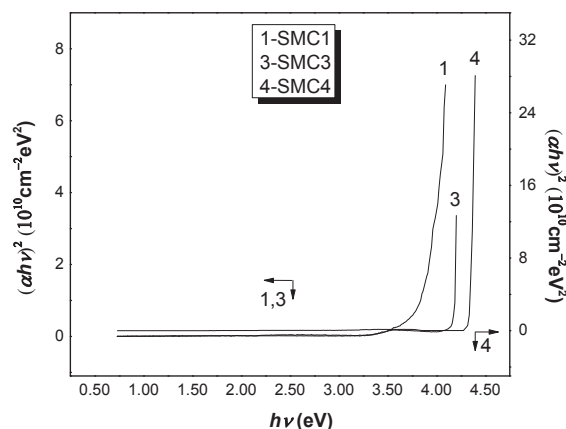


Fig. 7. Optical absorption of investigated organic films

We assumed that in the lower temperature range ($T < T_c$), the Mott's variable-range hopping (VRH) model (Mott and Davis, 1979; Mott et al., 1975; Pope and Swenberg, 1999; Shklovskii and Efros, 1984) may be used to adequately explain the temperature dependence of d. c. electric conductivity of the actual organic films. According to the VRH model, for three-dimensional systems, the conductivity-temperature dependence can be described by (Mott et al., 1975; Pope and Swenberg, 1999; Shklovskii and Efros, 1984) (Eqs. 6, 7).

$$\sigma = \sigma_0 \cdot \exp \left[- (T_0 / T)^{1/4} \right] \quad (6)$$

where:

$$\sigma_0 = e^2 R^2 \nu_0 N(E_F) \tag{7}$$

is a pre-exponential factor and R is the hopping distance, expressed as Eq. (8).

$$R^2 = [9 / 8\pi\alpha k_B N(E_F)]^{1/4} T^{1/2} \tag{8}$$

The parameter T_0 is a characteristic Mott temperature, characterizing the degree of disorder (Mott and Davis, 1979) (Eq. 9).

$$T_0 = \frac{\lambda\alpha^3}{k_B N(E_F)} \tag{9}$$

In the above relationships $N(E_F)$ represents the density of the localized states at the Fermi level E_F , α^{-1} ($\alpha=10^7 \text{ cm}^{-1}$) is the coefficient of exponential decay for a localized state wave function near Fermi level, λ denotes a dimensionless constant [of about 18 (Rusu et al., 2007)], ν_0 is the typical phonon frequency, e is electron charge, and k_B is the Boltzmann's constant. The parameter σ_0 can be expressed in the form of Eq. (10). (Mott et al., 1975).

$$\sigma_0 = \sigma^* T^{-1/2} \tag{10}$$

σ^* is a new pre-exponential factor and Eq. (6) may be written as Eq. (11), where σ^* and T_0 represent the Mott's characteristic parameters.

$$\sigma = \sigma^* T^{-1/2} \cdot \exp\left[-(T_0 / T)^{1/4}\right] \tag{11}$$

Assuming that σ_0 is not depending on temperature, in virtue of Eq. (6) the $\ln(\sigma T^{1/2})=f(T^{-1/4})$ curves have to be linear. For the organic compounds under study, these dependences, in the lower temperature range, $298 \text{ K} < T < T_c$, are presented in Fig. 8. As can be observed from the last figure, the obtained experimental dependences are linear, which indicates the validity of the VRH model in adequate explaining the temperature dependence of d. c. electric conductivity of actual organic compounds in thin films, in the lower temperature range.

By using data from Fig. 8 in Eq (11), the values of the Mott's parameters σ^* and T_0 have been calculated and listed in Table 5. We also checked suitability of investigated compounds for potential thermistor applications.

The working of a thermistor is essentially based on the temperature dependence of the electric resistance of a semiconductor material, within the intrinsic conduction regime, that can be described by Eq. (12), where R_T is the electric resistance at temperature T , R_∞ represents a parameter depending on the compound nature, and B characterizes the temperature sensitivity of the thermistor.

$$R_T = R_\infty \cdot \exp\left(\frac{B}{T}\right) \tag{12}$$

The temperature coefficient of the resistance, defined by Eq. (13)

$$\alpha_T = \frac{1}{R} \frac{dR}{dT} \tag{13}$$

can be expressed as a function of temperature, by means of Eq. (12) (Eq. 14).

$$\alpha_T = -\frac{B}{T^2} \tag{14}$$

The obtained values of the characteristic parameters α_T (at temperature $T=473 \text{ K}$) and B are listen in Table 6 for the examined organic films. It can be concluded that some of the compounds under study can be recommended for use as thermistor materials.

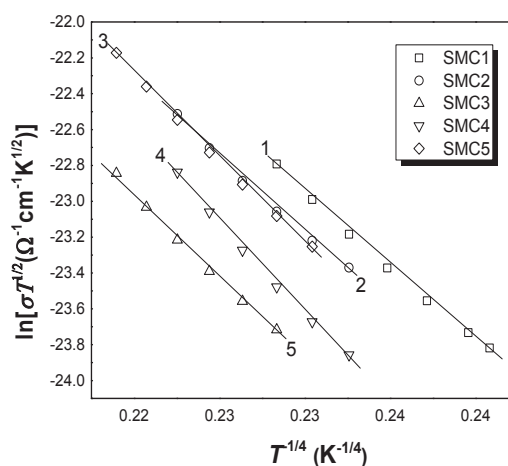


Fig. 8. Mott's variable-range hopping (VRH) conduction (lower temperature range, $298 \text{ K} < T < T_c$) in the heat-treated samples

Table 4. Typical results of optical measurements

Sample	d (nm)	E_{go}^d (eV)
SMC1	389	3.82
SMC3	478	4.18
SMC4	403	4.33

E_{go}^d -direct optical energy band gap

Table 5. Mott parameters, σ^* and T_0 , for five samples under study

Compound	d (μm)	ΔT (K)	T_0 (K)	σ^* ($\Omega^{-1}\text{cm}^{-1}\cdot\text{K}^{1/2}$) (at 353 K)
SMC1	0.38	298–353	1.10×10^8	2.27×10^0
SMC2	0.44	333–383	1.28×10^8	4.61×10^0
SMC3	0.47	353–403	1.82×10^8	2.17×10^1
SMC4	0.40	333–383	2.57×10^8	3.14×10^2
SMC5	0.45	343–403	1.92×10^8	6.03×10^1

ΔT -low temperature investigated temperature range

Table 6. Characteristic thermistor parameters of investigated compounds

Compound	D (μm)	$-\alpha$ (K^{-1}) ^a	B (K)
SMC1	0.38	0.013	2970
SMC2	0.44	0.011	2640
SMC3	0.47	0.010	2410
SMC4	0.40	0.013	3080
SMC5	0.45	0.012	2750

^a For $T=473$ K

4. Conclusions

The recently synthesized organic compounds, 4,7-phenanthroline-4-ium salts (SMC compounds) in thin films, behave as typical n -type polycrystalline semiconductors.

The electron transfer in the investigated compounds is strongly influenced by their specific molecular structures, enabling formation of extended conjugation systems, as well as their packing capacity.

In the higher temperature range ($T > T_c$), the d. c. electric conductivity of examined compounds can be described in terms of the band gap representation model. In the lower temperature domain ($298 \text{ K} < T < T_c$) the Mott's variable-range hopping model can be conveniently used.

Acknowledgements

This work was supported by the ANCS (National Authority for Scientific Research), Ministry of Economy, Trade and Business Environment, through the National Program Capacities, Project No. 257/28.09.2010 (Acronym CERNESIM), European Social Fund, Sectorial Operational Program Human Resources Development 2007–2013, through the strategic grant POSDRU/159/1.5/S/137750, project "Doctoral and Postdoctoral programs support for increased competitiveness in Exact Science research".

References

- Baccarani G., Riccò B., Spandini G.J., (1978), Transport properties of polycrystalline silicon films, *Journal of Applied Physics*, **49**, 5565-5570.
- Bernards D.A., Owens R.M., Malliaras G.G., (2008), *Organic Semiconductors in Sensor Applications* (Springer Series in Material Science), Springer-Verlag, Berlin-Heidelberg.
- Căplănuș I., (1999-2000), On the electrical properties of some purified enzymes in thin films, *Scientific Annals of Al. I. Cuza University of Iasi (Physics)*, **XLV-XLVI**, 224–228.

- Coropceanu V., Cornil J., da Silva Filho D. A., Olivier Y., Silbey R., Brédas J.-L., (2007), Charge transport in organic semiconductors, *Chemistry Review*, **107**, 926-952.
- Cullity B.D., Stock R.S., (2001), *Elements of X-Ray Diffraction*, 3rd Edition, Prentice Hall, New Jersey.
- Danac R., Leontie L., Carlescu A., Rusu G.I., (2012), DC electric conduction mechanism of some newly synthesized indolizine derivatives in thin films, *Materials Chemistry and Physics*, **134**, 1042-1048.
- Danac R., Leontie L., Girtan M., Preliceanu M., Graur A., Carlescu A., Rusu G. I., (2014), On the direct current electric conductivity and conduction mechanism of some stable disubstituted 4-(4-pyridyl)pyridiniumylides in thin films, *Thin Solid Films*, **556**, 216-222.
- Deleonibus S., (2009), *Electronic Device Architectures for the Nano-CMOS Era: From Ultimate CMOS Scaling to Beyond CMOS Devices*, Pan Stanford Publishing, Singapore.
- Facchetti A., Marks T.J., (2010), *Transparent Electronics: From Synthesis to Applications*, Wiley, Chichester.
- Fraxedas J., (2006), *Molecular Organic Materials. From Molecules to Crystalline Solids*, Cambridge University Press, Cambridge-New York-Melbourne-Madrid-Cape Town-Singapore-São Paulo.
- Greenaway D. L., Harbeke G., (1968), *Optical Properties and Band Structure of Semiconductors*, Pergamon, Oxford.
- Gutman F., Lyons L.E., (1981), *Organic Semiconductors, Part A*, Robert E. Publishing, Malabar, FL.
- Harbeke G., (1985), *Polycrystalline Semiconductors: Physical Properties and Applications*, Springer, Berlin.
- Horowitz G., (1998), Organic field-effect transistors, *Advanced Materials*, **10**, 365-377.
- Huang Y., Tian Y., Cheng W., (2014), Optimization of energy saving for wireless sensor networks, *Environmental Engineering and Management Journal*, **13**, 1057-1070.
- Iniewski K., (2011), *Nanoelectronics-Nanowires, Molecular Electronics, and Nanodevices*, McGraw Hill, New York.
- Karl N., (2003), Charge carrier transport in organic semiconductors, *Synthetic Metals* **133-134**, 649-657.

- Kazheva O.N., Kushch N.D., Aleksandrov G.G., Dyachenko O.A., (2002), Crystal structure and molecular packing in a new organic semiconductor-penta[bis(ethylenedithio)tetrathiafulvalene]-hexathiocyanatomononitratoyttrium(III)-ethanol, *Materials Chemistry and Physics*, **73**, 193-197.
- Kazmerski L.L., (1980), *Polycrystalline and Amorphous Thin Films and Devices*, Academic, New York.
- Kymissis I., (2009), *Organic Field Effect Transistors: Theory, Fabrication and Characterization*, Springer-Verlag, New York.
- Lebed A.G., (2008), *The Physics of Organic Superconductors and Conductors*, Springer Series in Materials Science, Vol. 110, Springer-Verlag, Berlin-Heidelberg-New York.
- Leontie L., Druta I., Alupoae R., Rusu G. I., (2003a), On the electronic transport in some new synthesized high resistivity organic semiconductors in thin films, *Materials Science and Engineering B*, **100**, 252-258.
- Leontie L., Roman M., Brinza F., Podaru C., Rusu G. I., (2003b), Electrical and optical properties of some new synthesized ylides in thin films, *Synthetic Metals*, **138**, 157-163.
- Leontie L., Druta I., Danac R., Prelipceanu M., Rusu G.I., (2005a), Electrical properties of some new high resistivity organic semiconductors in thin films, *Progress in Organic Coatings*, **54**, 175-181.
- Leontie L., Druta I., Danac R., Rusu G.I., (2005b), On the electronic transport properties of pyrrolo[1,2-a][1,10]phenanthroline derivatives in thin films, *Synthetic Metals*, **155**, 138-145.
- Leontie L., Danac R., (2006), Optical properties of some new synthesized organic semiconductors in thin films, *Scripta Materialia*, **54**, 175-179.
- Leontie L., Rusu G. I., (2006), On the electronic transport properties of bismuth oxide thin films, *Journal of Non-Crystalline Solids*, **352**, 1475-1478.
- Leontie L., Druta I., Danac R., (2006), Electrical conduction mechanism in N-(p-R-phenacyl)-4,5-diazafluorenum-9-one bromides thin films, *Synthetic Metals*, **156**, 224-229.
- Leontie L., Druta I., Furdul B., Rusu G. I., (2007), On the mechanism of electrical conduction in some new quaternary salts of bipyridine and indolizine pyridine in thin films, *Progress in Organic Coatings*, **58**, 303-311.
- Leontie L., Druta I., Rotaru Al., Apetroaei N., Rusu G. I., (2009), Electronic transport properties of some new monoquaternary salts of 4,4'-bipyridine in thin films, *Synthetic Metals*, **159**, 642-648.
- Leontie L., Danac R., Druta v., Carlescu A., Rusu G.I., (2010), Newly synthesized fused heterocyclic compounds in thin films with semiconductor properties, *Synthetic Metals*, **160**, 1273-1279.
- Leontie L., Danac R., Apetroaei N., Rusu G.I., (2011), Study of electronic transport properties of some new N-(p-R-phenacyl)-1,7-phenanthroline bromides in thin films, *Materials Chemistry and Physics*, **127**, 471-478.
- Leontie L., Danac R., Girtan M., Carlescu A., Rambu A. P., Rusu G. I., (2012), Electron transport properties of some new 4-tert-butylcalix[4]arene derivatives in thin films, *Materials Chemistry and Physics*, **135**, 123-129.
- Logothetidis S., (2012), *Nanostructured Materials and Their Applications*, Springer-Verlag, Berlin, Heidelberg.
- Meier H., (1974), *Organic Semiconductors*, Verlag Chemie, Weinheim.
- Metzger R.M., (2012), *Unimolecular and Supramolecular Electronics I: Chemistry and Physics Meet at Metal-Molecule Interfaces*, Springer, Heidelberg-Dordrecht-London-New York.
- Moss T.S., Balkanski M., (1994), *Handbook on Semiconductors, Optical Properties of Semiconductors*, North-Holland, Elsevier, Amsterdam.
- Mott N.F., Davis E.A., Street R.A., (1975), States in the gap and recombination in amorphous semiconductors, *Philosophia Magna*, **32**, 961-996.
- Mott N.F., Davis E.A., (1979), *Electron Processes in Non-Crystalline Materials*, Clarendon, Oxford.
- Ohtsu M., (2004), *Progress in Nano-electro Optics III*, Springer-Verlag, Berlin-Heidelberg.
- Pancove J., (1979), *Optical Processes in Semiconductors*, Prentice-Hall, Englewood Cliffs, NJ.
- Paraschiv L.S., Paraschiv S., Ion I.V., (2014), Experimental and theoretical analyses on thermal performance of a solar air collector, *Environmental Engineering and Management Journal*, **13**, 1965-1970.
- Pecharsky V.K., Zavalij P.Y., (2009), *Fundamentals of Powder Diffraction and Structural Characterization of Materials*, 2nd Edition, Springer, New York.
- Pope M., Swenberg C.E., (1999), *Electronic Processes in Organic Crystals and Polymers*, 2nd Edition, Oxford University Press, New York-Oxford.
- Prelipceanu M., Prelipceanu O.S., Leontie L., Danac R., (2007), Photoelectron spectroscopy investigations of pyrrolo[1,2-a][1,10]phenanthroline derivatives, *Physics Letters A*, **368**, 331-335.
- Rusu G.I., Căplănuș I., Leontie L., Airinei A., Butuc E., Mardare D., Rusu I.I., (2001), Studies on the electronic transport properties of some aromatic polysulfones in thin films, *Acta Materialia*, **49**, 553-559.
- Rusu G.I., Airinei A., Rusu M., Prepeliță P., Marin L., Cozan V., Rusu I.I., (2007), On the electronic transport mechanism in thin films of some new poly(azomethine sulfone)s, *Acta Materialia*, **55**, 433-442.
- Schols S., (2011), *Device Architecture and Materials for Organic Light-Emitting Devices: Targeting High Current Densities and Control of the Triplet Concentration*, Springer-Verlag, Dordrecht-Heidelberg-London-New York.
- Seeger K., (1999), *Semiconductor Physics*, Springer-Verlag, Berlin-Heidelberg-New York.
- Shklovskii B. I., Efros A. L., (1984), *Electronic Properties of Doped Semiconductors*, Springer-Verlag, Berlin.
- Smith R., (1980), *Semiconductors*, Cambridge University Press, London.
- Stallinga P., (2009), *Electrical Characterization of Organic Electronic Materials and Devices*, Wiley, Chichester.
- Sun S.-S., Saracftci N.S., (2005), *Organic Photovoltaics: Mechanisms, Materials, and Devices*, CRC Press, Taylor & Francis, Boca Raton-London-New York-Singapore.
- Szodrai F., Lakatos Á., (2014), Measurements of the thermal conductivities of some commonly used insulating materials after wetting, *Environmental Engineering and Management Journal*, **13**, 2881-2886.
- Şunel V., Rusu G. I., Rusu G. G., Leontie L., Şoldea L. C., (1995), Electrical characteristics of some derivatives of p-aminobenzoic acid in thin films, *Progress in Organic Coatings*, **26**, 53-61.
- Turbiez M., Frere P., Allain M., Videlot C., Ackermann J., Roncali J., (2005), Design of organic semiconductors:

tuning the electronic properties of π -conjugated oligothiophenes with the 3,4-ethylenedioxythiophene (EDOT) building block, *Chemistry-A European Journal*, **11**, 3742-3752.

Ueno N., Kera S., (2008), Electron spectroscopy of functional organic thin films: Deep insights into valence electronic structure in relation to charge transport property, *Progress in Surface Science*, **83**, 490-557.



“Gheorghe Asachi” Technical University of Iasi, Romania



DISTRIBUTION OF OXYGEN TRANSFER RATES IN STIRRED BIOREACTOR FOR DIFFERENT FERMENTATION BROTHS - OXYGEN-VECTOR DISPERSIONS

Anca-Irina Galaction¹, Alexandra Cristina Blaga², Corina Paraschiva Ciobanu²,
Marius Turnea¹, Dan Cașcaval^{2*}

¹“Grigore T. Popa” University of Medicine and Pharmacy of Iasi, Faculty of Medical Bioengineering,
Department of Biomedical Science, 9-13 M. Kogalniceanu Str., 700454 Iasi, Romania

²“Gheorghe Asachi” Technical University of Iasi, Faculty of Chemical Engineering and Environmental Protection,
Department of Organic, Biochemical and Food Engineering, 73 Prof. Dr. docent Dimitrie Mangeron Str., 700050 Iasi, Romania

Abstract

The oxygen transfer into the fermentation broths could be improved in presence of oxygen-vectors, without intensification of mixing or aeration. The experimental results for simulated, *P. shermanii* and *S. cerevisiae* broths indicated the significant increase of k_La , by adding *n*-dodecane, but the magnitude of this effect depends especially on the cells affinity for hydrocarbon droplets. Therefore, due to the higher affinity of yeasts cells for hydrocarbon droplets during their entire growth cycle, the increase of oxygen mass transfer rate was lower and the influence of specific power input was different than those recorded for simulated or bacterial broths. By means of the experimental data, mathematical correlations describing the influences of the main parameters on k_La have been proposed for each studied fermentation systems at different positions on the broths height, with an average deviations varying between $\pm 6.72\%$ and $\pm 6.93\%$.

Key words: bioreactor, *n*-dodecane, oxygen transfer, oxygen-vector

Received: November, 2014; *Revised final:* February, 2015; *Accepted:* February, 2015

1. Introduction

The oxygen supply into the broths constitutes one of the decisive factors of aerobic microorganisms' cultures, playing an important role in the scale-up and economy of large-scale fermentation systems. The aeration efficiency depends on the bioreactor capacity to generate high rate of oxygen diffusion from air to the broths, as well as of its transfer through the liquid phase to the microorganisms. Therefore, one of the priorities in designing and operating the aerobic bioreactor is to ensure the optimum oxygen transfer from the gaseous phase to the microbial cells (Dumont et al., 2006).

The biosynthesis processes of single-cell protein on various water insoluble hydrocarbon

substrates indicated that the addition of the nonaqueous organic phase may induce significant increase of oxygen transfer rate from air to microorganisms, without needing a supplementary intensification of mixing (Cașcaval et al., 2006; Clarke and Correia 2008; Dumont et al., 2006; Rols et al., 1990). Thus, the compounds which added to fermentation media improve the oxygen transfer towards the microorganisms have been defined as the oxygen-vectors (Cașcaval et al., 2006; Rols et al., 1990). The oxygen solubility in these compounds is for several times higher than in water, the main oxygen-vectors tested in biotechnology being hydrocarbons, perfluorocarbons, and oils used as antifoam agents (Cașcaval et al., 2006; Clarke et al., 2006; Clarke and Correia, 2008; Da Silva et al.,

* Author to whom all correspondence should be addressed: e-mail: dancasca@tuiasi.ro; dancasca@yahoo.com

2008; Dumont et al., 2006; Gomez et al., 2006; Lee et al., 2005; Li et al., 2012; Pilarek and Szewczyk, 2008; Rols et al., 1990; Xu et al., 2007). Oxygen-vectors exhibit no toxicity against the cultivated microorganisms, and could be used as supplementary sources of carbon and energy.

The addition of oxygen-vectors induces the appearance of four phases in the bioreactor: the gas phase (air), the aqueous phase, the liquid organic phase, and the solid phase (biomass), as well as the formation of new interfacial areas between the gas and liquid phases (Clarke and Correia, 2008; Li et al., 2012). In these systems, the oxygen transfer could occur directly to the microbial cells, or through oxygen-vectors adsorbed or not to the bubble surface (Caçcaval et al., 2006; Clarke and Correia, 2008; Rols et al., 1990). Moreover, the cells could be adsorbed to bubbles surface or to organic phase droplets. Among the possible mechanisms of oxygen transfer proposed in literature, the most plausible assumes that the hydrocarbon is adsorbed to bubbles surface, with or without formation of a continuous film, the oxygen diffusion from the gaseous phase to microorganisms occurring through oxygen-vector and then through aqueous phase or directly to the cells adsorbed to hydrocarbon droplets or film surface (Caçcaval et al., 2006; Clarke and Correia, 2008; Da Silva et al., 2008; Dumont et al., 2006; Li et al., 2012; Rols et al., 1990). Because the previous results indicated that the main resistance to oxygen transfer is due to the diffusion through aqueous boundary layer from hydrocarbon - aqueous phase interface, the oxygen mass transfer coefficient corresponding to aqueous film, $k_L a$, can also be used to describe the oxygen transfer in these systems (Caçcaval et al., 2006; Clarke and Correia, 2008; Galaction et al., 2005). This diffusional resistance can be counteracted both by increasing the interfacial area of oxygen transfer, especially by organic phase droplets adsorption to the bubble surface, and by accumulation of oxygen in organic phase, which acts as an oxygen reservoir (Caçcaval et al., 2006; Clarke et al., 2006; Dumont et al., 2006; Galaction et al., 2005; Rols et al., 1990).

Although the literature offers numerous correlations for $k_L a$, there are still many queries concerning the accuracy of $k_L a$ predictions, owing to the strong influence of bioreactor geometry and operating variable range for which the proposed models are adequate, as well as to the experimental methods used for $k_L a$ determination (Montes et al., 1999; Van't Riet and Tramper, 1991). Moreover, the applicability of these correlations is limited to certain microorganisms' cultures only, quantifying the system behavior for a given region without indicating the distribution of oxygen transfer rate in the whole bulk volume of the broth. These limitations become more important in the case of aerobic fermentation systems containing oxygen-vectors.

The literature underlined the possibility to characterize the performances of stirred bioreactors by means of the computation fluid dynamics method

(CFD), which has been previously applied for analyzing the distribution of the flow streams and velocity, gas hold-up, air bubble size, interfacial area, bubble coalescence or formation, and oxygen transfer rate in stirred vessels (Hjertager, 1998; Kerdouss et al., 2006; Kerdouss et al., 2008). However, although the oxygen transfer is directly related to the processes analyzed and modeled by CFD or other techniques, there is no information concerning the distribution of oxygen transfer rate inside the polyphasic media containing oxygen-vectors for stirred bioreactors with multiple impellers.

For this reason, the aim of these experiments is to analyze the distribution of the oxygen transfer rate in broths - oxygen-vector dispersions, for a stirred bioreactor and different fermentation broths without biomass (simulated broths) and with microorganisms (bacteria, *Propionibacterium shermanii*, and yeasts, *Saccharomyces cerevisiae*), using a large domain of operating variables. *n*-Dodecane has been used as oxygen-vector. For quantifying the effects of the considered factors (apparent viscosity, biomass concentration, affinity of different microorganisms for the hydrocarbon phase, concentration of *n*-dodecane, specific power input, and superficial air velocity) on $k_L a$ value and distribution on broth height, some mathematical correlations have been established for each considered position inside the bioreactor. The proposed equations could be useful for mass transfer optimization or scaling-up in fermentation systems containing hydrocarbons as oxygen-vectors.

2. Experimental

The experiments were carried out in 5 L (4 L working volume, ellipsoidal bottom) laboratory bioreactor (Biostat A, B. Braun Biotech International), with computer-controlled and recorded parameters. The bioreactor and impeller characteristics have been presented in the previous papers (Caçcaval et al., 2006).

The bioreactor mixing system consists of two Rushton turbine impellers and three baffles. The impeller diameter was of 64 mm. The inferior stirrer was placed at 64 mm from the bioreactor bottom. The superior stirrer was placed on the shaft at the optimum distance from the inferior one according to the type of the studied broth, namely at 128 mm for the simulated broths, respectively at 64 mm for the bacterial and yeasts broths, as it was demonstrated in the previous works (Caçcaval et al., 2007). The rotation speed was maintained below 600 rpm, this level of rotation speed avoiding the cavity formation at the broths surface.

The sparging system consists of a single ring sparger with 64 mm diameter, placed at 15 mm from the vessel bottom, having 14 holes with 1 mm diameter. The air volumetric flow rate was varied from 75 to 450 L h⁻¹, corresponding to the superficial air velocity of 0.84 - 5x10⁻³ m s⁻¹.

In the experiments, simulated and real broths have been used. The simulated broths were carboxymethylcellulose sodium salt solutions with pseudoplastic behavior and apparent viscosity in the domain of 10 - 96 cP. The following real broths have been studied:

- bacteria (*P. shermanii*), C_X being of 30.5 - 120.5 g d.w. l^{-1} , and apparent viscosity of 1.8 - 5.7 cP
- yeasts (*S. cerevisiae*), C_X being of 30 - 110 g d.w. l^{-1} , and apparent viscosity of 2.2 - 7.8 cP.

Owing to the difficulty of *in-situ* measurement of viscosity during the experiments, the viscosity was measured before and after each experiment using a rotary viscometer of Haake Viscometer 6 Plus type. Both the experiments and viscosity measurements were carried out at a temperature of 30°C. Any viscosity or morphology change was recorded during the experiments. *n*-Dodecane (SIGMA Chemie GmbH) was used as oxygen-vector (oxygen solubility 54.9 10^{-3} g L^{-1} at 35°C and atmospheric air pressure (Rols et al., 1990). Its maximum volumetric fraction into the broth was 0.20.

For k_La values determination the static method has been used (Caçaval et al., 2006; Montes et al., 1999; Van't Riet and Tramper, 1991). This method has the advantages that it can be applied for different media (for establishing the effect of media components on oxygen mass transfer) and does not involve chemical reactions that could affect the measurement accuracy. According to this method, the values of k_La were calculated from the slopes of the straight lines plotted by means of the dependence

$$\ln \frac{C_1^*}{C_1^* - C_1} \text{ vs. time (Van't Riet and Tramper, 1991).}$$

The solved oxygen concentrations in broth were measured using an oxygen electrode of InPro 6000 Series type (Mettler Toledo). As it was underlined in literature, because the k_La values were in all cases less than 0.1 s^{-1} , it was assumed that the response of the oxygen electrode to the change in the oxygen concentration is sufficiently fast and does not affect the determination accuracy (Montes et al., 1999; Ozbek and Gayik, 2001).

Because the static method is adequate for non-respiring systems only, the respiratory activity of microorganisms was inhibited by suspending the biomass in a solution of 0.2% pyrogalllic acid and 0.4% potassium hydroxide for about 20 min. Then, the biomass was filtered, washed with distilled water and used for the above mentioned suspensions preparation (Caçaval et al., 2006).

For analyzing the distribution of oxygen transfer rate inside the broth, the oxygen electrode was introduced at four different positions, placed vertically from bioreactor bottom as follows:

- position 1: at 20 mm
- position 2: at 70 mm
- position 3: at 120 mm
- position 4: at 170 mm.

The variations of dissolved oxygen concentration were recorded by the bioreactor computer-recorded system and were analyzed for calculating k_La . The mathematical correlations, which describe the influences of considered factors on k_La for the four positions inside the broths, were developed using MATLAB software. For the experimental data, a multiregression analysis was performed, the difference between the experimental and modeled value being reduced to the minimum by least-square fit method. By means of the MATLAB program, the regression coefficients and standard deviations were calculated.

Each experiment has been carried out for three times, for identical conditions, the average value of k_La being considered. The maximum experimental errors have varied between 3.72 and 5.91%.

3. Results and discussion

The increase of broths viscosity, mainly as the result of the biomass accumulation, reduces significantly the rate of oxygen mass transfer, due to the reduction of turbulence in the system. Moreover, the microbial cells exhibit significant effect on oxygen mass transfer, the biomass influence being the results of (Galaction et al., 2004; Ozbek and Gayik, 2001):

- modification of rheological characteristics of broths during fermentation process, especially by increasing of the apparent viscosity, effect that is less pronounced for bacterial cultures; besides the reduction of turbulence, the increase of viscosity leads to the perturbation of bubbles dispersion-coalescence equilibrium

- obstruction of mass transfer, due to both of the reduction of oxygen solubility and to the barrier effect created by cells adsorption to the air bubbles surface; however, the adsorbed solid particles can promote the surface renewal or direct consumption of oxygen with favorable effect on oxygen transfer rate.

The previous works indicated that the addition of hydrocarbons could increase the concentration of solved oxygen into the broths (Caçaval et al., 2006; Clarke and Correia, 2008; Da Silva et al., 2008; Dumont et al., 2006; Rols et al., 1990). The effect of oxygen-vectors has to be related to the broths characteristics, especially due to the above presented effect of biomass presence and accumulation on oxygen transfer. Furthermore, as the result of the different affinity of cells for hydrocarbon droplets, the cells could be absorbed to hydrocarbons droplets surface and the formed cells-droplets associations could be furthermore adsorbed to air bubbles surface. The formation and stability of the cells-droplets-air bubbles associations depends on biomass characteristics, especially cells affinity for hydrocarbon phase, mixing intensity, hydrocarbons droplets size, and tensides presence in broth (Caçaval et al., 2006; Clarke et al., 2006; Clarke and Correia, 2008; Dumont et al., 2006). Although in these systems the oxygen could be directly consumed

from air bubbles by microorganisms included in these associations, the barrier effect could become dominant, its relative importance depending on microorganisms' type and morphology.

Also in the fermentation systems containing hydrocarbons as oxygen-vectors, the bubbles dispersion-coalescence equilibrium is supplementary affected by the cells presence, which could amplify or hinder the coalescence process, depending on their concentration and morphological conformation (Li et al., 2012). Therefore, the appearance of small bubbles is promoted, this leading to the increase of the interfacial area for oxygen mass transfer. However, owing to the high retention time of these small bubbles into the broth, the oxygen concentration gradient between the gaseous and aqueous phases, or between the gaseous and hydrocarbon phases, and, implicitly, the oxygen mass flow are reduced (Galaction et al., 2004; Montes et al., 1999; Ozbek and Gayik, 2001). These phenomena induce the heterogeneous distribution of air bubbles, of gas-liquid interfacial area and, implicitly, of oxygen transfer rate inside the broths.

For these reasons, the use of a single mathematical model or of an average value for $k_L a$ corresponding to a given aerobic fermentation system does not offer the required accuracy for quantifying the effects of oxygen-vectors for operating the bioreactor at optimum conditions. Consequently, by means of the experimental data, it is necessary to plot "the map" of the distribution of oxygen transfer rate inside the microbial broths containing hydrocarbons.

4.1. Simulated broths

Although the shapes of the recorded curves are similar, Fig. 1 indicates different correlations between $k_L a$ and n -dodecane concentration depending on the broth apparent viscosity, specific power input, and position inside the bioreactor.

Therefore, regardless of the value of apparent viscosity of simulated broths, $k_L a$ is increased by increasing the volumetric fraction of oxygen-vector, but this effect has to be correlated with the viscosity of broths. At low apparent viscosity, 15 cP, two domains of $k_L a$ variation can be observed from Fig. 1.

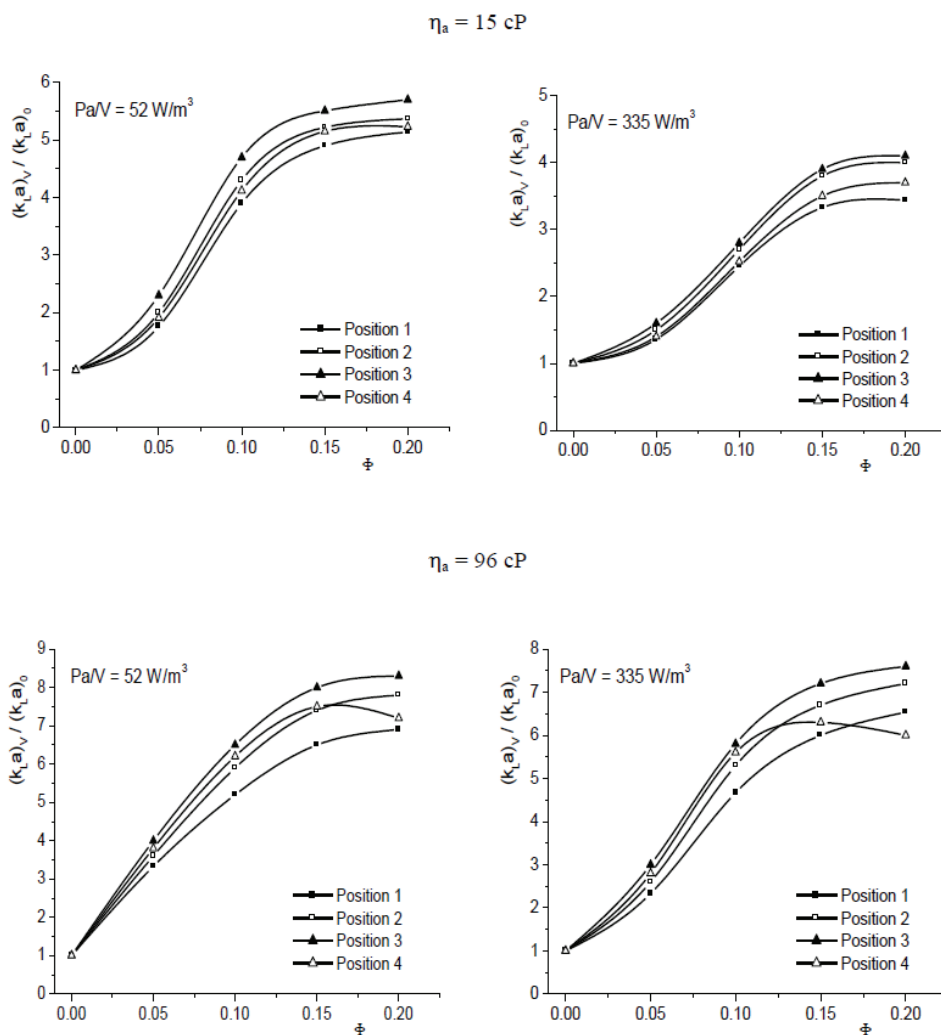


Fig. 1. Influence of n -dodecane concentration on oxygen mass transfer coefficient for different apparent viscosities of simulated broths and specific power inputs ($v_s = 8.4 \times 10^{-4} \text{ m s}^{-1}$)

For oxygen-vector concentration up to $\Phi = 0.1$ and the closest positions to the two impellers, corresponding to the bottom and top of the simulated broths, $k_L a$ initially increases with the increase of oxygen-vector concentration, reaching then a rather constant value. This dependence between the oxygen transfer rate and *n*-dodecane concentration is similar to those recorded for the intermediary positions of the oxygen electrode, but the value of volumetric fraction of oxygen-vector related to the constant level of $k_L a$ decreases from 0.15 to 0.10 by intensifying the mixing. For all considered positions inside the bioreactor, the analyzed variations are the consequence of the important influence of air - *n*-dodecane and *n*-dodecane - aqueous phase interfacial areas on oxygen transfer rate. The average size of hydrocarbon droplets is reduced by mixing intensification and, implicitly, the interfacial areas are strongly increased. Furthermore, the small droplets of hydrocarbon can be assimilated as rigid spheres which interact with the aqueous film surrounding the bubbles, amplifying the turbulence in this region and increasing supplementary the oxygen diffusion rate (Caçcaval et al., 2006; Clarke et al., 2006). The magnitude of these phenomena becomes more important in the regions with the highest turbulence, namely at the positions 1 and 4.

For more viscous broths, $k_L a$ increases continuously for the entire variation domain of *n*-dodecane concentration. Moreover, at higher specific power input and *n*-dodecane volumetric fraction over 0.05, the values of oxygen transfer rate recorded for position 2 exceeds those corresponding to position 4. This variation could be the result of the modification of the viscous broth flow, implicitly of the turbulence extent, in presence of air bubbles and hydrocarbon droplets in the region with intense mixing. Thus, at low rotation speed, the contribution of pneumatic mixing to the circulation of dispersion is important, the increase of rotation speed intensifying supplementary the broth agitation into the bioreactor. At higher rotation speed, the bubbles retention time increases, the gas-liquid dispersion or the two liquid phases flow becomes more complex and its circulation velocity is lower than that of the flow streams promoted by mechanical mixing in non-aerated media or in the regions placed between the impellers. Moreover, the retention of air diminishes the oxygen concentration gradient between the gaseous and liquid phases, this phenomenon affecting additionally the mass transfer.

The decisive influence of media hydrodynamics on oxygen transfer rate is underlined by the results obtained previously for the mixing time distribution into fermentation broths (Caçcaval et al., 2007). According to these studies, the maximum efficiency of mixing is reached for specific power input values close to those corresponding to maximum $k_L a$, and the distribution of mixing intensity on the broth height is similar to that of oxygen transfer rate (Caçcaval et al., 2011). For

higher apparent viscosity, the flow streams velocity is gradually reduced towards the bioreactor top, due to the diminution of the turbulence degree and to the increase of the distance from the sparger.

Compared to the system without oxygen-vectors, analyzed at similar experimental conditions, the addition of *n*-dodecane leads to the enhancement for several times of oxygen transfer rate. This intensification of mass transfer can be described by means of the *amplification factor*, which was defined as the ration between $k_L a$ in presence of oxygen-vector, $(k_L a)_V$, and in absence of oxygen-vector, $(k_L a)_0$, for similar experimental conditions (Galaction et al., 2004).

From Fig. 2 it can be seen that the positive effect of *n*-dodecane addition depends on the broth viscosity, mixing intensity, and position inside the bioreactor. For all cases, the reduction of apparent viscosity and the increase of specific power input lead to the diminution of the magnitude of hydrocarbon effect on oxygen mass transfer coefficient, due to the favorable influence of turbulence on oxygen solubilization and mass transfer. Thus, by varying the amount of dissipated energy by mixing from 52 to 335 W m⁻³, the maximum value of amplification factor was reduced from 5.1 - 5.7 to 3.4 - 4.1 for simulated broths having the apparent viscosity of 15 cP, respectively from 6.9 - 8.3 to 6 - 7.6 for simulated broths with 96 cP apparent viscosity.

This reduction of $(k_L a)_V / (k_L a)_0$ ratio could be attributed to the two phenomena that occur with mixing intensification. On the one hand, even in absence of oxygen-vector, the enhancement of turbulence generates the increase of interfacial area between the gas and liquid phases and, consequently, high oxygen transfer rate (Galaction et al., 2004). On the other hand, according to the mechanism assumed for oxygen transfer in presence of hydrocarbons, an important role on oxygen diffusion is attributed to adsorption of hydrocarbon droplets to bubbles surface, with or without coalescing with superficial film formation (Rols et al., 1990). Although the volumetric fractions of air and oxygen-vector are generally in the same order of magnitude, the average bubble diameter is significant higher than that of the hydrocarbon droplets (literature indicates that the average value of bubble diameter is for 100 times that of the oxygen-vector droplets (Rols et al., 1990). Therefore, a large number of hydrocarbon droplets is adsorbed on bubble surface and coalesce forming a continuous film of oxygen-vector. The hydrodynamic instabilities, induced by turbulence increase and by collisions between bubbles and hydrocarbon droplets, lead to the disruption of oxygen-vector superficial film or to the removal of the oxygen-vector droplets from the bubble surface. Moreover, the increase of apparent viscosity cumulated with mixing intensification determines the increase of time needed for coalescence of the hydrocarbon droplets adsorbed to the bubble surface. In both cases, the

covering degree of the bubble surface by hydrocarbon droplets decreases, thus reducing the oxygen diffusion rate from air to aqueous phase.

Regardless of the apparent viscosity and specific power input, the analysis of amplification factor distribution inside the broth suggests that its highest values are reached for the intermediary positions, the *n*-dodecane addition counteracting the lowest turbulence corresponding to these regions. Obviously, for the regions with high turbulence, namely positions 1 and 4, the positive effect of oxygen-vector is diminished, the lowest amplification factor being recorded either for position 1 in less viscous broths, or for position 4 in viscous ones (Fig. 2).

As it was above discussed, for apparent viscosity of 96 cP, due to the more complex hydrodynamics of broth related to position 4, the effect of *n*-dodecane on $k_L a$ becomes the least important in this region, especially at hydrocarbon volumetric fraction over 0.10. These results underline once again the major role of the *n*-dodecane droplets

size which controls the interfacial areas, according to the mechanism proposed for oxygen transfer in presence of oxygen-vectors.

Similar to the aerobic fermentation systems without oxygen-vectors, the increase of apparent viscosity of broth leads to the significant decrease of $k_L a$, this effect being attenuated by increasing the hydrocarbon concentration, due to the favorable effect on oxygen solubilization and to the acceleration of diffusion. The apparent viscosity influences also the value and distribution inside the broth of the amplification factor, its effect depending mainly on the mixing intensity (Fig. 3).

Thus, for a specific power input of 52 W m^{-3} , by increasing the apparent viscosity from 1 to 96 cP, the amplification factor is reduced to a minimum value, corresponding to 15 cP, then increasing continuously. In this case, due to the less intense mixing and, consequently, lower turbulence, the negative influence of viscosity on amplification factor is more pronounced compared to systems containing water (1 cP).

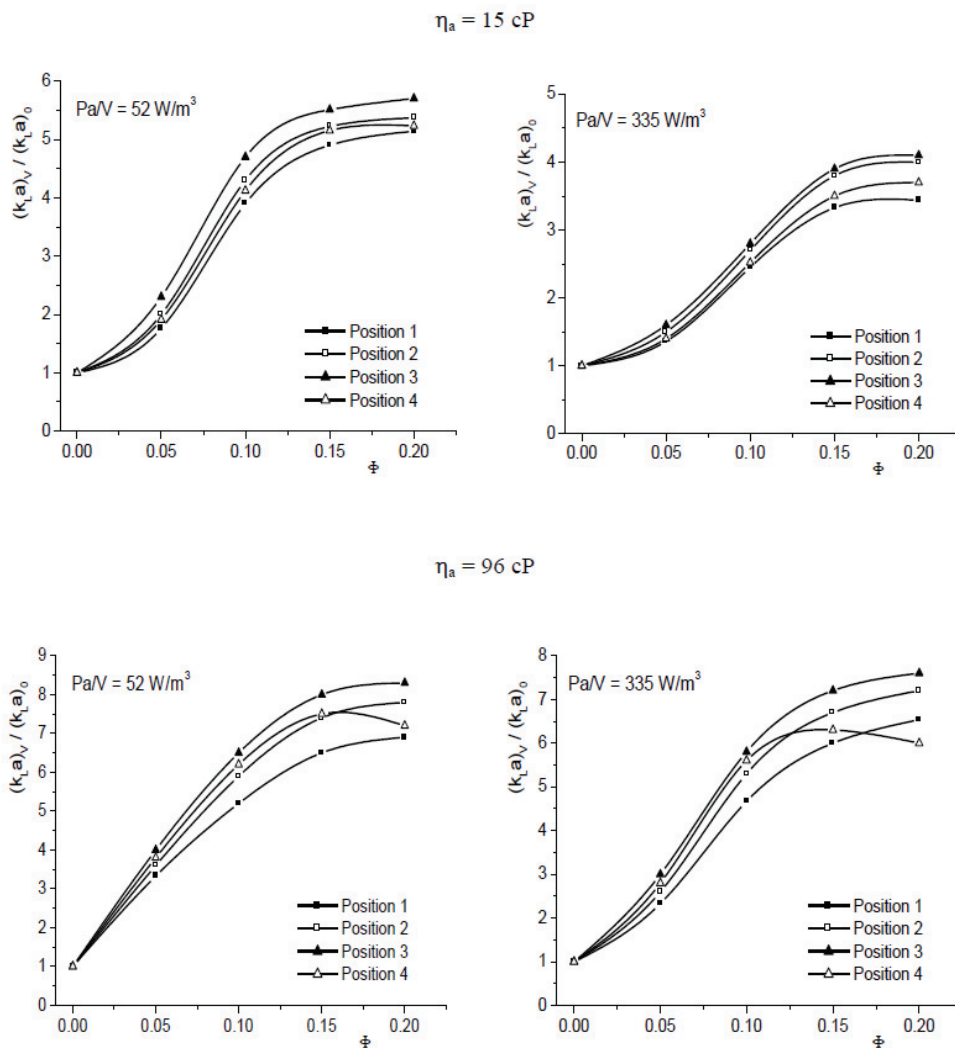


Fig. 2. Influence of *n*-dodecane concentration on amplification factor for different apparent viscosities of simulated broths and specific power inputs ($v_s = 8.4 \times 10^{-4} \text{ m s}^{-1}$, $\Phi = 0.20$)

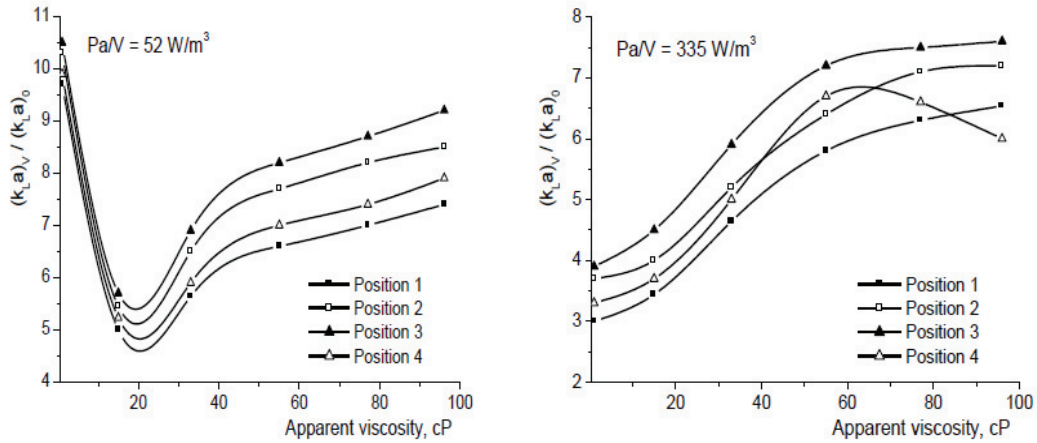


Fig. 3. Influence of apparent viscosity on amplification factor for different specific power inputs ($v_s = 8.4 \times 10^{-4} \text{ m s}^{-1}$, $\Phi = 0.20$)

Due to the increase of the interfacial area between the gaseous and liquid phases in presence of *n*-dodecane, the magnitude of the positive influence of oxygen-vector becomes more important by increasing the apparent viscosity of the broths, but the values of $(k_L a)_V / (k_L a)_0$ ratio for the four positions remain below those obtained for water (Fig. 3).

Because the intensification of mixing induces the fine dispersion of gaseous and *n*-dodecane phases, with favorable effect on oxygen transfer rate, the increase of energy dissipated by mechanical agitation in more viscous media leads to the continuous increasing of amplification factor (Fig. 3). This variation is valid for the entire bulk volume of the broth, excepting the top region. Although at lower specific power input, the variation of oxygen transfer rate obtained for position 4 is similar to those recorded for the other considered positions, at higher mixing intensity and apparent viscosity over 50 cP, the amplification factor for position 4 is reduced and becomes the lowest one. This particular variation is the result of the apparent viscosity influence on the turbulence extent and interfacial area value. Thus, for low-viscous broths, Newtonian broths or for media containing electrolytes, tensides, polymeric compounds, the bubbles coalescence is avoided, the average bubbles size being small.

For more viscous broths or exhibiting non-Newtonian behavior, the equilibrium between the dispersion and the coalescence of bubbles is perturbed, large size bubbles are formed, this phenomenon inducing the decrease of gas-liquid interfacial area and the heterogeneous distribution of air into the broth (Mattiasson and Adlercreutz, 1987). In this case, the bubbles coalescence occurs especially around the impeller placed closer to the sparger, namely that related to position 1. Due to the air accumulation around the inferior impeller and to the nonuniform rising of larger bubbles, the bubbles distribution in region 4 is heterogeneous, and the volumetric fraction of air is low. Consequently, although the second impeller is placed in this region, the positive effect of *n*-dodecane addition is reduced

and the amplification factor values recorded for position 4 become inferior to those for the other three positions.

The increase of aeration rate promotes the intensification of turbulence, the homogeneous distribution of air into the broth and the increase of oxygen concentration gradient between gaseous phase and media, thus exhibiting a favorable effect on oxygen mass transfer. As in the case of effect of energy dissipated by mechanical mixing, the intensification of aeration leads to the increase of $k_L a$, even in absence of *n*-dodecane. Besides the increase of air - broth interfacial area, the increase of aeration rate induces the amplification of turbulence with similar effects to those of the intensification of mechanical agitation. Furthermore, by increasing the aeration, the air volumetric fraction in broth increases, thus diminishing the covering degree of bubbles surface by hydrocarbon droplets. This phenomena is more pronounced for high viscous broths, owing to the high bubbles retention time into the broth and, consequently, to the increase of air volumetric fraction.

4.2. *Propionibacterium shermanii* broths

P. shermanii is the main aerobic bacteria producer of vitamin B12 at industrial scale. Although the effects of cells on rheological characteristics of the broth and oxygen transfer rate are less significant compared to the other microorganisms types, they cannot be neglected. Moreover, the affinity of cells for the hydrocarbon droplets represents an important factor controlling the oxygen transfer in fermentation system containing oxygen-vectors.

Generally, from Fig. 4 it can be observed for all positions that the oxygen transfer rate increases with the increase of *n*-dodecane concentration and specific power input. However, the shapes of the plotted dependences between $k_L a$ and volumetric fraction of oxygen-vector are changed by increasing the biomass concentration or mixing intensity.

At low bacterial cells concentration and low specific power input, the increase of *n*-dodecane concentration inside the *P. shermanii* broth leads to the continuous improvement of oxygen transfer. At higher rotation speed, the contribution of the mechanical agitation to the oxygen transfer becomes more important and compensates the negative effect of bubbles surface blockage, by redistributing the adsorbed cells and renewing the gas-liquid interface. Consequently, at higher mixing intensity, the value of oxygen mass transfer coefficient remains at a rather constant level for *n*-dodecane volumetric fraction over 0.15, regardless of the considered position inside the bioreactor.

The bacterial cells accumulation exhibits a negative influence on k_La , especially due to the increase of apparent viscosity and of extent of the bubbles blocking effect by cells adsorption (Galaction et al., 2004). Moreover, Fig. 4 indicates that by increasing the oxygen-vector amount inside the broth, k_La increases, reaches a maximum value, then remaining at a constant level. The minimum value of *n*-dodecane volumetric fraction corresponding to the constant level of oxygen mass transfer rate is reduced from 0.15 to 0.10 by intensifying the mixing from 110 to 440 Wm^{-3} . This behavior of the system is the result of the modification of bacterial cells affinity for the hydrocarbon droplets during the growth cycle of *P. shermanii* in direct relation with its biomass concentration in the broth (Caşcaval et al., 2006; Rols et al., 1990). According to the previous studies, unlike the simulated broths without biomass, the bacterial cells are adsorbed on oxygen-vector droplets surface, this phenomenon diminishing the favorable effect of oxygen-vector addition (Caşcaval et al., 2006).

However, as it was reported in literature, the bacteria cells are known to be hydrophobic only at the beginning of their growth, at lower biomass concentrations, the microorganisms growth and accumulation inducing their desorption from droplets surface and dispersion into aqueous phase (Rols et al., 1990). In these circumstances, the coverage degree of *n*-dodecane droplets surface by cells decreases, the droplets are adsorbed on air bubbles surface, with or without the formation of a continuous film, thus avoiding the blockage of the bubbles free surface by cells. Consequently, the magnitude of the effect of oxygen-vector becomes more important than in fermentation broths with lower bacterial cells concentration, and, implicitly, the *n*-dodecane amount required for reaching the maximum value of k_La is reduced.

The above results are confirming by the dependences between the amplification factor and *P. shermanii* cells concentration plotted in Fig. 5. For both considered specific power inputs, regardless of the positions inside the broth, the bacterial cells accumulation leads initially to the reduction of $(k_La)_V/(k_La)_0$ ratio, which reaches a minimum value followed by its significant increase at higher biomass

concentration. As it was above mentioned, the initial reduction of amplification factor is the result of the higher affinity of *P. shermanii* cells for the hydrocarbon droplets, especially at lower biomass concentration. For the studied fermentation system, the cells adsorption to the hydrocarbon droplets surface is more pronounced for cells concentration up to 10 - 30 g d.w. l^{-1} , depending on the mixing intensity. Therefore, the induced barrier effect hinders the oxygen transfer from the *n*-dodecane phase to the aqueous one, and reduces the amplification factor compared to the simulated broths without biomass. The growth of bacteria and, implicitly, the increase of the biomass amount in the broths, induce the cells desorption from the oxygen-vector droplets surface, thus exhibiting positive effect on oxygen transfer. The desorption process becomes more significant at higher bacterial cells concentration, being accelerated by increasing the specific power input. For this reason, the value of *P. shermanii* cells concentration related to the minimum $(k_La)_V/(k_La)_0$ ratio decreases by intensifying the mixing.

Furthermore, due to the nonuniform distribution on the broth height both of the biomass concentration, as the result of cells deposition at the bioreactor bottom, and of the mixing intensity, which is lower in the intermediary positions 2 and 3, the minimum values of amplification factor recorded for the positions 2 and 3 are below those for positions 1 and 4. For the same reasons, the $(k_La)_V/(k_La)_0$ ratio corresponding to the top position for biomass concentration over 96 g d.w. l^{-1} and specific power input of 440 $W m^{-3}$ reaches a value inferior to those recorded for the other three positions.

The increase of specific power input induces the fine dispersion of *n*-dodecane with favorable effect on oxygen transfer rate. From Fig. 6 it can be observed that the positive effect of mixing intensification is recorded only for the values of specific power input up to 240 Wm^{-3} , the further increase of energy dissipated by mechanical agitation leading to the reduction of k_La .

The mechanism responsible for this variation is the same as in the case of simulated broths. However, for bacterial suspensions, the coverage of the bubbles surface by hydrocarbon droplets is partially hindered by mixing intensification and the free bubbles surface could be occupied by *P. shermanii* cells absorption, the oxygen diffusion rate from air to aqueous phase via hydrocarbon phase being reduced. Due to the above discussed aspects, this phenomenon is more pronounced for lower biomass concentration and specific power input over 240 Wm^{-3} . For this reason, the maximum value of the graphical dependence between k_La and the energy dissipated by mechanical agitation is not recorded for concentrated bacterial cell broths, the influence of specific power input over 240 Wm^{-3} on oxygen mass transfer rate becoming insignificant in these systems.

Consequently, the increase of power consumption for mechanical mixing induces the

continuous reduction of $(k_L a)_V / (k_L a)_0$ ratio, effect that is more pronounced for lower volumetric fractions of *n*-dodecane. The influence of superficial air velocity on amplification factor is similar to that of mixing intensity. By increasing the aeration rate, the supplementary induced turbulence promotes the diminution of the covering degree of bubbles surface by hydrocarbon droplets. In the case of *P. shermanii* broths, this phenomenon becomes more important at

intense mixing for biomass concentration over 30 g d.w. l⁻¹.

Thus, due to the cumulated effect of mechanical and pneumatic mixing on the turbulence in the studied systems, by increasing the superficial air velocity from 8.4×10^{-4} to 5×10^{-3} m s⁻¹ the amplification factor was reduced for about 1.5 - 2.5 times (the effect was more pronounced at higher level of specific power input).

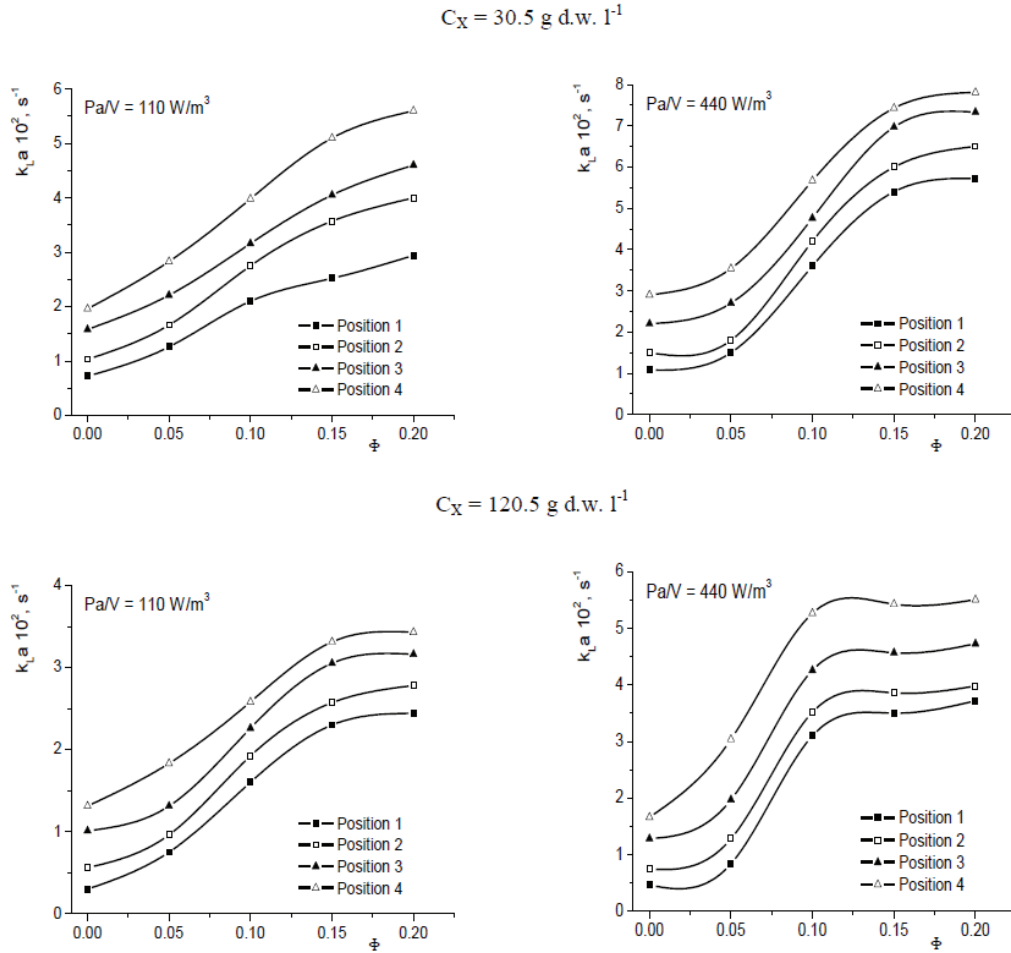


Fig. 4. Influence of *n*-dodecane concentration on oxygen mass transfer coefficient for different bacterial cells concentrations and specific power inputs ($v_s = 8.4 \times 10^{-4}$ m s⁻¹)

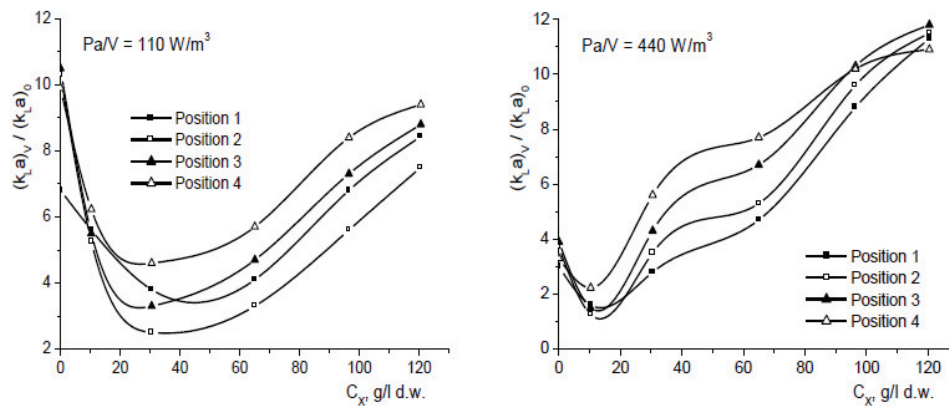


Fig. 5. Influence of bacterial cells concentration on amplification factor for different specific power inputs ($v_s = 8.4 \times 10^{-4}$ m s⁻¹, $\Phi = 0.15$)

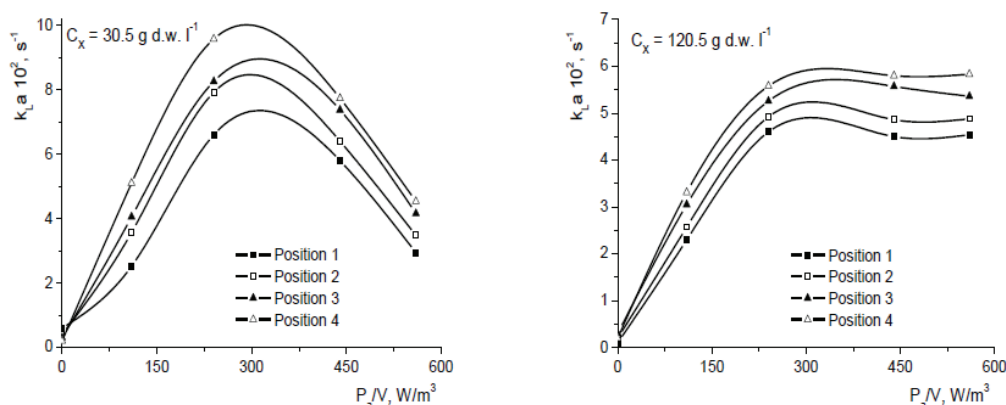


Fig. 6. Influence of specific power input on oxygen mass transfer coefficient for different bacterial cells concentrations ($v_s = 8.4 \times 10^{-4} \text{ m s}^{-1}$, $\Phi = 0.15$)

4.3. *Saccharomyces cerevisiae* broths

In absence of *n*-dodecane, due to the closer viscosities of the bacterial and yeasts broths at similar biomass concentrations, the variations of k_{La} with bioreactor operating parameters, as well as the phenomena inducing these variations for *S. cerevisiae* cultures are similar to those recorded for *P. shermanii* ones (Galaction et al., 2004). However, the higher affinity for hydrocarbon phase of yeasts induces different behavior compared to that of bacteria, the yeasts cells being adsorbed to oxygen-vectors droplets during the entire fermentation cycle (Mimura et al., 1971; Rols et al., 1990).

Generally, from Fig. 7 it can be observed that the values of oxygen transfer rate in yeasts broths containing oxygen-vectors are lower than those recorded in bacterial broths, for identical experimental conditions. However, although the increase of *n*-dodecane concentration leads to the increase of k_{La} , the affinity of yeasts cells for oxygen-vector droplets and the mixing intensity control the shape of the dependence between the oxygen mass transfer rate and hydrocarbon volumetric fraction (Fig. 7). At lower biomass concentration (30 g d.w. l^{-1}) and less intense mixing, k_{La} is slowly enhanced by increasing the oxygen-vector concentration up to 10% vol., due to the yeasts cells adsorption to the hydrocarbon droplets surface. The further increase of the *n*-dodecane amount inside the broths partially counteracts the cells adsorption phenomenon, the oxygen mass transfer being accelerated for Φ over 0.10.

The mixing intensification induces the increase of turbulence and, implicitly, the cells desorption from the hydrocarbon droplets surface, generating an important positive effect on k_{La} for volumetric fraction of oxygen vector up to 0.10. For the same reasons as in the above discussed systems of bacterial fermentation, the supplementary addition of *n*-dodecane leads to the slower acceleration of oxygen transfer from the hydrocarbon to aqueous phase.

At higher *S. cerevisiae* concentration ($110 \text{ g d.w. l}^{-1}$), its cells affinity for hydrocarbon phase exhibits a stronger negative effect. Thus, according to Fig. 7, for specific power input of 110 W m^{-3} , the oxygen-vector effect on k_{La} is less important for its volumetric fraction below 0.10, becoming significant at higher concentrations. The increase of specific power input induces effects comparable to the case of lower biomass concentration.

As the result of the distribution of mixing intensity and biomass concentration on the broth height (Caçcaval et al., 2011), the highest values of oxygen mass transfer coefficient are recorded for positions 4 and 1, respectively, while the lowest ones correspond to the intermediary positions 2 and 3.

Similar to the oxygen mass transfer inside the bacterial broths, the yeasts concentration influences the k_{La} mainly by means of the broth apparent viscosity, and additionally by cells adsorption on the *n*-dodecane droplets surface. However, contrary to the effect of *P. shermanii* concentration, the strongest reduction of oxygen mass transfer coefficient with *S. cerevisiae* biomass accumulation from 30 to $110 \text{ g d.w. l}^{-1}$ was recorded for higher amounts of *n*-dodecane (for $\phi = 0.20$, k_{La} was reduced for about 1.15 to 1.3 times at specific power input of 110 W m^{-3} , and for about 1.2 to 1.33 times at 440 W m^{-3} , the most important reduction corresponding to positions 1 and 4). For the same experimental conditions, but without *n*-dodecane, k_{La} was reduced for 1.3 to 3.2 times by increasing the yeasts concentration in the mentioned domain. In this case, the most important diminution of the oxygen transfer rate was recorded for the intermediary positions.

The variation of amplification factor during the yeasts accumulation inside the broth is completely different from that previously observed for bacteria suspensions. Therefore, in the case of *S. cerevisiae* suspensions, $(k_{La})_v/(k_{La})_0$ ratio reaches a maximum value, decreasing then (Fig. 8). This variation is the consequence of two opposite phenomena induced by increasing the biomass concentration. On the one hand, the addition of *n*-

dodecane leads to the intensification of oxygen transfer from gaseous phase to the broth, effect which is more important in the regions with higher mixing intensity, namely positions 1 and 4. On the other hand, due to the affinity of yeasts cells for the hydrocarbons droplets, the biomass is adsorbed to the droplets surface and blocks the interface of oxygen transfer from aqueous to organic phase. Moreover, the cells-droplets associations could be adsorbed to the air bubbles surface, inducing an additional resistance to the oxygen diffusion.

On the basis of these considerations, according to Fig. 8, the maximum value of amplification factor becomes more obvious for the intermediary positions 2 and 3, due to the related poor broth circulation intensity (Caçaval et al., 2007). Furthermore, the maximum values of $(k_L a)_V / (k_L a)_0$ ratio corresponding to positions 2 and 3 is recorded for lower biomass concentration compared to those related to positions 1 and 4, also as a result of lower intensity of mixing in the intermediary positions cumulated with the affinity of yeasts cells for hydrocarbon.

The influence of mixing intensity has to be correlated with the stronger affinity of yeasts cells for the hydrocarbon phase. As it can be observed from

Fig. 9, the variation of oxygen transfer rate with the specific power input depends on the *S. cerevisiae* concentration and position inside the broth.

Regardless of the biomass concentration, the mixing intensification induces initially the enhancement of oxygen transfer. However, depending on the *S. cerevisiae* cells concentration and position inside the broth, the oxygen transfer rate decreases or increases slowly over a certain value of specific power input. Therefore, for less concentrated suspensions of *S. cerevisiae*, the oxygen transfer rate is continuously increased for positions 1 and 4 by intensifying the mixing, but this variation becomes less pronounced for specific power input over 240 W m^{-3} . In the case of the same suspensions of yeasts, the maximum value of $k_L a$ is reached at specific power input of 440 W m^{-3} . For higher amount of yeast cells, the maximum $k_L a$ is reached at 440 W m^{-3} for positions 1 and 4, while for the intermediary positions the value of specific power input corresponding to the maximum $k_L a$ is reduced to 240 W m^{-3} . As it was above discussed, the intensification of mixing induces the fine dispersion of air and of *n*-dodecane, with the increase of interfacial area, as well as the disruption of cells-droplets and cells-droplets-air bubbles associations.

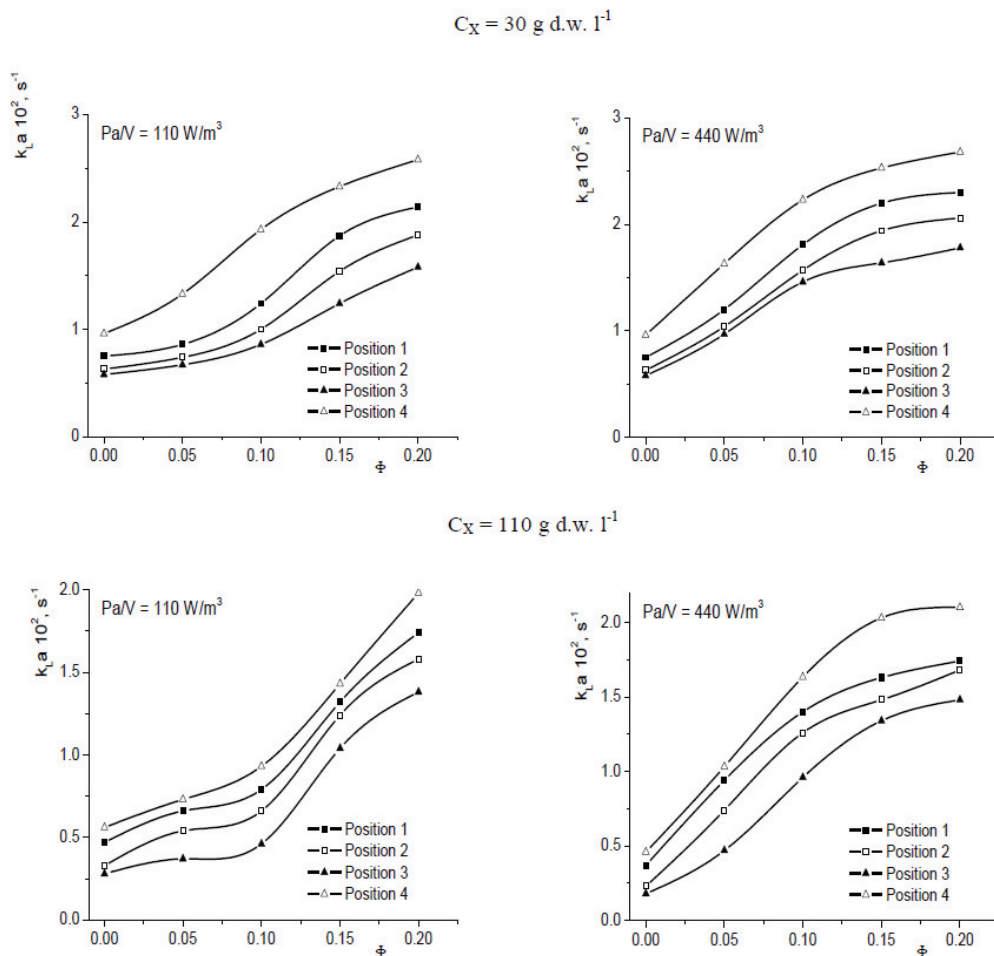


Fig. 7. Influence of *n*-dodecane concentration on oxygen mass transfer coefficient for different yeasts cells concentrations and specific power inputs ($v_s = 8.4 \times 10^{-4} \text{ m s}^{-1}$)

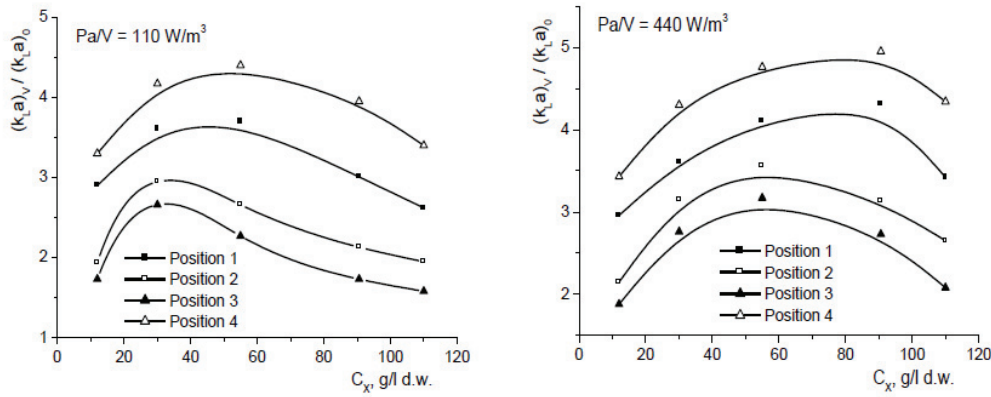


Fig. 8. Influence of yeasts cells concentration on amplification factor for different specific power inputs ($v_s = 8.4 \times 10^{-4} \text{ m s}^{-1}$, $\Phi = 0.15$)

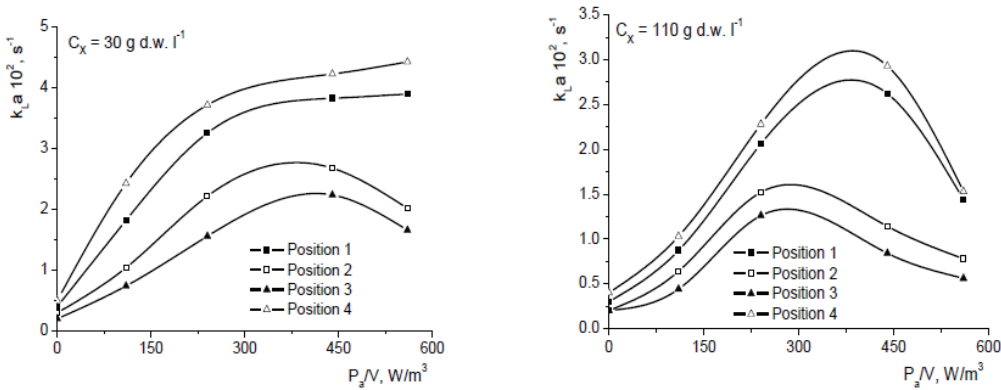


Fig. 9. Influence of specific power input on oxygen mass transfer coefficient for different yeast cells concentrations ($v_s = 8.4 \times 10^{-4} \text{ m s}^{-1}$, $\Phi = 0.15$)

Both phenomena induce initially a positive effect on oxygen transfer rate. In the same time, due to the stronger affinity of yeast cells for the hydrocarbon droplets compared to that of bacterial ones, the surface of the finely dispersed bubbles and droplets can be easily occupied by *S. cerevisiae* cells adsorption, thus amplifying the resistance to the oxygen mass transfer and, consequently, reducing k_{La} . The negative effect of surface blockage is more important at higher biomass concentration and leads to the reduction of specific power input related to the maximum value of oxygen transfer rate for all considered positions in the bioreactor.

Although the intensification of aeration induces similar effect as the increase of specific power input, it also leads to the increase of the air volumetric fraction in broth and to the diminution of the covering degree of bubbles surface by hydrocarbon droplets. Consequently, the amplification factor is reduced. Owing to these opposite effects, the influence of aeration rate on amplification factor for *S. cerevisiae* suspensions is different to that recorded for simulated and bacterial broths. In this case, the maximum value of $(k_{La})_V / (k_{La})_0$ ratio is reached for the superficial air velocity of $3.35 \times 10^{-3} \text{ m s}^{-1}$ and decreases from 4.4 to 2.2 with

S. cerevisiae biomass accumulation from 30 to 110 g d.w. l^{-1} .

4.4. Correlations for oxygen transfer

By means of the experimental data obtained for the studied simulated and real broths, mathematical correlations describing the influence of oxygen-vector concentration, apparent viscosity or biomass concentration, specific power input and air superficial velocity on k_{La} have been established for the four positions inside the broths. Depending on the studied system, two general expressions have been considered (Eqs. 1-2).

$$k_{La} = \alpha \cdot \eta_a^\beta \cdot \left(\frac{P_a}{V}\right)^\gamma \cdot v_s^\delta \quad (1)$$

for simulated broths, or

$$k_{La} = \alpha \cdot C_x^\beta \cdot \left(\frac{P_a}{V}\right)^\gamma \cdot v_s^\delta \quad (2)$$

for bacterial and yeasts broths. The coefficients β , γ and δ values are function of *n*-dodecane concentration.

The values of α , β , γ and δ coefficients were calculated by the multiregression method using MATLAB software. Thus, the following correlations have been obtained:

a. simulated broths (Eqs. 3-6):

• Position 1

$$k_L a = 1.18 \cdot \left[\frac{\eta_a^{1.27}}{v_S^{2.12} \cdot \left(\frac{P_a}{V}\right)^{3.11}} \right]^\phi, s^{-1} \quad (3)$$

• Position 2

$$k_L a = 1.12 \cdot \left[\frac{\eta_a^{3.63}}{v_S^{0.85} \cdot \left(\frac{P_a}{V}\right)^{2.35}} \right]^\phi, s^{-1} \quad (4)$$

• Position 3

$$k_L a = 1.72 \cdot \left[\frac{\eta_a^{1.91}}{v_S^{0.35} \cdot \left(\frac{P_a}{V}\right)^{3.10}} \right]^\phi, s^{-1} \quad (5)$$

• Position 4

$$k_L a = 2.17 \cdot \left[\frac{\eta_a^{2.67}}{v_S^{0.31} \cdot \left(\frac{P_a}{V}\right)^{3.77}} \right]^\phi, s^{-1} \quad (6)$$

b. bacteria (*P. shermanii*) (Eqs. 7-10):

• Position 1

$$k_L a = 0.76 \cdot \left[\frac{C_X^{1.61}}{v_S^{0.46} \cdot \left(\frac{P_a}{V}\right)^{3.33}} \right]^\phi, s^{-1} \quad (7)$$

• Position 2

$$k_L a = 2.38 \cdot 10^{-2} \cdot \left[\frac{C_X^{2.27}}{v_S^{0.66} \cdot \left(\frac{P_a}{V}\right)^{8.19}} \right]^\phi, s^{-1} \quad (8)$$

• Position 3

$$k_L a = 3.81 \cdot 10^{-2} \cdot \left[\frac{C_X^{0.31} \cdot \left(\frac{P_a}{V}\right)^{0.15}}{v_S^{0.66}} \right]^\phi, s^{-1} \quad (9)$$

• Position 4

$$k_L a = 3.74 \cdot 10^{-2} \cdot \left[\frac{C_X^{0.15} \cdot \left(\frac{P_a}{V}\right)^{0.25}}{v_S^{8.72 \cdot 10^{-3}}} \right]^\phi, s^{-1} \quad (10)$$

c. yeasts (*S. cerevisiae*) (Eqs. 7-10):

• Position 1

$$k_L a = 8.91 \cdot 10^{-2} \cdot \left[\frac{C_X^{8.46 \cdot 10^{-2}}}{v_S^{0.39} \cdot \left(\frac{P_a}{V}\right)^{0.17}} \right]^\phi, s^{-1} \quad (11)$$

• Position 2

$$k_L a = 7.10 \cdot 10^{-2} \cdot \left[\frac{C_X^{1.95}}{v_S^{0.74} \cdot \left(\frac{P_a}{V}\right)^{3.81}} \right]^\phi, s^{-1} \quad (12)$$

• Position 3

$$k_L a = 6.12 \cdot 10^{-3} \cdot \left[\frac{C_X^{0.81} \cdot \left(\frac{P_a}{V}\right)^{0.11}}{v_S^{1.60 \cdot 10^{-2}}} \right]^\phi, s^{-1} \quad (13)$$

• Position 4

$$k_L a = 9.16 \cdot 10^{-3} \cdot \left[\frac{C_X^{0.33} \cdot \left(\frac{P_a}{V}\right)^{0.32}}{v_S^{6.26 \cdot 10^{-2}}} \right]^\phi, s^{-1} \quad (14)$$

The proposed equations offer a good agreement with the experimental data, the maximum deviations being of 6.92% for simulated broths, 8.40% for *P. shermanii* broths, and 9.73% for *S. cerevisiae* broths.

The above discussed influences of the considered parameters and their importance are suggested by the sign and value of the corresponding exponents. Therefore, regardless of the position inside the bioreactor, the specific power input exhibits negative influence in the case of simulated broths. For broths containing biomass, the negative influence of mixing intensity is observed only for the positions placed at the bioreactor bottom, namely positions 1 and 2, due to the higher amount of solid phase in this region, which could block the hydrocarbon droplets or bubbles surface by adsorption. The influence of superficial air velocity is positive in all studied systems, but is more important in the absence of the blockage of the oxygen mass transfer surface by cells (simulated and bacterial broths).

4. Conclusions

The addition of oxygen-vector, namely *n*-dodecane, leads to the enhancement for several times of oxygen transfer rate compared to the conventional aerobic fermentations, without supplementary mixing or aeration intensification. However, the influence of oxygen-vector on $k_L a$ value and distribution inside the broths has to be analyzed in relation with the broth characteristics (apparent viscosity or biomass concentration), bioreactor operating parameters, and, most important, affinity of cells for hydrocarbon

droplets. Moreover, the amplitude of the considered factors influences differs from one region inside the broth to another. The oxygen mass transfer has been analyzed for a stirred bioreactor by means of k_La and amplification factor, $(k_La)_V / (k_La)_0$, for viscous simulated broths without biomass, *P. shermanii* and *S. cerevisiae* broths.

Generally, the increase of apparent viscosity or of biomass concentration induces the significant decrease of k_La , the magnitude of this influence being diminished by increasing the volumetric fraction of *n*-dodecane. The positive effect of *n*-dodecane addition was recorded for all four positions considered inside the bioreactor, being more important for simulated and *P. shermanii*, due to the absence or low affinity of cells for hydrocarbon droplets.

The different affinity of bacterial and yeasts cells for hydrocarbon phase induces different variations of amplification factor during the accumulation of biomass. Thus, for *P. shermanii* broths, the amplification factor initially decreases from the value reached in the absence of cells, increasing then strongly with the biomass accumulation. This phenomenon is the result of the modification of cells affinity for hydrocarbon droplets during the biomass growth and accumulation. The variation of amplification factor with the increase of *S. cerevisiae* concentration is completely different from that obtained for bacteria suspensions, due to the higher affinity of yeasts cells for organic phase. This parameter reached a maximum value, followed by its decrease. For positions 1 and 4, the maximum $(k_La)_V / (k_La)_0$ ratio corresponds to higher biomass concentration compared to the intermediary positions.

Although the shapes of the dependences between the oxygen transfer rate and specific power input are rather similar for the three studied fermentation systems, the influence of mixing intensification also depends on broths type. Therefore, the increase of specific power input influences positively the oxygen transfer rate for simulated broths and yeasts suspensions containing low cell concentrations, especially at the bottom and top regions of the bioreactor. For bacterial broths, regardless of the position inside the bioreactor, k_La increases with mixing intensification, reaches a maximum value followed by its decreasing. This variation is more pronounced for less concentrated suspensions.

In all studied cases, the influence of superficial air velocity on amplification factor was similar to that of mixing intensity. Thus, by increasing the aeration rate, the promoted turbulence leads to the diminution of the amplification factor, as the result of the reduction of covering degree of bubbles surface by hydrocarbon droplets.

The influences of the considered factors have been included in some mathematical correlations which allow predicting the oxygen mass transfer coefficient in different regions of the bioreactor for

simulated, bacterial, and yeasts, and offer a good concordance with the experimental results (the average deviation varied between $\pm 6.72\%$ for simulated broths and $\pm 6.93\%$ for *P. shermanii* cultures).

Nomenclature

C_1 - oxygen concentration in the broth, mol l⁻¹
 C_1^* - maximum oxygen concentration in the broth, mol l⁻¹
 C_X - biomass concentration, g d.w. l⁻¹
 k_La - oxygen mass transfer coefficient, s⁻¹
 $(k_La)_0$ - k_La in absence of oxygen-vector, s⁻¹
 $(k_La)_V$ - k_La in presence of oxygen-vector, s⁻¹
 $(k_La)_V / (k_La)_0$ - amplification factor,
 P_a - power consumption for mixing of aerated broths, W
 P_a/V - specific power input, W m⁻³
 v_S - superficial air velocity, m s⁻¹
Greek symbols
 $\alpha, \beta, \gamma, \delta$ - parameters of Eqs. (1) and (2)
 ϕ - volumetric fraction of oxygen-vector
 η_a - apparent viscosity, Pa·s

References

- Caşcaval D., Galaction A.I., Folescu E., Turnea M., (2006), Comparative study on the effects of *n*-dodecane addition on oxygen transfer in stirred bioreactors for simulated, bacterial and yeasts broths, *Biochemical Engineering Journal*, **31**, 56-66.
- Caşcaval D., Galaction A.I., Turnea M., (2007), Comparative analysis of mixing distribution in aerobic stirred bioreactor for simulated, yeasts and fungus broths, *Journal of Industrial Microbiology and Biotechnology*, **34**, 35-47.
- Caşcaval D., Galaction A.I., Turnea M., (2011), Comparative analysis of oxygen transfer rate distribution in stirred bioreactor for simulated and real fermentation broths, *Journal of Industrial Microbiology and Biotechnology*, **38**, 1449-1466.
- Clarke K.G., Williams P.C., Smit M.S., Harrison S.T.L., (2006), Enhancement and repression of the volumetric oxygen transfer coefficient through hydrocarbon addition and its influence on oxygen transfer rate in stirred tank bioreactors, *Biochemical Engineering Journal*, **28**, 237-242.
- Clarke K.G., Correia L.D.C., (2008), Oxygen transfer in hydrocarbon-aqueous dispersions and its applicability to alkane bioprocesses: a review, *Biochemical Engineering Journal*, **39**, 405-429.
- Da Silva T.L., Reis A., Roseiro J.C., Hewitt C.J., (2008), Physiological effects of the addition of *n*-dodecane as an oxygen-vector during steady-state *Bacillus licheniformis* thermophilic fermentations perturbed by a starvation period or a glucose pulse, *Biochemical Engineering Journal*, **42**, 202-216.
- Dumont E., Andres Y., Le Cloirec P., (2006), Effect of organic solvents on oxygen mass transfer in multiphase systems: Application to bioreactors in environmental protection, *Biochemical Engineering Journal*, **30**, 245-252.
- Galaction A. I., Caşcaval D., Oniscu C., Turnea M., (2004), Prediction of oxygen transfer coefficients in stirred bioreactors for bacteria, yeasts and fungus broths, *Biochemical Engineering Journal*, **20**, 85-94.
- Galaction A.I., Caşcaval D., Turnea M., Folescu E., (2005), Enhancement of oxygen mass transfer in stirred bioreactors using oxygen-vectors. 2.

- Propionibacterium shermanii* broths, *Bioprocess and Biosystems Engineering*, **27**, 263-271
- Gomez E., Santos V.E., Alcon A., Garcia-Ochoa F., (2006), Oxygen transport rate on *Rhodococcus erythropolis* cultures: Effect on growth and BDS capability, *Chemical Engineering Science*, **61**, 4595-4604.
- Hjertager B.H., (1998), Computational fluid dynamics (CFD) analysis of multiphase chemical reactor, *Trends in Chemical Engineering*, **4**, 45-92.
- Kerdouss F., Bannari A., Proulx P., (2006), CFD modeling of gas dispersion and bubble size in a double turbine stirred tank, *Chemical Engineering Science*, **61**, 3313-3322.
- Kerdouss F., Bannari A., Proulx P., Bannari R., Skrga M., Labrecque Y., (2008), Two-phase mass transfer coefficients prediction in a bioreactor with a CFD model, *Computer & Chemical Engineering*, **32**, 1943-1955.
- Lee B.S., Kim E.K., (2004), Lipopeptide production from *Bacillus* sp. GB16 using a novel oxygenation method, *Enzyme and Microbial Technology*, **35**, 639-647.
- Li M., Meng X., Diao E., Du F., Zhao X., (2012), Productivity enhancement of S-adenosylmethionine in *Saccharomyces cerevisiae* using n-hexadecane as oxygen vector, *Journal of Chemical Technology and Biotechnology*, **87**, 1379-1384.
- Mattiasson B., Adlercreutz P., (1987), Perfluorochemicals in biotechnology, *Trends in Biotechnology*, **5**, 250-254.
- Mimura A., Watanabe S., Takeda I., (1971), Biochemical engineering analysis of hydrocarbon fermentation III. Analysis of emulsification phenomena, *Journal of Fermentation Technology*, **49**, 255-262.
- Montes F.Y., Catalan J., Galan M.A., (1999), Prediction of $k_L a$ in yeasts broths, *Process Biochemistry*, **34**, 549-555.
- Ozbek B., Gayik S., (2001), The studies on the oxygen mass transfer coefficient in a bioreactor, *Process Biochemistry*, **36**, 729-741.
- Pilarek M., Szewczyk K.W., (2008), Effects of perfluorinated oxygen carrier application in yeast, fungi and plant cell suspension cultures, *Biochemical Engineering Journal*, **41**, 38-42.
- Rols J. L., Condoret J.S., Fonade C., Goma G., (1990), Mechanism of enhanced oxygen transfer in fermentation using emulsified oxygen-vectors, *Biotechnology and Bioengineering*, **35**, 427-435.
- Van't Riet K., Tramper J., (1991), *Basic Bioreactor Design*, New York, M. Dekker Inc.
- Xu F., Yuan Q. P., Zhu Y., (2007), Improved production of lycopene and β -carotene by *Blakeslea trispora* with oxygen-vectors, *Process Biochemistry*, **42**, 289-293.



“Gheorghe Asachi” Technical University of Iasi, Romania



ION EXCHANGE PROCESSES ON WEAK ACID RESINS FOR WASTEWATER CONTAINING COPPER IONS TREATMENT

**Cristina Modroga^{*}, Alexandra Raluca Miron, Oanamari Daniela Orbulet,
Cristina Costache, Giani Apostol**

*University “Politehnica” of Bucharest, Faculty of Applied Chemistry and Materials Science,
Department of Analytical Chemistry and Environmental Engineering, 1-7 Polizu Str., Bucharest, Romania*

Abstract

The capacity of ion exchange resins, MN 500 and C100 H, for the removal of copper ions from aqueous solution has been investigated under different conditions, namely: initial solution pH, initial metal-ion concentration and contact time.

The adsorption of Cu(II) on these resins follows the first-order reversible kinetic. The film diffusion of Cu (II) in these ion exchange resins was shown to be the main rate limiting step. The studies showed that these cation exchange resins can be used as efficient adsorbent material for the removal of Cu (II) from aqueous solutions. The adsorption process, which is pH dependent, shows maximum removal of copper in the pH range 2-7 for an initial copper concentration of 10 mg/L.

The adsorption rate constants for all these kinetic models have been calculated. Results showed that the intraparticle diffusion and initial Cu(II) sorption into resins was the main rate limiting step. The uptake of copper by the ion exchange resins is reversible and thus has good potential for the removal/recovery of copper from aqueous solutions. After the experiments we concluded that such ion exchange resins can be used for the efficient removal of copper from water and wastewater.

Key words: copper, ion exchange, Purolite MN 500, Purolite C 100 H, sorption capacity

Received: November, 2014; *Revised final:* February, 2015; *Accepted:* February, 2015

1. Introduction

Copper is a reddish metal that occurs naturally in rock, soil, water, sediment and air. Copper also occurs naturally in plants and animals. Copper is necessary for good health. It is an essential trace element that facilitates the activity of several enzymes. The element provides a role in the development and maintenance of the cardiovascular system, including the heart, arteries and the blood vessels, the skeletal system, and the structure and function of the nervous system, including the brain (Adhoum et al., 2004; Ahmaruzzaman et al., 2011; Basha et al., 2011).

Copper is found in varying amounts in all tissues and about 50 percent of the total copper content of the body are found in the bones and

muscles. The highest concentration of copper is found in the brain and liver.

However, very large single or daily intakes of copper can harm human health. Long term exposure to copper dust can irritate the nose, mouth, eyes and cause headaches, dizziness, nausea and diarrhea. Victims of Wilson's disease will steadily accumulate it in the liver, central nervous system and kidneys.

Copper is toxic to aquatic life and certain microorganisms potentially disrupting nutrient cycling processes. Hazards depend upon the form and bio availability of copper (Basha et al., 2011). In order to protect the public health and aquatic life, it is necessary to remove copper from industrial effluent before discharging it to public wastewater treatment plant or receiving waters.

^{*} Author to whom all correspondence should be addressed: e-mail: c_modroga@yahoo.com

The average concentration of copper in ground water is similar to that in lakes and rivers. However, monitoring data indicates that some ground waters contain higher levels of copper. This is generally strongly attached to the particles in the water. Lakes and reservoirs recently treated with copper compounds for algae control or the ones receiving cooling water from a power plant may have high concentrations of dissolved copper. Once in natural water, much of this copper soon attaches to particles or converts to forms that cannot easily enter the body (EPA, 2002; Imamoglu et al., 2008; Kononova et al., 2014; Sousa et al., 2010).

Soil generally contains between 2 and 250 ppm copper, although concentrations close to 7,000 ppm have been found near copper production facilities. High concentrations of copper may be found in soil because dust from these industries settles out of air, or waste from mining and other copper industries are disposed of on the soil.

Copper is quite malleable and good conductor of heat and electricity. In terms of electrical conductivity, only silver is more effective, thus it is used in electrical industry. Copper is widely used in the production of wire, brass, boiler pipe, cooking utensils and fertilizers etc.

The potential sources of pollution with copper are: smelting and refining industries, copper wire manufacturing, coal burning, iron and steel industries, metal cleaning operations, plating baths, rinses and manufacturing of printed circuit. Copper is found in industrial discharge and is used as an algacide in reservoirs.

Various methods exist for the removal of toxic metal ions from aqueous solutions (Bohdana et al., 2008; Delvaux et al., 2000; Crini et al., 2014; Helfferich et al., 1995; Pollution Databse, 2004; Weber et al., 2008). Ion exchange is widely used and with good performance in the removal and recovery of metals from natural water and industrial wastewater (Fu et al., 2014; Samarghandi et al., 2013). Copper usage and pollution should be reduced wherever possible.

2. Experimental

All chemicals used during experiments were purchased from Merck (Germany). All the experiments conducted were carried out in duplicate sets. All measurements were performed in parallels in each set. The removals reported are the average of the parallel measurements of the duplicate sets and the parallel measurements.

Ion exchange studies were done by contacting synthetic aqueous solutions containing $1 \div 100 \text{ mg} \cdot \text{L}^{-1}$ Cu (II), with an ion exchange resin, in a batch system. In these studies, a strongly basic anion exchanger, sort MN 500 and C 100 H (Purolite – Romania), was used. MN 500 is a hypercrosslinked strong acid resin and C 100 H is a premium gel, polystyrenic, strong acid cation exchange resins. In this paper, the influence of water pH and the

exchange anion onto Cu (II) retention kinetic was studied. The solutions containing Cu (II) ions have been prepared using CuSO_4 and deionised water. For the adjustment of the pH value, a 1N sulphuric acid solution has been used.

During the kinetic study, aqueous solutions containing $100 \text{ mg} \cdot \text{L}^{-1}$ were used. Thus, 50 mL of solution were contacted with $1 \pm 2 \cdot 10^{-4}$ g of resin, under batch conditions, at different contact times as follows: 2, 4, 6, 8, 10 and 12 minutes. The temperature control was done using an incubator FOC 225E –Velp Scientifica.

The influence of the exchange ion nature was studied at a pH value of 5 ± 0.2 . The pH control was done by using a pH meter Consort C830. The Cu (II) concentration in aqueous phase was determined by the colorimetric method using a spectrophotometer model CINTRA 5.

3. Results and discussion

The $\text{H}^+/\text{Cu}^{2+}$ ion exchange rates on the gel-like weak acid resin MN 500 and C 100H were measured under conditions favouring a particle diffusion controlled mechanism, namely in concentrated external solutions using an efficient stirring. The experiments were performed at constant temperature (20°C) and two stirring speed (500 and 600 min^{-1}) for different size fractions. The resin was initially in H^+ form, and the outgoing proton in the external solution after replacement by Cu^{2+} ion was monitored with of pH meter at appropriate time intervals, Δt .

The proton activity coefficient is considered constant and the ratio of the activity differences in equation 1 could be taken equal to the ratio of the concentration differences defining the fractional attainment equilibrium.

The pH at time zero was considered as the first value read after the addition $\text{Cu}(\text{SO}_4)_2$ solution under efficient stirring, varying in the range of 2.7 - 1.8. The ion exchange rate was measured for systems with an external solution of $0.997 \text{ M Cu}(\text{SO}_4)_2$.

The mean radius of the swollen beads in metal form was measured microscopically. The results are given as the mean of 50 determination and 99.9 % confidence limits according to Student distribution: $(0.359 \pm 0.025) \times 10^{-3}$, $(0.331 \pm 0.022) \times 10^{-3}$, $(0.294 \pm 0.016) \times 10^{-3}$ for MN 500 and respectively $(0.507 \pm 0.025) \times 10^{-3}$, $(0.502 \pm 0.022) \times 10^{-3}$, $(0.495 \pm 0.016) \times 10^{-3}$ for C 100 H.

The experimental results obtained for $\text{H}^+/\text{Cu}^{2+}$ ion exchange rate on MN 500 and C 100 H, for different sizes of particles and constantly stirring, are given in Figs. 1 and 2. The experiment show that the decreasing of the mean radius of the swollen beads an increase of the stirring speed on the ion exchange rate within experimental errors. The obtained results support an ion done at different time intervals in order to collect data for the entire range of time of the ion exchange process.

The apparent ion exchange capacity Q_{app} (2) was estimated from the experimental pH at time $t = 0$ and at equilibrium with Eq. (1), where V_s is the solution volume with correction for swelling, pH_{eq} is the pH at equilibrium, pH_i initial, f_{H^+} is the proton activity factor and $m_{sat\ resin}$ is the mass of resin saturated with water vapours (g).

$$Q_{app} = \frac{V_s (10^{-pH_{eq}} - 10^{-pH_i}) \cdot f_{H^+}}{m_{sat\ resin}} \quad (1)$$

For the H^+/Cu^{2+} ion exchange process on MN 500 and C 100 H in concentrated external solution (0.997 M) at 20 °C, the degree of dissociation, γ , of the weak acid functional groups and the apparent ion exchange capacity, Q_{app} , were evaluated using the Eqs. (2, 3). The results are given in Table 1.

Several kinetic functions were fitted to the experimental F vs. t curves. The best fit was selected for the highest coefficient of determination and F-statistic parameters of the goodness of fit, and has the physical meaning of an empirical kinetic equation. For all the experiments for this system the best fitted function was the empirical Eq. (3).

$$F = a(1 - \exp(-bt)) + c[1 - 1/(1 + cdt)] \quad (2)$$

Table 2 gives the coefficients of the empirical equation 3 for H^+/Cu^{2+} ion exchange process on MN 500 and C 100 H resin for different size fraction, at 500 min^{-1} and 20°C. The empirical kinetic equations were used to interpolate points for $F \rightarrow 0$, to calculate the interdiffusion coefficients also at low fraction of exchange.

In order to verify which mechanism describe better the experimental points the Eq. (3) for film diffusion control, the experimental data for H^+/Cu^{2+} ion exchange kinetics on a weak acid resin were also used for modeling, where F is the fractional attainment of equilibrium at time t and $k = -3DC/R\delta\bar{C}$; C – the molar concentration of the external solution; \bar{C} – the molar concentration of fixed ionic groups, D – the interdiffusion coefficient in the film, R – the mean

radius of the swollen resin beads, δ – the thickness of the Nernst film of liquid phase.

$$n(1 - F) = -k \cdot t \quad (3)$$

The results presented in Figs. 3 and 4 showed that the hypothesis of film diffusion mechanism is not supported by the experimental data.

The intraparticle integral interdiffusion coefficients were obtained with quasi-homogeneous resin phase kinetic models. The H^+/Cu^{2+} integral interdiffusion coefficients were calculated for different fractional attainment of equilibrium using Eqs. (4 – 8). Knowing the time t for the considered F , and the mean radius of the swollen resin particles, the diffusion coefficient \bar{D} can be calculated. The convergence of series 4 and 6 was considered to be achieved when the difference between two consecutive values of \bar{D} was equal to or smaller than 0.1%. The results are presented in Figs. 3 - 6. All experiments were performed for $\dot{u} < 0.1$, justifying the use of both ISV and FSV conditions.

In Figs. 3 and 4 it is presented the variation of H^+/Cu^{2+} integral interdiffusion coefficients on MN 500 and C 100 H resin, calculated with Eq. (4), $n = 10$ and the simplified Eqs. of Reichenberg, (4) and (5) (Reichenberg, 1953).

$$F(t) = 1 - \frac{\bar{Q}_A(t)}{\bar{Q}_A^0} = 1 - \frac{6}{\pi^2} \sum_{n=1}^{\infty} \frac{1}{n^2} \exp\left(-\frac{\bar{D}t\pi^2 n^2}{r_0^2}\right) \quad (4)$$

$$F(t) = 1 - \frac{6}{\pi^2} \sum_{n=1}^{\infty} \frac{1}{n^2} \exp(-n^2 \pi^2 \tau)$$

where $\bar{Q}_A(t)$ is the amount of A in the exchanger at time t ; \bar{Q}_A^0 – the initial amount of A in the ion exchanger; $F(t)$ is the fractional attainment of equilibrium, defined by $F(t) = \frac{(\bar{Q}_A^0 - \bar{Q}_A(t))}{(\bar{Q}_A^0 - \bar{Q}_A^\infty)}$; \bar{Q}_A^∞ –

the amount of A left in the exchanger when equilibrium is attained.

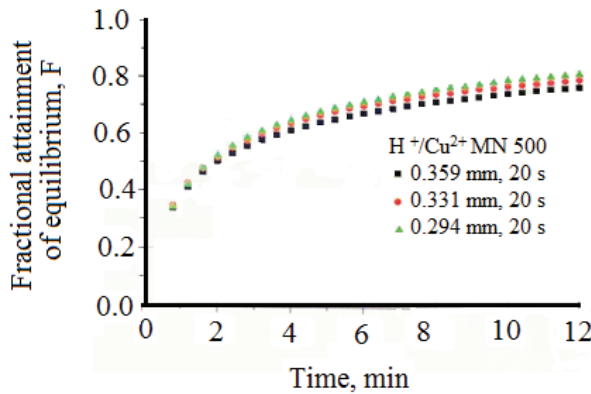


Fig. 1. Fractional attainment of equilibrium vs. time for H^+/Cu^{2+} ion exchange process on MN 500; 20°C; 0.997 M Cu $(SO_4)_2$; 500 min^{-1} .

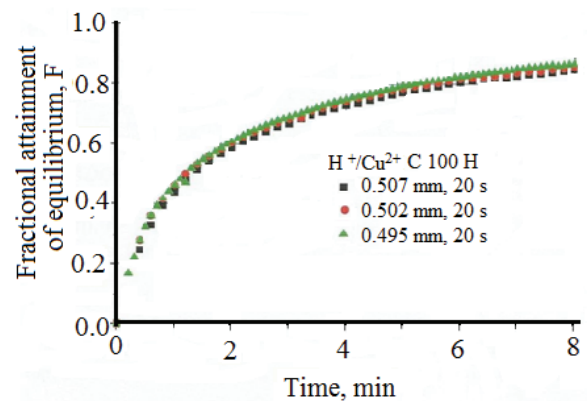


Fig. 2. Fractional attainment of equilibrium vs. time for H^+/Cu^{2+} ion exchange process on C 100 H resin; 20°C; 0.997 M Cu $(SO_4)_2$; 500 min^{-1} .

Table 1. Experimental and theoretical evaluations of the apparent ion exchange capacity and the degree of dissociation of the weak acid resin MN 500 and C 100 H for H⁺/Cu²⁺ ion exchange; 20 °C

$R \cdot 10^{-3}$ (m)	Resin mass (g)	Vs (L)	pH _i	pH _{eq}	μ mol/L	Moisture %	[X] mol/L	Q _{app} exp. (meq/g)	Q _{app} calc. (meq/g)	γ exp.	γ calc.
MN 500											
0.359	0.9630	0.05	2.70	1.80	1.495	51.0	11.55	0.653	0.116	0.056	0.011
0.359	1.0548	0.05	2.51	1.80	1.495	51.0	11.55	0.541	0.116	0.046	0.011
0.359	1.0501	0.05	2.50	1.80	1.495	51.0	11.55	0.526	0.111	0.046	0.011
0.359	1.0236	0.05	2.71	1.80	1.495	51.0	11.55	0.578	0.115	0.050	0.011
0.359	1.0312	0.05	2.41	1.78	1.495	51.0	11.55	0.510	0.116	0.040	0.011
0.331	0.9612	0.05	2.65	1.77	1.495	51.7	12.01	0.639	0.117	0.052	0.010
0.331	0.9910	0.05	2.34	1.80	1.495	51.7	12.01	0.505	0.119	0.038	0.011
0.331	0.9624	0.05	2.68	1.80	1.495	51.7	12.01	0.590	0.121	0.050	0.011
0.331	1.0080	0.05	2.42	1.78	1.495	51.7	12.01	0.510	0.117	0.038	0.011
0.331	0.9676	0.05	2.66	1.80	1.495	51.7	12.01	0.590	0.120	0.048	0.011
0.294	0.7961	0.05	2.70	1.83	1.495	51.5	11.35	0.666	0.120	0.058	0.011
0.294	0.5974	0.05	2.50	1.88	1.495	51.5	11.35	0.70	0.126	0.061	0.011
C 100 H											
0.507	1.0562	0.05	2.70	1.80	1.120	51.0	11.55	0.198	0.184	0.0176	0.015
0.507	1.2340	0.05	2.56	1.80	1.120	51.0	11.55	0.216	0.192	0.0181	0.015
0.507	0.9034	0.05	2.65	1.80	1.120	51.0	11.55	0.216	0.192	0.0181	0.015
0.507	1.0610	0.05	2.41	1.78	1.120	51.0	11.55	0.215	0.178	0.0180	0.015
0.507	0.9000	0.05	2.58	1.88	1.120	51.0	11.55	0.233	0.190	0.0191	0.015
0.502	1.0162	0.05	2.68	1.83	1.120	51.0	11.55	0.212	0.185	0.0179	0.015
0.502	1.0429	0.05	2.60	2.281	1.120	51.0	11.55	0.217	0.180	0.0186	0.015
0.502	1.0701	0.05	2.55	1.88	1.120	51.0	11.55	0.210	0.183	0.0183	0.015
0.502	1.0664	0.05	2.65	1.80	1.120	51.7	12.01	0.210	0.191	0.0171	0.014
0.502	1.0664	0.05	2.70	1.78	1.120	51.7	12.01	0.210	0.192	0.0171	0.014
0.495	1.0616	0.05	2.70	1.80	1.120	51.7	12.01	0.218	0.194	0.0178	0.014
0.495	1.0810	0.05	2.42	1.83	1.120	51.5	11.35	0.211	0.181	0.0178	0.015

Table 2. The coefficients of the empirical equation 3 on F vs. t experimental curves for H⁺/Cu²⁺ ion exchange process on weak acid resin MN 500 and C 100 H

R (mm)	No. of exp. Points	a	b	c	d	Coef. det.	F statistic
MN 500							
0.359	284	0.632±0.040	0.046±0.008	0.388±0.031	0.007±0.0008	0.9968	22496
0.331	280	0.584±0.050	0.068±0.020	0.477±0.050	0.00666±0.0005	0.9966	40340
0.294	200	0.742±0.030	0.033±0.004	0.344±0.015	0.0037±0.0005	0.9974	21787
C 100 H							
0.507	300	0.653±0.030	0.054±0.003	0.446±0.030	0.147±0.023	0.9975	38744
0.502	290	0.737±0.040	0.073±0.003	0.561±0.040	0.291±0.087	0.9949	47571
0.495	158	0.930±0.043	0.044±0.001	0.462±0.044	1.9e+5	0.9988	21812

The fractional attainment of equilibrium $F(t)$ depends only on the magnitude of the dimensionless time parameter $\tau = \frac{\bar{D}t}{r_0^2}$. When $\frac{\bar{D}t}{r_0^2}$ is small, the series 6 does not converge rapidly. In the range $F(t) < 0.85$, Reichenberg (Reichenberg, 1953) introduces the approximation (Eq. 5):

$$F(t) = \frac{6}{\pi^{3/2}}(Bt)^{1/2} - \frac{3}{\pi^2}(Bt), \text{ where } B = \frac{\bar{D}\pi^2}{r_0^2} \quad (5)$$

$$F(t) = \frac{6}{\pi^{3/2}}(\pi^2\tau)^{1/2} - \frac{3}{\pi^2}(\pi^2\tau)$$

For $F(t) > 0.6$ Reichenberg's had shown that (Eq. 6):

$$F(t) = 1 - \frac{6}{\pi} \exp(-Bt) \quad (6)$$

Less accurate than Eq. (4), but more convenient for practical use is Vermeulen's approximation (Vermeulen, 1953) which fits the whole range $0 \leq F(t) \leq 1$ (Eq. 7):

$$F(t) \cong \left[1 - \exp\left(-\frac{\bar{D}\pi^2 t}{r_0^2}\right) \right]^{1/2} \quad (7)$$

Eqs. (7) for (10) terms is not convergent when $F < 0.1$. The mean radius of the swollen resin particles in H⁺ form is higher than that in Cu²⁺ form. The size of the particles varies during the ion exchange process from the value corresponding to H⁺ form to that in the Cu²⁺ form.

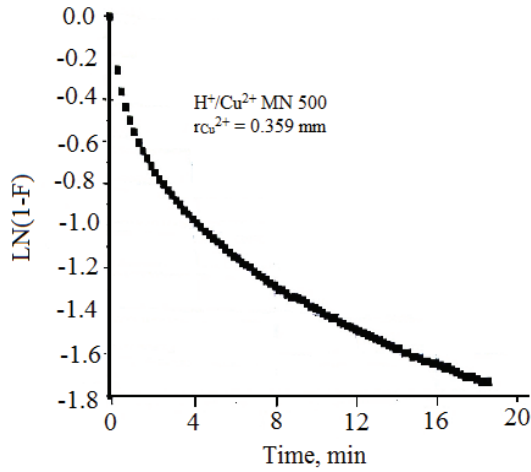


Fig. 3. Testing of the model for film diffusion controlled kinetic on H^+/Cu^{2+} ion exchange process on MN 500 at $20C$; 500 min^{-1}

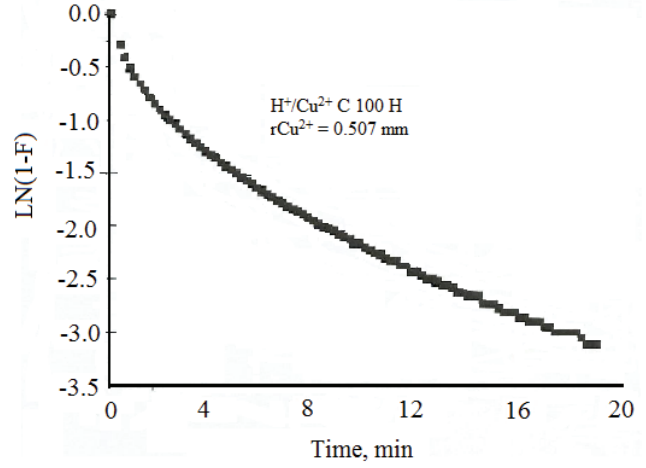


Fig. 4. Testing of the model for film diffusion controlled kinetic on H^+/Cu^{2+} ion exchange process on C 100H at $20C$; 500 min^{-1}

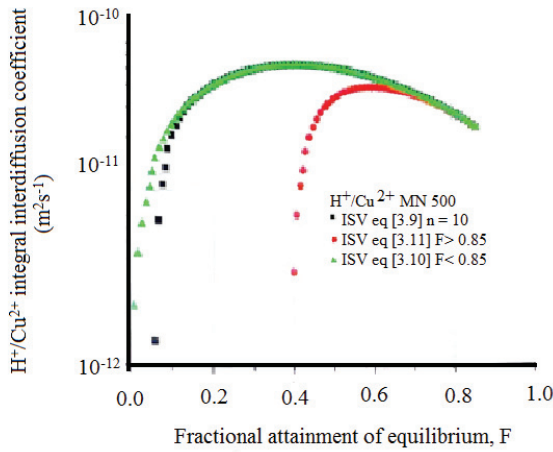


Fig. 5. The H^+/Cu^{2+} integral interdiffusion coefficients vs. fractional attainment of equilibrium calculated with QHRP models; $20C$; 0.359 mm ; 500 min^{-1} (MN 500)

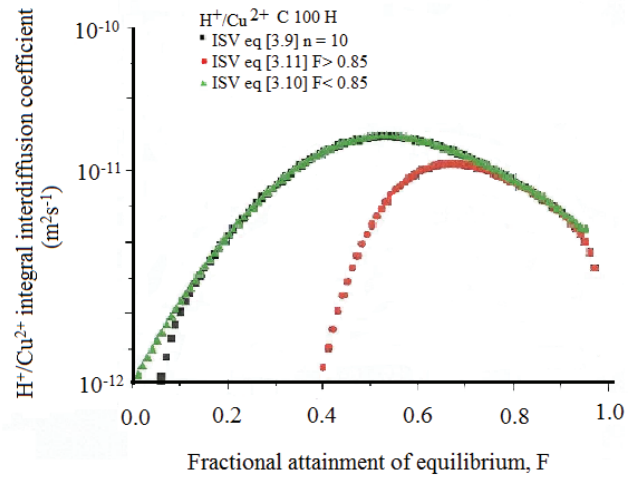


Fig. 6. The H^+/Cu^{2+} integral interdiffusion coefficients vs. fractional attainment of equilibrium calculated with QHRP models; $20C$; 0.507 mm ; 500 min^{-1} (C 100 H)

The H^+/Cu^{2+} integral interdiffusion coefficients were calculated with Eq. 8 for all size fractions using the mean radii of the swollen resin particles in H^+ and Cu^{2+} forms, being reported in Figs. 5 and 6.

$$F(t) = \frac{\omega + 1}{\omega} \left\{ 1 - \frac{1}{\alpha - \beta} \left[\frac{\alpha \exp(\alpha^2 \tau) (1 + \text{erf} \alpha \tau^{1/2})}{\beta \exp(\beta^2 \tau) (1 + \text{erf} \beta \tau^{1/2})} \right] \right\} \quad (8)$$

where α and β are the roots of the equation $x^2 + 3\omega x - 3\omega = 0$ and erf is the error function.

It can be observed that the variation of the radius beads from H^+ to Cu^{2+} form produces a small variation of the values of the interdiffusion coefficients, for the same size fractions. The interdiffusion coefficients decrease if the size fractions decreases supporting a higher resistance to diffusion in small particles compared with larger ones due to a higher degree of cross linking in small particles.

The H^+/Cu^{2+} integral interdiffusion coefficients increase with the fractional attainment of equilibrium according to the Helfferich minority rule.

4. Conclusions

The present paper was devoted to the investigation of ion exchange kinetics of systems important in waste water treatment on a weak acid gel-like resin with significantly importance in industrial packed bed applications. The investigated systems were H^+/Cu^{2+} on Purolite MN 500 and C 100H. The ion exchange rates were measured in batch systems using a potentiometric method. A procedure diminishing the interference of the electrolyte desorbition during the measurement of the ion exchange rate was established.

The experiments were performed in conditions favouring a particle diffusion controlled mechanism. The kinetic measurements were done for each system for different size fractions of the resin and different

stirring speeds in order to assign the ion exchange mechanism. The results support for all the investigated systems an ion exchange mechanism in which the ion interdiffusion inside the resin particle is the controlling step. The value of the interdiffusion coefficients inside the ion exchangers are influenced by many factors sometimes in opposite ways, with different magnitudes and it is very difficult to predict their variation in the given conditions. The integral interdiffusion coefficients calculated with Paterson approximation are in very good agreement with those obtained with the rigorous analytical solution for FSV and avoids the convergence problem and can be used to compute values for integral interdiffusion coefficients for $F < 0.1$.

The results obtained with the simplified equation proposed by Reichenberg for $F = 0.85$ are in very good agreement with those obtained with the rigorous analytical solution for ISV and avoid the problem of the series convergence.

The H^+/Cu^{2+} interdiffusion coefficients on the weak acid resin are not very well discriminated by the resin matrix of the different size fractions, having close numerical values, probably due to the close values for the radius of the hydrated ion in the resin phase.

$$\overline{D}_{H^+/Cu^{2+}} \text{ on C 100 H} > \overline{D}_{H^+/Cu^{2+}} \text{ MN 500.}$$

Acknowledgements

The work has been funded by the Sectoral Operational Programme Human Resources Development 2007-2013 of the Ministry of European Funds through the Financial Agreement POSDRU/159/1.5/S/134398.

References

- Aber S., Ayoubi-Feiz B., Salari D., (2013), Investigation of isothermal and fixed-bed column sorption of Cu (II) onto almond shell, *Environmental Engineering and Management Journal*, **12**, 3, 435-441
- Adhoum N., Monser L., Bellakhal N., Belgaied J.E., (2004), Treatment of electroplating wastewater containing Cu^{2+} , Zn^{2+} and Cr^{6+} by electrocoagulation, *Journal of Hazardous Materials*, **112**, 3, 207-213,
- Ahmaruzzaman M., (2011), Industrial wastes as low-cost potential adsorbents for the treatment of wastewater laden with heavy metals, *Advances in Colloid and Interface Science*, **166**, 36-59
- Anis M., Haydar S., Bari A.J., (2013), Adsorption of lead and copper from aqueous solution using unmodified wheat straw, *Environmental Engineering and Management Journal*, **12**, 11, 2117-2124
- Basha A.C., Somasundaram M., Kannadasan T., Lee C.W., (2011), Heavy metals removal from copper smelting effluent using electrochemical filter press cells, *Chemical Engineering Journal*, **171**, 563-571
- Bensacia N., Fechete I., Moulay S., Debbih-Boustila S., Boos A., Garin F., (2014), Removal of cadmium (II) from aqueous media using cooh/tud-1 mesoporous solid. Kinetic and thermodynamic studies, *Environmental Engineering and Management Journal*, **13**, 10, 2675-2686
- Bohdana C., Cantea D.S., Dale J.A., Pincovschi E., Oancea AMS., (2008), Polymeric ion exchangers based on styrene-divinylbenzene matrix. Textural and structural modifications after grafting different functional groups, *Proceedings IEX Cambridge*, 427-434
- Crini G., Morin-Crini N., Fatin-Rouge N., Déon S., Fievet P., (2014), Metal removal from aqueous media by polymer-assisted ultrafiltration with chitosan, *Arabian Journal of Chemistry*, doi:10.1016/j.arabjc.2014.05.020.
- Delvaux B., Kruyts N., Cremers A., (2000), Rhizosphere mobilization of radiocesium in soils, *Environmental Science and Technology*, **34**, 1489-1493
- Fu L., Shuang C., Liu F., Li A., Li Y., Zhou Y., Song H., (2014), Rapid removal of copper with magnetic polyacrylic weak acid resin: Quantitative role of bead radius on ion exchange, *Journal of Hazardous Materials*, **272**, 102-111.
- Helfferich F., (1995), *Kinetics, Ion Exchange*, Dover Publications INC., New York, 250-319.
- Imamoglu M., Tekir O., (2008), Removal of copper (II) and lead (II) ions from aqueous solutions by adsorption on activated carbon from a new precursor hazelnut husks, *Desalination*, **228**, 108-113.
- Kononova O.N., Kuznetsova M.A., Mel'nikov A.M., Karplyakova N.S., Kononov Y.S., (2014), Original scientific paper Sorption recovery of copper (II) and zinc (II) from chloride aqueous solutions, *Journal of the Serbian Chemical Society*, **79**, 1037-1049.
- Oancea A.M.S., Drinkal C., Höll W.H., (2008), Evaluation of exchange equilibria on strongly acidic ion exchangers with gel, -type, macroporous and macronet structure, *Reactive and Functional Polymers*, **68**, 492-506
- Pollution Database, (2004), Copper and its compounds, European Pollutant Emission Register, On line at: <http://pollution.unibuc.ro/?substance=20>.
- Reichenberg D., (1953), Properties of ion-exchange resins in relation to their structure, III: Kinetics of exchange, *Journal of the American Chemical Society*, **75**, 596
- Samarghandi M.R., Zarrabi M., Amrane A., Soori M.M., Sepehr M.N., (2013), Removal of acid black dye by pumice stone as a low cost adsorbent: kinetic, thermodynamic and equilibrium studies, *Environmental Engineering and Management Journal*, **12**, 2137-2147.
- Sousa F.W., Oliveira A.G., Ribeiro J.P., Rosa M.F., Keukeleire D., Nascimento R.F., (2010), Green coconut shells applied as adsorbent for removal of toxic metal ions using fixed-bed column technology, *Journal of Environmental Management*, **9**, 1634-1640
- Weber V., Popescu A.R., Oancea AMS., (2008), Interdiffusion coefficients in gel and macroporous weak acid resins, *Revista de Chimie*, **59**, 5, 519-524.
- Yahaya N.K.E.M., Abustana I., Latiff M.F.P.M., Bello O.S., Ahmad M.A., (2011), Fixed-bed column study for Cu(II) removal from aqueous solutions using rice husk based activated carbon, *International Journal of Engineering & Technology*, **11**, 186-190.



"Gheorghe Asachi" Technical University of Iasi, Romania



BIOSORPTION OF ANTIMONY BY BROWN ALGAE

S. muticum AND *A. nodosum*

Gabriela Ungureanu, Sílvia Santos*, Rui Boaventura, Cidália Botelho

LSRE – Laboratory of Separation and Reaction Engineering, Associate Laboratory LSRE/LCM, Faculdade de Engenharia da Universidade do Porto, Rua Dr. Roberto Frias, 4200-465 Porto, Portugal

Abstract

Environmental contamination by antimony has been described as a critical issue in many articles. In this study, the Sb(III) removal by two brown algae, *Sargassum muticum* and *Aschophylum nodosum*, has been tested. Algae were collected in Viana do Castelo beach (Portugal). Preliminary tests were carried out and, based on the results, *Sargassum muticum* was chosen for subsequent experiments. Kinetic data were described by pseudo second order model. After about four hours contact time the equilibrium was achieved. A slight effect of pH was observed in the removal efficiency of Sb by *S. muticum*. Adsorption equilibrium isotherm was determined for pH 5. Langmuir model predicted a maximum adsorption capacity of 5.4 ± 0.8 mg/g. The present study revealed that the alga *S. muticum* can be used as a low-cost adsorbent for antimony removal from aqueous solution.

Key words: algae, antimony, biosorption, low cost adsorbents, oxyanions

Received: November, 2014; *Revised final:* February, 2015; *Accepted:* February, 2015

1. Introduction

Antimony is a natural occurring metalloid, but can also be introduced in environment by anthropogenic sources since it is used in brake linings, in semiconductor components, flame retardants, as catalyst in plastics, addictive in glassware and ceramics and in ammunition.

In aqueous solution, antimony is present as oxyanion and speciation is defined by pH and pE conditions. Antimony can exist in four oxidation states, Sb(V), Sb(III), Sb(0) and Sb(-III), but in the environment it is usually present in the oxidation state (+5), antimonate, in aerobic environments, and (+3), antimonite, in anaerobic environments (Wilson et al., 2010). Sb(III) is considered ten times more toxic than Sb(V) (Bencze, 1994; Stemmer, 1976). The guideline of the World Health Organization is a maximum concentration of 5 µg/L antimony in water for human consumption (WHO, 2011). The most common form of a body being exposed to contamination by antimony is through the ingestion

of food and water. Antimony is classified as a toxic pollutant, potentially carcinogenic to humans and therefore considered a pollutant of priority interest by entities such as the Environmental Protection Agency of the United States (USEPA, 1979) and the European Union (UE, 1976).

References for purification of water containing antimony, especially for drinking water, are quite limited. The most common studied methods for antimony removal are coagulation/flocculation (Guo et al., 2009; Wu et al., 2010), membrane processes (Kang et al., 2000; Saito et al., 2004), electroprocesses (Koparal et al., 2004; Zhu et al., 2011) and adsorption (Sarı et al., 2010; Shan et al., 2014; Xi et al., 2013). Adsorption has been viewed as a simple and relative low-cost process, suitable for removing low levels of contaminants and applicable for point-of-use treatment. A broad range of adsorbents comprising metal oxides, hydroxides and minerals (Li et al., 2012; Xu et al., 2011), sorbents based on residues and waste materials (Biswas et al., 2009) and biomaterials (Sun et al., 2011;

* Author to whom all correspondence should be addressed: e-mail: scrs@fe.up.pt; Phone: (351) 22 508 1885; Fax: (351) 22 508 1674

Vijayaraghavan and Balasubramanian, 2011) have been studied for antimony removal from water. A good adsorbent should have a low cost while providing high removal efficiency. Biosorption has been increasingly studied in recent years because this technique has the great advantage to have a lower cost compared to conventional methods. The biosorbents capacity improvement has been evaluated by surface modification treatments such as protonation or iron pre-treatment (Davis et al., 2003).

Algae are divided into three broad categories: brown algae (Phaeophyta), red algae (Rhodophyta) and green algae (Chlorophyta) (Dunn, 1998). Brown algae are classified into about 265 genera of more than 1500 species are all multicellular, present chloroplasts (golden brown) containing chlorophyll a and c, and β -carotenoid fucoxanthin (pigment), which masks the green color of chlorophyll. Polysaccharides represent more than 65% of the cellular constituents of the algae and alginic acid is the major polysaccharide from brown algae (Davis et al., 2003).

Algal biomass is an available natural material with a very low cost. Algae, especially the brown type, have been extensively used as biosorbents for heavy metals, and several studies have demonstrated the good adsorption ability for metal cations (Cazón et al., 2012; Dittert et al., 2013; Freitas et al., 2008; Kleinubing et al., 2011; Lupea et al., 2012; Sheng et al., 2004). However, its use as biosorbent for metal or metalloids anions is scarcely studied (Vijayaraghavan and Balasubramanian, 2011). In this research, the antimony removal by marine brown macroalgae *Sargassum muticum* and *Aschophyllum nodosum*, has been tested. *Sargassum muticum* belongs to domain Eukaryota, kingdom Chromalveolata, phylum Heterokontophyta, class Phaeophyceae, order Fucales, family Sargassaceae, and genus *Sargassum*. *Aschophyllum nodosum* belong to kingdom Chromalveolata, phylum Heterokontophyta, class Phaeophyceae, order Fucales, family Fucaceae and genus *Aschophyllum*. Araujo et al. (2006) characterized the existing macroalgae communities in the pools in the intertidal zone and rocks, over 60 km from the northwest coast of Portugal. The authors found that the *Sargassum muticum* is located preferably in the pools in the intertidal zone (98.8%) and *Aschophyllum nodosum* is almost entirely on the rocks (99.1%). Chemical characterization of biosorbents under study was performed. The algae were previously tested in virgin form and pre-treated with nitric acid. Equilibrium and kinetic studies were performed in batch, testing the effect of pH and concentration.

2. Experimental methods

2.1. Chemicals

Antimony standard solutions were prepared from a standard solution 1000 mg/L Sb(III) solution (*CarloErba*). The pH was adjusted to the required

values using HNO₃ and NaOH aqueous solutions, prepared from HNO₃ 65% PA (*Sigma Aldrich*) and NaOH pellets 99% purity (*Merck*). All the solutions were prepared in ultrapure water produced by *Millipore system (Direct-Q model)*.

2.2. Glassware preparation

All the glassware and plastic material used in experimental tests were washed by soaking for 24 hours in HNO₃ 20% solution, rinsed with distilled water and dried in the oven.

2.3. Biomass preparation

The two brown seaweeds, *Sargassum muticum* and *Aschophyllum nodosum*, were collected in Viana do Castelo beach (Portugal) in February of 2013. The seaweeds were firstly washed with tap water and following with distilled water until achieving a low conductivity. The seaweeds were air-dried during 2 days, and then dried overnight in the oven at 60°C, milled in 5 mm granulometry and stored in a desiccator. In this paper these seaweeds, without further treatment, will be named as virgin algae: virgin *S. muticum* (VM) and virgin *A. nodosum* (VN).

It was also decided to perform a protonation of the seaweeds. The main purpose of this chemical treatment is to facilitate the contact of the functional groups responsible for metal binding, creating new groups and reinforce biomass capacity. Untreated biomass generally contains light metal ions (potassium, sodium, calcium, magnesium). The protons in the strong acid treatment displace these light metals from the binding sites (Davis et al., 2003). However, the use of pretreatments is economically unadvisable in cases where the increase in process efficiency is not significant.

The virgin seaweed (8 g/L) was contacted for 6h with 1M solution of HNO₃, under agitation (150-200 rpm). After contact, the alga was washed with distilled water in several cycles until the wash water achieved a pH about 4 – 4.5. This protonated alga was also dried in the oven at 60°C and stored in desiccator. In this paper, the acid treated algae were designated as protonated *S. muticum* (PM) and protonated *A. nodosum* (PN).

2.4. Analytical procedures

Atomic adsorption spectrometry (AAS; spectrophotometer *GBC 932 Plus*) was the technique used to determinate the concentration of antimony in aqueous solution. Analyses were done using the following technical parameters: air/acetylene flame, 10mA lamp current, 217.6 nm wavelength, 2 nm slit, deuterium background correction, with triplicate readings and a detection limit of 0.4 mg/L. Before AAS analysis the samples were filtered using cellulose acetate membrane filters (45 μ m porosity).

Total antimony concentrations in algae were also measured. Samples were analyzed by graphite

furnace (*GBC SenAA Dual*) due to the very low levels of antimony detected. The analysis was performed with 217.6 nm wavelength, slit 0.2 nm, 10 mA lamp current and background correction. The detection limit was 3 µg/L.

2.5. Chemical characterization

Volatile matter was analyzed by calcination at 550°C for 2 hours (Method no. 2540E; APHA, 1999). Metals contents (Fe, Mn, Al, K, Mg, Na, Ca, Sb) present in virgin and protonated algae were determined by digesting 1.5 g of biomass in glass tubes at 150°C for 2h with 5.0 ml of distilled water, 12 ml of HCl (*Merck*) and 4ml of HNO₃ (*Merck*). After digestion, solutions were filtered through cellulose acetate membrane filters (*SantoriusStedim*). Samples were digested in duplicate and a blank digestion was also performed.

Metal concentrations were determined by flame AAS and antimony concentration by graphite furnace.

2.6. FTIR - Fourier transform infrared analysis

Infrared spectroscopy (*Shimadzu FTIR IRAffinity*) was performed in order to identify the predominant functional groups on the biosorbent surface. The algae were ground and used in solid form using diffuse reflectance accessory. Spectra were registered between 4000 and 400 cm⁻¹.

2.7. Screening adsorption tests

These simple adsorption tests were conducted to evaluate the adsorption ability of the different seaweeds (in virgin and treated forms). Adsorption tests were performed in Erlenmeyer flasks containing 50 mL of 10 mg Sb/L solution, at different pH (2, 3, 4 and 5), and 100 mg of VM, VN, PM and PN, accurately weighed. The suspensions were stirred (*PlacaMulti 15 Stirrer, Velp*), at 200 rpm, under room temperature (23°C±1).

pH was monitored regularly and readjusted if necessary, in order to maintain a constant value (±0.5). After a 6h contact time, samples were filtered and concentrations of antimony in liquid phase analyzed by AAS. The amount of antimony adsorbed in the equilibrium (q , mg/g) was calculated by a mass balance equation (Eq. 1):

$$q = \frac{C_0 - C}{C_s} \quad (1)$$

where C_0 is the initial Sb concentration in the liquid phase (mg/L), C is the concentration after adsorption (mg/L) and C_s is the sorbent dosage (g/L).

2.8. Adsorption kinetic studies

Based on the results of screening tests, the algae VM was selected for further equilibrium and kinetics studies. Adsorption kinetic studies were done

in Erlenmeyer flasks containing 50 mL of 10 mg Sb/L solution in contact with 2 g/L of VM, under magnetic agitation (*PlacaMulti 15 Stirrer, Velp*, at 200 rpm) and room temperature (23°C±1). The stirring rate values considered sufficient to ensure that all active centers of biomass are available for metal removal, ranges between 150 rpm (Martins et al, 2006) and 300 rpm (Yang and Volesky, 1996). It is considered therefore that the effect of external diffusion in the film can be assumed as negligible.

The dynamic kinetic study was conducted for various constant pH values (2; 3; 4 and 5), adjusted on the beginning of the test and corrected when necessary. The content of each Erlenmeyer flask was let in agitation for previously established time intervals in order to obtain the Sb concentration decay at different contact times. The quantity of antimony removed from the solutions by algae material was determined by the difference between the initial concentration of antimony on that sample and the final concentration in the same sample, measured by AAS and calculated with Eq. (1).

2.9. Adsorption equilibrium studies

Sorption isotherms were performed at pH 5 and room temperature (23°C±1). The initial antimony concentration ranged between 2-20 mg/L. Equilibrium studies were performed in Erlenmeyer flasks. The volume of antimony solution in each flask was 50 mL and the biomass concentration 2 g/L (accurately weighed for each sample). The contact between the sorbent and antimony solution was under constant magnetic stirring (200 rpm). After the equilibrium point reached (about 4 hours), the residual antimony concentration (C) was determined by AAS and the amount of Sb adsorbed per algebra mass unity (q) calculated by Eq. (1).

3. Results and discussion

3.1. Chemical characterization

The values obtained for the volatile matter concentrations were calculated based on the dry weight of samples. Table 1 presents the results of volatile matter contents for algae *Sargassum muticum* and *Aschophylum nodosum*, in virgin and protonated forms, expressed in percentage of loss of weight.

Table 2 presents metallic elements content in virgin and protonated algae. Predominant elements are sodium, potassium, calcium and magnesium, which are in fact the predominant elements in the constitution of seawater. After the acid treatment, the concentration of all components decreased by dissolution in the aqueous phase. The values obtained for antimony concentration in seaweeds are negligible.

3.2. FTIR – Fourier transform infrared analysis

The Infrared Spectroscopy by Fourier Transform allows identifying functional groups

present in the biosorbents surface that can help to evaluate the adsorption mechanism. The functional groups are identified by the presence of bands at certain characteristic frequencies. Fig. 1 shows the FTIR spectra of both the virgin biosorbents.

Table 3 summarizes the dominants stretching frequencies observed in seaweeds. The broad band between 3000-3750 cm^{-1} confirms the presence of the O-H group of glucose, constituent of the cell wall of a vegetal cell, and the N-H groups of proteins (Deng et al., 2007). The absorption band at 3000-2800 cm^{-1} may be due to C-H distention of aliphatic chains, asymmetric and symmetric respectively (Murphy et al, 2007; Sheng et al., 2004). The small band detected at about 1700-1680 cm^{-1} and those at 1550 and 1460 cm^{-1} correspond to the distention C=O of chelate and to the distention C=O of carboxyl groups (Fourest and Volesky, 1996). The band at 1180 cm^{-1} may be due to C-N distention in proteins (Park et al., 2005). The 830 cm^{-1} band suggests the presence of S=O bonds (Fourest and Volesky, 1996).

The IR spectrum indicates that several types of functional groups are present in the structure of VM and VN and these groups can interact with metal ions from aqueous solutions during the sorption process. Therefore, metal ions can be bound by specific chemical interactions.

3.3. Screening Tests results

Preliminary tests were performed with VM, PM, VN and PN for pH 2, 3, 4 and 5. Fig. 2 shows the results of these preliminary tests.

Antimony concentration in the solid phase, q (mg/g), evaluates the capacity of the algae to adsorb antimony from aqueous solutions. The results of screening tests suggest that the best biosorbents for antimony are VM and PM at pH 4 and 5. A slight increase in the adsorbed amount was observed with the increase in pH from 2 to 4-5, especially for VM and PN algae.

Table 1. Percentage of volatile matter in studied algae

<i>Sargassum muticum</i>	VM	74 %
	PM	98 %
<i>Aschophylum nodosum</i>	VN	79 %
	PN	99 %

Table 2. Metals content in virgin and protonated algae

	Fe (mg/g)	Mn (mg/g)	Al (mg/g)	K (mg/g)	Mg (mg/g)	Na (mg/g)	Ca (mg/g)	Sb ($\mu\text{g/g}$)
VM	0.24	<0.05	<0.05	83	11	14	12	< 0.7
PM	0.15	<0.05	<0.05	0.27	0.28	0.55	1.10	< 0.7
VN	0.09	<0.05	0.06	25	10	25	16	< 0.7
PN	0.21	<0.05	0.09	0.76	0.48	0.47	0.21	< 0.7

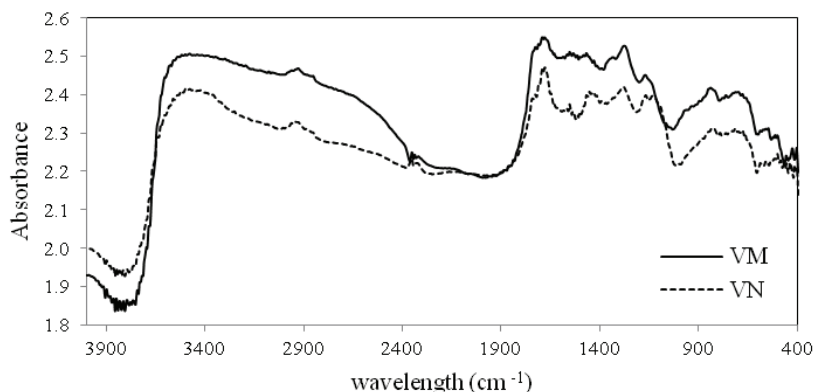


Fig. 1. FTIR spectra of VM and VN

Table 3. Dominants stretching frequencies in seaweeds FTIR spectra

Band	Symbol of functional groups	Name of functional groups
3750 - 3000	O-H	Hydroxyl
3000 - 2800	C-H	Methyl
1680 - 1700	C=O	Carboxyl
1550	C=O	Carboxyl
1460	C=O	Carboxyl
1290	S=O	Sulfate
1180	C-N / C-O	Ether
830	S=O	Sulfate

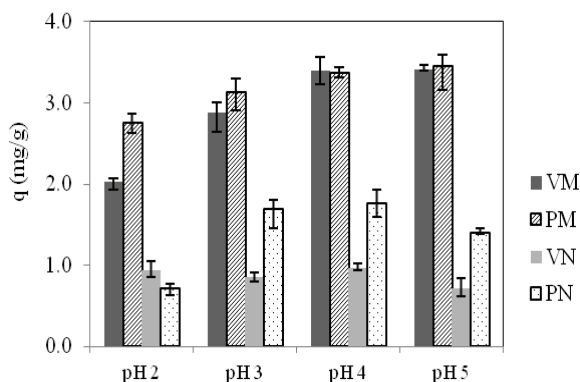


Fig. 2. Adsorbed amount of Antimony by *VM*, *PM*, *VN* and *PN* using 10mg/L Sb solution, 2g/L algae concentration and different pHs

This behavior can be explained considering the charge of both adsorbent and adsorbate in different pH conditions. According to speciation diagrams available in literature (Filella et al., 2002), Sb(III) occurs in water under the form of $\text{Sb}(\text{OH})_2^+$ (extreme acidic pH), H_3SbO_3 or $\text{Sb}(\text{OH})_3$ (pH 2-10) and H_2SbO_3^- or $\text{Sb}(\text{OH})_4^-$ (strong alkaline pH). On the other side, the charge of the adsorbent tends to be more positive for lower pH values. At extreme acidic pH values, alga and Sb appeared as positively charged and adsorption was then limited by repulsion. In the present study, pH values higher than 5 were not studied, since it was expected that the majority of the wastewaters contaminated with antimony (from mining, for example) are acidic.

VM and *PN* algae showed the most interesting results with similar adsorbed amounts at pH 4-5. However, *PN* performance at pH 2 was significantly worse than *VM*. *PN* also requires a pre-treatment step (with strong acid) which implies higher costs. *VM* was then selected, instead of *PM*, for kinetic and equilibrium studies.

3.4. Adsorption kinetic studies

The kinetic study represents the first step in determining the inter-dependencies between equilibrium phenomenon and mass transfer, establishing a predictive model of the sorption behavior. Experimental results obtained in the kinetic study of Sb(III) biosorption by *VM* seaweed are presented in Fig. 3.

The kinetic curves can be divided into two phases, a first phase fast enough (0 - 30 minutes) and a second slower phase (30-480 minutes). More than 35% of the biosorption equilibrium capacity occurs in the first 15 min. In 30 minutes of biosorption, more than 50% of the equilibrium capacity was achieved. The equilibrium time, for the different systems is about 4h, since there were no further significant changes on the biosorbed amount of Sb. Several authors have reported fast kinetics for antimonite removal, with contact times lower than

few hours (Uluozlu et al., 2010; Vijayaraghavan and Balasubramanian, 2011; Wu et al., 2012).

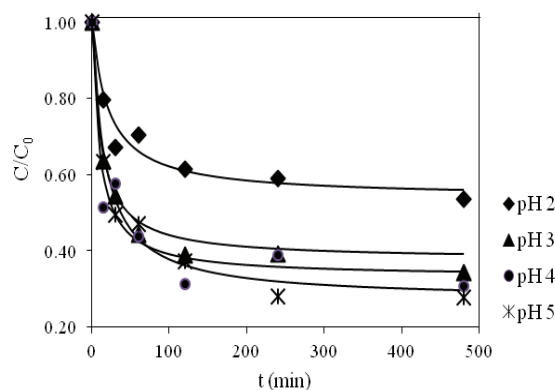


Fig. 3. Kinetics for Sb(III) biosorption on *VM* at different pH (initial concentration 10mg/L Sb solution, alga dosage 2g/L and 23°C): experimental data and pseudo-second order model

In fact, the fast biosorption kinetics of metals present a very significant practical importance, allowing the use of smaller columns with continuous operation, in an efficient and economical way (Aksu, 2001).

The most commonly used models to describe adsorption kinetics are the pseudo 1st order and pseudo 2nd order models. The pseudo 1st order model or Lagergren (1898) considers that the occupancy rate of the active centers by the metal in aqueous solution is proportional to the number of available centers. It also assumes that the surface is homogeneous and active centers have the same affinity for the metal ion. Pseudo-1st order model is expressed by Eq. (2), where q (mg g^{-1}) is the biosorption capacity for a determined contact time t (min), q_e (mg g^{-1}) the biosorption capacity in equilibrium and k_1 (min^{-1}) is the kinetic constant.

$$q = q_e(1 - e^{-k_1 t}) \quad (2)$$

In accordance, the initial uptake rate, h_1 ($\text{mg g}^{-1} \text{min}^{-1}$) is given by Eq. (3).

$$h_1 = k_1 q_e \quad (3)$$

The pseudo 2nd order model (Ho et al., 1996) is based on the sorption capacity of the solid phase and assumes a homogeneous surface and metal binds to two active centers. Pseudo 2nd model is represented by the Eq. (4), where k_2 ($\text{g mg}^{-1} \text{min}^{-1}$) is the kinetic constant of second order.

$$q = \frac{k_2 q_e^2 t}{1 + k_2 q_e t} \quad (4)$$

The initial biosorption rate, h_2 ($\text{mg g}^{-1} \text{min}^{-1}$) is determined by Eq. (5):

$$h_2 = k_2 q_e^2 \tag{5}$$

Pseudo 1st and pseudo 2nd order models were fitted to experimental kinetic data by non-linear regression using *CurveExpert* software. The obtained parameters for the models are presented in Table 4. Fig. 4 presents the modeled curves for the experimental data obtained for pH 5.

It was found that the models of pseudo 1st order and pseudo 2nd order adequately represent the experimental results, with coefficients of determination values (R^2) exceeding 0.9. Pseudo-second order model presented however the best determination coefficients. It also predicted q_e values closer to the experimental ones. Fig. 3 presents modeled curves (pseudo-second order model) for the different pH conditions data.

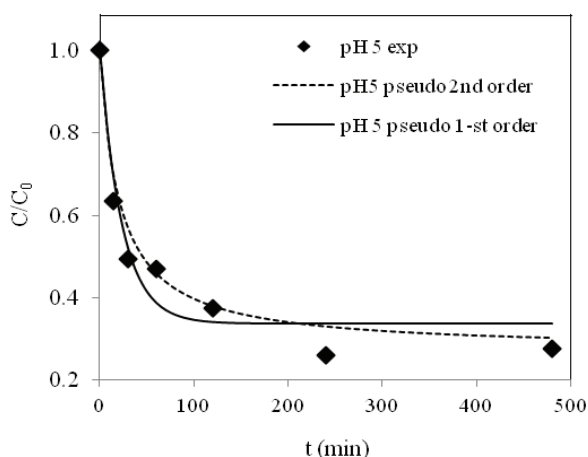


Fig. 4. Kinetics for Sb biosorption on VM at pH 5 (initial concentration: 10mg/L Sb solution; alga dosage: 2g/L alga and 23°C): experimental data and modeling

It is observed that as the pH increased from 2 to 4, maximum biosorbed amount also increased. Similar values (3.3 ± 0.5 mg/g and 3.5 ± 0.1 mg/g) were obtained at pH 4 and 5. This is in agreement with the results obtained in the screening tests. In the present study, pH above 5 was not tested, since most important effluents containing antimony (mine effluents) present pH typically in acidic range. Although different maximum adsorbed amounts were achieved in different pH conditions, kinetic constants are relatively close.

Considering the pseudo-second order model, initial biosorption rates (evaluated by Eq. 5) are 0.095, 0.25, 0.33 and 0.25 $\text{mg g}^{-1} \text{min}^{-1}$, at pH 2, 3, 4 and 5, respectively. However, considering the

corresponding 95% confidence interval, the initial biosorption rates do not vary significantly with pH, lying in the range 0.06-0.8 $\text{mg g}^{-1} \text{min}^{-1}$.

3.5. Adsorption equilibrium studies

Equilibrium isotherms represent the relation between the concentration of a solute in the liquid phase and the equilibrium concentration on the biosorbent particles, at a given temperature. The isotherms give information about the affinity of adsorbent to the adsorbate and the maximum biosorption capacity.

The biosorption isotherm for Sb(III) adsorption by VM seaweed is presented in Fig. 5. Results were obtained at 23°C, using an adsorbent dosage of 2 g/L and varying the initial concentration of antimony from 2 to 20 mg/L. Langmuir and Freundlich models were adjusted to experimental data. The Langmuir model (1918) assumes: the active centers are uniformly distributed over the surface of the adsorbate, with constant adsorption energy and the same affinity; a monolayer coverage of adsorbed species; no interactions between the adsorbed species in adjacent sites. The expression of Langmuir model is given by the Eq. (6).

$$q_e = \frac{K_L Q_{max} C_e}{1 + K_L C_e} \tag{6}$$

where q_e (mg g^{-1}) the equilibrium concentration of solute in the solid phase, C_e (mg L^{-1}) the equilibrium concentration of solute in the liquid phase, Q_{max} (mg g^{-1}) the maximum biosorption capacity and K_L (mg L^{-1}) Langmuir constant.

According to Hall et al. (1966), Langmuir isotherm can be expressed in terms of a dimensionless constant, separation factor (R_L), defined by the following Eq. (7).

$$R_L = \frac{1}{1 + K_L C_0} \tag{7}$$

Therefore, it is possible to predict, from the profile of the isotherm, if the biosorption system is favorable ($0 < R_L < 1$), unfavorable ($R_L > 1$), linear ($R_L = 1$) or irreversible ($R_L = 0$).

The Freundlich isotherm (1906) is an empirical expression given by Eq. (8). This model assumes a heterogeneous sorption surface with different energy active centers.

Table 4. Parameters for kinetic models (value \pm interval for 95% confidence)

	Pseudo first order			Pseudo second order		
	q_e (mg/g)	k_1 (min^{-1})	R^2	q_e (mg/g)	k_2 ($\text{g mg}^{-1} \text{min}^{-1}$)	R^2
pH 2	1.79 \pm 0.01	0.04 \pm 0.01	0.92	2.08 \pm 0.09	0.022 \pm 0.006	0.96
pH 3	2.65 \pm 0.08	0.056 \pm 0.008	0.98	2.85 \pm 0.03	0.031 \pm 0.002	0.99
pH 4	3.1 \pm 0.6	0.06 \pm 0.05	0.89	3.3 \pm 0.6	0.03 \pm 0.02	0.93
pH 5	3.2 \pm 0.4	0.04 \pm 0.02	0.94	3.5 \pm 0.1	0.021 \pm 0.003	0.98

$$q_e = K_F C_e^{1/n_F} \quad (8)$$

where K_F ($(\text{mg g}^{-1})(\text{L m}^{-1})^{1/n_F}$) is a constant for the adsorbate-adsorbent system and n_F is a constant that indicates the intensity of adsorption ($n_F > 1$ favorable isotherm; $n_F \leq 1$ unfavorable isotherm).

Model fitting to Eqs. (6) and (8) was performed by non-linear regression using *CurveExpert* software and the model parameters are presented in Table 5.

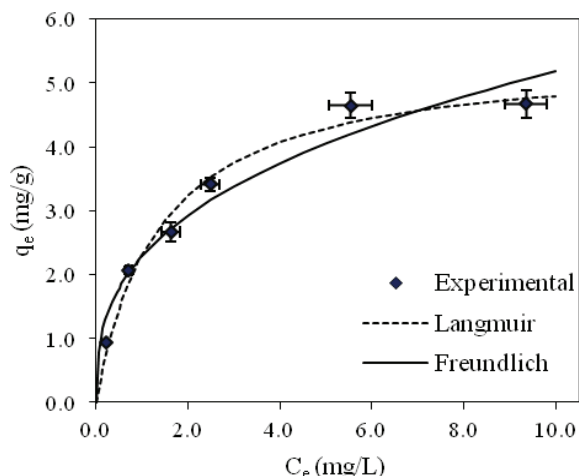


Fig. 5. Equilibrium isotherm for Sb biosorption on VM at pH 5, 2g/L alga and 23°C: experimental data and modeling

Table 5. Parameters for equilibrium models (value ± interval for 95% confidence)

Langmuir	Freundlich
$Q_{max} = 5.5 \pm 0.8 \text{ mg/g}$	$1/n_F = 0.36 \pm 0.04$
$K_L = 0.7 \pm 0.3 \text{ L/mg}$	$K_F = 2.3 \pm 0.1 \text{ mg g}^{-1}(\text{mg.L}^{-1})^{1/n}$
$R^2 = 0.99$	$R^2 = 0.97$

Both models represent quite well the experimental data, with values for the determination coefficients higher than 0.97. Even so, the Langmuir model best describes equilibrium data, with a correlation coefficient of 0.99, and predicted a maximum biosorption capacity close to that obtained experimentally. Also, the separation factor R_L calculated by Eq. (7), and using the highest initial Sb concentration is 0.07, a value between 0 and 1, which indicates a favorable process.

The Langmuir model revealed a maximum biosorption capacity of 5.5 mg/g for the VM seaweed. Wu et al. (2012) used *Microcystis* biomass and obtained an adsorption capacity of 4.88 mg/g for Sb(III), at pH 4. This value is quite similar to the one reported in present study, but it was obtained using much higher initial concentration ranges (0 to 400 mg/L). Cyanobacteria *Synechocystis sp.* was tested by Mu (2011) and a maximum biosorption capacity of 4.68 mg/g, using a initial concentration range from 5 to 100 mg/L Sb(III) was reported. Other authors presented higher adsorption capacities, such as 81.1 mg/g, for lichen, *PhysciaTribacia* (Uluozlu et al.,

2010), 14.9 mg/g (at pH 6) for *Sargassum sp.* (brown alga) (Vijayaraghavan and Balasubramanian, 2011). Much higher adsorption capacities have been obtained by binary metal oxides, for example 214 mg/g, at pH 3, for a Fe-Mn oxide (Xu et al., 2011); this kind of material requires however synthesis and then costs of preparation.

4. Conclusions

Algae are effective biosorbents for the removal of antimony(III) from aqueous solutions. The maximum adsorption capacity of the *Sargassum muticum* is 5.5 mg/g, at pH 5 and 23 °C. Equilibrium data was adequately described by both Langmuir and Freundlich models. The biosorption equilibrium was reached in approximately 4 hours.

The pseudo-second order kinetic model reasonably described the biosorption kinetics. It is important to note that this study was conducted using a biosorbent found in abundance in nature that requires no preparation. The study was conducted in a range of Sb concentration found in typical conditions in liquid effluents contaminated with antimony.

Acknowledgements

This work was partially supported by project Pest-C/EQB/LA0020/2013 financed by FCT and FEDER through COMPETE, and by QREN, ON2 and FEDER. G. Ungureanu acknowledges her PhD scholarship (SFRH/BD/77471/2011) by FCT. S. Santos acknowledges her postdoctoral scholarship by ON2 (NORTE-07-0124-FEDER-000008 RL1-P3).

References

- Aksu Z., (2001), Equilibrium and kinetic modelling of cadmium(II) biosorption by *C. vulgaris* in a batch system: effect of temperature, *Separation and Purification Technology*, **21**, 285-294
- APHA, (1999), Standard methods for the examination of water and wastewater, APHA/AWWA/WEF, American Public Health Association (APHA), 20th Ed., Washington, DC.
- Araujo R., Sousa-Pinto I., Barbara I., Quintino V., (2006), Macroalgal communities of intertidal rock pools in the northwest coast of Portugal, *Acta Oecologica*, **30**, 192-202.
- Benze K., (1994), *Antimony. Handbook on Metals*, In: *Clinical and Analytical Chemistry*, Seiler H.G., Sigel A., Sigel H. (Eds.), New York, Marcel Dekker, 227-236.
- Biswas B.K., Inoue J., Kawakita H., Ohto K., Inoue K., (2009), Effective removal and recovery of antimony using metal-loaded saponified orange waste, *Journal of Hazardous Materials*, **172**, 721-728.
- Cazón J.P.H., Benítez L., Donati E., Viera M., (2012), Biosorption of chromium(III) by two brown algae *Macrocystispyrifera* and *Undariapinnatifida*: equilibrium and kinetic study, *Engineering in Life Sciences*, **12**, 95-103.
- CEC, (1976), Council Directive 76/substances discharged into aquatic environment of the community, Council

- of the European Communities, *Official Journal, L*, **129**, 23–29.
- Davis A.T., Voleskya B., Mucci A., (2003), A review of the biochemistry of heavy metal biosorption by brown algae, *Water Research*, **37**, 4311–4330.
- Deng L., Su Y., Su H., Wang X., Zhu X., (2007), Sorption and desorption of lead (II) from wastewater by green algae *Cladophora fascicularis*, *Journal of Hazardous Materials*, **143**, 220-225.
- Dittert I., Vilar V., Silva E., Souza S., Souza A., Botelho C., Boaventura R., (2013), Turning *Laminaria digitata* Seaweed into a Resource for Sustainable and Ecological Removal of Trivalent Chromium Ions from Aqueous Solutions, *Clean Technologies and Environmental Policy*, **15**, 955-965.
- Dunn C.E., (1998), *Seaweeds as Hyperaccumulators*. In: *Plants that Hyperaccumulate Heavy Metals. Their Role in Phytoremediation, Microbiology, Archaeology, Mineral Exploration and Phytomining*, Brooks R.R. (Ed.), CAB International, New York, 119-125.
- Filella M., Belzile N., Chen Y.W., (2002), Antimony in the environment: a review focused on natural waters I. Occurrence, *Earth-Science Reviews*, **57**, 125-176.
- Fourest E., Volesky B., (1996), Contribution of sulfonate groups and alginate to heavy metal biosorption by the dry biomass of *Sargassum fluitans*, *Environmental Science Technology*, **30**, 277-282.
- Freitas O.M.M., Martins R.J.E., Delerue-Matos C.M., Boaventura R.A.R., (2008), Removal of Cd(II), Zn(II) and Pb(II) from aqueous solutions by brown marine macro algae: kinetic modeling, *Journal of Hazardous Materials*, **153**, 493–501.
- Guo X.J., Wu Z.J., He M.C., (2009), Removal of antimony(V) and antimony(III) from drinking water by coagulation-flocculation-sedimentation (CFS), *Water Research*, **43**, 4327-4335
- Hall K.R., Eagleton L.C., Acrivos A.E., Vemeulen T., (1966), Pore and solid diffusion kinetics in fixed bed adsorption under constant pattern conditions, *Industrial and Engineering Chemistry Fundamentals*, **5**, 212-223.
- Ho Y.S., Wase D.A.J., Forster C.F., (1996), Kinetic studies of competitive heavy metal adsorption by sphagnum moss peat, *Environmental Technology*, **17**, 71-77.
- Kang M., Kawasaki M., Tamada S., Kamei T., Magara Y., (2000), Effect of pH on the removal of arsenic and antimony using reverse osmosis membranes, *Desalination*, **131**, 293-298.
- Kleinubing S.J., Silva E.A., Silva M.G., Guibal E., (2011), Equilibrium of Cu(II) and Ni(II) biosorption by marine alga *Sargassum filipendula* in a dynamic system: competitiveness and selectivity, *Bioresource Technology*, **102**, 4610–4617.
- Koparal A.S., Ozgur R., Ogutveren U.B., Bergmann H., (2004), Antimony removal from model acid solutions by electrodeposition, *Separation and Purification Technology*, **37**, 107-116.
- Lagergren S., (1898), About the theory of so-called adsorption of soluble substances, *Kungliga Svenska Vetenskapsakademiens Handlingar*, **24**, 1-39.
- Langmuir I., (1918), The adsorption of gases on plane surfaces of glass, mica and platinum, *Journal American Chemical Society*, **40**, 1361-1403.
- Li X., Dou X., Li J., (2012), Antimony(V) removal from water by iron-zirconium bimetal oxide: performance and mechanism, *Journal of Environmental Sciences (China)*, **24**, 1197-203.
- Lupea M., Bulgariu L., Macoveanu M., (2012), Biosorption of Cd(II) from aqueous solution on marine green algae biomass, *Environmental Engineering and Management Journal*, **11**, 607-615.
- Martins B.L., Cruz C.C.V., Luna A.S., Henriques C.A., (2006), Sorption and desorption of Pb²⁺ ions by dead *Sargassum* sp. Biomass, *Biochemical Engineering Journal*, **27**, 310-314.
- Murphy V., Hughes H., McLoughlin P., (2007), Cu(II) binding by dried biomass of red, green and brown macroalgae, *Water Research*, **41**, 731-740.
- Park D., Yun Y.S., Park J.M., (2005), Studies on hexavalent chromium biosorption by chemically-treated biomass of *Ecklonia* sp., *Chemosphere*, **60**, 1356-1364.
- Saito T., Tsuneda S., Hirata A., Nishiyama S., Saito K., Saito K., Sugita K., Uezu K., Tamada M., Sugo T., (2004), Removal of antimony(III) using polyol-ligand-containing porous hollow-fiber membranes, *Separation Science and Technology*, **39**, 3011-3022.
- Sari A., Citak D., Tuzen M., (2010), Equilibrium, thermodynamic and kinetic studies on adsorption of Sb(III) from aqueous solution using low-cost natural diatomite, *Chemical Engineering Journal*, **162** 521–527.
- Shan C., Ma Z.Y., Tong M.P., (2014), Efficient removal of trace antimony(III) through adsorption by hematite modified magnetic nanoparticles, *Journal of Hazardous Materials*, **268**, 229-236.
- Sheng P.X., Ting Y.P., Chen J.P., Hong L., (2004), Sorption of lead, copper, cadmium, zinc, and nickel by marine algal biomass: characterization of biosorptive capacity and investigation of mechanisms, *Journal of Colloid and Interface Science*, **275**, 131–141.
- Stemmer K.L., (1976), Pharmacology and Toxicology of Heavy-Metals – Antimony, *Pharmacology and Therapeutics. Part A*, **1**, 157-160.
- Sun F.H., Wu F.C., Liao H.Q., Xing B.S., (2011), Biosorption of antimony(V) by freshwater cyanobacteria *Microcystis* biomass: Chemical modification and biosorption mechanisms, *Chemical Engineering Journal*, **171**, 1082-1090.
- Uluozlu O.D., Sari A., Tuzen M., (2010), Biosorption of antimony from aqueous solution by lichen (*Physciatribacia*) biomass, *Chemical Engineering Journal*, **163**, 382–388.
- USEPA, (1979), *Water Related Fate of the 129 Priority Pollutants*, vol. 1, USEPA, Washington, DC Doc. 745-R-00-007.
- Vijayaraghavan K., Balasubramanian R., (2011), Antimonite Removal Using Marine Algal Species, *Industrial and Engineering Chemistry Research*, **50**, 9864-9869.
- WHO, (2011), *Guidelines for drinking-water quality*, 4th Edition, World Health Organization, Geneva, On line at: http://www.who.int/water_sanitation_health/en/.
- Wilson S.C., Lockwood P.V., Ashley P.M., Tighe M., (2010), The chemistry and behaviour of antimony in the soil environment with comparisons to arsenic: A critical review, *Environmental Pollution*, **158**, 1169–1181.
- Wu F.C., Sun F.H., Wu S., Yan Y.B., Xing B.S., (2012), Removal of antimony(III) from aqueous solution by freshwater cyanobacteria *Microcystis* biomass, *Chemical Engineering Journal*, **183**, 172-179.
- Wu Z.J., He M.C., Guo X.J., Zhou R.J., (2010), Removal of antimony (III) and antimony (V) from drinking water by ferric chloride coagulation: Competing ion

- effect and the mechanism analysis, *Separation and Purification Technology*, **76**, 184-190
- Xi J.H., He M.C., Wang K.P., Zhang G.Z., (2013), Adsorption of antimony(III) on goethite in the presence of competitive anions, *Journal of Geochemical Exploration*, **132**, 201-208.
- Xu W., Wang H.J., Liu R.P., Zhao X., Qu J.H., (2011), The mechanism of antimony(III) removal and its reactions on the surfaces of Fe-Mn Binary Oxide, *Journal Of Colloid And Interface Science*, **363**, 320-326.
- Yang J., Volesky B., (1996), Intraparticle diffusivity of Cd ions in a new biosorbent material, *Journal of Chemical Technology and Biotechnology*, **66**, 355-364.
- Zhu J., Wu F.C., Pan X.L., Guo J.Y., Wen, D.S., (2011), Removal of antimony from antimony mine flotation wastewater by electrocoagulation with aluminum electrodes, *Journal of Environmental Sciences China*, **23**, 1066-1071.



“Gheorghe Asachi” Technical University of Iasi, Romania



PRELIMINARY ECOTOXICOLOGICAL EVALUATION OF ERYTHROSIN B AND ITS PHOTOCATALYTIC DEGRADATION PRODUCTS

Laura Carmen Apostol^{1,2*}, Camelia Smaranda², Mariana Diaconu², Maria Gavrilescu^{2,3*}

¹“Stefan cel Mare” University of Suceava, Faculty of Food Engineering, 13 Universitatii Str., 720229 Suceava, Romania

²“Gheorghe Asachi” Technical University of Iasi, Faculty of Chemical Engineering and Environmental Protection,
Department of Environmental Engineering and Management, 73 Prof.dr.docent D. Mangeron Str., 700050 Iasi, Romania

³Academy of Romanian Scientists, 54 Splaiul Independentei, RO-050094 Bucharest, Romania

Abstract

The class of xanthene dyes has a complex chemical structure, which showed to be toxic for mixed culture of microorganisms (i.e. anaerobic granular sludge). Because of the unwanted effects of Erythrosin B (Ery B) on environmental components and some food confirmed previously, the dye was chosen in this study to evaluate its ecotoxicity. Also, the Ery B photocatalytic degradation products were assessed in terms of their ecotoxicity.

Three-days of seed germination and root growth tests were conducted using a dicotyledonous plant that is the garden cress (*Lepidium sativum* L.), in the presence of different dye concentration and its photodegradation products. Dye affected mostly the roots of the plant. According to toxic effects on root growth, toxicity of the dye indicated a 72h exposition average Effective Concentration EC₅₀ value corresponding to 25 mgL⁻¹ Ery B.

The presence of the Ery B photocatalytic degradation products in the aqueous solution leads to a higher efficiency on *Lepidium sativum* L. germination, favoring the stem length growth.

Key words: dye degradation, *Lepidium sativum* L., toxicity test

Received: November, 2014; *Revised final:* February, 2015; *Accepted:* February, 2015

1. Introduction

Dyes constitute one of the pollutants class causing a variety of environmental problems: they can generate eco-risks beside the dyes itself, by toxic by-products produced naturally through oxidation or reduction pathways assisted by environmental conditions (Abo-Farha, 2010; Fatta-Kassinos et al., 2010; Gaya and Abdullah, 2008; Luenloi et al., 2011).

Food Red 14 (Erythrosin B), authorised as a food additive in the EU is a water-soluble dye of xanthene class widely used as a colorant since 1973 in different industries, such in foodstuffs (baked

goods, fruits cocktails), cosmetics (lipsticks, bubble baths) or drugs (tablet, capsule), but their presence in the environment is of increased worry, since they may produce severe environmental and public health risks due to possible mutagenic or carcinogenic effects (Apostol et al., 2012). This class of compounds has a complex chemical structure, and showed to be toxic for mixed cultures of microorganisms (i.e. anaerobic granular sludge), enzymes, aquatic and terrestrial organisms, fungi, (Apostol et al., 2012; Carpenter et al., 1984; Krasnoff et al., 1999; Mizutani, 2009; Uesugi et al., 2006; Walthall and Stark, 1999). This is the reason for that there are numerous researches addressing the

* Author to whom all correspondence should be addressed: e-mail: laura.apostol@fia.usv.ro, mgav@tuiasi.ro

removal of dyes from aqueous effluents so as to minimize the ecological and health risks.

The photocatalytic processes have been applied successfully in the removal of organic pollutants from different classes (pesticides, pharmaceuticals and personal care compounds, halogenated compounds, dyes), where biodegradation of recalcitrant pollutants demonstrated to be inefficient due to the compounds toxicity (Caliman and Gavrilescu, 2009; Gavrilescu et al., 2014; Perreira et al., 2009; Van der Zee and Cervantes, 2009).

Heterogeneous photocatalysis has significant advantages over many processes used in the treatment of aqueous effluents polluted with dyes. The majority of the researchers reported that the process can induce the break of the dye molecule, but rarely complete mineralization can be achieved in an economically and environmental friendly way (Betianu et al., 2008; Caliman et al., 2008; Kumar, 2010). Those considerations conducted to a limited number of reported materials regarding the reaction mechanism and intermediates, and open door for new research. Although only few studies reported the total removal of dyes by photocatalysis, the method can result in the mineralization of the hazardous pollutants rather than transferring them to another phase, as in the case of adsorption on different materials (Apostol and Gavrilescu, 2009; Brinza et al., 2009; Satuf et al., 2011). In 2007, two papers were published addressing preliminary studies on Erythrosin B photodegradation, but no information were provided on the toxicity of dye degradation products (Hasnat et al., 2007; Uddin et al., 2007).

In order to evaluate the toxicity of the degradation products of Erythrosin B in our study, the dye was subject of UV photocatalytic degradation in the presence of the catalyst Degusa TiO₂ Aeroxide P25. In the first step, the experiments were conducted in order to evaluate the influence of different parameters on the removal efficiency of the dye (data not shown). The resulted effluent was used to perform toxicity tests, carried out using *Lepidium sativum* L. as the test organism and food chain indicator.

2. Materials and methods

2.1. Materials

The compound investigated in this study (Ery B) was chosen because of its use in different industries, in particular the food industry, despite the toxic and carcinogenic effects demonstrated in the context of research conducted on this topic. The acid dye, Erythrosin B is a red odourless powder or granules with a calculated Log P (octanol-water) of 4.95 at 25°C (Molinspiration, 2007), soluble in water ($\leq 9\%$ w/w) and ethanol. The chemical was purchased from Sigma-Aldrich (C.I. Acid Red 51, 45430).

Phytotoxicity tests were carried out with garden cress seeds (*Lepidium sativum* L.) from commercial source (AGROSEL garden cress seeds).

2.2. Methods

2.2.1. Toxicity tests

The growth of *Lepidium sativum* L. roots is a parameter frequently used to assess the ecotoxic risks from river pollution, wastewater sources, and leachates of industrially polluted soils (Studzińska and Buszewski, 2009). *Lepidium sativum* L. was selected as the test organism because of the advantage offered by some morphological and physiological properties (small, high growth rates and vegetative propagation) and due to its capacity to grow in a wide range of pH-values (Gyekye, 2013; Pavel et al., 2013).

Toxicity tests were carried out according to a standardized protocol (ISO/DIS 15 799, (1999): three-days of seed germination and root growth tests were conducted using the dicotyledonous garden cress *Lepidium sativum* L. as indicator. This method was tested first for the assesment of the effects of substances contained in residues applied to soil on plant emergence and growth.

The sensitivity of *Lepidium sativum* L. germination to Erythrosin B and its degradation by-products was investigated using dye solutions of different concentration. The toxicity tests were conducted in triplicate using 20 seeds each for germination on Petri dishes. Volumes of 3mL solution of a certain concentration of Ery B, and the corresponding degradation products, respectively were used to wet the paper supporting the seeds. The Petri dishes were kept at room temperature ($\sim 25^{\circ}\text{C}$) for 72 hours. The number of seeds germinated, formed biomass, stem length and root length were measured to determine the germination degree.

The dye was tested in a concentration series (1 to 50 mgL⁻¹) in order to obtain the 72 h exposition average Effective Concentration (72 h-EC₅₀), which is the concentration where 50% of the plants were affected.

2.2.2. Separation of Ery B degradation products from reaction mixture

In order to identify the by-products resulted from Erythrosin B photodegradation, 500mg L⁻¹ Ery B were degraded for 8h in the presence of 5 g L⁻¹ TiO₂ according to the procedure described previously (Pereira et al., 2013). All chemicals and solvents were obtained from Sigma-Aldrich, Merck and Chemical Company. The final solution was purified by column chromatography using silica gel 60.70-230 mesh. The resulted solution was filtered using a 0.2 μm filter in order to remove the catalyst particles. First, the filtered solution containing the degradation by-products was treated by liquid-liquid extraction with ethyl acetate (Iovu and Nicolescu, 2009). The following step consisted in a solid-liquid extraction on silica gel.

The thin layer chromatography (TLC) screening was conducted and several solvents were tested in order to prepare the sample for NMR analysis (Iovu and Nicolescu, 2009; Tataru and Vata, 1999). Visualization was performed in short- and long- wavelength UV-light. The samples were refrigerated at 4°C and kept in the dark from the time of collection until analyzes.

3. Results and discussion

3.1. Ecotoxicological tests

Toxicity tests were conducted in order to evaluate the ecotoxicity of Ery B dye and its photodegradation products using an indirect acute toxicity bioassay on the dicotyledonous plant *Lepidium sativum* sp. according to the standard procedure. The number of seeds germinated, formed biomass, stem length and root length were measured to determine the germination degree (Fig. 1).

Table 1 presents the results of the toxicity tests. It can be observe that dye affect especially the roots of the plant. The presence of the by-products in the aqueous solution leads to a higher efficiency on *Lepidium sativum* sp. germination if the growth stem length is considered.

Toxicity data are usually expressed either as a concentration causing a specific effect (e.g. death or growth) in 50% of the tested organisms (Effect Concentration, EC₅₀). EC₅₀ stands for the concentration of a test compound that reduces root growth to 50% of control (Enderlein et al., 2007; Pavel et al., 2013).

The experimental data were analyzed by regression analysis following logarithmic transformations and EC₅₀ values for Erythrosin B were expressed as toxicant concentrations. According to toxic effects on root growth, toxicity of the dye indicated EC₅₀ corresponded to 25 mg L⁻¹ Ery B.

3.2. Separation of the products from reaction mixture

Two compounds were isolated by liquid-liquid extraction. P1 is a pale yellow compound with a crystalline structure, which is soluble in acetone. The TLC chromatogram indicated that the product P1 is not a pure compound.

P2 is a white powder compound. It was eluted with different mobile phases: chloroform, ethylic ether, acetone, ethyl acetate, hexane. The mixture of n-hexane with ethyl acetate was the best for migration on silica - gel plate in TLC analysis.

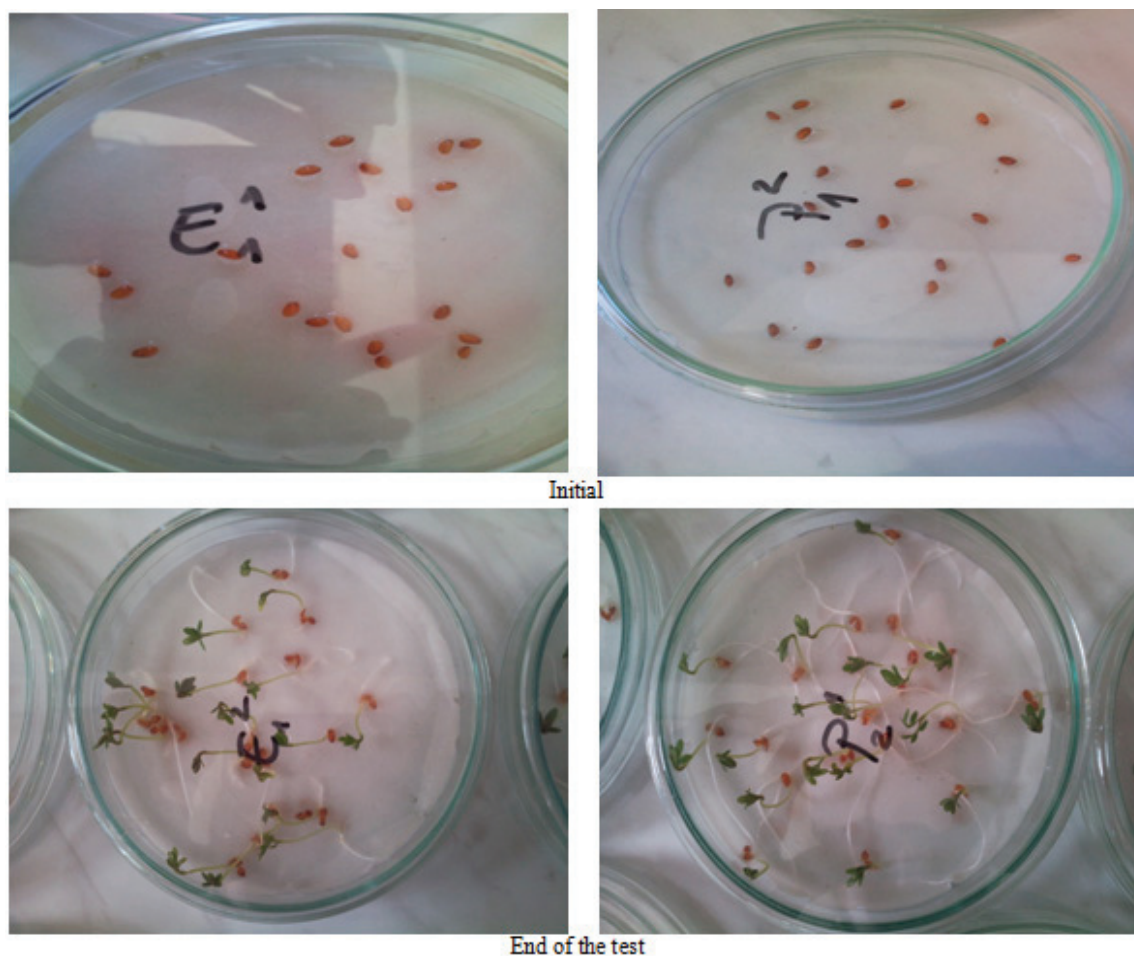


Fig. 1. *Lepidium sativum* sp germination in the presence of Erythrosin B and photodegradation products

Table 1. Erythrosin B and photodegradation by-products effects on *Lepidium sativum* L.

Tested substance	Stem length (mm)	Root length (mm)	Biomass (g)		
			Stem	Root	Total
Blank	16.0333 ± 0.55	34.9833 ± 1.06	0.1009 ± 0.007	0.0316 ± 0.017	0.3674 ± 0.04
Ery B ₁ (25 mg L ⁻¹)	15.0667 ± 0.93	17.6333 ± 1.53	0.1086 ± 0.008	0.0332 ± 0.006	0.3239 ± 0.02
Ery B ₂ (50 mg L ⁻¹)	10.35 ± 0.46	5.9333 ± 0.48	0.0848 ± 0.006	0.0142 ± 0.002	0.1717 ± 0.146
By-products (25 mg L ⁻¹)	18.2833 ± 3.41	32.9833 ± 9.07	0.1182 ± 0.021	0.0563 ± 0.011	0.3806 ± 0.06
By-products (50 mg L ⁻¹)	18.8833 ± 2.53	32.3333 ± 2.23	0.1238 ± 0.014	0.0556 ± 0.006	0.3718 ± 0.03

Unfortunately the NMR data were not encouraging because of the sensitivity of the methods and the compound could not be identified.

3.3. UV-Vis analysis

The UV-Vis analysis of the sample containing the dissolved by-products was performed between 200 and 700 nm with a T60 UV-Visible spectrophotometer. The sample was diluted with distilled water. The adsorption spectra showed two distinct adsorption peaks, at ~224 nm and ~524 nm (Fig. 2). The band A₀ represents the UV-Vis spectrum of initial Erythrosin B solution before starting the photocatalytic degradation. After the beginning of the degradation process it is observed a decrease in peak intensity corresponding to 524 nm. As the reaction progress, at the value of 224 nm a new peak is formed, that increases in intensity while the reaction time increases. The monitorization stopped after 8 h of irradiation. In this solution the presence of I⁻ ionic species was also evidenced by reaction with AgNO₃ (Fig. 3).

Because the data obtained from our analysis does not allow a proper identification of the products formed during photocatalytic degradation, a literature analysis was carried out for xanthene dyes available mechanism in order to propose a degradation pathway for Erythrosin B. This survey addressed the following frameworks: the products isolated and identified by chromatographic methods in conjunction

with a spectral study performed by Jain et al. (2005), resulted from electrochemical degradation of Erythrosin B; the possible mechanisms for azo dye

X-GRL degradation by three processes based on the degradation intermediates detected by GC/MS reported by Zho and He (2007); the study of Mai et al. (2007) on the reaction products and intermediates of 2,4,6-triiodoresorcinol formed during the synthesis of color additive FD&C Red No. 3 (Erythrosin) using high performance liquid chromatography; mechanism and pathway intermediates resulted from the degradation of Rhodamine B in MPC in the presence of H₂O₂ detected by GC/MS by He et al. (2009); the study of Mehrdad and Hashemzadeh (2009) for the determination of activation energy for Rhodamine B degradation in the presence of hydrogen peroxide and some metal oxide.

The results obtained from UV-Vis analysis, TLC products characterization and the literature data helped us to propose a degradation mechanism for Erythrosin B (Fig. 4). The compounds proposed as Erythrosin B photodegradation by-products were subject of some ecotoxicological studies.

In order to explain the effect of the solution containing the Ery B photodegradation by-products on *Lepidium sativum* Table 2 present some tested species and the effects of Ery B degradation products on their development. For example, phthalic acid in solution determines population/ biomass growth of *Scenedesmus subspicatus* and *Chilomonas paramecium*.

A solution of 4-hydroxybenzoic acid inhibits the organism growth and induces the death of *Oncorhynchus mykiss* (Rainbow trout) and of *Daphnia magna*, but in higher concentrations compared to those resulted from Erythrosin B degradation. A similar behaviour is found for terephthalic acid solutions (Table 2).

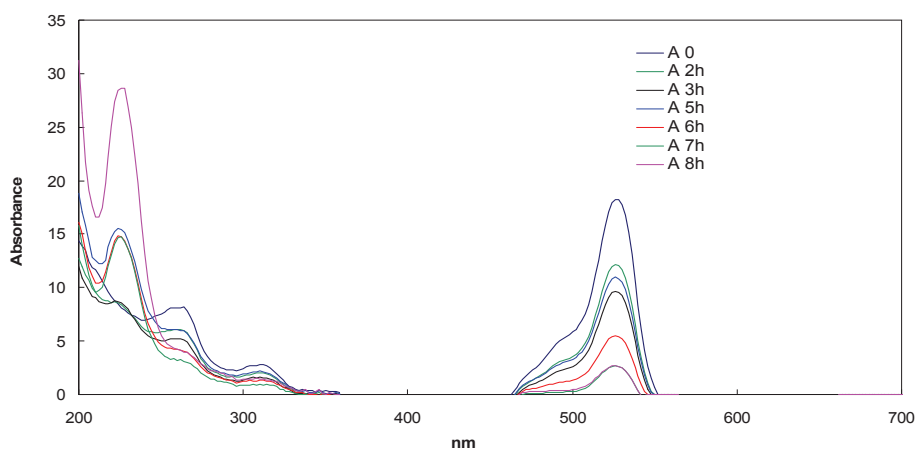
**Fig. 2.** UV-Vis spectra of final photodegradation solution of Erythrosin B



Fig. 3. The presence of I⁻ in solution after Erythrosin B photodegradation

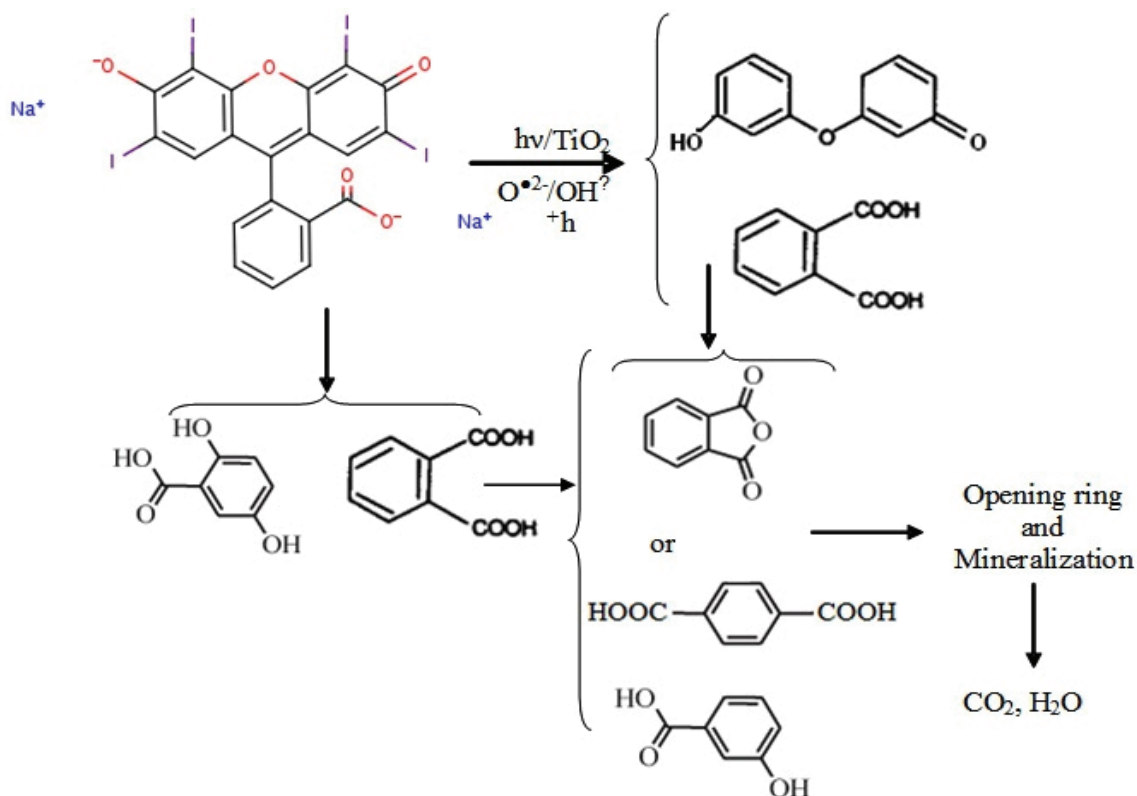


Fig. 4. The most probable degradation mechanism of Erythrosin B in the presence of UV/TiO₂

Table 2. Relevant ecotoxicity studies of Erythrosin B potential photodegradation byproducts

Compound	Tested species	Effects	Reference
2,5-dihydroxybenzoic acid	<i>Hydrilla</i> sp.	Growth, general	Martin and Martin (1988)
	<i>Chlorella vulgaris</i>	Population changes, general	Dedonder and Van Sumere (1971)
phthalic acid	<i>Scenedesmus subspicatus</i>	Population/ Biomass Growth	Kuhn and Pattard (1990)
	<i>Chilomonas paramecium</i>	Population growth rate	Bringmann and Kuhn (1981)
phthalic anhydride	<i>Selenastrum capricornutum</i>	Population – Biomass Growth	Michael et al. (1989)
	<i>Oedogonium cardiacum</i>	Accumulation	Lu and Metcalf (1975)
terephthalic acid	<i>Tetrahymena pyriformis</i> (Ciliate)	36-h IC ₅₀ = 55 mg/L	Yoshioka et al. (1985)
4-hydroxybenzoic acid	<i>Oncorhynchus mykiss</i> (Rainbow trout)	72-h EC ₅₀ = 68.5 mg/L	Verschueren (2001)
	<i>Daphnia magna</i>	48-h EC ₅₀ = > 100 mg/L	Kuehn (1989)

The main compounds resulted from the degradation process which have similar effects to those found in other studies correspond to phthalic anhydride/phthalic acid and 2,5-dihydroxybenzoic acid.

4. Conclusions

The toxicity of Erythrosin B dye against the garden cress *Lepidium sativum* L. was evaluated in a preliminary trial. The experiments performed using seeds cultivated on Petri dishes showed that the dye affected especially the roots of the plant.

Also, Ery B was the subject of UV photocatalytic degradation in the presence of the catalyst Degusa TiO₂ Aeroxide P25 in order to evaluate the toxicity of its degradation products. Photocatalytic degradation of Erythrosin B led to a complete detoxification of the compounds but the complete mineralization was not achieved. The presences of at least two compounds isolated by liquid-liquid extraction, as main by-products in the aqueous solution, led to a higher efficiency on *Lepidium sativum* sp germination according to stem length growth.

This study confirmed the opportunity of toxicological assays related to dye decolorization experiments. The results are the basis for further investigations essential to obtain the data necessary in the assessment of ecological and health risks.

Acknowledgements

This paper was elaborated with the support of a grant of the Romanian National Authority for Scientific Research, CNCS – UEFISCDI, project number PN-II-ID-PCE-2011-3-0559, Contract 265/2011. The scientific support of Professor Dan Scutaru is highly acknowledged.

References

- Abo-Farha S.A., (2010), Photocatalytic degradation of monoazo and diazo dyes in wastewater on nanometer-sized TiO₂, *Journal of American Science*, **6**, 130-142.
- Apostol L.C., Gavrilescu M., (2009), Application of natural materials as sorbents for persistent organic pollutants, *Environmental Engineering and Management Journal*, **8**, 243-252.
- Apostol L.C., Pereira L., Pereira R., Gavrilescu M., Alves M.M., (2012), Biological decolorization of xanthene dyes by anaerobic granular biomass, *Biodegradation*, **23**, 725-737.
- Betianu C., Caliman A.F., Gavrilescu M., Cretescu I., Cojocaru C., Poullos I., (2008), Response surface methodology applied for Orange II photocatalytic degradation in TiO₂ aqueous suspensions, *Journal of Chemical Technology & Biotechnology*, **83**, 1454-1465.
- Bollman M.A., Baune W.K., Smith S., DeWhitt K., Kapustka L., (1989), Report on algal toxicity tests on selected Office of Toxic Substances (OTS) chemicals, U.S. Environmental Protection Agency, Environmental Research Laboratory, Report Number EPA/600/3-90/041.
- Bringmann G., Kuhn R., (1981), Comparison of the effect of toxic substances on the flagellate organisms such as ciliates and the holozoic bacteria-devouring organisms such as saprozoic protozoans (Vergleich der Wirkung von Schadstoffen auf Flagellate), *Gwf-Wasser Abwasser*, **122**, 308-313.
- Brinza L., Nygard C.A., Dring M.J., Gavrilescu M., Benning L.G., (2009), Cadmium tolerance and adsorption by the marine brown alga *Fucus vesiculosus* from the Irish Sea and the Bothnian Sea, *Bioresource Technology*, **100**, 1727-1733.
- Caliman F.A., Curteanu S., Betianu C., Gavrilescu M., Poullos I., (2008), Neural networks and genetic algorithms optimization of the photocatalytic degradation of Alcian Blue 8GX, *Journal of Advanced Oxidation Technologies*, **11**, 316-326.
- Caliman F.A., Gavrilescu M., (2009), Pharmaceuticals, personal care products and endocrine disrupting agents in the environment – A review, *Clean – Soil, Air, Water*, **34**, 277-303.
- Carpenter T.L., Respicio N.C., Heitz J.R., (1984), Acute light-dependent toxicity of free-acid formulations of xanthene dyes to larval *Culex pipiens quinquefasciatus* say (Diptera: Culicidae), *Environmental Entomology*, **13**, 1366-1370.
- Dedonder A., Van Sumere C.F., (1971), The effects of phenolics and related compounds on the growth and respiration of *Chlorella vulgaris*, *Z. Pflanzenphysiol.*, **65**, 70-80.
- Enderlein U.S., Enderlein R.E., Williams W.P., (2007), *Water quality requirements*, In: *Water pollution control*, On line at: http://www.who.int/water_sanitation_health/resources/quality/wpcchap2.pdf.
- Fatta-Kassinos D., Hapeshi E., Malato S., Mantzavinos D., Rizzo L., Xekoukoulotakis N.P., (2010), *Removal of Xenobiotic Compounds from Water and Wastewater by Advanced Oxidation Processes*, In: *Xenobiotics in the Urban Water Cycle: Mass Flows, Environmental Processes, Mitigation and Treatment Strategies*, Fatta-Kassinos D., Bester K., Kummerer K. (Eds.), Springer, Netherlands, 387-412.
- Gavrilescu M., Demnerová K., Aamand J., Agathos S., Fava F., (2014), Emerging pollutants in the environment: present and future challenges in biomonitoring, ecological risks and bioremediation, *New Biotechnology*, **32**, 147-156.
- Gaya U.I., Abdullah A.H., (2008), Heterogeneous photocatalytic degradation of organic contaminants over titanium dioxide: A review of fundamentals, progress and problems, *Journal of Photochemistry and Photobiology C: Photochemistry Reviews*, **9**, 1-12.
- Gyekye K.A., (2013), An assessment of toxic in urban soils using garden cress (*Lepidium sativum*) in Vasileostrovsky Ostrov and Elagin Ostrov, Saint Petersburg, Russia, *Journal of Geography and Geology*, **5**, 63-70.
- He Z., Sun C., Yang S., Ding Y., He H., Wang Z., (2009), Photocatalytic degradation of rhodamine B by Bi₂WO₆ with electron accepting agent under microwave irradiation: Mechanism and pathway, *Journal of Hazardous Materials*, **162**, 1477-1486.
- Iovu M., Nicolescu T.O., (2009), *Organic Chemistry - Experimental Methods*, Carol Davila University Publishing House, Bucharest, Romania.
- ISO/DIS 15 799, (1999), Soil Quality — Guidance on the ecotoxicological characterization of soils and soil materials. Annex A.1.2.2 Determination of the effects

- of pollutants on soil flora— Part 2: effects of chemicals on the emergence and growth of higher plants. Switzerland: International Organisation for Standardisation. Geneva, Switzerland.
- Jain R., Bhargave M., Sharma N., (2005), Electrochemical degradation of Erythrosin in pharmaceuticals and food product industrial effluent, *Journal of Scientific and Industrial Research*, **64**, 191-197.
- Krasnoff S.B., Faloon D., Williams J.E., Gibson D.M., (1999), Toxicity of xanthene dyes to entomopathogenic fungi, *Biocontrol Science and Technology*, **9**, 215-225.
- Kuehn R., Pattard M., Pernak K.-D., Winter A., (1989), Results of the harmful effects of selected water pollutants (anilines, phenols, aliphatic compounds) to *Daphnia Magna*, *Water Research*, **23**, 495-500.
- Kuhn R., Pattard M., (1990), Results of the harmful effects of water pollutants to green algae (*Scenedesmus subspicatus*) in the cell multiplication inhibition test, *Water Research*, **24**, 31-38.
- Kumar P., (2010), *Photocatalytic degradation of Procion Yellow Dye*, Master of Technology Thesis, Thapar University, Dublin, Ireland.
- Lu P.Y., Metcalf R.L., (1975), environmental fate and biodegradability of benzene derivatives as studied in a model aquatic ecosystem, *Environmental Health Perspectives*, **10**, 269-284.
- Luenloi T., Chalermisinsuwan B., Sreethawong T., Hinchiranan N., (2011), Photodegradation of phenol catalyzed by TiO₂ coated on acrylic sheets: Kinetics and factorial design analysis, *Desalination*, **274**, 192-199.
- Mai H.T., Brodie D.L., Meyers M.B., Baldo A.L., Krantz Z., Weisz A., (2006), Determination of 2,4,6-triiodoresorcinol and other side reaction products and intermediates in the color additive FD & C Red No. 3 (Erythrosin) using high-performance liquid chromatography, *Food Additives and Contaminants*, **23**, 547-551.
- Mehrdad A., Hashemzadeh R., (2009), Determination of activation energy for the degradation of Rhodamine B in the presence of hydrogen peroxide and some metal oxide, *Journal of the Chemical Society of Pakistan*, **31**, 738-743.
- Mizutani T., (2009), Toxicity of xanthene food dyes by inhibition of human drug-metabolizing enzymes in a noncompetitive manner, *Journal of Environmental and Public Health*, Article ID 953952, <http://dx.doi.org/10.1155/2009/953952>.
- Pavel V.L., Sobariu D.L., Diaconu M., Stătescu F., Gavrilesco M., (2013), Effects of heavy metals on lepidium sativum germination and growth, *Environmental Engineering and Management Journal*, **12**, 727-733.
- Pereira L., Coelho A.V., Viegas C.A., dos Santos M.M.C., Robalo M.P., Martinsa L.O., (2009), Enzymatic biotransformation of the azo dye Sudan Orange G with bacterial CotA-laccase, *Journal of Biotechnology*, **139**, 68-77.
- Pereira L., Pereira R., Oliveira C.S., Apostol L., Gavrilesco M., Pons M.N., Zahraa O., Alves M.M., (2013), UV/TiO₂ photocatalytic degradation of xanthene dyes, *Photochemistry and Photobiology*, **89**, 33-39.
- Satuf M.L., Pierrestegui M.J., Rossini L., Brandi R.J., Alfano O.M., (2011), Kinetic modeling of azo dye photocatalytic degradation in aqueous TiO₂ suspension. Toxicity and biodegradability evaluation, *Catalysis Today*, **161**, 121-126.
- Studzńska S., Buszewski B., (2009), Study of toxicity of imidazolium ionic liquids to watercress (*Lepidium sativum* L.), *Analytical and Bioanalytical Chemistry*, **393**, 983-990.
- Tataru L., Vata M., (1999), *Methods for Separation and Purification of Chemical Substance*, (in Romanian), Cermi Publishing House, Iasi, Romania.
- Uesugi N., Furumiya K., Mizutani T., (2006), Inhibition mechanism of UDP-glucuronosyltransferase 1A6 by xanthene food dyes, *Journal of Health Science*, **52**, 549-557.
- Van der Zee F.P., Cervantes F.J., (2009), Impact and application of electron shuttles on the redox (bio)transformation of contaminants: a review, *Biotechnology Advances*, **27**, 256-277.
- Verschueren K., (2001), *Handbook of Environmental Data on Organic Chemicals*, Vol. 1-2, 4th Ed., John Wiley & Sons, New York.
- Walthall W.K., Stark J.D., (1999), The acute and chronic toxicity of two xanthene dyes, fluorescein sodium salt and phloxine B, to *Daphnia pulex*, *Environmental Pollution*, **104**, 207-215.
- Zhou M., He J., (2007) Degradation of azo dye by three clean advanced oxidation processes: Wet oxidation, electrochemical oxidation and wet electrochemical oxidation-A comparative study, *Electrochimica Acta*, **53**, 1902-1910.



“Gheorghe Asachi” Technical University of Iasi, Romania



PORE STRUCTURE CHARACTERIZATION OF CHEMICALLY MODIFIED BIOCHAR DERIVED FROM RICE STRAW

Sobhy M. Yakout^{1,2*}, Abd El Hakim M. Daifullah², Sohair A. El-Reefy²

¹King Saud University, College of Science, Biochemistry Department, Riyadh 11451 Saudi Arabia

²Atomic Energy Authority, Hot Laboratories Centre, 13759, Egypt

Abstract

Biochar derived from agricultural biomass waste is increasingly recognized as multifunctional material for various applications according to its characteristics. It is therefore essential to investigate biochar properties before large-scale application. In this study, rice straw-derived biochars produced at different temperatures (550, 650, 750 °C). The resulting biochars were subjected to liquid-phase oxidation by different agents including KOH, HNO₃, H₂SO₄, H₂O₂ and KMnO₄ to obtain biochar with different properties. Pore structure characteristics including surface area, micro and meso pore volume, and pore size distribution were studied. Biochar surface is sensitive to the type of modifying reagent. Biochars treated by KOH, KMnO₄ and H₂O₂ give higher nitrogen uptake in the range of micropores and mesopores. The rice straw-derived biochars especially produced at 650°C and treated by KOH have the highest surface area (179.7 m²/g) and micropore volume (0.081 cc/g) than the rest of biochars. In contrast, biochars treated by H₂SO₄ and HNO₃ give lower nitrogen uptake and lead to loss of the biochar's porosity. Loss of micropore volume is as low as 10-40% of pore volume in H₂SO₄ and HNO₃ treated biochars. Biochars exhibit wide pore size distribution, from narrow micropores to wide mesopores. One modal distribution was obtained with peak oscillation in the region of 1.0 to 1.3 nm in the case of micropore region. However, for the mesopore region, two minima at about 3.0 nm and 5.0 nm were observed. More homogeneous micropore distribution was produced from KOH and H₂O₂ treatment in contrast to that of HNO₃ and H₂SO₄ treatment, which give heterogeneous micropore distribution.

Key words: activated biochar, pore size distribution, pore volume, rice straw, surface area

Received: March, 2013; *Revised final:* April, 2014; *Accepted:* April, 2014

1. Introduction

Biomass is a renewable energy resource and has a growing interest as a chemical feedstock source. The pyrolysis conversion of biomass into value-added products namely; solid char (bio-char), liquid (bio-oil) and gas (bio-gas) has attracted tremendous research interest, mainly due to the rising energy demands and concerns over greenhouse gas emissions (Heo et al., 2010). Many applications use the liquid product (bio-oil), however no attention has been received for char.

Biochar is a new scientific term with various definitions in the literature. On the word of Lehmann and Joseph (2009), biochar can be well-defined as “a

carbon rich product when biomass such as wood, manure or leaves is heated in a closed container with little or unavailable air”.

Shackley et al. (2012) described biochar in more words as “the porous carbonaceous solid produced by the thermochemical conversion of organic materials in an oxygen depleted atmosphere that has physicochemical properties suitable for safe and long-term storage of carbon in the environment”.

Indeed, various types of biomass containing animal wastes, crop residues and sewage sludge used to prepare useful biochars via slow to intermediate pyrolysis processes (Ahmad et al., 2014). Agricultural wastes or residues are wide available low-cost raw material to produce biochar, as well as

* Author to whom all correspondence should be addressed: e-mail: sobhy.yakout@gmail.com; Phone: +966558448693; Fax: +96614675931

biooil and gases (Chen et al., 2011a).

Rice straw is one of the main categories of agricultural by-products. Large quantities of straws accumulate due to agricultural practices in Egypt. Although some residues are used as feed, fuel or straw returned to the fields, millions of tons of rice straws are burnt annually in Egypt through wildfires, post-harvest burning of cultivation fields, and domestic uses for cooking and heating. This represents a main source of source of air pollution.

The main harmful of burning agricultural by-products is carbon dioxide gas emission. Carbon dioxide gas is considered as the most significant greenhouse gas created by human activities. Pyrolysis of straw agricultural wastes to give charcoal and biochar like product has been proposed to decrease undesirable effects of direct burning on human health and environment. As result of the biochar is opposing to biological decomposition, it is remain for much longer time in the terrestrial systems and then their useful effects are prolonged (Lehmann et al., 2011).

In the past five years, several researchers began to focus on developing biochar from straw (Chen et al., 2011b; Hameed and El-Khaiary, 2008; Lima et al., 2010; Qiu et al., 2009; Sun et al., 2011; Xu et al., 2011). However, limited knowledge is available for the surface modification of biochar. The surface modifications result in variation of surface reactivity, physicochemical and structural properties.

Surface modification of biochar using alkali or acid results in changing of surface areas plus functional groups characteristics on biochar. Further investigation on biochar modification is important owing to necessity to develop it for special application.

Bio-char has various applications for soil amendment, removal of toxic materials and production of value-added products (Azargohar et al., 2014). To evaluate each type of bio-char for any particular application, the bio-char should be characterized for its composition, porous structure and surface chemistry (Azargohar et al., 2014).

The objectives of this work consist in the examination of the modification of biochar prepared from Rice straw by using various liquid-phase oxidation methods, the investigation of the

modification effects on the pore structure and surface properties of the products, and the determination of the optimum experimental conditions for the preparation of materials with desired surface properties and adsorption capacities

2. Experimental

2.1. Preparation of biochar

Rice straw biochar was prepared according to our previous study (Daifullah et al., 2007), briefly, dried Rice Straw (500 gm) was heated at 50°C/10 min in fluidized bed reactor under flow 300ml/min of nitrogen. When temperature reached 350 °C, steam at a rate of 5 ml/min was introduced. Heating continued up to 550, 650, 750 °C, with one hour hold. After cooling, biochars were left to cool, washed with distilled water, and dried at 120 °C. Biochar at 550, 650 and 750°C took the abbreviations of RS₁, RS₂, and RS₃ respectively.

2.1.1. Oxidative modification of biochar (RS₁, RS₂, RS₃)

Obtained biochars were subjected to liquid-phase oxidation using different oxidizing agents in order to obtain materials with various surface characters.

The experiemntail procedures using different oxidizing agents were summarized in Table 1. After each modification biochar then washed with deionized water, decanted and the samples were dried overnight in an oven at 110 °C and stored in a desiccator for latter use.

2.2. Pore structure characterization

In order to determine surface areas and pore characteristics of various samples, nitrogen adsorption/desorption isotherms were measured at 77 K on an automatic adsorption instrument (Quantachrome Instruments, Model Nova1000e series, USA) in relative pressure in the range of 10⁻⁶ to 0.999. Before measurement, biochar samples were crushed and powdered to shorten the time required for reaching equilibrium in the isotherm study and degassed at 250°C under nitrogen flow for 16 hours.

Table 1. Experiemntail procedur for modification of RS biochars by different agents

<i>Agent</i>	<i>Procedure</i>	<i>Symbole</i>
KOH	RS biochars were treated with 1M KOHwith boiling for 2h. The oxidized biochars were washed and then dried over night at 50 °C (Shim et al., 2001).	RS ₁ /KOH
HNO ₃	50g of RS biochars were treated with 50cm ³ of 65% nitric acid at 60 °C with stirring for 3 h (El-Hendawy, 2003).	RS ₁ /HNO ₃
H ₂ SO ₄	RS biochars were treated with 2% H ₂ SO ₄ (v/v) at 150 °C for 24 h. then washed with deionized water until pH was stable. Afterwards, the material soaked in 1% sodium bicarbonate solution overnight to remove residual acid (Babel and Kurniawan, 2004).	RS ₁ /H ₂ SO ₄
H ₂ O ₂	RS biochars were immersed in 30% H ₂ O ₂ with a ratio of H ₂ O ₂ to RS of 10 ml /g at room temperature until complete degradation of the H ₂ O ₂ (when there was no further gas evolution)(Pereira et al., 2003).	RS ₁ /H ₂ O ₂
KMnO ₄	1g of RS biochars were treated by 50ml 0.1 N KMnO ₄ solution at 50 °C for 48h (Youssef et al., 1982).	RS ₁ /KMnO ₄

The cross section area, i.e the area occupied by an adsorbate molecule in completed monolayer for the N₂ molecule at 77K was taken as 16.2 Å². The surface area of the biochar samples was obtained by means of standard methods, pore volume and pore size distribution were subsequently calculated from the N₂ adsorption data using NOVA Win 2.0 software. BET equation and Langmuir equation in the range of relative pressure 0.05 up to 0.3 was used to calculate the apparent surface area (S_{BET}, S_L).

The total pore volume (V_{t,0.95}) estimated from amount of nitrogen adsorbed at relative pressure of 0.95 and the mean pore radius from $r_{BET} = 2V_t/S_{BET}$, assuming cylindrical pore opens at both ends (NOVAWin2 / 2-P Ver. 2.1 Operation Manual). DFT method was used to calculate the total surface area (S_{DFT}) and total pore volume (V_{t,DFT}) of investigated samples as well as those parameters of respective types of pore, e.g. the micropore, mesopore surface area (S_{mic,DFT}, S_{mes,DFT}), micropore and mesopore volume (V_{mic,DFT}, V_{mes,DFT}).

3. Results and discussion

3.1. Nitrogen adsorption isotherms (comparative plots)

According to BDDT classification, the nitrogen isotherms in Fig. 1 are type I and IV with mesoporous hysteresis loop (Brunauer, 1943). In the present investigation, although the adsorption isotherms for all samples are similar, the adsorption capacities are significantly different according to the carbonization temperature and strength of modifying agent. In the case of samples treated by KOH, the upward shift is maximum in RS₁ and RS₂ series while samples oxidized by KMnO₄ give the maximum shift in RS₃ series. Only H₂SO₄ treated biochars slightly shifted downward in all biochar series.

3.2. Pore parameters analysis

It is clear from Table 2 that surface area resulting from micropores was over 80% of total surface area. It is well recognized that micropores are characterized by high surface area due to their tremendous number and depth (Girgis et al., 2002). The increase of temperature has a little effects on the surface area of products (RS₁, RS₂, RS₃) while upon oxidation treatment the total surface area is highly increased using KOH followed by H₂O₂ and KMnO₄, whereas treatment with HNO₃ decreases the surface area while H₂SO₄ treatment highly decreases the surface area. Decrease the micropore surface area in case of acid treatment due to great part of oxygen functional groups are located at the entrance of the pores, which hinder nitrogen molecules to go inside the pores (Pradhan and Sandles, 1999). According to Guo et al. (2005), the reduction of surface area is great in case of H₂SO₄ treatment due to high

destruction effect results from the surplus water vapor released via H₂SO₄ dehydration. This produce an over-gasification of parent biochar by converting micropores into meso- and macropores, and therefore causes a detrimental effect on the BET and micropore surface areas (Guo and Lua, 1999).

Table 2 show that Rice Straw based biochars prepared at 650 °C (RS₂) give surface area little higher than that carbonized at 550 and 750 °C. These results are in good agreement with the total pore volume due to increasing micropore and mesopore volume. However, for carbonization temperatures higher than 650 °C the surface areas decreased due to the severe reaction of C-H₂O and the burnt off of increased amount of biochar, resulting in the conversion of microporosities into mesoporosities or even macroporosities. Thus, carbonization at 650 °C can be considered as the temperature at which the reaction of steam with Rice Straw under our experimental conditions is the optimum. Pore-drilling and pore-widening by steam as a carbonizing agent occur simultaneously up to 650 °C to increase the micro and mesopore volumes. However, the pore-widening effect is more dominant by the gasification above 650 °C which destroys the pore wall of micropores (Yun et al., 2001). Upon increasing the temperature of carbonization the pore wide increases. Increasing temperature leads to the destruction of pore to larger one, increasing fraction percentage of mesopores and decreasing of micropores.

As can be seen from Table 2, there is a considerable increase in the pore diameter particularly for biochars modified by HNO₃, H₂SO₄ and KMnO₄. This means that treatment of parent biochar leads to some destruction of micropores forming mesopores and increase pore diameter. The same results are supported when the fraction percentage of micropore and mesopores volume are compared. The fraction of micropore decreased especially in case of HNO₃ and H₂SO₄-oxidized samples, while mesopores fraction increased. The decrease of total surface area of samples treated by H₂SO₄ and HNO₃ was mainly ascribed to the decrease of micropore volume i.e H₂SO₄ and HNO₃ treatments result in extensive widening of the pores, breaking of pore wall and destroying of pore structure, leading to a decrease of surface area. Considering the parent samples as reference, the loss of micropore volume is as low as 10-40% of pore volume in nitric and sulfuric acid treated samples.

Thus, one can conclude that liquid-phase oxidation, especially when carried out under severe acidic conditions such as reported here, leads to the fixation of a large amount of oxygen functionalities on the biochar surface, with the simultaneous partial destruction or degradation of the porous structure of biochars.

Treatment by KMnO₄ leads to increase of mesopores and micropores volumes. Therefore, the micropore and external surface area are increased with subsequent increase of the total surface area.

This conformed by increasing pore radius from the parent samples but still lower than in case of acid treatments. For H₂O₂-treatment samples, a development of micropores and loss of mesopores volume are observed leading to increase of the micropore and the total surface area. This conformed by the reduction of pore radius. Similar results were obtained by Domingo-Garcia et al. (2000) and Korili and Gil (2001). In the case of KOH treatment, pore structure seems to depend on the carbonization

temperature of the parent samples. RS₂/KOH has the highest surface area and micropore volume than all rest samples.

This means that its surface area concentrated in micropores. RS₁/KOH has high micropore and mesopore volume that make the total pore volume reach its maximum in this sample while its micropore volume still lower than RS₂/KOH so its surface area is lower than RS₂/KOH but great compared to all other samples.

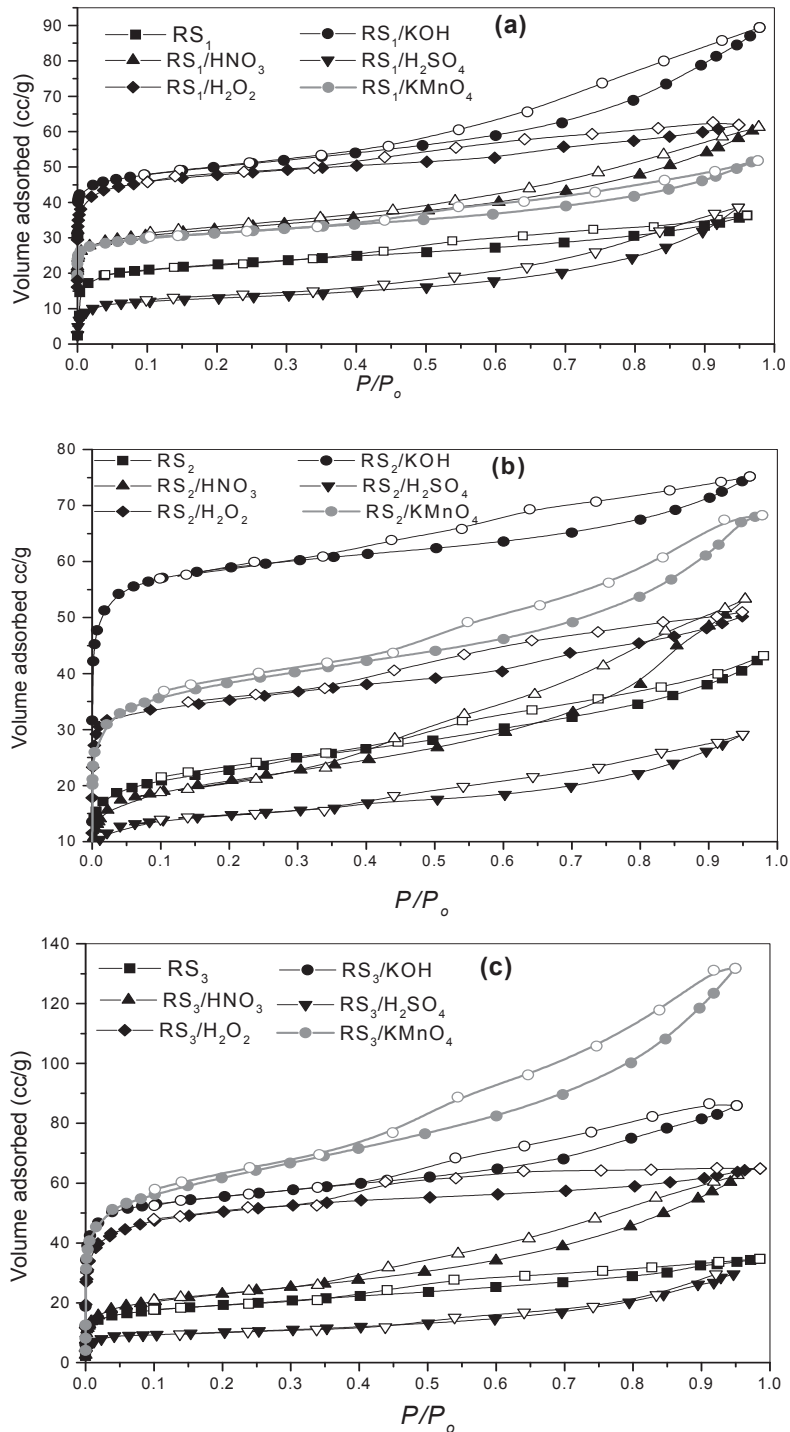
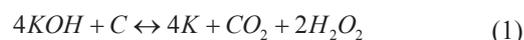


Fig. 1. (a) Nitrogen adsorption isotherms for RS₁ biochar series, (b) nitrogen adsorption isotherms for RS₂ biochar series and (c) Nitrogen adsorption isotherms for RS₃ biochar series (Solid symbols: adsorption; open symbols: desorption)

Table 2. Pore structure parameters of RS biochars

Method	BET			DFT					
	Residue	SBET (m ² /g)	V _{p(0.95)} (cc/g)	r _{BET} (nm)	S _{DFT} (m ² /g)	S _{mic} (m ² /g)	S _{mes} (m ² /g)	V _{p(DFT)} (cc/g)	V _{mic} (cc/g,%)
RS ₁	71.35	0.055	1.55	59.5	51.5	8.0	0.054	0.03(55)	0.024(45)
RS1/KOH	143.3	0.175	2.45	137.1	100	37.1	0.165	0.065(25)	0.1(75)
RS1/HNO ₃	87.2	0.118	2.7	59.4	30	29.4	0.11	0.02(18)	0.09(82)
RS1/H ₂ SO ₄	56.9	0.082	2.9	43.9	29.2	14.7	0.08	0.02(25)	0.06(75)
RS1/H ₂ O ₂	110.9	0.078	1.4	107.3	98.0	9.3	0.076	0.05(66)	0.026(34)
RS1/KMnO ₄	87.75	0.095	2.2	71.6	51.3	20.3	0.094	0.03(32)	0.064(68)
RS ₂	76.2	0.063	1.6	65.3	52.8	12.5	0.064	0.034(53)	0.03(47)
RS2/KOH	179.7	0.115	1.3	186.6	180	6.4	0.105	0.081(77)	0.024(23)
RS2/HNO ₃	68.8	0.083	2.4	56.4	39.7	16.7	0.074	0.021(28)	0.053(72)
RS2/H ₂ SO ₄	46.9	0.045	1.9	40.4	33.2	7.17	0.047	0.02(44)	0.025(56)
RS2/H ₂ O ₂	96.8	0.06	0.9	120.9	97.5	23.4	0.057	0.05(88)	0.007(12)
RS2/KMnO ₄	122.9	0.1	1.7	114.1	99.2	14.88	0.099	0.05(50)	0.049(50)
RS ₃	63.0	0.052	1.65	53.8	43.6	10.2	0.047	0.02(47)	0.025(53)
RS3/KOH	86.3	0.066	1.5	85.1	77.4	7.75	0.063	0.04(63)	0.023(37)
RS3/HNO ₃	66.3	0.081	2.45	50.7	32.3	18.4	0.077	0.02(26)	0.057(74)
RS3/H ₂ SO ₄	47.5	0.065	2.7	37.0	24.2	12.8	0.054	0.014(26)	0.04(74)
RS3/H ₂ O ₂	85.1	0.053	1.2	76.5	71.4	5.1	0.051	0.04(78)	0.011(22)
RS3/KMnO ₄	91.5	0.092	2.0	78.1	60.6	17.5	0.086	0.032(37)	0.054(62)

It has been reported that metals, and specially potassium may be intercalate to the biochar matrix, resulting in increase of pore volume and alkali might catalyze this process (Martin-Gullon et al., 2004). The potassium hydroxide is reduced by the biochar producing potassium metal which is removed by washing (Lillo-Rodenas et al., 2003) (Eq. 1).



We can conclude that the highest modification effect is produced by KOH and its treated biochars have very important properties i.e. it posses higher surface area and micropore volume than other treated biochars.

Generally, modified biochars give different micro and mesopore concentration compared to the original biochar. It may be considered that pores are formed by etching the lattice by different etchants so different sizes of pores are formed. By the use of such modifying solutions the fixation of oxygen

groups on the wall of mesopores converting those previously classified as mesopores into micropores i.e micropores increased (Korili and Gil, 2001). Together with the process of oxygen fixation, there is indication that some pores were destroyed because of the loss of pore wall results in increase of mesoporosity. Change to the physical morphology of modified biochar depends on the strength of the oxidizing agent. In summation, sever oxidation practically destroy the porous structure of the original biochar due to erosion of the pore wall, while oxidation carried out in moderate condition promotes some modification in the original texture characteristics.

3.3. Pore size distribution

Figs. 2 and 3 depict DFT pore size distribution of the biochar samples. It is clear that the samples exhibit wide pore size distribution, from narrow micropores to wide mesopores.

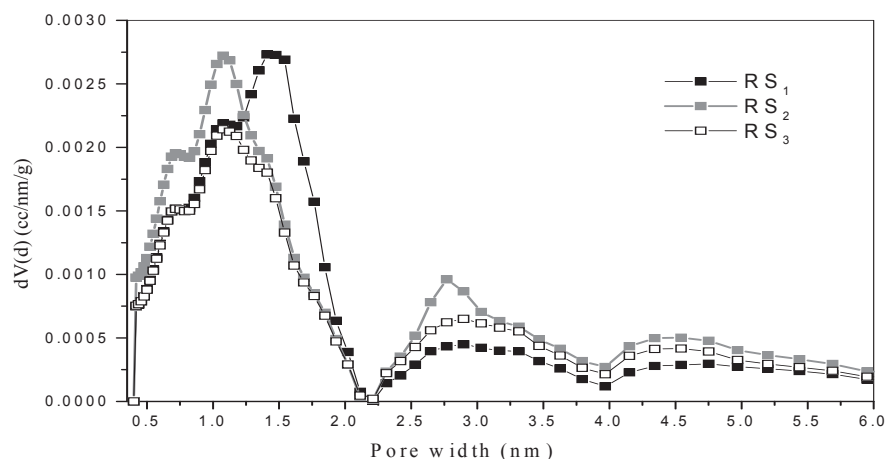


Fig. 2. DFT pore size distribution of biochar samples

Regarding of micropore region, one modal distribution of pore size is gained in all biochar samples with peak in fluctuate in range of 1.0 to 1.3 nm. For mesopore region, a wide pore size distribution was detected with two minima at about 3.0 nm and 5.0 nm corresponding to the transition from pore wide accommodating one adsorbed layer to two, and two layer to three, respectively (Villar-Rodile et al., 2002).

The results illustrate that carbonization temperature appears to affect pore size distribution (Fig. 2). The micropore of carbonized Rice Straw at 550 °C concentrated in peak at 1.5 nm while increasing carbonization temperature shifts this peak to lower pore width at 1.0 nm.

In mesopore range there are two broad peaks at 2.7 and 4.5 nm, its intensity increased by increasing carbonization temperature up to 650 °C.

Thus we can say that increasing carbonization temperature enhancing micro and mesoporosity.

The effect of increasing porosity with temperature occur up to 650 °C but by increasing temperature to 750 °C, there is remarkable contrast in the micropore volume and little decrease of mesopore volume. This indicates that increasing temperature above 650 °C lead to destruction of micropores and some mesopores. Thus Rice Straw carbonized at 650 °C has the highest developed micro and mesoporosity.

For samples treated by HNO₃ or H₂SO₄ (Fig. 3), the micropore size distribution is destroyed by oxidation, with great reduction of micropore volume and shifting in direction of larger pore size in comparison with parent biochar, which is a highly pronounced with increasing carbonization temperature of the parent biochar.

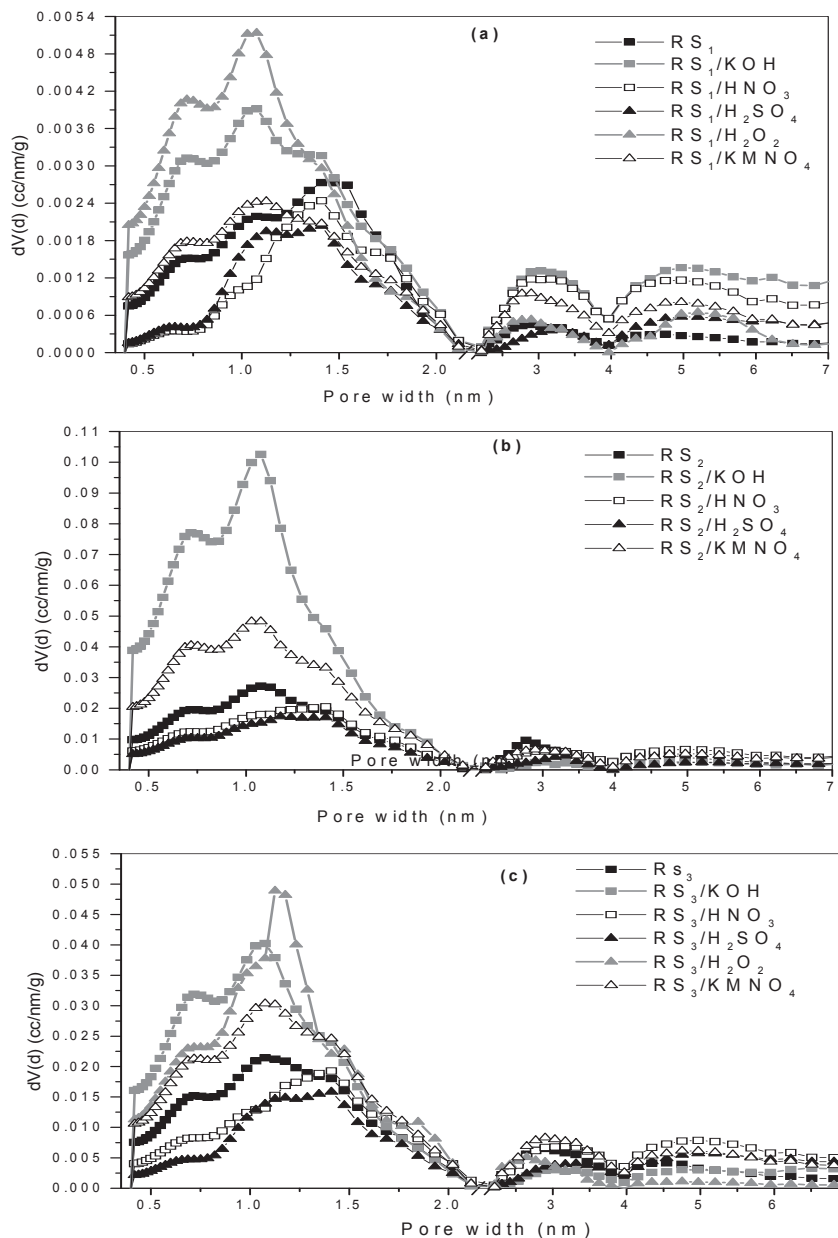


Fig. 3. (a) DFT pore size distribution of biochar samples (a) RS₁ series, (b) DFT pore size distribution of biochar samples (b) RS₂ series and (c) DFT pore size distribution of biochar samples (c) RS₃ series

In mesopore range, HNO₃ gives mesopores greater than H₂SO₄ and this effect is highly appeared at high carbonization temperature where RS₃/HNO₃ gives the highest mesoporosity of all samples.

Generally the peak height in case of HNO₃ treatment is greater than that of H₂SO₄ treatment in both micropore and mesopore ranges. This means that the main effect of H₂SO₄ treatments on microporosity is to open the preexistent pores while HNO₃ fix more oxygen groups converting mesopores to micropores, i.e. the destruction effect is predominate in H₂SO₄ treatment while group fixation effect is predominate in HNO₃ treatment. This is probably one of the reasons why the mesopores volume increases in case of HNO₃ in spite of it has comparable micropore volume with H₂SO₄ treatment.

In contrast, in the KOH and H₂O₂ treatment, the micropore peak height increases which reflect the enhancement of micropore volume. Especially at lower carbonization temperature the peaks of KOH and H₂O₂ are shifted to lower micropore diameter and KOH gives the greatest contribution of mesoporosity. So we can conclude that HNO₃ and H₂SO₄ treatment give high developed mesoporosity, H₂O₂ give highest microporosity while KOH give both high micro and mesoporosity.

The distribution of the peaks in samples treated by KOH and H₂O₂ are sharper than that of the starting biochar, while the peaks of samples treated by HNO₃ and H₂SO₄ are broader. These results indicate that more homogenous micropore distribution produced from KOH and H₂O₂ treatment in contrast of HNO₃ and H₂SO₄ treatment, which give heterogeneous micropore distribution (Korili and Gil, 2001).

In practice, more micropores are necessary for biochars application in gas phase adsorption because almost of gaseous pollutant molecules diameters range from 0.4 to 0.9 nm (Guo and Lua, 2000). On the other hand, biochars application for liquid phase adsorption must have mesopores owing to larger sizes of liquid molecules. This development in microporosities of biochars prepared from Rice Straw points to potential applications in both gas-phase and liquid-phase adsorption for air and water pollution control.

4. Conclusions

Biochars porosity was significantly different according to the carbonization temperature and modifying agent strength. Under our experimental conditions 650 °C can be considered as optimum for biochar preparation. Surface area of biochars prepared at 650 °C (76m²/g) higher than that carbonized at 550 °C (71m²/g) and 750°C (63m²/g). Considering parent samples as reference, KOH treatment increases the surface area followed by H₂O₂ and KMnO₄ whereas H₂SO₄ decreases the surface area followed by HNO₃. Increasing temperature shifts peak from 1.5 nm to lower pore

width at 1.0 nm and increases intensity of two peaks at 2.7 and 4.5 nm in mesoporous range.

Acknowledgments

The authors would like to extend their sincere appreciation to the Deanship of Scientific Research at King Saud University for its funding of this research through the Research Group Project No RGP-VPP-184.

References

- Ahmad M., Rajapaksha A.U., Lim J.E., Zhang M., Bolan N., Mohan D., Vithanage M., Lee S.S., Ok Y.S. (2014), Biochar as a sorbent for contaminant management in soil and water: A review, *Chemosphere*, **99C**, 19-33.
- Azargohar R., Nanda S., Kozinski J.A., Dalai A.K., Sutarto R., (2014), Effects of temperature on the physicochemical characteristics of fast 4 pyrolysis biochars derived from Canadian waste biomass, *Fuel*, **125**, 90-100.
- Babel S., Kurniawan T.A., (2004), Cr(VI) removal from synthetic wastewater using coconut shell charcoal and commercial activated carbon modified with oxidizing agents and/or chitosan, *Chemosphere*, **54**, 951-67.
- Brunauer S., (1943), *The adsorption of gases and vapors - Physical adsorption*, vol. I, Princeton University Press.
- Chen B., Chen Z., Lv S., (2011a), A novel magnetic biochar efficiently sorbs organic pollutants and phosphate, *Bioresource Technology*, **102**, 716-23.
- Chen X., Chen G., Chen L., Chen Y., Lehmann J., McBride M.B., Hay A.G., (2011b), Adsorption of copper and zinc by biochars produced from pyrolysis of hardwood and corn straw in aqueous solution, *Bioresource Technology*, **102**, 8877-84.
- Daifullah A.A., Yakout S.M., Elreefy S.A., (2007), Adsorption of fluoride in aqueous solutions using KMnO₄-modified activated carbon derived from steam pyrolysis of rice straw, *Journal of Hazardous Materials*, **147**, 633-43.
- Domingo-Garca M., Lopez-Garzon F.J., Perez-Mendoza M., (2000), Effect of some oxidation treatments on the textural characteristics and surface chemical nature of an activated carbon, *Journal of Colloid and Interface Science*, **222**, 233-240.
- El-Hendawy A.A., (2003), Influence of HNO₃ oxidation on the structured and adsorptive properties of corncob activated carbon, *Carbon*, **41**, 713-722.
- Girgis B.S., Yunis S.S., Soliman A.M., (2002), Characteristics of activated carbon from peanut hulls in relation to conditions of preparation, *Materials Letters*, **57**, 164-172.
- Guo J., Lua A.C., (1999), Textural and chemical characterizations of activated carbon prepared from oil-palm stone with H₂SO₄ and KOH impregnation, *Microporous Mesoporous Materials*, **32**, 111-117.
- Guo H., Lua A.C., (2000), Preparation of activated carbons from oil-palm-stone chars by microwave induced carbon dioxide activation, *Carbon*, **38**, 1985-1993.
- Guo J., Xu W.S., Chen Y.L., Lua A.C., (2005), Adsorption of NH₃ onto activated carbon prepared from palm shells impregnated with H₂SO₄, *Journal of Colloid and Interface Science*, **281**, 285-290.
- Hameed B.H., El-Khaiary M.I., (2008), Kinetics and equilibrium studies of malachite green adsorption on

- rice straw-derived char, *Journal of Hazardous Materials*, **153**, 701-708.
- Heo H.S., Park H.J., Yim J.H., Sohn J.M., Park J., Kim S.S., Ryu C., Jeon J.K., Park Y.K., (2010), Influence of operation variables on fast pyrolysis of *Miscanthus sinensis* var. *purpurascens*, *Bioresource Technology*, **101**, 3672-7.
- Korili S.A., Gil A.A., (2001), On the applications of various methods to evaluate the microporous properties of activated carbons, *Adsorption*, **7**, 249-264.
- Lehmann J., Joseph S., (2009), *Biochar for environmental management: an introduction*, Earthscans.
- Lehmann J., Rillig M.C., Thies J., Masiello C.A., Hockaday W.C., Crowley D., (2011), Biochar effects on soil biota –a review, *Soil-biology-and-biochemistry*, **43**, 1812–1836.
- Lillo-Rodenas M.A., Cazorla-Amoros D., Linares-Solano A., (2003), Understanding chemical reactions between carbons and NaOH and KOH, An insight into the chemical activation mechanism *Carbon*, **41**, 267–275.
- Lima I.M., Boateng A.A., Klasson K.T., (2010), Physicochemical and adsorptive properties of fast-pyrolysis biochars and their steam activated counterparts, *Journal of Chemical Technology and Biotechnology*, **85**, 1515-1521.
- Martin-Gullon I., Marco-Lozar J.P., Cazorla-Amoros D., Linares-Solano A., (2004), Analysis of the microporosity shrinkage upon thermal post-treatment of H₃PO₄ activated carbons, *Carbon*, **42**, 1339–1343.
- Novawin2/2-P VER. 2.1, (2003), Operation Manual Quantachrome Instruments.
- Pereira M.F.R., Soares S.F., Órfão J.J.M., Figueiredo J.L., (2003), Adsorption of dyes on activated carbons: influence of surface chemical groups, *Carbon*, **41**, 811-821.
- Pradhan B.K., Sandles N.K., (1999), Effect of different oxidizing agent treatments on the surface properties of activated carbons, *Carbon*, **37**, 1323-1332.
- Qiu Y., Zheng Z., Zhou Z., Sheng G.D., (2009), Effectiveness and mechanisms of dye adsorption on a straw-based biochar, *Bioresource Technology*, **100**, 5348-5351.
- Shackley S., Carter S., Knowles T., Middelink E., Haeefele S., Sohi S., Cross A., Haszeldine S., (2012), Sustainable gasification-biochar systems? A case-study of rice-husk gasification in Cambodia, Part 1: Context, chemical properties, environmental and health and safety issues, *Energy Policy*, **42**, 49–58.
- Shim J.W., Park S.J., Ryu S.K., (2001), Effect of modification with HNO₃ and NaOH by pitch-based activated carbon fibers, *Carbon*, **39**, 1635-1642.
- Sun K., Ro K., Guo M., Novak J., Mashayekhi H., Xing B., (2011), Sorption of bisphenol A, 17 α -ethinyl estradiol and phenanthrene on thermally and hydrothermally produced biochars, *Bioresource Technology*, **102**, 5757-5763.
- Villar-Rodile S., Denoye R., Rouquero J., Martinez-Alonso A., Tascon J.M.D., (2002), Porous Texture Evolution in Nomex-Derived Activated Carbon Fibers, *Journal of Colloid and Interface Science*, **252**, 169-176.
- Xu R.K., Xiao S.C., Yuan J.H., Zhao A.Z., (2011), Adsorption of methyl violet from aqueous solutions by the biochars derived from crop residues, *Bioresource Technology*, **102**, 10293-10298.
- Youssef A.M., Ghazy T.M., El-Nabaiuwy T.H., (1982), Moisture sorption by modified-activated carbons, *Carbon*, **20**, 113-116.
- Yun C. H., Park Y. H., Park C.R., (2001) Effects of pre-carbonization on porosity development of activated carbons from rice straw, *Carbon*, **39**, 559–567.



“Gheorghe Asachi” Technical University of Iasi, Romania



TRANSFORMATION OF TECHNOGENIC Cu AND Zn COMPOUNDS IN CHERNOZEM

Tatiana M. Minkina¹, Tatiana V. Bauer¹, Abdulmalik A. Batukaev²,
Saglara S. Mandzhieva^{1*}, Marina V. Burachevskaya¹, Svetlana N. Sushkova¹,
Tatiana V. Varduni¹, Alexey K. Sherstnev¹, Valery P. Kalinichenko³

¹Southern Federal University, 105 Bolshaya Sadovaya St., 344006 Rostov-on-Don, Russia

²The Chechen State University, Chechen Republic, 32 Sheripov St., 364907 Grozny, Russia

³Institute of Soil Fertility of South Russia, 2 Krivoshlykov St., 346493 Persianovka, Russia

Abstract

The influence of exogenous form of heavy metals intake on their transformation in the soil is determined during model experiments. Distinctions in quantity of extracted mobile compounds of heavy metals in the soil depending on a form of addition various connections of Cu and Zn are established. The smallest mobility of Cu and Zn at addition of heavy metal oxides is observed. It is established that Cu accumulates mainly in the fraction connected with organic matter; Zn accumulates in residual fraction and in the fraction connected with ferric oxide and manganese oxide by consecutive fractionation technique.

Key words: attendant anion, chernozem ordinary, fractionation, heavy metals compounds, transformation

Received: July, 2014; *Revised final:* November, 2014; *Accepted:* November, 2014

1. Introduction

Soil contamination adversely affecting agroecosystems occurs from different sources, however, the heavy metals (HM) ranking among the first. In case of technogenic contamination, the HM input to soil leads to their accumulation in the topsoil and the quite different interaction with soil components in dependence of adsorbent properties and chemical peculiar features of the metal.

In the course of further transformation, HM are involved into different chemical and physical-chemical processes that have an influence on their behavior in soil (Kar and Berenjian, 2013; Ma et al., 2013; Minkina et al., 2008; 2013; Wiatrak, 2014). Numerous mechanisms responsible for interaction between HM and soil components depend on different HM forms, which determine their mobility, migration capacity and toxicity (Abdulla et al., 2013; Endovitsky et al., 2014; Minkina et al., 2012).

As a rule, HM are present in soil in easily and difficultly soluble forms. The easily soluble forms can effectively react with soil components, whereas due to further transformation the hardly soluble forms are subject to dissolution (Ladonin and Karpukhin, 2011).

The metal oxides and salts in soils can represent different potential threats for the environment and living organisms. In soils contaminated with metal oxides the concentration of metal mobile forms is lower than in soil contaminated with metals in the form of easily soluble salts (Minkina et al., 2014). Therefore, the metal oxides in the soil should induce a lower environmental hazard per unit of metal mass than easily soluble salts (Pinskii et al., 2014).

The present study is aimed at identifying the regularities in transformation processes of exogenic Zn and Cu compounds in ordinary chernozems.

* Author to whom all correspondence should be addressed: e-mail: msaglara@mail.ru; Phone: +7 988 896 9553; Fax: +7 863 2975070

2. Materials and methods

2.1. Soil characteristics

Soil samples were taken in the 0-20cm topsoil of the heavy-textured ordinary chernozem on loess-like loam (Haplic Chernozem, FAO) in the virgin area.

The soil had a clay content of 286 g kg⁻¹ and a physical clay content of 471 g kg⁻¹, pH_(water) of 7.3, organic C content of 23 g kg⁻¹, CaCO₃ content of 1 g kg⁻¹, cation exchange capacity of 37.1 mmolc kg⁻¹ and exchangeable Ca, Mg and Na contents of 29.5, 5.5 and 0.1 mmolc kg⁻¹, respectively.

The soil was air dried, homogenized and sieved to a 1 mm fraction for the experiment.

2.2. Pot experiment

In order to study transformation of Zn (II) and Cu (II) cations absorbed by soil we conducted the pot experiment. The soil (1 kg) was mixed with dry metal salts and placed into plastic pots with ceramsite drainage. We used Zn and Cu salts of oxides, acetates, sulfides, chlorides, nitrates and phosphates. These salts are the main forms in which metals entered in soil from technogenic sources. Zn and Cu salts were added in soil separately in three replicates.

The dose 300 mg kg⁻¹ of Zn and Cu corresponds to the level of soil contamination by these metals in the Rostov region (Russia). The soil was irrigated to the field water capacity and this moisture level remained for the whole period of experiment (1 year).

2.3. Extraction procedures

Parallel extractions were employed to study Zn and Cu mobile forms (Minkina et al., 2008; 2013), using the following reagents: 1 N ammonium acetate buffer (NH₄OAC) at pH 4.8 for extraction of the exchangeable forms; 1% EDTA in NH₄OAC at pH 4.8 for the exchangeable and complex forms. The amount of complex compounds was calculated as differences between the HM content in extract of the mixed reagent and NH₄OAC. 1 N HCl extracted acid soluble forms.

The difference between the Zn and Cu content in HCl and NH₄OAC extract permitted to determine the amount of specifically sorbed compounds. The sum of the exchangeable, complex and specifically sorbed forms is weakly bound compounds. They are the most important from ecological viewpoint and capable to enter adjacent areas and the plants in particular. The data obtained by sequential extraction show a trend of transformation processes of an exogenic metal in soil and mechanisms responsible for this transformation. In order to study the interaction between HM and soil components the fractional analysis by Tessier's method (Tessier et al., 1979) was made in soil samples contaminated with metal acetate salts (Table 1). The salts of acetic

acid were preferred because they are the most soluble and capable to interact quickly with the soil components. The Tessier's method is one of the most used methods of sequential fractionation (Minkina et al., 2008). The Tessier's procedure of fractionating metals is largely similar to other methods used for the analysis of soils, sediments, and bottom sediments. This procedure ensures the separation of five fractions of HM compounds:

(1) The exchangeable fraction contains metal ions mainly retained by electrostatic forces on the surface of clay and other minerals, organic substances, and amorphous compounds with the low pH values of zero charge. The fraction is affected by the ionic composition of soil solution. The exchangeable forms of HM extractable from soils by neutral salt solutions mainly correspond to adsorbed forms weakly bound to the soil matrix (Mandzhieva et al., 2014; Pinskii et al., 2014).

(2) The carbonate-bound fraction contains HM ions specifically sorbed on Ca and Mg carbonates. Partial dissolution of metal phosphates is also possible (Perelomov and Pinsky, 2003).

(3) The hydroxide-bound fraction contains HM ions occluded by amorphous Fe and Mn hydroxides or adsorbed on their surface. Metals from organic complexes and amorphous sulfides can be released during extraction.

(4) The organic matter-bound fraction contains HM ions retained by organic substances or organomineral compounds. Sulfides can undergo partial decomposition.

(5) The residual fraction contains HM ions strongly fixed in the crystal lattices of primary and secondary minerals.

This fraction can also include metals from stable sulfides and, in small amounts, stable organomineral substances. After each extraction step, the liquid and solid phases are separated by centrifugation. Metal concentration in solutions was determined by atomic-absorption spectroscopy (AAS).

3. Results and discussion

In the uncontaminated soil the distribution of Zn and Cu forms were given in the following sequence: specifically sorbed > complex > exchangeable. The content of the most mobile exchangeable forms is very low – less than 1 mg kg⁻¹ (Tables 2, 3), what may be explained by the presence of carbonates in soil, their highly dispersed mycelial form and slightly alkaline pH (Minkina et al., 2013). The weakly bound Zn and Cu compounds are mainly represented by specifically sorbed forms.

Due to artificial soil contamination with Zn and Cu in the rate of 300 mg kg⁻¹ their content in extracted forms reveals changes caused by chemical properties of these metals. The Zn distribution in the group of weakly bound compounds can be ranked in the following order: specifically sorbed > exchangeable > complex.

Table 1. Sequential fractionation of metals (Tessier et al., 1979)

<i>Metal compounds</i>	<i>Extractant</i>	<i>Soil : solution ratio</i>	<i>Extraction conditions</i>
Exchangeable	1 M MgCl ₂ , pH 7.0	1:8	shaking at room temperature for 1 h
Bound to carbonates	1 M NaCH ₃ COO, pH 5.0 (with CH ₃ COOH)	1:8	shaking at room temperature for 5 h
Bound to Fe, Al, and Mn (hydr)oxides	0.04 M NH ₂ OH·HCl in 25% CH ₃ COOH	1:20	heating at 96±3°C under periodical shaking for 8 h
Bound to organic matter	0.02 M HNO ₃ + 30% H ₂ O ₂ , pH 2.0 (with HNO ₃), then 3.2 M NH ₄ CH ₃ COO in 20% HNO ₃	1:20	heating at 85±2°C under periodical shaking for 5 h
Residual fraction	HF+HClO ₄ , then conc. HNO ₃	1:25	evaporation

Table 2. The content of weakly bound Zn compounds (mg kg⁻¹) in ordinary chernozem contaminated with this metal (300 mg kg⁻¹) in the form of different compounds

<i>Exchangeable compounds</i>	<i>Complex compounds</i>	<i>Specifically adsorbed compounds</i>	<i>Weakly bound compounds</i>
no metal addition			
0.3±0.01	1.4±0.1	10.9±1.2	12.6±1.4
ZnO			
83.8±7.7	19.1±2.6	111.2±10.5	214.1±18.0
Zn(CH ₃ COOH) ₂			
34.5±3.9	51.8±4.7	146.5±15.2	232.8±20.0
ZnSO ₄			
105.5±9.1	16.7±1.3	120.7±9.9	242.9±19.2
Zn(NO ₃) ₂			
96.8±8.2	27.3±2.1	163.3±14.8	287.4±23.1
ZnCl ₂			
102.0±8.7	47.0±5.1	209.5±11.9	358.5±32.4
Zn ₃ (PO ₄) ₂			
101.8±9.0	63.5±7.6	192.8±18.0	358.1±22.9

An insignificant Zn concentration in complex forms is explained by its greater binding to carbonates and oxides as compared to the organic matter (Minkina et al., 2008; Pinskii et al., 2014). The Cu distribution in forms of compounds within the uncontaminated and contaminated soils is identical and can be presented according to the following order: specifically sorbed > complex > exchangeable. In the studied soil the metal mobility increases due to its complex formation with the organic matter. The data of fractional composition of Cu compounds in soil were shown that the organic matter plays a primary role in absorption of this metal (Ladonin and Karpukhin, 2011; Minkina et al., 2008; Pinskii et al., 2010).

When introducing different metal compounds into the soil, it was possible to define the difference in the amount of extracted Zn and Cu that is explained by varying solubility of their compounds (Pinskii et al., 2014). For instance, the Zn input to soil in the form of hardly soluble compounds showed that after incubation for a 1 year the content of its mobile compounds seemed to be lower by 5-7 units as compared to that applied in the form of easily soluble salts. As regards Cu, its content was decreased by 1.0-3.5 units. The Cu oxide (K_{sp} 4,79×10⁻²¹) is soluble to a lesser extent than Zn oxide

(K_{sp} 2,19×10⁻¹⁷). When comparing the influence of anions on extraction of HM cations from soil, it seemed reasonable to show that the amount of weakly bound Zn compounds becomes decreased according to the following order: PO₄²⁻ ≈ Cl⁻ > NO₃⁻ > SO₄⁻ > CH₃COO⁻ > O⁻. The content of Cu compounds was presented as follows: NO₃⁻ > Cl⁻ > SO₄²⁻ > PO₄²⁻ > CH₃COO⁻ > O⁻. According to the results of experiment to study the salts solubility, it was found that zinc phosphate unlike copper dissolves in NH₄OAC at pH 4.8, 1% EDTA in NH₄OAC at pH 4.8 and 1 N HCl. The solution's pH changes in contact with the soil depending on the content of the adsorbed HM cations and the attendant anions. The values of the pH for the soil suspensions after the addition of HM salts are reduced by 0.2-0.5 units (Pinskii et al., 2014).

One of the methods to study the metal forms in soil is chemical sequential extraction permitting to distribute HM according to their binding with the main soil components as bearers of these metals. Just this method is more informative as compared to selective extracts, because it allows partitioning even conservative metal fractions containing in metal crystalline litters (Ladonin and Plyaskina, 2009). The results of the sequential extraction of initial uncontaminated soil served as evidence of the

following distribution of Cu forms: residual fraction > bound to the organic matter > bound to Fe and Mn oxides > bound to carbonates > exchangeable fraction. For Zn is quite another picture: residual fraction > bound to Fe and Mn oxides > bound to the organic matter > bound to carbonates > exchangeable (Table 4). The peculiar feature of the fractional composition of Zn and Cu compounds in initial soil is that the residual fraction is found to be dominant (for Zn – 67% of the total content, for Cu – 38%). Such are the regional biogeochemical features of the soil microelement composition in Rostov oblast (south of Russia) and of the mineralogical composition of the parent rocks. The yellow brown loess like loams and clays of the PreCaucasian Plain inherited the stable minerals of the initial rocks with the typical microelement composition of the minerals (Minkina et al., 2013).

Distribution of HM fractions in non-contaminated soils is a result of soil formation processes and chemical properties of metals determining their affinity with different soil components (Ladonin and Karpukhin, 2011). The prevalence of residual fraction parallel with the low content of the other two fractions bound to soil to a lesser extent, serves as evidence that the initial soil has no HM of technogenic origin. Having analyzed the distribution of Zn and Cu fractions in the contaminated soil, it should be concluded that the fractions are differently distributed (Table 4). In case of artificial soil contamination with HM acetates (300 mg kg⁻¹) the exchangeable fraction seems to be increased by 25 for Zn and 16 for Cu. Besides, the relative content of metals in the given fraction increases insignificant: 3% and 1% respectively (Table 5).

Table 3. The content of weakly bound Cu compounds (mg kg⁻¹) in ordinary chernozem contaminated with this metal (300 mg kg⁻¹) in the form of different compounds

<i>Exchangeable compounds</i>	<i>Complex compounds</i>	<i>Specifically adsorbed compounds</i>	<i>Weakly bound compounds</i>
no metal addition			
0.3±0.01	0.5±0.1	2.2±0.3	3.0±0.6
CuO			
9.7±1.2	58.8±5.3	101.2±9.9	169.7±12.3
Cu(CH ₃ COOH) ₂			
13.3±1.4	63.9±5.9	107.6±11.7	184.8±11.8
Cu ₃ (PO ₄) ₂			
31.3±2.7	76.3±8.1	141.0±11.2	248.6±12.3
CuSO ₄			
32.5±3.4	100.5±10.2	146.5±11.3	279.5±12.9
CuCl ₂			
61.3±4.1	109.2±10.6	145.7±10.3	316.2±11.5
Cu(NO ₃) ₂			
68.3±6.2	112.9±8.6	146.7±11.0	327.9±16.7

Table 4. Fractional Zn and Cu distribution in ordinary chernozem, mg kg⁻¹

<i>Dose of metal, mg kg⁻¹</i>	<i>The exchangeable fraction</i>	<i>The carbonate-bound fraction</i>	<i>The hydroxide-bound fraction</i>	<i>The organic matter-bound fraction</i>	<i>The residual fraction</i>	<i>Sum of fraction</i>
Zn(CH ₃ COOH) ₂						
no metal addition	0.6±0.2	1.8±0.3	14.2±2.1	11.5±3.5	56.9±6.0	85.0
300	15.2±1.9	24.6±2.2	144.5±10.2	30.7±2.6	153.0±12.8	368.0
Cu(CH ₃ COOH) ₂						
no metal addition	0.4±0.1	1.2±0.3	10.0±2.2	16.1±4.3	17.3±2.4	45.0
300	6.5±1.1	27.8±3.2	116.4±10.4	110.1±9.9	80.2±8.6	341.0

Table 5. Relative content of Zn and Cu forms in ordinary chernozem, % of the sum of fractions

<i>Dose of metal, mg kg⁻¹</i>	<i>The exchangeable fraction</i>	<i>The carbonate-bound fraction</i>	<i>The hydroxide-bound fraction</i>	<i>The organic matter-bound fraction</i>	<i>The residual fraction</i>
Zn(CH ₃ COOH) ₂					
no metal addition	1	2	17	13	67
300	4	7	39	8	42
Cu(CH ₃ COOH) ₂					
no metal addition	1	3	22	36	38
300	2	8	34	32	24

The fraction bound to carbonates becomes enhanced by 14 for Zn and by 23 for Cu with the metal introducing into the soil. Fe-Mn oxides play a dominating role in accumulation of this HM. In this case the relative content of Cu shows an increase by 12%. The Zn amount in the fraction bound to Fe-Mn oxides and hydroxides is the greatest as compared to the residual fraction increased by 22% (Table 4). Zn is characteristic of rather great affinity to reactionary center of mineral soil components (Guisti, 2011; Minkina et al., 2008; Nimirciag, 2012; Pinski et al., 2014).

In case of contaminating the soil with Cu in the dose of 300 mg kg⁻¹ a share of the organic fraction gets decreased by 4%. The Zn amount in the given fraction increases by 2.7 units. In view of this, the percentage content of Zn decreases by 5%. Zn is capable to form stabile complexes to a lesser extent. The organic matter plays a significant role in Zn immobilization in view of forming the unstable out- or intrasphere complex compounds capable to transfer into the other forms of compounds (Mandzhieva et al., 2014; Perelomov and Pinsky, 2003; Pinski et al., 2010; Rodríguez-Oroz et al., 2012).

The HM input to soil in the doze of 300 mg kg⁻¹ reveals decreasing a share of the firmly bound residual fraction in the total content of the metal extracted from soil (14% for Cu and 25% for Zn). This serves as evidence that this metal is weakly involved into the structure of the most stable soil components. Such a peculiarity in distribution of HM fractions can be used as a diagnostic criterion for natural or anthropogenic contamination of soils and the level of their contamination (AL-Sharafat et al., 2012; Minkina et al., 2013).

4. Conclusions

1. The form of applied metal exerts an impact on its mobility in soil. Cu and Zn become mobile to a lesser extent when the soil is supplemented with HM oxides. The influence of attendant anions upon the content of weakly bound HM forms shows a decrease in the following order: PO₄²⁻ ≈ Cl⁻ > NO₃⁻ > SO₄²⁻ > CH₃COO⁻ > O⁻ for Zn and NO₃⁻ > Cl⁻ > SO₄²⁻ > PO₄²⁻ > CH₃COO⁻ > O⁻ for Cu.

2. The main role in the interaction with soil components and hence in the distribution according to the HM compounds plays the specific characteristics of the metal, not the attendant anion. Based upon a model experiment it has been established that in non-contaminated soils the main HM share is predominantly concentrated in crystalline litters of the primary and secondary minerals. In contaminated soils the HM are found to be in the following fractions: Cu – in the fraction bound to the organic matter; Fe and Mn oxides take an active part in accumulation of this metal. Zn – in the residual fraction as well as in the fraction bound to Fe-Mn oxides. The regularity in Zn and Cu

distribution according to mobile forms in control and contaminated soils with Cu is in the sequence: specifically sorbed > complex > exchangeable. In soils contaminated with Zn the initial position of mobile forms reveals a change: specifically sorbed > exchangeable > complex.

Acknowledgments

This research was supported by projects of Ministry of Education and Science of Russia, no. 5.885.2014/K; Leading scientific school, no. 5548.2014.5; Russian Foundation for Basic Research, 14-05-00586_A; the President of Russia, no. MK-6448.2014.4. Analytical work was carried out on the equipment of Centers for collective use of Southern Federal University "High Technology", no. RFMEFI59414X0002.

References

- Abdulla N.I., Al-Haidary A.M.A., Al-Jeboori M.I., Zanganah F.H.H., Al-Azawi S.R.F., Al-Dujaili A.H. (2013), Kinetics and equilibrium adsorption study of lead (II) onto low cost clays, *Environmental Engineering and Management Journal*, **12**, 483-491.
- AL-Sharafat A., Altarawneh M., Altahat E., (2012), Effectiveness of agricultural extension activities, *American Journal of Agricultural and Biological Science*, **7**, 194-200.
- Endovitsky A.P., Minkina T.M., Kalinichenko V.P., Batukaev A.A., Dikaev Z.S., Sushkova S.N., (2014), The association of ions in the soil solution of saline soils, *American Journal of Agricultural and Biological Science*, **9**, 238-244.
- Guisti L., (2011), Heavy metals in urban soils of Bristol (UK), Initial screening for contaminated land, *Journal of Soils and Sediments*, **11**, 1385-1398.
- Kar S.Z., Berenjian A., (2013), Soil formation by ecological factors: Critical review, *American Journal of Agricultural and Biological Science*, **8**, 114-116.
- Ladonin D.V., Karpukhin M.M., (2011), Fractional composition of nickel, copper, zinc, and lead compounds in soils polluted by oxides and soluble metal salts, *Eurasian Soil Science*, **8**, 874-885.
- Ladonin D.V., Plyaskina O.V., (2009), Heavy metal pollution of urban soils, *Eurasian Soil Science*, **42**, 816-823.
- Ma Y., Chen J., Wu X., (2013), Assessment of heavy metals contaminations from solidified waste drilling mud landfilling pond in ordos plateau (semi-arid region), China, *Environmental Engineering and Management Journal*, **12**, 1837-1842.
- Mandzhieva S.S., Minkina T.M., Sushkova S.N., Motuzova G.V., Bauer T.V., Chaplugin V.A., (2014), The group composition of metal compounds in soil as an index of soil ecological state, *American Journal of Agricultural and Biological Science*, **9**, 19-24.
- Minkina T.M., Mandzhieva S.S., Chaplugin V.A., Motuzova G.V., Sushkova S.N., Fedorov Y.A., Kolesnikov S.I., Bauer T.V., (2014), Accumulation and distribution of heavy metals in plants within the technogenesis zone, *Environmental Engineering and Management Journal*, **13**, 1535-1543.
- Minkina T.M., Motusova G.V., Mandzhieva S.S., Nazarenko O.G., (2012), Ecological resistance of the soil-plant system to contamination by heavy metals, *Journal of Geochemical Exploration*, **123**, 33-40.

- Minkina T.M., Motuzova G.V., Mandzhieva S.S., Nazarenko O.G., Burachevskaya M.V., Antonenko E.M., (2013), Fractional and group composition of the Mn, Cr, Ni, and Cd compounds in the soils of technogenic landscapes in the impact zone of the Novocherkassk power station, *Eurasian Soil Science*, **46**, 375-385.
- Minkina T.M., Motuzova G.V., Nazarenko O.G., Kryshchenko V.S., Mandzhieva S.S., (2008), Forms of heavy metal compounds in soils of the steppe zone, *Eurasian Soil Science*, **41**, 708-716.
- Nimirciag R., (2012), Heavy metals in the soils of Rodna mining area, Romania and zeolite efficiency for remediation, *Environmental Engineering and Management Journal*, **11**, 421-426.
- Perelomov L.V., Pinsky D.L., (2003), Mn, Pb, and Zn compounds in gray forest soils of the Central Russian Upland, *Eurasian Soil Science*, **6**, 610-618.
- Pinskii D.L., Minkina T.M., Gaponova Y.I., (2010), Comparative analysis of mono-and polyelement adsorption of copper, lead and zinc by an ordinary chernozem from nitrate and acetate solutions, *Eurasian Soil Science*, **43**, 748-756.
- Pinskii D.L., Minkina T.M., Mandzhieva S.S., Fedorov U.A., Nevidomskaya D.G., Bauer T.V., (2014), Adsorption features of Cu(II), Pb(II), and Zn(II) by an ordinary chernozem from nitrate, chloride, acetate, and sulfate solutions, *Eurasian Soil Science*, **47**, 10-17.
- Rodríguez-Oroz D., Lasheras E., Aldabe J., Elustondo D., Santamaría J.M., Garrigó J., (2012), Heavy metals mobility in experimental disturbed and undisturbed acid soil columns in Spanish Pyrenees, *Environmental Engineering and Management Journal*, **11**, 1149-1158.
- Tessier A., Campbell P.G.C., Bisson M., (1979), Sequential extraction procedure for the speciation of particulate trace metals, *Analytical Chemistry*, **51**, 844-850.
- Wiatrak P., (2014), Evaluation of nitrogen application methods and rates with nutrisphere-n on soil nitratennitrogen in southeastern coastal plains, *American Journal of Agricultural and Biological Science*, **9**, 64-71.



“Gheorghe Asachi” Technical University of Iasi, Romania



HEALTH RISK ASSESSMENT OF HEAVY METALS AND POLYCYCLIC AROMATIC HYDROCARBONS IN SOIL AT COKE OVEN GAS PLANTS

Hou Wei¹, Zhang Le¹, Li Shuxian², Wu Dan^{1,3,4*}, Li Xiaojun⁵, Ji Lan², Ma Xiping¹

¹Liaoning University, College of Environmental Science, 110036 Shenyang, China

²Shenyang Academy of Environmental Sciences, 110016 Shenyang, China

³Harbin Institute of Technology, State Key Lab of Urban Water Resources and Environment, 150090 Harbin, China

⁴Liaoning Academy of Environmental Sciences, 110161 Shenyang, China

⁵Chinese Academy of Sciences, Institute of Applied Ecology, 110016 Shenyang, China

Abstract

Sites contaminated with hazardous materials pose serious risks to human health and ecological environments. Quantitative health risk assessment is a site-specific complex procedure requiring evaluation of all possible pathways. Several studies have focused on the evaluation of heavy metals or organic pollutants; however, only few studies focused on the evaluation of diverse pollutants such as heavy metals and organics. In this study, the health risk of heavy metals and organic pollutants in the soils near coke oven gas plants, China, was assessed according to three human exposure pathways (peroral intake soil, skin exposure to soil, inhale soil.). The carcinogenic and noncarcinogenic risk values of the heavy metals and organic pollutants in each grid (divided into three zones and 60 grids) and grid layer (divided into three layers and 128 samples) were calculated. The total carcinogenic and noncarcinogenic risk values were calculated cumulatively as per the grid and grid layer. The grid area and the volume of contaminated soil corresponding to various risk factors were calculated. The results of the health risk assessment show that 49 out of the 60 grids have a carcinogenic risk factor $>10^{-5}$ with a total area of 103,340 m². This site has extremely high health risk if 10^{-5} is regarded as the assessment standard for causing cancer. These results show that coke oven gas plants can pose serious risk to human health, and carcinogenic effects should cause more attention.

Key words: carcinogenic risk assessment, contaminated site, noncarcinogenic risk assessment, organic contaminant, soil

Received: July, 2013; *Revised final:* September, 2014; *Accepted:* September, 2014

1. Introduction

Sites contaminated with hazardous materials are a current and urgent problem globally (Stezar et al., 2011). Contaminated site refers to industrial zones where the hazardous material concentration in soil exceeds the standard value, and the soil or water pollution caused by industrial activities pose potential danger to human health and ecological environments. The pollutions caused by contaminated sites have become a major environmental problem for every nation, and the number of contaminated sites has been increasing (Sousa, 2001). Contaminated sites, particularly the

megasites, have become an issue of major concern because of their worldwide occurrence and the related extensive environmental and socio-economic effects (EEA, 2000; Stezar et al., 2011). Local contamination is one of the main threats to soil identified by the EU Soil Communication (COM, 2002). To date, 300,000 sites across the EU have been identified as definitely or potentially contaminated; however, the European Environment Agency estimated the existence of as many as 1.5 million contaminated sites (EEA, 2000).

Not all metals in soil are bioavailable and cause adverse effects to human health or the environment (Chapman et al., 2003; Jensen et al.,

* Author to whom all correspondence should be addressed: e-mail: inuwudan@126.com; Phone: +8615840379989

2006; Vasseur et al., 2008; Pizzol et al., 2011). However, even trace quantities of heavy metals, such as cadmium (Cd), arsenic (As), lead (Pb), and mercury (Hg), can cause adverse health effects (Ferré-Huguet et al., 2008; Martí-Cid et al., 2008; Martorell et al., 2011).

Organisms in different trophic levels are also believed to be suffering from metal toxicities (Popita et al., 2014; Rand et al., 1995); therefore, human health is under threat from the exposure to heavy metals by seafood intake (Hansen, 1981; Hansen et al., 1990). Organic pollutants, such as polycyclic aromatic hydrocarbons (PAHs), are also a major reason for deformity and cancer. The presence of some PAHs has shown increased incidence of skin, lung, and bladder, liver, and stomach cancers in laboratory animals (Armstrong et al., 2004; Boffetta et al., 1997; Bosetti et al., 2007; Kogevinas et al., 2003). Total cyanide and volatile organic compounds (VOCs) are also considered as trace substances harmful to human health.

The human health risk assessment (HHRA) is a useful approach for quantifying the potential harmful index of environmental contaminants. Depending on land use, risks exist for human health, ecosystems (including ecosystem services), and groundwater (Swartjes et al., 2012). In recent years, extensive research has been focused on this area (Christopher et al., 2014; Health, 1994; Health, 2007; Khillare et al., 2012; MOE, 2005; Richardson, 1997; Stezar et al., 2011; Torretta et al., 2014; Xia et al., 2010; Zhenxing et al., 2011; Zhiyuan et al., 2014). However, many studies focused on heavy metals or organic pollutants, while fewer studies (Saedi et al., 2012) focused on diverse pollutants such as heavy metals and PAHs.

In this study, health risk assessment was conducted based on a comprehensive analysis of the risk assessment methods, such as pollution recognition, exposure assessment, toxicity parameters, and risk characterization, followed in the USA and developed European countries. The purpose of this study were (1) to perform environmental survey and risk assessment of original production sites and health risk assessment by monitoring data that can provide scientific references for site management, restoration, site development, and utilization decisions and (2) to use the quantitative risk assessment methods for heavy metals and PAHs in order to evaluate the health risk for both adults and children by three different exposure pathways.

2. Materials and methods

2.1. Study area

Shenyang Coke Oven Gas Co. Ltd., located at the intersection of Beisi Road and Zhaogong Street in Tiexi district and in the west of Shenyang downtown in Liaoning province, with -130,000 m² areas, 3,800 m maximum length, and 3,400 m maximum width, was chosen as the study site. This company was

established in 1958, which is the only manual gas production company, providing 30% of Shenyang's daily gas requirement. The designed production capability of the company is 450,000 tons of coke, 23,000 tons of tar, 6,000 tons of ammonium sulfate, and 6,000 tons of crude benzene. Major products of the company are metallurgical coke and coke oven gas, and the by-products are ammonium sulfate, tar, and crude benzene. The specific pollutants of the study area are hydrocarbon organic matter and heavy metals.

2.2. Sampling

Seven points and thirteen soil samples were collected from the original Shenyang Coke Oven gas factory on April 12th, 2011 (Fig. 1). Table 2 lists the monitoring methods used in our laboratory for the soil testing, and the results indicate the presence of pollutants such as heavy metal, cyanide, PAH, mononuclear aromatics, petroleum, and hydrocarbons in the soil samples.

Considering the complexity of pollution, comprehensive sampling and monitoring methods were used for the soil analysis. According to the preliminary survey results and the functional use of the original sites, the factory was divided into three zones: (i) chemical product recovery zone (zone A), (ii) coal preparation zone (zone B), and (iii) public zone (zone C). Grids were drawn in the three zones, and the areas of grids increased from zone A to C. Zone A has 25 grids with an area of ~900 m² for each grid; zone B has 18 grids with an area of ~1,600 m² for each grid; and zone C has 17 grids with an area of ~4,600 m² for each grid.

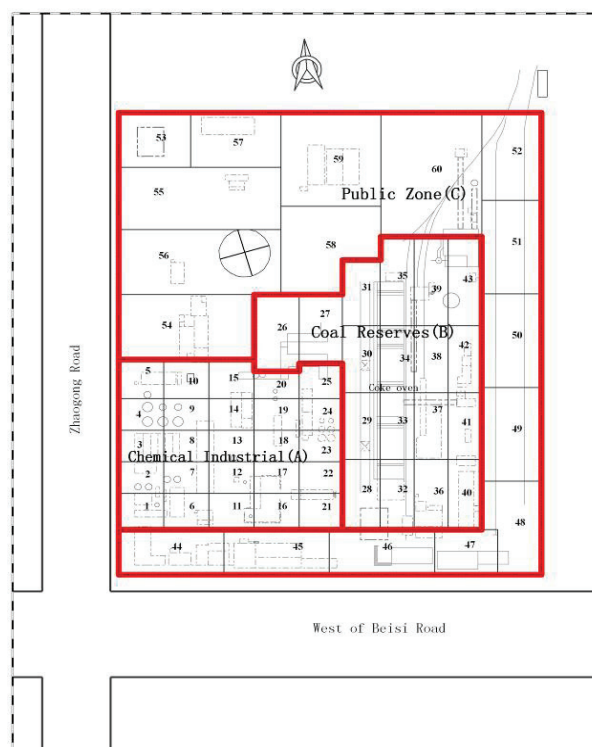


Fig. 1. Study site and sample points

A fixed point in the center of each grid was selected for sampling arrangement principle for zones A and B. However, for the removal project of the original factory, the original site was damaged significantly; therefore, in principle, the samples could be collected nearby the central point. The sampling point arrangement principle for zone C was selected based on the original sites of facilities that caused most of the pollution. From June 28th to July 1st, 2011, 60 points and 128 samples were collected from the site.

In zone A, the soil samples were collected from three layers, and the layer depths from the top to the bottom were 0–0.2 m surface soil, 0.2–0.4 m, and 0.4–1 m (Peijun, et al., 2009). In zone B, the soil samples were collected from two layers, and the sample depths from the top to the bottom were 0–0.2 m surface soil and 0.2–0.4 m. In zone C, the soil samples were collected from one layer, and the sample depth was 0.4–1 m. The samples for metals analyses were stored in closed polyethylene bags at <4 °C. The samples for PAHs (organic matter) were stored in PTFE (polytetrafluoroethylene) gasket brown jar.

2.3. Analytical methods

Pebbles, plant branches, etc. were removed from the collected wet soil samples, and then drying, grinding, and screening were performed using a 100-mesh stainless steel sieve. Soil was mixed and then stored in plastic bags at 0–4 °C after sealing. Sample analysis was conducted by the standard monitoring methods developed by Aoshi Analysis and Detection (Shanghai) Co. Ltd. as shown in Table 1. All the samples including blank, parallel samples, and standard recoveries were analyzed in duplicates for quality assurance/quality control (QA/QC) of laboratory analyses. For PAHs, the QA/QC was performed by field and laboratory blanks and standard spiked recoveries.

The recoveries of SRM (standard reference materials) and internal standards varied from 88% to 107%. The degree of precision was analyzed by the standard parallel experiments to reflect the random error of the analysis method. The relative standard deviations of PAHs, VOCs, and heavy metals in the parallel samples ranged from 1.29% to 25.6%, approaching the standard US EPA RSD <30%, thus demonstrating good precision in the experimental data.

2.4. Risk assessment method

The possible exposure scene of this study was a sensitive residential land. According to the site environment research studies and different functional plannings of different regions, many situations were analyzed where the concerned pollutants may cause harm to human health. Various exposure approaches of the concerned pollutants confirmed the pollutants' migration exposure model for environment and

human body, and then relevant parameter values corresponding to the exposed quantities under various exposure approaches were calculated. For heavy metals, where humans were exposed to site pollutants, the main approaches include three computation modules: peroral intake soil, skin exposure to soil, inhale soil. The exposure dosage was calculated by Eqs. (1) and (2), adapted from (Celebi et al., 2014; US EPA 1989; US EPA 1997).

$$ADD_i = \frac{C_w \times IR \times EF \times ED}{BW \times AT} \quad (1)$$

where ADD_i is the daily exposure dose of the heavy metals or PAHs through three pathways $\mu\text{g}/(\text{kg d})$, C_w is the concentration of heavy metals or PAHs (mg/kg), IR is the ingestion rate (including three exposures: peroral intake soil, skin exposure to soil, inhale soil.) (mg/d), EF is the exposure frequency which is 350 d/year in this study. ED is the exposure duration (year), BW is the body weight (adult: 55.9 kg; child: 15.9 kg). AT is the averaging time (d), which is calculated as 72 (expectation of life) \times 365 = 26,280 d in this study (Ruzhong et al., 2012).

$$LADD = \frac{c \cdot EF}{AT} \left[\frac{CR_{child} \cdot ED_{child}}{BW_{child}} + \frac{CR_{adult} \cdot ED_{adult}}{BW_{adult}} \right] \quad (2)$$

$LADD$ is the daily exposure dose ($\text{mg}/(\text{kg d})$) and CR is the intensity of three exposures. CR refers to intake rate for peroral intake soil (mg/d). CR refers to respiratory rate for inhale soil (m^3/d). $CR = \text{skin exposure area} \times \text{skin adhesion} \times \text{dermal absorption factor} (\text{mg}/\text{d})$. Based on pollutant identification and exposure assessment, the carcinogenic and noncarcinogenic hazards of the concerned pollutants were analyzed. The toxicity parameter values such as reference dose, reference concentration, carcinogenic slope factor, and unit carcinogenic factor of the concerned pollutants were also determined according to the relevant toxicity assessment parameter data of the US EPA, which mainly focuses on the pollutant's physiochemical, carcinogenic and noncarcinogenic properties, and the hazard effects on human health by different pathways and the corresponding reaction dosages (Table 2).

According to the toxicity parameters (Steven et al., 2010) and partial literature of the Ministry of Environmental Protection (SFo, SFi, and SFd refer to the slope factor of direct ingestion, inhalation, and dermal absorption; URF: unit carcinogenic factor; RfDo, RfDi, and RfDd refer to the reference dose of direct ingestion, inhalation, and dermal absorption; and RfC: reference concentration) Based on the exposure and toxicity assessments, each sample was analyzed for the concentration of concerned pollutants, and the carcinogenic risk value and hazard quotient were calculated based on the risk assessment of each type of exposure's risk value of the same type of pollutant and the total risk value of all the pollutants from all the exposure pathways.

Table 1. Monitoring methods for test index

No.	Test index	Test method	Detection limit (mg/kg)
1	Metals (8) (As, Pb, Cd, Cr, Hg, Zn, Cu, and Ni)	US EPA 6010C US EPA 7470A	As:1 Hg:0.05 others:0.5
2	PAHs	US EPA 8270D	0.1–0.2

Table 2. Partial toxicity parameters of concerned pollutants

Pollutants	SFo	SFi	SFd	URF	RfDo	RfDi	RfDd	RfC
Arsenic			1.5			0.0003	0.0003	
Mercury						0.0003	0.0003	
Benzene	0.055	0.027	0.055	0.008	0.004	0.009	0.004	0.030
Naphthalene		0.12		0.034	0.020	0.001	0.020	0.003
Chrysene	0.007	0.039	0.007	0.011				
Fluorene					0.040	0.040	0.040	
Fluoranthene					0.040	0.040	0.040	
Phenanthrene					0.040	0.040	0.040	
anthracene					0.040	0.040	0.040	
Benzo(g,h,i)pyrene					0.040	0.040	0.040	
Benzo(a)pyrene	7.300	3.850	7.300	1.100				
Dibenzo(a, h)anthracene	7.300	4.20	7.300	1.200				
Benzo(a)anthracene	0.73	0.385	0.730	0.110				
Benzo(b)fluoranthene	0.730	0.385	0.730	0.110				
Indene(1,2,3-cd)pyrene	0.730	0.385	0.730	0.110				
Benzo(k)fluoranthene	0.073	0.385	0.073	0.110				

The carcinogenic risk (CR) associated with ingestion and dermal exposure was calculated by Eqs. (3) and (4) adapted from US EPA (1989) and (2004), where *HI* is the probability of developing cancer over a lifetime because of exposure to a contaminant, *LADD* is the daily exposure dosage obtained from Eqs. (1) and (2), and *SF* is the slope factor.

$$HI_i = \sum_{j=1}^{17} LADD_{ij} \times SF_{ij} \tag{3}$$

$$THI = \sum_{i=1}^3 HI_i \tag{4}$$

The total *HI* values for children and adults were calculated by adding the *HI*s calculated from three pathways.

For the non-carcinogens, the dosages calculated for each element and exposure pathway were subsequently divided by the corresponding reference dosage (*RfD*) to afford the hazard quotient (*HQ*), and the hazard index (*THQ*) is equal to the sum of *HQ*s (Eqs. 5-6).

$$HQ_i = \frac{ADD_{ij}}{RfD_i} \tag{5}$$

$$THQ = \sum_{i=1}^{17} \sum_{j=1}^3 HQ_i \tag{6}$$

In general, the value of *HQ* or *HI* < 1 indicates no significant risk of noncarcinogenic effects; the value of *HQ* or *HI* > 1 indicates significant noncarcinogenic effects, which increased with increasing value of *HQ* or *THQ* (Siyue et al., 2010; US EPA, 2001).

3. Results and discussion

3.1. Site pollution status assessment

During the sampling at the polluted site of coking gasworks, 128 samples of 60 grids were collected. The relevant indexes of 19 plot layers' pollutants were lower than the limiting values formulated by the *Exhibition land Standard* (Table 3), which covered 16.1% of the total plot layers. The 19 plot layers include: 6-3, 8-3, 10-3, 11-3, 13-3, 15-3, 27-1, 35-1, 37-1, 37-2, 40-2, 41-1, 41-2, 45, 48, 50, 51, 52, and 53. The total polluted area of 112 plot layers was ~113,040 m², and the total soil volume was 168,425 m³. The soil in Coke Oven gas factory was polluted by organic pollutants for a long time (since the factory was established). The main pollutants identified were cyanide, PAH, and total petroleum hydrocarbon. The pollution characteristics were complexity in pollutant types, pollution areas, pollutant migration, transformation downward, etc.

The laboratory test analysis of seven sampling sites showed the major total cyanide pollution, PAH pollution, and TPH pollution in soil samples of Coke Oven gas factory, and lighter heavy metal pollution

in several grids. All the grids except 27, 30, 41, 49, 50, 51, and 52 showed total cyanide pollution with the highest level >2136.5 times of the standard; all the grids except grid 48 showed PAH pollution with the highest level >7961.48 times of the standard; all the grids except 13, 17, 28, 30, 34–37, 39–41, 44–53, 55, and 57–59 showed TPH pollution with the highest level >219.83 times of the standard; four grids showed slight excess of heavy metals such as As, Cu, Pb, and Hg (Fig. 2).

The pollution level and pollution area intensity decreased successively in the sequence of recovery zone, coal preparation zone, and public zone. The concentration of heavy metals was higher than the surrounding surface soil concentration (Wanxia et al., 2012), but lower than the concentration of soil previously irrigated with industrial wastewater (Peijun et al., 2009). The concentration of TPH was lower than the concentration of the soil at the petroleum-contaminated sites (In-Sun et al., 2011). The concentration of PAHs was higher than that of vegetables grown in the vicinity of thermal power plants (Khillare et al., 2012).

3.2. Risk assessment results of three zones

Notably, an excess lifetime cancer risk of $\geq 10^{-6}$ has been consistently considered as insignificant and $\geq 10^{-4}$ as significant (Man et al., 2013). Through risk assessment on the site in zone A grids, where the pollution indexes exceed value B in *Exhibition land Standard* (HJ350-2007), the pollutants with a relatively higher risk are naphthalene, benzantracene (a), benzofluoranthrene (b), benzopyrene (a), indenopyrene (1,2,3-cd), dibenzanthracene (a, h), and benzene.

Naphthalene and benzene showed extremely high carcinogenic and noncarcinogenic risks, respectively, and some grids' carcinogenic risk even reached 10^{-2} , which was similar to the study of Lake Chaohu (Ning et al., 2013). Some grids' carcinogenic risk even reached 10^{-3} , illustrating extremely high environmental risk in zone A soil (Fig. 3). During the sampling process, some sampling grids' soil was black and had several oily substances with pungent smell. Therefore, zone A is a heavy pollution zone, and some grids in zone A are heavy pollution grids.

In zone B, the pollutants with relatively higher concentrations are naphthalene, fluoranthene, benzantracene (a), chrysene, benzofluoranthrene (b), benzofluoranthrene (k), benzopyrene (a), indenopyrene (1,2,3-cd), and dibenzanthracene (a, h). Benzantracene (a), benzofluoranthrene (b), and benzopyrene (a) showed relatively high carcinogenic risk, and some grids' carcinogenic risk even reached 10^{-3} , indicating that zone B soil (Fig. 3) has a relatively higher environmental risk. The result is similar as the PAHs in soil of the Chenzhou industrial zone. The PAHs in soil of pyroelectric industrial sites exceed the standard (0.3 mg/kg) 60 times with high risk environment (Ganghui et al.,

2012). During the sampling process, some sampling grids' soil had traces of oily substance with slight pungent smell. Therefore, zone B is mid-level pollution zone, and some grids in zone B are mid-level pollution grids.

In zone C, the pollutants with a relatively higher risk are naphthalene, fluoranthene, benzantracene (a), chrysene, benzofluoranthrene (b), benzofluoranthrene (k), benzopyrene (a), indenopyrene (1,2,3-cd), and dibenzanthracene (a, h). Benzopyrene (a) showed a relatively higher carcinogenic risk, and some grids' carcinogenic risk even reached 10^{-4} . Grid 56 showed a relatively higher carcinogenic risk, indicating that some soil in this zone still has environmental risk. However, zone C (Fig. 3) showed a relatively lower environmental risk as a whole, thus belonging to mild-contamination zone and a part of the grids are mild-contamination grids.

By the risk value calculation, 49 grids among 60 monitored grids with area of 103,340 m² showed carcinogenic risk $>10^{-5}$, confirming that PAHs can cause cancer. However, the minimum PAH concentrations for causing cancer are different for different areas and different intake approaches. Canadian soil quality guidelines for the protection of environmental and human health consider a cancer risk of $\leq 10^{-5}$ at contaminated sites as insignificant (CCME, 2010). Most regulatory bodies cite an incremental lifetime cancer risk (ILCR) between 10^{-6} and 10^{-4} for potential risk (Xia et al., 2010). In zone A, the risk value was extremely high as the whole. The risk value of most grids exceeded 10^{-3} , and some even reached 10^{-2} . The risk value of grid 18 was the highest which reached 4.041E-02. In zone B, the risk value was relatively higher as the whole. The risk value of some grids exceeded 10^{-4} , and some even reached 10^{-3} . The risk value of grid 43 was the highest which reached 2.152E-03. In zone C, only few grids showed environmental risk with risk value $>10^{-4}$, in which the carcinogenic risk exceeded 10^{-4} . The risk value of grid 56 was the highest which reached 1.925E-04. B[a]P_{eq}-based (B[a]P_{eq} was calculated by the multiplication of the individual PAH concentration by its PEF) lifetime lung cancer risks estimated for both the exposure groups were 4.35×10^{-2} and 5.42×10^{-2} exposed to the PAHs in a carbon black manufacturing industry, respectively, for palletizing and packaging workers. For dermal exposure, B[a]P_{eq}-based lifetime skin cancer risks for both the exposure groups were estimated to be 1.13×10^{-3} and 1.56×10^{-3} , respectively (Tsai et al., 2001).

The average upper-bound B[a]P_{eq}-based inhalation incremental lifetime cancer risk for three age groups was 1.57×10^{-4} (3.10×10^{-7} – 4.46×10^{-4}), whereas for dermal incremental lifetime cancer risk was 1.19×10^{-4} (2.19×10^{-6} – 2.99×10^{-4}) (Szuchich et al., 2006). The US Environmental Protection Administration indicated a different unit risk of 6.4×10^{-7} (ng/m³)⁻¹ based on the total PAH content (US

EPA, 1984). If the magnitude 10^{-5} is taken as the evaluation standard for causing cancer, the health risk of this site was extremely high.

The noncarcinogenic risk value of 25 grids was >1.0 in the 60 monitored grids. The noncarcinogenic risk value of some grids was very high. The total area of the 25 grids was $35,120 \text{ m}^2$, and the carcinogenic risk of the grids with noncarcinogenic risk >1.0 exceeded 10^{-5} .

3.3. Risk assessment result of layer

A total of 128 grid layers were evaluated. Using the equations and parameters in risk assessment guide rule and assuming that each grid layer is a surface layer and the pollutant concentration of the upper layer soil (Fig. 3) is the same as that of the lower layer soil (Figs. 4 and 5), the definite carcinogenic risk and noncarcinogenic risk values of each grid layer were calculated. Calculated risk value was considered as the main basis of soil classification, governance, and restoration technical solutions, which fully considered the comprehensive effects of various pollutants in polluted soil on human health and the environment and is a more scientific definite risk value of grid layers with indexes exceeding A value in Exhibition land Standard. Through layer

assessment and calculation, the surface soil was found to have larger pollution area and heavier pollution level. The definite carcinogenic risk of 18 grids in the upper layer exceeded 10^{-3} , and that of 20 grids even exceeded 10^{-4} (Fig. 3). The definite carcinogenic risk of 12 grids in the middle layer exceeded 10^{-3} , and that of 16 grids even exceeded 10^{-4} (Fig. 4). The definite carcinogenic risk of 10 grids in the bottom layer exceeded 10^{-3} , and that of two grids even exceeded 10^{-4} (Fig. 5). The definite carcinogenic risk of surface soil of most grids in zones A and B exceeded 10^{-4} by rigorous technical method for sites' environment management.

The definite noncarcinogenic risk of 22, 20 and 11 grids in the upper, middle and bottom layer exceeded 1.0, respectively (Figs. 3, 4, 5). The total soil volume of grid layers, with absolute carcinogenic risk value $>1 \times 10^{-3}$, was $69,310 \text{ m}^3$. The total soil volume of grid layers, with an absolute carcinogenic risk value between 1×10^{-3} and 1×10^{-4} , was $42,105 \text{ m}^3$, whereas $30,695 \text{ m}^3$ of it was the earth volume of parcel layers with the absolute noncarcinogenic risk value >1.0 . The total earth volume of grid layers where the absolute carcinogenic risk value was between 1×10^{-4} and 1×10^{-5} was $62,720 \text{ m}^3$, and $18,935 \text{ m}^3$ of it was the earth volume of grid layers with the absolute noncarcinogenic risk value >1.0 .

Table 3. Exhibition land Standard

	Pollutant	A level	B level
PAH	Naphthalene	54	530
	Chrysene	9	40
	Fluorene	210	8200
	Fluoranthene	310	8200
	Phenanthrene	2300	61000
	anthracene	2300	10000
	Benzo(g,h,i) pyrene	230	6100
	Benzo(a) pyrene	0.3	0.66
	Diphenyl(a,h)anthracene	0.3	0.66
	Benzo(a) anthracene	0.9	4
	Benzo(b)fluoranthene	0.9	4
	Indene (1,2,3-cd) pyrene	0.9	4
	Benzo(k)fluoranthene	0.9	4
	Mononuclear aromatics	Benzene	0.2
Heavy metals	Arsenic	20	80
	Mercury	1.5	50

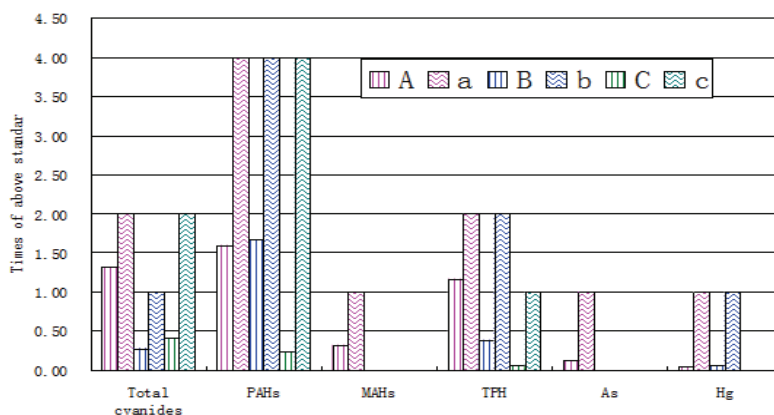


Fig. 2. Times of above standard of six factors (A: average of Zone A; a: maximum of Zone A; B: average of Zone B; b: maximum of Zone B; C: average of Zone C; c: maximum of Zone C)

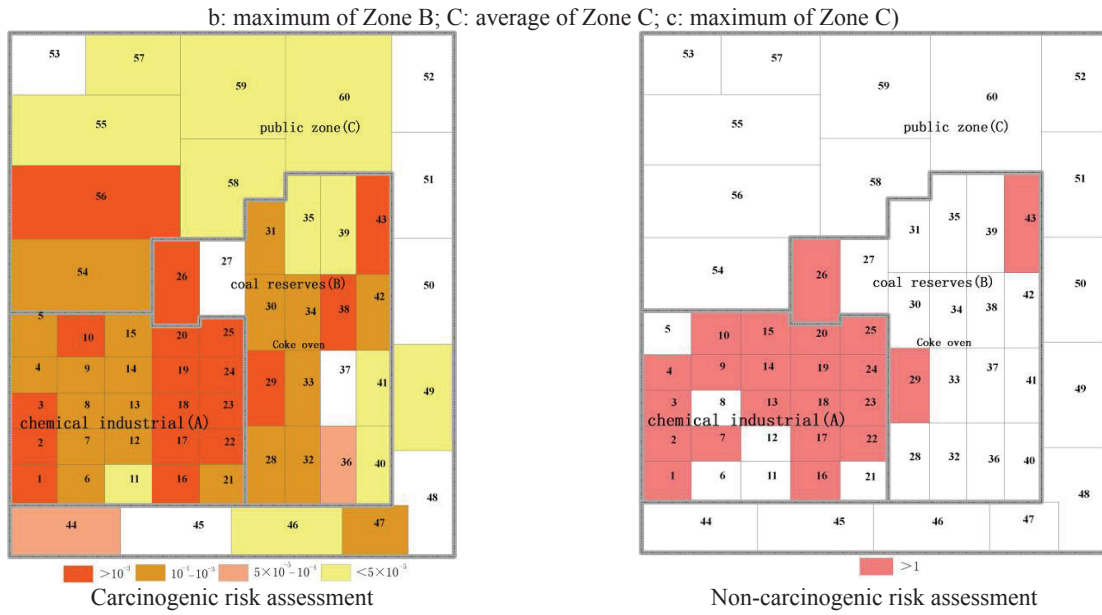


Fig. 3. Risk assessment result of upper layer (A, B, C)

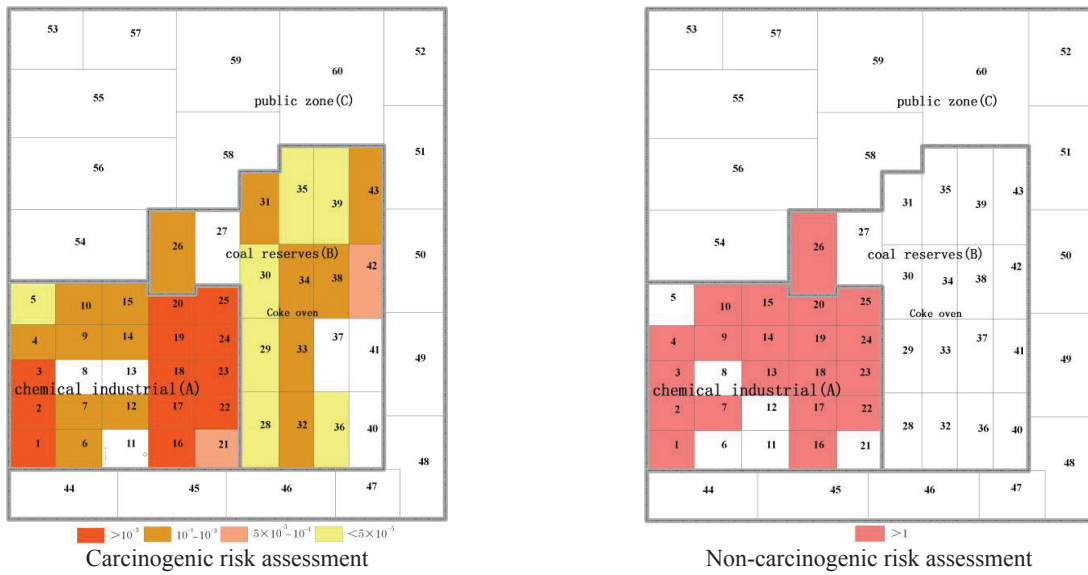


Fig. 4. Risk assessment result of middle layer (A, B, C)

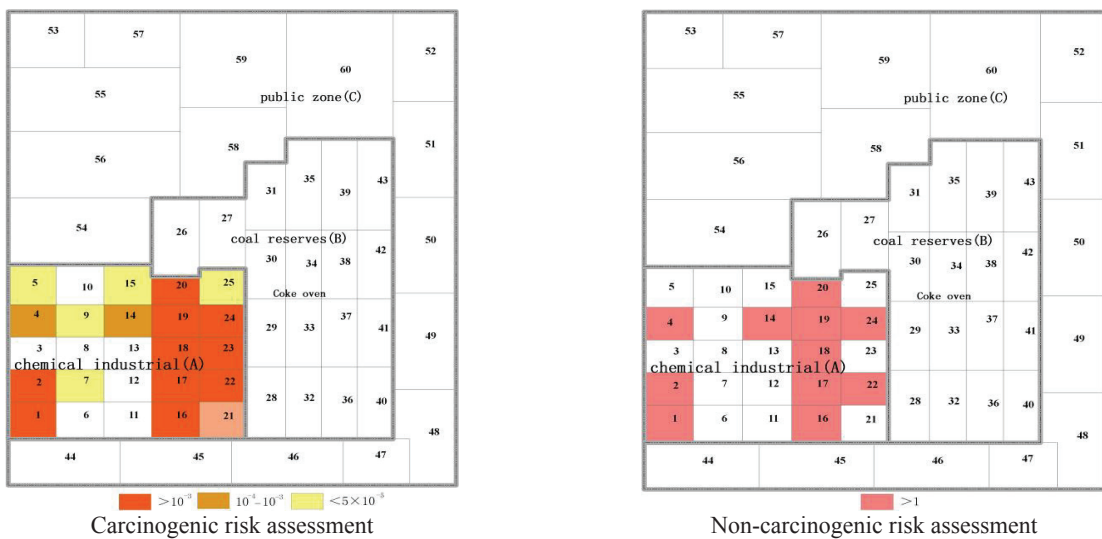


Fig. 5. Risk assessment result of bottom layer (A, B, C)

The total earth volume of grid layers with the absolute carcinogenic risk value $<1 \times 10^{-5}$ was 9,514 m³, and 2,910 m³ of it was the earth volume of grid layers with the absolute noncarcinogenic risk value >1.0 .

4. Conclusions

Sites contaminated with hazardous materials pose serious risks to human health, and the health risk assessment caused by contaminated sites will be the focus of future research. Combining the site's future planning uses and assessing contaminated site's environmental risk may provide a scientific basis for the implementation of environment management decision and restoration engineering.

The pollution level and pollution area intensity decreased successively in the order of chemical industrial zone, coal reserve zone, and public zone. The soil was contaminated by heavy metals, TPH, and PAHs, clearly indicating that the soil should be remediated immediately.

The health risk assessment indicates that 49 out of the 60 grids have a carcinogenic risk factor $>10^{-5}$ with a total area of 103,340 m², and grid 18 has the highest value-at-risk of 0.0404. This site has extremely high health risk if 10^{-5} is regarded as the assessment standard for causing cancer.

The heavy and mid-level contaminated soils of the grid layers with a risk value $>5 \times 10^{-5}$ should be dug out and transferred to conditional disposal facilities for remote centralized processing; mild-contaminated soil of the grid layers with a risk value $<5 \times 10^{-5}$ can be processed collectively in the site.

Acknowledgments

This research is supported by NSFC (Natural Science Foundation of China (31100349)).

References

- Armstrong B., Hutchinson E., Unwin J., Fletcher T., (2004), Lung cancer risk after exposure to polycyclic aromatic hydrocarbons: a review and meta-analysis, *Environmental Health Perspectives*, **112**, 970-978.
- Boffetta P., Jourenkova N., Gustavsson P., (1997), Cancer risk from occupational and environmental exposure to polycyclic aromatic hydrocarbons, *Cancer Causes Control*, **8**, 444-472.
- Bosetti C., Boffetta P., La Vecchia C., (2007), Occupational exposures to polycyclic aromatic hydrocarbons, and respiratory and urinary tract cancers: a quantitative review to 2005, *Annals Oncology*, **18**, 431-446.
- CCME, (2010), *Canadian soil quality guidelines for the protection of environmental and human health: carcinogenic and other PAHs*, In: *Canadian Environmental Quality Guidelines 1999*, Canadian Council of Ministers of the Environment, Winnipeg.
- Celebi A., Sengorur B., Klave B., (2014), Human health risk assessment of dissolved metals in groundwater and surface waters in the Melen watershed, Turkey, *Journal of environmental science and health, Part A: Toxic/hazardous substances and environmental engineering*, **49**, 153-161.
- Chapman P.M., Wang F., Janssen C.R., Goulet R., Kamunde C.N., (2003), Conducting ecological risk assessments of inorganic metals and metalloids: current status, *Human and Ecological Risk Assessment*, **9**, 641-697.
- Christopher A., Ollson Loren D., Knopper, Melissa L., Whitfield A., Jayasinghe R., (2014), Site specific risk assessment of an energy-from-waste thermal treatment facility in Durham Region, Ontario, Canada, Part A: Human health risk assessment, *Science of the Total Environment*, **466-467**, 345-356.
- COM., (2002), Communication from the commission to the council, the European parliament, the economic and social committee and the committee of the regions, Towards a Thematic Strategy for Soil Protection, Brussels, 16.4.
- EEA, (2000), Management of contaminated sites in Western Europe, European Environment Agency Copenhagen, Denmark.
- Ferré-Huguet, N., Martí-Cid, R., Schuhmacher, M., Domingo, J.L., (2008), Risk assessment of metals from consuming vegetables, fruits and rice grown on soils irrigated with waters of the Ebro River in Catalonia, *Biological Trace Element Research*, **123**, 1-14.
- Ganghui Z., Lu S., Xiaoyong L., Xiulan Y., Lixiang Z., (2012), Combined pollution of heavy metals and PAHs and its risk assessment in industrial sites of Chenzhou City, *Geographical research*, **31**, 831-839.
- Hansen J.C., (1981), A survey of human exposure to mercury, cadmium and lead in Greenland, *Monographs on Greenland, Man & Society*, **3**, 1-36.
- Hansen J.C., Tarp U., Bohm J., (1990), Prenatal exposure to methyl mercury among Greenlandic Polar Inuits, *Archives of Environmental Health*, **45**, 355-358.
- Health Canada, (1994), Human Health Risk Assessment for Priority Substances: Canadian Environmental Protection Act. Ottawa, ON: Canada Communication Group—Publishing.
- Health Canada, (2007), Federal Contaminated Risk Assessment in Canada Part I: Guidance on Human Health Preliminary Quantitative Risk Assessment (PQRA). Version 2.0. Ottawa, ON: Health Canada, Environmental Health Assessment Services, Safe Environments Programme.
- In-Sun P., Jae-Woo P., (2011), Determination of a risk management primer at petroleum-contaminated sites: developing new human health risk assessment strategy, *Journal of Hazardous Materials*, **185**, 1374-1380.
- Jensen J., Mesman M., Loibner A. P., Erlacher E., Rutgers M., Archibald G., Ehlers C., Dirvenvan Breemen L., Bogolte B. T., Sorokin N., Celis R.L., TerLaak T., Hartnik T., Bierkens, J., (2006), Ecological risk assessment of contaminated land-decision support for site specific investigations, RIVM Report no. 711701047, On line at: <http://dce.au.dk/fileadmin/Attachments/Prefaceetc.pdf>.
- Khillare P.S., Jyethi D.S., Sarkar S., (2012), Health risk assessment of polycyclic aromatic hydrocarbons and heavy metals via dietary intake of vegetables grown in the vicinity of thermal power plants, *Food and Chemical Toxicology*, **50**, 1642-1652.
- Kogevinas M., Mannetje A., Cordier S., Ranft U., Gonzalez C.A., Vineis P., (2003), Occupation and

- bladder cancer among men in Western Europe, *Cancer Causes Control*, **14**, 907-914.
- Man Y.B., Kang Y., Wang H.S., Lau W., Li H., Sun X.L., Giesy J.P., Chow K.L., Wong M.H., (2013), Cancer risk assessments of Hong Kong soils contaminated by polycyclic aromatic hydrocarbons, *Journal of Hazardous Materials*, **261**,770-776.
- Martí-Cid, R., Llobet, J. M., Castell, V., Domingo, J. L., (2008), Dietary intake of arsenic, cadmium, mercury, and lead by the population of Catalonia, *Biological Trace Element Research*, **125**, 120-132.
- Martorell I., Perelló G., Martí-Cid R., Llobet J.M., Castell V., Domingo J.L., (2011), Human exposure to arsenic, cadmium, mercury, and lead from foods in Catalonia, Spain: temporal trend, *Biological Trace Element Research*, **142**, 309-322.
- MOE, (2005), Procedures for the Use of Risk Assessment under Part XV.1 of the Environmental Protection Act, Ontario Ministry of the Environment, On line at: <https://dr6j45jk9xcmk.cloudfront.net/documents/2330/124-procedures-for-the-use-of-risk-assessment-en.pdf>.
- Ning Q., Wei H., Xiang-Zhen K., Wen-Xiu L., Qi-Shuang H., Bin Y., Hui-Ling O., Qing-Mei W., Fu-Liu X., (2013), Ecological risk assessment of polycyclic aromatic hydrocarbons (PAHs) in the water from a large Chinese lake based on multiple indicators, *Ecological Indicators*, **24**, 599-608.
- Peijun L., Xin W., Allinson G., Xiaojun L., Xianzhe X., (2009), Risk assessment of heavy metals in soil previously irrigated with industrial wastewater in Shenyang, China, *Journal of Hazardous Materials*, **161**, 516-521.
- Pizzol L., Critto A., Agostini P., Marcomini A., (2011), Regional risk assessment for contaminated sites Part 2: Ranking of potentially contaminated sites, *Environment International*, **37**, 1307-1320.
- Popita G.E., Varga I., Gurzau A., Bence F., Yuzhakova T., Hategan R.M., Redey A., Popovici A., Marutoiu C., (2014), Environmental impact and risk assessment in the area of "Pata Rât" landfill site, Cluj-Napoca, Romania, *Environmental Engineering and Management Journal*, **13**, 435-447.
- Rand G.M., Wells P.G., McCarty L.S., (1995), *Introduction to Aquatic Toxicology*, In: *Fundamentals of Aquatic Toxicology: Effects, Environmental Fate, and Risk Assessment*, Rand G.M. (Ed.), Taylor and Francis, Washington, DC.
- Richardson G.M., (1997), Compendium of Canadian Human Exposure Factors for Risk Assessment, O'Connor Associates Environmental Inc., Ottawa, Canada, On line at: <http://www.usask.ca/toxicology/docs/cef>.
- Ruzhong L., Chengrong P., Jing C., Yanmin J., Guizhen D., (2012), Heavy metal contamination and health risk assessment for urban topsoil and dust in Tongling City, *China Environmental Science*, **32**, 2261-2270.
- Saeedi M., Loretta Y.L., Salmanzadeh M., (2012), Heavy metals and polycyclic aromatic hydrocarbons: Pollution and ecological risk assessment in street dust of Tehran, *Journal of Hazardous Materials*, **227-228**, 9-17.
- Siyue L., Quanfa Z., (2010), Risk assessment and seasonal variations of dissolved trace elements and heavy metals in the Upper Han River, China, *Journal of Hazard Material*, **181**, 1051-1058.
- Sousa C.D., (2001), Contaminated sites: The Canadian situation in an international context, *Journal of Environmental Management*, **62**, 131-154.
- Steven D.S., Laird B.D., Lemieux C.L., (2010), Polycyclic aromatic hydrocarbons are enriched but bioaccessibility reduced in brown field soils adhered to human hands, *Chemosphere*, **80**, 1101-1108.
- Stezar I.C., Modoi O.C., Török Z., Ajtai N., Crişan A.D., Coşara G.V., Senzacconi F., Ozunu A., (2011), Preliminary investigation and risk assessment of contamination on an industrial site in maramures county, *Environmental Engineering and Management Journal*, **10**, 65-73.
- Swartjes A., Rutgers M., Lijzen J.P.A., Janssen P.J.C.M., Otte P.F., Wintersen A., Brand E., Posthuma L., (2012), State of the art of contaminated site management in The Netherlands: Policy framework and risk assessment tools, *The Science of the Total Environment*, **15**, 427-428.
- Szuchich C., Chungmn L., (2006), Health risk assessment on human exposed to environmental polycyclic aromatic hydrocarbons pollution sources, *Science of the Total Environment*, **366**, 112-123.
- Torretta V., Raboni M., Copelli S., Capodaglio A.G., (2014), A theoretical approach of a new index-based methodology for risk assessment of pipelines (I), *Environmental Engineering and Management Journal*, **13**, 2643-2652.
- Tsai P.J., Shieh H.Y., Lee W.J., Lai S.O., (2001), Health risk assessment for workers exposed to polycyclic aromatic hydrocarbons (PAHs) in carbon black manufacturing industry, *Science of the Total Environment*, **278**, 137-150.
- US EPA., (1984), Health effects assessments for polycyclic aromatic hydrocarbons (PAHs), US Environmental Protection Agency (EPA), Environmental Criteria and Assessment Office, EPA 549/1-86-013, Cincinnati, On line at: <http://cfpub.epa.gov/ncea/cfm/recorddisplay.cfm?deid=38617>.
- US EPA, (1989), Risk Assessment Guidance for Superfund Volume I Human Health Evaluation Manual (Part A). EPA/540/1-89/002, Office of Emergency and Remedial Response U.S. Environmental Protection Agency, Washington, D.C., On line at: http://www.epa.gov/oswer/riskassessment/ragsa/pdf/rags_a.pdf.
- US EPA, (1997), Exposure Factors Handbook, National Center for Environmental Assessment Office of Research and Development, U.S. Environmental Protection Agency, Washington, D.C., On line at: <http://www.epa.gov/ncea/efh/pdfs/efh-frontmatter.pdf>.
- US EPA, (2001), Supplemental Guidance for Developing Soil Screening Levels for Superfund Sites. OSWER 9355.4-24, Office of Solid Waste and Emergency Response, On line at: http://www.epa.gov/superfund/health/conmedia/soil/pdfs/ssg_main.pdf.
- US EPA, (2004), Risk Assessment Guidance for Superfund Volume I: Human Health Evaluation Manual (Part E, Supplemental Guidance for Dermal Risk Assessment). EPA/540/R/99/005, Office of Superfund Remediation and Technology Innovation U.S. Environmental Protection Agency, Washington, DC, On line at: <http://www.epa.gov/oswer/riskassessment/ragsel/>.
- Vasseur P., Bonnard M., Palais F., Eom I. C., Morel J. L., (2008), Bioavailability of chemical pollutants in contaminated soils and pitfalls of chemical analyses in hazard assessment, *Environmental Toxicology*, **23**, 652-656.
- Wanxia R., Bing X., Zhixiao M., Yong G., Lin S., Yunsong Z., (2012), Characters and potential

- ecological risks of heavy metals in soil of Chinese brownfield redevelopment site - Case of Tiexi old industrial area, Shenyang City, *Sustainable Development*, **2**, 159-166.
- Xia Z., Duan X., Qiu W., Liu D., Wang B., Tao S., Jiang Q., Lu B., Song Y., Hu X., (2010), Health risk assessment on dietary exposure to polycyclic aromatic hydrocarbons (PAHs) in Taiyuan, *Science of the Total Environment*, **408**, 5331-5337.
- Zhenxing W., Jianqun C., Liyuan C., Zhihui Y., Shunhong H., Yu Z., (2011), Environmental impact and site-specific human health risks of chromium in the vicinity of a ferro-alloy manufactory, China, *Journal of Hazardous Materials*, **190**, 980-985.
- Zhiyuan L., Zongwei M., van der Kuijp T.J., Zengwei Y., Huang L., (2014), A review of soil heavy metal pollution from mines in China: Pollution and health risk assessment, *Science of the Total Environment*, **468-469**, 843-853.



“Gheorghe Asachi” Technical University of Iasi, Romania



EXPERIMENTAL STUDY ON THE AERATION OXYGENATION INTO PRINTING AND DYEING WASTEWATER USING JET AERATOR

Chunsheng Lei*, Xiaofeng Zhu, Meicheng Zhou, Liangfei Dong*, Feng e Zhang

School of Environmental and Safety Engineering, Changzhou University, Changzhou Jiangsu 213164, China

Abstract

This study focused on the use of jet aeration to treat printing and dyeing wastewater. The related environmental factors influencing the dynamical efficiency of a jet aerator were investigated. Results showed that an ideal linear relation existed between dynamical efficiency and working pressure ($R^2 > 0.98$), with dynamical efficiency decreasing gradually as the working pressure increased. When the gas-liquid ratio was approximately 0.6:1 to 1.4:1, more bubbles were formed by the gas-liquid mixture in the jet aerator. Dynamical frequency increased steadily when gas-liquid was mixed uniformly and the injection depth was deeper than 6 m. The treatment performed with the hydraulic retention time (HRT) lasted 3 h, and the dissolved oxygen was maintained above 3 mg/L.

Key words: aeration oxygen-rich, environmental factors, jet aeration, textile wastewater

Received: January, 2013; *Revised final:* July, 2013; *Accepted:* August, 2013

1. Introduction

Aeration is an important step in sewage aerobic biochemical treatment. This step provides sufficient dissolved oxygen (DO) for reaction in the reactor, aside from maintaining the organism and the substrate, and keeping the adequate oxygen mixture (Thalasso et al., 1995). The energy consumption of aeration accounts for approximately 60% to 70% of the total consumption in wastewater treatment plants (WWTPs) (Flores-Cotera and García-Salas, 2005). Thus, a high dynamic efficiency of aerating equipment is essential in saving energy.

Conventional aerating equipment requires gas to pass through fixed gas pipelines and diffusion devices. Therefore, nozzles are prone to blocking and are costly to maintain. Mechanical aeration is conducted at the expense of considerable energy consumption. The manufacture of a mechanical aerator is also relatively complicated. Mechanical and conventional aerators have low efficiencies and

oxygen utilization rates, long aerating time, difficult maintenance, and high infrastructure costs. By contrast, jet aeration is an advanced aerating technology with advantages such as high oxygen utilization ratio ranging from 15% to 30%, effective gas diffusion, high mass transfer coefficient, uniform DO and bubble mixture (Morchain et al., 2000), simple construction, and convenient maintenance (Havelka et al., 1997, 2000; Zahradník et al., 1997). Moreover, a properly installed jet aerator is suitable for treating highly concentrated industrial wastewater (Chedeville et al., 2007; Petruccioli et al., 2002).

The effects of working pressure, gas-liquid ratio, and working depth of the jet device on improving oxygen transfer power efficiency were comprehensively investigated with textile wastewater as the research object.

Based on the experimental results, a reasonable design and operation parameters were proposed to provide technical support for the engineering and operation of a jet aerator.

* Author to whom all correspondence should be addressed: e-mail: 463272501@qq.com, qiuyu_lei@126.com; Phone: +86-519-68983809; Fax: +86-519-81290376

2. Experimental

2.1. Experimental device

Fig. 1 shows the pilot device, which is a $4\text{ m} \times 15\text{ m} \times 9\text{ m}$ jet aerator. A small amount of activated sludge is found at the bottom. Synergistic nozzles (DN150×210) are installed based on the experimental requirements. The diameter of the branch tubes attached to the synergistic nozzles is 150 mm. Five branch pipes, arranged in a mutually staggered manner, are connected to each side of the main collection tube. The diameter of the main collection tube is 200 mm. The GW1200 jet aerator model has a flow rate of approximately $140\text{ m}^3/\text{h}$ to $480\text{ m}^3/\text{h}$, inlet pressure of approximately 0.034 MPa to 0.482 MPa, and maximal inspiratory capacity of $1556\text{ m}^3/\text{h}$ under 0.016 MPa. The inlet is connected to the air-compressed pipe, and the tail pipe is connected to the gas–liquid mixing main tube. The working pump is a self-suction pump with a flow rate of $210\text{ m}^3/\text{h}$. The pump head is 11 m with an 18.5 kW of power. A regulator, a pressure reducing valve, and a flow gauge are installed in the pump flow and air-compressed pipes. Pressure gauges are installed at both ends of the jet aerator.

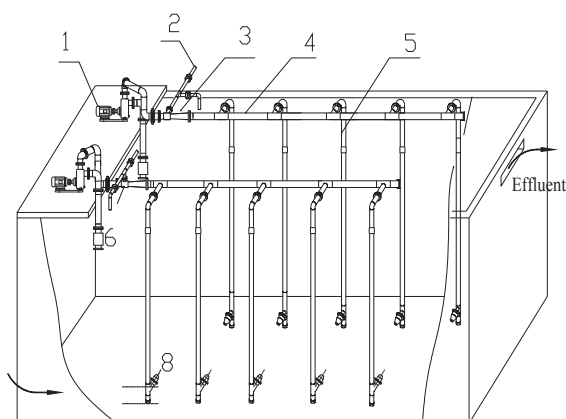


Fig. 1. Jet aeration oxygen-rich pilot test device for printing and dyeing wastewater treatment (1: self-suction pump; 2: air-compressed pipe; 3: jet aerator; 4: gas–liquid mixing main tube; 5: gas–liquid mixing branch tubes; 6: wastewater absorption mouth; 7: pressure reducing valve; and 8: efficient nozzle)

2.2. Experimental method

The experiment was conducted in a continuous feed mode. Effluent from the working pump passed through the nozzles of the jet device. The decreased diameter of the branch pipes resulted in high flow velocity. The high-speed flow passed through the inspiratory room into the throat pipes, forming a partial vacuum. After a large amount of air was drawn into the throat pipes using an air-compressed pipe (the pressure of the supplied gas was 0.016 MPa), the pressure from the water jet generated many small bubbles while the activated sludge was cut into tiny particles with full contact

with air bubbles and with a large specific surface area. A mist-shaped gas–liquid mixture was released from the synergistic jet nozzle because of the second jet. The experiment was conducted in a textile WWTP in Nantong City, Jiangsu Province, China. Wastewater was first hydrolyzed, acidified, and stored in the jet aeration tank. The necessary parameter (i.e., DO) was recorded before measuring the oxygen transfer power efficiency of the jet device. Air jet aeration was compared with pure oxygen jet aeration.

2.3. Measurement

The measurements used were regular indices and bubble photographs with different gas–liquid ratios. The regular indices were pH and DO. DO was measured using a DO meter (YSI Pro20), and pH was determined using a pH Meter (-2 to 18 measurement range with uncertainty of less than 1%). Bubble photographs were scanned with an electron microscope (JSM 6390).

3. Results and discussion

3.1. Effect of working pressure on oxygen transfer power efficiency

Jet aerators are classified as either high-pressure or low-voltage types based on the pressure of the working medium. The working pressure and nozzle flow velocity of high-pressure and low-pressure jets are 0.2 MPa, 20 m/s and 0.07 MPa, 12 m/s, respectively. Energy consumption of the low-pressure type is one-third higher than the high-pressure type in theory. However, the actual energy consumption is less than the energy consumption in theory. The low-pressure jet was chosen in this experiment because of the abovementioned characteristics. A large working pressure means more water passed through the jet and more gas was inhaled. Considering the specific amount of oxygen demanded, the number of jets required was relatively few, and the cost of the equipment was low.

The effects of the working pressure at different depths on the oxygen transfer coefficient are shown in Fig. 2. The pressure of the supplied gas was 0.016 MPa, and the gas–liquid ratio was 0.6. Although the power of the pump increased as the working pressure increased, the dynamical efficiency decreased based on a linear relation. Correlations (R^2) with different water depths were 0.9971, 0.9903, and 0.9850. Increasing water depth under the same pump power increased the dynamical efficiency. At water depths of 3 m and 5 m, the down-slope trend of the dynamical efficiency was almost consistent. At a water depth of 7 m, the dynamical efficiency slightly increased by $0.3719\text{ kgO}_2/\text{kWh}$ compared with the measured value at 5 m depth. When the working pressure was 0.07 MPa and depth was 7 m, the oxygen transfer dynamical efficiency was $2.44\text{ kgO}_2/\text{kWh}$.

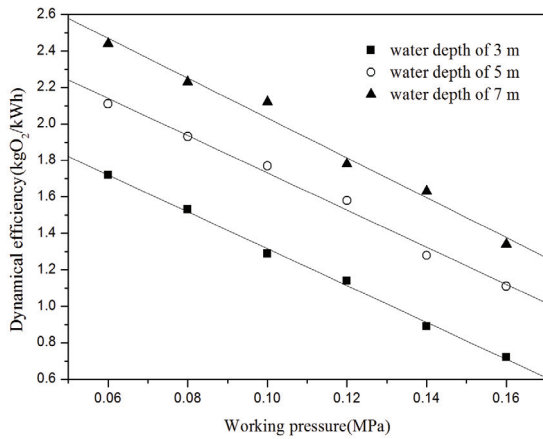


Fig. 2. Effect of the working pressure of the jet device on dynamical efficiency

3.2. Effect of the gas-liquid ratio on oxygen transfer dynamical efficiency

The use of bubble diffusion and hydraulic shear to achieve aeration and mixture differentiates a jet aeration device from mechanical aeration and bubble diffusion devices. The interaction between gas and liquid facilitates ejection, which forms a pulsed surface wave and causes the flow to drip liquid into the device interior (Gamisans et al., 2004; Kandakure et al., 2005; Little, 1995). This process facilitates the collision of compressed air and the formation of small bubbles (Fig. 3). Smaller bubbles mix more easily with liquid droplets to form a creamy mixture. Bubbles are compressed in the water after entering the diffusion tube.

The effects of different gas-liquid ratios on the dynamical efficiency of air jet aeration and pure oxygen aeration are shown in Figs. 4 and 5.

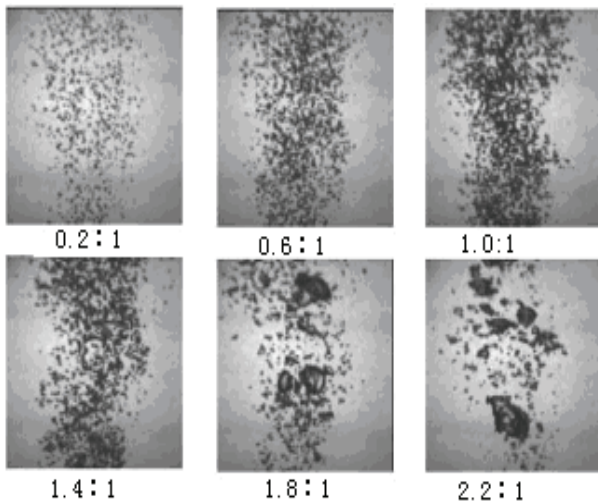


Fig. 3. Images of bubbles at different gas-liquid ratios

As shown in Fig. 3, the size and the degree to which small bubbles are mixed and formed by high-speed fluid droplets varied with different gas-liquid ratios (Q_{gas}/Q_{liquid}). Larger gas-liquid ratios resulted in larger particle sizes.

When the gas-liquid ratio was 0.2:1, particle size was at an extreme value, whereas the amount of bubbles in per unit area was at minimum.

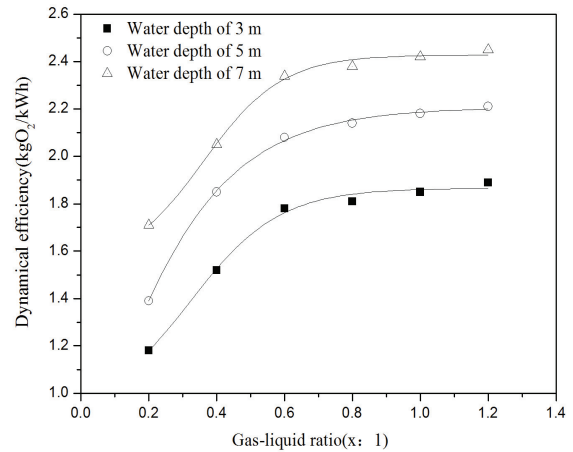


Fig. 4. Effect of different gas-liquid ratios on the dynamical efficiency of air jet aeration

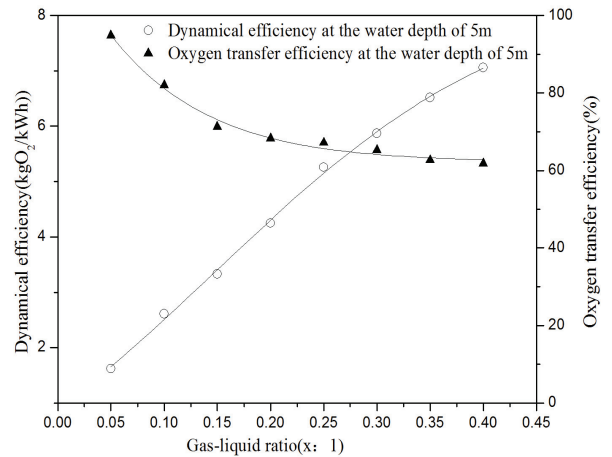


Fig. 5. Effect of different gas-liquid ratios on the dynamical efficiency of pure oxygen jet aeration

When the gas-liquid ratio was 1.8:1, the particle size was large and appeared as a speckle, which was in incomplete contact with the liquid. When the gas-liquid ratio was 1:1, the particle size was smaller, with a maximum number of bubbles in per unit area. When aeration with gas-liquid was 1:1, water, gas, and the organism completely contacted with each other.

Figs. 4 and 5 show that under the same working pressure, a larger gas-liquid ratio resulted in more gas per unit of water inhaled by the jet aerator and an increased dynamical efficiency. However, the oxygen transfer efficiency decreased despite air or pure oxygen aeration. At the water depth of 5 m and a gas-liquid ratio of 0.4:1, the dynamical efficiency of pure oxygen jet aeration was 7.06 kgO₂/kWh, which is far higher than the dynamical efficiency of air jet aeration (1.85 kgO₂/kWh). Dynamical efficiency increased as the ejection depth increased. When the gas-liquid ratio was higher than 0.6:1, the dynamical efficiency increased steadily, as shown in

Fig. 3. When the gas–liquid ratio was between 0.6:1 and 1.4:1, the amount of bubbles per unit area was almost stable.

3.3. Effect of the working depth on oxygen transfer dynamical efficiency

Synergistic nozzles were installed at different depths to examine the dynamical efficiency and the oxygen transfer efficiency at 0.088 MPa working pressure and 1:1 gas–liquid ratio. Results are shown in Fig. 6.

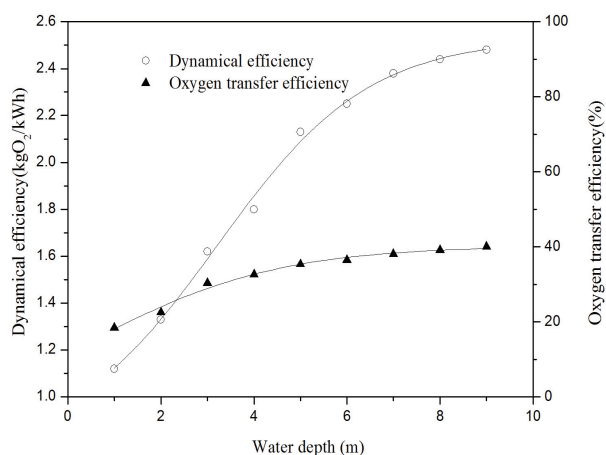


Fig. 6. Variation in the dynamical efficiency of air jet aeration at different water depths

Fig. 6 shows that as the water depth increased, the dynamical efficiency and the oxygen transfer efficiency curves of the jet aerator correspondingly increased. However, the dynamical efficiency increased more rapidly than the oxygen transfer efficiency, which became steadier after the water depth reached 5 m. This observation shows that the dynamical and oxygen transfer efficiencies of the jet aerator are related to the volume of aerated water. These parameters were stable under the surface area and were closely linked to water depth.

Based on the relationship between oxygen mass transfer coefficient K_{La} and the water depth of the aeration tank, results showed that a deeper water level resulted in a lower oxygen mass transfer coefficient. Thus, we conclude that at a deeper water level, the jet aerator is more useful, and its dynamical efficiency becomes higher.

3.4. Variations in DO over time

DO is a reflection of the treatment effect of jet aeration. At a working pressure of 0.088 MPa, water depth of 9 m, and gas–liquid ratio of 0.8:1, two selected aerators were used to treat 100 m³ printing and dyeing wastewater. The average DO in the front-end of the aeration tank was 1.43 mg/L, and the verified range was from 1.02 mg/L to 4.2 mg/L.

The other DO peak was 2.96 mg/L, which was measured after installing the jet aerator. DO decreased rapidly afterwards. After 25 d, DO in the

wastewater stabilized at approximately 1.21 mg/L. The DO average in the back-end of the aeration tank was 3.33 mg/L, and the verified range was from 0.99 mg/L to 5.08 mg/L. The peak was similar to the concentration in front-end of the aeration tank. The lowest concentration appeared after 2 d, when the DO in the front-end of the aeration tank was higher than that in the back-end. This condition could have been caused by the organism entering a logarithmic proliferation period during which a great deal of DO was consumed. After 18 d, the DO of the effluent exceeded 3 mg/L (Fig. 7).

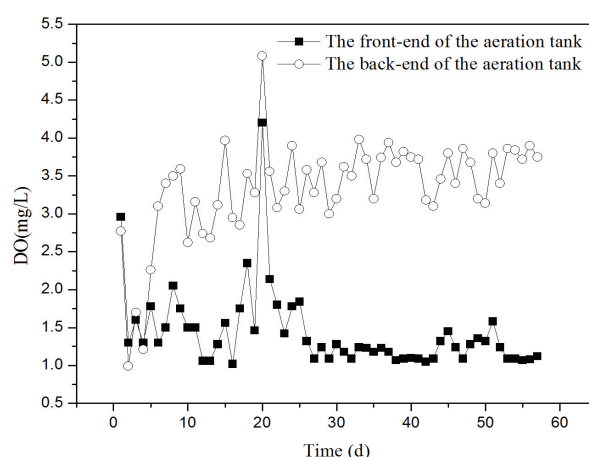


Fig. 7. Variations in DO over time

4. Conclusions

Dynamical efficiency of the jet aerator decreased as the working pressure increased. When the gas–liquid ratio was between 0.6 and 1.4, a greater amount of bubbles formed per unit area of the gas–liquid mixture in the jet aerator’s interior. When the gas–liquid ratio was 1:1, the dynamical efficiency slowly increased as the gas–liquid ratio increased.

Oxygen utilization and dynamical efficiency increased with the jet aeration water depth.

Acknowledgements

This work was supported by the National Natural Science Funds (Grant No. 51208068).

References

- Chedeville O., Debaq M., Ferrante Almanza M., Porte C., (2007), Use of an ejector for phenol containing water treatment by ozonation, *Separation and Purification Technology*, **57**, 201-208.
- Flores-Cotera L.B., García-Salas S., (2005), Gas holdup, foaming and oxygen transfer in a jet loop bioreactor with artificial foaming media and yeast culture, *Journal of Biotechnology*, **116**, 387-396.
- Gamisans X., Sarrà M., Lafuente F.J., (2004), Fluid flow and pumping efficiency in an ejector-venturi scrubber, *Chemical Engineering and Processing: Process Intensification*, **43**, 127-136.
- Havelka P., Linek V., Sinkule J., Zahradník J., Fialova M., (1997), Effect of the ejector configuration on the gas suction rate and gas hold-up in ejector loop reactors, *Chemical Engineering Science*, **52**, 1701-1713.

- Havelka P., Linek V., Sinkule J., Zahradník J., Fialová M., (2000), Hydrodynamic and mass transfer characteristics of ejector loop reactors, *Chemical Engineering Science*, **55**, 535-549.
- Kandakure M.T., Gaikar V.G., Patwardhan A.W., (2005), Hydrodynamic aspects of ejectors, *Chemical Engineering Science*, **60**, 6391-6402.
- Little J.C., (1995), Hypolimnetic aerators: Predicting oxygen transfer and hydrodynamics, *Water Research*, **29**, 2475-2482.
- Morchain J., Maranges C., Fonade C., (2000), CFD modelling of a two-phase jet aerator under influence of a crossflow, *Water Research*, **34**, 3460-3472.
- Petruccioli M., Cardoso Duarte J., Eusebio A., Federici F., (2002), Aerobic treatment of winery wastewater using a jet-loop activated sludge reactor, *Process Biochemistry*, **37**, 821-829.
- Thalasso F., Naveau H., Nyns E.H., (1995), Design and performance of a bioreactor equipped with a Venturi injector for high gas transfer rates, *The Chemical Engineering Journal and the Biochemical Engineering Journal*, **57**, B1-B5.
- Zahradník J., Fialová M., Linek V., Sinkule J., Řezníčková J., Kaštánek F., (1997), Dispersion efficiency of ejector-type gas distributors in different operating modes, *Chemical Engineering Science*, **52**, 4499-4510.



INSTRUCTIONS FOR AUTHORS

1. Introduction

Environmental Engineering and Management Journal (EEMJ) is an international medium for publication of Original Papers, Reviews, Case Studies, Book Reviews on the fundamentals, applications in environmental engineering and technologies, applied environmental sciences, environmental health, management, sustainable development, education for sustainability. Advertising is also accepted with contractual payment forms.

Submission of a manuscript implies that the work described has not been published before (except in the form of an abstract or as part of a published lecture, or thesis); that it is not under consideration for publication elsewhere; that its publication has been approved by all coauthors, if any, as well.

Papers, books for review, offers to review, suggestions and commercials (advertising) should be submitted to the *Editor-in-Chief*. All papers will be published in English. Non-English speaking authors should seek the advice of a professional language expert or an English speaker to help translate the paper.

2. Legal requirements

The author(s) guarantee(s) that the manuscript is/will not be published elsewhere in any language without the consent of the copyright holders, that the rights of third parties will not be violated, and that the publisher will not be held legally responsible should there be any claims for compensation. Authors wishing to include figures or text passages that have already been published elsewhere are required to obtain permission from the copyright holder(s) and to include evidence that such permission has been granted when submitting their papers. Any material received without such evidence will be assumed to originate from the authors. The author(s) are encouraged to transfer the copyright of the article to the publisher upon acceptance of an article by the journal, using the Authors' Warranty and Assignment of Copyright agreement. This transfer enables the Editor to protect the copyrighted material for the authors, but does not relinquish the author's proprietary rights. The publication of an article is conditioned by the signature of the author to whom correspondence should be addressed on this Authors'

Warranty and Assignment of Copyright that is provided by the Editor.

Ethics in Publishing

For information on ethics in publishing for journal publication see <http://omicron.ch.tuiasi.ro/EEMJ/plagiarism.htm>

Conflict of interest

All authors are requested to disclose any actual or potential conflict of interest such as any financial, personal or other relationships with other people or organizations concerning the submitted work that could inappropriately influence, or be perceived to influence, their work.

3. Editorial procedure

For original papers, an upper limit of 7000 words is recommended (including Abstract, Keywords, References, Figures and Tables), processed with MS editing facilities.

For review papers (critical evaluation of existing data, defined topics or emerging fields of investigation, critical issues of public concern), an upper limit of 15000 words is recommended (including Abstract, Keywords, References, Figures and Tables).

Manuscripts should be written in English (American or British usage is accepted, but not a mixture of these) and submitted **electronically**, in .doc format (please do not use .docx) to the *Editor-in-Chief*, at **one (and only one)** of the following e-mail addresses: **eemjournal at yahoo dot com; eem_journal at yahoo dot com; eemjeditor at yahoo dot com; eemj_editor at yahoo dot com; eemjournal at gmail dot com; eemjeditor at gmail dot com; eemjoffice at gmail dot com.**

Please be sure to include your full affiliation and e-mail address (see Sample manuscript).

When submitting the manuscript, it is mandatory to include a cover letter to the editor. The cover letter must state:

- that all authors mutually agree that the manuscript can be submitted to EEMJ;
- that the manuscript contains the original work of the authors;

- the novelty in results/findings, or significance of results;
- that the manuscript has not already been published, or is not under consideration for publication elsewhere.

Manuscripts are evaluated first in the Editorial Office (as a preliminary condition for acceptance) in terms of meeting the requirements of the journal, including attempts of plagiarism. The authors are responsible for the accuracy of the whole paper and references. Authors will be notified about the registration of their contribution. Only those contributions, which conform to the following instructions, can be considered for the peer-review process. Otherwise, the manuscripts are returned to the authors, with observations, comments and annotations.

The peer review process is decisive for paper acceptance. It could be done in several stages, depending on the revision quality of the manuscript in accordance with the requirements of paper evaluators. Please do not transmit electronic data or requirements to the publisher until your manuscript has been reviewed and accepted for publication. Please follow the instructions below.

A minimum of four suitable *potential reviewers* should be provided by the authors. Please provide their name, email addresses, and institutional affiliation. When compiling this list of potential reviewers please consider the following important criteria: they must be knowledgeable about the manuscript subject area of the manuscript; they must not be from the authors' own institution or country; they should not have recent (less than five years) joint publications with any of the authors. However, the final choice of reviewers is at the editors' discretion.

4. Manuscript preparation

General:

Authors must follow the Instructions for authors strictly, failing which the manuscripts would be rejected without review. Editors reserve the right to adjust the formatting style to conform to the standards of the journal.

Manuscripts should be concise, in 1.5 line spacing, and should have 2 cm all over margins. The font should be Times New Roman of size 12 points. The numbering of chapters should be in decimal form. Ensure that each new paragraph is clearly indicated, using TAB at 1.25 pts.

The text layout should be in single-column format. Keep the layout of the text as simple as possible. Most formatting codes will be removed and replaced on processing the manuscript. However, do use bold face, italics, subscripts, superscripts etc. Add line numbering and page numbers. To avoid unnecessary errors it is strongly advised to use the 'spell-check' and 'grammar-check' functions of your word processor.

Title page will contain:

- A concise and informative title (Times New Roman bold, all caps of size 14 points); the maximum length

of the title should be maximum 100 letters and spaces; The full name(s) of the author(s) (first name, then last name, with Times New Roman bold 12 points) should be written below the title. The affiliation(s) and complete postal address(es) of the author(s) will be provided immediately after the full name of the authors and will be written with Times New Roman 12 points. When the paper has more than one author, their name will be followed by a mark (Arabic numeral) as superscript; for the corresponding author, an asterisk will be added using *Word_Insert_Reference_Footnote_Symbol* sequence. Also, the full and e-mail addresses, telephone and fax numbers of the corresponding author will be provided in the footer of the first page, as: Author to whom all correspondence should be addressed: email....., Phone....., Fax.....

- **Abstract:** each paper must be preceded by an abstract presenting the most important results and conclusions in no more than 250 words. Do not include citations in the Abstract.
- **Keywords:** three to five keywords should be supplied after the Abstract for indexing purposes, separated by comma, **ordered alphabetically**, using American spelling and avoiding general and plural terms and multiple concepts (avoid, for example, "and", "of"). Be sparing with abbreviations: only abbreviations firmly established in the field may be eligible.
- The text of the paper should be divided into **Introduction, Materials and methods (or Experimental), Results and discussion, Conclusions, References** (for papers dealing with environmental management, policy, education etc., the Experimental part can be replaced by case-studies presentation).

1. Introduction

State the objectives of the work and provide an adequate background, avoiding a detailed literature survey or a summary of the results.

2. Material and methods (or 2. Experimental)

Provide sufficient detail to allow the work to be reproduced. Methods already published should be indicated by a reference: only relevant modifications should be described.

3. Results and discussion

Results should be clear and concise. Discussion should explore the significance of the results of the work, not repeat them. Avoid extensive citations and discussion of published literature.

4. Conclusions

The main conclusions drawn from results should be presented in a short Conclusions section. Do not include citations in this section.

Formulae, symbols and abbreviations:

Formulae will be typeset in Italics (preferable with the Equation Editor of Microsoft Office 2003) and should be written or marked as such in the manuscript, unless they require a different styling. The formulae should be numbered on the right side, between brackets:

$$a^3 = 3M / 4N \quad (1)$$

Always refer in the text to Equations as (Eq. 1), Eqs. (1-4) etc.

The more complex Chemical Formulae should be presented as Figures.

Abbreviations should be defined when first mentioned in the abstract and again in the main body of the text and used consistently thereafter.

SI units must be used throughout.

Footnotes should be avoided.

References:

The list of References should only include works that are cited in the text and that have been published. References should be cited in the text in brackets (**Harvard style**) as in the following examples:

(Chisti, 1989), (Gavrilescu and Roman, 1996), (Moo-Young et al., 1999).

References should be alphabetically listed at the end of paper, with complete details, as follows:

Books: Names and initials of authors, year (between brackets), chapter title, title of the book (*italic*), editors, edition, volume number, publisher, place, page number:

Mauch K., Vaseghi S., Reuss M., (2000), *Quantitative Analysis of Metabolic and Signaling Pathways in Saccharomyces cerevisiae*, In: *Bioreaction Engineering*, Schügerl K., Bellgardt K.H. (Eds.), Springer, Berlin Heidelberg New York, 435-477.

Faber K., (2000), *Biotransformations in Organic Chemistry – A Textbook*, vol. VIII, 4th Edition, Springer, Berlin-Heidelberg-New York.

Handbook, (1951), *Handbook of Chemical Engineer*, vol. II, (in Romanian), Technical Press, Bucharest, Romania.

Symposia volumes: Names and initials of authors, year (between brackets), paper title, symposium name, volume number, place, date, page numbers:

Clark T.A., Steward D., (1991), *Wood and Environment*, Proc. 6th Int. Symp. on Wood and Pulping Chemistry, Melbourne, vol. 1, 493-498.

Journal papers: Names and initials of authors, year (between brackets), full title of the paper, full name of the journal (*italic*), volume number (**bold**), first and last page numbers:

Tanabe S., Iwata H., Tatsukawa R., (1994), Global contamination by persistent organochlorines and their ecotoxicological impact on marine mammals, *Science of the Total Environment*, **154**, 163-177.

Patents: Names and initials of authors, year (between brackets), patent title, country, patent number (*italic*):

Grant P., (1989), *Device for Elementary Analyses*. USA Patent, No. 123456.

Dissertations: Names and initials of authors, year (between brackets), title, specification (PhD Thesis, MSc Thesis), institution, place:

Aelenei N., (1982), *Thermodynamic study of polymer solutions*, PhD Thesis, Institute of Macromolecular Chemistry Petru Poni, Iasi, Romania.

Star K., (2008), *Environmental risk assessment generated by natural hazards*, MSc Thesis, Institute of Hazard Research, Town, Country.

Legal regulations and laws, organizations:

Abbreviated name, year (between brackets), full name of the referred text, document type, author, URL address:

ESC, (2007), Improving access to modern energy services for all fundamental challenge, Economic and Social Council, ENV/DEV/927, On line at: <http://www.un.org/News/Press/docs/2007/envdev927.doc.htm>.

EPA, (2007), Biomass Conversion: Emerging Technologies, Feedstocks, and Products, Sustainability Program, Office of Research and Development, EPA/600/R-07/144, U.S. Environmental Protection Agency, Washington, D.C., On line at: <http://www.epa.gov/Sustainability/pdfs/Biomass%20Conversion.pdf>.

EC Directive, (2000), Directive 2000/76/EC of the European Parliament and of the Council of 4 December 2000, on the incineration of waste, Annex V, *Official Journal of the European Communities*, L 332/91, 28.12.2000, Brussels.

GD, (2004), Governmental Decision No. 1076/2004 surnamed SEA Governmental Decision, regarding the procedure for strategic environmental impact assessment for plans or programs, *Romanian Official Monitor*, Part I, No. 707 from 5th of August, 2004.

Web references

The full URL should be given in text as a citation, if no other data are known. If the authors, year, title of the documents are known and the reference is taken from a website, the URL address has to be mentioned after these data:

Burja C., Burja V., (2008), Adapting the Romanian rural economy to the European agricultural policy from the perspective of sustainable development, MPRA, Munich Personal RePEc Archive, On line at: http://mpa.ub.uni-muenchen.de/7989/1/MPRA_paper_7989.pdf

Web references must not be listed separately, after the reference list.

All references must be provided in English with a specification of original language in round brackets.

Citation in text

Please ensure that every reference cited in the text is also present in the reference list (and vice versa). Do not cite references in the abstract and conclusions.

Unpublished results, personal communications as well as URL addresses are not recommended in the references list.

Citation of a reference as "in press" implies that the item has been accepted for publication.

Papers which have been accepted for publication should be included in the list of references with the name of the journal and the specification "in press".

References style

Text: All citations in the text may be made directly (or parenthetically) and should refer to:

- *single author:* the author's name (without initials, unless there is ambiguity) and the year of publication: "as previously demonstrated (Smith, 2007)"; "as Smith (2007) demonstrated"
- *two authors:* both authors' names and the year of publication: (Arnold and Sebastian, 2008; Smith and Hansel, 2006; Stern and Lars, 2009)
- *three or more authors:* first author's name followed by "et al." and the year of publication: "As has recently been shown (Werner et al., 2005)...", "Kramer et al. (2000) have recently shown"

Citations of groups of references should be listed first alphabetically, then chronologically.

Examples: "...as demonstrated (Aden, 1996a, 1996b, 1999; Allan and Jones, 1995; Han et al., 2007; Weiss and Schmidt, 1988)".

Abbreviations

Define all abbreviations at their first mention in the text. Ensure consistency of abbreviations throughout the article.

Acknowledgements

Include acknowledgements in a separate section at the end of the article before the references and do not, therefore, include them on the title page, as a footnote to the title or otherwise. List here those individuals who provided help during the research (e.g., providing language help, writing assistance or proof reading the article, funding supports etc.).

Footnotes

Footnotes must be avoided. Do not include footnotes in the Reference list.

Table footnotes

Indicate each footnote in a table with a superscript lowercase letter.

Tables

Draw the Tables in grid format using a basic, solid line style without shadows.

Ensure that the data presented in Tables do not duplicate results described in Figures or elsewhere in the paper.

Figures

Number Figures consecutively in accordance with their appearance in the text. All illustrations should be provided in camera-ready form, suitable for reproduction, which may include reduction without retouching.

Photographs, charts and diagrams are all to be referred to as Figure(s) and should be numbered consecutively, in the order to which they are referred.

Figures may be inserted preferably as black line drawings. They should be pasted on, rather than taped, since the latter results in unclear edges upon reproduction.

Ensure that each illustration has a caption, placed below the Figure. Supply also captions separately, not attached to the figure. A maximum limit of 8 Figures are allowed per manuscript.

A caption should comprise a brief title (**not** on the Figure itself) and a description of the illustration. Keep text in the illustrations themselves to a minimum but explain all symbols and abbreviations used. Multiple Figures can be expressed as one Figure (for e.g. 1a, 1b, 1c etc...), while retaining the maximum limit of 6.

ALL Figures must be submitted in either .jpg or .tiff format with a very good resolution (but do not submit graphics that are disproportionately large for the content).

Figures and Tables must be embedded in the text.

Proofs

Proofs will be sent to the corresponding author (by e-mail) and should be returned within 72 hours of receipt. Corrections should be restricted to typesetting errors; any other changes may be charged to the authors.

Paper in Electronic Format:

Authors are asked to submit their final and accepted manuscript as an attachment to one of the above-mentioned e-mail addresses. Use the .doc format (not .docx!).

5. Page charge

There is no charge per printed page for regular papers.

6. Reprints

The corresponding author will be provided with a .pdf file of the paper via e-mail, free of charge. A hard copy of the issue containing the paper can be provided on request, for a fee. This request will be formulated when the final form of the manuscript (the electronic one) is provided.

7. Additional procedures for the editorial management of *Environmental Engineering and Management Journal*

Starting with volume 13/2014, the members of the Scientific Advisory Board and the Corresponding authors will receive each issue of the journal in electronic .pdf format. Printed copies can be delivered on request.

An author cannot appear on more than two papers per regular issue. An author cannot appear on more than three papers in a Guest Editor/ Conference issue.

The evaluation/peer-review process of manuscripts submitted for Guest Editor / Conference issues published according to journal *Editorial Procedure and Policy* will be handled and evaluated as with regular manuscripts, so that only consistent papers will be published. The manuscripts must be sent at least six months before the presumed date of publication. Those manuscripts which do not fulfill the journal requirements will be rejected. This is to discourage superficiality in the development of the manuscript, from formal and scientific points of view. No amount of money will be refunded following the rejection of manuscripts.

No more than 160 pages and no more than 20 papers are acceptable for regular issues. No more than 180 pages and no more than 25 papers are opportune for special issues. The number of pages is based on the published version of an article, not on the submitted version (for instance, when page breaks are changed and when images are enlarged for easier viewing).

An issue can include, as an exception, a number of 25-30 papers as a maximum. This situation could appear when the authors of an already accepted paper need and ask for early publication, from the position in the list of accepted papers. In this circumstance, a yearly submission to our journal (500 Euro) will be asked for each already accepted paper, for its publication in advance.

A newly-received manuscript can be evaluated by priority, when a deposit of 200 Euro shall be paid by authors in advance. If the manuscript is deemed

unsuitable for publication, the authors will not be eligible for a refund.

Failure to pay mandatory charges may result in the paper being withheld from early publication.

In all cases, the corresponding author will sign an agreement with the *Editor-in-Chief*, and the *Director* of the *EcoZone* Publishing House according to journal *Editorial Procedure and Policy*.

Automated software is used for checking against plagiarism. In order to avoid false results, the generated reports are cautiously checked and confirmed by journal staff. We do not send plagiarism reports to authors. Any manuscripts which do not prove to be at least 90% original will be rejected. The rejection for plagiarism may arise at any phase of the editorial / review process, even if the manuscript was accepted for publication. The authors are solely responsible for the originality of their submission. Therefore, any manuscript should be carefully checked for such inconsistencies before submitting to EEMJ.

The authors are required to follow academic publishing rules, to adhere to the principles of scientific ethics and to sign the Authors' warranty and Copyright transfer.

Detailed information concerning these issues may be found of the EEMJ website, under *Editorial Procedure and Policy*.

Environmental Engineering and Management Journal is edited by the
Publishing House **ECOZONE** of the
Academic Organization for Environmental Engineering and Sustainable Development (OAIMDD)
within the **Department of Environmental Engineering and Management – Faculty of Chemical Engineering and
Environmental Protection under the aegis of "Gheorghe Asachi" Technical University of Iasi**
73 Prof.Dr.docent Dimitrie Mangeron Street, 700050-Iasi, Romania



"Gheorghe Asachi" Technical University of Iasi